Identification of novel avirulence effectors in the Dothideomycete plant pathogens, *Venturia inaequalis* and *Cladosporium fulvum*

A thesis presented in partial fulfilment of the requirements for the degree of

Doctor of Philosophy (PhD)

in

Plant Sciences

at Massey University, Manawatū

New Zealand

Silvia de la Rosa

2022

Abstract

Venturia inaequalis and *Cladosporium fulvum* are important fungal pathogens of crop species, causing scab and leaf mould disease of apple and tomato, respectively. Resistance to these pathogens is governed by *Rvi* (apple) and *Cf* (tomato) resistance (*R*) genes. These *R* genes encode immune receptors that recognize specific pathogen virulence factors, termed avirulence (Avr) effectors, to activate plant defenses. Notably, isolates or strains of *V. inaequalis* and *C. fulvum* have emerged that can overcome resistance mediated by specific *R* genes in their respective hosts. To better understand how these pathogens cause disease or overcome resistance, and to monitor the occurrence of resistance-breaking isolates or strains in the field, Avr effectors from *V. inaequalis* and *C. fulvum* must be identified and functionally characterized. Using a combined comparative genomics and phenotyping approach based on progeny from a sexual cross between *V. inaequalis* isolates that differ in their ability to overcome *Rvi4* resistance in apple, a strong candidate for the corresponding *AvrRvi4* effector gene was identified (Chapter 2). Similarly, using a comparative genomics approach based on *in planta*-expressed effector candidates from *C. fulvum* strains that differ in their ability to overcome *Cf-9B* resistance in tomato, combined with functional assays, the corresponding *Avr9B* effector gene was identified (Chapter 4). In the resistance-breaking isolates or strains studied, the candidate *AvrRvi4* gene was disrupted, while the *Avr9B* gene had been deleted. Consistent with most fungal Avr effectors and their genes, both the *AvrRvi4* candidate and *Avr9B* are highly expressed *in planta*, and encode small, secreted cysteine-rich proteins. The AvrRvi4 candidate forms part of an expanded protein family in *V. inaequalis*, with members predicted to adopt a β-sandwich fold similar to structurally characterized fungal effectors. Avr9B, however, is predicted to adopt a novel protein fold. Finally, using a heterologous expression approach, three *in planta*-expressed candidate effectors from *V. inaequalis* were found to trigger defense responses in non-host plants (*Nicotiana* spp.), suggesting they are recognized by R proteins in these species (Chapter 3). Taken together, this thesis has increased our understanding of the molecular mechanisms responsible for the activation and circumvention of resistance by *V. inaequalis* and *C. fulvum*, which will in turn direct host cultivar deployment and disease control strategies in the field.

Acknowledgements

First and foremost, I would like to thank my supervisor Dr Carl Mesarich, for giving me the opportunity to be part of his research team as his first PhD student. I truly value the time, effort, and patience you invested in me and my project. I could not forget thanking you for all the jokes that brought me into happy tears during lunch time, those moments eased the stress I was going through. I also thank my Co-supervisor Prof. Rosie Bradshaw, for all her input, suggestions, and guidance. Special thanks to Dr Joanna Bowen for allowing me to perform some of my experiments at Plant and Food Research, for offering a place to stay in Auckland, for her advice and critical review of my PhD thesis. Thanks also to Saadiah Arshed and Brogan McGreal for their contribution to my project regarding bioinformatic methods. My gratitude to Dr Vincent Bus for his input and for providing apple seeds, grafted trees, and *V. inaequalis* parent isolates and progeny for my experiments. Thanks to David Jones for kindly providing Cf-9 and Cf-9B constructs for my agroinfiltration experiments.

Thanks to Assoc. Prof. Matthieu Joosten for his valuable feedback and ideas for the *C. fulvum* project, and to Christiaan Schol for his time and effort by completing some of my experiments at Wageningen University. My gratitude as well to the collaborators from INRAE in France: Bruno LeCam for allowing me to use data from his *V. inaequalis* isolate EU-B04 for my screening experiments, and to Mélanie Sannier for sequencing *V. inaequalis* race 4 isolates. Thanks to Kim Plummer for her brilliant ideas and her hospitality during my visit to the Stromlo Plant Pathology conference in Australia. I would also like to thank the team at the MMIC, Matthew Savoian and Raoul Salomon for their help and guidance.

To the following people that have been part of this long and challenging path, full of ups and downs. Without all of you, it would have been almost impossible to have the strength and willingness to continue. I am extremely grateful to have shared the lab with exceptional scientists, thanks for your friendship, help with my experiments and for being there for me in difficult moments; Mariana Tarallo, Ellie Bradley, Mercedes Rocafort, Melissa Guo, Simren Brar, Hannah McCarthy, Ashleigh Mosen, Berit Hassing and Lukas Hunziker. I'm also grateful for the incredible friends that always had comforting words, an advice, or a simple funny anecdote that made me smile; Rayén León, Alejandra Alfaro, Mario Alayón, Paul Ogbuigwe and Sebastián Rivera. Special thanks to Carlos Santa Cruz, for preparing the best Mexican food and for sharing with me all those delicious meals that made me feel like home. Thank you, Diana Cabrera, for always being there for me and for cheering me up in decisive moments of my life and PhD.

My sincere appreciation to my friends in Mexico and Europe, thanks for your friendship, love and support despite the distance and time apart, Beatriz Alvarado, Rolando Moreno, Thalia Parra, José Angel Monsivais and Gina Samaniego. Thank you, Dr Felipe Reyes, for all your support during both of my scholarship applications, I am sure we will meet again.

To my family: Gracias mamá y papá por su amor, por haberme dado el mejor ejemplo, la mejor educación, y por apoyarme siempre en todas mis decisiones. Sin ustedes no habría logrado lo que hasta ahora. Los amo tanto y me siento muy afortunada de ser su hija. Espero estén orgullosos de mi, esto se los dedico principalmente a ustedes. Espero verlos pronto y poder compensar todo este tiempo que he estado tan lejos de casa. Gracias a mis tías, primas y sobrinos, especialmente a Brenda Saucedo. Perlita, aún nos quedan muchas carcajadas y momentos por compartir, estás en mis pensamientos y confío que vas a ganar esta lucha. Admiro tu fortaleza!

Table of contents

List of figures

List of tables

List of Abbreviations

aa	amino acid(s)
ADPR	adenosine diphosphate ribose
AF	apoplastic fluid
Amp	ampicillin
APS	ammonium persulfate
ATP	adenosine triphosphate
ATR1	*Arabidopsis thaliana* Recognized 1
ATTA	*Agrobacterium tumefaciens* transformation assay(s)
Avr	avirulence
BAC	bacterial artificial chromosome
BAK1	Brassinosteroid Insensitive 1-Associated Kinase 1
bp	base pair(s)
BLAST	basic local alignment search tool
BSA	bulk segregant analysis
°C	degrees Celsius
CC	coiled-coil
CBM	carbohydrate-binding module
cDNA	complementary DNA
cds	coding sequence
CfCEs	*Cladosporium fulvum* candidate effectors
CE	candidate effector
Cin	cellophane-induced
cm	centimetre(s)
CPPs	cerato-platanin(s)
CTAB	cetyltrimethyl ammonium bromide
CWDEs	cell wall-degrading enzymes
Cys	cysteine
DAMP	damage-asssociated molecular pattern
DMI	demethylation inhibitor
DMSO	dimethyl sulfoxide
DNA	deoxyribunocleic acid
dNTP	deoxyribonucleic triphosphate
dpi	days post-inoculation
DTT	dithiothreitol
ECPs	extracellular proteins
ED	ectodomain
EDTA	ethylenediaminetetraacetic acid
ER	endoplasmic reticulum

ETI	effector-triggered immunity
ETS	effector-triggered susceptibility
fgl	flagellin
FLS2	flagellin-sensing 2
FPMK	fragments per million per kilobase
g	gram
g	gravitational force
GFP	green fluorescent protein
GH	glycosyl hydrolase
GPI	glycosylphosphatidylinositol
GWAS	genome-wide association study
h	hour(s)
ha	hectare
HABS	high-affinity binding sites
HR	hypersensitive response
ID	integrated domain
IDR	intrinsically disordered region
IM	induction medium
IP	invasion pattern
IPR	invasion pattern receptor
IPTG	Isopropyl β-D-1-thiogalactopyranoside
IPTR	invasion pattern-triggered response
JGI	Joint Genome Institute
KD	kinase domain
kDa	kilodalton(s)
L	litres
LB	lysogeny broth
LPMOs	lytic polysaccharide monooxygenase(s)
LPS	lipopolysaccharide
LRR	leucine-rich repeat
LysM	lysin motif
M	molar
MAMP	microbe-associated molecular pattern
MAPK	mitogen-activated protein kinase
MBC	methyl benzimidazole carbamate
mg	milligram
min	minute(s)
ml	millilitre(s)
mm	millimetre(s)
mM	millimolar

MM	minimal medium
MMT	million metric tons
MS	Murashige and Skoog
MTI	MAMP-triggered immunity
MW	molecular weight
NB	nucleotide-binding site
NCBI	National Centre for Biotechnology Information
NEP1	necrosis and ethylene-inducing peptide 1
NGS	next generation sequencing
NLPs	necrosis and ethylene-inducing peptide 1-like proteins
NLS	nuclear localization signal
nt	nucleotide(s)
NZ	New Zealand
µg	microgram(s)
µl	microlitre(s)
µM	micromolar
OD	optical density
PAGE	polyacrylamide gel electrophoresis
PAMP	pathogen-associated molecular pattern
PCR	polymerase chain reaction
PDA	potato dextrose agar
PDB	protein data bank
PDB	potato dextrose broth
PEP1	protein essential during penetration 1
pLDDT	predicted local-distance difference test
PNPL	plant natriuretic peptide-like
PR	pathogenesis-related
PR1α	pathogenesis-related protein 1α
PRR	pattern recognition receptor
PTI	PAMP-triggered immunity
PVDF	polyvinylidene fluoride
PVP	polyvinylpyrrolidone
PVX	potato virus X
QoI	quinone outside inhibitor
QTL	quantitative trait locus
R	resistance
RCPs	repeat-containing protein(s)
RH	relative humidity
RIP	repeat-induced mutation

RiPPs	ribosomally and post-translationally modified peptide(s)
RLCKs	receptor-like cytoplasmic kinase(s)
RLKs	receptor-like kinase(s)
RLPs	receptor-like protein(s)
RNA	ribonucleic acid
ROS	reactive oxygen species
rpm	revolutions per minute
RPP1	recognition of *Peronospora parasitica* 1
RT	room temperature
RT-qPCR	quantitative reverse transcription PCR
SA	salicylic acid
SDHI	succinate dehydrogenase inhibitor
SDS	sodium dodecyl sulfate
sec	second(s)
SERK3	somatic embryogenesis receptor kinase 3
SNPs	single nucleotide polymorphism(s)
SNVs	single nucleotide variant(s)
SOBIR1	suppressor of BAK1-interacting receptor-like kinase 1
SP	signal peptide
SRA	sequence read archive
SSPs	small secreted protein(s)
TAE	tris-acetic acid EDTA
TBST	tris-buffered saline and Tween 20
TBSV	tomato bushy stunt virus
T-DNA	transfer DNA
TEMED	tetramethylethylenediamine
TIR	toll/interleukin-receptor
TM	transmembrane domain
UV	ultraviolet
V	volt(s)
VICE	*Venturia inaequalis* candidate effector
VIGS	virus-induced gene silencing
WA	water agar
X-gal	5-bromo-4-chloro-3indolyl-β-D-galactopyranoside
XopQ	*Xanthomonas* outer protein Q
YFP	yellow fluorescent protein

Chapter 1: General introduction

Fungal plant pathogens are a global threat to food security as they cause diverse crop diseases that result in high agricultural yield losses each year. Estimations of global annual agricultural production losses from fungal diseases range from 10 to 23% (Steinberg & Gurr, 2020) and in some cases can reach up to 30% (Savary et al., 2019). Such losses are anticipated to increase with climate change, as the warmer and wetter weather conditions favour disease, but also the spread of fungal species further north into the Northern hemisphere and further south into the Southern hemisphere (Bebber et al., 2013; Chaloner et al., 2021). Many diseases affecting and threatening crops are caused by fungal pathogens belonging to the phylum Ascomycota, and in particular, the Dothideomycetes, which is the largest and most ecologically diverse class in the kingdom Fungi (Haridas et al., 2020; Kirk et al., 2008). The Dothideomycete class can be divided into more than 23 orders comprised of 110 families, 1,261 genera and about 19,000 species (Wijayawardene et al., 2017). The Pleosporales, Capnodiales and Venturiales are three Dothideomycete orders that include many of the most devastating pathogens worldwide (Ohm et al., 2012). Among the main crop diseases caused by these orders of fungi are Septoria nodorum blotch of wheat (caused by *Parastagonospora nodorum*) (Quaedvlieg et al., 2013), net blotch of barley (caused by *Pyrenophora teres* f. *maculata*) (Backes et al., 2021), blackleg disease of brassicas (caused by *Leptosphaeria maculans*) (Becker et al., 2017), scab disease of apple (caused by *Venturia inaequalis*) (Bowen et al., 2011), leaf mould disease of tomato (caused by *Cladosporium fulvum*) (Mesarich et al., 2018), black sigatoka disease of banana (caused by *Pseudocercospora fijiensis*) (Arango et al., 2016), and septoria leaf blotch of wheat (caused by *Zymoseptoria tritici*) (Kildea et al., 2021) (Fig. 1.1). Depending on the fungus, the lifestyle of these Dothideomycetes can be biotrophic, necrotrophic or hemibotrophic. Biotrophs, such as *V. inaequalis* and *C. fulvum*, depend on living tissue to acquire nutrients and colonize their hosts. Hemibiotrophs, such as *L. maculans*, *P. fijiensis* and *Z. tritici* initially have a biotrophic phase, where they require living host tissue, but then later shift to a necrotrophic lifestyle, whereby they kill the host to obtain nutrients. Finally, necrotrophs, such as *P. nodorum* and *P. teres* f. *maculata*, steadily decompose their host

cells to obtain nutrients for growth (Pradhan et al., 2021; Vleeshouwers & Oliver, 2014). It should be noted, however, that some biotrophic pathogens are sometimes referred to as hemibiotrophs, despite not having a necrotrophic phase. Indeed, the term hemibiotroph is also often used to describe pathogens that switch from a biotrophic to saprophytic mode of growth, such as *V. inaequalis* (Bowen et al., 2011). *C. fulvum*, too, is also sometimes referred to as a hemibiotroph (e.g., Ökmen et al., 2017). This is because, under some conditions, disease lesions become chlorotic or necrotic late in the infection cycle. This is thought to be due to the production and aggregation of conidiophores that block stomata, limiting respiration, that in severe infections, leads to the death of the host (Thomma et al., 2005).

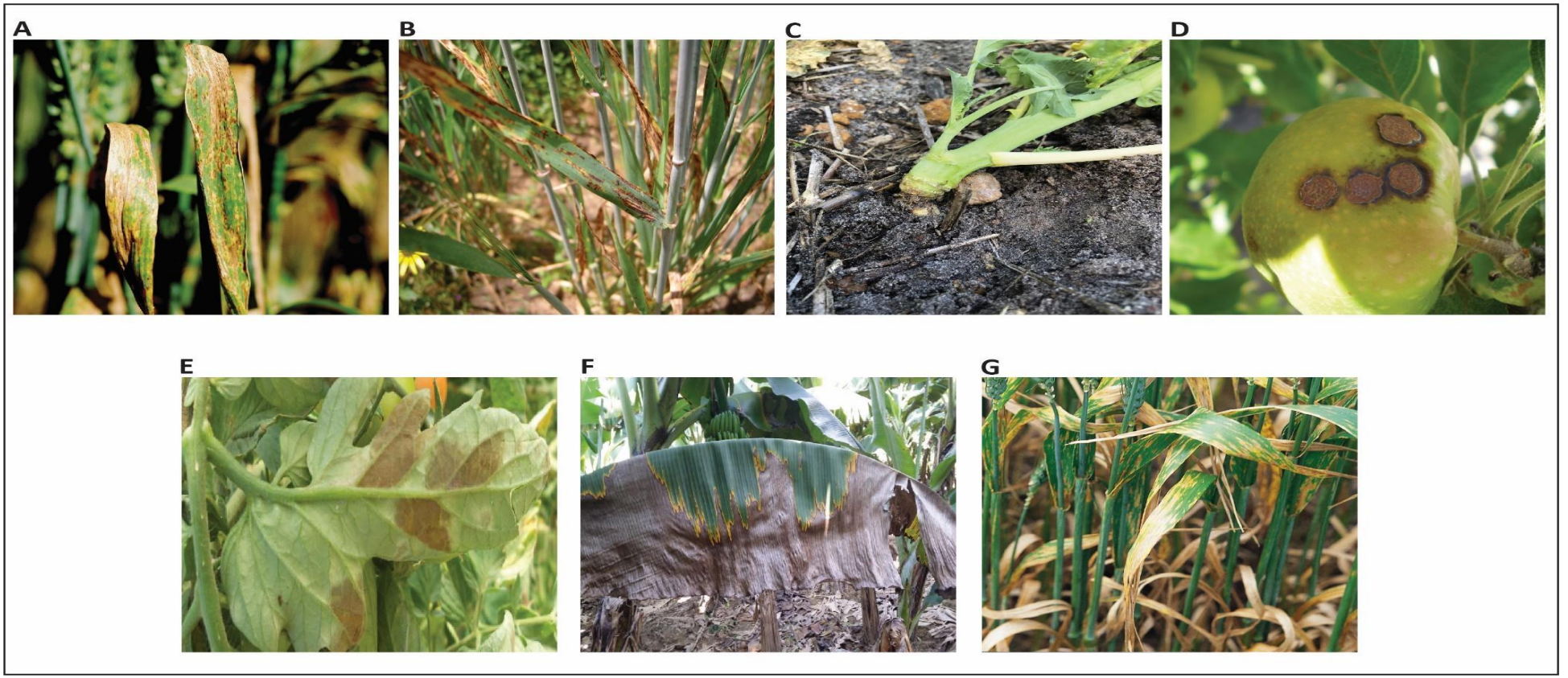

Figure 1.1. Crop diseases caused by fungal pathogens belonging to the Dothideomycetes class. (A) Septoria nodorum blotch disease of wheat caused by *Parastagonospora nodorum* (Department of Agriculture and Food Western Australia, DAFWA (2013)). **(B)** Net blotch disease of barley caused by *Pyrenophora teres* f. *maculata* (Geoff Thomas, DAFWA (2021)). **(C)** Blackleg disease of Brassicas caused by *Leptosphaeria maculans* (Justin Kudnig, Advanta Seeds (2018)). **(D)** Scab or black spot disease of apple caused by *Venturia inaequalis* (Department of Primary Industries and Regional Development, DPIRD (2021)). **(E)** Leaf mould disease of tomato caused by *Cladosporium fulvum* (Nexles® EU). **(F)** Black Sigatoka disease of banana caused by *Pseudocercospora fijiensis* (Prof. André Drenth, University of Queensland). **(G)** Septoria leaf blotch disease of wheat caused by *Zymoseptoria tritici* (South Australian Research and Development Institute (1992)).

1.1 Plant-pathogen interactions

To cause disease, plant-pathogenic fungi must enter their hosts. To do this, they first need to circumvent preformed physical and chemical barriers at the plant surface. Physical barriers include stomata, the cuticle and in some instances, the cell wall (Wang & Wang, 2018), whereas chemical barriers include phytoanticipins, which are secondary metabolites stored in plant tissues (Zaynab et al., 2018). Such barriers serve as a basic level of defence against invading organisms. Thus, as soon as contact is made, pathogenic fungi sense such physical and chemical components on the plant surface (e.g. stomatal pores, wax, cellulose and cutin), to stimulate the processes of germination and penetration required for host entry (Lo Presti et al., 2015; Toruno et al., 2016). The Dothideomycete*s* *Alternaria alternata* and *Alternaria brassicicola*, as well as the Sordariomycete *Fusarium solani*, for example, deploy cutinases to penetrate the cuticle, whereas *L. maculans* and *C. fulvum* use the topography signals of stomatal pores and wounds to enter into leaves (Asai & Shirasu, 2015; Kim et al., 1998; Stotz et al., 2014; Tanaka et al., 2017). Some fungi use specialized infection structures named appressoria to penetrate the plant tissue. To penetrate, the appressorium must adhere firmly to the host surface and form an infection peg that breaks into the cuticle and cell wall (Huang, 2001). *V. inaequalis* can breach the cuticle using appressoria combined with enzymatic activity (Koller et al., 1991). Contrarily, the Basidiomycota fungus *Ustilago maydis* and the Sordariomycete *Colletotrichum higginsianum*, use appressoria to accumulate turgor pressure and facilitate the entry into the host through mechanical force (Giraldo & Valent, 2013; Ryder & Talbot, 2015).

Once physical and pre-formed chemical barriers have been breached or overcome by plant-pathogenic fungi, plants must rely on their immune system to provide protection against infection and disease. Over recent years, several models have been put forward to describe the plant immune system. The most well-known of these is the Zigzag Model (Fig. 1.2) (Jones & Dangl, 2006). This model separates the plant immune system into two layers; the first layer relies on pattern recognition receptors (PRRs) at the cell surface, which recognize conserved pathogen-associated molecular patterns (PAMPs), such as chitin in fungi or flagellin of bacteria to give PAMP-triggered immunity (PTI). PTI defence responses include callose deposition, production of reactive oxygen species (ROS), ion fluxes at the plasma membrane, accumulation of defence hormones

and antimicrobial compounds, and the expression of other pathogenesis-related (PR) genes (Boller & Felix, 2009; Couto & Zipfel, 2016; Giraldo & Valent, 2013). To successfully infect their hosts, invading plant pathogens must then deliver virulence factors, termed effectors, into host cells to suppress PTI to give effector-triggered susceptibility (ETS). If the pathogen does not have the right toolkit of effector proteins, then PTI cannot be overcome. In the second layer of the plant immune system, certain plants have evolved to recognize one or more of these effector proteins to trigger effector-triggered immunity (ETI), rendering the plant resistant. This recognition relies on intracellular immune receptors called resistance (R) proteins, with the recognized effectors termed avirulence (Avr) effector proteins, as the pathogen is rendered avirulent. ETI is characterized by a strong localized cell death reaction at the pathogen infection site, termed the hypersensitive response (HR), which halts the growth of the pathogen (Heath, 2000). To successfully cause infection and disease, plant pathogens then need to suppress ETI through an expansion of their effector repertoire or through, for example, deletion or modification of the gene encoding the recognized Avr effector, such that recognition can no longer occur (Jones & Dangl, 2006). These interactions between R and Avr proteins are the ongoing result of a molecular arms race between plant pathogens and their hosts to evade and regain recognition, respectively.

Over recent years, however, it has become increasingly clear that the Zigzag Model has several key shortfalls. For example, the Zigzag Model does not accommodate fungal pathogens with necrotrophic or hemibiotrophic lifestyles. Furthermore, it does not acknowledge the involvement of endogenous damage-associated molecular patterns (DAMPs) (e.g. plant cell wall fragments released by fungal cell wall-degrading enzymes) in triggering PTI, or the fact that some PTI responses are strong, while some ETI responses are weak or do not involve an HR. Notably, the distinction between PAMPs and effectors has also become increasing ambiguous, with a number of conserved effectors from plant-pathogenic fungi now known to be recognized by PRRs as PAMPs (Boller & Felix, 2009; Thomma et al., 2011). PRRs, too, have been shown to function as R proteins outside of the cell, where they recognize effector proteins from, for example, *C. fulvum*, to trigger ETI (see section 1.5.5). With these points in mind, an alternative view of the plant immune system, called the Invasion Model was proposed (Fig. 1.3) (Cook et al., 2015). This model states that molecules with any function, be that a PAMP,

effector or DAMP, are collectively called invasion patterns (IPs). IPs are perceived by invasion pattern receptors (IPRs) which include both extracellular and intracellular immune receptors, leading to IP-triggered responses (IPTRs) of various strengths, depending on the IP and IPR involved. The outcome of an IPTR can either be the continuation or the end of the symbiosis (infection) due to the success or failure to suppress IPTR, respectively.

Figure 1.2. The Zigzag Model of the plant immune system. In phase 1, the plant immune system recognizes and responds to conserved pathogen-associated molecular pattern (PAMPs), via pattern recognition receptors (PRRs) leading to PAMP-triggered immunity (PTI). In phase 2, pathogens secrete effectors to suppress PTI, or enable pathogen nutrition and dispersal, resulting in effector-triggered susceptibility (ETS). In phase 3, an effector is recognized by an intracellular resistance (R) protein to trigger effector-triggered immunity (ETI) that results in a hypersensitive cell death response (HR). The recognized effector is termed an avirulence (Avr) protein. In phase 4, pathogens have lost, mutated, or gained new effectors through horizontal gene flow (in blue), to suppress ETI. Selection favors new plant R protein alleles that can recognize the altered or new effectors, resulting again in ETI. Figure from Jones & Dangl (2006).

Figure 1.3. **The Invasion Model of the plant immune system.** Invasion patterns (IPs), whether pathogen-associated molecular patterns (PAMPs), damage-associated molecular patterns (DAMPs) or effectors, are perceived by plant invasion pattern receptors (IPRs), leading to an IP-triggered defence response (IPTR). In the case of biotrophs, this IPTR may stop the symbiosis (infection). Invading pathogens however can use effectors to suppress IPTRs. In the case of necrotrophs, these can utilize the IPTR for their own advantage (e.g. nutrient acquisition) and continue the symbiosis. Figure from Cook et al. (2015).

From this point forward, I will use the term Avr effector in the context of being an IP, extracellular and intracellular R proteins in the context of being an IPR, and HR or another R protein-mediated response in the context of being an IPTR, consistent with the Invasion Model.

At the simplest level, the interaction between pathogen Avr effector proteins and plant R proteins is governed by pathogen *Avr* effector genes and plant *R* genes, and is best described by the Gene-for-Gene Model proposed by Flor (1971). This model suggests that the occurrence of matching genes in the host (*R* genes) and pathogen (*Avr* genes) are required for host resistance, leading to incompatibility. Furthermore, this model points out that the absence, alteration or loss of either the *R* or *Avr* gene compromises host resistance, leading to disease or compatibility. However, Avr–R

interactions are not always this simple. Complex interactions between Avr and R proteins have been described in cases where two Avr proteins are recognized by a single R protein, when an Avr protein is recognized by more than one R protein, and when another effector is able to mask the presence of another Avr protein (Anh et al., 2018; Ghanbarnia et al., 2018; Petit-Houdenot et al., 2019).

For example, the *Avr* gene encoding AvrLm10 from *L. maculans* and the *R* gene encoding Rlm10 from *Brassica nigra* do not interact in a typical gene-for-gene manner, but instead display a 'genes-for-gene' interaction (Petit-Houdenot et al., 2019). More specifically, the AvrLm10 avirulence is conferred by two adjacent *Avr* genes, *AvrLm10A* and *AvrLm10B*, which are both necessary to trigger *Rlm10*-mediated resistance (Petit-Houdenot et al., 2019). In another example, a 'gene-for genes' interaction is observed between the *Avr* gene *AVR–Rmg8* from the Sordariomycete *Pycularia oryzae* and the wheat *R* genes *Rmg8* and *Rmg7,* which encode R proteins that can both recognize the Rmg8 Avr effector (Anh et al., 2018). Finally, the *L. maculans* gene encoding the AvrLm4-7 effector protein can block the recognition of the AvrLm5-9 Avr protein by the corresponding *B. napus* Rlm9 resistance protein (Ghanbarnia et al., 2018). To the contrary, necrotrophic fungi follow the Inverse Gene-for-Gene Model. Under this model, fungi instead have effector genes that encode host-selective toxins (HSTs). These HSTs interact with the product of plant susceptibility (*S*) genes to cause disease susceptibility instead of resistance (Friesen et al., 2007). These examples illustrate how complex and dynamic the interactions between plants and fungal pathogens are. In both cases, the Avr and HST can be thought of as IPs and the R and S proteins as IPRs.

1.2 Invasion pattern receptors (IPRs)

Activation of plant immune responses depend on the recognition of IPs by extracellular or intracellular IPRs.

1.2.1 Extracellular IPRs

Extracellular IPRs are highly conserved transmembrane proteins that are activated upon recognition of apoplastic IPs. PRRs are divided into main two classes: the receptor-like kinases (RLKs) and the receptor-like proteins (RLPs) (Zipfel, 2014). RLKs possess a ligand-binding domain (ectodomain), a transmembrane (TM) domain and a cytoplasmic

kinase domain, whereas RLPs contain an extracellular domain and a short cytoplasmic tail without a kinase domain (Fig. 1.4) (Wang et al., 2018; Zipfel, 2014). Lacking an intracellular kinase domain, the majority of RLPs must interact constitutively with the adaptor kinase Suppressor of BAK1-Interacting Receptor-like Kinase 1 (SOBIR1) (Gust & Felix, 2014), and then recruit the Brassinosteroid Insensitive 1-Associated Kinase 1/Somatic Embryogenesis Receptor Kinase 3 (BAK1/SERK3) for immune signaling upon recognition of the IP. For example, the tomato RLP Cf-4 is constitutively associated with SOBIR1 to provide stability and perceive Avr4, an Avr effector protein from *C. fulvum*, and then SERK1 and BAK1/SERK3 associate to induce an HR (Postma et al., 2016). In the same way, the tomato RLP Ve1, which recognizes Ave1, an effector protein from the Sordariomycete *Verticillium dahliae*, depends on SERK1 and BAK1/SERK3 to activate an HR (Fradin et al., 2011; Fradin et al., 2009). Receptor-like cytoplasmic kinases (RLCKs) associate with RLK complexes and trigger intracellular signaling through mitogen-activated protein kinase (MAPK) cascades that, upon phosphorylation of different substrates, regulate plant immunity (Fig. 1.4) (Xu & Zhang, 2015). RLKs and RLPs are classified according to their ectodomain, with the leucine-rich repeat (LRR) ectodomain, which recognises peptides or proteins, being the largest subfamily (He et al., 2018). A well characterized LRR-RLK is the Flagellin-Sensing 2 (FLS2) that perceives the bacterial elicitor flagellin (fgl22) (Gómez-Gómez & Boller, 2000). There are other examples of extracellular domains in IPRs, such as the lysin motifs (LysM) that sense chitin and bacterial peptidoglycans, and the lectin-S domains that recognize bacterial lipopolysaccharide (LPS) (Ranf et al., 2015; Wan et al., 2012).

Figure 1.4. Extracellular invasion patter receptor (IPR) activation and subsequent signal transduction in plants. Plasma membrane-localized receptor-like kinase (RLK) and receptor-like protein (RLP) invasion pattern (IP) receptors (IPRs), recognize IPs (shown as stars) of invading pathogens. At the basic level, RLKs contain an extracellular ectodomain (ED), a transmembrane domain (TM), and a cytoplasmic kinase domain (KD). Upon binding of an IP to a RLK receptor, hetero-dimerization of the receptor with a regulatory RLK is induced, which leads to phosphorylation and activation of both RLKs. On the contrary, RLPs lack the kinase domain often associated with RLKs. The activation of an RLP-RLK complex usually requires a ligand or IP-dependent interaction with another RLK. Receptor-like cytoplasmic kinases (RLCKs) associate with RLK complexes to initiate mitogen-activated protein kinase (MAPK) cascades that further phosphorylate (P) diverse protein substrates to regulate not only plant immunity, but also other processes such as plant growth and development. Figure from He et al. (2018).

1.2.2 Intracellular IPRs

Intracellular IPRs frequently consist of a non-conserved amino (N)-terminal domain, central nucleotide-binding and oligomerization site (NB) and a carboxyl (C)-terminal leucine-rich repeat (LRR) (Ma et al., 2020). These proteins, called NLRs, are classified depending on their N-terminal domain whether a Toll/interleukin 1 receptor (TIR), coiled-coil (CC) or (RPW8)-like coiled-coil domain (Martin et al., 2020; Petit-Houdenot & Fudal, 2017; Takken & Goverse, 2012). NLR proteins are not designated to a single location in the cell, but have been found to localize to the cytoplasm, nuclear compartments, plasma membrane, and endomembranes (Heidrich et al., 2012; Kapos et al., 2019). Different effector detection strategies by NLR receptors have been shown.

Direct recognition can occur when the effector interacts directly with the NLR, activating a defence response (Fig. 1.5A) (Dodds et al., 2006). Indirect recognition can be described by the Guard Model which proposes that the effector interacts with targets guarded by the NLR (Fig. 1.5B) (Dangl & Jones, 2001). A third model, the Integrated Decoy Model, proposes that the NLR possesses an extra integrated domain (ID) that acts as a functional effector target that recognizes the effector indirectly (Fig. 1.5C) (Baggs et al., 2017). Direct or indirect effector recognition by NLRs trigger defence responses that generally give rise to an HR (Jones et al., 2016).

Recently, the activation mechanisms of CC-NLRs and TIR-NLRs upon effector recognition have been described (Ma et al., 2020; Martin et al., 2020; Wang et al., 2019). Wang et al. (2019) studied the activation of the CC-NLR ZAR1 (HopZ-Activated Resistance 1) from *Arabidopsis* by the AvrAC effector from the bacterium *Xanthomonas campestris* pv. *campestris.* ZAR1 in an inactive state is in a complex with the RLCK RKS1. Upon uridylation of the PBS1-like protein 2 (PBL2) by AvrAC, PBL2 activates RKS1 to induce conformational changes in ZAR1 to bind dATP or ATP which further facilitates structural remodelling of ZAR1. This structural remodeling results in the formation of a pentameric ZAR1-RKS1-PBL2 complex, also called a resistosome (Fig. 1.6A-B) (Wang et al., 2019). This funnel-shaped complex promotes ZAR1 integration into the plasma membrane to induce an immune response (i.e., HR-associated cell death) by disturbing the integrity of the plasma membrane or ionic homeostasis (Wang et al., 2019).

Martin et al. (2020) studied the activation of the TIR-NLR ROQ1 (Recognition of XopQ1) from *Nicotiana benthamiana* by the effector XopQ (*Xanthomonas* outer protein Q) from *Xanthomonas euvesicatoria*. Upon physical interaction and recognition of XopQ, the LRR and post-LRR domains form a special 'horseshoe-shape' scaffold that encloses the effector and inhibits its ligand-binding function. Such recognition and activation lead to tetramerization of ROQ1 through the NB-ARC domains, bringing the TIR domains closer to form a resistosome (Fig. 1.6C). Such oligomerization exposes the NADase active site, in which the subsequent NAD^+ cleavage leads to the release of adenosine diphosphate ribose (ADPR) that modulates cytosolic Ca^{2+} influx leading to cell death (Martin et al., 2020).

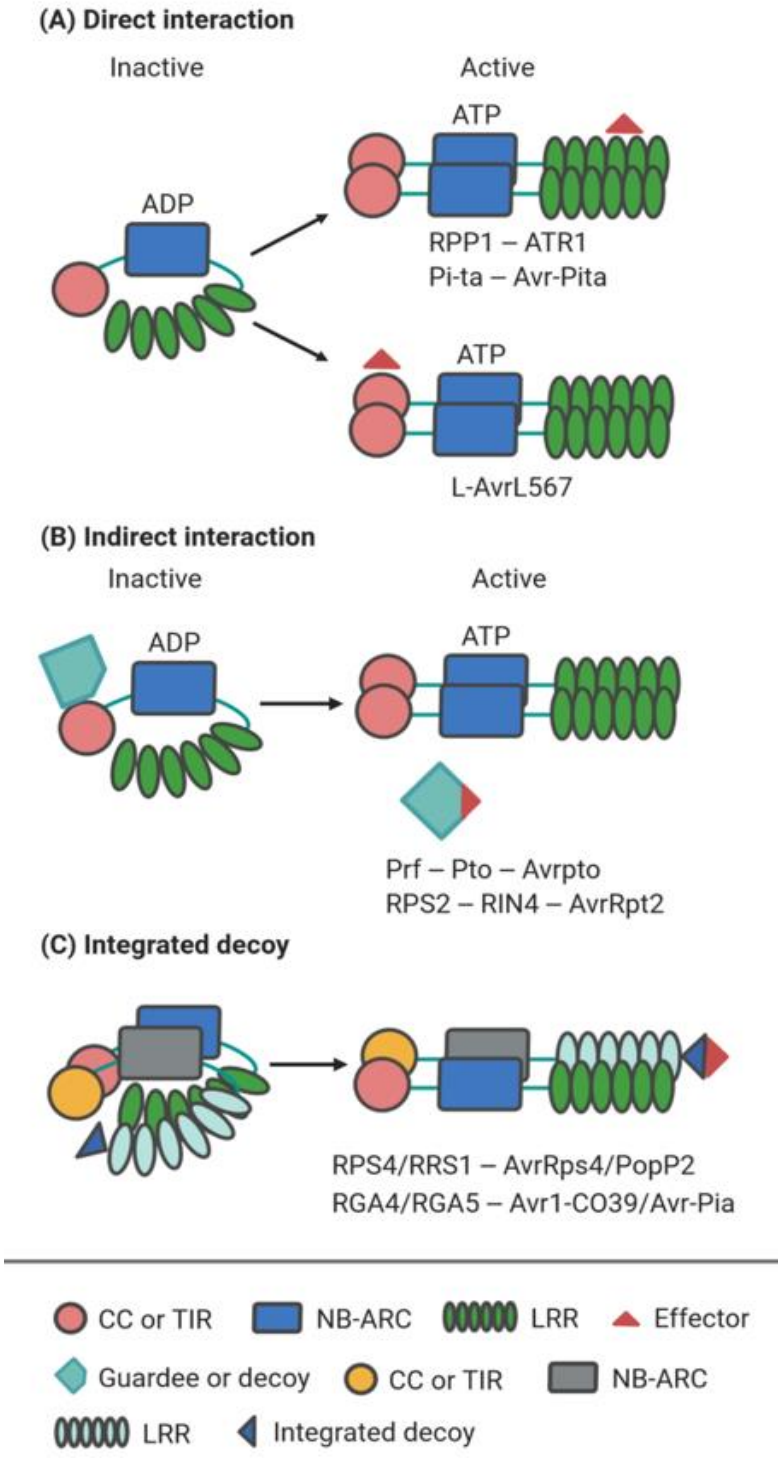

Figure 1.5. Intracellular receptors (NLRs) recognize pathogen effector proteins through different strategies. Inactive NLRs bind adenosine diphosphate (ADP). Upon effector recognition, NLRs change to an activated conformation by binding adenosine triphosphate (ATP). Examples appear below each figure. **(A)** Direct effector recognition by interaction with the leucine-rich repeat (LRR) domain or the amino (N)-terminus of the NLR. Direct recognition of the ATR1 (*Arabidopsis thaliana* Recognized 1) effector from *Hyaloperonospora arabidopsidis*, by the C-terminal leucine-rich repeat (LRR) domain of the RPP1 (Recognition of *Peronospora parasitica* 1). Similarly, the Pi-ta NLR protein from rice recognizes directly the Avr-Pita effector from *Magnaporthe oryzae.* Direct recognition of the AvrL567 effector from *Melampsora lini* by

the Toll/interleukin 1 receptor (TIR) domain from the L NLR protein of flax. **(B)** Indirect effector recognition by the NLR upon modification of the plant guardee or decoy by the effector. The tomato NLR protein Prf forms a complex with the intracellular kinase Pto. Pto interacts with the bacterial effector AvrPto from *Pseudomonas syringae,* activating the NLR and leading to an immune response. In a similar way, the *A. thaliana* NLR protein RPS2 detects the *P. syringae* effector AvrRpt2 recognition via the guardee protein RIN4 to trigger plant defences. **(C)** Indirect effector recognition by the NLR via integrated decoys often functioning in pairs with canonical NLRs. The *Arabidopsis* R protein pair RPS4 and RRS1 respond to the bacterial effectors AvrRps4 and PopP2 (from *P. syringae* and *Ralstonia solanacearum*, respectively), via an integrated decoy at the C-terminus of RRS1 to trigger a defence response. Figure from Sun et al. (2020).

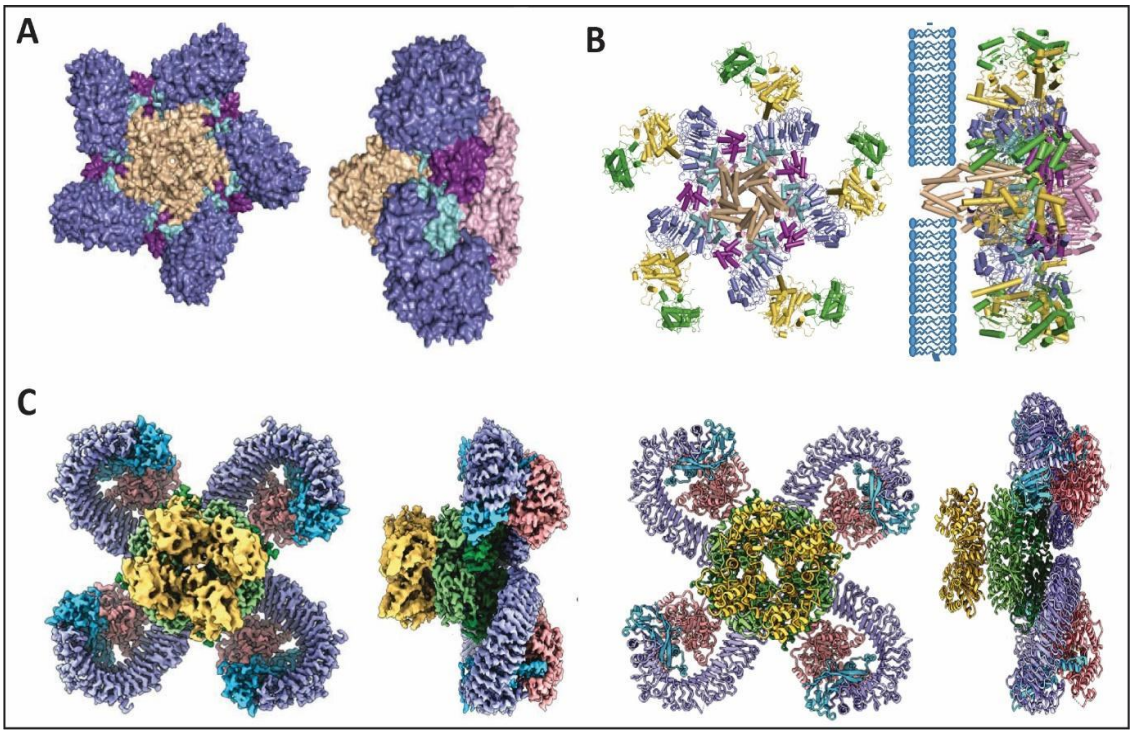

Figure 1.6. Coiled-Coil (CC) and Toll-Interleukin 1 (TIR) nucleotide-binding site (NB) and leucine-rich repeat (LRR) receptor (NLR) oligomerize to form a resistosome. (A) Overall structure of the ZAR1 NLR from *Arabidopsis*. CC, beige; NB-ARC, pink, purple and light blue; LRR, blue. **(B)** Structure of ZAR1 resistosome and association with or integration into the plasma membrane. CC, beige; NB-ARC, pink, purple and light blue; LRR, blue; RKS1, yellow and PBL2 green. **(C)** Overall structure of the ROQ1 (*Nicotiana benthamiana* NLR)-XopQ (*Xanthomonas euvesicatoria* effector) complex. TIR, yellow; NB-ARC, light to dark green; LRR, violet; post-LRR domain, light blue and XopQ, salmon. Figures adapted from Wang et al. (2019) and Martin et al. (2020).

1.3 Features and functions of fungal effector proteins

While fungal effectors can be secondary metabolites or small RNAs (Rodriguez-Moreno et al., 2018), the majority of fungal effectors identified to date are proteinaceous. Typically, these proteinaceous effectors are small in size (<300 amino acid [aa] residues in length), highly expressed *in planta*, and contain an even number of cysteine residues involved in disulphide bond formation for protection against plant proteases (Dalio et al., 2018; Mesarich et al., 2018). They also often possess an amino N-terminal signal peptide for secretion to the host environment (Mesarich et al., 2014), but tend to lack a transmembrane domain (TM) for integration into the fungal plasma membrane, or glycophosphatidylinositol (GPI) anchor modification site for attachment to the fungal plasma membrane or cell wall. Nevertheless, there are examples of effector proteins that do not possess these common characteristics, such as Vdlsc1, an unconventionally secreted effector protein from *V. dahliae*, which lacks a signal peptide (Liu et al., 2014), or VPS9, a conventionally secreted effector protein from the Basidiomycota fungus *Puccinia graminis* f. sp. *tritici* that is 744 aa in size (Nirmala et al., 2011).

Some effector proteins are race-specific, while others are highly conserved across fungi, also known as ‘‘core effectors’’ (Stergiopoulos et al., 2010; Wang & Wang, 2018). Necrosis and ethylene-inducing peptide 1 (Nep1)-like proteins (NLPs), for example, are conserved effector proteins secreted by fungal species with necrotrophic lifestyles to trigger tissue necrosis for successful colonization (Bashi et al., 2010; Bohm et al., 2014). These include SsNep1 and SsNep2 from *Sclerotinia sclerotiorum*, which induce cell death when transiently expressed in tobacco leaves (Bashi et al., 2010), and both MpNep1 and MpNep2 from *Moniliophthora perniciosa*, which induce necrosis and ethylene emission in tobacco and cacao leaves (Garcia et al., 2007). Avr4 and Ecp2 from *C. fulvum* are examples of core effectors with functional orthologs widely distributed among other Dothideomycete species. Effectors can act in the plant apoplast (apoplastic effectors) or inside plant cells (cytoplasmic effectors). Some examples are detailed below.

1.3.1 Apoplastic effector proteins

The apoplast is the narrow space between the pathogen cell wall and the plant plasma membrane (Rocafort et al., 2020; Wang et al., 2020) that offers a nutrient supply for the pathogen to proliferate. However, this narrow space is also armed with plant proteases and hydrolases that interfere with pathogen infection. In response, fungal pathogens deploy apoplastic effectors to protect their cell walls against hydrolysis by host chitinase enzymes, or to sequester fungal cell wall oligosaccharides that are released by plant hydrolases to prevent their recognition as PAMPs by PRRs. An example is Avr4 from *C. fulvum*, which protects against plant chitinases by binding to chitin in the fungal cell wall (van den Burg et al., 2006). Avr4 homologs have been identified in other Dothideomycete plant pathogens such as *Dothistroma septosporum*, *Pseudocercospora fijiensis, Cercospora apii, Cercospora beticola* and *Cercospora nicotianae* (de Wit et al., 2012; Stergiopoulos et al., 2010). Other examples include the LysM domain effectors, which sequester chitin oligosaccharides to prevent their recognition by host LysM IPRs (de Jonge & Thomma, 2009; Kombrink et al., 2011; Mentlak et al., 2012). Slp1 from *M. oryzae*, for instance, sequesters chitin-oligosaccharides in order to suppress chitin-induced plant immune responses (Mentlak et al., 2012).

During colonization of the apoplast, plant-pathogenic fungi also need to overcome defences mediated by plant proteases. Inhibition of these enzymes is one of the strategies used by these organisms to overcome plant defence. For example, the biotrophic fungus *Ustilago maydis* inhibits maize cysteine proteases by secreting the effector Pit2, which is essential for fungal virulence (Mueller et al., 2013). In addition, the same fungus secretes the effector Pep1 (Protein essential during penetration 1) to inhibit maize peroxidases and thus interfere with the oxidative burst that generates ROS as a defence response (Hemetsberger et al., 2012). Another barrier to colonizing the apoplast is the presence of anti-microbial compounds. Therefore fungal pathogens secrete enzymes as a strategy for detoxification of these compounds. For example, *C. fulvum* secretes CfTom1, a glycosyl hydrolase that hydrolyses α-tomatine (a major saponin of tomato) into the non-toxic tomatidine (Ökmen et al., 2013).

1.3.2 Cytoplasmic effector proteins

Cytoplasmic effectors are translocated inside host cells where they modulate plant immunity and physiology. Once inside the cells they can affect processes such as hormone signaling, secondary metabolite synthesis, transcription systems, and can inactivate important components in PRRs, hence disturbing MAPK cascades (Asai & Shirasu, 2015; Liu et al., 2014; Lo Presti et al., 2015). As mentioned, there are effectors that influence hormone signaling by manipulating, for example, salicylic acid (SA) production. Such is the case of the *V. dahliae* effector Vdlsc1 that hydrolyses isochorismate, the precursor of SA, to suppress its accumulation in the host (Liu et al., 2014). Similarly, the chorismate mutase effector protein Cmu1 is delivered into host cells by *U. maydis* to reduce the production of SA (Djamei et al., 2011). Another example is AvrLm4-7 from *L. maculans* that also manipulates the signaling pathways involved in the biosynthesis of SA and ethylene (Nováková et al., 2016). Unlike other fungal pathogens such as rusts and powdery mildews that produce haustoria likely involved in effector translocation, the effector delivery mechanism into plant cells by filamentous pathogens that are restricted to the apoplast remains unknown. Interestingly, plant cell-to-cell movement of cytoplasmic effectors has been reported. The *F. oxysporum* effectors Avr2 and Six5 interact at and manipulate plasmodesmata to facilitate cell-to-cell movement of Avr2 (Cao et al., 2018).

1.3.3 Avirulence effector proteins

As mentioned in section 1.1, effector proteins of plant-pathogenic fungi can sometimes be recognized as Avr effectors by plant R proteins to trigger IPTRs. Such Avr–R recognition events can help to identify new *R* genes to incorporate into new cultivars, as well as to understand how fungal pathogens cause disease. Hence, it is fundamental to identify new Avr effector proteins as a base to improve future plant disease control strategies (Zhang & Coaker, 2017). Many Avr effector proteins have been identified from plant-pathogenic fungi over recent years using different approaches, including proteomics or reverse genetics, map-based cloning, homology-based searches, association mapping, comparative genomics and transcriptomics (Kanja & Hammond-Kosack, 2020).

The *C. fulvum* avirulence effectors Ecp1, Ecp2-1, Ecp4, Ecp5, Ecp6, Avr4, Avr4E and Avr9 were identified using reverse genetics (Joosten et al., 1994; Joosten & de Wit, 1988; Laugé. et al., 2000; Schottens-Toma & de Wit, 1988; Van den Ackerveken, Van Kan, et al., 1993; van Kan et al., 1991; Westerink et al., 2004; Wubben et al., 1994). Avr2 was identified using an effectoromics approach (Luderer et al., 2002), and Avr5 was identified through a bioinformatics and transcriptome sequencing approach (Mesarich et al., 2014). The avirulence effector AvrStb6 from *Z. tritici* was identified using a genome-wide association study (GWAS) in combination with quantitative trait locus (QTL) mapping (Zhong et al., 2017). AvrLm1, AvrLm6, AvrLm4-7, AvrLm5-9, AvrLm10, AvrLm11 and AvrLm14 from *L. maculans* were identified using a map-based cloning approach (Balesdent et al., 2013; Degrave et al., 2021; Fudal et al., 2007; Gout et al., 2006; Parlange et al., 2009; Petit-Houdenot et al., 2019; Van de Wouw et al., 2014). AvrLm2 was identified through comparative genomics (Ghanbarnia et al., 2015), and the laborious identification of AvrLm3 included genetic mapping, RNA-seq, next generation sequencing (NGS) of bacterial artificial chromosome (BAC) clones and *de novo* assembly approaches (Plissonneau et al., 2016). Characterized Avr effector proteins identified from Dothideomycete plant-pathogenic fungi, and their cognate R proteins, are summarized in Table 1.1.

Table 1.1. Identified Avirulence (Avr) effector proteins from plant-pathogenic Dothideomycete fungi and their corresponding plant resistance (R) proteins.

Plant pathogen	Disease	Avirulence effector protein	Size (aa)[a]	Cys No.[b]	Corresponding R protein[c]	Reference
Leptosphaeria maculans	Black leg disease of *Brassica* crops	AvrLm1	205	1	LepR3 (RLP)	(Gout et al., 2006; Ma & Borhan, 2015)
		AvrLm2	232	8	Rlm2 (RLP)	(Ghanbarnia et al., 2015; Larkan et al., 2015)
		AvrLm3	160	10	Rlm3	(Plissonneau et al., 2016)
		AvrLm4-7	143	8	Rlm4 and Rlm7 (WAKL)	(Haddadi et al., 2021; Parlange et al., 2009)
		AvrLm5-9	141	6	Rlm9 and Rlm5 (WAKL)	(Ghanbarnia et al., 2018; Larkan et al., 2020; Plissonneau et al., 2018; Van de Wouw et al., 2014)
		AvrLm6	144	6	Rlm6	(Fudal et al., 2007)
		AvrLm10A AvrLm10B	120 178	7 1	Rlm10	(Petit-Houdenot et al., 2019)
		AvrLm11	95	1	Rlm11	(Balesdent et al., 2013)
		AvrLm14	134	4	Rlm14	(Degrave et al., 2021)
Zymoseptoria tritici	Septoria tritici blotch of wheat	AvrStb6	82	12	Stb6 (RLK)	(Saintenac et al., 2018; Zhong et al., 2017)
		Avr3D1	92	8	Stb7	(Meile et al., 2018)

Table 1.1. Continued.

Plant pathogen	Disease	Avirulence effector protein	Size (aa)[a]	Cys No.[b]	Corresponding R protein[c]	Reference
Cladosporium fulvum	Leaf mould of tomato	Ecp1	96	8	Cf-Ecp1	(Laugé et al., 1997)
		Ecp2-1	165	4	Cf-Ecp2	(Laugé et al., 1997)
		Ecp4	119	6	Cf-Ecp4	(Laugé. et al., 2000)
		Ecp5	115	5	Cf-Ecp5	(Laugé et al., 2000)
		Ecp6	222	8	Cf-Ecp6	(Bolton et al., 2008)
		Avr2	78	8	Cf-2.1 and Cf-2.2 (RLP)	(Dixon et al., 1996; Luderer et al., 2002; Rooney, 2005)
		Avr4	135	8	Cf-4 (RLP)	(Joosten et al., 1994; Thomas et al., 1997)
		Avr4E	121	6	Cf-4E (RLP)	(Takken et al., 1999; Westerink et al., 2004)
		Avr5	103	10	Cf-5 (RLP)	(Mesarich et al., 2014; Dixon et al., 1998)
		Avr9	63	6	Cf-9 (RLP)	(Jones et al., 1994; van Kan et al., 1991)

[a]Length in amino acids (aa), including signal peptide.
[b]Cysteine number in mature protein.
[c]RLP, receptor-like protein; RLK, receptor-like kinase; WAKL wall associated kinase-like.

1.4 The New Zealand horticulture industry

In 2020, the total value of the New Zealand horticultural industry was estimated to exceed $10 billion, including a record high of $6.65 billion worth of exports (http://freshfacts.co.nz, issue 2020). The export value has increased more than 60% in the past 10 years thanks to the investment from research to post-harvest practices. Apple and tomato are two crops produced in New Zealand for local and international consumption, contributing greatly to its economy. Apple, for instance, was the second largest horticultural export of New Zealand in 2020, in the fresh fruit category. More specifically, in the same year, New Zealand exported 402,000 tonnes of apple, reaching a record value of $876 million. Apple statistics show a stable growth of the apple fruit industry year-on-year (Table 1.2), which is anticipated to reach a value of 1 billion by 2022.

In total, 125 tomato greenhouses, with a planted area of 120 ha are present in New Zealand. The domestic sales of tomato reached a value of $120 million in 2020, and a value of $11.2 million for export the same year (http://freshfacts.co.nz, issue 2020) (Table 1.3).

Table 1.2. New Zealand apple industry overview. Source: FreshFacts, issue 2020 (http://freshfacts.co.nz)

Year	2005	2010	2015	2018	2019	2020
National export production ('000 tonnes)	315	260	331	377	395	402
Exports ($ million, fob[1])	387	324.6	561.8	732.9	828.8	876.3
Area planted (ha[2])	10,764	8,630	8,566	9,139	10,179	10,396

[1]Exports given as free on-board (fob) values.
[2]ha; hectares.

Table 1.3. New Zealand tomato industry overview. Source: FreshFacts, issue 2020 (http://freshfacts.co.nz).

Year	2005	2010	2015	2018	2019	2020
Total crop volume[1] (tonnes)	40,000	40,000	42,400	42,400	n/a	42,000
Exports ($ million, fob[2])	8.5	10.1	8.1	9.6	11.2	11.2
Domestic sales ($ million, fob)	105	108	91.2	200	176	120

[1]Greenhouse production.
[2]Exports given as free on-board (fob) values.
n/a: not available

Climate change has brought many challenges for apple growers such as colour development (red color reduction), sunburn and increased pests and diseases (FreshFacts NZ, issue 2019). Regarding tomato greenhouse production, it is less influenced by climatic factors. However, with increasing rainfall and humidity in some regions, traditional farming of tomatoes in the open field could also be at risk (Silva et al., 2017). Biotic factors, such as pathogens that cause disease, are a major threat for apple and tomato production. Many of these diseases are caused by Dothideomycete fungi. Two prime examples are apple scab disease caused by *V. inaequalis* and tomato leaf mould disease caused by *C. fulvum*. Future challenges in the horticulture industry of New Zealand include responding to current and future plant disease outbreaks, in order to meet the qualitative and quantitative demands of the industry. Research priorities must include plant-pathogen interactions to provide knowledge for the development of long-lasting resistant plant varieties. The focus of this thesis is these two important pathogens to better understand the molecular mechanisms they use to invade their respective hosts, as well as the molecular mechanisms their hosts use to detect them.

1.5 *Cladosporium fulvum*

Tomato (*Solanum lycopersicum*) leaf mould is caused by the asexual, non-obligate biotrophic Dothideomycete fungus *C. fulvum* (syn. *Passalora fulva* and *Fulvia fulva*) (Braun et al., 2003; Thomma et al., 2005). *C. fulvum* affects tomato plants worldwide, but it is in greenhouses and high-tunnel environments where the main problem persists due to the favorable conditions, such as moderate temperatures and a high relative humidity (Mesarich et al., 2018). This fungal disease was first described by Cooke (1883) and its origin is presumably in South America, where the provenance of cultivated tomato has been corroborated (Jenkins, 1948).

1.5.1 Infection cycle of *C. fulvum*

Infection starts when conidia, with the aid of wind or water, spread and land on the abaxial side of a tomato leaf. When high relative humidity conditions are present, conidia germinate and form a thin runner hypha that grows over the leaf surface (Bond, 1938; De Wit, 1977; Lazarovits & Higgins, 1976). Then, the main germ tube or a lateral hyphal branch is able to enter the leaf when an open stoma is encountered. After the inner leaf is reached, the hypha enlarges and continues growing between the mesophyll cells (Fig. 1.7C), forming long and branched hyphal structures that form hyphal aggregations in the substomatal spaces approximately 10-14 days after the initial infection. After aerial mycelia are formed, conidiophores are released to the exterior through stomata, where they produce conidia, which are subsequently dispersed to spread the disease (Fig. 1.7D) (de Wit et al., 2012; Thomma et al., 2005). The disease symptoms are characterized by pale green to yellow spots on the adaxial leaf surface that turn brown after sporulation (Fig. 1.7 A-B), leaf wilting, and partial defoliation that in severe infections can lead to plant death (Thomma et al., 2005). Besides affecting leaves, *C. fulvum* can also infect stems, flowers and fruits (Butler & Jones, 1949).

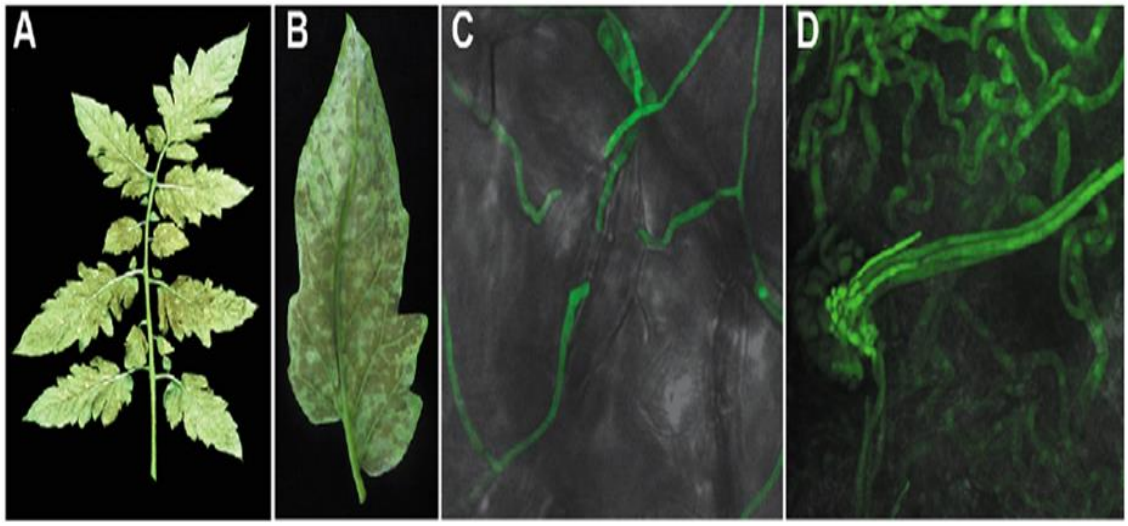

Figure 1.7. Tomato leaf mould disease symptoms and development. (A) *Cladosporium fulvum* sporulating on the abaxial side of a tomato (*Solanum lycopersicum*) plant two weeks-post inoculation; **(B)** *C. fulvum* sporulating on the abaxial side of a leaflet at two weeks post-inoculation; **(C)** *C. fulvum* (transgenic strain expressing green fluorescent protein; GFP) runner hyphae at the surface of the leaf and penetrating a stoma of tomato at four days post-inoculation. **(D)** *C. fulvum* (GFP-transgenic strain) conidiophores emerging from a stoma at 10 days post-inoculation. Figure adapted from de Wit et al. (2012).

1.5.2 Leaf mould control methods

Leaf mould disease is controlled in different ways. Cultural methods rely on keeping the relative humidity in greenhouses below 85%, providing enough ventilation and light, adequate spacing between rows and plants, and avoiding persistent moisture on leaves. Additionally, it is important to reduce the primary inoculum by removing and destroying remaining plant debris. Along with the mentioned cultural practices, fungicide spray programmes are used to help control the disease (Veloukas et al., 2007). Among these are the demethylation inhibitors (DMIs) which bind to the heme iron of the cytochrome P450 sterol 14α-demethylase (Cyp51) to inhibit sterol biosynthesis in the fungal membranes (Yuzo & Yuri, 1987). As observed in other fungal pathogens, resistance to this type of fungicide could be the result of mutations or overexpression of the *CYP51A1* gene in *C. fulvum* (Cordero-Limon et al., 2021; Köller, 1992; Ma et al., 2006; Villani et al., 2016; Wang et al., 2015). A specific type of DMI, the triazoles, are effective fungicides against *C. fulvum* (Wang et al., 2017). So far, no resistance to triazoles have been reported in *C. fulvum*. Another class of fungicides used are the methyl benzimidazole

carbamate (MBC) fungicides that bind the β-tubulin in order to prevent fungal mitosis and cell division (Ma & Michailides, 2005). *C. fulvum* isolates resistant to MBC fungicides have been reported through point mutation at codons 198 and 200, leading to Glu-to-Ala and Phe-to-Tyr amino acid substitutions, respectively, in the β-tubulin protein (Yan et al., 2008). Finally, strobirulin or quinone outside inhibitors (QoI), which unpair the ability of the pathogen to produce energy through inhibition of mitochondrial respiration (i.e. binding to the cytochrome bc1 [CYTB] enzyme complex at the outer quinone oxidizing site [QoI site] (Gisi et al., 2002). However, resistance to QoI fungicides in *C. fulvum* has been reported, and results from a Phe-to-Leu amino acid substitution at position 129 of CYT B (Watanabe et al., 2017). In addition to cultural and fungicide control methods, cultivars of tomato with *R* genes active against *C. fulvum* are used.

1.5.3 Molecular aspects of the *C. fulvum*-tomato interaction

The *C. fulvum*-tomato interaction has been used as a pathosystem model for understanding gene-for-gene interactions between pathogen *Avr* effector genes and host plant *R* genes. The products of tomato *R* genes, designated as (Cf) for resistance to *Cladosporium fulvum*, mediate recognition of corresponding *Avr* effector gene products from *C. fulvum* (van den Burg et al., 2006). When the matching *Cf* and *Avr* genes are present, a resistance response is triggered in the plant; in this manner the fungus is avirulent and can no longer infect the host (incompatible interaction). If no matching *Cf* and *Avr* genes are present, then there is no recognition by the plant, and thus the fungus is virulent and can successfully colonize the host (compatible interaction) (de Wit et al., 1997).

1.5.3.1 Compatible interaction

Under optimum relative humidity and temperature conditions, conidia germinate and subsequently differentiate runner hyphae. Then, runner hyphae enter tomato leaves through open stomata (Joosten & de Wit, 1999). *C. fulvum* does not form haustoria to feed off the plant. Instead, it remains in the leaf apoplast in order to obtain nutrients such as sugars and amino acids, where it secretes effector proteins to interfere with plant defence responses and promote colonization (Joosten et al., 1990). These include at least 75 small secreted proteins (SSPs) of less than 300 aa residues in length (Mesarich et al., 2018), most of which have an even number of cysteines residues that

form disulphide bridges that provide stability in the harsh protease-rich tomato apoplast. Effector proteins of *C. fulvum* can be divided into extracellular proteins (ECPs) produced by all strains, and avirulence proteins (Avrs) that are race-specific (Rooney, 2005; van Esse et al., 2008). As mentioned in Section 1.5.1, approximately 14 days after infection, hyphal aggregations form in the substomatal spaces and release conidia through stomata leads to spread of the disease (Thomma et al., 2005). A compatible interaction is illustrated in (Fig. 1.11A) (Ökmen, 2013).

1.5.3.2 Incompatible interaction

Regarding conidial germination, runner hyphae differentiation and stomatal penetration, there is no difference between a compatible and incompatible interaction. It is when the runner hyphae enter the apoplast that host defence responses are activated to halt the growth of the fungus. These responses involve collapse of the host mesophyll cells that are proximate to the fungal hyphal cells and callose formation (De Wit, 1977). At the molecular level, there is a fast accumulation of PR proteins such as β-1,3-glucanases, chitinases and cysteine proteases (Wubben et al., 1993). However, the most efficient outcome of the incompatible interaction is the HR, already described in Section 1.1 which halts the growth of the fungus (de Wit et al., 2009). An incompatible interaction is illustrated in (Fig. 1.11B) (Ökmen, 2013).

1.5.4 *Cladosporium fulvum effectors*

A large number of *C. fulvum* effectors have been identified using different approaches (Section 1.3.3). From these, only Avr2, Avr4, Ecp6 and CfTom1 have been functionally characterized.

1.5.4.1 Characterized *C. fulvum* effectors

Avr2 is a pre-protein of 78 aa in length with a 20 aa predicted signal sequence and contains eight cysteine residues. Avr2 inhibits diverse tomato cysteine proteases including Rcr3 (required for *C. fulvum* resistance) (Dixon et al., 2000; Kruger et al., 2002; Rooney, 2005), and the close relative Pip1 (*Phytophthora*-inhibited protease 1) (van Esse et al., 2008). Heterologous expression of Avr2 in *Arabidopsis thaliana* enhances susceptibility to *Botrytis cinerea* and *V. dahliae*. In the same way, tomato lines expressing Avr2 increase susceptibility to race 2 *C. fulvum* strains (lacking *Avr2*), showing

that Avr2 is required for virulence (van Esse et al., 2008). Recently, it has been shown that Rcr3 homologs in tomato, potato, eggplant, pepper and petunia can be inhibited by Avr2; however, only Rcr3 homologs from tomato and potato can trigger an HR in the presence of Cf-2 and Avr2, illustrating the evolution of Rcr3 (Kourelis et al., 2020). Such Cf-2-dependent Avr2 recognition is correlated with the evolutionary distance to tomato; as the phylogenetic distance to tomato Rcr3 increases, the likelihood of a Cf-2-dependent HR decreases (Kourelis et al., 2020).

The mature Avr4 protein contains 86 aa with eight cysteine residues involved in disulphide bridge formation (Joosten et al., 1994). Avr4 protects the hyphae against plant chitinases by binding to the fungal cell walls and in doing so, prevents the release and recognition of chitin fragments by PRRs (van den Burg et al., 2006). The chitin-binding ability of Avr4 is mediated by the carbohydrate-binding module family 14 (CBM14) domain (van den Burg et al., 2006). The solved crystal structure of CfAvr4 revealed structural similarity to other CBM14 family members (Fig. 1.8A) (Hurlburt et al., 2018). In the same study, an effector-ligand co-crystallization of Avr4-chitohexaose [$(GlcNAc)_6$] uncovered that two Avr4 molecules dimerize and form a sandwich structure by encapsulating two molecules of chitohexahose $(GlcNAc)_6$ (Fig. 1.8B) (RSCB protein data bank (PDB) ID: 6BN0) (Hurlburt et al., 2018).

The role of Avr4 in virulence has been demonstrated (van Esse et al., 2007); heterologous expression of Avr4 in *A. thaliana* increased susceptibility to *B. cinerea* and *Plectosphaerella cucumerina*. In addition, the silencing of this effector resulted in less colonization and biomass production by *Avr4*-silenced *C. fulvum* strains on tomato leaves (van Esse et al., 2007). Avr4 homologues have been identified in other Dothideomycete fungi such as *P. fijiensis* and *Cercospora* species (Stergiopoulos et al., 2010). The *M. fijiensis* Avr4 is a functional ortholog that protects fungi against plant chitinases in the same way as *C. fulvum* Avr4 and induces a strong Cf-4-dependent HR (Stergiopoulos et al., 2010). Interestingly, a recently described paralog of Avr4 from *Pseudocercospora fuligena,* PfAvr4-2, was found to contain a non-functional chitin-binding domain. Instead, this paralog interacts with pectin in plant cell walls and interferes with Ca^{2+}-mediated cross-linking at the cell-cell junction zones. In this manner, it affects the structure of the plant cell wall and makes it more accessible for enzymatic degradation (Chen et al., 2021).

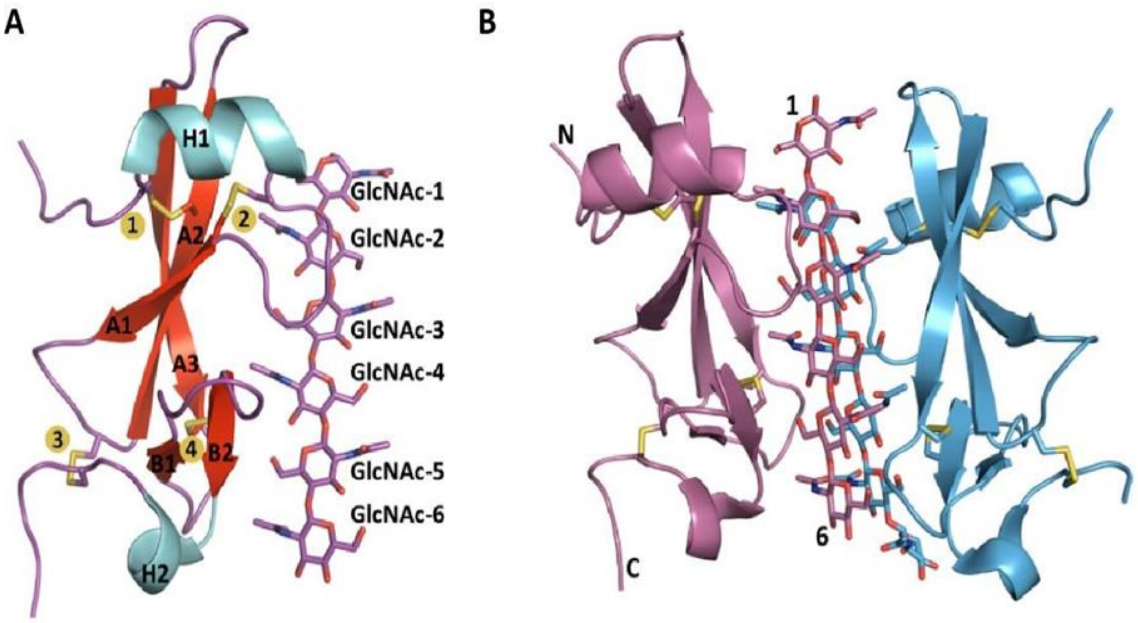

Figure 1.8. Crystal structure of the Avr4 effector protein from *Cladosporium fulvum.* (RSCB protein data bank (PDB) ID: 6BN0) **(A)** The Avr4 monomer is composed of an amino (N)-terminal α-helix (H1), an unorganized β-sandwich fold with three anti-parallel β-strands (A1-A3), two anti-parallel β-strands (B4 and B5) forming a small β-sheet, and a carboxyl (C)-terminal α-helix (H2). Avr4 is bound to a chitohexaose $(GlcNAc)_6$ molecule (shown in sticks). **(B)** The CfAvr4-$(GlcNAc)_6$ dimeric structure is composed by two Avr4 monomers (shown in purple and blue), binding to two molecules of $(GlcNAc)_6$ (shown in sticks). Disulfide bonds in both structures are shown in yellow. Figures adapted from Hurlburt et al. (2018).

Ecp6 is a well characterized protein of 222 amino acids, with a signal peptide of 18 amino acids, eight cysteines and contains three LysM carbohydrate binding domains (LysM1-LysM3) (Fig. 1.9) (RSCB protein data bank (PDB) ID: 4B8V) (Bolton et al., 2008; Sanchez-Vallet et al., 2013). Unlike Avr4 that prevents hydrolysis of fungal cell walls, Ecp6 sequesters chitin fragments released by plant chitinases and thus prevents the activation of defence responses (de Jonge et al., 2010). More specifically, the binding of chitin is mainly enabled by the dimerization of domains LysM1 and LysM3 to form a chitin-binding groove which outcompetes host PRRs for the binding of chitin (de Jonge et al., 2010; Sanchez-Vallet et al., 2013). Silencing of the *Ecp6* gene demonstrated its role in virulence, with silenced transformants having less biomass *in planta* (Bolton et al., 2008). Interestingly, Ecp6 orthologs are not only present in other Dothideomycetes such as *L. maculans*, *Z. tritici* and *P. fijiensis,* but also in the Sordariomycete *M. oryzae*, and the Leotiomycetes *Sclerotinia sclerotiorum* and *B. cinerea*, indicating the importance

of avoiding chitin-triggered plant defence responses across distinct classes of fungal pathogens (Bolton et al., 2008).

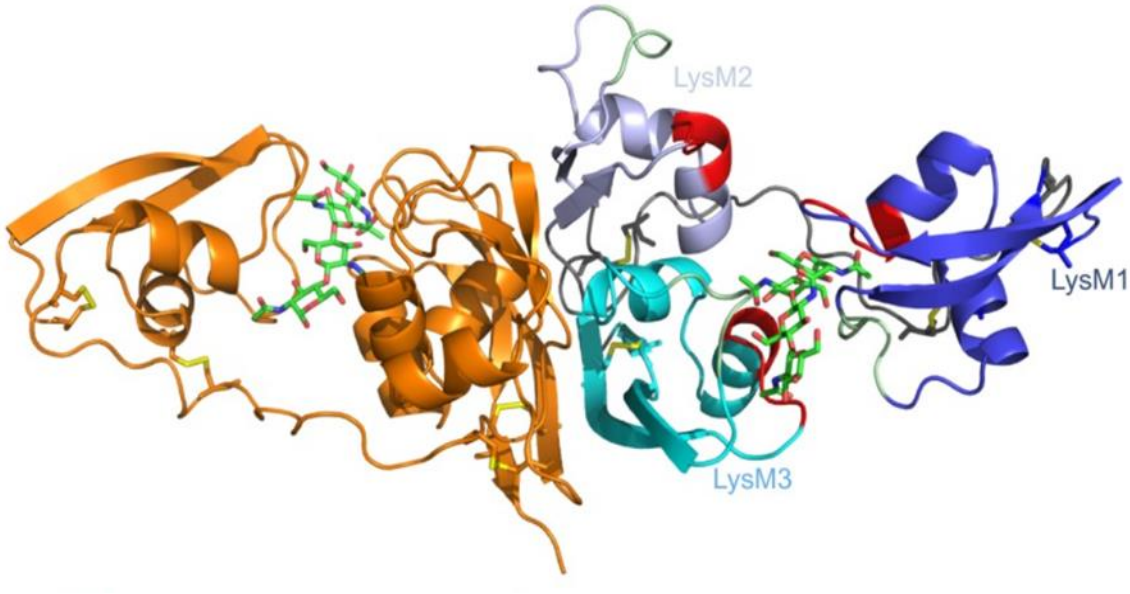

Figure 1.9. Crystal structure of the Ecp6 effector protein from *Cladosporium fulvum*. (RSCB protein data bank (PDB) ID: 4B8V). Structure of an Ecp6 dimer (left monomer in orange) and three LysM domains (in three shades of blue) of the right monomer with flexible loop (grey) between LysM1 and LysM2. The chitin tetramer and the four disulfide bridges are indicated in green and yellow sticks, respectively. In the right monomer the two chitin-binding loops are shown in red and green for each of the LysM domains. Figure from Sánchez-Vallet et al. (2013).

CfTom1 is a secreted enzyme and part of glycosyl hydrolase 10 family (GH10). It contains 345 amino acids with a predicted secretion signal of 19 amino acids, and two cysteines. This effector degrades the fungitoxic α-tomatine into tomatidine, a less toxic metabolite. The requirement of CfTom1 for full virulence was demonstrated by a targeted gene deletion, where a reduction of fungal biomass of Δ*cftom* mutants was observed at 10 dpi onwards (Ökmen et al., 2013).

1.5.4.2 Uncharacterized *C. fulvum* effectors

The *Ecp1* gene encodes a precursor protein of 96 aa in size, which after the removal of its secretion signal and the activity of plant proteases results in a stable protein of 65 aa with eight cysteine residues. Ecp2 has a 165 aa precursor protein that is processed similarly to Ecp1 and results in a protein of 142 aa with four cysteines (Joosten & de Wit, 1988; Van den Ackerveken, Van Kan, et al., 1993; Wubben et al., 1994). Using a gene

replacement approach, *Ecp1* and *Ecp2* were found to be involved in virulence. *Ecp1* and *Ecp2*-deficient strains resulted in poor colonization and lower secretion of *in planta*-produced proteins as well as more severe plant defence responses such as accumulation of PR proteins (Laugé et al., 1997). Ecp2 homologs have been found in *P. fijiensis* and *Z. tritici* (Stergiopoulos et al., 2010), suggesting an elemental virulence function that has not been elucidated so far. The *Ecp4* gene encodes a 119 aa protein with a predicted 18 aa secretion signal and 6 cysteines. Ecp5 encodes a 115 aa protein with a secretion signal of 17 aa, resulting in a mature protein of 98 aa with 6 cysteine residues (Laugé. et al., 2000). Ecp7 is a mature protein of 100 aa residues with six cysteine residues that was determined to have a redundant role in virulence (Bolton et al., 2008).

Avr4E is a mature protein of 101 aa with six cysteines (Westerink et al., 2004) whose function is yet to be determined. The Avr9 pre-protein of 63 aa is processed into a stable protein of 28 aa due to the activity of plant proteases (Van den Ackerveken, Vossen, et al., 1993; van Kan et al., 1991). Through N-terminal Iodine-125 labeling of Avr9, high-affinity binding sites (HABS) on the plasma membrane of tomato were identified regardless of the presence of the matching Cf-9 receptor (Kooman-Gersmann et al., 1996). Further studies could not detect a direct interaction between Avr9 and Cf-9; thus, it has been hypothesized that Avr9 interacts with host another target to trigger a Cf-9-dependent HR (Luderer et al., 2001). The function of Avr9 remains to be elucidated, but its functional redundancy has been implied, as disruption of the gene does not compromise virulence (de Wit, 2016). Avr5 is a mature protein of 81 aa with ten cysteine residues (Mesarich et al., 2014). The role of Avr5 in virulence was determined by inoculating an *Avr5*-complemented *C. fulvum* race 5 strain on susceptible tomato, resulting in a significant increase of fungal biomass as measured by qRT-PCR (Mesarich et al., 2014). In addition, 70 *in planta*-induced SSPs were identified using RNA-Seq transcriptome and proteomic data from a compatible *C. fulvum*–tomato interaction (Mesarich et al., 2018); 41 were selected, based on their expression levels, and used to perform an effectoromics-based screening. Effectoromics is the use of effector or candidate effectors to identify new *R* genes in plant germplasm by association with an HR (Vleeshouwers & Oliver, 2014). Ten of the 41 selected SSPs triggered HR in wild tomato. These included Ecp8, Ecp9-1, Ecp10-1, Ecp11-1, Ecp12, Ecp13, Ecp14-1, Ecp15, Ecp16 and Ecp17. All 10 of these SSPs are cysteine-rich and contain a predicted secretion

signal (Mesarich et al., 2018). Interestingly, the structure of Ecp11-1 (RSCB protein data bank (PDB) ID: 6ZUS) (Fig. 1.10) has been elucidated and it shares structural similarity to Avr effector proteins from *L. maculans*, specifically AvrLm3, AvrLm5-9 and AvrLm4-7 (Lazar et al., 2021; Mesarich et al., 2018).

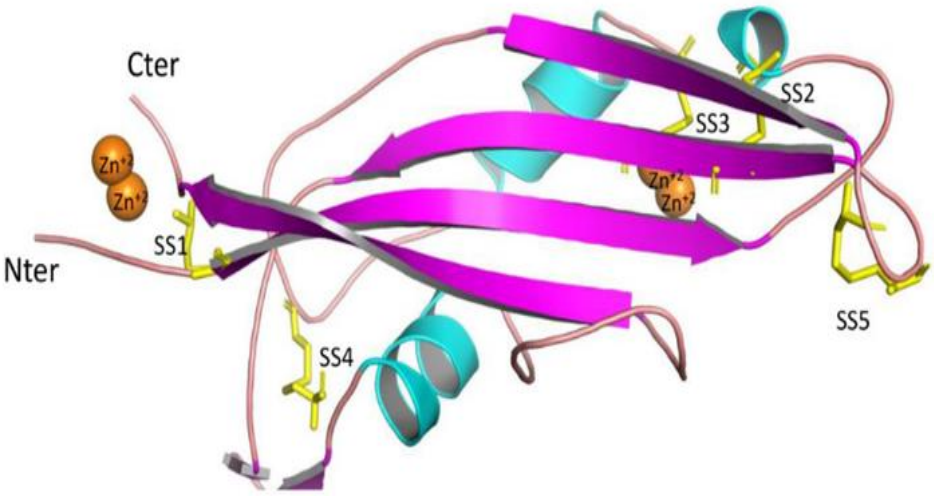

Figure 1.10. Crystal structure of the Ecp11-1 effector from *Cladosporium fulvum*. (RSCB protein data bank (PDB) ID: 6ZUS). Zn^{+2} ions involved in crystal packing are shown as orange spheres. α-helix is represented in cyan, β-strand in magenta. N- and C-termini are labelled. Numbered disulfide bonds are represented by yellow sticks. Figure from Lazar et al. (2021).

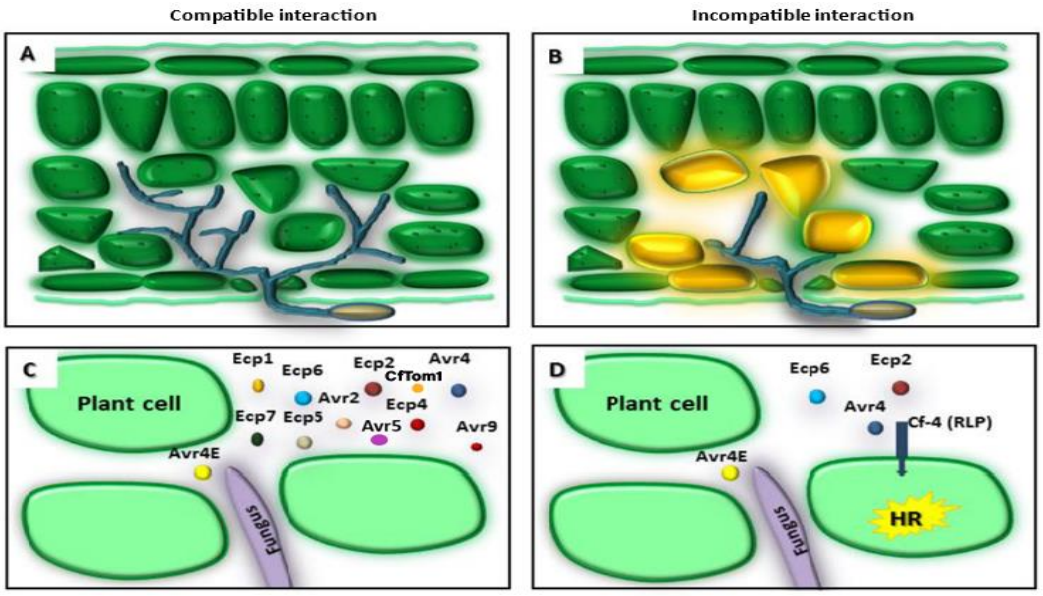

Figure 1.11. Compatible and incompatible *Cladosporium fulvum*–tomato interactions. (A) Compatible interaction. After the conidium germinates, a runner hypha enters through an open stoma then colonizes and remains in the tomato leaf apoplast. **(B)** Incompatible interaction. The fungus is recognized by tomato, leading to a hypersensitive response (HR; shown by yellow cells), which halts growth of the fungus. **(C)** *C. fulvum* secretes effector proteins to manipulate and colonize the host during a compatible interaction. **(D)** Resistant plants possess Cf resistance (R) proteins that recognize avirulence (Avr) effector proteins to activate an immune response involving an HR. Image adapted from Ökmen (2013).

1.5.5 Tomato Cf resistance proteins

Cf genes encoding R proteins originate from different wild *Solanum* species, such as *S. piminellifolium, S. peruvianum* and *S. hirsutum*, and have been incorporated into cultivated tomato since the 1930s (de Wit et al., 2009). All *Cf* genes encode transmembrane RLPs that confer race-specific resistance against *C. fulvum*. They are members of *Hcr9* and *Hcr2* gene clusters designated as homologues of *Cladosporium* resistance gene 9 and 2, respectively. The *Cf-4*, *Cf-4E*, *Cf-9*, *Cf-9B* and *Cf-9E* genes belong to the *Hcr9* gene family, mapping to tomato chromosome 1 (Haanstra et al., 1999; Jones et al., 1994; Kruijt et al., 2004; Panter et al., 2002; Parniske et al., 1999; Soumpourou et al., 2007; Takken et al., 1999; Thomas et al., 1997), whereas *Cf-2* and *Cf-5* belong to the *Hcr2* gene family, mapping on tomato chromosome 6 (Dixon et al., 1996; Rivas & Thomas, 2005). All known Cf proteins are summarized in Table 1.4. So far, the resistance

traits mediated by all *Cf* genes have been overcome due to modifications or deletions of the cognate *Avr* genes (Iida et al., 2015; Stergiopoulos et al., 2007).

Previous reports suggest that the LRRs of RLPs are involved in the recognition of Avr effector proteins from *C. fulvum*. Experiments using chimeric versions of the Cf-2 and Cf-5 resistance proteins have shown that their specificity relies on LRRs 3 to 27 and LRRs 3 to 21, respectively (Seear & Dixon, 2003). Furthermore, domain swaps between Cf-4 and Cf-9 showed that Cf-4 specificity relies on variant amino acids in two LRRs (11 and 12), whereas Cf-9 specificity is dispersed along a wider number of LRRs (10 to 18) (Wulff et al., 2001). All together, these studies concluded that recognition of *C. fulvum* Avrs by Cf proteins relies on LRR number and specific amino acid variations within some of the LRRs.

Table 1.4. Features of tomato Cf resistance (R) proteins, mediating resistance to *Cladosporium fulvum*.

Cf R protein name	R protein class[a]	*Hcr* gene family	Protein length (aa)	Number of LRRs	Corresponding avirulence (Avr) effector protein	References
Cf-2.1	RLP	2	1,112	38	Avr2	(Dixon et al., 1996; Luderer et al., 2002; Rooney, 2005)
Cf-2.2	RLP	2	1,112	38	Avr2	(Dixon et al., 1996; Luderer et al., 2002; Rooney, 2005)
Cf-4	RLP	9	806	25	Avr4	(Joosten et al., 1994; Thomas et al., 1997)
Cf-4E	RLP	9	855	27	Avr4E	(Takken et al., 1999; Westerink et al., 2004)
Cf-5	RLP	2	968	32	Avr5	(Dixon et al., 1998; Mesarich et al., 2014)
Cf-9	RLP	9	863	27	Avr9	(Jones et al., 1994; van Kan et al., 1991)
Cf-9B	RLP	9	865	27	Avr9B[b]	(Jones et al., 1994; Parniske et al., 1997)
Cf-9E	RLP	9	862	27	Avr9E[b]	(Jones et al., 1994; Parniske et al., 1997)

[a]RLP, receptor like proteins. [b]Unidentified Avr effector proteins. *Hcr*: homologues of *C. fulvum R* gene.

1.5.6 Avoidance of Cf-mediated resistance

Virulent isolates of *C. fulvum* avoid Cf-mediated recognition through deletions, point mutations or transposon insertions in the *Avr* coding sequence, leading to an alteration or complete loss of the Avr protein. This transition from avirulence to virulence is mainly caused by the strong selection pressure imposed on the fungus to avoid resistance due to the introduction of *Cf* genes into commercial tomato cultivars (Stergiopoulos et al., 2007). *Cf-2* mediated resistance was disrupted due to insertions or deletions in the coding sequence of the *Avr2* gene that subsequently resulted in a truncated Avr2 protein. In addition, multiple nonsynonymous polymorphisms and other modifications altering the protein sequence have been reported (Table 1.5) (Luderer et al., 2002). *Cf-4*-mediated resistance has been broken in different ways. A single nucleotide deletion led to a frameshift in the coding sequence of Avr4, resulting in a truncated protein (Joosten et al., 1997). Single nucleotide changes resulted in aa substitutions (Tyr67His and Thr66Ile) in different isolates, facilitating the circumvention of *Cf-4*-mediated resistance. In addition, other point mutations resulted in Cys-to-Tyr substitutions at different positions of the Avr4 protein (Cys-64, Cys-70 and Cys-109) (Joosten et al., 1994; Joosten et al., 1997). As cysteines are involved in disulphide bonding, these Avr4 isoforms are unstable and more sensitive to proteases, and thus cannot accumulate in the apoplast to activate a Cf-4-dependent HR (van den Burg et al., 2003). Cys-to-Phe and Cys-to-Ser substitutions have been also reported at position 64 of the amino acid sequence (Iida et al., 2015; Yoshida et al., 2021).

Evasion of *Cf-4E*-mediated resistance has been achieved by deletion or mutation of the *Avr4E* gene (Lucentini et al., 2021; Westerink et al., 2004). The amino acid substitutions correspond to Phe82Leu, Met93Thr and Met93Tyr (Iida et al., 2015; Lucentini et al., 2021; Westerink et al., 2004).

C. fulvum isolates that do not possess *Avr9* are virulent on *Cf-9* plants by avoiding Cf-9 mediated recognition (Bernal-Cabrera et al., 2021; Iida et al., 2015; van Kan et al., 1991; Yoshida et al., 2021).

To avoid *Cf-5*-mediated resistance, the *Avr5* gene had been deleted or pseudogenized as a result of a premature stop codon (Mesarich et al., 2014), and also a (c.268G>C) mutation leading to a Gly90Arg substitution was observed in Japanese

isolates (Iida et al., 2015). Deletions of *Avr* genes in *C. fulvum* can be attributed to their close location to repetitive elements. The deletion mechanism likely involves homologous recombination between repetitive elements that flank the *Avr* genes (Mesarich et al., 2014). Such is likely the case of the *Avr5* gene that is surrounded by repetitive elements (Mesarich et al., 2014).

Fewer modifications have been found in *Ecp* effector genes compared to *Avr* effector genes. The polymorphisms found in *Ecp* effector genes have been rarely found in the protein coding sequence as there is no strong selection pressure on them considering no *Cf-Ecp* genes have been widely used in commercial tomato lines (Stergiopoulos et al., 2007). However, recently more DNA modifications leading to nonsynonymous substitutions of Ecp protein sequences have been reported in strains from Argentina (Lucentini et al., 2021; Medina et al., 2015). All polymorphisms at the DNA level of Avr effectors and the effect of these polymorphisms on *C. fulvum*, in terms of evading *Cf*-mediated resistance, are summarized in Table 1.5

Table 1.5. Allelic variation in the avirulence (*Avr*) and extracellular protein (*Ecp*) effector genes of *Cladosporium fulvum*.

Avr/Ecp gene	Polymorphism at DNA level	Effect on protein	Loss of Cf-mediated HR	Reference
Avr2	gene deletion	no protein	Yes	Medina et al., 2015
	c 2T>C	Met1?	Yes	Stergiopoulos et al., 2007
	c. 1 A>G	Met1Val	Yes	Iida et al., 2015
	c. 28 T>G	Trp10Gly	No	Medina et al., 2015; Lucentini et al., 2021
	c. 29 G>T	Trp10Leu	No	Medina et al., 2015; Lucentini et al., 2021
	c. 50 ins. T	Ile18ThtfsX24	Yes	Iida et al., 2015
	c. 52 A>C	Ile18Leu	No	Iida et al., 2015
	c. 56 del. CAGCAGCCAA	Ala19GlufsX38	Yes	Iida et al., 2015
	c. (64_69)del. A	Lys22AsnfsX11	Yes	Luderer et al., 2002
	c. (64-69) ins. A	leu24TyrfsX18	Yes	Luderer et al., 2002; Iida et al., 2015
	c. 117_119 ins. A	Tyr41ValfsX1	Yes	Luderer et al., 2002; Novak et al., 2021
	c.127T>G	Leu43Val	N.d.	Stergiopoulos et al., 2007
	c.158+12_*60del179	Asp54_Gly78del	Yes	Stergiopoulos et al., 2007

Table 1.5. Continued.

Avr/Ecp gene	Polymorphism at DNA level	Effect on protein	Loss of Cf-mediated HR	Reference
Avr2	c.158+26_158+28delTGA	-	No	Luderer et al., 2002
	c. 242 G>T	Cys63Phe	Yes	Iida et al., 2015
	c.196C>T	Gln67X	Yes	Stergiopoulos et al., 2007
	c.57_58ins5kb	p.Cys72AlaX?	Yes	Luderer et al., 2002
	Transposon insertion	no protein	Yes	Iida et al., 2015
Avr4	c. 54 C>A	Synonymous	No	Medina et al., 2015
	c.-57G>A	-	No	Stergiopoulos et al., 2007
	c. 118 T>C	Cys40Arg	Yes	Iida et al., 2015
	c.124delC	p.Gln42LysfsX63	Yes	Joosten et al., 1994; Joosten et al., 1997
	c. 191 G>T	Cys64Phe	Yes	Iida et al., 2015
	c. 191 G>C	Cys64Ser	Yes	Iida et al., 2015; Yoshida et al., 2021
	c. 191 G>A	Cys64Tyr	Yes	Iida et al., 2015; Joosten et al., 1994
	c.197C>T	p.Thr66Ile	Yes	Joosten et al., 1994; Joosten et al., 1997
	c.199T>C	p.Tyr67His	Yes	Joosten et al., 1994; Joosten et al., 1997
	c.209G>A	Cys70Tyr	Yes	Joosten et al., 1994; Joosten et al., 1997
	c.257G>T	Cys86Phe	Yes	Stergiopoulos et al., 2007
	c.265G>A	Gly89Arg	N.d.	Stergiopoulos et al., 2007
	c. 318 del. G	Ser107ValfsX4	Yes	Iida et al., 2015
	c.326G>A	Cys109Tyr	Yes	Stergiopoulos et al., 2007
	357 G>A	Synonymous	No	Lucentini et al., 2021
Avr4E	gene deletion	no protein	Yes	Westerink et al., 2004; Iida et al., 2015; Yoshida et al., 2021
	c. 244 T>C	Phe82Leu	Yes	Westerink et al., 2004; Iida et al., 2015; Yoshida et al., 2021
	c. 278 T>C	Met93Tyr	Yes	Westerink et al., 2004; Iida et al., 2015
	c. 278 C>T	Met93Thr	No	Lucentini et al., 2021
Avr5	gene deletion	no protein	Yes	Mesarich et al., 2014; Iida et al., 2015
	c. 11 ins. TC	stop7(SP)	Yes	Mesarich et al., 2014
	c. 268 G>C	Gly90Arg	Yes	Iida et al., 2015

Table 1.5. Continued.

Avr/Ecp gene	Polymorphism at DNA level	Effect on protein	Loss of Cf-mediated HR	Reference
Avr9	gene deletion	no protein	Yes	Iida et al., 2015; Yoshida et al., 2021; Bernal-Cabrera et al., 2021
	c. 23T>C	Val8Ala	No	Stergiopoulos et al., 2007; Iida et al., 2015
	137 T>G	-	No	Medina et al., 2015; Lucentini et al., 2021
Ecp1	c.171+33T>C	-	-	Stergiopoulos et al., 2007
	969 T>G	Asp62Asn	N.d.	Medina et al., 2015; Lucentini et al., 2021
	979 ins. A	frameshift	N.d.	Medina et al., 2015; Lucentini et al., 2021
Ecp2-1	257 T>C	Synonymous	No	Medina et al., 2015; Lucentini et al., 2021
	305 C>A	Synonymous	No	Medina et al., 2015; Lucentini et al., 2021
	409 G>T	Arg64Ile	No	Laugé et al., 1998; Medina et al., 2015; Lucentini et al., 2021
	414 T>G	Ser66Ala	N.d.	Medina et al., 2015; Lucentini et al., 2021
	663 ins. A	frameshift	N.d.	Medina et al., 2015; Lucentini et al., 2021
	680 ins. G	frameshift	N.d.	Medina et al., 2015; Lucentini et al., 2021
Ecp4	c.323 G>T	Gly90Val	No	Laugé et al., 2000
	380 G>T	Cys108Trp	N.d.	Medina et al., 2015; Lucentini et al., 2021
	395 ins. A	Gly109Val	N.d.	Medina et al., 2015; Lucentini et al., 2021
	408 ins. A	frameshift	N.d.	Medina et al., 2015; Lucentini et al., 2021
Ecp5	c.86+146 G>A	-	-	Stergiopoulos et al., 2007
	65 A>T	stop	Yes	Medina et al., 2015; Lucentini et al., 2021
	516 del. G	frameshift	N.d.	Medina et al., 2015; Lucentini et al., 2021
	541 G>A	Cys48Tyr	N.d.	Medina et al., 2015; Lucentini et al., 2021
	691 ins. G	frameshift+stop	Yes	Medina et al., 2015; Lucentini et al., 2021

Ins. (insertion), del. (deletion), N.d. (not determined).

1.6 *Venturia inaequalis*

Scab, or black spot, the most economically important disease of apple, is caused by the non-obligate biotrophic Dothideomycete fungus *V. inaequalis* (Cooke) G. Winter (MacHardy, 1996). The two states of the fungus are the saprophytic sexual state (*V. inaequalis* Cke.) and the parasitic asexual state (*Spilocaea pomi* Fr.) (Agrios, 1988). *V. inaequalis* mainly affects cultivated apple, *Malus* x *domestica*, as well as other members of the Rosaceae family such as *M. sieversii* (wild apple), *M. sylvestris* (European crab apple) and *M. floribunda* (Japanese flowering crabapple), as well as *Crataegus oxyacantha* (hawthorn), *Sarcocephalus esculentus, Cotoneaster integerrima, Pyracantha*, *Viburnum* sp., and *Eriobotrya japonica* (loquat) (MacHardy, 1996; Sutton et al., 2014). Based on the ability or inability to infect different hosts, it has been proposed, although not yet widely accepted, that *V. inaequalis* can be further divided into three formae speciales: *V. inaequalis* f. sp. *pomi* (infecting *Malus* spp.), *V. inaequalis* f. sp. *pyracanthae* (infecting *Pyracantha* spp.) and *V. inaequalis* f. sp. *eriobotryae* (infecting *Eriobotrya*) (Gladieux et al., 2010a; Le Cam et al., 2002). The disease is present in all apple-growing regions worldwide, but it is more severe in regions that have a temperate climate with cool and moist conditions during spring (Gladieux et al., 2010b). Previous studies focusing on population genetics have revealed that *V. inaequalis* emerged in Central Asia, the centre of origin of apple, and subsequently invaded Europe, North and South America, South Africa and New Zealand (Cornille et al., 2012; Gladieux et al., 2008). The fungal genus *Venturia* includes members that infect other cropping trees: *V. pyrina* (European pear), *V. nashicola* (Asian pear), *V. cerasi* (cherry), *V. carpophila* (peach and almond), *V. effusa* (pecan) and *V. oleaginea* (olive) which are host-specific pathogens (Gonzalez-Dominguez et al., 2017).

1.6.1 Life cycle of *V. inaequalis*

During its lifecycle, the fungus undergoes both sexual saprobic and asexual biotrophic stages (Fig. 1.12) (MacHardy, 1996). The saprobic phase occurs during winter, where sexual reproduction takes place between two opposite mating types to form sexual fruiting bodies, called pseudothecia, in fallen leaf litter (Gladieux et al., 2008). The biotrophic phase starts in spring and early summer, when ascospores are released from pseudothecia mainly during or after rain events and dispersed by wind (Gladieux et al.,

2008; Gonzalez-Dominguez et al., 2017). It is during this time of the growing season that the infection risk is higher, as leaves and fruit are young and, therefore, most susceptible (Xu & Robinson, 2005). When ascospores land on fruit or leaves, they germinate, produce an appressorium to penetrate through the cuticle, and then differentiate subcuticular runner hyphae and pseudoparenchymatous structures called stromata in the subcuticular environment without invading plant cells. Stromata and the production of conidia that burst through the cuticle lead to the characteristic scab lesions (Fig. 1.13) (Bowen et al., 2011). These circular lesions on leaves and fruit are initially light green in colour, then later increase in size and become olive-brown coloured and velvety, which then often become cracked and torn (Fig. 1.13). Conidia cause secondary infections within the orchard during the growing season by means of wind and rain dispersion (Bowen et al., 2011; MacHardy, 1996).

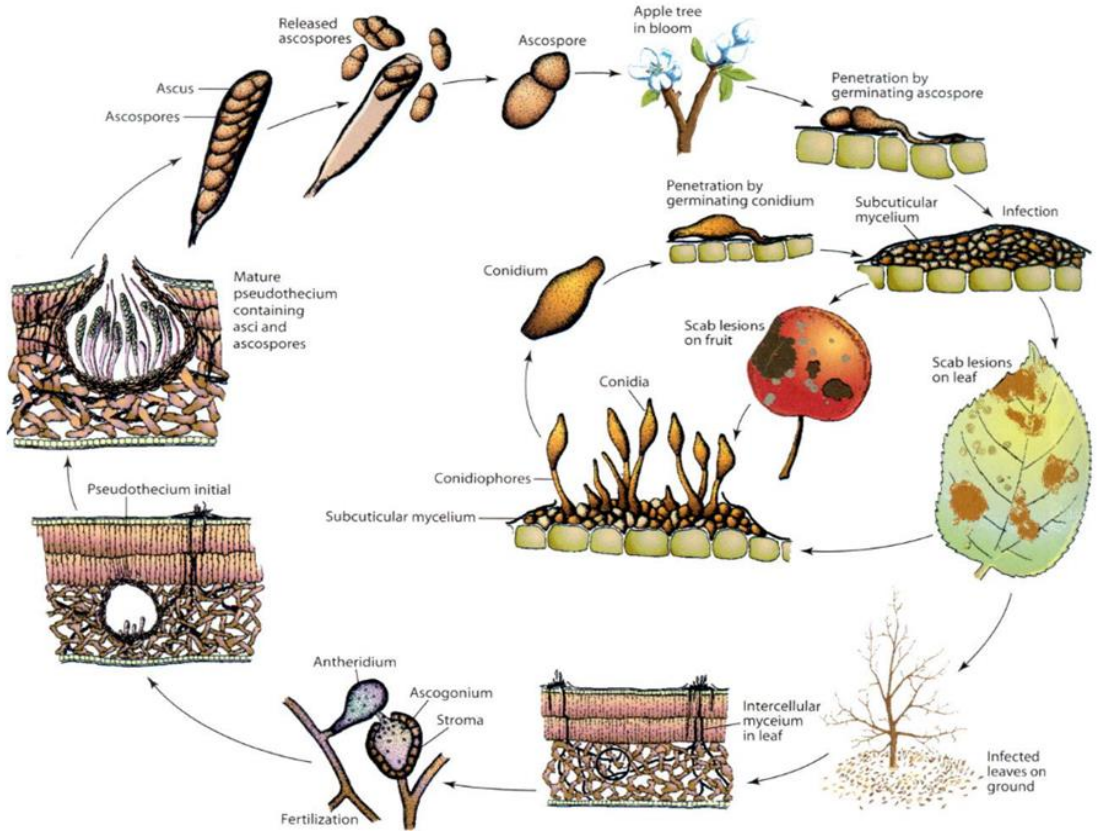

Figure 1.12. *Venturia inaequalis* life cycle. Figure from Agrios, *Plant Pathology*, p. 506. Copyright Elsevier 2005.

Figure 1.13. Symptoms of scab or blackspot disease on apple plants caused by *Venturia inaequalis*. Picture taken by C. Mesarich at the Massey University orchard in Palmerston North, New Zealand.

1.6.2 Scab control methods

Scab disease causes up to a 70% reduction in apple production, which can be attributed to fruit infection that renders the fruit unmarketable (i.e. through deformations and spots), as well as defoliation that reduces growth and yield (Thakur et al., 2013). If the infection is severe, leaves or fruit are prone to fall from the tree (Thakur et al., 2013). The disease can be controlled with sanitation and cultivation measures (i.e., leaf mulching accompanied with urea applications, and reducing humidity in tree canopies through proper pruning and tree spacing). But the primary method of control is fungicide applications (Bowen et al., 2011; Gauthier, 2018). Around 15 fungicide applications per season are needed to control scab, leading to high costs to the apple industry (Khajuria et al., 2018; Patocchi et al., 2004). In New Zealand, fungicide applications alone cost the apple industry around $1,200 per hectare each season (http://www.plantandfood.co.nz/growingfutures/case-studies/residue-free-apples/controllingblackspot). With over 10,396 hectares of commercial apple grown in New Zealand (Table 1.2), this equates to over $12.4 million per annum, without considering costs associated with yield losses and unmarketable product.

Not only costs related to fungicide are concerning for the apple industry but also fungicide resistance. So far, *V. inaequalis* isolates resistant to Strobirulin or QoIS, DMIs, succinate dehydrogenase inhibitors (SDHIs), MBC and dodine fungicides have been reported worldwide (Beresford et al., 2012; Fiaccadori et al., 2011; Lichtner et al., 2020; Polat & Bayraktar, 2021; Sallato et al., 2006). Resistance to those fungicides are the result of diverse mechanisms. Reduced sensitivity to QoI fungicides is conferred by a single G143A substitution in the cyt b protein (Fiaccadori et al., 2011; Gisi et al., 2002). Resistance to DMIs in *V. inaequalis* is probably due to the overexpression of the *CYP51A1* gene (Cordero-Limon et al., 2021; Schnabel & Jones, 2001; Villani et al., 2016). Moderate, high and low level of resistance to MBC fungicides are the result of mutations at codons 198, 200 and 240 respectively, in the *β-tubulin* gene (Polat & Bayraktar, 2021). SDHIs interfere with cellular respiration by targeting the succinate dehydrogenase reductase enzyme at complex II of mitochondria (Avenot & Michailides, 2010). Resistance to SDHIs in other fungal pathogens (e.g. *A. alternata*, *Z. tritici* and *B. cinerea*) has been as a result of different mutations in the succinate dehydrogenase gene (*sdh*) complex (Sierotzki & Scalliet, 2013). So far, resistance to SDHIs in *V. inaequalis* has not been reported (Ayer et al., 2020; Ayer et al., 2019). The specific mode of action for dodine fungicides remains uncertain. However, it has been reported that it affects and disrupts the plasma membrane (Schuster & Steinberg, 2020). To date, resistance to dodine has been reported in other countries, but not in New Zealand, and the molecular mechanisms involved in resistance remain to be elucidated (Carbone et al., 2021; Köller et al., 1999; Lichtner et al., 2020). The frequent and erroneous use of single-site fungicides to control apple scab increases the selection pressure to overcome this control method, and results in beneficial mutations in major genes, leading to the emergence of new fungicide-resistant isolates of *V. inaequalis* (Polat & Bayraktar, 2021). In addition to cultural methods and fungicide applications, the discovery and stacking of multiple *R* genes remains the most effective disease management strategy in apple orchards.

1.6.3 Molecular aspects of the *V. inaequalis*-apple interaction

The *V. inaequalis*-apple pathosystem follows a gene-for-gene interaction between pathogen *Avr* effector genes and host *R* genes. According to this interaction, the apple scab *R* genes are named *Rvik* (where *R* is for resistance gene, *vi* is for *V. inaequalis* and *k* is for the differential host), whereas the corresponding *Avr* genes are named *AvrRvik* (Bowen et al., 2011; Bus et al., 2011). So far, more than 20 *R* genes have been genetically identified in apple, whereas only a few *Avr* genes have been genetically identified in *V. inaequalis* (Khajuria et al., 2018). Similarly to *C. fulvum*, when an isolate of *V. inaequalis* is able to overcome an *R* gene in an apple host, it is defined as a race (Bowen et al., 2011). Therefore, there are predicted to be up to 20 physiological races (or more if lost more than one *Avr*) of *V. inaequalis* that correspond to the 20 known *R* genes in apple (Table 1.6).

Table 1.6. Scab immune receptor (*R*) genes in apple and their corresponding avirulence (*Avr*) effector genes from *Venturia inaequalis*.

R gene	Corresponding avirulence gene	Resistance reaction
Rvi1	*AvrRvi1*	Necrosis
Rvi2	*AvrRvi2*	Stellate necrosis
Rvi3	*AvrRvi3*	Stellate necrosis
Rvi4	*AvrRvi4*	Hypersensitive response
Rvi5	*AvrRvi5*	Hypersensitive response
Rvi6	*AvrRvi6*	Chlorosis
Rvi7	*AvrRvi7*	Hypersensitive response
Rvi8	*AvrRvi8*	Stellate necrosis
Rvi9	*AvrRvi9*	Stellate necrosis
Rvi10	*AvrRvi10*	Hypersensitive response
Rvi11	*AvrRvi11*	Stellate necrosis/chlorosis
Rvi12	*AvrRvi12*	Chlorosis
Rvi13	*AvrRvi13*	Stellate necrosis
Rvi14	*AvrRvi14*	Chlorosis
Rvi15	*AvrRvi15*	Hypersensitive response
Rvi16	*AvrRvi16*	Hypersensitive response
Rvi17	*AvrRvi17*	Chlorosis
Rvi18	*AvrRvi18*	Hypersensitive response
Rvi19	*AvrRvi19*	All classes of resistance reactions
Rvi20	*AvrRvi20*	All classes of resistance reactions

1.6.3.1 Compatible interaction

Under optimum moisture conditions, the conidium adheres and forms a germ tube on the leaf or fruit surface, then breaches the cuticle directly or by appressorial differentiation (Fig. 1.14A) (Smereka et al., 1987). An initial stroma forms beneath the penetration site, from which runner hyphae emerge (Fig. 1.14B). From these runner hyphae, new stromata then form (Fig. 1.14C), followed by the abundant production of conidia and conidiophores (Fig. 1.14D) (Bowen et al., 2011). *V. inaequalis* does not form specialized feeding structures such as haustoria; however, it has been hypothesized that it acquires nutrients via the stromata in the subcuticular space (Bowen et al., 2011). To suppress plant immune responses and successfully colonize the host, it is assumed that stromata also deliver effector proteins into the subcuticular environment (Deng et al., 2017). However, there could be an unknown mechanism in which these effectors are taken up by the plant cells, as one of the Rvi R proteins identified in apple belongs to the TIR-NBS-LRR family (section 1.6.5) (Bowen et al., 2009; Khajuria et al., 2018; Schouten et al., 2013).

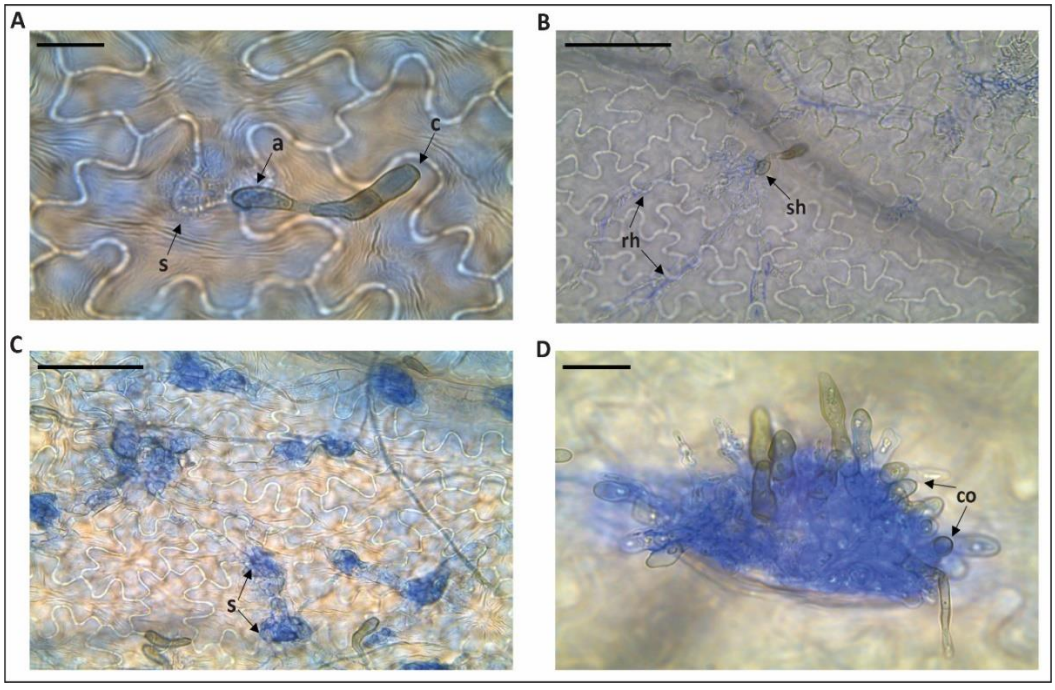

Figure 1.14. Apple leaf infection by *Venturia inaequalis* (compatible interaction). **(A)** A conidium germinating and forming an appressorium on the surface of the leaf. A stroma forms beneath the penetration site. Bar = 5 µm; **(B)** Subcuticular runner hyphae. Bar = 20 µm; **(C)** Stromata. Bar = 20 µm; **(D)** Production of conidia and conidiophores. Bar = 5 µm; Key: a = appressorium; c = conidium; co = conidiophores; rh = runner hyphae; sh = subcuticular hyphae; s = stroma. The fungus is stained with aniline blue. Figures from Rocafort et al. (in preparation).

1.6.3.2 Incompatible interaction

Limited sporulation and a resistance response characterize an incompatible interaction in apple. Resistance to *V. inaequalis* has been divided into three classes according to the reaction observed in leaves. The highly resistant class 1 reaction is characterized by a typical HR visible as pinpoint pits due to a rapid localized cell death (Fig. 1.15B). The resistant class 2 reaction is characterized by collapsed epidermal cells (Fig. 1.15C). Class 3 is divided into 3a (Fig. 1.15D), which is weakly resistant, and 3b (Fig. 1.15E), which is weakly susceptible as subcuticular sporulating stromata of the fungus and modified epidermal cells are present. The class 2, 3a and 3b resistance reactions can be macroscopically observed with symptoms such as chlorosis (Fig. 1.15C), necrosis (Fig. 1.15H) and stellate necrosis, which is a ''star-like'' collapse of cells (Fig. 1.15G) (Bus et al., 2005a; Chevalier et al., 1991; Gessler et al., 2006). These differences, and intensity in resistance reactions, likely depend on the *Rvi* gene and the induced downstream signaling pathways involved (Bowen et al., 2011). The class 4 reaction is included, but as a susceptible response, where no changes are visible as the epidermis does not appear to undergo changes compared to uninfected tissue (Fig. 1.15F) (Chevalier et al., 1991; Gessler et al., 2006; Jänsch et al., 2013).

Figure 1.15. Scab reaction classes on apple leaves after inoculation with *Venturia inaequalis*. Macroscopic symptoms differ depending on the resistance gene carried by the host. **(A)** No macroscopic symptoms; **(B)** class 1 or pinpoint pits; **(C)** class 2; **(D)** class 3a; **(E)** class 3b; **(F)** class 4 or susceptibility; **(G)** stellate necrosis; **(H)** necrosis. Pictures taken approximately 21 days post- inoculation. Image from (Gessler et al., 2006).

1.6.4 *V. inaequalis* effectors

So far, only one *Avr* effector gene, *AvrRvi6*, which corresponds to the *Rvi6 R* gene of apple, has been cloned, but the sequence of this gene has not yet been published (Le Cam et al., unpublished). In addition to this, the region covering the *AvrRvi1 Avr* effector gene was identified using a map-based cloning strategy, but the gene itself has not yet been identified (Broggini et al., 2007). Thus, little is known about effector genes from *V. inaequalis*. Different strategies have been deployed to identify *V. inaequalis* effector

candidates such as map-based cloning, expressed sequence tag (EST) libraries, *in vitro* growth using liquid culturing or cellophane membranes (section 1.6.4.1), transcriptome and whole genome sequencing. A bioinformatic analysis of ESTs derived from cDNA libraries of infected plant material (*in planta*), potato dextrose broth (PDB) and cellophane membranes (in culture), led to the identification of 16 *V. inaequalis* candidate effectors (VICE) (Bowen et al., 2009). Furthermore, using a proteomics approach, eight proteins were identified from a *V. inaequalis* liquid culture filtrate that triggered necrosis in different apple accessions (Mesarich et al., unpublished; Win et al., 2003).

Specific candidate effectors previously identified are Cin1 (Cellophane-induced 1) and Cin3 (Cellophane-induced 3), which were identified from growth of *V. inaequalis* on cellophane membranes (Fig. 16) (Kucheryava et al., 2008). Both *Cin* genes were found to be highly expressed in culture during growth in cellophane membranes and *in planta*. *Cin1* encodes a mature protein of 442 amino acids, with seven or eight imperfect repeats of approximately 60 amino acids that each fold into a three-helix bundle stabilized by two disulphide bonds. Additionally, two *Cin1* paralogs have also been identified: *Cin1L1* (*Cin1-Like 1*) and *Cin1L2* (*Cin1-Like 2*) (Kucheryava et al., 2008; Mesarich et al., 2012). The encoded Cin1L1 and Cin1L2 mature proteins are 149 and 85 amino acids in length respectively, with both containing 4 cysteine residues and a single Cin1-like repeat (Mesarich et al., 2012). Cin3 encodes a 212 amino acid ribosomally synthesized and post-translationally modified peptide (RiPP) precursor protein with four or five repeats and no cysteine residues (Kucheryava et al., 2008; Hassing and Mesarich et al., unpublished).

A secretome comparison of four *V. inaequalis* isolates uncovered many genes encoding predicted secretomes ranging from 1131 to 1622 proteins in size. From these, over 245 putative candidate effectors (SSPs <500 amino acids) were identified (Deng et al., 2017). Interestingly, among these SSPs were those with sequences with similarities to fungal hydrophobins, and to other fungal effectors such as Ecp6 from *C. fulvum* (to be discussed in Chapter 3), Ave1 from *Verticillium* species and AvrLm6 from *L. maculans* (Deng et al., 2017). Previously, fifteen *AvrLm6*-like genes were identified in *V. inaequalis*. The closest homolog to AvrLm6 from *L. maculans* was shown to be up-regulated during infection and, using an eYFP-fusion protein, was found to localize to the subcuticular stromata of infected apple hypocotyls (Shiller et al., 2015).

1.6.4.1 An *in vitro* model to mimic *in planta* growth

Cellophane membranes overlaying potato-dextrose agar (PDA) have been used to analyze the morphological differentiation related to the infection structures formed by *V. inaequalis in planta*, and to identify relevant fungal genes in the *V. inaequalis*-apple pathosystem (Kucheryava et al., 2008). Interestingly, it was observed that *V. inaequalis* spores can germinate and form appressoria to penetrate cellophane in a similar way as on the plant surface (Fig. 1.16A-B). After penetrating the cellulose sheet, subcuticular-like hyphae and stroma-like structures differentiate (Fig. 1.16A-C-D-E). The hyphal differentiation and thus stromata formation is suggested to derive from a sensing mechanism triggered by the texture or pressure of the surrounding medium, and not to a chemical response (Kucheryava et al., 2008). As mentioned in the previous section, two cellophane-induced (*Cin*) genes were identified using this *in vitro* model and provided the first insights into genes that are likely involved in apple infection.

Figure 1.16. *Venturia inaequalis* inside a cellophane membrane as an in culture model for *in planta* growth. (A) A germinating conidium forming an appressorium on the membrane surface and differentiating subcuticular-like hyphae inside the membrane itself. Bar = 10 µm. **(B)** Hypha emerging from the cellophane membrane. Bar = 10 µm. **(C)** Stroma-like structure formed inside the cellophane membrane. Bar = 100 µm. **(D)** Stroma-like structure formed inside the cellophane membrane stained with aniline blue. Bar = 10 µm. **(E)** Immuno-stained stroma-like structure formed inside the cellophane membrane. Bar = 10 µm. **(F)** Stroma-like structures formed inside a cellophane membrane. Bar = 5 mm. Key: a = appressorium; c = conidium; eh = emerging hypha; sclh = sub-cuticular-like hyphae; sl = stroma-like. Image from Kucheryava et al. (2008).

1.6.5 Apple Rvi resistance proteins

Practically all *Rvi R* genes deployed in apple orchards have been derived from wild *Malus* species such as *M. floribunda*, *M. micromalus*, *M. pumila* and *M. sieversii* (Bus et al., 2011). So far, 20 *Rvi* genes have been genetically identified and two of them have been cloned, *Rvi6* (Belfanti et al., 2004) and *Rvi15* (Schouten et al., 2013). *Rvi6*, formerly called *Vf*, was identified from an *HcrVf* (homologues of *Cladosporium fulvum* resistance genes) cluster (Vinatzer et al., 2001). This was the first scab *R* gene to be cloned and is the most widely used *Rvi* gene in cultivated apple varieties (Belfanti et al., 2004; Parisi et al., 1994). Rvi6 belongs to the RLP family (Belfanti et al., 2004), whereas the intracellular receptor Rvi15 belongs to the TIR-NBS-LRR family (Schouten et al., 2013). The *Rvi15* gene from the accession GMAL 2473 was cloned with its native promoter and inserted into the susceptible cultivar 'Gala' using *Agrobacterium tumefaciens*-mediated transformation. Transformed plants were inoculated with *V. inaequalis* (carrying *AvrRvi15*), triggering a HR (Schouten et al., 2013). Some of the remaining *Rvi* genes have been genetically identified from diverse cultivars and their location has been mapped for future cloning attempts (Khajuria et al., 2018).

1.6.6 Avoidance of Rvi-mediated resistance

Due to the limited information regarding *V. inaequalis* effectors, a precise example of the molecular mechanism behind a specific resistance-breaking strain is lacking. However, hypotheses can be formulated with the understanding of other fungal pathogen-host relationships. The heterothallic nature of *V. inaequalis* contributes to high genetic diversity and effective adaptation to selection pressures imposed on the fungus due to monocultural practices in orchards (Padder et al., 2013). Monogenic resistance, governed by single *Rvi* genes in apple, has been overcome and led to the rapid evolution of *V. inaequalis*, presumably by using similar strategies to other plant pathogens such as mutations, insertions or deletions in the *Avr* genes or promoters (Broggini et al., 2007). Repeat-induced mutations (RIPs) occurring during sexual crossing can also lead to the transition from avirulence to virulence (Fudal et al., 2009). *V. inaequalis* candidate effectors have been found to be located close to repetitive sequences and, as mentioned previously, the close location of *Avr* genes to repetitive elements can facilitate gene deletions due to homologous recombination between

repetitive elements that flank these *Avr* genes (Deng et al., 2017; Mesarich et al., 2014). With exception of *Rvi11*, and the *Rvi15* to *Rvi20* genes whose resistance has not been overcome yet, *V. inaequalis* isolates overcoming all the remaining resistance genes have been reported (Khajuria et al., 2018; Patocchi et al., 2020).

1.7 Aims and objectives

Isolates or strains of *V. inaequalis* and *C. fulvum* have evolved to overcome resistance mediated by one or more *R* genes in apple (*Rvi* genes) and tomato (*Cf* genes), respectively, and are increasingly being identified in New Zealand and other countries worldwide. These strains are of great concern, because many have circumvented resistance mediated by *R* genes present in commercially deployed apple and tomato cultivars, and therefore have the potential to cause significant crop losses. To develop effective, durable control strategies against these resistance-breaking isolates or strains, a better understanding of how *V. inaequalis* and *C. fulvum* interact with their hosts at the molecular level is required.

The focus of the current research was therefore to identify and characterize Avr effectors from *V. inaequalis* and *C. fulvum* that have broken resistance in apple and tomato, respectively, as well as to identify and characterize effectors from *V. inaequalis* that are recognized by R proteins in the non-host species *Nicotiana benthamiana* and *Nicotiana tabacum* (i.e. to gain insights into effectors that might be recognized by R proteins in apple). For this purpose, the following aims and objectives were pursued:

Aim 1: Identify the *AvrRvi4* effector gene of *V. inaequalis*, which corresponds to the *Rvi4* *R* gene of apple. For this aim, the specific objectives were to:

1) Sequence the genomes of the New Zealand *V. inaequalis* isolates J222 (possesses a functional copy of the *AvrRvi4* gene) and NZ203.1 (lacks a functional copy of the *AvrRvi4* gene) using Illumina genome sequencing.
2) Identify *in planta*-expressed SSP effector candidates from a pre-prepared six-frame translation of *in planta* RNA-Seq transcriptome sequence from *V. inaequalis* reference strain MNH120 (possesses a functional copy of the *AvrRvi4* gene) using web- and software-based prediction tools.
3) Phenotype the progeny of a previously prepared sexual cross between isolates J222 and NZ203.1 on an apple cultivar carrying the *Rvi4* gene using infection assays and bright-field microscopy.
4) Assess whether other regions of the isolate NZ203.1 genome, and the genomes of progeny that lack a functional copy of the *AvrRvi4* gene, are

deleted or modified using web-, software-and other bioinformatic-based tools.

5) Assess the expression profile of the *AvrRvi4* gene during growth of isolate MNH120 on a susceptible apple cultivar lacking the *Rvi4* gene and in culture using pre-existing RNA-Seq transcriptome sequencing data.
6) Assess the level of *AvrRvi4* gene allelic variation across isolates of *V. inaequalis* collected from around the world using polymerase chain reaction (PCR) amplicon sequencing and public sequence database searches.
7) Use web-based prediction tools to gain insights into the function of the AvrRvi4 effector.
8) Complementation of isolate NZ203.1 with a functional copy of *AvrRvi4* to determine if avirulence is restored.

Aim 2: Identify and characterize candidate effector proteins of *V. inaequalis* reference isolates MNH120 and EU-B04 in the non-host plants *N. benthamiana* and *N. tabacum* using an effectoromics approach. For this aim, the specific objectives were to:

1) Generate a list of *in planta*-expressed candidate effector proteins from pre-existing transcriptomic data of isolate EU-B04 and pre-existing in-culture proteomics data of isolate MNH120 using web-based prediction tools.
2) Express *V. inaequalis* candidate effectors in *N. benthamiana* and *N. tabacum* using *Agrobacterium tumefaciens*-mediated transient expression assays (ATTAs) to determine whether they have the ability to trigger a resistance response (e.g. chlorosis or cell death).
3) Use web-based prediction tools to gain insights into the function of the effector candidates triggering cell death and/or chlorosis.
4) Assess the expression profile of the candidate effector-encoding genes using pre-existing RNA-Seq data.

Aim 3: Identify and characterize the *Avr9B* effector gene of *C. fulvum*, which corresponds to the *Cf-9B R* gene of tomato. The specific objectives were to:

1) Sequence the genome of *C. fulvum* strain IPO 2679 from New Zealand, which is known to overcome Cf-9B-mediated resistance in tomato, using Illumina sequencing technology.
2) Compare the nucleotide and protein sequences of all previously identified in *planta*-expressed apoplastic SSP effectors and effector candidates from an Avr9B-producing reference strain of *C. fulvum* (0WU) with the corresponding genes and proteins from *C. fulvum* strain IPO 2679, to identify Avr9B effector candidates.
3) Co-express the Avr9B effector candidates with the corresponding Cf-9B immune receptor in *N. tabacum* using ATTAs to determine which of these candidates triggers an HR upon recognition by Cf-9B.
4) Assess the level of *Avr9B* gene allelic variation across strains of *C. fulvum* collected from around the world using PCR amplicon sequencing.
5) Identify homologs of the Avr9B effector from other fungi, and co-express a subset of these with the Cf-9B immune receptor in *N. tabacum* using ATTAs to determine whether they are able to trigger a Cf-9B-dependent HR.
6) Assess the expression profile of the *Avr9B* gene during growth of a *C. fulvum* strain in planta and in culture using RT-qPCR.
7) Complement the NZ IPO 2679 strain with a functional copy of *Avr9B* to determine if avirulence is restored.
8) Investigate the localization of the Avr9B effector *in planta* using ATTAs in conjunction with GFP and mCherry fusions in *N. tabacum* using confocal microscopy.
9) Use web-based prediction tools to gain insights into the function of the Avr9B effector.

Chapter 2: Identification of the AvrRvi4 avirulence effector from *Venturia inaequalis*

2.1 Introduction

Apple is the crop with the third highest global fruit yields in the world after bananas (116 Million Metric Tons; MMT) and watermelons (100 MMT) (http://faostat.fao.org). With a production of 87 MMT, apples are threatened by the scab pathogen *Venturia inaequalis.* Host specificity of *V. inaequalis* is reportedly divided into three formae speciales: *V. inaequalis* f. sp. *pomi* infecting *Malus* spp. (including apple), *V. inaequalis* f. sp. *pyracanthae* infecting *Pyracantha* spp (firethorn) (Le Cam et al., 2002), and *V. inaequalis* f. sp. *eriobotryae* infecting *Eriobotrya japonica* (loquat) (Gladieux et al., 2010a). Races of *V. inaequalis* are defined by their ability to overcome resistance mediated by a specific *Rvi* gene to cause infection. These races are thought to carry a mutated version of the corresponding *Avr* gene in their genomes (Bus et al., 2011). Host plants are defined based on the *Rvi* gene they carry. For example, the host (0) 'Royal Gala' cultivar does not carry any known *Rvi* genes, whereas host (6) carries the *Rvi6* gene (Bus et al., 2011).

The first *Rvi* gene cloned, *Rvi6* (formerly *Vf*), was identified from the crabapple species *Malus floribunda* 821 (Belfanti et al., 2004; Gessler et al., 2006). *Rvi6* encodes a membrane-anchored extracellular R protein from the leucine-rich receptor-like protein (LRR-RLP) class, like the Cf R proteins from tomato (Vinatzer et al., 2001), and mediates recognition of the AvrRvi effector AvrRvi6 from *V. inaequalis*. The *AvrRvi6* gene encodes a secreted protein that triggers a chlorotic resistance reaction upon recognition by Rvi6 (Bus et al., 2011). Notably, due to the intensive use of cultivars carrying single *Rvi* genes, resistance-breaking isolates of *V. inaequalis* have continually emerged. For example, use of *Rvi6* as the major source of resistance in apple breeding programmes resulted in the emergence of *V. inaequalis* race (6) isolates virulent on host (6) *Rvi6* cultivars in Europe as early as the 1990s (Parisi et al., 1994; Roberts & Crute, 1994) and, more recently, in North America (Papp et al., 2020). It is understood that different mutations in the

AvrRvi6 gene have resulted in the circumvention of *Rvi6*-mediated resistance in race (6) isolates (Bruno Le Cam, personal communication).

The second *Rvi* gene cloned, *Rvi15* (formerly *Vr2*) (Schouten et al., 2013), was identified from the accession GMAL 147 (a clone of the Russian seedling R12740-7A) (Patocchi et al., 2004; Patocchi et al., 2003; Vinatzer et al., 2001). The *Rvi15* gene encodes an intracellular R protein from the toll interleukin 1-nucleotide binding site-LRR (TIR-NBS-LRR) class (Schouten et al., 2013), and mediates recognition of the AvrRvi effector AvrRvi15 from *V. inaequalis*. The Rvi15-mediated resistance reaction is characterized by a pinpoint pit HR (Bus et al., 2011). To date, however, there are no reports of *V. inaequalis* race (15) isolate overcoming Rvi15-mediated resistance in host (15) plants, and AvrRvi15 has not yet been identified (Patocchi et al., 2020).

The *Rvi4* gene (formerly *Vh4*, *Vx* and *Vr1*) (Boudichevskaia et al., 2004; Bus et al., 2009; Bus et al., 2005b; Ranatunga et al., 1999) is present in the Russian apple *Malus pumila* R12740-7A (Shay & Williams, 1956), accession PRI 478-33 (also known as X 2249, W7AR44T20 and TSR33T239, an F2 derivative of R12740-7A) (Bus et al., 2005b; Hemmat et al., 2002; Parisi et al., 1993), accession A185R04T093 (a cross between cultivar 'Granny Smith' and accession PRI 478-33), and some specific apple cultivars, including 'Regia'(Boudichevskaia et al., 2006). Although *Rvi4* has not yet been cloned, it has been mapped to linkage group 2 (LG2) of accession PRI 478-33 (Bus et al., 2005b; Jänsch et al., 2015). The R protein encoded by the *Rvi4* gene elicits a class 1 resistance response, visualized by a pinpoint pit HR upon recognition of the yet-unidentified AvrRvi effector AvrRvi4 (Bus et al., 2011). Reports of *V. inaequalis* overcoming Rvi4-mediated resistance are still scarce, with only a few reports of race (4) isolates in Europe and the USA (Bus et al., 2011; Caffier et al., 2015; Masny, 2017; Patocchi et al., 2020; Sandskär & Liljeroth, 2005). Many of the race (4) isolates identified to date, however, do not appear to be completely compatible with host (4) plants. For example, the race (4) isolate 1638 from France first triggers an HR on Rvi4 plants before sporulating (Bus, 2006; Bus et al., 2011). In 2009, a New Zealand isolate of *V. inaequalis* (NZ203.1) overcoming Rvi4-mediated resistance was identified in an orchard at the New Zealand Institute for Plant and Food Research in Havelock North. Unlike other race (4) isolates previously identified, NZ203.1 sporulates abundantly on plants carrying *Rvi4,* suggesting complete compatibility. Identification of the *AvrRvi4* gene is crucial to enhance our understanding of how

V. inaequalis interacts with apple at the molecular level, and to determine the molecular mechanisms leading to resistance-breaking isolates. Identification of *AvrRvi4* will also enable the appearance or presence of Rvi4-resistance breaking isolates to be tracked over time, so that decisions on deployment of *Rvi4* in a pyramided resistant apple cultivar (≥3 *Rvi* genes) can be made, as recommended by Patocchi et al. (2020).

V. inaequalis possesses several characteristics that are useful for dissecting gene-for-gene interactions with apple. Firstly, the genomes of multiple *V. inaequalis* isolates have been sequenced (Deng et al., 2017; Le Cam et al., 2019; Lichtner et al., 2020; Passey et al., 2020; Passey et al., 2018). Secondly, *V. inaequalis* can be cultured easily on cellophane membranes overlaying potato-dextrose agar (PDA) (see section 1.6.4.1), enabling the rapid preparation of spore suspensions for infection assays on differential apple cultivars. Thirdly, isolates of *V. inaequalis*, representing different mating types of the fungus, can be crossed easily *in vitro*, resulting in genetically non-uniform and phenotypically stable progenies that can be subcultured multiple times (Jha et al., 2009). Taking advantage of these characteristics, this chapter describes the identification of a candidate *AvrRvi4* effector gene using a whole genome sequencing and phenotyping approach based on progeny derived from a sexual cross between the *V. inaequalis* race (1,4) isolate NZ203.1 and a *V. inaequalis* race (1) isolate J222.

2.2 Materials and methods

2.2.1 Biological materials

Fungal isolates and plants used in the work described in this chapter are listed in Table 2.1. *V. inaequalis* isolates J222 and NZ203.1, as well as progeny derived from a J222 x NZ203.1 cross, were kindly provided by Dr Vincent Bus (the New Zealand Institute for Plant and Food Research, Havelock North), while *V. inaequalis* isolate MNH120 was kindly provided by Dr Joanna Bowen (the New Zealand Institute for Plant and Food Research, Auckland). Apple seed from cultivar 'Royal Gala' were kindly provided by Dr. Bowen, while apple seed, derived from a cross between apple cultivar 'Royal Gala' and apple accession TSR33T239 were kindly provided by Dr. Bus.

Table 2.1. Biological materials used in this chapter.

Organism	Characteristics	Reference
Venturia inaequalis		
MNH120 (ICMP 13258, Vi1)	Wild type race 1 isolate (overcomes resistance in apple cultivars mediated by the *Rvi1* resistance (*R*) gene). Source: leaf tissue of apple cultivar 'Granny Smith', Huapai, Auckland, New Zealand, 1996	Deng *et al*. (2017); Stehmann *et al*. (2001)
J222	Wild type race 1 isolate (overcomes resistance in apple cultivars mediated by the *Rvi1 R* gene). Source: leaf tissue of an unknown apple tree at a New Zealand Institute for Plant and Food Research orchard, Nelson, New Zealand, 1996	Bus *et al*. (2005a,b)
NZ203.1	Wild type race 1,4 isolate (overcomes resistance in apple cultivars mediated by the *Rvi1* and *Rvi4 R* genes). Source: fruit of BK255 (A022R16T173 x PRI 478-33) at a New Zealand Institute for Plant and Food Research orchard, Havelock North, New Zealand, 2007	V. Bus, unpublished[a]
J222 x NZ203.1 (S001–S107)	107 progeny from a cross between isolates J222 and NZ203.1	V. Bus, unpublished[a]
Malus* x *domestica		
'Royal Gala'	Seeds from apple cultivar 'Royal Gala' (carries no *Rvi R* genes)	
'Royal Gala' x TSR33T239	Seeds from a cross between apple cultivar 'Royal Gala' and apple accession TSR33T239 (carries only the *Rvi4 R* gene) that have segregated for the *Rvi4 R* gene	V. Bus, unpublished[a] Jansch *et al.* (2015) Baldi *et al*. (2004)

[a]The New Zealand Institute for Plant & Food Research, Havelock North.

2.2.2 Growth conditions

2.2.2.1 Apple seed germination

Apple seeds were surface-sterilized with 75% (v/v) ethanol for 5 min, rinsed five times with sterile deionized water, and then imbibed in sterile water overnight at room temperature (RT). The seed coat or testa was subsequently removed with forceps and each seed placed into 0.5x Murashige and Skoog (MS)-medium (Duchefa Biochemie, Haarlem, The Netherlands) containing 1% (w/v) phytagel (Plant Media, Dublin, Ireland). Here, the white embryo of the seed was positioned downwards, with only half of the seed submerged into the MS-phytagel medium. Seeds were then germinated at 21°C with a 16 h light / 8 h dark photoperiod for approximately 7 days. Finally, germinated seeds with a radicle of approximately 8–10 cm were transferred into small TEKU® pots (Pöppelmann, Lohne, Germany) containing Dalton's Potting Mix (Fruitfed, New Zealand) and grown as seedlings under the same controlled conditions.

2.2.2.2 Preparation and maintenance of detached apple leaves

Fully expanded apple leaves from seedlings in section 2.2.2.1 were detached at the base of the petiole (i.e. where the petiole meets the stem) using scissors, surface-sterilized with 1% (v/v) hypochlorite for 5 min, washed three times with sterile deionized water, and then placed onto 2% (w/v) water agar (WA) (Acumedia®, Michigan, USA). A small portion of the petiole at the cut end was subsequently covered with sterile cotton wool soaked in sterile water to ensure hydration, immediately inoculated with *V. inaequalis* (see section 2.2.4) and maintained under the controlled conditions described in section 2.2.2.1 for up to 5 days.

2.2.2.3 Fungal isolates

Monospore-derived cultures of *V. inaequalis* were stored as dehydrated mycelia grown on filter paper or cellophane membranes at –20°C and were used to initiate new cultures. When solid cultures were required, filter paper or cellophane membranes harbouring *V. inaequalis* were placed onto potato dextrose agar (PDA; Scharlab, Barcelona, Spain) plates, rehydrated with approximately 70 µl of sterile water, sealed with Parafilm® M (Pechiney Plastic Packaging; Chicago, IL, USA), and grown until conidia were observed (typically 7–10 days post-rehydration) in clear boxes maintained at 22°C

under a cyclic 16 h period of white fluorescent light and 8 h dark. Upon sporulation, the PDA plates were flooded with sterile water, the conidia dislodged using a sterile glass L-shaped spreader and then the conidia separated from other fungal debris by filtration through glass wool (Sigma-Aldrich, Missouri, USA), with 100 µl of the spore suspension subsequently spread onto sterile cellophane membranes (Waugh Rubber Bands; Wellington, New Zealand; autoclaved in sterile water twice before use) overlaying PDA. For liquid cultures of *V. inaequalis*, conidia were prepared as above, and inoculated into potato dextrose broth (PDB; Scharlab) and cultured at 22˚C on a rotary shaker at 180 rpm (Bio-Line Incubator Shaker, Edwards Instrument Company, Wisconsin, USA) for 4–5 weeks. Short-term storage of *V. inaequalis* plates was at 4˚C. For long-term storage, dehydrated mycelia grown on cellophane membranes were air-dried in a laminar flow overnight and stored at –20°C in 50 ml Falcon™ tubes (Corning, New York, USA).

2.2.3 Mating of J222 and NZ203.1

In vitro mating of *V. inaequalis* isolates J222 (race (1)) and NZ203.1 (race (1,4)) was performed by Dr Vincent Bus as per Bus et al. (2005a). Mature leaves of apple cultivar 'Royal Gala' were washed under running tap water to remove any debris and cut into 2 x 2 cm squares away from the midrib of the leaf. Leaf pieces were autoclaved and then placed in Petri dishes containing 2% (w/v) WA. A plug of mycelium from each isolate was taken from 3-week-old PDA cultures and mixed on the leaf pieces with a scalpel. Plates were sealed with two layers of Parafilm® M and placed in a sealed plastic bag. Cultures were incubated at RT under natural (night/day) conditions for 2 weeks. Then, plates were inverted and maintained in the dark at 8˚C for 4 months. Following this period, cultures were checked for the production of pseudothecia by eye. Once pseudothecia produced asci with mature ascospores (ascertained using bright field microscopy), individual ascospores were isolated then cultured on PDA as per section 2.2.2.3.

2.2.4 *V. inaequalis* infection assays

2.2.4.1 Identification of apple seedlings carrying the *Rvi4 R* gene

Apple seeds derived from a cross between the susceptible cultivar 'Royal Gala' (which carries no *Rvi R* genes) and the accession TSR33T239 (which carries the *Rvi4 R* gene), were assessed by Dr Joanna Bowen at the New Zealand Institute for Plant and

Food Research, Auckland, for whether they possessed the *Rvi4 R* gene, so that they could be used in an HR-screening assay with *V. inaequalis* (see section 2.2.4.2). For this purpose, progeny of the above-mentioned cross were germinated and the first three fully expanded leaves harvested according to sections 2.2.2.1 and 2.2.2.2, respectively. Next, conidia spores of *V. inaequalis* isolate MNH120 (which possesses a functional copy of the *AvrRvi4* gene) were prepared as per section 2.2.2.3 and adjusted to a final concentration of 10^5 conidia ml^{-1} with sterile water using a hemocytometer. From this spore suspension, 5 µL droplets were placed on the adaxial leaf surface, making sure that the droplets did not merge, and at 4 days post-inoculation (dpi), the presence or absence of an HR (i.e. following the recognition of the AvrRvi4 Avr effector of *V. inaequalis* by the Rvi4 R protein of apple) was first assessed by eye and then under a binocular microscope (bright field microscopy) to identify seedlings that carried the *Rvi4 R* gene. Those seedlings that produced an HR were taken though to subsequent *V. inaequalis* infection assays involving progeny of a cross between isolates J222 and NZ203.1 in section 2.2.3.

2.2.4.2 Phenotyping of *V. inaequalis* progeny

To determine which progeny of *V. inaequalis*, derived from a cross between isolates J222 and NZ203.1 (Table 2.1 and section 2.2.3), carry a functional copy of the *AvrRvi4 Avr* effector gene, each was screened, along with the two parental isolates, for their ability to trigger an HR on apple seedlings containing the corresponding *Rvi4 R* gene from section 2.2.4.1. For this purpose, detached leaves from apple seedlings carrying the *Rvi4 R* gene were prepared and inoculated with the parental isolates and progeny according to sections 2.2.2.2 and 2.2.4.1, respectively. More specifically, each leaf was inoculated with both parental isolates and two progeny (i.e., a quarter of the leaf each for each isolate) (Fig. 2.1). At 4 dpi, leaves were harvested and stained according to Bruzzese and Hasan (1983) and observed under a compound microscope (bright field microscopy) to visualize the HR or subcuticular infection structures (subcuticular runner hyphae and stromata) (see section 2.2.4.3).

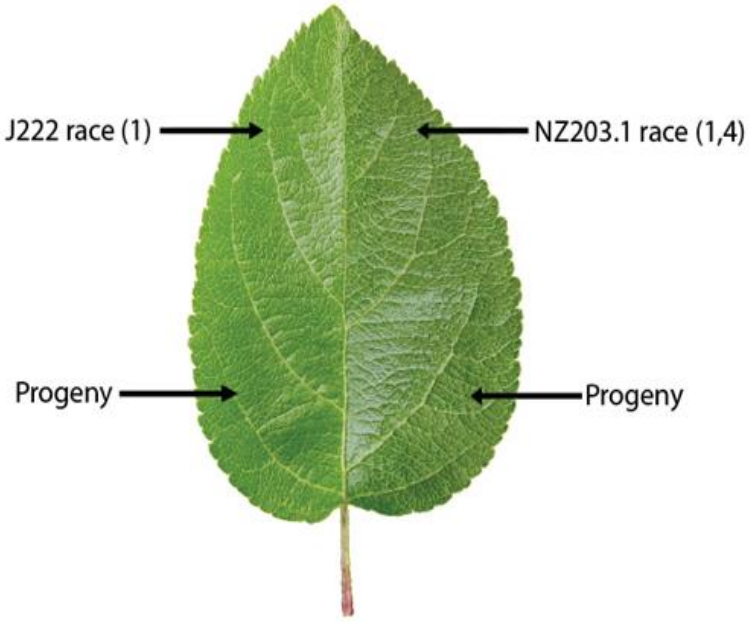

Figure 2.1. Arrangement of *Venturia inaequalis* isolates in the phenotyping experiment on detached leaves of apple from a cross between cultivar 'Royal Gala' and accession TSR33T239 carrying the *Rvi4* resistance gene. The *V. inaequalis* race (1) isolate J222 was used as a positive control for the hypersensitive response (HR), as it contains a functional copy of the *AvrRvi4* gene (i.e. an HR should be triggered). The *V. inaequalis* race (1,4) isolate NZ203.1 was used as a negative control, as it lacks a functional copy of the *AvrRvi4* gene (i.e. no HR should be triggered. Instead, sporulation or the production of subcuticular infection structures should be observed). Two different progeny isolates were tested per detached leaf (an HR would only be triggered if they contained a functional copy of the *AvrRvi4* gene inherited from isolate J222).

2.2.4.3 Microscopy

Whole apple leaves were immersed in approximately 30 ml of clearing-staining solution (30% v/v ethanol, 15% v/v chloroform, 12.5% v/v [90% lactic acid], 15% w/v phenol, 45% w/v chloral hydrate, 0.06% w/v aniline blue) for 48 h at RT, de-stained in a concentrated chloral hydrate solution (2.5 g/ml of water) for 12–24 h, rinsed in distilled water, and then observed by bright field microscopy under a compound microscope (Leica DM 1000 LED, Leica Microsystems CMS GmbH). Images were captured with a digital camera Leica DFC 295 and visualized using the Leica software Leica Application Suite X (LAS X).

2.2.5 DNA manipulation

2.2.5.1 Genomic DNA extraction

V. inaequalis progeny, derived from a cross between isolates J222 and NZ203.1, were grown on cellophane membranes for 10 days as per section 2.2.2.3 in preparation for genomic DNA extraction. For each of the progeny, genomic DNA was then extracted from fungal biomass present on two cellophane membranes according to the method described by Schwessinger and McDonald (2017). For the parental isolates J222 and NZ203.1, fungal biomass was instead harvested from 4- to 5-week-old PDB liquid cultures, grown according to section 2.2.2.3. For genomic DNA extraction, samples were first freeze-dried, then ground to a powder in liquid nitrogen for 2 min, transferred to 14 ml of lysis buffer ((0.35 M sorbitol, 0.1 M Tris-HCl, 5 mM EDTA pH 8.0), (50 mM EDTA, 2 M NaCl, 2% [w/v] CTAB, pH 8.0), 5% [w/v] Sarkosyl N-lauroylsarcosine sodium salt, 10% w/v] PVP40, 10% [w/v] PVP10 and 10 U of RNAse A (Thermo Fisher)) in a 50 ml Falcon™ tube, vortexed and incubated for 30 min at RT with mixing by inversion every 5 min. Following incubation, 200 µl (800 U/ml) of Proteinase K (New England Biolabs, Massachusetts, USA) were added to the mix and incubated for 30 min, with mixing by inversion every 5 min. The samples were then cooled on ice for 5 min. Finally, 2.8 ml of potassium acetate (5 M) were added and mixed by inversion, with the samples then incubated for 5 min on ice, and the fungal debris collected by centrifugation at 5,000 *g* for 12 min at 4°C. Following centrifugation, the supernatant was transferred to a fresh 50 ml Falcon™ tube containing 17 ml of phenol:chlorophorm:isoamyl alcohol (P:C:I) in a ratio of 25:24:1 (v/v), mixed by inversion for 2 min and centrifuged at 4°C and 4,000 *g* for 10 min. The supernatant was then transferred to a fresh Falcon™ tube, and the P:C:I step repeated an additional two times. To precipitate the genomic DNA, the supernatant was subsequently mixed with a 0.1 volume of sodium acetate (3 M, pH 5.2) and 1 volume of isopropanol, incubated for 5 min at RT, and then centrifuged at 4°C and 8,000 *g* for 30 min. After pouring off the supernatant, the pellet was washed with 5 ml of 70% ethanol and centrifuged at 5,000 *g* for 5 min. The pellet was transferred to a 1.6 ml microcentrifuge tube (Eppendorf), washed with 1.5 ml of 70% ethanol and centrifuged at 13,000 *g* for 5 min. The pellet was then air-dried for 3 min and dissolved in 10 mM Tris, pH 8.5. Finally, to remove other contaminants that might be present in the extracted genomic DNA that may interfere with quantification, quality assessments, or

sequencing (e.g. polysaccharides), each sample was further purified using an E.Z.N.A. ®HP Plant DNA Mini Kit (Omega Bio-tek, Georgia, USA) according to the manufacturer's instructions. Purified genomic DNA samples were resolved by 1% (w/v) agarose gel electrophoresis to confirm absence of degradation and/or RNA contamination, and both quantity (ng/µl) and quality (absorbance [A] 260 280 nm ratio [A260/280]) data collected by Nanodrop (Thermo Fisher Scientific).

2.2.5.2 Agarose gel electrophoresis

Genomic DNA was mixed with 0.25 volumes of SDS loading dye (0.2% [w/v] Bromophenol Blue (Avantor Sciences Inc., Pennsylvania, USA), 20% [w/v] sucrose, 1% [w/v] SDS and 5 mM EDTA, pH 6.8) and resolved on a 1% (w/v) agarose (HyAgaroseTM, HydraGene) gel in 1x Tris/acetic acid/EDTA (TAE) buffer, pH 8.3 (190 mM Tris, 342 mM acetic acid [Emsure®, Merck, New Jersey, USA], 2.5 mM EDTA) at 80 V for 50 min. Lambda DNA/*Hind*III ladder (Invitrogen, Massachusetts, USA) was used as a size marker. DNA was stained with ethidium bromide (1 µg/ml) for 15 min. DNA was visualized with the Molecular Imager® Gel Doc™ XR system and the Image LabTM Software (Bio-Rad, California, USA).

2.2.6 Genome sequencing

In preparation for genome sequencing, genomic DNA samples from section 2.2.5.1 were first supplied to the Massey Genome Service (MGS) facility (Palmerston North, New Zealand) with an A260/280 ratio of 1.8–2.0, and no obvious DNA degradation or RNA contamination (see section 2.2.5.2). The quality and quantity of the genomic DNA samples from section 2.2.5.1 were then validated by the MGS facility using a Qubit assay (Thermo Fisher Scientific), with samples required to have a genomic DNA quality score (GQS) of at least 3.0 (out of 5.0). Following these quality assurance steps, genomic DNA samples were shipped to Novogene (Beijing, China), who then carried out library preparation and Illumina Novaseq™ paired-end 150 bp (PE150) sequencing on the NovaseqTM platform, with the aim of providing 100x coverage (6 Gb of raw data) for the parental isolates J222 and NZ203.1, and 50x coverage (3 Gb of raw data) for the 50 J222 x NZ203.1 progeny isolates (MGS project number MGS00251).

2.2.7 Bioinformatic methods

2.2.7.1 Genome assembly for isolates J222 and NZ203.1 of *V. inaequalis*

Genome assemblies were performed by David Winter (Massey University, Palmerston North) as follows. As a starting point for genome assembly, fastp v.0.20.0 (Chen et al., 2018) was used to remove all low-quality bases from the sequencing reads of *V. inaequalis* parental isolates J222 and NZ203.1 obtained in section 2.2.6. At the same time, this step was also performed on the sequencing reads corresponding to the 50 J222 x NZ203.1 progeny isolates. A *de novo* genome sequence was then assembled for each of the parental isolates using SPAdes v3.11.1 (Bankevich et al., 2012), with each of the final assemblies generated from a set of different kmers (21,33,55,77,99,127). Final genome assemblies were assessed for quality using QUAST v5.0.2 (Gurevich et al., 2013) and searched for potential adapter (Illumina oligonucleotide sequence) contamination at the National Center for Biotechnology Information (NCBI) UniVec database using the Basic Local Alignment Search Tool (BLAST) (ftp://ftp.ncbi.nlm.nih.gov/pub/UniVec/). Genome sequences were visualized using Geneious v. 9.1.8 software (www.geneious.com) (Kearse et al., 2012).

2.2.7.2 Determination of *V. inaequalis* isolate mating type

Mating type determination was performed by Saadiah Arshed (New Zealand Institute for Plant and Food Research, Auckland) as follows. The nucleotide sequences for the *V. inaequalis* mating type genes were retrieved from NCBI (the *MAT1-1* and *MAT1-2* gene sequence IDs in NCBI are MG818328.1 and MG818329.1, respectively). The mating-type of the progeny was determined by identifying the presence or absence of the alpha box at the mating type locus. The alpha box is present in isolates that carry the *MAT1-1* locus and absent in isolates that carry the *MAT1-2* locus (Turgeon & Yoder, 2000). In order to identify the presence or absence of the *MAT1-1* alpha box within the progeny, filtered Illumina sequencing reads were mapped to the unmasked isolate EU-B04 (*MAT1-1*) reference genome (GenBank PRJNA407103; Le Cam et al., 2019). Briefly, sequencing reads were trimmed to their longest contiguous region using BBDuk with reads longer than 50-bp retained for downstream analysis. The trimmed reads were mapped to the unmasked EU-B04 reference genome using the Burrows-Wheeler Aligner (BWA) (version 0.7.17) (Li & Durbin, 2010). Sequence variants in the progeny were

identified relative to the EU-B04 reference genome using the bcftools and vcftools software embedded within the SAMtools package (v. 1.9) (Li & Durbin, 2010). The alignment files were then input into the Intergrative genomics viewer (IGV) software for visualisation of the mapped reads (Robinson et al., 2011). The presence or absence of the alpha box within the progeny sequences were assessed in the location of the alpha box in EU-B04 found at genome co-ordinates QWWT01000001.1:4,765,219-4,766,287.

2.2.7.3 Identification of small secreted proteins (SSPs) from *V. inaequalis* isolate MNH120

Transcriptome sequencing reads from an RNA-Seq infection time course of *V. inaequalis* isolate MNH120 on susceptible apple cultivar 'Royal Gala' at 12- and 24-hours post-inoculation, as well as 2, 3, 5 and 7 dpi, each with four biological replicates, were available during this project (Rocafort et al., in preparation). As isolate MNH120 is known to carry a functional copy of the *AvrRvi4* effector gene (Deng et al., 2017), and because *AvrRvi4* must be expressed during host colonization to trigger an *Rvi4*-dependent HR, it was reasoned that a subset of these reads would correspond to *AvrRvi4*. With this in mind, a *de novo* assembly of *in planta* RNA-Seq reads was generated by Brogan McGreal (The New Zealand Institute for Plant and Food Research, Auckland), to identify candidate *AvrRvi4* effector genes. More specifically, the quality of reads were checked using FastQC/0.11.7 and raw reads were filtered and trimmed with AfterQC v. 0.9.5 (S. Chen et al., 2017). The front 15 bp of the raw reads were trimmed and trimmed reads below 50 bp in length were removed. An RNA-Seq *de novo* assembly was generated using trinityrnaseq v. 2.6.5 (Grabherr et al., 2011). A six-frame translation of all assembled transcripts was produced using transeq from the emboss suite (Madeira et al., 2019).

AvrRvi4 is likely an small secreted protein (SSP), as effectors of plant-pathogenic fungi are typically SSPs of <300 amino acid residues in length, without a transmembrane domain or a glycophosphatidylinositol (GPI) anchor modification site (Mesarich et al., 2014). Thus, the six-frame translation from above was set up as a BLAST-compatible database using Geneious v. 9.1.8 software (Kearse et al., 2012). Using this database, all SSPs that were previously predicted to be encoded by genes present in the genome of *V. inaequalis* isolate MNH120 (Deng et al., 2017) were screened for their presence in the

six-frame translation database using BLASTp. Here, only hits of 100% amino acid sequence identity, spanning at least 90% of the translated sequence present in the database, were taken as evidence of presence. In some cases, the MNH120 genome sequence was used to identify the amino (N) or carboxyl (C) terminus of the putative SSP, which was missing from the six-frame translation database. At the same time, an exhaustive reciprocal BLASTp analysis was performed to identify all homologs of the putative SSPs present in the six-frame translation database that did not have a gene model in the current genome annotation (Deng et al., 2017). This is because many SSPs of *V. inaequalis* are known to form part of expanded families and are poorly predicted by gene annotation software (Deng et al., 2017; Shiller et al., 2015). Here, a BLASTp Expect (E)-value or percentage identity was not applied, but rather similar proteins were retained if they contained a similar or identical cysteine spacing profile. Based on the long-list of putative SSPs identified using these two approaches, only those with a predicted N-terminal signal peptide, plus no putative transmembrane domain of GPI anchor modification site were retained. For this purpose, SignalP v4.0 (Nielsen, 2017), TMHMM v2.0 (Krogh et al., 2001) and Big-PI (Eisenhaber et al., 1999) were used to predict the presence of N-terminal signal peptides, transmembrane domains and GPI anchor modification sites, respectively.

2.2.7.4 Identification of candidate AvrRvi4 SSPs

To identify candidate AvrRvi4 proteins, the SSPs from section 2.2.7.3 were assessed for sequence conservation across the genomes of all non-race (4) *V. inaequalis* isolates present at NCBI, as well as the NZ203.1 race (1,4) isolate from section 2.2.7.1, using tBLASTn in conjunction with Geneious v. 9.1.8 (Kearse et al., 2012). More specifically, the genomes from NCBI used in this analysis were from the phenotyped *V. inaequalis* isolates 104, 1066e, 1639, 1680, 2199, 301 and EU-B04 (Bénaouf & Parisi, 2000; Caffier et al., 2015; Gladieux et al., 2008; Le Cam et al., 2019; Parisi et al., 2004). Based on this analysis, only those SSPs with mutations present exclusively in the NZ203.1 race (1,4) isolate were retained as candidate AvrRvi4 proteins.

2.2.7.5 Genome sequence variant calling and trait association

To provide further evidence that one of the candidates in section 2.2.7.4 corresponds to *AvrRvi4*, or to identify other genes in the genome that may be this gene

(e.g. it could be possible that *AvrRvi4* encodes a protein that does not have a signal peptide, or it encodes a secondary metabolite), the following approach was performed by David Winter (Massey University, Palmerston North). To identify genome sequence variants that are potentially associated with the inability of *V. inaequalis* to trigger an Rvi4-dependent HR, sequencing reads from the parental isolates J222 and NZ203.1, as well as the 50 J222 x NZ203.1 progeny isolates (section 2.2.7.1), were first aligned to the assembled NZ203.1 genome sequence using BWA-MEM v0.7.17 (Li, 2013). Single nucleotide variants (SNVs) were then identified in the NZ203.1 and 50 J222 x NZ203.1 progeny isolates by comparison to the assembled NZ203.1 genome using SAMtools mpileup v1.2 (Li et al., 2009) and BFCtools v1.7-2 (Narasimhan et al., 2016). Low quality SNVs were removed by filtering out SNVs (a) where the called genotype for the NZ203.1 parent did not match the corresponding site in the NZ203.1 genome (as these sites are likely the result of mis-mapped reads in repetitive regions of the genome), (b) SNVs with a minor allele frequency <0.2 (as the expected frequency of a variant allele in this design is 0.5) and (c) sites with a mean mapping quality score <30. In addition to SNVs, potential segregating deletions from the sequencing data were identified by calculating depth-of-coverage for each site in the reference genome using Mosdepth v0.2.2 (Pedersen & Quinlan, 2018) and treating regions of >100 bp containing <2 sequencing depth as indel variants.

To identify genetic variants that co-segregate with phenotype (i.e. the inability of an isolate to trigger an HR on resistant apple seedlings carrying the *Rvi4* resistance gene), the frequency of non-reference alleles (i.e. alleles not shared with the NZ203.1 genome) in isolates that failed to trigger an HR on resistant Rvi4 plants was calculated using vcfR v1.12.0 (Knaus & Grünwald, 2017) and adegenet v.2.1.3 (Jombart & Ahmed, 2011). A Fisher's exact test was then performed using the R programming language (Team, 2013) to determine the significance of any association between SNV genotypes and phenotypes.

2.2.7.6 Gene prediction

A search for genes in the genomic regions derived from the SNV analysis (section 2.2.7.5) was performed using the AUGUSTUS gene prediction web server (Stanke &

Morgenstern, 2005). Here, *Aspergillus oryzae* gene annotation parameters were used for the prediction.

2.2.7.7 Single nucleotide polymorphism (SNP) confirmation in *V. inaequalis* progeny and the NZ203.1 parent

SNP analysis was performed by Mercedes Rocafort (Massey University, Palmerston North) as follows. Sequencing reads from the progeny were aligned to the assembled contig NODE 617 of the parental isolate J222 using BWA-MEM v. 0.7.17 (Li, 2013). Mapped reads (both paired-end reads) were extracted using SAMtools v1.12 (Danecek et al., 2021). The resulting BAM files were loaded into Geneious v. 9.0.5 and all progeny sequences were visualized to investigate the presence of SNPs in the *AvrRvi4* candidate gene *atg6122*.

2.2.7.8 Candidate *AvrRvi4* promoter and insertion sequence analysis

Nucleotide motifs present in the promoter region of the candidate *AvrRvi4* gene were identified 500 bp of nucleotide sequence upstream of the candidate *AvrRvi4* effector gene family from *V. inaequalis* using the Multiple Em for Motif Elicitation (MEME Suite v. 5.4.1, https://meme-suite.org/meme/tools/meme) (Bailey et al., 2015), using the classic motif discovery mode with default settings.

To elucidate the presence of transposable elements in the candidate *AvrRvi4* gene, the ~12.2 kb insertion present in this gene of isolate NZ203.1 was translated in all six frames using the EMBOSS Transeq web tool (Madeira et al., 2019), and analyzed for protein sequence homology using the BLASTp tool in NCBI with a 1e-50 E value cut off.

2.2.8 Allelic variation in the candidate *AvrRvi4* gene

tBLASTn and BLASTn were used to identify the candidate *AvrRvi4* gene and its paralogs in 88 isolates of *V. inaequalis* (Bénaouf & Parisi, 2000; Caffier et al., 2015; Deng et al., 2017; Gladieux et al., 2008; Gladieux et al., 2010b; Le Cam et al., 2019; Lichtner et al., 2020; Papp et al., 2020; Parisi et al., 1993; Passey et al., 2020; Passey et al., 2018; Roberts & Crute, 1994; Shiller et al., 2015), as well as homologs of this gene in other *Venturia* species present in publicly available genome sequences at NCBI and the Joint Genome Institute (JGI) (Bock et al., 2016; Chen et al., 2017; Deng et al., 2017; Jaber et al., 2020; Johnson et al., 2019; Le Cam et al., 2019; Prokchorchik et al., 2019; Winter et

al., 2020; Zhou et al., 2021). Nucleotide and protein sequence alignments were performed using Clustal Ω (Madeira et al., 2019) to identify polymorphisms in the candidate *AvrRvi4* gene and protein, respectively. A neighbour-joining phylogenetic tree based on 1,000 bootstrap replicates was constructed with Geneious v. 9.1.8 software (Kearse et al., 2012) based on the amino acid sequence alignment of the AvrRvi4 effector family and homologs found in other *Venturia* species.

2.2.9 Structural prediction of the candidate AvrRvi4 effector family

Structural predictions were performed using AlphaFold2 and the ColabFold server (Jumper et al., 2021; Mirdita et al., 2021). For this purpose, a multiple sequence alignment using Clustal Ω of all members of the candidate AvrRvi4 protein family from *V. inaequalis* (without the predicted N-terminal signal peptides and stop codons), was used as input. To assess confidence, the predicted local-distance difference test (pLDDT) and global superposition metric template modelling score (TM-score) were used. pLDDT can range from 0 to 100, with pLDDT values of 70 to 90 indicating reasonable confidence and a value of >90 depicting very high confidence. TM-score ranges from 0 to 1, where a value of 0.5 or higher indicates a similar fold between structures, whereas a value of 1 indicates a perfect match between structures. Structural comparisons were performed with the DALI server (Holm, 2020), with significant similarities measured by a Z-score above 2. Structural superimposition, electrostatic potential (surface charge) analysis and visualization were performed using the Alignment and APBS Electrostatics Plugins, respectively, in PyMol v2.5 (https://pymol.org/2/) (The PyMOL Molecular Graphics System, 2015) DeLano (2002).

To predict and/or to confirm intrinsically disordered regions (IDR), protein sequences were analysed with the Predictor of Natural Disordered Regions (PONDR®) server (http://www.pondr.com) (Molecular Kinetics, Inc., Washington State University and the WSU Research Foundation).

2.3 Results

2.3.1 Whole genome sequencing provides two new *V. inaequalis* reference genomes

As a starting point for the identification of *AvrRvi4*, the genomes of *V. inaequalis* parental isolates J222 and NZ203.1, as well as 50 of their progeny were sequenced. The total sizes of the assembled genomes for *V. inaequalis* parental isolates J222 and NZ203.1 were 66.8 and 70 Mb, respectively (Table 2.2). The N50 value was 83 kb for isolate J222 and 21 kb for isolate NZ203.1, while the number of scaffolds was 21,244 for isolate J222 and 3,408 for isolate NZ203.1 (Table 2.3). Both isolates had approximately the same GC content of 43% (Table 2.3). The cumulative genome length as a function of contig number and size is shown in (Fig. 2.2). The genomes of the 50 progeny were sequenced to a sequencing depth of between 22x and 69x coverage, but not assembled.

Table 2.2. Genome assembly statistics for *Venturia inaequalis* parental isolates J222 and NZ203.1

Isolate	Total length	N50	no. of scaffolds	GC content
J222 race (1)	66.8 Mb	83.18 kb	21,244	43.3
NZ203.1 race (1,4)	70.2 Mb	21.75 kb	3,408	43

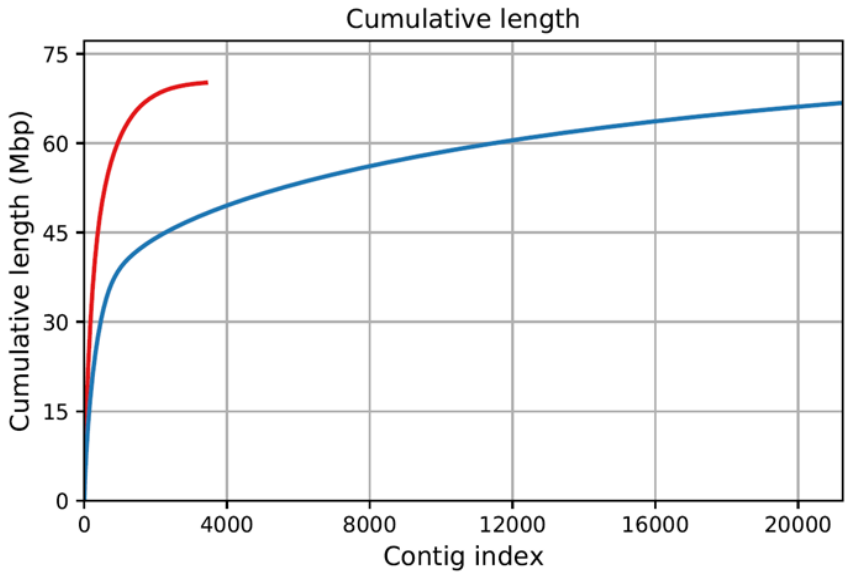

Figure 2.2. Cumulative genome length as a function of contig number and size for the parental isolates J222 (red) and NZ203.1 (blue) of *Venturia inaequalis*.

2.3.2 Mating-type assessment of *V. inaequalis* isolates

To provide confidence that there was no unintentional mix-up or cross-contamination among parental and progeny isolates during culturing, genomic DNA extraction or sequencing, the *V. inaequalis* mating-type locus was assessed across all samples. The parental isolate J222 carries mating-type gene *MAT1-1* at the mating-type locus, whereas the parental isolate NZ203.1 carries mating-type gene *MAT1-2* (Fig. 2.3). The assessment resulted in 20 progeny carrying *MAT1-1* and 30 progeny carrying *MAT1-2* (Table 2.3). Hence, no mixture in any of the isolates based on the presence of both mating-type genes in a single sample was observed.

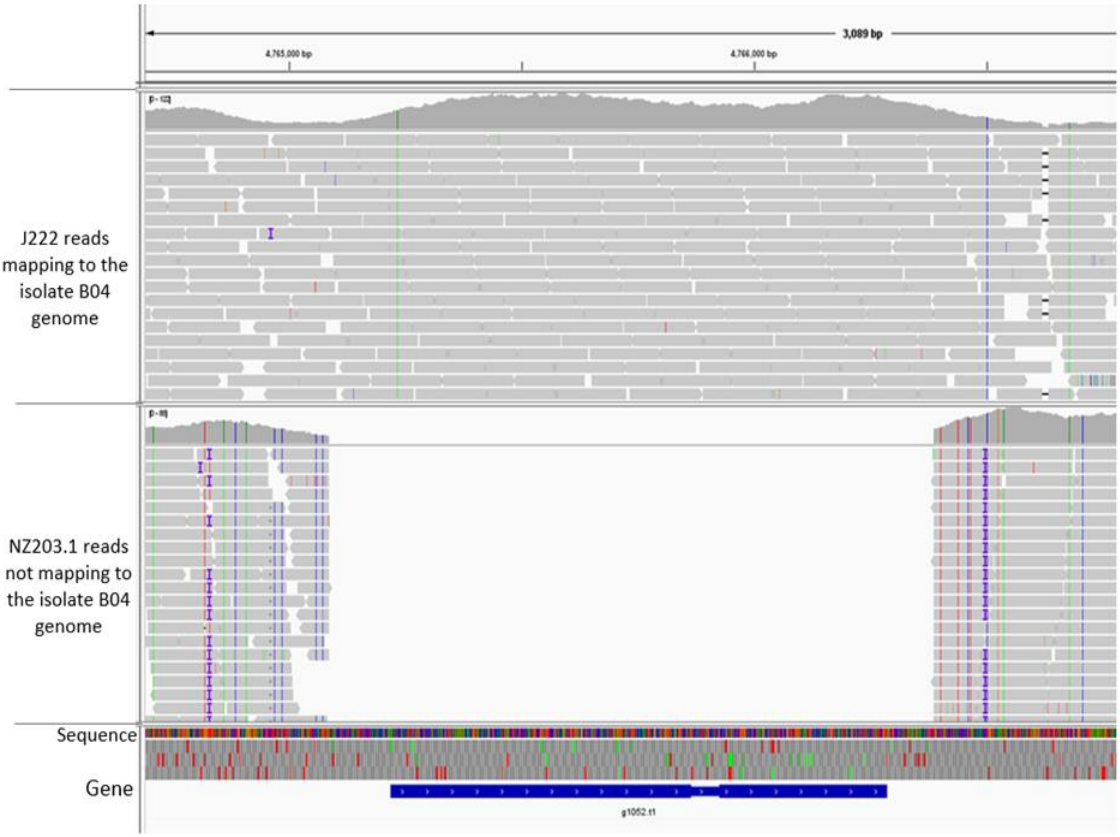

Figure 2.3. Presence and absence of the alpha box associated with mating-type gene *MAT1-1* in *Venturia inaequalis* isolates J222 and NZ203.1. J222 and NZ203.1 sequencing reads were mapped to the isolate EU-B04 genome (Le Cam et al., 2019).

Table 2.3. Mating-type gene present in the parental isolates J222 and NZ203.1 of *Venturia inaequalis,* as well as 50 progeny (S001–S107) from the J222 x NZ203.1 cross. Isolates with *MAT1-1* gene are highlighted in white, while isolates with *MAT1-2* gene are highlighted in grey.

Isolate	Mating-type gene present	Isolate	Mating-type gene present
J222	*MAT1-1*	**S052**	*MAT1-2*
NZ203.1	*MAT1-2*	**S053**	*MAT1-2*
S001	*MAT1-2*	**S056**	*MAT1-2*
S002	*MAT1-1*	**S057**	*MAT1-2*
S004	*MAT1-1*	**S059**	*MAT1-2*
S006	*MAT1-1*	**S061**	*MAT1-2*
S008	*MAT1-1*	**S062**	*MAT1-2*
S009	*MAT1-2*	**S063**	*MAT1-1*
S010	*MAT1-2*	**S064**	*MAT1-2*
S012	*MAT1-2*	**S065**	*MAT1-2*
S013	*MAT1-1*	**S067**	*MAT1-2*
S014	*MAT1-1*	**S068**	*MAT1-1*
S016	*MAT1-2*	**S069**	*MAT1-2*
S019	*MAT1-1*	**S074**	*MAT1-2*
S021	*MAT1-2*	**S079**	*MAT1-2*
S022	*MAT1-1*	**S081**	*MAT1-2*
S025	*MAT1-1*	**S085**	*MAT1-2*
S026	*MAT1-1*	**S087**	*MAT1-2*
S027	*MAT1-1*	**S088**	*MAT1-1*
S032	*MAT1-2*	**S091**	*MAT1-1*
S036	*MAT1-2*	**S092**	*MAT1-2*
S038	*MAT1-1*	**S095**	*MAT1-2*
S040	*MAT1-2*	**S097**	*MAT1-1*
S041	*MAT1-1*	**S099**	*MAT1-1*
S048	*MAT1-1*	**S104**	*MAT1-2*
S049	*MAT1-2*	**S107**	*MAT1-2*

2.3.3 SSP comparisons between isolates of *V. inaequalis* reveal 16 AvrRvi4 effector candidates

Based on the analysis as per Section 2.2.7.3, only 16 AvrRvi4 effector candidates (named candidate 1–16) were identified (Table 2.4). Candidate 1 (NCBI gene ID: *KAE9977539*) is a 1,416 nucleotide (nt) gene with no introns and encodes a protein of 471 amino acids in length, with ten cysteines and a predicted signal peptide of 18 amino acids in *V. inaequalis* isolate MNH120 and other isolates. In isolate NZ203.1, a 30 nt

deletion was observed, leading to a shorter protein of 461 amino acids. In addition to this, 31 nt mutations were identified, leading to 8 amino acid substitutions and one amino acid insertion. Candidate 2 (JGI gene number: *atg11569*) is a 444 nt gene with no introns, and encodes a protein of 148 amino acids with six cysteines and a predicted signal peptide of 21 amino acids. In isolate NZ203.1, T26C and C52T mutations were discovered, leading to V9A and P18S amino acid substitutions, respectively. As these amino acid substitutions occurred in the signal peptide, and are unlikely to affect secretion, this AvrRvi4 candidate was discarded.

Candidate 3 (JGI gene number: atg10296) is 291 nt in length with no introns, and encodes a protein of 97 amino acids with six cysteines and a predicted signal peptide of 18 amino acids. In isolate NZ203.1, 14 mutations were identified, leading to 11 amino acid substitutions, specifically H2Y, L8P, P15S, T16A, F34Y, A42G, Q44H, T56M, D60N, K61R and Q68E. Candidate 4 (no gene ID available) is a gene of 380 nt in length with one intron (50 nt), and encodes a protein of 109 amino acids in length with six cysteines and a predicted signal peptide of 19 amino acids. This gene appears to be deleted in isolate NZ203.1. Candidate 5 (NCBI gene ID: *KAE9973409*) is 352 nt in length with a predicted intron of 52 nt. The gene encodes a protein of 99 amino acids in length, with six cysteine residues and a predicted signal peptide of 18 amino acids. Two mutations were discovered in isolate NZ203.1, leading to two amino acid substitutions: D66E and N74S. Candidate 6 (JGI gene number: *atg12048*) is a gene of 334 nt containing an intron of 52 nt. This gene encodes a protein of 93 amino acids with six cysteines and a predicted signal peptide of 19 amino acids. Four mutations at the nucleotide level were found in isolate NZ203.1, leading to A77T and A87L amino acid substitutions in the protein sequence. Candidate 7 (JGI gene number: *atg7793*) is a gene consisting of 443 nt and two introns of 87 and 92 nt, respectively. It encodes a protein of 87 amino acids with six cysteines and a putative signal peptide of 18 amino acids. The loss of the start codon was identified in NZ203.1, that subsequently would lead to no protein production.

Candidate 8 (JGI gene number: *atg3658*) is encoded by a gene of 377 nt with two introns of 57 and 62 nt, respectively. The encoded protein is 85 amino acids in length with six cysteines and a predicted signal peptide of 18 amino acids. Only one mutation at position 185 was identified, leading to a T43I amino acid substitution. Candidate 9 (JGI gene number: *atg12027*) is encoded by a 354 nt gene with two introns of 74 and 63

nt, respectively. The encoded protein consists of 83 amino acids, eight cysteines and a predicted signal peptide of 19 amino acids. A nucleotide insertion (T) at position 37 of the coding sequence (cds) produced a frameshift mutation, leading to a premature stop codon in isolate NZ203.1. Candidate 10 (JGI gene number: *atg8503*) is 387 nt, with two introns of 75 and 63 nt, respectively. This gene encodes a protein of 82 amino acids in length with eight cysteines and a putative signal peptide of 19 amino acids. The gene sequence in isolate NZ203.1 contains an 18 nt insertion in the first intron, and 20 mutations in the cds affecting the protein sequence. These mutations lead to multiple amino acid substitutions, specifically S7P, A8V, F9I, T34L, G35R, D46N, T47I, C53Y, H55N, G57R, D72N, G73R, K74Y and V75L.

The eleventh candidate (no gene ID available) is encoded by a 240 nt gene with no introns. The gene encodes a protein of 80 amino acids with eight cysteines and a predicted signal peptide of 16 amino acids. The gene sequence in isolate NZ203.1 contains a mutation in start codon (ATG to ATA), resulting in a (M1I) amino acid substitution, compromising the production of the protein. Candidate 12 (NCBI gene ID: *KAE9966577*) consists of a gene containing 617 nt and two introns of 153 and 56 nt, respectively. The encoded protein is 135 amino acids in length with eight cysteines and a predicted signal peptide of 18 amino acids. One nucleotide mutation was found in the cds, leading to a H62R amino acid substitution in isolate NZ203.1. Candidate 13 (JGI gene number: *atg6122*) is 769 nt with one intron of 49 nt. The encoded protein possesses 240 amino acids, a predicted signal peptide of 25 amino acids and six cysteines. The three mutations identified in the cds led to two amino acid substitutions in isolate NZ203.1, specifically a F78S and an A101V. In addition, a 12, 216 bp insertion was found to disrupt the gene in the same isolate.

Candidate 14 (NCBI gene ID: *KAE9981873*) is 369 nt, with only one intron of 66 nt. The encoded protein is 100 amino acids in length with a predicted signal peptide of 20 amino acids and contains no cysteine residues. Six mutations in the cds unique to NZ203.1 led to one amino acid substitution (I18V) in the signal peptide, and five more (T22A, I30T, Y58F, T81A and S87I) in the mature protein. Candidate 15 (JGI gene number: *atg6605*) is encoded by a 351 nt gene without introns. The encoded protein is 116 amino acids in length, with no cysteines and a predicted signal peptide of 21 amino acids. In isolate NZ203.1, seven unique mutations were observed, but only five of them altered

the protein sequence. More specifically, the observed amino acid substitutions were S36P, F43S, N73S, K75N and T90R. The last candidate, candidate 16 (no gene ID available), is 391 nt in length, with one intron of 46 nt. The encoded protein consists of 114 amino acids with three cysteines in the mature protein. The predicted signal peptide cleavage site is at amino acid residue 25. A cytosine insertion at position 211 of the cds caused a frameshift mutation that led to a premature stop codon in isolate NZ203.1. All corresponding sequences of the AvrRvi4 candidates appear in Figure A.5

Table 2.4. AvrRvi4 avirulence effector candidates identified through a small secreted protein (SSP) sequence comparison across isolates of *Venturia inaequalis*.

Candidate number	NCBI ID/JGI number[a]	gene size (nt) [b]	protein length (aa) [c]	No. of cysteines[d]	differences observed
1	*KAE9977539*	1519	470	10	Non-synonymous substitutions, deletions and one insertion
2	*atg11569*	444	147	6	Non-synonymous substitutions
3	*atg10296*	291	96	6	Non-synonymous substitutions
4	No ID	381	109	6	deleted
5	*KAE9973409*	300	99	6	Non-synonymous substitutions
6	*atg12048*	334	93	6	Non-synonymous substitutions
7	*atg7739*	443	87	6	Loss of start codon
8	*atg3658*	377	85	6	Non-synonymous substitutions
9	*atg12027*	354	83	8	Non-synonymous substitutions
10	*atg8503*	387	82	8	Non-synonymous substitutions
11	No ID	240	79	8	loss of start codon
12	*KAE9966577*	617	135	8	Non-synonymous substitutions
13	*atg6122*	769	240	6	Non-synonymous substitutions/Insertion
14	*KAE9981873*	369	100	0	Non-synonymous substitutions
15	*atg6605*	351	116	0	Non-synonymous substitutions
16	No ID	391	114	4	Premature stop codon

[a]NCBI, National Centre for Biotechnology Information; JGI, Joint Genome Institute. [b]nt, nucleotides. [c]aa, amino acids. [d]number of cysteine residues in the predicted mature protein (i.e. after the predicted signal peptide cleavage site). *V. inaequalis* isolates used in the comparison correspond to EU-B04, 104, 1066e, 1639, 2199, 301, MNH120, J222 and NZ203.1.

2.3.4 Phenotyping of *V. inaequalis* progeny

Forty-four out of 50 progeny, derived from a cross between *V. inaequalis* isolates J222 race (1) and NZ203.1 race (1,4), were inoculated onto resistant apple seedlings carrying the *Rvi4 R* gene to determine which of these progeny carry a functional copy of the corresponding *AvrRvi4* effector gene (six of the 50 progeny isolates could not be phenotyped due to a lack of sporulation). Here, inoculation sites were assessed at 4 dpi for the presence of a localized cell death response (i.e. an HR), indicative of *AvrRvi4* presence and disease resistance (incompatibility), or the formation of subcuticular runner hyphae and/or stromata, indicative of *AvrRvi4* absence and disease susceptibility (compatibility). For this purpose, leaves were first assessed macroscopically, and if no conclusion could be drawn, were then assessed by bright field microscopy under a compound microscope. As expected, the J222 parental isolate triggered a macroscopically or microscopically visible HR at the inoculation site of apple seedlings carrying the *Rvi4* gene, confirming that this isolate does indeed carry a functional, expressed copy of the *AvrRvi4* gene (Figs. 2.4 and 2.5A, and Table 2.5). In the case of the microscopic observations, this HR was characterized by yellow-brown, granular, disorganized, or collapsed epidermal cells (Fig. 2.5A). Also as expected, the NZ203.1 parental isolate was unable to trigger a macroscopically or microscopically visible HR at the inoculation site of apple seedlings carrying the *Rvi4* gene, but instead showed abundant growth on the leaf surface (Fig. 2.4 and Table 2.5), as well as both runner hyphae and stromata under the apple cuticle (Fig. 2.5E and Table 2.5), confirming that this isolate does indeed lack a functional, expressed copy of the *AvrRvi4* gene (*avrRvi4*). To check similar or dissimilar phenotypes, all progeny were inoculated onto susceptible 'Royal Gala' leaves, as a control.

Of the 44 progeny isolates tested, 12 triggered a strong and visible HR in seedlings carrying the *Rvi4* gene (example shown in Fig. 2.4), while a further seven triggered an HR that was only visible under the compound microscope (examples shown in Fig. 2.5B–D). An additional two progeny isolates were found to possibly trigger an HR. However, as these results were not clear, they were instead classified as ambiguous (Table 2.5). Thus, out of the 44 progeny isolates tested, 19 were deemed to potentially carry the *AvrRvi4* gene (Table 2.5). Like that observed for the NZ203.1 parental isolate, 15 of the progeny isolates displayed abundant, macroscopically visible growth at inoculation sites

on the surface of leaves from apple seedlings carrying the *Rvi4* gene (example shown in Fig. 2.4), with infection by these 15 isolates confirmed microscopically (examples shown in Fig. 2.5E-H). One additional isolate (S092) with low surface growth, showed the presence of stromata under the compound microscope (Table 2.5), suggesting that it lacks a functional copy of the *AvrRvi4* gene (*avrRvi4*). A further six progeny isolates with limited stromata production were classified as ambiguous, since it was not clear whether these isolates had started to form stromata before infection was halted (i.e. upon recognition of AvrRvi4 by Rvi4) (Table 2.5). Thus, out of the 44 progeny isolates tested, 16 were deemed to potentially lack a functional copy of the *AvrRvi4* gene (*avrRvi4*) (Table 2.5). It should be noted that one of the progeny isolates (S104) could not be classified as virulent (*avrRvi4*) or avirulent (*AvrRvi4*), as neither a macroscopically or microscopically visible HR was produced, nor was there any subcuticular runner hyphae or stromata formed (Table 2.5). A summary of observations for the 44 progeny phenotyped in this experiment are detailed in Table 2.5. Microscopy photos of other progeny not shown in Figure 2.5 appear in Figure A.6.

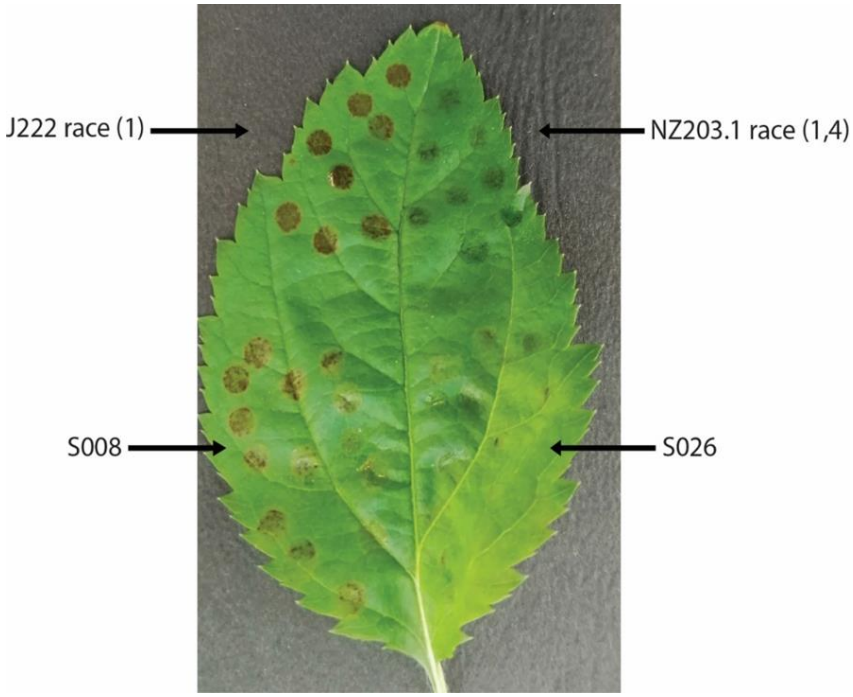

Figure 2.4. Macroscopic observations of *Venturia inaequalis* isolates inoculated on *Rvi4* apple leaves. Hypersensitive response (HR) triggered by parental isolate J222 (race (1)) and progeny isolate S008, which carry a functional copy of the *AvrRvi4* gene. Sporulation on leaves inoculated with parental isolate NZ203.1 (race (1,4)) and progeny isolate S026, which lack a functional copy of the *AvrRvi4* gene. Progeny isolates S008 and S026 are derived from a cross between parental isolates J222 and NZ203.1. Photograph taken at 4 days post-inoculation.

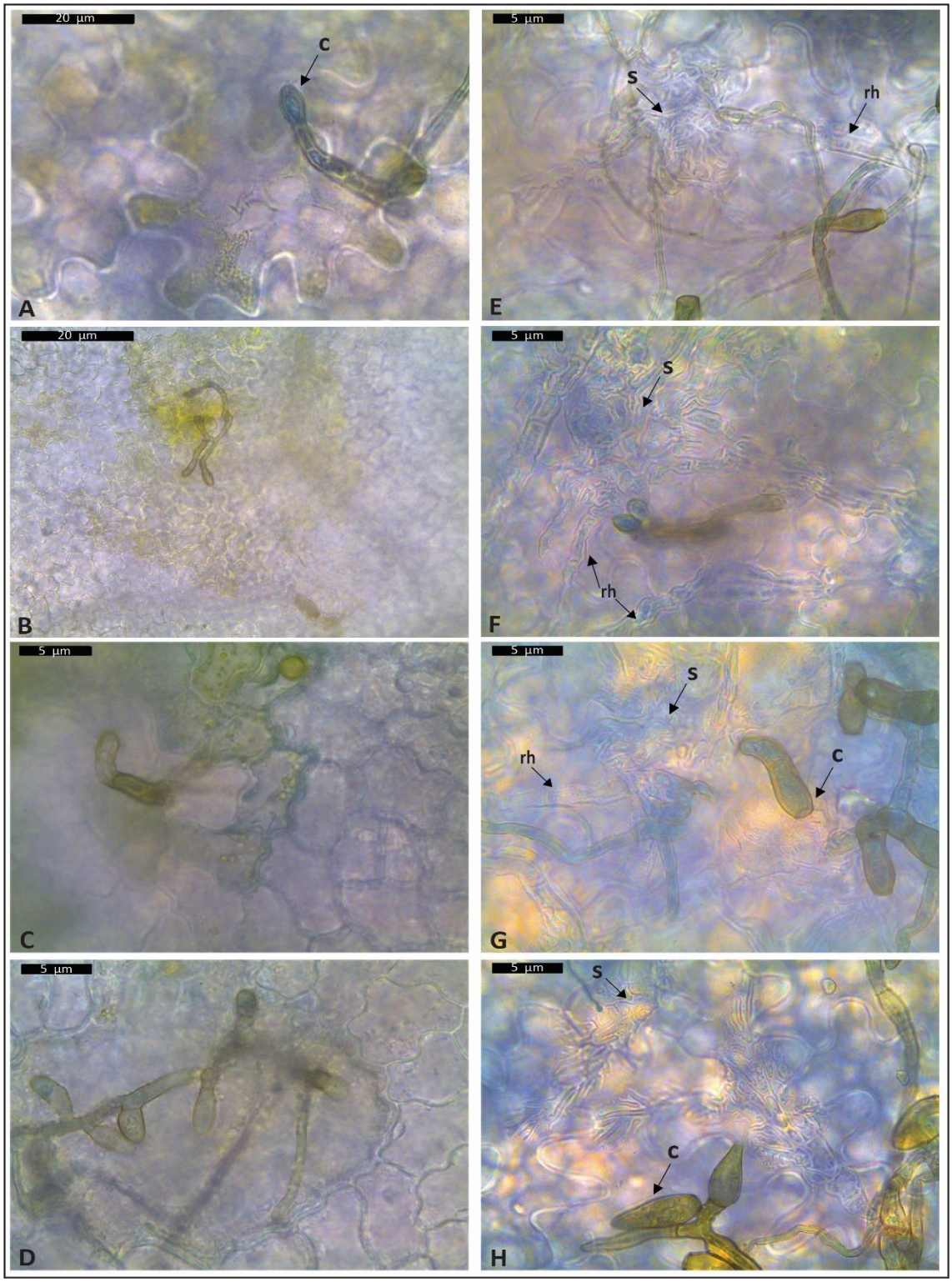

Figure 2.5. Microscopic observations of *Venturia inaequalis* isolates inoculated on *Rvi4* apple leaves. (A) Hypersensitive response (HR) triggered by parental isolate J222 (race (1)), which carries a functional copy of the *AvrRvi4* gene. **(B, C, D)** HR triggered by progeny isolates S021, S069 and S099, which carry a functional copy of the *AvrRvi4* gene. **(E)** Subcuticular stroma and runner hyphae formed by parental isolate NZ203.1 (race (1,4)), which lacks a functional copy of the *AvrRvi4* gene. **(F, G, H)** Subcuticular stromata (s) and runner hyphae (rh) formed by progeny isolates S053, S067 and S006, which lack a functional copy of the *AvrRvi4* gene. Arrows indicate infection structures. (c) conidium. All progeny isolates are derived from a cross between parental isolates J222 and NZ203.1. Samples observed correspond to leaves at 4 days post-inoculation.

Table 2.5. Prediction of which progeny (S001–S107) from a cross between parental isolates J222 and NZ203.1 of *Venturia inaequalis* contain a functional copy of the *AvrRvi4* effector gene. HR; hypersensitive response.

Isolates predicted to possess a functional AvrRvi4 gene	Observation	Isolates predicted to lack a functional AvrRvi4 gene	Observation	Ambiguous	Observation
J222	Macroscopically visible hypersensitive response (HR)	NZ203.1	Macroscopically abundant surface growth and microscopically visible stromata	S016	Possible HR visible by bright field microscopy
S001	Macroscopically visible HR	S002	Macroscopically abundant surface growth and microscopically visible stromata	S026	Limited stromata visible by bright field microscopy
S004	Macroscopically visible HR	S006	Macroscopically abundant surface growth and microscopically visible stromata	S041	Limited stromata visible by bright field microscopy
S008	Macroscopically visible HR	S009	Macroscopically abundant surface growth and microscopically visible stromata	S048	Limited stromata visible by bright field microscopy
S012	HR visible by bright field microscopy	S010	Macroscopically abundant surface growth and microscopically visible stromata	S052	Visible surface growth
S013	HR visible by bright field microscopy	S019	Macroscopically abundant surface growth and microscopically visible stromata	S061	Possible HR visible by bright field microscopy
S021	Macroscopically visible HR	S022	Macroscopically abundant surface growth and microscopically visible stromata	S062	Limited stromata visible by bright field microscopy
S025	HR visible by bright field microscopy	S053	Macroscopically abundant surface growth and microscopically visible stromata	S088	Limited stromata visible by bright field microscopy
S027	Macroscopically visible HR	S057	Macroscopically abundant surface growth and microscopically visible stromata	S104	No evidence of cell death or stromata by bright field microscopy
S032	Macroscopically visible HR	S059	Macroscopically abundant surface growth and microscopically visible stromata		

Isolates predicted to possess a functional AvrRvi4 gene	Observation	Isolates predicted to lack a functional AvrRvi4 gene	Observation	Ambiguous	Observation
S036	Macroscopically visible HR	S063	Macroscopically abundant surface growth and microscopically visible stromata		
S038	HR visible by bright field microscopy	S067	Macroscopically abundant surface growth and microscopically visible stromata		
S049	HR visible by bright field microscopy	S079	Macroscopically abundant surface growth and microscopically visible stromata		
S056	Macroscopically visible HR	S081	Macroscopically abundant surface growth and microscopically visible stromata		
S065	HR visible by bright field microscopy	S087	Macroscopically abundant surface growth and microscopically visible stromata		
S069	Macroscopically visible HR	S091	Macroscopically abundant surface growth and microscopically visible stromata		
S074	Macroscopically visible HR	S092	Stromata visible by bright field microscopy		
S085	Macroscopically visible HR				
S097	HR visible by bright field microscopy				
S099	Macroscopically visible HR				

Progeny isolates S014, S040, S064, S068, S095 and S107 could not be phenotyped due to a lack of sporulation.

2.3.5 Four regions of the *V. inaequalis* NZ203.1 race (1,4) genome contain single nucleotide variants (SNVs) that co-segregate with an inability of the fungus to trigger an HR on *Rvi4* apple

To identify mutations in the genomes of *V. inaequalis* isolate NZ203.1 race (1,4) and its progeny that co-segregate with an inability of the fungus to trigger an HR on *Rvi4* apple, an SNV analysis was performed. For this purpose, all reads from the parental isolates J222 and NZ203.1, as well as the 50 J222 x NZ203.1 progeny isolates were aligned to the assembled NZ203.1 genome sequence, and SNVs genotypes not present in the assembled J222 genome identified. This was made possible by the fact that all available genomes corresponding to the parental and progeny isolates were sequenced to high depth. SNV calling on these data produced a total of 744,271 putative SNVs across the entire NZ203.1 genome. SNVs co-segregating with an inability of progeny isolates to trigger an HR on Rvi4 apple were then analysed at a genome-wide scale. A Fisher's exact test was performed using the R programming language to determine the significance of any association between SNV genotypes and phenotypes. From this analysis, 656 positions across four scaffolds of the NZ203.1 genome containing SNVs with an adjusted p-value of <0.01 (i.e. having the best association between SNVs and a loss of the HR phenotype) were identified (summarised in Table 2.6). Data for all 656 positions are shown in Table A.3.

Table 2.6. Summary of regions in the *Venturia inaequalis* NZ203.1 race (1,4) genome that have the best correlation between single nucleotide variants (SNVs) and an inability of progeny from a cross between isolates J222 and NZ203.1 to trigger a hypersensitive response (HR) on Rvi4 apple.

number of J222 race (1) alleles in stromata-forming progeny of a J222 x NZ203.1 cross (range)	number of J222 race (1) alleles in HR-eliciting progeny of a J222 x NZ203.1 cross (range)	number of J222 race (1) alleles in progeny of a J222 x NZ203.1 cross for which a phenotype could not be concluded (ambiguous)	NZ203.1 genome scaffold	Number of positions identified	SNV positions (first to last)	p-value (range)	adjusted p-value (range)
0–1	19	7–11	NODE_510_length_33946_cov_13.0851	86	659–32,671	1.08E-10–5.39E-10	0.000401–0.00802
0–1	18–19	8–11	NODE_84_length_156639_cov_13.546	453	229–86, 645	5.39E-10–1.08E-08	0.000401–0.00802
0–1	18–19	9–10	NODE_31_length_236765_cov_12.7941	104	214,554–236,630	8.62E-09–1.08E-08	0.006416–0.00802
1	19	9–10	NODE_175_length_104725_cov_13.1158	13	92,705–103,286	1.08E-08	0.00802

2.3.6 A single candidate *AvrRvi4* gene is present in the NZ203.1 race (1,4) isolate genome

To determine whether the four genome regions of the NZ203.1 race (1,4) isolate identified in section 2.3.5 contained a mutated *AvrRvi4* gene candidate, an extensive search for genes in the four genomic regions was performed using the AUGUSTUS gene prediction web server (Stanke & Morgenstern, 2005). Based on this analysis, only five genes were predicted to encode an SSP of less than 300 amino acids. One is located on NODE_175_length_104725_cov_13.1158, the second located on NODE_31_length_236765_cov_12.7941, three more located on NODE_84_length_156639_cov_13.546 and a further one located on NODE_510_length_33946_cov_13.0851 of NZ203.1.

Of these, only one had mutations (located on NZ203.1 genome scaffold NODE_510_length_33946_cov_13.0851) that were exclusive to the NZ203.1 race (1,4) isolate, when compared to the corresponding sequence in the race (1) isolates MNH120 and J222. This gene corresponds to gene *atg6122* in the isolate MNH120 reference genome (Deng et al., 2017). The mutations exclusively identified in the *atg6122* gene of the NZ203.1 race (1,4) isolate, when compared to the corresponding gene in the J222 race (1) isolate, were a TT to AG dinucleotide change at positions 232–233, a G to A change at position 304, and a 12,216 bp insertion following position 280 (Fig. 2.6). Importantly, each of these mutations was identified as a significant co-segregating mutation in the SNV analysis (locations 1,103, 1,104 and 13,391 in exon 1, and 2,056–13,391 in the inserted sequence).

To confirm that the mutations co-segregate with a loss in the ability to trigger *Rvi4*-mediated resistance, the TT to AG dinucleotide change at positions 232–233, and the G to A change at position 304 were tracked across the genomes of the phenotyped progeny. In support of *atg6122* being *AvrRvi4*, all 19 progeny that triggered an HR on *Rvi4* apple had the allele from the J222 race (1) isolate, while all but one progeny (15 of 16; progeny isolate S063) that failed to trigger an HR on *Rvi4* apple had the allele from the NZ203.1 race (1,4) isolate (Table 2.7). Contrary to the macroscopic and microscopic observations where abundant surface growth and visible stromata were present, progeny isolate S063, had the allele of the J222 race (1) isolate (Table 2.7). Strikingly, the

atg6122 gene was also one of the 16 original *AvrRvi4* candidates (candidate 13) derived from the MNH120 SSP sequence comparison in section 2.3.3 (Table 2.4), providing further support that *atg6122* is indeed *AvrRvi4*. Regarding the progeny isolates that gave an ambiguous phenotype on *Rvi4* apple, six had the allele from the J222 race (1) and two had the allele from the NZ203.1 (Table 2.7).

A closer inspection of the *atg6122* gene in the NZ203.1 race (1,4) isolate revealed that disruption by the 12,216 bp sequence is the only mutation in this gene that could be responsible for circumvention of *Rvi4*-mediated resistance, since the TT to AG dinucleotide change at positions 232–233 is also present in the non-race (4) isolate 104 while the G to A change at position 304 is also present in the non-race (4) isolate MNH120 (Fig. 2.6). To determine whether the 12,216 bp insertion is a repetitive element, it was searched against the MNH120 genome using BLASTn in the local Geneious database. This analysis revealed that there are at least 7 copies (E value range from 3.34 e-160 to 4.99 e-5) of the insertion sequence in the MNH120 genome, confirming that it is a repetitive element. Moreover, a BLASTp analysis of the 6-frame translation of the ~12.2 kb insertion element uncovered hits to DNA helicases and helicase-like proteins, indicating that the repetitive element is likely a transposable element.

The complete sequence of the candidate *AvrRvi4* gene, including 500 bp of the upstream and downstream sequence containing the promoter and terminator regions, and the predicted protein sequence is shown in Fig. 2.7. The *AvrRvi4* candidate gene has two exons of 529 and 191 bp respectively, and one intron of 49 bp. The gene encodes an SSP of 240 amino acids in length with six cysteines, and a predicted N-terminal signal peptide of 25 amino acids (Fig. 2.7). Following the signal peptide, the AvrRvi4 candidate has a putative pro-domain of 17 amino acids, ending with a possible Kex2 protease cleavage motif (LXPR) (Fig. 2.7). Moreover, it is predicted to contain a C-terminal intrinsically disordered region (Figs. 2.9 and 2.10).

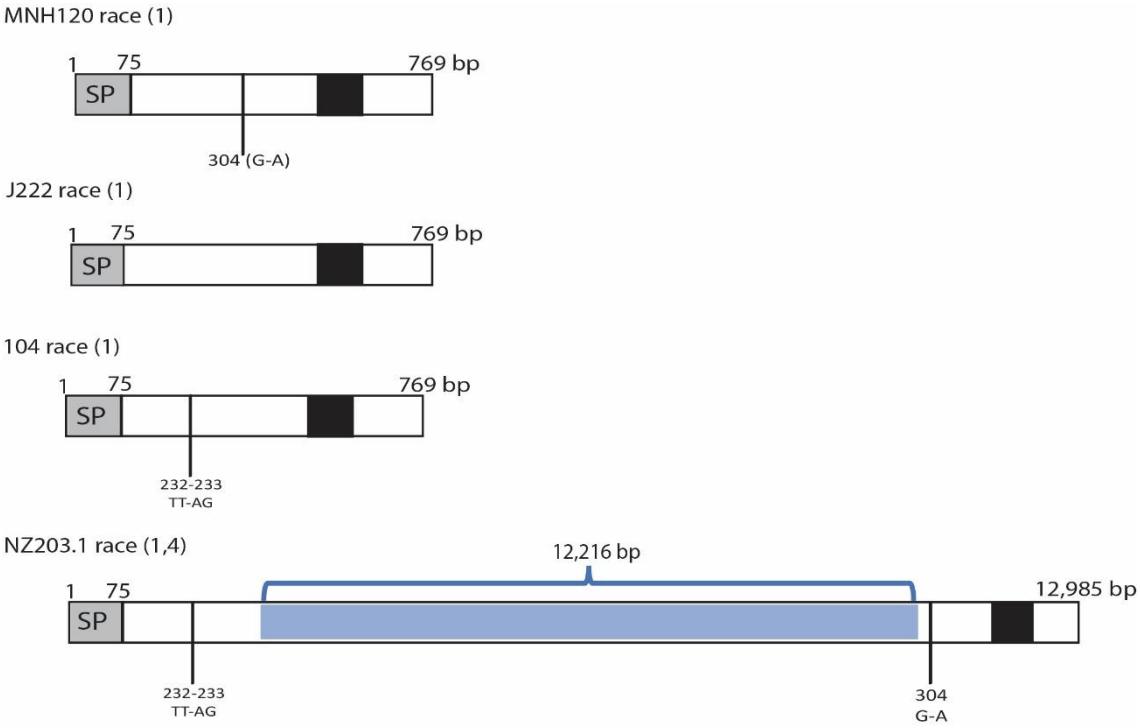

Figure 2.6. Schematic representation of the *atg6122* (candidate *AvrRvi4*) gene from *Venturia inaequalis* across four isolates. The wild type allele from the race (1) isolates MNH120, J222 and 104 is 769 base pairs (bp) in length. The gene is disrupted by a long repetitive element of 12,216 bp (highlighted in blue) after nucleotide position 280 in the NZ203.1 race (1,4) isolate. It additionally contains a TT to AG dinucleotide change at positions 232-233, as in isolate 104, and a G to A change at the equivalent position 304 of the isolate MNH120. The predicted N-terminal signal peptides (SP) are highlighted in grey, and the introns are highlighted in black

Table 2.7 Correlation between the genotype of *Venturia inaequalis* J222 race (1)/NZ203.1 race (1,4)/J222 x NZ203.1 progeny isolates and their phenotype on *Rvi4* apple. Bold fonts represent the expected phenotype-genotype correlation if the *atg6122* gene of *V. inaequalis* is *AvrRvi4*. Cells in grey shading represent no phenotype-genotype correlation. Flanking single nucleotide polymorphisms (SNPs) refer to the TT to AG dinucleotide change at positions 232–233, and the G to A change at position 304 across genomes of the progeny.

Functional *AvrRvi4* gene			**Non-functional *AvrRvi4* gene**			**Ambiguous**		
Isolate	**Phenotype**	**Genotype (flanking SNPs in *atg6122*)**	**Isolate**	**Phenotype**	**Genotype (Flanking SNPs in *atg6122*)**	**Isolate**	**Phenotype**	**Genotype (Flanking SNPs in *atg6122*)**
J222	**Macroscopically visible HR**	**NO**	**NZ203.1**	**Macroscopically abundant surface growth and microscopically visible stromata**	**YES**	**S016**	**Possible HR visible by bright field microscopy**	**NO**
S001	**Macroscopically visible HR**	**NO**	**S002**	**Macroscopically abundant surface growth and microscopically visible stromata**	**YES**	**S026**	**Limited stromata visible by bright field microscopy (likely AvrRvi4)**	**NO**
S004	**Macroscopically visible HR**	**NO**	**S006**	**Macroscopically abundant surface growth and microscopically visible stromata**	**YES**	**S041**	**Limited stromata (likely lacks AvrRvi4)**	**YES**
S008	**Macroscopically visible HR**	**NO**	**S009**	**Macroscopically abundant surface growth and microscopically visible stromata**	**YES**	S048	Limited stromata visible by bright field microscopy (likely lacks AvrRvi4)	NO
S012	**Microscopic HR**	**NO**	**S010**	**Macroscopically abundant surface growth and microscopically visible stromata**	**YES**	S052	Unavailable photo. Visible surface growth on leaves	NO

Functional *AvrRvi4* gene			Non-functional *AvrRvi4* gene			Ambiguous		
Isolate	Phenotype	Genotype (flanking SNPs in *atg6122*)	Isolate	Phenotype	Genotype (Flanking SNPs in *atg6122*)	Isolate	Phenotype	Genotype (Flanking SNPs in *atg6122*)
S013	**Microscopic HR**	**NO**	**S019**	**Macroscopically abundant surface growth and microscopically visible stromata**	**YES**	**S061**	**Possible HR visible by bright field microscopy**	**NO**
S021	**Macroscopically visible HR**	**NO**	**S022**	**Macroscopically abundant surface growth and microscopically visible stromata**	**YES**	**S062**	**Limited stromata visible by bright field microscopy (likely lacks AvrRvi4)**	**YES**
S025	**Microscopic HR**	**NO**	**S053**	**Macroscopically abundant surface growth and microscopically visible stromata**	**YES**	**S088**	**Limited stromata visible by bright field microscopy (likely lacks AvrRvi4)**	**YES**
S027	**Macroscopically visible HR**	**NO**	**S057**	**Macroscopically abundant surface growth and microscopically visible stromata**	**YES**	**S104**	**No evidence of cell death or stromata**	**NO**
S032	**Macroscopically visible HR**	**NO**	**S059**	**Macroscopically abundant surface growth and microscopically visible stromata**	**YES**			
S036	**Macroscopically visible HR**	**NO**	S063	Macroscopically abundant surface growth and microscopically visible stromata	NO			
S038	**Microscopic HR**	**NO**	**S067**	**Macroscopically abundant surface growth and microscopically visible stromata**	**YES**			

Functional *AvrRvi4* gene			Non-functional *AvrRvi4* gene			Ambiguous		
Isolate	Phenotype	Genotype (flanking SNPs in *atg6122*)	Isolate	Phenotype	Genotype (Flanking SNPs in *atg6122)*	Isolate	Phenotype	Genotype (Flanking SNPs in atg6122)
S049	Microscopic HR	NO	S079	Macroscopically abundant surface growth and microscopically visible stromata	YES			
S056	Macroscopically visible HR	NO	S081	Macroscopically abundant surface growth and microscopically visible stromata	YES			
S065	Microscopic HR	NO	S087	Macroscopically abundant surface growth and microscopically visible stromata	YES			
S069	Macroscopically visible HR	NO	S091	Macroscopically abundant surface growth and microscopically visible stromata	YES			
S074	Macroscopically visible HR	NO	S092	Stroma visible under microscope	YES			
S085	Macroscopically visible HR	NO						
S097	Microscopic HR	NO						
S099	Macroscopically visible HR	NO						

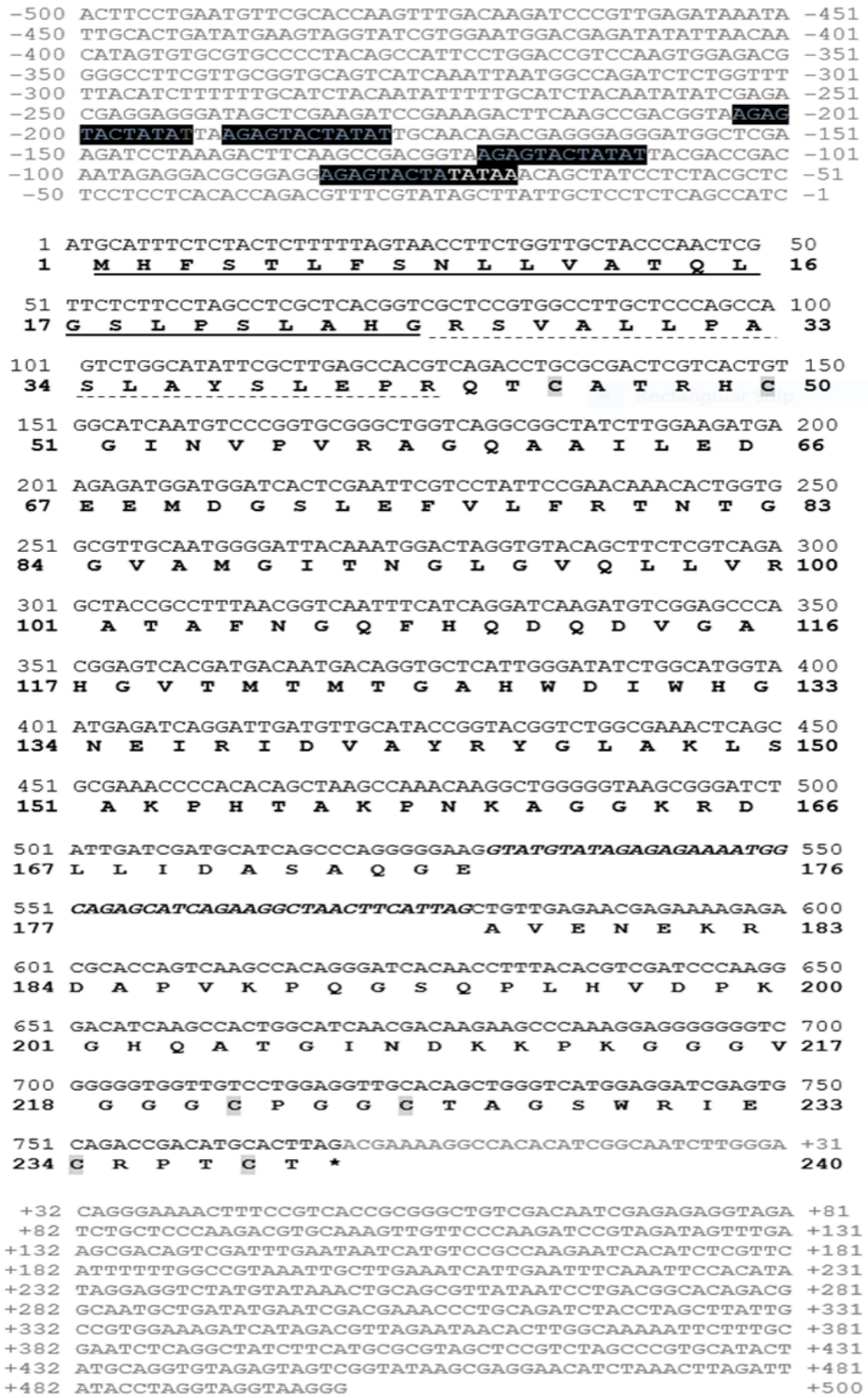

Figure 2.7. Nucleotide sequence of the candidate *AvrRvi4* gene from *Venturia inaequalis* and the protein it encodes. The TATAA box and a repetitive 12-bp promoter motif are highlighted in black, and the intron sequence is italicized. The translated amino acid sequence is presented underneath the nucleotide sequence. The predicted signal peptide is underlined with a solid line, whereas the putative pro-domain is underlined with a dashed line. Cysteine residues are highlighted in grey.

2.3.7 The candidate *AvrRvi4* gene is surrounded by repetitive elements

To investigate the genomic location of the candidate *AvrRvi4* gene in isolate NZ203.1, the genome scaffold carrying this gene in isolate MNH120 was examined. The *AvrRvi4* gene is located on a 51,493 nt scaffold (scaffold_791) and is flanked by repetitive elements. The relatively small size of the scaffold suggests that it is surrounded by further repeats, which have prevented the assembly of the scaffold into a larger scaffold. The G+C content across the entire scaffold ranges from 16.18 to 64.73%, and the specific G+C content of the candidate *AvrRvi4* gene is 52.7% (Fig. 2.8).

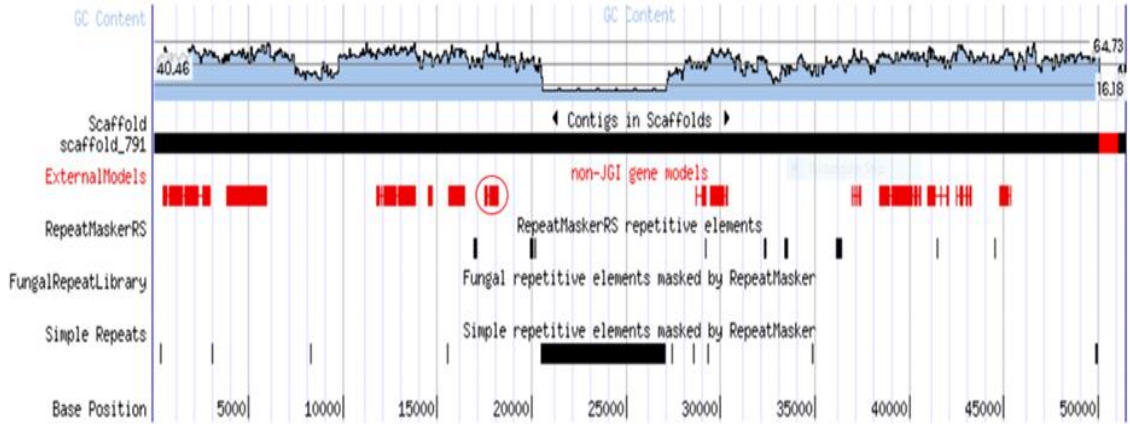

Figure 2.8. Genomic location of the candidate *AvrRvi4* gene. The candidate *AvrRvi4* gene is located on genome scaffold_791 in isolate MNH120. Genes are shown in red and repetitive elements are shown in black. The candidate *AvrRvi4* gene is circled in red. The red block in the scaffold_791 represents a gap of unknown sequence (996 nt) between contig 1 (50,022 nt) and contig 2 (475 nt) used to assemble scaffold_791. Screen shot obtained from the the Joint Genome Institute (JGI) Mycocosm site.

2.3.8 The candidate *AvrRvi4* gene contains a high level of polymorphism among *V. inaequalis* isolates

To analyse polymorphisms in the candidate *AvrRvi4* gene, 88 *V. inaequalis* isolates from a worldwide collection present in NCBI (Table A.4), representing *V. inaequalis* f. sp. *pomi*, *V. inaequalis* f. sp. *pyracanthae* and *V. inaequalis* f. sp. *eriobotryae,* were analyzed for allelic variation. Based on nucleotide sequence alignments, a total of 77 DNA modifications across all isolates were identified (Table 2.8 and Fig. 2.9). Seventy-three

are single-nucleotide polymorphisms (SNPs), and four are indels (insertions or deletions). From these modifications, sequence alignments revealed that 45 of the DNA modifications altered the predicted amino acid sequence of the candidate AvrRvi4 protein (Table 2.8 and Fig. 2.9).

Table 2.8. Allelic variation in the candidate *AvrRvi4* gene and the protein it encodes across isolates of *Venturia inaequalis* that infect apple, loquat and pyracantha. Polym: Polymorphism.

Polym. in gene	Polym. in protein	Polym. in gene	Polym. in protein	Polym. in gene	Polym. in protein
64T>C	Leu22Phe	233T>C	Phe78Thr	463A>G	Thr155Ala
85G>T	Val28Leu	233T>G	Phe78Ser	DEL. 474-489	del. AsnLysArgGlyGly
92T>G	Leu31Arg	ins. 239-240 C-C	-	511G>.T	-
98C>T	Ala33Val	del. 244 A	Asn81Gln	515C>T	Arg171Ser
104G>C	Leu35Pro	del. 246 T	-	518C>T	Ser172Leu
109T>C	Tyr37His	257C>G	-	556C>T	-
110A>C	-	262G>A	-	563A>T	-
111T>C	-	263G>T	-	565G>C	-
140C>T	Thr47Arg	276A>T	-	581G>A	Val178Ile
152G>A	Gly51Asp	279A>C	-	597G>C	Arg183Thr
154A>G	Ile52Ala	284T>C	Val95Aala	603C>T	Arg185Val
155T>C	-	302C>T	Aala101Val	608G>A	Val187Ile
157A>G	-	304A>G	Thr102Aala	646C>A	-
158A>C	-	315C>T	-	652A>G	-
162C>T	-	388A>G	Ile130Val	673C>T	-
163C>A	Pro55Lys	397G>A	Gly133Asn	694G>C	-
164C>A	Pro55Lys	398G>A	Gly133Asn	699T>C	Val217Ala
170G>T	-	399T>C	-	699T>G	Val217Gly
171G>C	-	420T>G	-	700C>A	Val217Gly
172G>A	-	428G>A	Arg143Gln	733G>C	-
173C>A	Ala58Asn	437T>G	Leu146Arg	473A>T	Ile232Tyr
181G>T	Ala61Ser	493G>A	Ala147Arg	744T>A	Ile232Tyr
192G>C	Leu64Phe	440C>G	-	744T>C	Ile232Thr
210T>C	-	444A>G	-	753G>A	Arg235Lys
229C>T	-	452C>G	Ala151Gly	759C>G	Thr237Arg
232T>A	Phe78Thr	456C>G	-		

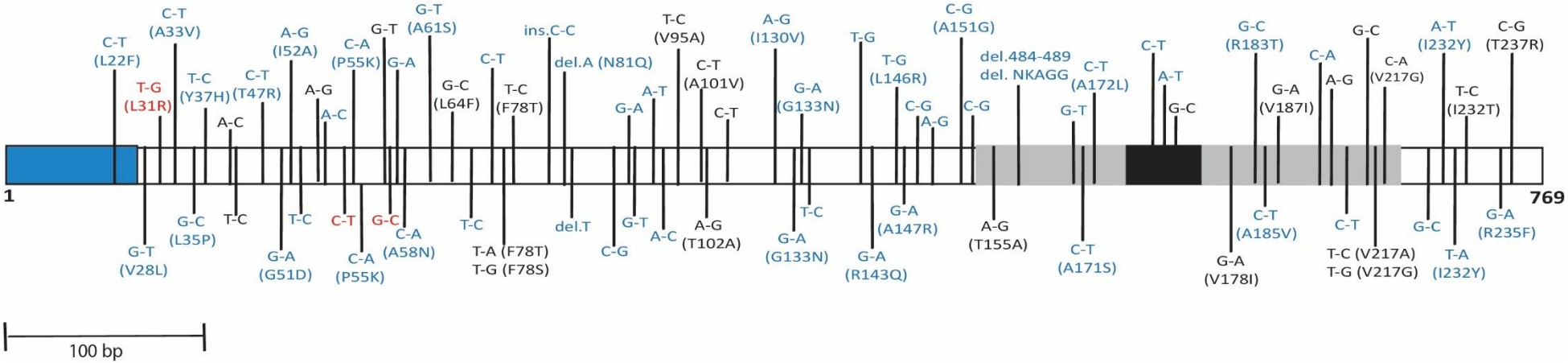

Figure 2.9. Sequence variation in the candidate *AvrRvi4* gene across a worldwide collection of *Venturia inaequalis* f. sp. *pomi*, *V. inaequalis* f. sp. *pyracanthae* and *V. inaequalis* f. sp. *eriobotryae* isolates. The blue box indicates the nucleotide sequence encoding the predicted signal peptide. The predicted intron is shown as a black box. The predicted intrinsically disordered region (IDR) is shown in grey shading. DNA polymorphisms resulting in an amino acid sequence alteration in the protein are indicated underneath or beside nucleotides. Scale bar = 100 base pairs (bp). DNA polymorphisms specific to one or more isolates of *V. inaequalis* f. sp. *pyracanthae* are shown in red. DNA polymorphisms specific to one or more isolates of *V. inaequalis* f. sp. *eriobotryae* are shown in blue and DNA polymorphisms specific to one or more isolates of *V. inaequalis* f. sp. *pomi* are shown in black.

2.3.9 *V. inaequalis* is anticipated to circumvent *Rvi4*-mediated resistance through different mechanisms

To investigate whether other race (4) isolates of *V. inaequalis* overcome *Rvi4*-mediated resistance through the same gene disruption as observed in NZ203.1, PCR amplifications of the candidate *AvrRvi4* gene were carried out in three European race (4) isolates; the amplicons were sequenced and compared to the alleles from strains J222 and 203.1 (Table 2.9). Amplicon sequencing revealed both isolates 141 and 405 share the same TT-AG dinucleotide substitutions at positions 232-233, as observed in isolate NZ203.1. Furthermore, isolate 405 shares a G-A substitution at position 304 which is also observed in isolate MNH120 (Table 2.9 and Fig. 2.6). Notably, isolate 141 carries unique point mutations leading to non-synonymous substitutions. Specifically, a G to T substitution at position 170, and a C to T substitution at position 302, leading to Arg-to-Leu and an Ala-to-Val amino acid substitution at positions 57 and 101 of the protein, respectively. In addition, a cytosine deletion at position 486, led to a frameshift mutation resulting in four amino acid substitutions and a premature stop codon at position 168.

Isolate 405 carries three unique point mutations leading to non-synonymous substitutions. Specifically, a TT to AG dinucleotide substitution at positions 582-583 leading to a Val-to-Lys amino acid change at position 178 of the protein, and a G-T substitution at position 584, leading to a premature stop codon at position 179. Isolate 1634 also carries single point mutations including a G-T substitution at position 149 and a A-G substitution at position 304, leading to a Cys-to-Phe and a Thr-to-Ala amino acid substitution at positions 50 and 102 of the protein, respectively. A TC-AG dinucleotide substitution was observed at positions 689-690 that led to a Val-to-Glu amino acid substitution at position 217. Interestingly, the orthologue in this isolate possesses multiple insertions leading to frameshift mutations altering the C-terminal sequence of the protein. All polymorphisms are summarized in Table 2.9.

Taken together, the race (4) isolates analyzed have specific mutations in the candidate *AvrRvi4* gene that are consistent with an ability of these isolates to overcome *Rvi4*-mediated resistance in apple.

Table 2.9. Polymorphisms in candidate *AvrRvi4* genes from three *Venturia inaequalis* isolates overcoming *Rvi4*-mediated resistance.

Isolate	Apple accession isolated from	Country isolated	Community	Year of isolation	Polymorphism in gene	Polymorphism in protein
141	TSR33T239	France	Beaucouzé	1985	G170T	R57L
					T232A	F78S
					T233G	F78S
					C302T	A101V
					486delC	frameshift (VSGIYstop)
405	TSR33T239	France	Toulenne	1988	G170T	R57L
					T232A	F78S
					T233G	F78S
					G304A	A101V
					T582A	V178K
					T583G	V178K
					G584T	179stop
1634	TSR33T239	France	Beaucouzé	2001	G149T	C50F
					G170T	R57L
					C302T	A101V
					A304G	T102A
					580insT	frameshift V178I
					T689A	V217E
					C690G	V217E
					insGGG	frameshift
					723insG	frameshift

2.3.10 The candidate AvrRvi4 effector forms part of an expanded family in *V. inaequalis*

To determine whether the candidate *AvrRvi4* effector gene is present as a singleton in the *V. inaequalis* genome, the protein it encodes was screened against the MNH120 genome using tBLASTn. Based on this analysis, six paralogs of the *AvrRvi4* gene were identified, of which five are predicted to encode a protein present in the MNH120 protein catalogue, (protein ID 16340 (*atg140*) [53% amino acid identity], protein ID 21509 (*atg478*) [56% amino acid identity], protein ID 19167 (*atg5171*) [47% amino acid identity], protein ID 18274 (*atg8679*) [50% amino acid identity], and protein ID 13790 (*atg12431*) [57% amino acid identity]). The remaining paralogue has a TGG to TAG codon change at position 386, leading to a truncated protein based on a premature stop codon at position 129 (hereafter referred to as Truncated AvrRvi4-Like Protein 1; TALP1) (Fig. 2.10). All proteins in the family possess a highly conserved N-terminal signal peptide, a pro-domain ending in a putative Kex2 protease cleavage site (LXPR, LXAR or FXPR), an IDR at the C-terminal, and six strictly conserved cysteines (all except the *AvrRvi4* candidate and *atg478* contain an additional cysteine residue) (Fig. 2.10). Interestingly, all seven members of the family are also present in *V. inaequalis* f. sp. *pyracanthae* and *V. inaequalis* f. sp. *eriobotryae*, with some strains of the three formae speciales containing the full length TALP1.

All genes of the *AvrRvi4* effector family are expressed during infection, with *atg478* and *atg8679* having the lowest expression, whereas *atg140* and *atg12431* being moderately expressed, reaching their highest expression at 5 dpi. The second most highly expressed gene, *atg5171*, is highly expressed at 3 dpi, reaching its highest expression at 5 dpi, and then is downregulated at 7 dpi. Strikingly, *atg6122* (candidate *AvrRvi4*) is by far the most highly expressed gene of all the family members, reaching the highest expression at 3 dpi (Fig. 2.11).

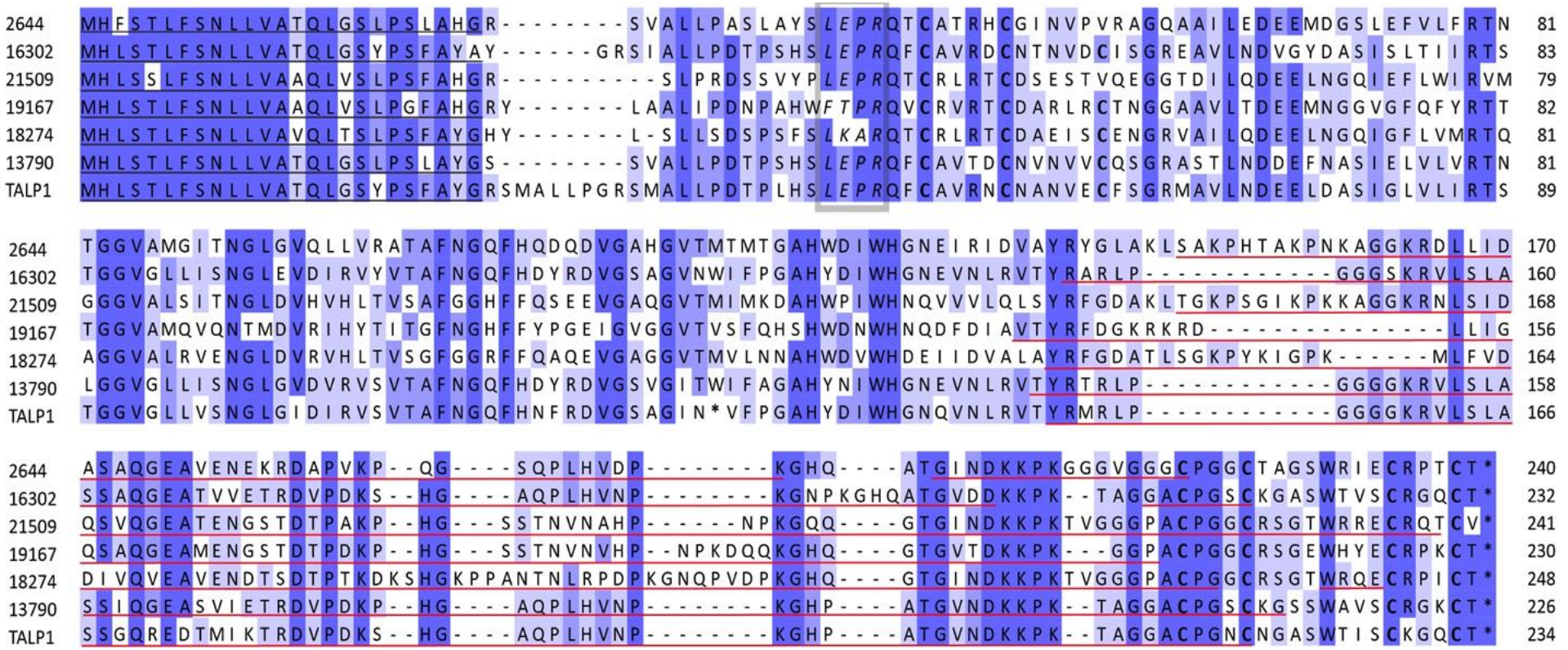

Figure 2.10. Alignment of proteins from the candidate AvrRvi4 effector family of *Venturia inaequalis* MNH120. Protein sequences were aligned using Clustal Ω. The Joint Genome Institute (JGI) protein ID numbers are as follows: 20644 (*atg6122*; candidate AvrRvi4 protein), 16302 (*atg140*), 21509 (*atg478*), 19167 (*atg5171*), 18274 (*atg8679*), 13790 (*atg12431*) and TALP1 (Truncated AvrRvi4-Like Protein 1). Predicted signal peptides are underlined in black. Intrinsically disordered regions (IDR) predicted with Predictors of Natural Disordered Regions (PONDR®) are underlined in red. Putative LxPR, LxAR and FTPR Kex2 cleavage sites appear in italics inside a grey box. Cysteine residues are shown in bold font. Amino acid conservation is shown in blue, with dark blue representing strict conservation.

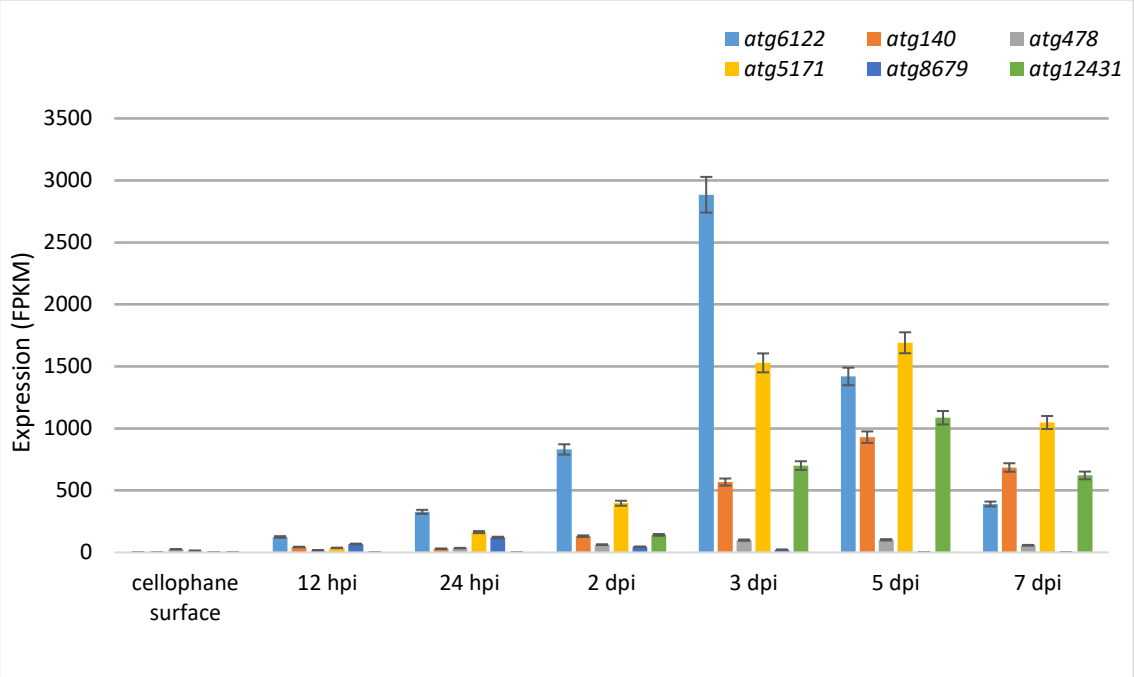

Figure 2.11. Expression levels of the candidate *AvrRvi4* effector gene family from *Venturia inaequalis* isolate MNH120. The transcriptome data for each gene is derived from *V. inaequalis* isolate MNH120 during growth in culture (cellophane surface overlaying PDA) at 7 days post-inoculation (dpi) or during infection of apple cultivar 'Royal Gala' at 12 and 24 hours post-inoculation (hpi), as well as 2, 3, 5 and 7 days post-inoculation (dpi), and presented as fragments per million per kilobase (FPMK) values. Error bars represent standard deviation between four biological replicates.

2.3.11 The *AvrRvi4* candidate contains a tandemly-repeated promoter element

To better understand why the candidate *AvrRvi4* gene is expressed almost twice as highly as the next most-highly expressed paralog of this family at 3 dpi, the presence of duplicated motifs in the promoter region of *AvrRvi4* was investigated. The promoter region of the candidate *AvrRvi4* gene was found to contain four perfect repeats of a 12-bp sequence located between -204 and -71 nt relative to the translation start site (5' AGAGTACTATAT 3'), one of which overlaps with the putative TATAA box at position -74 (Figs. 2.7 and 2.12). Furthermore, three of these motifs were found to reside in a much larger imperfect repeat of ~2.25 units located between -262 and -91 relative to the translation start site, with repeats 1 and 2 of 82 and 67 nt in length, respectively (Fig.

2.12). To determine whether the 12-bp motif was present in the upstream regions of other members from the candidate *AvrRvi4* gene family, a search for the same or similar motif was performed within the -500 bp region of each gene using the MEME motif search tool (Bailey et al., 2015). An identical copy of the 12-bp motif was not present in any upstream region of the paralogous genes, although one similar 12-bp motif (5' AGAGCACCATAT 3') was found in *atg5171.* This motif is located in the same region as in the candidate *AvrRvi4* gene promoter, -144 bp relative to the start codon. Interestingly, *atg5171* and *AvrRvi4* are the two most highly expressed genes of the family (Fig. 2.11). Together, these results suggest that the duplicated 12-bp motif, and/or the larger duplicated promoter element that three of the 12-bp motifs are embedded in, may be responsible for overexpressing the candidate *AvrRvi4* gene relative to other family members at 3 dpi. However, this hypothesis requires further investigation.

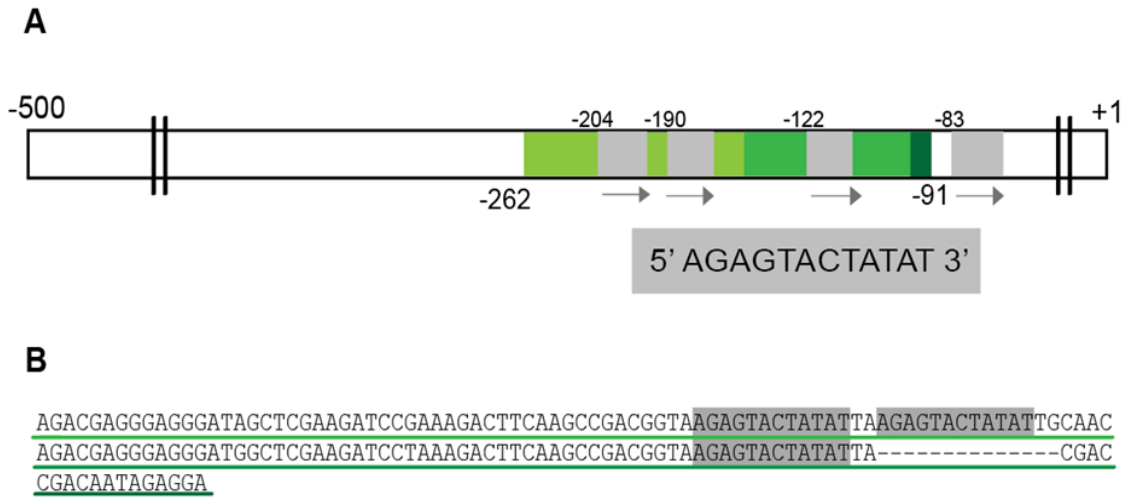

Figure 2.12. Tandem repeats present in the promoter region of the candidate *AvrRvi4* effector gene from *Venturia inaequalis.* (A) The large imperfect repeats appear in light to dark green. The 12-base pair repeat element located in the promoter region of the candidate *AvrRvi4* gene is shown as grey boxes. The numbers indicate the nucleotide positions relative to the translation start site. **(B)** Nucleotide alignment of the larger repeats in the promoter region including three of the four 12-bp repeat elements.

2.3.12 Members of the candidate AvrRvi4 effector family are predicted to adopt a β-sandwich fold with a large intrinsically disordered region

To gain further insights into the tertiary structure and virulence function of the candidate AvrRvi4 effector family from *V. inaequalis*, the tertiary structures of all members (excluding the truncated protein encoded by the pseudogenised gene) were predicted using AlphaFold2 (Jumper et al., 2021). For the main member of the family, the candidate AvrRvi4 protein (*atg6122*), AlphaFold2 predicted a tertiary structure with a pLDDT score of 67.20 and a predicted TM-score of 0.5715 (Fig. 2.13A-B). Structural prediction uncovered a β-sandwich fold with two antiparallel β-sheets composed of four and five strands respectively and a single turn α-helix, stabilized by two disulfide bonds. In addition, no obvious positively or negatively charged surfaces were identified in the predicted AvrRvi4 candidate's structure (Fig. 2.14)

Comparison of the predicted tertiary structure of the candidate AvrRvi4 protein with previously solved structures present in the RCSB Protein Data Bank (PDB) using the Dali server (Holm, 2020) revealed that this protein has structural similarity to a speckle-type POZ protein (RSCB protein data bank (PDB) ID: 3HQI-A) (Zhuang et al., 2009), and a ubiquitin carboxyl-terminal hydrolase 7 (RSCB protein data bank (PDB) ID: 2F1Z-B) (Hu et al., 2006). Interestingly, other structures with a similar fold include the host-selective toxin ToxA from *Pyrenophora tritici-repentis* (RSCB protein data bank (PDB) ID: 1ZLE) (Fig. 2.13C) (Sarma et al., 2005) and the Avr2 effector protein from *Fusarium oxysporum* f sp. *lycopersici* (RSCB protein data bank (PDB) ID: 5OD4) (Fig. 2.13D) (Di et al., 2017). These structures also adopt a β-sandwich fold stabilised by disulfide bonds (Di et al., 2017; Sarma et al., 2005), but possess different strand/sheet topology (i.e. order of β-sheets) and disulfide locations to the candidate AvrRvi4. Alignment with the predicted structure of the candidate AvrRvi4 effector protein is shown in Fig. 2.13E. In addition to the β-sandwich fold, the candidate AvrRvi4 protein is also predicted to contain a large C-terminal IDR (Fig. 2.13A), matching the previous IDR prediction determined by PONDR®. Similar to the candidate AvrRvi4 effector protein, the other five members of the family were predicted to adopt the same β-sandwich fold with large C-terminal IDRs (Fig. 2.12F-J). pLDTT values for these members ranged from 35 to 44, specifically: 13790

(*atg12431*)=43.6, 16302 (*atg140*)=44.2, 21509 (*atg478*)=35.2, 18274 (*atg8679*)=41.4 and 19167 (*atg5171*)=35.5.

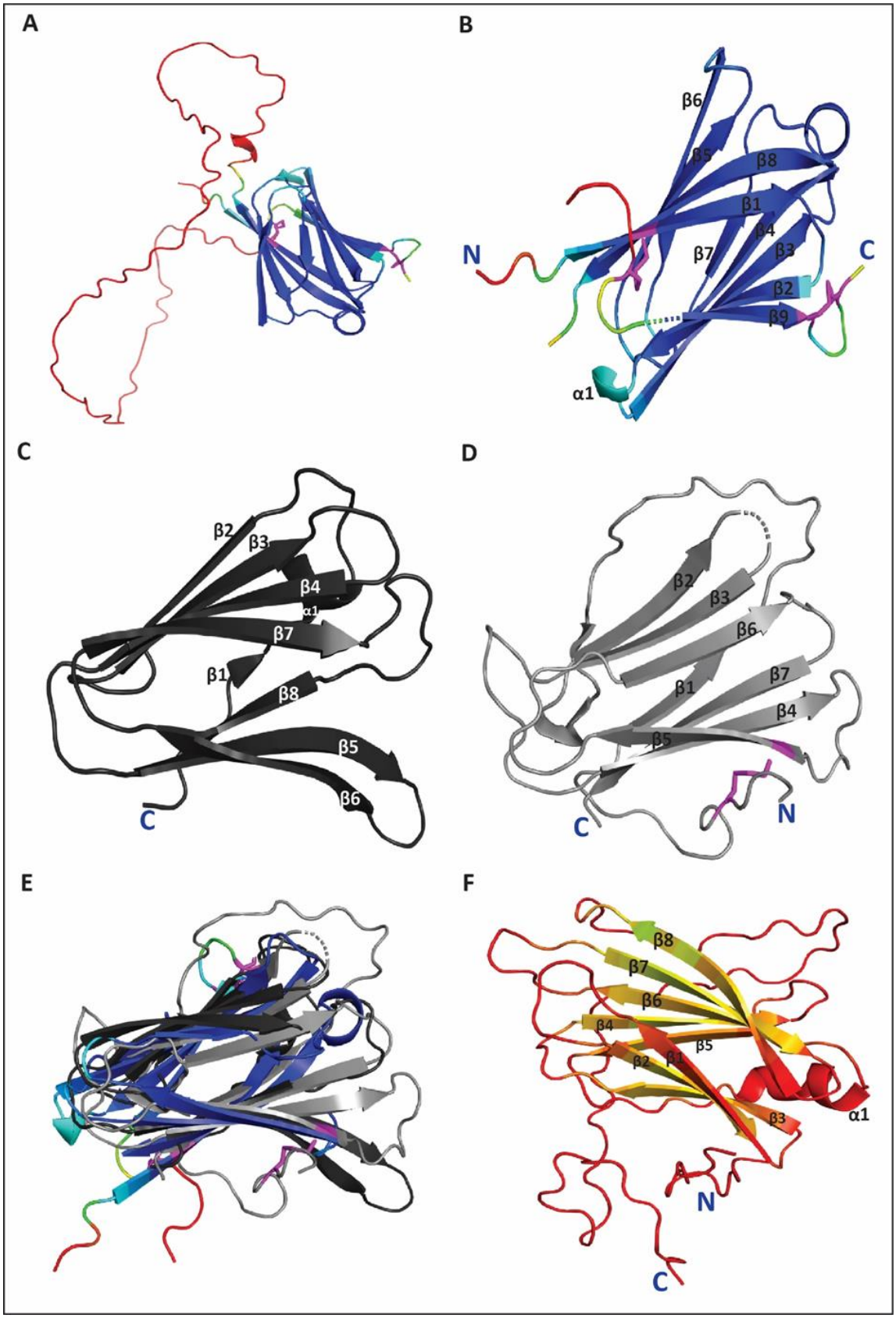

Figure 2.13. Legend in the next page.

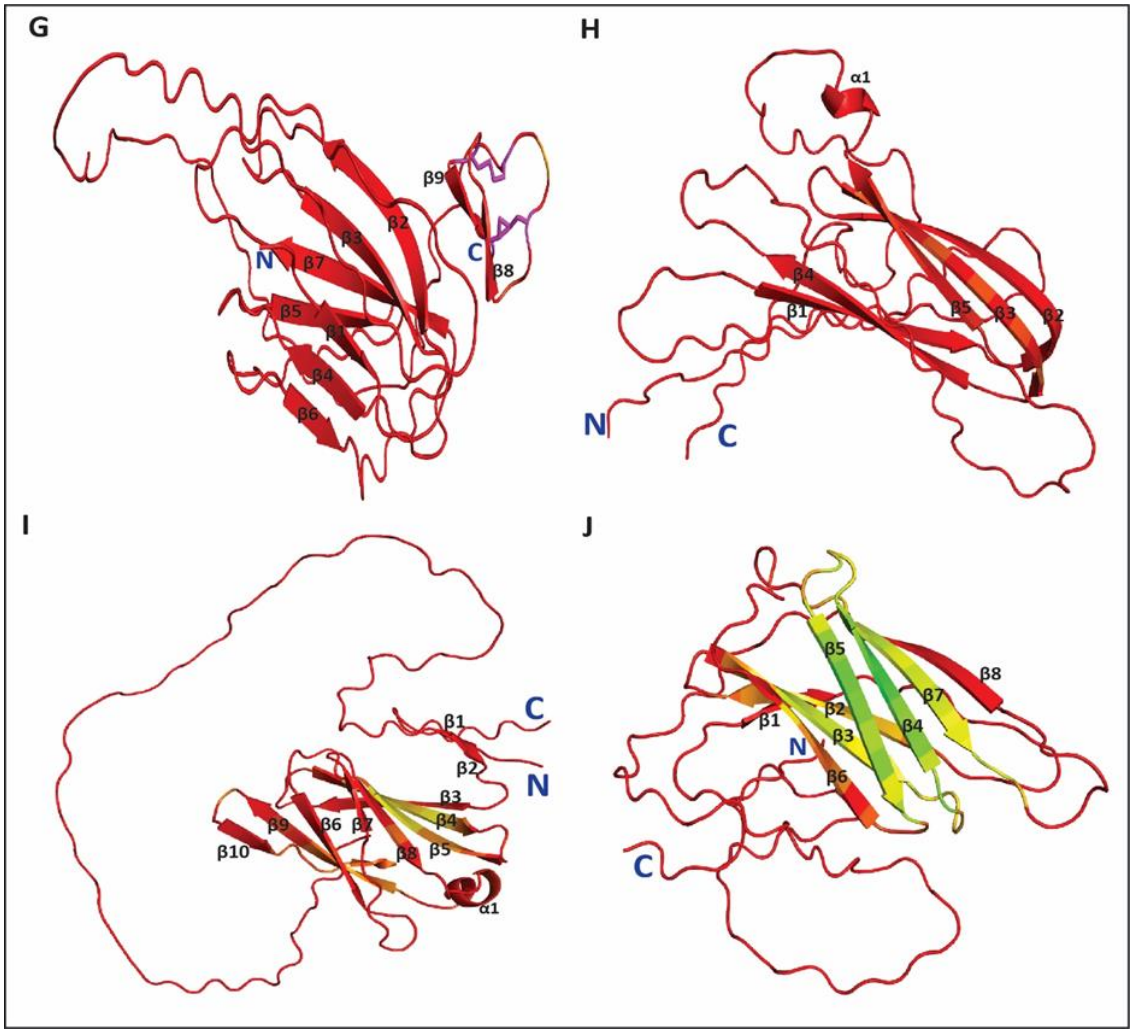

Figure 2.13. Predicted tertiary structure of candidate AvrRvi4 effector family members from *Venturia inaequalis.* **(A)** Overall tertiary structure of the candidate AvrRvi4 effector protein predicted by AlphaFold2 (Jumper et al., 2021). **(B)** Tertiary structure of the candidate AvrRvi4 effector protein without the predicted intrinsically disordered region (IDR). **(C)** Solved crystal structure of the host-selective toxin ToxA from *Pyrenophora tritici-repentis* (RSCB protein data bank (PDB) ID: 1ZLE) (Sarma et al., 2005). **(D)** Solved crystal structure of the Avr2 effector protein from *Fusarium oxysporum* (RSCB PDB ID: 5OD4) (Di et al., 2017). **(E)** Structural superimposition of the candidate AvrRvi4 effector, ToxA (black) and Avr2 (grey) proteins. **(F)** Tertiary structure of the 16302 (*atg140*) protein predicted by AlphaFold2 **(G)** Tertiary structure of the 21509 (*atg478*) protein predicted by AlphaFold2. **(H)** Tertiary structure of the 19167 (*atg5171*) protein predicted by AlphaFold2. **(I)** Tertiary structure of the 18274 (*atg8679*) protein predicted by AlphaFold2. **(J)** Tertiary structure of the 13790 (*atg12431*) protein predicted by AlphaFold2. For AlphaFold2 predictions, structures are coloured according to the pLDDT score: dark blue for highly confident predicted regions; light blue and green for regions of low confidence and red for very low confidence (incuding intrinsically disordered) regions. The β strands and α helices are numbered sequentially. Disulfide bonds are shown as purple sticks. The N- and C-termini are labelled in each panel. Tertiary structures were superimposed, visualized and rendered using PyMol (https://pymol.org/2/) (The PyMOL Molecular Graphics System, 2015) (DeLano, 2002).

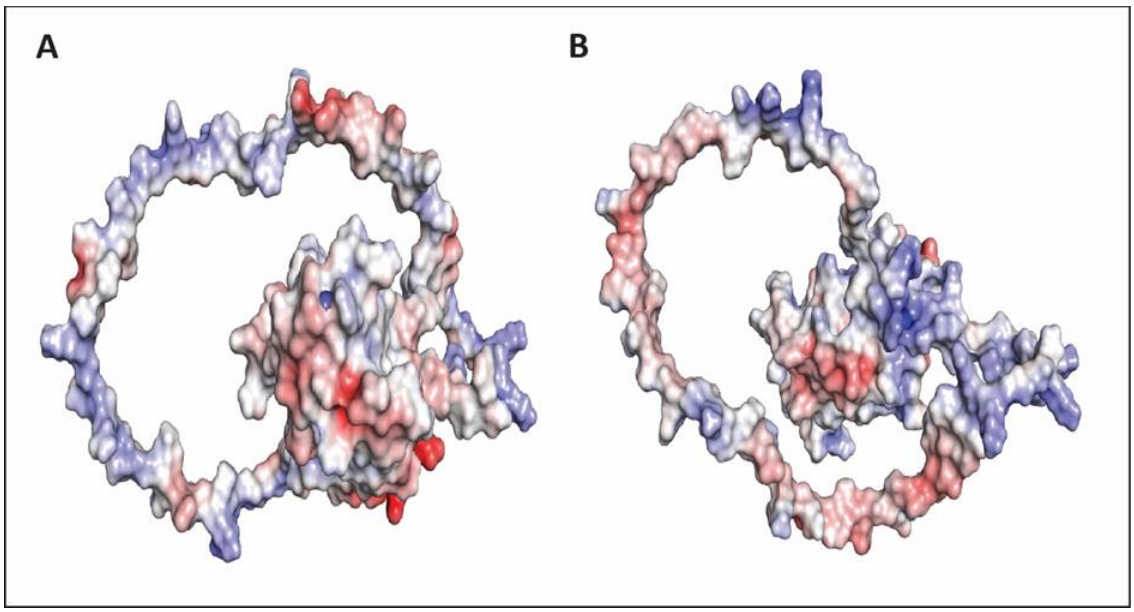

Figure 2.14. Surface charge potential of the candidate AvrRvi4 effector protein from *Venturia inaequalis*. Surface charge potential (rotated 180° around the y axis). Blue represents positive charge and red negative charge. Tertiary structures were visualized and rendered using PyMol (https://pymol.org/2/) (The PyMOL Molecular Graphics System, 2015) (DeLano, 2002).

2.3.13 Homologs of the candidate AvrRvi4 effector are restricted to *Venturia* species infecting members of the Malinae subtribe of host plants

Other *Venturia* pathogens for which genomes are available are *V. pyrina* (Deng et al., 2017; Le Cam et al., 2019), *V. nashicola* (Johnson et al., 2019), *V. asperata* (Le Cam et al., 2019), *V. orbiculata* (Le Cam et al. 2019), *V. oleaginea* (Jaber et al., 2020), *V. carpophila* (C. Chen et al., 2017; Zhou et al., 2021) and *V. effusa* (Young et al., 2019). To identify homologs of the candidate AvrRvi4 effector in other *Venturia* species, these genome resources were retrieved from NCBI. Using the tBLASTn tool, as part of the Geneious v. 9.1.8 software, seven AvrRvi4 homologs were identified (at least 25% amino acid identity) (Fig. 2.15), made up of one in *V. asperata* [36% amino acid identity], three in *V. orbiculata* [39, 45 and 39% amino acid identity, respectively], two in *V. pyrina* [39 and 28% amino acid identity, respectively], and one in *V. nashicola* [26% amino acid

identity]. No homologs were identified in the *V. oleaginea*, *V. carpophila*, a sequenced saprotroph from the Venturiaceae, or any other fungus outside the *Venturia* genus. All members are short (237-280 amino acid) proteins with a N-terminal signal peptide, followed by a conserved LxPR, LxGR, LxVR or LxAR Kex2 protease cleavage site motif, a C-terminal IDR and 6 to 8 cysteine residues. These *Venturia* species contain at least one homolog of the candidate AvrRvi4 protein, and are pathogens of apple (*V. asperata*), Rowan (*V. orbiculata*), European pear (*V. pyrina*) and Asian pear (*V. nashicola*) (Caffier et al., 2012; Le Cam et al., 2019; Sivanesan, 1977). Interestingly, these *Venturia* species, together with *V. inaequalis* f. sp. *pomi* (*Malus* spp.), *V. inaequalis* f. sp. *pyracanthae* (firethorn) and *V. inaequalis* f. sp. *eriobotryae* (loquat) (Gladieux et al., 2010a; Le Cam et al., 2002), are pathogenic to members of the Malinae subtribe of host plants in the Rosaceae family. Taken together, homologs of the candidate AvrRvi4 effector family appear to be restricted to members of the *Venturia* genus affecting host plants of the Malinae subtribe.

A phylogenetic tree constructed based on amino acid alignments of the AvrRvi4 effector family and homologs present in *V. asperata*, *V. nashicola*, *V. orbiculata* and *V. pyrina* showed that members of the AvrRvi4 family from *V. inaequalis* cluster in separate groups to the other members present in other *Venturia* species (Fig. 2.16), suggesting several gene duplication events have occurred in *V. inaequalis* or an ancestral fungus to this species.

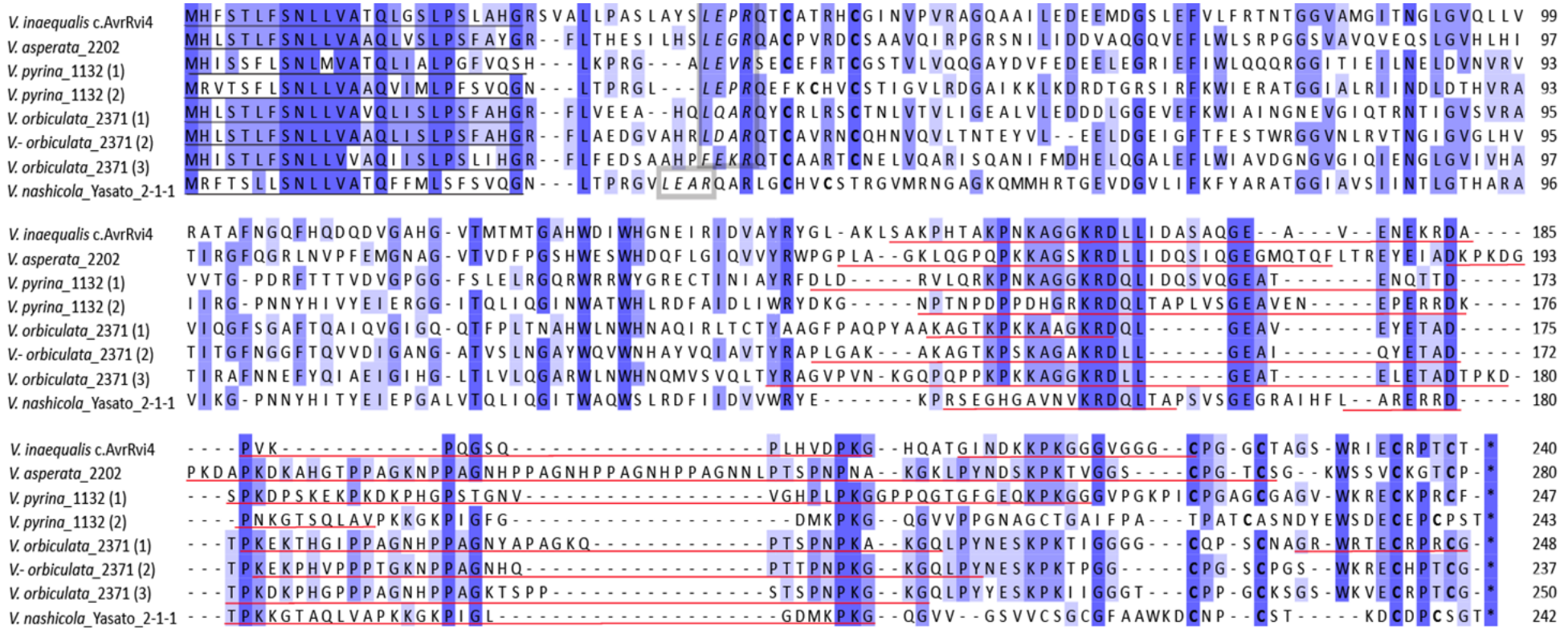

Figure 2.15. Alignment of homologs of the candidate AvrRvi4 effector family in *Venturia* species. Species and Isolates are as follows: *Venturia inaequalis* isolate MNH120 candidate AvrRvi4, *Venturia asperata* isolate 2202 (Le Cam et al., 2019), *Venturia pyrina* isolate 1132, proteins 1 and 2 (Le Cam et al., 2019), *Venturia orbiculata* isolate 2371, proteins 1, 2 and 3 (Le Cam et al., 2019), and *Venturia nashicola* isolate Yasato 2-1-1 (Johnson et al., 2019). Predicted signal peptides are underlined in black. Predicted intrinsically disordered regions (IDRs) are underlined in red. Putative LxGR, LxAR, LxKR, FxKR, LxVR and LxPR Kex2 cleavage sites appear in italics inside a grey box. Cysteine residues are shown in bold font. Amino acid conservation is shown in blue, with dark blue representing strict conservation.

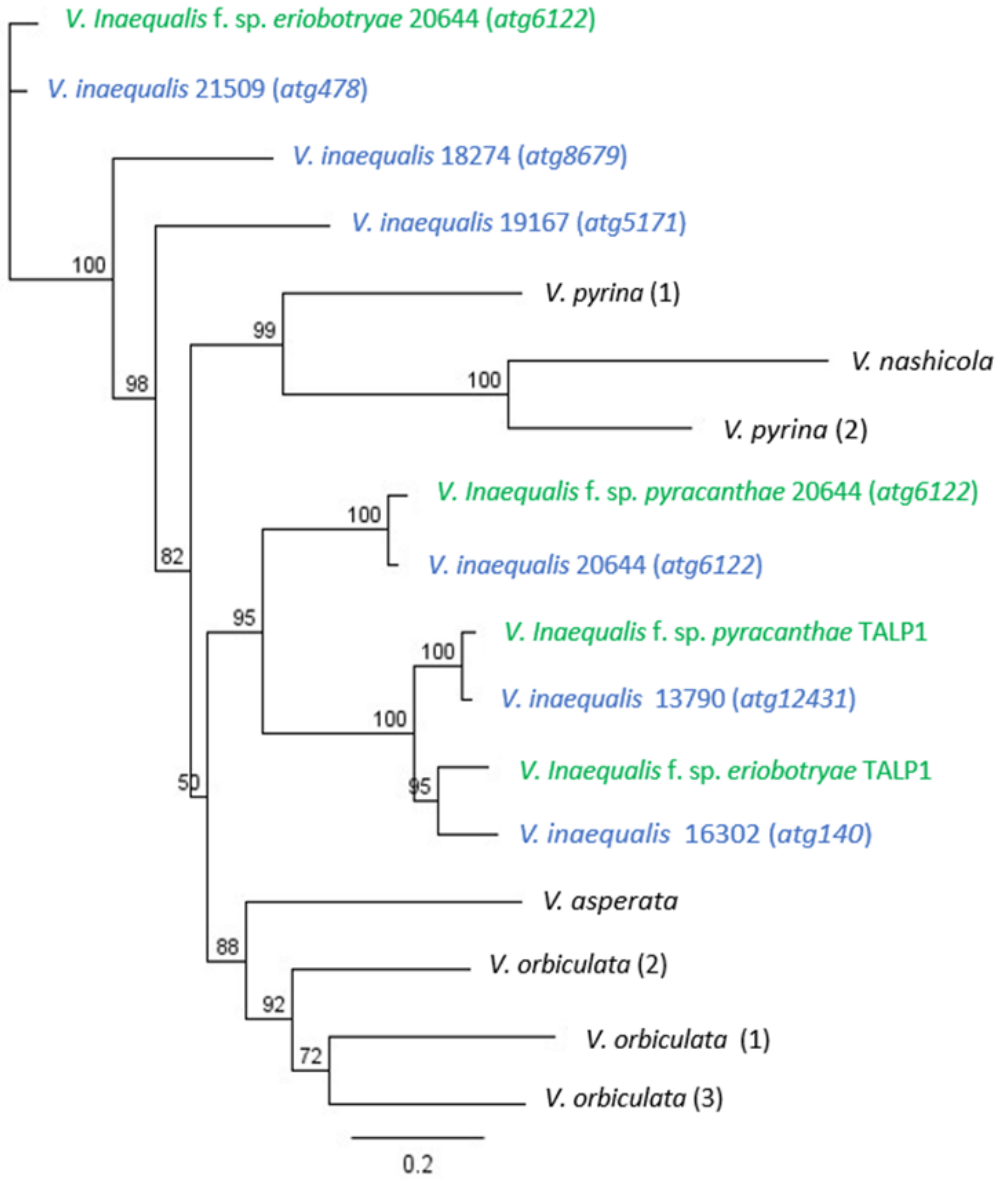

Figure 2.16. Phylogenetic tree of the AvrRvi4 effector family and homologs in other *Venturia* species. Neighbor-joining tree obtained from the amino acid alignment of AvrRvi4 proteins. Protein numbers in brackets after other *Venturia* species indicate the orthologue number (as in Fig. 2.15). *V. inaequalis* f. sp. *pomi* appears in blue, followed by the Joint Genome Institute (JGI) protein ID number, and the corresponding gene in brackets. *V. inaequalis* f. sp. *pyracanthae* and *V. inaequalis* f. sp. *eriobotryae* are shown in green. Numbers near the branches correspond to the bootstrap values. The tree was built in Geneious Software v. 9.1.8.

2.4 Discussion

Apple cultivars carrying the *Rvi4 R* gene have been used in some apple growing regions to control apple scab. Effective control relies on the ability of the encoding Rvi4 R protein to recognize the Avr effector AvrRvi4, leading to an HR that stops fungal proliferation. However, virulent isolates have been reported in different regions in Europe, North America and New Zealand. Hence, molecular identification and characterization of the *AvrRvi4* gene is fundamental to better understand how the pathogen overcomes *Rvi4*-mediated resistance. First, to identify *AvrRvi4*, parental isolates and other non-race (4) isolates with available genomes were compared to identify 16 candidate AvrRvi4 proteins. Then, a phenotyping strategy on plants carrying *Rvi4* using progeny from a cross of two *V. inaequalis* isolates was pursued. In addition, a whole genome sequencing approach was followed to associate the phenotype with genotype among parental and progeny isolates tested. Overall, 44 progeny obtained from a sexual cross between the *V. inaequalis* J222 race (1) isolate (containing a functional copy of *AvrRvi4*) and the *V. inaequalis* NZ203.1 race (1,4) isolate (lacking a functional copy of *AvrRvi4*), inoculated on resistant apple plants (carrying *Rvi4*), allowed the identification of progeny segregating for the *AvrRvi4* gene. Phenotyping infections resulted in 19 progeny isolates inducing HR (i.e. carrying *AvrRvi4*) and 15 progeny forming infection structures (i.e. lacking *AvrRvi4*). The limited number of available plants with a strong resistance phenotype, required the use of moderately resistant ones for infection assays. Certainly, all the equivocal phenotypes (i.e. from progeny isolates S048, S052, S063 and S104) were derived from leaves from moderately resistant plants, explaining the variability of the phenotyping.

Using a SNV analysis at the whole genome level, it was possible to identify four genomic regions with the best phenotype-genotype correlation. In one of these regions, a single candidate gene coding for one of the 16 AvrRvi4 candidates was identified. All evidence obtained in the study so far, including an analysis of the corresponding gene sequence from other race (4) isolates collected from France, suggest that this candidate is indeed AvrRvi4. However, a complementation experiment in which a functional copy of the candidate gene from either of the race (1) isolates used in this study (J222 or MNH120) is introduced ectopically into the genome of the NZ203.1 race (1,4) isolate, is now required. If the complemented isolate is able to trigger an HR on *Rvi4* apple, only

then will identification of AvrRvi4 be confirmed. This experiment is now underway in association with collaborators from the New Zealand Institute for Plant and Food Research.

The first approach pursued to identify AvrRvi4, leading to 16 candidates, is indeed time consuming as it requires identification and validation of the mutations responsible for the loss of HR. Therefore, to speed up and complement the identification of the best AvrRvi4 candidate, a bulked segregant analysis approach (BSA) was added to this study. This involves the pooling of mutant and wild type segregants derived from a sexual cross, using the SNPs of the parents as markers (Michelmore et al., 1991; Niu et al., 2020). Using a BSA has made it possible to map and identify pathogenicity genes. For example, a BSA based on the genome comparison of parental (a non-pathogenic and a highly aggressive) and progeny isolates led to the mapping and identification of a gene responsible for sporulation, sclerotia production and pathogenicity in *Botrytis cinerea* (Acosta Morel et al., 2021).

The candidate *AvrRvi4* gene, like most other *Avr* effector genes identified to date from plant-pathogenic fungi (Kanja & Hammond-Kosack, 2020), encodes a small, secreted, cysteine-rich protein, and is both highly expressed and induced during infection. In the *V. inaequalis* NZ203.1 race (1,4) isolate, the candidate *AvrRvi4* gene is disrupted by a long repetitive element of 12,216 bp. Gene disruption is one of the mechanisms by which fungal pathogens can overcome resistance mediated by *R* genes. Examples of *Avr* genes disrupted by repetitive elements have been reported in other plant-pathogenic fungi (Luderer et al., 2002; Olukayode et al., 2019; Wu et al., 2015; Zhou et al., 2007). More specifically, a 5 kb insertion in the *Avr2* gene from the tomato leaf mould pathogen *C. fulvum* allowed the circumvention of resistance mediated by the *Cf-2 R* gene from tomato. Other insertion events in three different *Avr* genes from the rice blast pathogen *Magnaporthe oryzae* have also been described. First, a transposon was identified in the coding region of the *Avr* gene *Avr-Pita*, allowing the fungus to evade recognition mediated by the *Pi-ta R* gene from rice (Zhou et al., 2007). Secondly, a 480 bp transposable element in the *Avr* gene *AvrPi9* was discovered that enabled the emergence of virulent isolates capable of circumventing *Pi9*-mediated resistance (Wu et al., 2015). And thirdly, a transposon insertion was identified in the promoter region of

AvrPib, permitting highly virulent isolates to cause disease on rice cultivars carrying the corresponding *Pib R* gene (Olukayode et al., 2019).

An analysis of the candidate *AvrRvi4* gene in other race (4) isolates of *V. inaequalis* revealed that this fungus likely not only overcomes *Rvi4*-mediated resistance through a single disruption event, but also through point mutations and indels, altering the amino acid sequence, leading to a truncated or possibly an unstable AvrRvi4 protein. For example, the Cys-to-Phe change in the candidate AvrRvi4 protein from the French isolate 1634, could have a similar outcome to that observed in *C. fulvum* where Cys-to-Tyr substitutions lead to an unstable Avr4 protein, that is rapidly degraded in the apoplast, thereby evading *Cf-4*-mediated resistance (van den Burg et al., 2003). Resistance mediated by single *R* genes has been overcome by other fungal pathogens through different modes. As mentioned, strains of *C. fulvum* have overcome *Cf-2*-mediated resistance not only by transposon insertion, but also through deletion of the corresponding *Avr2* gene, indels leading to a truncated protein, and multiple point mutations resulting in non-synonymous substitutions (Iida et al., 2010; Iida et al., 2015; Lucentini et al., 2021; Luderer et al., 2002; Novak et al., 2021; Stergiopoulos et al., 2007). Insertion events are facilitated by the close genomic location of *Avr* genes to transposable elements (TEs) (Möller & Stukenbrock, 2017). Genomic studies of plant-pathogenic fungi have revealed that effector genes are located in TE-rich regions, allowing high mutation rates that support effector diversification advantageous for the pathogen (Möller & Stukenbrock, 2017). Indeed, *V. inaequalis* SSPs have been found to be closely associated with TEs (Deng et al., 2017), which is also the case for the candidate *AvrRvi4* gene that was found to be located between repetitive elements in the genome. In addition, the hits to helicases and helicase-like proteins in the ~12.2 kb insertion on the allele from isolate NZ203.1, supports this premise.

The high level of polymorphism observed in the candidate *AvrRvi4* gene across all *V. inaequalis* isolates is probably influenced by the single sexual cycle and multiple asexual cycles they undergo per season that allow high recombination and mutation rates (Khajuria et al., 2018). This sequence variation is essential for overcoming *Rvi*-mediated resistance. Indeed, these features have been studied in the Septoria leaf blotch Dothideomycete pathogen, *Zymoseptoria tritici,* whose population's ability to thrive on new host varieties is also facilitated by frequent sexual reproduction that

creates large populations displaying high recombination rates that facilitate mutations, and in some cases, these mutations are advantageous (Zhan et al., 2003). The numerous mutations in the candidate *AvrRvi4* gene specific to *V. inaequalis* f. sp. *eriobotryae* could correspond to host specificity involving loquat.

The predicted secretome of *V. inaequalis* isolate MNH120 consists of approximately 850 SSPs, of which more than half form part of expanded protein families ranging in size from five to 75 members (Deng et al., 2017; Rocafort et al., in preparation). These protein families are the result of duplication of an ancestral gene, and may allow the fungus to evolve new SSP functionalities (Nei & Rooney, 2005). The candidate AvrRvi4 protein forms part of one of the expanded SSP families, which consists of six proteins with a similar predicted structural fold. Whether these family members have the same function during host colonization remains to be determined. Sequence analysis of other reference genomes from selected *Venturia* species revealed that they also contain one or more copies of a gene encoding an AvrRvi4 candidate homolog. More specifically, three full-length homologs were identified in *V. nashicola,* three in *V. orbiculata*, two in *V. pyrina* and one in *V. asperata*. All of these pathogens, together with the three formae speciales of *V. inaequalis*, infect members of the Malinae subtribe, which may signify a role in promoting colonization of these host plants. The latter is consistent with lineage-specific SSPs that belong to expanded gene families, found strictly in the *Venturia* genus determining host–*Venturia* interactions (Deng et al., 2017; Shiller et al., 2015).

The finding that the candidate AvrRvi4 effector forms part of an expanded family is not unusual, given that Avr effectors belonging to expanded families in other plant-pathogenic fungi have been reported. Examples of these include the MAX (*Magnaporthe* Avrs and ToxB-like) (de Guillen et al., 2015) and PWL (Pathogenicity on Weeping Lovegrass) effectors from in *M. oryzae* (Kang et al., 1995; Sweigard et al., 1995), the LARS (for *Leptosphaeria* AviRulence-Suppressing) effectors from *Leptosphaeria maculans* (Lazar et al., 2021), the AvrM (Catanzariti et al., 2005), AvrM14 (Anderson et al., 2016), AvrL2 (Anderson et al., 2016) and AvrL567 (Dodds et al., 2006) effectors from *Melampsora lini*, as well as the RALPH (RNase Like Proteins expressed in Haustoria) effectors from *Blumeria graminis* f. sp. *hordei* (Pennington et al., 2019; Spanu, 2017) and the Ecp4/7, Ecp9 and Ecp10 effectors from *C. fulvum* (Mesarich et al., 2018).

Fungal effector proteins often have low sequence similarity and lack characterized functional domains, making predictions about the functions in virulence more difficult. In some cases, tertiary structures of these effectors can provide more insights into their functional roles (Franceschetti et al., 2017). The recently awarded 2021 Science Breakthrough of the Year (https://www.science.org/content/article/breakthrough-2021), artificial intelligence (AI)-driven software AlphaFold2 (Jumper et al., 2021), has made it possible to predict the 3D tertiary structures of proteins with high accuracy. Using AlphaFold2, the candidate AvrRvi4 protein was predicted to adopt a β-sandwich fold stabilized by three disulfide bonds, with a large intrinsically disordered region (IDR). Effectors with a similar β-sandwich fold include ToxA from the necrotrophic fungus *P. tritici-repentis* and Avr2 from *F. oxysporum* f. sp. *lycopersici* (Di et al., 2017; Sarma et al., 2005).

ToxA is a proteinaceous host-selective toxin that induces cell death on wheat varieties carrying the susceptibility gene *Tsn1* (Ciuffetti et al., 1997; Strelkov & Lamari, 2003; Tomas et al., 1990). The *Tsn1*-associated necrosis requires ToxA internalization into host cells allegedly through an arginyl-glycyl-aspartic (RGD) motif (Manning et al., 2008; Meinhardt et al., 2002). Tsn1 is an intracellular susceptibility (S) IPR of the NBS-LRR type that includes N-terminal serine/threonine kinase domains (Faris et al., 2010). Nevertheless, the specific function of Tsn1 or a possible Tsn1–ToxA direct interaction remain unknown (Faris et al., 2010). Different ToxA–protein interactions facilitating cell death have been reported. First, it was demonstrated that the association of ToxA with the chloroplast-localised protein of wheat, ToxABP1, interrupted the physiological function of the chloroplast, leading to oxidative stress and cell death (Ciuffetti et al., 2010; Manning et al., 2007). Then, a TAI (Tox Interactor) chloroplast plastocyanin was also found to interact with ToxA and induce cell death (Tai et al., 2007). In addition, a PR-1 protein of wheat was suggested to be a potential target of ToxA after a PR-1-ToxA interaction was demonstrated (Lu et al., 2014). Questioning the different outcomes of the latter studies, it has recently been demonstrated that ToxA directly interacts with a HIN1-like protein (TaNHL10), an integral membrane protein of wheat to facilitate *Tsn1*-mediated cell death (Dagvadorj et al., 2021). This interaction specifically occurs in the apoplast, rather than in the cell, through the surface exposed C-terminus of TaNHL10, and does not require the RGD motif as stipulated before by Manning et al. (2008) and

Meinhardt et al. (2002). This interaction would facilitate pathogen perception to activate a defence response, as NHL proteins have been reported to have a role in plant immunity (Varet et al., 2003).

Avr2 (avirulence factor 2, also referred to as secreted in xylem; Six3) (Houterman et al., 2009), in conjunction with another effector from *F. oxysporum* f. sp. *lycopersici*, Six5, activates an immune response in tomato carrying the corresponding *I-2 R* gene. Like Tsn1, the I-2 is an NBS-LRR type of R protein (Ori et al., 1997; Simons et al., 1998). Six5 interacts with Avr2 at plasmodesmata and facilitates cell-to-cell movement of Avr2, contributing to virulence in susceptible plants, whereas in resistant plants carrying *I-2*, an immune response is triggered (Cao et al., 2018; Ma et al., 2015).

Avr2, ToxA and the candidate AvrRvi4 effector protein share only 5% sequence identity. They all share, however, a β-sandwich fold consisting of two antiparallel β-sheets composed of three to five strands each, enclosing a hydrophobic core (Fig. 2.13A–E) (Di et al., 2017; Sarma et al., 2005). In contrast to Avr2 and ToxA that contain only one disulfide bond, AvrRvi4 is stabilised by three disulfide bonds. Whether these proteins share a common evolutionary ancestor, as has been proposed for other fungal effectors with similar structures (Franceschetti et al., 2017), or overlaps in functions during host colonization, remain to be determined. Certainly, the fact that the AvrRvi4 candidate has a different overall strand/sheet topology to Avr2 and ToxA suggests a common shared ancestral protein or a conserved function is unlikely. Interestingly, similarly to ToxA (Ciuffetti et al., 1997) and Avr2 (Houterman et al., 2009), members of the candidate AvrRvi4 effector family have an N-terminal pro-domain ending in a putative Kex2 protease cleavage site that is likely removed by a Kex2-like homologue prior to secretion. This is likely also the case for many other fungal effector proteins (e.g. Six1, Six4 and Six6 from *F. oxysporum* f. sp. *lycopersici*), irrespective of whether they are produced by a biotrophic, hemibiotrophic or necrotrophic fungus (Outram et al., 2021). The roles of pro-domains remain largely unknown; however, they have been implicated in stabilisation, proper folding and localisation (Baker et al., 1993; Outram et al., 2021; Tuori et al., 2000). Hence, it can be speculated that pro-domain removal is essential for the correct folding and function of each member of the candidate AvrRvi4 effector family.

In addition to the presence of a pro-domain, members of the candidate AvrRvi4 effector family are predicted to possess a large IDR at their C-terminus. IDRs lack a fixed or ordered three dimensional structure but remain biologically active (Uversky et al., 2005), and provide advantages such as flexibility to interact with several targets, a wider interaction surface area, folding upon binding to targets and accessibility of posttranslational modification sites (Yang et al., 2020). Intriguingly, the candidate AvrRvi4 effector protein contains numerous mutations in its putative IDR, which is in line with versatility of proteins containing IDRs that are more tolerant to mutations, providing evolutionary advantages compared with ordered proteins (Babu et al., 2012; Nilsson et al., 2011). For example, effector PWL2 from *Magnaporthe oryzae* can evade the host immune system just by transitioning from an ordered to a disordered structure (Schneider et al., 2010). Recently, a sequence comparison of the Avr2 effector between virulent and avirulent *Phytophtora infestans* strains uncovered a difference in protein structure amongst them (Yang et al., 2020). Virulent strains possessed disordered interfaces both at the N- and C-terminal domains of Avr2, leading to an unstable protein, which in turn, altered the interaction with StBSL1 (without losing its biological activity), to avoid R2-mediated resistance response (Saunders et al., 2012; Yang et al., 2020). The presence of IDRs in the candidate AvrRvi4 effector family suggests that such long and flexible regions are important for effector translocation, virulence function during host colonization, or evasion of recognition by the plant immune system, as described previously in bacterial effectors from plant pathogens (Marín et al., 2013). Indeed, more research is required to elucidate the importance and function of IDRs in effectors from plant pathogens.

The high levels of expression of the candidate *AvrRvi4* effector gene could be explained by the presence of multiple repeats of 12 bp in length in the promoter region of this gene. This phenomenon has been previously described in the expression of the *Avr* effector gene *PWL2* from *M. oryzae* (Zhu et al., 2021). *PWL2* expression requires three tandem repeats of a 12-bp motif present in the promoter region (between -331 and -182 nt) (Sweigard et al., 1995; Zhu et al., 2021). Moreover, this 12-bp (5'-TTATGCAAGCTT-3') motif was also present in the upstream region of the *Avr* effector gene *AVR-Pik* and other effector genes, exhibiting similar expression patterns: induction at 25 hpi, repression at 33 hpi and re-induction at 38 hpi (Zhu et al., 2021). According to

this, the 12-bp regulatory element has a significant role in the expression of genes specific to the biotrophic stage of the fungus (Zhu et al., 2021). Similar to the observations by Zhu et al., (2021), the candidate *AvrRvi4* and *atg5171* genes share a similar 12-bp motif in their promoter regions that may play a role in their expression patterns, specifically inducing expression at 2 dpi, when the fungus has breached the leaf cuticle. Then, reaching the highest expression from 3 to 7 dpi, which coincides with the differentiation of stromata from sub-cuticular runner hyphae, when effectors are delivered to promote host colonization (Bowen et al., 2011; Kucheryava et al., 2008). This is also consistent with the high expression levels and localization of an AvrLm6-like protein in stromata at 7 dpi (Shiller et al., 2015).

In summary, this study has identified a very strong candidate for the AvrRvi4 effector of *V. inaequalis*, recognized by the Rvi4 R protein of apple. Despite the economic importance of *V. inaequalis* and other pathogens from the same genus, the molecular interactions with their respective hosts remain largely unknown (Bowen et al., 2009; Deng et al., 2017). Further studies using high quality genome assemblies are required to better understand these interactions (Le Cam et al., 2019), evolution and emergence of new pathogen variants. The identification of AvrRvi4 will allow the recognition of resistance-breaking isolates and direct apple breeding and selection programmes for protection against *V. inaequalis.* The identification of this effector will also enable targeted experiments that aim to determine the function of AvrRvi4 in apple plants lacking *Rvi4* and, in doing so, will provide valuable information on how effectors from this fungus function to promote host colonization.

Chapter 3: Identification of candidate effector proteins from the apple scab pathogen *Venturia inaequalis* that trigger cell death in non-host plant species

3.1 Introduction

To date, just over 60 effectors have been functionally characterized across filamentous plant pathogens (Kanja & Hammond-Kosack, 2020), which is a small portion of all the effector repertoires these pathogens carry and utilize to cause disease. For example, *V. inaequalis* produces approximately 850 SSPs during infection (Chapter 2), none of which have been functionally characterized. In the second layer of the plant immune system, plants use IPRs termed R proteins, whether intracellular nucleotide-binding domain leucine-rich repeat containing proteins (NLRs) or extracellular PRRs, to directly or indirectly recognize specific effectors. Such recognition generally leads to a localized chlorotic or necrotic cell death response, the hypersensitive response (HR), which halts pathogen growth, rendering the plant resistant (see section 1.1 of Chapter 1) (Cook et al., 2015; Heath, 2000; Jones & Dangl, 2006). Unlike many PRRs, these R proteins can be specific to certain plant species, accessions or cultivars (Kapos et al., 2019).

To better understand the underlying molecular mechanisms that filamentous pathogens use to manipulate and evade plant immune responses, as well as to understand how these pathogens activate the plant immune system, a greater emphasis needs to be put on effector identification and functional characterization. Such information will enable the identification of novel sources of resistance, as well as the implementation of new strategies to combat fungal diseases in important crops.

Effectoromics is a high-throughput screening approach to facilitate and accelerate the identification of novel *R* genes in plant germplasm (Vleeshouwers & Oliver, 2014). This approach relies on the expression of candidate effectors (CEs) in host or non-host plants (e.g. the model species *Nicotiana benthamiana* and *Nicotiana tabacum*), with a

possible outcome of a necrotic cell death or chlorotic response (i.e. HR), indicating a potential recognition by a plant R protein (Vleeshouwers & Oliver, 2014). For studies involving *N. benthamiana* or *N. tabacum*, CEs can be expressed through well-established *Agrobacterium tumefaciens*-mediated transient expression assays (ATTAs), also called agroinfiltration. This simple and versatile tool relies on the infiltration of an *A. tumefaciens* cell suspension carrying the desired *CE* gene in a binary expression vector into a small leaf area (Krenek et al., 2015). The binary expression system is composed of two different plasmids containing the genetic information for DNA transfer (T-DNA) and the desired insert (i.e. the *CE* gene). The T-DNA along with the *CE* gene is integrated into the plant genome, transforming the plant cells and allowing the transient expression of *CE* genes in the infiltrated zone (Debler et al., 2021; Ma et al., 2012).

Agroinfiltration has been used for CE screening and to study effector-receptor interactions in *N. benthamiana*. A notable example include the discovery of 13 cell death elicitors from a subset of 64 CEs from the Dothideomycete wheat pathogen *Zymoseptoria tritici*. Interestingly, the cell death-inducing activity of 12 of the 13 CEs was dependent on their apoplastic localization using an amino (N)-terminal secretion signal (signal peptide) and, as such, are likely recognized by extracellular R proteins (Kettles et al., 2017). Effector–R protein interactions, were studied with the co-expression of the avirulence (*Avr*) effector genes *Avr4* and *Avr9* from *Cladosporium fulvum* with the corresponding *R* genes of tomato *Cf-4* and *Cf-9*; these experiments resulted in chlorosis and necrotic responses in *N. benthamiana*, demonstrating that effector–R protein interactions can be studied in a non-host plant (Van der Hoorn et al., 2000). More recently, an effectoromics screen based on ATTAs in combination with the viral vector Potato Virus X (PVX) was carried out using 41 *C. fulvum* SSPs in wild tomato species (Mesarich et al., 2018). From this set of 41 SSPs, ten triggered an HR, indicating that the wild species carry novel *R* genes that could be incorporated into new tomato cultivars (Mesarich et al., 2018). Effectoromics has also enabled the rapid identification and cloning of single *R* genes. For example, a set of 54 RXLR candidate effectors from the late blight oomycete *Phytophthora infestans* were screened using a PVX approach in late blight-resistant *Solanum* species for elicitation of an HR (Vleeshouwers et al., 2008).

These HR events uncovered R–Avr interactions that subsequently led to the identification and cloning of two *R* genes (Vleeshouwers et al., 2008).

Given the success of the experiments described above, it was reasoned that a high-throughput effectoromics approach based on ATTAs could be used to facilitate the identification of CEs from *V. inaequalis* that are potentially recognized by R proteins in non-host *Nicotiana* species (i.e. as a consequence of their ability to trigger a visual cell death response). This may in turn, give clues into which effectors of *V. inaequalis* are potentially recognized as Avrs by R proteins in apple. While it is possible that these effectors could be recognized directly by an R protein in *Nicotiana* species, it is also possible that they are recognized indirectly through their modulation of a conserved virulence target in both host and non-host plants. Thus, by using an effectoromics approach, it was deemed possible that effector proteins of *V. inaequalis* could be identified that potentially play an important role in promoting apple colonization. With this in mind, 133 CEs of *V. inaequalis* were selected and screened for their ability to trigger a visual chlorotic or cell death response in *N. benthamiana* and *N. tabacum*.

3.2 Materials and methods

3.2.1 Biological materials

Bacterial strains and plants used in this chapter are listed in Table 3.1. Primers and plasmids used in this chapter are listed in Table A.1 and Table A.2, respectively.

Table 3.1. Biological materials used in this chapter.

Organism/strain	Characteristics	Reference/Source
Escherichia coli		
DH5α	*F⁻ endA1 glnV44 thi-1 recA1 relA1 gyrA96 deoR nupG* Φ80d*lacZ*ΔM15 Δ(*lacZYA-argF*)U169, *hsdR17*(r_K^- m_K^+), λ–	Taylor *et al*. (1993); Invitrogen
JM110	*rpsL thr leu thi lacY galK galT ara tonA tsx dam dcm glnV44 Δ(lac-proAB) e14- [F' traD36 proAB⁺ lacI^q lacZΔM15] hsdR17($r_K^-m_K^+$)*	Agilent
Agrobacterium tumefaciens		
GV3101::pMP90	Disarmed strain carrying pMP90 (pTiC58) helper plasmid; C58C1; Rif^R ,$Gent^R$	Koncz & Schell (1986); Hellens *et al*. 2000
Plants		
Nicotiana benthamiana	Wild type	Dr. K. Sohn[a]
Nicotiana tabacum	Wisconsin 38	Dr. K. Sohn[a]

[a] Previously School of Agriculture and Environment (SAE), Massey University.

3.2.2 Growth conditions

3.2.2.1 Plant material

Nicotiana benthamiana and *Nicotiana tabacum* seeds were surface-sterilized with 70% ethanol for 5 min, rinsed with sterile water and germinated in TEKU® pots (Pöppelmann, Lohne, Germany) containing Dalton's Premium Seed Mix (Fruitfed, New Zealand) at 21°C in a controlled growth room with 70% humidity and a 12 h light/12 h dark photoperiod. At two weeks post-sowing, seedlings were transferred to individual pots containing Dalton's Potting Mix (Fruitfed, New Zealand) and grown at 21°C with the same photoperiod and light intensity conditions.

3.2.2.2 Bacterial strains

3.2.2.2.1 *Escherichia coli*

E. coli cells were cultured overnight in Lysogeny Broth (LB; 0.5% tryptone, 1% yeast extract, 0.5% NaCl) on a rotary shaker at 180 rpm (Bio-Line Incubator Shaker, Edwards Instrument Company, Wisconsin, USA) or on LB agar (0.5% tryptone, 1% yeast extract, 0.5% NaCl, 1.5% bacteriological agar (Acumedia®, Michigan, United States of America (USA)) at 37°C supplemented with 100 µg/ml ampicillin (ACTGene, New Jersey, USA) or 50 µg/ml kanamycin (ACTGene). For short-term storage, *E. coli* strains were streaked onto LB agar plates, incubated overnight at 37°C and stored at 4°C. For long-term storage, cells were stored in 30% (v/v) glycerol (Ajax lab chemicals, New South Wales, Australia) and stored at -80°C.

3.2.2.2.2 *Agrobacterium tumefaciens*

A. tumefaciens cells were cultured overnight in LB on a rotary shaker (180 rpm) (Ecotron, INFORS-HT, Bottmingen, Switzerland), or on LB agar for 48 h, at 28°C. For selection of transformants, kanamycin (ACTGene), rifampicin (Duchefa Biochemie, Haarlem, The Netherlands) and gentamicin (ACTGene) were added to a final concentration of 50 µg/ml, 10 µg/ml and 30 µg/ml, respectively. For short-term storage, *A. tumefaciens* strains were streaked onto LB agar plates, incubated for 48 h at 28°C and stored at 4°C. For long-term storage, cells were stored in 30% (v/v) glycerol (Ajax lab chemicals, New South Wales, Australia) and stored at -80°C.

3.2.3 *E. coli* and *A. tumefaciens* electrocompetent cell preparation

E. coli DH5α, JM110 or *A. tumefaciens* GV3101 cells from a glycerol stock were streaked onto LB agar plates and grown overnight at 37°C (*E. coli*) or for 48 h at 28°C (*A. tumefaciens*). A single colony was then inoculated into 25 ml of LB medium and cultured overnight at 180 rpm at 37°C (*E. coli*) or 28°C (*A. tumefaciens*). The next day, flasks containing 500 ml LB were inoculated with 10-20 ml of the overnight cultures and grown at 180 rpm until an OD_{600} 0.65-0.75 was reached. Cultures were then poured into pre-cooled sterile centrifuge tubes, left on ice for 20-30 min and collected by centrifugation at 4,700 *g* (Heraeus Megafuge 16R, TX-400 rotor, Thermo Scientific) for 20 min at 4°C. The supernatant was subsequently discarded, an equal volume (to the original volume

spun down) of 10% (v/v) sterile, chilled glycerol was added, and cells were gently resuspended by inversion. This step was repeated four times resuspending the cells (in half of the original volume spun down) in 10% (v/v) glycerol, until cells were collected in a single tube forming a thick cell suspension. From this cell suspension, 40 µl aliquots were placed into pre-chilled sterile 0.6 ml microtubes and snap-frozen in liquid nitrogen. Tubes were stored at -80°C until required.

3.2.4 DNA manipulation

3.2.4.1 Gene synthesis

CE genes of *V. inaequalis* were synthesized in the pTWIST plasmid (Fig. A.1) (with *Bsa*I restriction sites at both ends for subsequent cloning into the pICH86988 expression vector), or directly into pICH86988 (Fig. A.2); Addgene plasmid #48076; http://n2t.net/addgene:48076;RRID:Addgene_48076; Weber et al., (2011), by Twist Bioscience (San Francisco, California, USA), for use in ATTAs involving *N. benthamiana* and *N. tabacum* (see section 3.2.5). Here, the nucleotide sequence encoding each mature CE protein was fused to the nucleotide sequences encoding the *N. tabacum* Pathogenesis-Related protein 1α (PR1α) signal peptide sequence (for secretion into the plant apoplast) and a 3xFLAG (3xDYKDDDDK) tag (for detection by Western blotting) at its N-terminus (Hopp et al., 1988; Kamoun et al., 1998). pTWIST plasmids were propagated in the dam-/dcm- *E. coli* strain JM110, to prevent the methylation of the *Bsa*I sites that can occur in other strains.

3.2.4.2 Measurement of DNA concentration

DNA concentration was measured with a Spectrophotometer (DeNovix, Delaware, USA) according to the manufacturer's instructions.

3.2.4.3 Agarose gel electrophoresis

DNA was mixed with 0.25 volumes of SDS loading dye (0.2% (w/v) Bromophenol Blue (Avantor Sciences Inc., Pennsylvania, USA), 20% (w/v) sucrose, 1% (w/v) SDS and 5 mM EDTA, pH 6.8) and resolved on a 1% (w/v) agarose (HyAgaroseTM, HydraGene) gel in 1x Tris/acetic acid/EDTA (TAE) buffer pH 8.3 (190 mM Tris, 342 mM acetic acid (Emsure®, Merck, New Jersey, USA), 2.5 mM EDTA) at 80 V for 50 min. A 1 kb plus DNA

ladder (Invitrogen, Massachusetts, USA) was used as a size marker. DNA was stained with ethidium bromide (1 µg/ml) for 15 min then visualized with the Molecular Imager® Gel Doc™ XR system and the Image LabTM Software (BioRad, California, USA).

3.2.4.4 Plasmid DNA extraction

A single *E. coli* colony was grown overnight, as described in section 3.2.2.2.1, in 5 ml of LB with appropriate antibiotics. Plasmid DNA was isolated from harvested cells using the E.Z.N.A.® Plasmid Mini Kit I (Omega Bio-tek, Georgia, USA), as per the manufacturer's instructions.

3.2.4.5 Golden Gate Assembly

Plasmids generated using Golden Gate assembly were constructed using a one-step reaction (example in Fig. A.3). A 20 µl total volume of master mix reaction was prepared with 1 µl of T4 DNA ligase (New England Biolabs, Massachusetts, USA), 2 µl T4 DNA Ligase Buffer (10X), 1 µl *Bsa*IHF-v2 restriction enzyme (New England Biolabs), and 2 µl of bovine serum albumin (BSA) (10X) buffer. In addition, 10 fmol of each insert was added (pTWIST vector with *Bsa*I sites flanking the gene of interest and pICH86988 backbone). The reaction was performed in a Thermocycler (Eppendorf, Hamburg, Germany) with the following conditions: 25 cycles at 37°C for 3 min and 16°C for 4 min, followed by two inactivation cycles at 50°C and 80°C for 5 min each. A colony PCR (section 3.4.2.7) and custom DNA sequencing (Massey Genome Service, Massey University, Palmerston North, New Zealand) were performed to confirm sequence authenticity of each plasmid insert. Plasmids with the correct insert sequence were transformed into electrocompetent *A. tumefaciens* GV3101 (section 3.2.4.8) for agroinfiltration experiments.

3.2.4.6 Sepharose filtration

To remove contaminants from the Golden Gate reactions, a sepharose filtration was performed. A 600 µl microtube (with a small needle hole in the bottom) was inserted into a 1.6 ml microtube. Subsequently, 150 µl of resuspended Sepharose® 4B beads (Merck, Darmstadt, Germany) were added into the 600 µl microtube and centrifuged at 2,000 *g* for 3-5 min, until the Sepharose beads appeared dry. Following centrifugation, the microtube containing the dry beads was placed inside a clean 1.6 ml

microtube and the total Golden Gate reaction volume was added. Tubes were centrifuged at 2,000 *g* for 1 min to filter and collect the reaction into the 1.5 ml microtube.

3.2.4.7 Colony PCR

PCRs were set up in a final volume of 25 µl containing 0.5 µl of each (10 mM) forward and reverse primer, 0.5 µl of (10 mM) dNTPs, 2.5 µl of 10X ThermoPol® Reaction Buffer (New England Biolabs), 0.125 µl Taq DNA polymerase (New England Biolabs) and nuclease-free water to 25 µl. A few cells of each selected colony were carefully added into a tube containing all the reagents. The PCR cycling conditions were as follows: initial denaturation for 30 sec at 95°C, followed by 30 cycles of 15 sec at 95°C, 30 sec at 55°C, 1 min/kb at 68°C, and a final extension at 68°C for 5 min.

3.2.4.8 Transformation of *E. coli* and *A. tumefaciens*

E. coli and *A. tumefaciens* electrocompetent cells were transformed by electroporation using a MicroPulser (Bio-Rad, California, USA) according to the following protocol: 40 µl of cell suspension, thawed on ice, was mixed with 5 ng of plasmid DNA and incubated for 1-2 min. The mixture of cells and plasmid DNA was transferred to an ice-cold 0.2 mm electroporation cuvette, and a single pulse (2.5 kV) was applied. Following electroporation, 1 ml of LB was immediately added to the cuvette; cells were gently resuspended and transferred to a 1.6 ml microfuge tube and incubated for 1 h at 180 rpm (Bio-Line Incubator Shaker) and 37°C (*E. coli*) or 2 h at 180 rpm (Ecotron INFORS-HT) and 28°C (*A. tumefaciens*). Cells were then plated and incubated on LB agar using the appropriate selective antibiotics and temperature (see section 3.2.2).

3.2.5 *Agrobacterium tumefaciens* transformation assays (ATTAs)

Glycerol stocks of *A. tumefaciens* GV3101 harboring the desired plasmids were streaked onto LB agar plates containing the appropriate antibiotics and grown for 48 h at 28°C. A single *A. tumefaciens* colony was then inoculated into 3 ml of LB, supplemented with the appropriate antibiotics, and incubated at 28°C at 180 rpm overnight (until an OD_{600} of 0.4 to 2 was reached). The following day, cells were collected by centrifugation at 2,500 *g* for 5 min and resuspended in 1 ml infiltration buffer containing 10 mM $MgCl_2$:$6H_2O$ (BDH Ltd), 10 mM MES-KOH (Sigma, Missouri, USA) and

100 µM acetosyringone (Sigma, Missouri, USA). Resuspended cultures were adjusted to an OD_{600} of 0.5 and incubated at room temperature for 2-3 h. Cultures were infiltrated into the underside of 5- to 6-week-old *N. benthamiana* and *N. tabacum* fully extended leaves using a 1 ml needleless syringe (Terumo, Tokio, Japan). Infiltrated sites were marked with large circles (*N. benthamiana*) or small dots (*N. tabacum*). Photographs were taken 7 days post-infiltration.

3.2.6 Protein extractions

Two days after infiltration with *A. tumefaciens* GV3101 harboring the plasmid of interest (section 3.2.5), *Nicotiana* leaves were collected and flash frozen in liquid nitrogen. Frozen samples were ground to a fine powder in liquid nitrogen using a mortar and pestle. The powder was transferred to a 2 ml Eppendorf tube and resuspended in an equal volume of GTEN buffer (10% v/v glycerol, 100 mM Tris pH 7.5, 1 mM EDTA, 150 mM NaCl, 10 mM DTT, 0.2% IGEPAL CA360, 10 µl/ml protease inhibitory cocktail (Sigma-Aldrich, Missouri, USA), 1% w/v PVP). Then, samples were incubated at 4˚C on a Heidolph rotator (John Morris Scientific) at 60 rpm for 30 min. Samples were collected by centrifugation at 4˚C, 5,000 *g* for 20 min and the supernatant was collected and transferred to a 1.5 mL microtube through a small piece of miracloth (Merck, New Jersey, USA) and stored at -20˚C.

3.2.7 SDS polyacrylamide gel electrophoresis (PAGE)

Each crude protein sample was concentrated to half of the original volume using a SpeedVac vacuum concentrator (Savant SPD131DDA, Thermofisher Scientific, Massachusetts, USA) and mixed (in a 2:1 ratio) with 3x SDS protein loading dye (30% v/v glycerol, 3% w/v SDS, 94 mM v/v Tris (pH 7.5), 0.05% w/v bromophenol blue, 24 mM v/v DTT, in sterile water). The samples were boiled for 5 min and 15 µl were loaded onto 12% Tris-glycine gel prepared in two stages: firstly, the 12% resolution gel (12% v/v acrylamide (Bio-Rad, California, USA), 390 mM Tris v/v (pH 8.8), 0.1% SDS v/v, 0.1% v/v ammonium persulfate (APS) and 0.04% v/v tetramethylethylenediamine TEMED (Sigma); secondly the 5% stacking gel (5.1% v/v acrylamide, 130 mM v/v Tris (pH 6.8), 0.1% v/v SDS, 0.1% v/v ammonium persulfate, 0.001% v/v TEMED). Gels were immersed

in SDS running buffer (25 mM Tris, 192 mM glycine, 0.1% w/v SDS, pH 8.3) and resolved at 30 V for 30 min (stacking gel) and at 80 V for 90 min (resolving gel).

3.2.8 Western blotting

After SDS-PAGE, proteins were transferred to an Immun-Blot® polyvinylidene fluoride (PVDF) membrane (Bio-Rad), submerged in transfer buffer (25 mM v/v Tris, 190 mM v/v glycine, 20% v/v methanol (pH 8.3)) at 30 V and 4°C overnight. The PVDF membrane was blocked with Tris-Buffered saline and Tween 20 buffer TBST (20 mM Tris, 136 mM NaCl (pH 7.6), 10% v/v Tween 20) with 5% w/v skim milk for 1 h at room temperature with gentle shaking on a Heidolph rotator (John Morris Scientific, Sydney, Australia). The blocking solution was discarded and the membrane was incubated with 1:5,000-diluted anti-FLAG® M antibody (Sigma-Aldrich) produced in mouse, for 1.5 h, followed by three washes with TBST buffer for 10 min each. Then, the membrane was incubated with 1:20,000-diluted secondary antibody (chicken anti-mouse (Santa Cruz Biotechnology, Texas, USA)) for 1 h, followed by three washes with TBST for 10 min each. The membrane was incubated on 0.5 ml of SuperSignal™ West Pico Chemiluminescent Substrate (Thermo Fisher Scientific, Massachusetts, USA) for 5 min. The blots were visualized with an Azure c600 imager (Azure Biosystems, California, USA).

3.2.9 Selection and bioinformatic analysis of candidate effectors (CEs) from *Venturia inaequalis*

CE proteins were selected from pre-existing transcriptome sequencing (RNA-Seq) and proteomic data derived from *V. inaequalis* grown in culture on cellophane membranes overlying potato dextrose agar (PDA) and in potato dextrose broth (PDB), and during infection of apple leaves (*in planta*). Four CE proteins were derived from previous investigations of the morphogenic differentiation of *V. inaequalis* isolate MNH120 using cellophane membranes (Deng et al., 2017; Kucheryava et al., 2008; Mesarich et al., 2012). Eight CE proteins were derived from the analysis of *V. inaequalis* isolate MNH120 liquid cultures (at 30 days post-inoculation; dpi) that elicited a cell death response in different apple cultivars upon infiltration (Win et al., 2003; Mesarich et al., unpublished). A total of 121 CE proteins were identified from RNA-Seq data using two isolates of *V. inaequalis* (MNH120 and EU-B04) (Deng et al. 2017; Bowen et al.

unpublished, Le Cam et al. unpublished). Infections of isolate MNH120 were performed in 'Royal Gala' apple leaves, and samples collected at six time points: 12 and 24 h post-inoculation (hpi), as well as 2, 3, 5 and 7 dpi. EU-B04 infections were also performed in 'Royal Gala' apple leaves.

Bioinformatic analyses were performed using a pipeline that mainly involved the use of different bioinformatic tools available online. ApoplastP was used to predict if a CE localizes to the apoplast or inside host cells (Sperschneider et al., 2018). EffectorP 3.0, which uses features such as protein length, net charge, molecular weight, serine, cysteine and tryptophan content, was used to predict whether or not a CE is in fact an effector protein (Sperschneider & Dodds, 2021). SignalP 4.1 was used to predict the presence of an N-terminal SP (Nielsen, 2017), and then TargetP 2.0 to confirm these results by prediction of potential CEs entering the secretory pathway (Emanuelsson et al., 2000). Transmembrane helices of membrane proteins were predicted with the TMHMM server v. 2.0 (Krogh et al., 2001); proteins that contain a TM helix possibly have a fixed function in the cellular membrane (Sonah et al., 2016) so if a TM helix was predicted outside of the region covering the predicted signal peptide that CE was discarded. Big-PI was used to predict glycosylphosphatidylinositol (GPI)-anchored proteins targeted to the plasma membrane (Eisenhaber et al., 1999); the presence of this membrane anchor is another criterion to discard a CE. Similarity searches using the BLAST server (tBLASTn and BLASTp) (Altschul et al., 1997) were carried out in non-curated publicly available databases at the National Center for Biotechnology Information (NCBI) and the Joint Genome Institute (JGI). BLASTp similarity searches were performed using a cut off E-value of $1e^{-5}$. Identification of functional protein domains was performed using InterPro 86.0 (Blum et al., 2020).

3.2.10 Structural prediction of CE proteins

Structural predictions were performed using AlphaFold2 (Jumper et al., 2021) and the ColabFold server (Mirdita et al., 2021). To assess confidence, the predicted local-distance difference test (pLDDT) and global superposition metric template modelling score (TM-score) were used. pLDDT can range from 0 to 100, with pLDDT values of 70-90 indicating reasonable confidence, and a value of >90 depicting very high confidence.

TM-score ranges from 0 to 1. A value of 0.5 or higher indicates a similar fold between structures, whereas a value of 1 indicates a perfect match between structures. Structural comparisons were performed with the DALI server (Holm, 2020), with significant similarities measured by a Z-score above 2. Structural superimposition, electrostatic potential (surface charge) analysis and visualization were performed using the Alignment and APBS Electrostatics Plugins, respectively, in PyMol 2.5 (https://pymol.org/2/) (The PyMOL Molecular Graphics System, 2015) (DeLano, 2002)

3.2.11 Allelic variation of candidate effectors

tBLASTn was used to identify *CE* genes present in publicly available genome sequences of 88 *V. inaequalis* isolates (Bénaouf & Parisi, 2000; Caffier et al., 2015; Deng et al., 2017; Gladieux et al., 2008; Gladieux et al., 2010b; Le Cam et al., 2019; Lichtner, 2018; Parisi et al., 1994; Passey & Armitage, 2018; Roberts & Crute, 1994; Shiller et al., 2015) present at NCBI, and in two *V. inaequalis* isolates from this thesis (Chapter 2) present in a local Geneious database. Sequence alignments were performed using Clustal Ω (Madeira et al., 2019) to identify polymorphisms in these gene sequences and the proteins they are predicted to encode.

3.3 Results

3.3.1 Bioinformatic analysis of CE proteins from *Venturia inaequalis*

A total of 133 CEs of *V. inaequalis* were selected for use in ATTA experiments in the non-host plants *N. benthamiana* and *N. tabacum* prior to this project based on genes that were highly expressed or detected in three different culture conditions (see section 3.2.9). These proteins were first investigated using web-based bioinformatic tools to confirm that they had one or more features typical of characterized fungal effectors; that is, they are small (i.e. <300 amino acid residues in length), secreted (i.e. they possess an N-terminal SP), and are cysteine-rich (i.e. they contain four or more cysteine residues after the signal peptide cleavage site) (Franceschetti et al., 2017) (Table A.5). All of the CE proteins prioritized for investigation in this study were less than 300 aa residues in length except for CE1 (463 amino acids). Of all CEs, 118 contained one or more cysteine residues. Extracellular targeting was confirmed for all CEs by predicting an N-terminal secretion signal using the SignalP 4.1 server. Of the 133 CEs, 100 were predicted to be effectors using the EffectorP 3.0 server, five were defined as unlikely-effectors and 28 as non-effectors. A total of 130 CEs were predicted to enter the secretory pathway using the TargetP 2.0 server. Using the TMHMM 2.0 and Big-PI servers, none of the proteins were predicted to possess a transmembrane helix or a GPI anchor (Table A.5).

To determine which CEs have similarity to other proteins present in publicly available databases, a BLAST analysis using the NCBI and JGI databases was performed. Of the 133 CEs, 127 were similar to hypothetical proteins of unknown function (Table A.5). This result was expected, as a large number of effector proteins have low or no sequence similarities to proteins of known function. A brief overview of the CEs with sequence similarity to other functionally characterised proteins is given below. Based on BLASTp analyses, CE10 belongs to the hydrophobins, and thus was renamed ViHyd1. Although a BLASTp analysis in JGI returned no significant sequence identity to other proteins, in NCBI, 35 significant hits to hypothetical proteins and hydrophobin-like proteins with up to 30% amino acid identity were obtained, although restricted to Dothideomycetes. Consistent with what is known for hydrophobins (Wösten, 2001), all similar proteins possessed a conserved cysteine spacing profile (Fig. 3.1).

Using the BLASTp tool in the JGI database for CE11 resulted in the prediction of three lysin motif (LysM) domains. These domains have been previously characterized in the Ecp6 effector from *C. fulvum* (see section 1.5.4.1). CE11 has 30 to 40% amino acid identity to hypothetical proteins of Dothideomycetes (*Leptosphaeria maculans* and *Z. tritici*) and Eurotiomycetes (*Aspergillus niger* and *Aspergillus kawachi*). Based on BLASTp in NCBI, CE11 shares sequence similarity with hypothetical proteins and putative peptidoglycan-binding proteins in Dothideomycetes (120 hits; up to 70% amino acid identity), Eurotiomycetes (21 hits; up to 30% amino acid identity) and Sordariomycetes (7 hits; up to 30% amino acid identity). The closest similarity was observed to proteins from members of the *Venturia* genus (Fig. 3.2). Due to the mentioned features of this protein, it was renamed ViEcp6.

BLASTp analyses on CE12 and CE13 in NCBI, place these proteins in the plant natriuretic peptide-like (PNPL) family, and therefore were renamed ViPNPL5 and ViPNPL9, respectively. Using both ViPNPL5 and ViPNPL9 as BLASTp queries resulted in significant hits (45; up to 80% amino acid identity) to hypothetical proteins and PNPLs from members of the *Venturia* genus only (Fig. 3.3). In addition, a BLASTp analysis in JGI uncovered hits to other expansin-like domain-containing proteins of Sordariomycetes and plants.

Figure 3.1. Clustal Ω protein alignment of *Venturia inaequalis* (MNH120) candidate effector 10 (CE10) with similar proteins from other fungi. CE10 was aligned with the top nine similar proteins identified in the non-redundant (nr) protein database of NCBI using BLASTp. Protein IDs and species names are as follows: CE10 ViHyd1 *V. inaequalis*, hypothetical protein QDS70025 (*Venturia effusa*) (Young et al., 2019), hydrophobin-like protein 1 KAF4548267 (*Elsinoe fawcettii*) (Jeffress et al., 2020), hydrophobin-like protein 3 KAF4547054 (*E. fawcetti*) (Jeffress et al., 2020), hydrophobin-like protein 5 KAF4547255 (*E. fawcettii*) (Jeffress et al., 2020), hydrophobin-like protein 4 KAF4547248 (*E. fawcettii*) (Jeffress et al., 2020), hydrophobin 1 CAC43386 (*Xanthoria parietina*) (Scherrer & Honegger, 2003), uncharacterized protein XP_007673867 (*Baudoinia panamericana*) (Ohm et al., 2012), hydrophobin-like proteins KAF4547273 and KAF4548263 (*E. fawcettii*) (Jeffress et al., 2020). Predicted signal peptides are underlined. Cysteine residues are in bold font and amino acid conservation is shown in blue, with dark blue representing strict conservation.

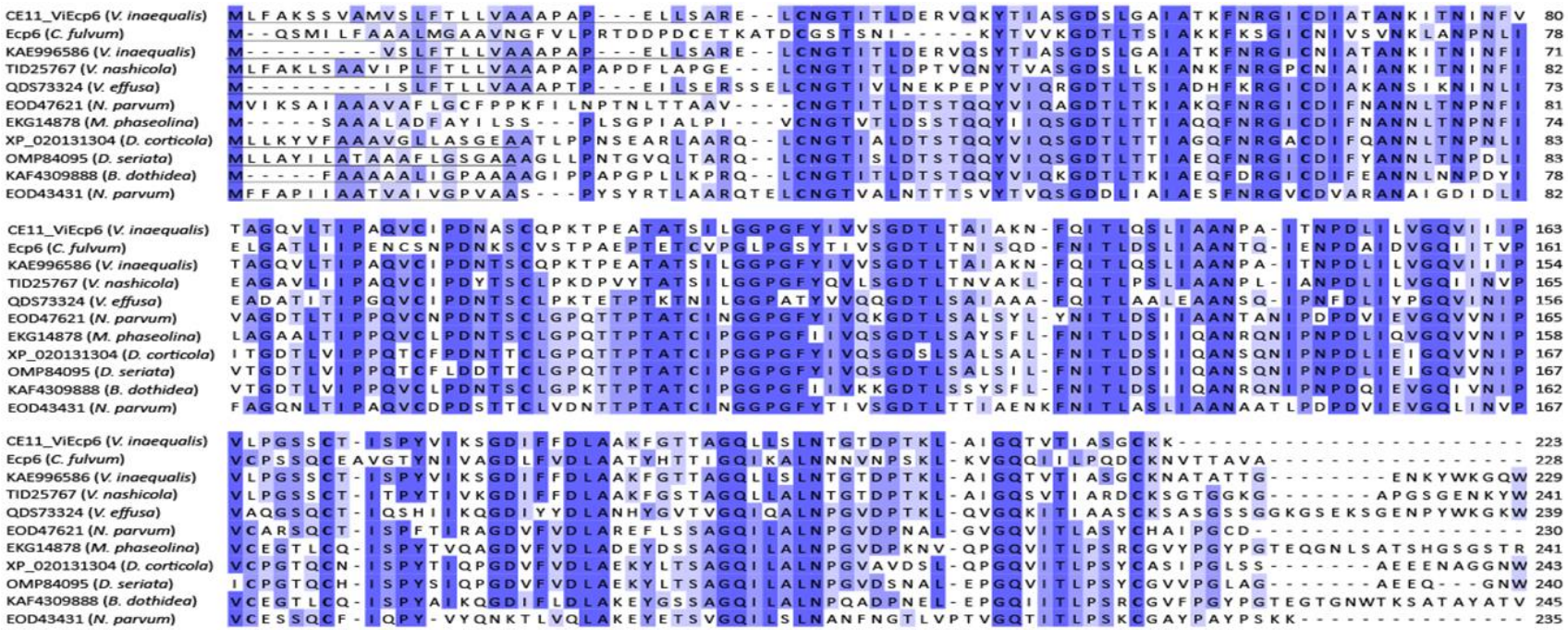

Figure 3.2. Clustal Ω protein alignment of *Venturia inaequalis* (MNH120) candidate effector 11 (CE11) with similar proteins from other fungi. CE11 was aligned with top ten similar proteins identified in the non-redundant (nr) protein database of NCBI using BLASTp. Protein IDs and species names are as follows: CE11 ViEcp6 (*V. inaequalis*) Ecp6 (*Cladosporium fulvum*) (Zaccaron & Stergiopoulos, 2021), hypothetical protein KAE9965866 (*V. inaequalis*) (Lichtner, 2018), putative peptidoglycan-binding lysin protein TID25767 (*Venturia nashicola*) (Prokchorchik et al., 2019), hypothetical protein QDS73324 (*Venturia effusa*) (Young et al., 2019), putative peptidoglycan-binding lysin protein EOD47621 (*Neofusicoccum parvum*) (Blanco-Ulate et al., 2013), peptidoglycan-binding lysin subgroup EKG14878 (*Macrophomina phaseolina*) (Islam et al., 2012), carbohydrate-binding module family 50 protein XP_020131304 (*Diplodia corticola*) (Fernandes et al., 2016), intracellular hyphae protein 1 OMP84095 (*Diplodia seriata*) (Robert-Siegwald et al., 2017), Intracellular hyphae protein 1 KAF4309888 (*Botryosphaeria dothidea*) (Yu et al., 2020), putative peptidoglycan-binding lysin protein EOD43431 (*N. parvum*) (Blanco-Ulate et al., 2013). Predicted signal peptides are underlined. Cysteine residues are in bold font and amino acid conservation is shown in blue, with with dark blue representing strict conservation. dark blue representing strict conservation.

Figure 3.3. Clustal Ω protein alignment of *Venturia inaequalis* (MNH120) candidate effectors 12 (CE12) and 13 (CE13) to similar proteins from members of the *Venturia* genus. CE12 and CE13 (*V. inaequalis* plant natriuretic peptide-likes, ViPNPLs) were aligned with the top eight similar proteins identified in the non-redundant (nr) protein database of NCBI using BLASTp. Protein IDs and species names are as follows: CE12 (ViPNPL-5) and CE13 (ViPNPL-9) (*V. inaequalis*), hypothetical protein RDI76995 (*V. inaequalis*) (Passey et al., 2018), ViPNPL-8 QDH43452 (*V. inaequalis*) (Wheeler et al., 2019), hypothetical protein RDI85909 (*V. inaequalis*) (Passey et al., 2018), ViPNPL-4 QDH43450, ViPNPL-2a QDH43447, ViPNPL-3 QDH43449 and ViPNPL-10 QDH43454 (*V. inaequalis*) (Wheeler et al., 2019), VpPNPL-7 QDH43462 (*Venturia pyrina*) (Wheeler et al., 2019). Predicted signal peptides are underlined. Cysteine residues are in bold font and amino acid conservation is shown in blue, with dark blue representing strict conservation.

3.3.2 Three CE proteins of *V. inaequalis* trigger chlorosis and/or cell death in *Nicotiana* species

To assess whether any of the *V. inaequalis* CEs are potentially recognized as IPs by IPRs IN non-host plants, each was expressed in leaves of *N. benthamiana* and *N. tabacum* using ATTAs (agroinfiltrations), and their ability to trigger necrotic cell death or chlorotic responses examined 7 days post-infiltration. In total, 132 out of the 133 CE proteins of *V. inaequalis* were successfully screened for their ability to trigger chlorosis or cell death in both *Nicotiana* species using ATTAs. The only CE protein that could not be screened was CE1, which contained a long repetitive sequence in its encoding gene that prevented its synthesis by Twist Bioscience and cloning by Golden Gate assembly. As expected, INF1, a *Phytophthora infestans* elicitin protein (Bos et al., 2006; Kamoun et al., 1998) used as the positive control in this study, consistently triggered cell death in both *Nicotiana* species (Fig. 3.4). INF1 was chosen as the positive control as it is known to trigger cell death upon recognition by a cell surface lectin-like receptor kinase pattern recognition receptor (PRR) in *Nicotiana* species (e.g. NbLRK1 in *N. benthamiana*) (Kanzaki et al., 2008). Also as expected, the empty vector pICH86988, used as the negative control in this study, did not trigger chlorosis or cell death in either *Nicotiana* species (Fig. 3.4). Here, only a ring of necrosis associated with mechanical damage at the infiltration site (i.e. when pressure was applied by the tip of the needleless syringe to facilitate infiltration) was observed.

Of the 132 CE proteins of *V. inaequalis* screened, only three triggered a consistent response based on chlorosis and/or cell death (i.e. across three or more biological replicates) in one or both of the *Nicotiana* species. The first of these three, CE17, induced a strong cell death response in *N. tabacum*, where the entire infiltration zone was necrotic, while in *N. benthamiana*, the same CE only induced patchy cell death across approx. 25% of the infiltration site (Fig. 3.4). The second CE protein, CE93, triggered a chlorotic response across the entire infiltration zone in *N. benthamiana*, but no chlorosis or cell death in *N. tabacum* (Fig. 3.4). The third CE protein, CE126, induced a strong cell death response in *N. tabacum* only, covering the complete infiltration site, but no chlorosis or cell death in *N. benthamiana* (Fig. 3.4). These results suggest that

CE17, CE93 and CE126 are recognized as IPs by IPR proteins in *N. benthamiana* and/or *N. tabacum* to activate the immune system of these model non-host plants.

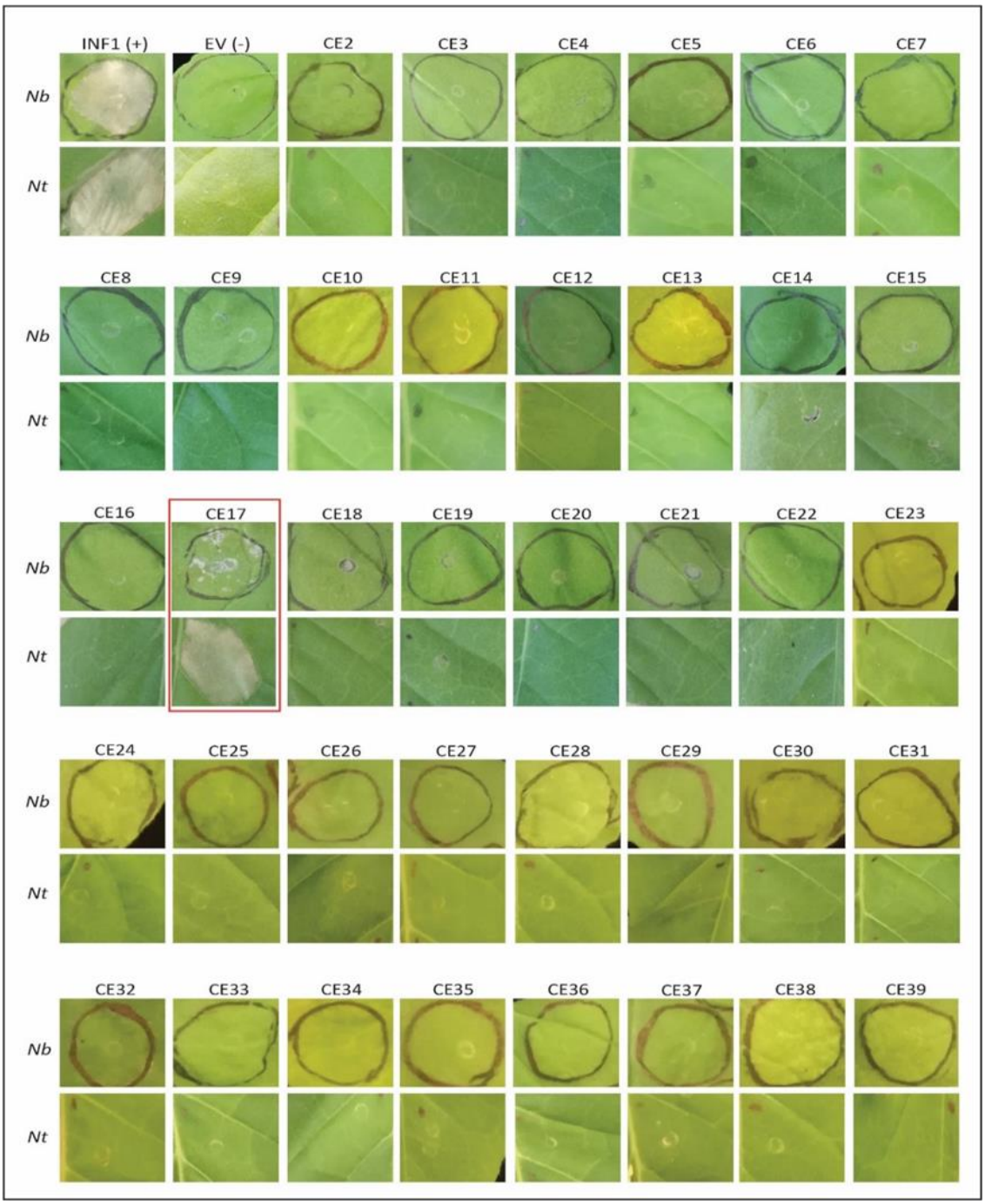

Figure 3.4. Three candidate effectors (CEs) of *Venturia inaequalis* trigger chlorosis and/or cell death in the model non-host species *Nicotiana benthamiana* (*Nb*) and *Nicotiana tabacum* (*Nt*) using an *Agrobacterium tumefaciens*-mediated transient expression assay (ATTA). The INF1 elicitin protein from *Phytophthora infestans* was used as a positive control and empty vector pICH86988 (EV) as a negative control. CE proteins of *V. inaequalis* that triggered chlorosis and/or cell death in *Nb* and/or *Nt* are boxed in red. All proteins were directed to the apoplast using the pathogenesis-related protein 1 (PR1α) signal peptide. Photos were taken at 7 days post-infiltration and are representative of at least three independent ATTA experiments.

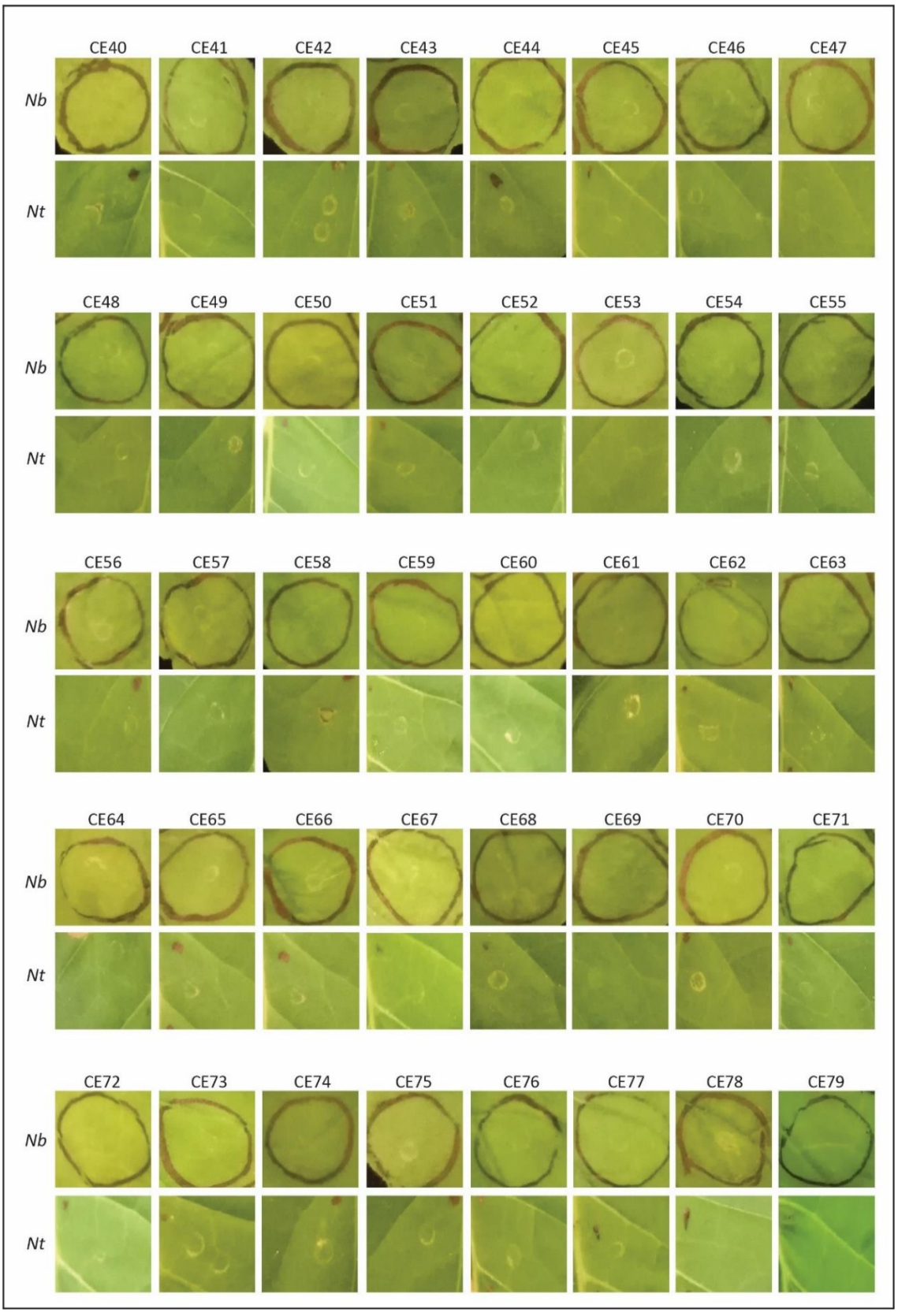

Figure 3.4 (continued).

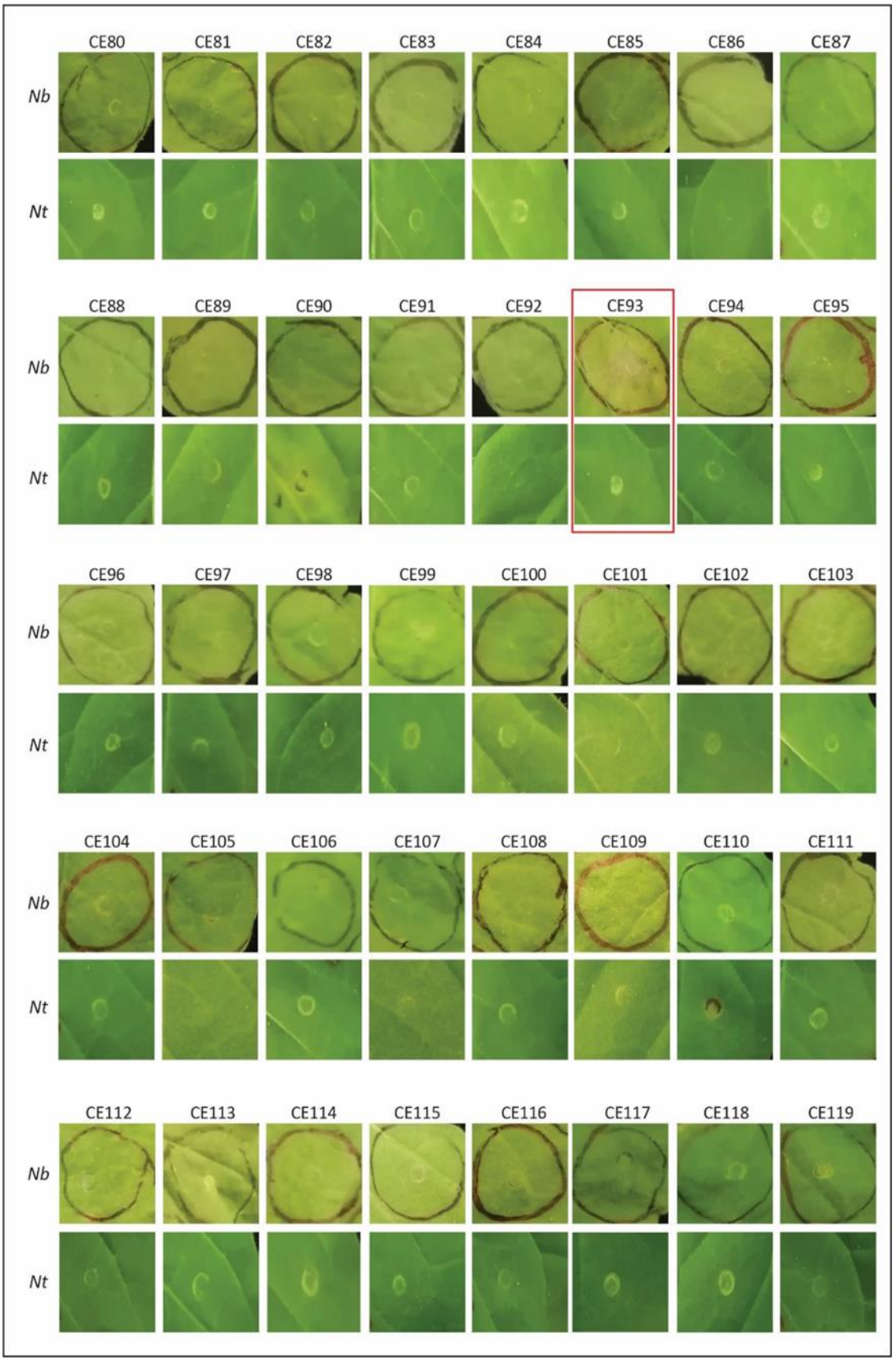

Figure 3.4 (continued).

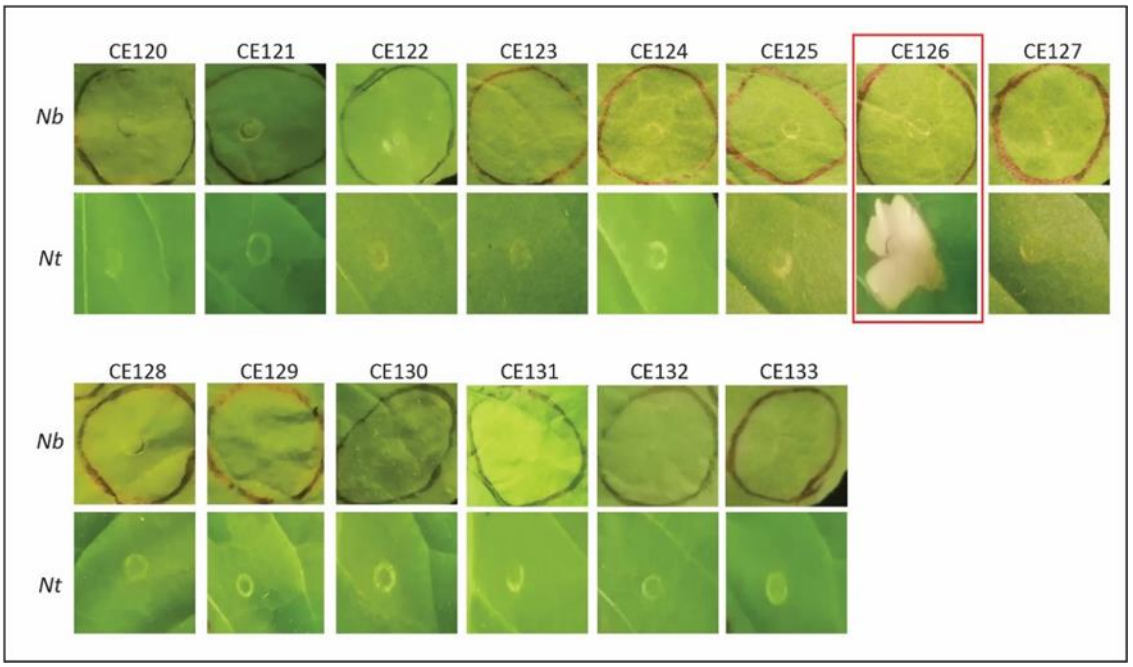

Figure 3.4 (continued).

3.3.3 Apoplastic localization is required for CE proteins of *V. inaequalis* to trigger chlorosis and/or cell death in *Nicotiana* species

In the ATTAs of section 3.3.2, the PR1α signal peptide of *N. tabacum* was used to deliver *V. inaequalis* CE proteins into the apoplast of *N. benthamiana* and *N. tabacum* leaves. While the CE proteins CE17, CE93 and CE126 were identified that trigger chlorosis and/or cell death in *N. benthamiana* and/or *N. tabacum* using this approach, this experiment did not provide any information on whether these responses are dependent on apoplastic localization (i.e. it remains possible that CE17, CE93 and CE126 triggered chlorosis and/or cell death prior to secretion, while still inside the plant cell). To determine whether apoplastic localization is required for the ability of CE17, CE93 and CE126 to trigger chlorosis and/or cell death in *N. benthamiana* and/or *N. tabacum*, each CE was expressed using an ATTA as before, but without the PR1α signal peptide. Consistent with that observed previously, the INF1 positive control protein triggered a strong cell death response in both *Nicotiana* species, while the EV negative control protein triggered no response (Fig. 3.5A). However, unlike that observed in section 3.3.2., versions of the CE17, CE93 and CE126 proteins without a signal peptide (ΔSP) failed to trigger chlorosis and/or cell death in *N. benthamiana* and/or *N. tabacum* (Fig.

3.5A). This inability to trigger chlorosis and/or cell death was not due to absence of the CE protein, as each could be detected from agroinfiltrated plants by Western blotting; the predicted molecular weights are CE17 ~15 kDa; CE93 ~22 kDa and CE126 ~22 kDa. The multiple bands observed in Western blots with protein versions containing a signal peptide are likely due to the post-translational modifications that occur at the ER-Golgi pathway (Fig. 3.5B). Taken together, these results suggest that apoplastic localization is required for the ability of the CE17, CE93 and CE126 proteins to trigger chlorosis and/or cell death in *N. benthamiana* and/or *N. tabacum.*

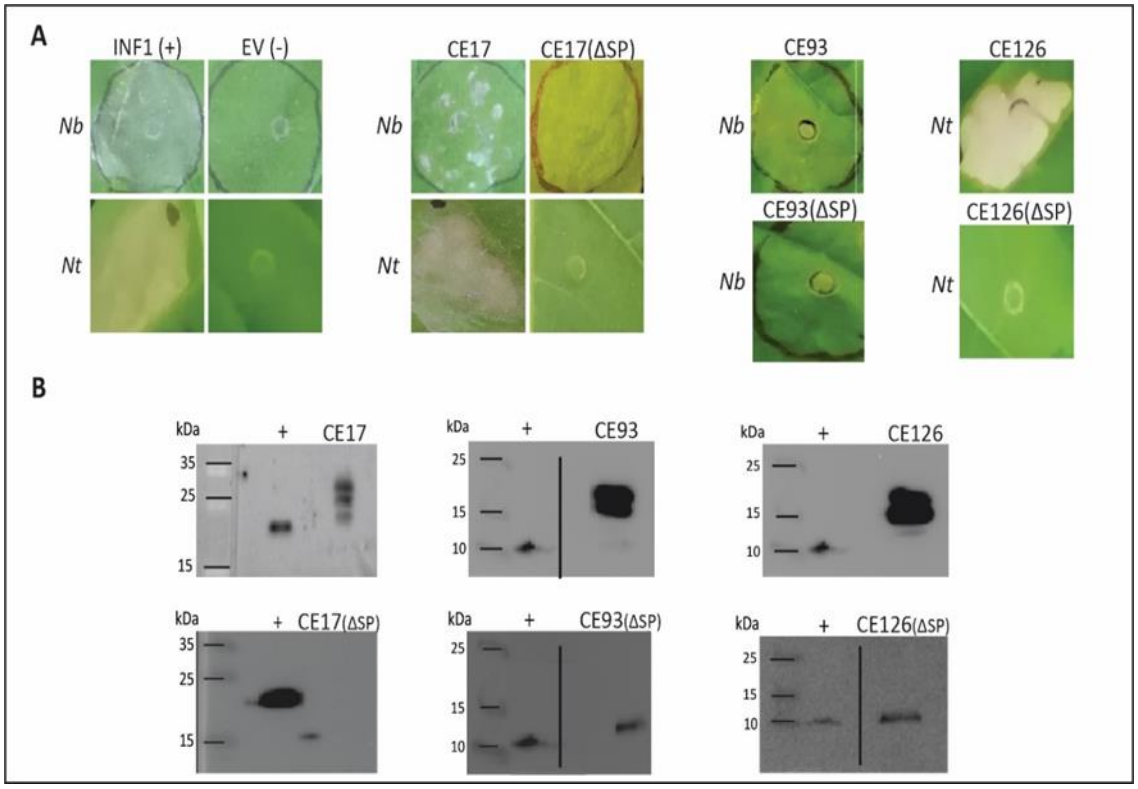

Figure 3.5. Apoplastic localization is required for candidate effector (CE) proteins of *Venturia inaequalis* to trigger chlorosis and/or cell death in *Nicotiana benthamiana* (*Nb*) and *Nicotiana tabacum* (*Nt*). (A) The *V. inaequalis* proteins CE17, CE93 and CE127 were expressed in *Nb* and *Nt* with or without the pathogenesis-related protein 1α (PR1α) signal peptide (SP or ΔSP, respectively) using an *Agrobacterium tumefaciens*-mediated transient expression assay (ATTA), and the presence or absence of chlorosis or cell death assessed at 7 days post-infiltration. Photos are representative of at least three independent ATTA experiments. **(B)** Protein detection by Western blotting. Protein samples were collected from leaf samples and the 3xFLAG tag was used for detection. Positive controls are a *Dothistroma septosporum* CE MW=10 kDa (Tarallo, unpublished), and a *Phytophthora agathidicida* RxLR effector MW=24 kDa (Guo et al., 2020) . Horizontal lines in the blots indicate blots that were cropped for figure simplification, original blots appear in Figure A.8.

3.3.4 CE proteins of *V. inaequalis* that trigger chlorosis and/or cell death in *Nicotiana* species are cysteine-rich and encoded by genes that are expressed during infection of apple leaves

Inspection of the sequences corresponding to the three *V. inaequalis* CE proteins that induced chlorosis and/or cell death in *N. benthamiana* and/or *N. tabacum* revealed that CE17 is 165 amino acid residues in length, with a predicted signal peptide of 20 amino acids, and contains five cysteine residues. CE93 is 241 amino acid residues in length, has a predicted signal peptide of 24 amino acids, and has 6 cysteines, while CE126 is 240 amino acid residues in length, has a predicted signal peptide of 19 amino acids, and contains 6 cysteine residues (Fig. 3.6A).

Pre-existing transcriptome sequencing (RNA-Seq) data from *V. inaequalis* grown in culture on the surface of cellophane membranes overlaying PDA at 7 days post-inoculation (dpi), as well as *in planta* during infection of susceptible apple leaves from cultivar 'Royal Gala' at 12- and 24-hours post-inoculation (hpi), as well as 2, 3, 5 and 7 dpi, has been collected in the Mesarich laboratory (Rocafort et al. unpublished). Using these data, expression of the genes encoding the three *V. inaequalis* CE proteins that induced chlorosis and/or cell death in *N. benthamiana* and/or *N. tabacum* was inspected. This revealed that the *CE17* gene is most highly expressed on cellophane but it is also highly expressed during the first two days of apple leaf infection, with expression peaking at 12 hpi (Fig. 3.6B). The expression of the *CE93* gene peaks at 12 hpi and reduced after 24 hpi (Fig. 3.6B). Finally, *CE126* is the lowest expressed of the three *CE* genes during infection, with the highest expression occurring during the early stage of infection at 12 hpi (Figure 3.6B).

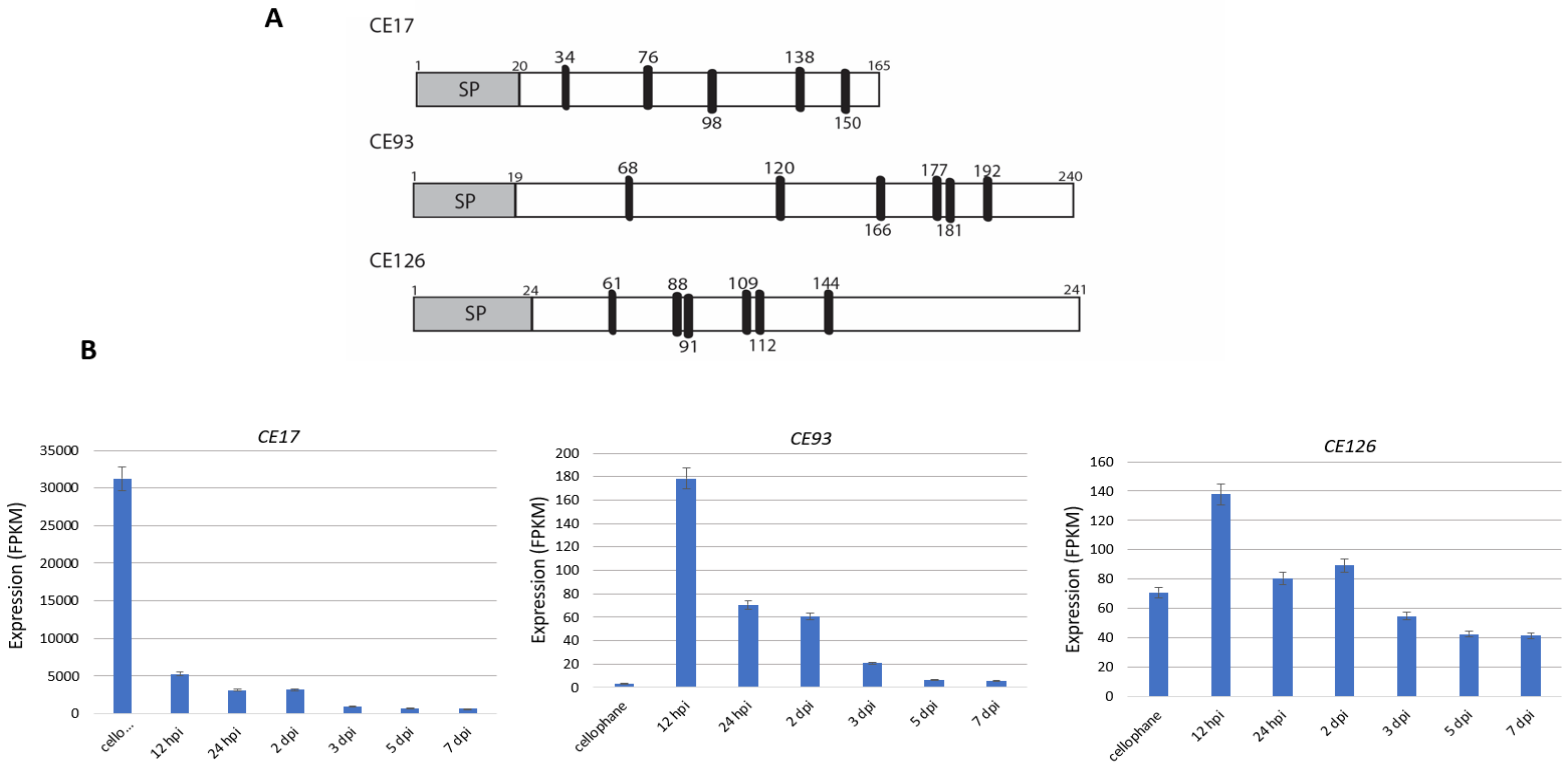

Figure 3.6. Candidate effectors (CEs) of *Venturia inaequalis* (MNH120) that trigger chlorosis and/or cell death in the model non-host species *Nicotiana benthamiana* and *Nicotiana tabacum* are small secreted cysteine-rich proteins, and are encoded by genes that are expressed *in planta*. (A) Schematic representation of the three CE proteins from *V. inaequalis* that trigger chlorosis and/or cell death in the model non-host species *N. benthamiana* and/or *N. tabacum*. All three CE proteins contain a putative signal peptide (SP) for secretion (predicted cleavage sites shown by thin vertical bars) and are cysteine-rich (shown by thick vertical bars and numbered according to their position in the full-length protein sequence). The full protein length is also shown at the end of each schematic. **(B)** RNA-Seq transcriptome data for the three CE genes presented as fragments per million per kilobase (FPMK) values. Hpi, hours-post inoculation; dpi, days post-inoculation. Error bars represent the standard deviation of four biological replicates.

3.3.5 CE proteins of *V. inaequalis* that trigger cell death in *Nicotiana* species have sequence similarity to effector proteins from plant-pathogenic fungi

To determine whether similar proteins to the three CE proteins from *V. inaequalis* that induce chlorosis and/or cell death in *N. benthamiana* and/or *N. tabacum* are present in other fungi, and if so, whether these proteins are restricted to fungal pathogens, each was screened for similar proteins present in NCBI and JGI using BLASTp. Based on this analysis, CE17 was found to have similarity to hypothetical proteins as well as putative Alt a 1-like proteins in Dothideomycetes such as *Alternaria* and *Cercospora* species, and the Sordariomycete *V. dahliae*, with the top hit to an Alt a 1-like protein in *Lasiodiplodia theobromae* (40% amino acid sequence identity) (Félix et al., 2019) (Fig. 3.7). Notably, similar proteins included Alt a 1 from the opportunistic broad host-range leaf spot, rot and blight pathogen of plants, *Alternaria alternata* (38% amino acid identity) (Troncoso-Rojas & Tiznado-Hernández, 2014), Ste b 1 from the sugar beet leaf spot pathogen *Cercospora beticola* (39% amino acid sequence identity) (De Jonge et al., 2018; Weiland & Koch, 2004), and PevD1 from the Verticillium wilt pathogen, *V*. *dahliae* (24% amino acid identity) (Song et al., 2020; Wang et al., 2012) (Fig. 3.7). To gain further insights into the function of CE17, InterPro was used to identify possible functional domains in the protein. This analysis revealed that CE17 belongs to the Alt a 1 family of proteins found exclusively in fungi that are characterized by a domain containing 2 conserved intramolecular disulfide bonds.

A BLASTp analysis in NCBI and JGI using CE93 as a query resulted in sequence similarity to hypothetical proteins in Dothideomycetes, with the top hits in *V. inaequalis* (98% amino acid identity) (Lichtner et al., 2020) and the Asian pear pathogen *Venturia nashicola* (89% amino acid identity) (Prokchorchik et al., 2019) (Fig. 3.8). Interestingly, similar proteins are also present in fungi that cause human diseases such as *Verruconis gallopava* (74% amino acid identity) (Cuomo et al., 2016), responsible for skin infections (phaeohyphomycosis) and in some cases, cardiac and endovascular infections (Jennings et al., 2016). Similar proteins are also present in fungal epiphytes such as *Microthyrium microscopicum* (70% amino acid identity) (Haridas et al., 2020; Wu et al., 2011), and the freshwater saprobic fungus *Clohesyomyces aquaticus* (65% identity) (Hyde, 1993;

Mondo et al., 2017) (Fig. 3.8). InterPro analysis revealed that this candidate belongs to the *Erysiphe graminis* f. sp. *hordei* 16-like (Egh16-like) family of proteins that are likely involved in germination and appressorium formation (Justesen et al., 1996).

Similarity searches in JGI using CE126 as a query uncovered low sequence similarity (~50% amino acid identity) to hypothetical proteins in the Dothideomycetes *L*. *maculans* and *Pyrenophora tritici*-r*epentis* (Birren et al., 2008; Rouxel et al., 2011), and putative cellulases in the Eurotiomycetes *Aspergillus fumigatus* and *Aspergillus niger* (~50% amino acid identity) (Andersen et al., 2011; Nierman et al., 2005). According to NCBI, CE126 possesses sequence similarity to hypothetical proteins, barwin-like endoglucanases, and carbohydrate-binding module family proteins of fungal pathogens from the Dothideomycete, Eurotiomycete and Sordariomycete classes. Among the top hits are a hypothetical protein in *V. inaequalis* (98% amino acid identity) (Lichtner, 2018) (Fig. 3.9), a barwin-like endoglucanase from the *V. nashicola* (75% amino acid identity) (Ishii & Yanase, 2000; Prokchorchik et al., 2019), and a carbohydrate-binding module family protein from the destructive fungus *Bipolaris victoriae*, causal agent of Victoria blight of oats (Condon et al., 2013; Taylor, 2020) (50% amino acid identity) (Fig. 3.9). InterPro analysis revealed matches to the RlpA-like domain superfamily of proteins that possess a unique double-psi beta barrel (DPPB) domain (section 3.3.6).

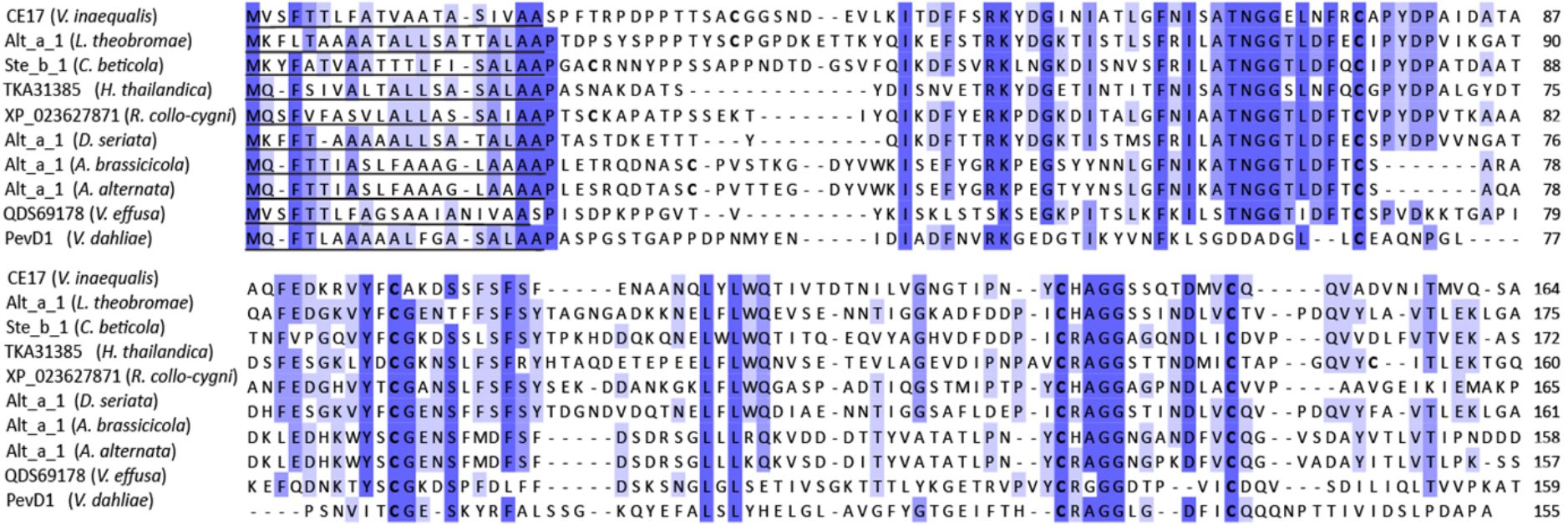

Figure 3.7. Candidate effector 17 (CE17) of *Venturia inaequalis* (MNH120) has sequence similarity to proteins from other fungi. CE17 was aligned with top nine similar proteins identified in the non-redundant (nr) protein database of NCBI using BLASTp. Protein IDs and species names are as follows: CE17 (*V. inaequalis*), Alt_a_1 KAB2573166 (*Lasiodiplodia theobromae*) (Félix et al., 2019), allergen Ste b 1 XP_023454096 (*Cercospora beticola*) (De Jonge et al., 2018), hypothetical protein TKA31385 (*Hortaea thailandica*) (Coleine et al., 2019), uncharacterized protein XP_023627871 (*Ramularia collo-cygni*) (Guldener, 2018), putative major allergen Alt a 1 KKY13371 (*Diplodia seriata*) (Morales-Cruz et al., 2015), Alt a 1 AAM18717 (*Alternaria brassicicola*) (Cramer & Lawrence, 2003), major allergen Alt a 1 QVK09752 (*Alternaria alternata*) (Pieczul, 2021), hypothetical protein QDS69178 (*Venturia effusa*) (Young et al., 2019), PevD1 (*Verticillium dahliae*) (Wang et al., 2012). Predicted signal peptides are underlined. Cysteine residues are in bold font and amino acid conservation is shown in blue, with dark blue representing strict conservation.

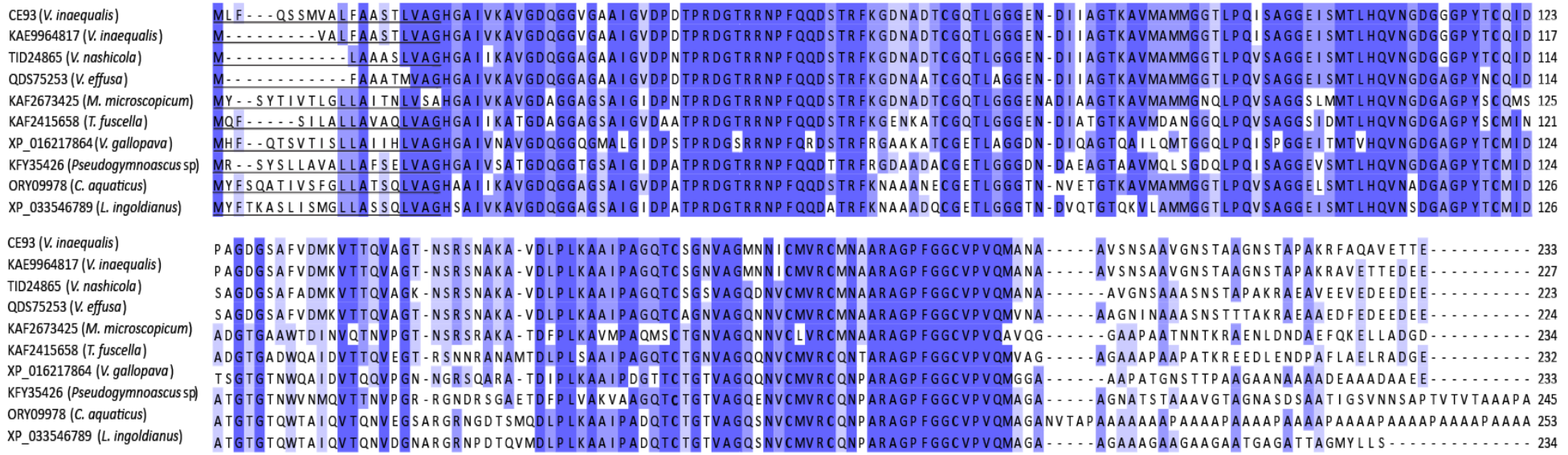

Figure 3.8. Candidate effector 93 (CE93) of *Venturia inaequalis* (MNH120) has sequence similarity to hypothetical proteins from other fungi. CE93 was aligned with top nine similar proteins identified in the non-redundant (nr) protein database of NCBI using BLASTp. Hypothetical protein IDs and species names are as follows: CE93 (*V. inaequalis*), KAE9964817 (*V. inaequalis*) (Lichtner, 2018), TID24865 (*Venturia nashicola*) (Prokchorchik et al., 2019), QDS75253 (*Venturia effusa*) (Young et al., 2019), KAF2673425 (*Microthyrium microscopicum*) (Haridas et al., 2020), KAF2415658 (*Tothia fuscella*) (Haridas et al., 2020), XP_016217864 (*Verruconis gallopava*) (Cuomo et al., 2016), KFY35426 (*Pseudogymnoascus sp.*) (Leushkin et al., 2015), ORY09978 (*Clohesyomyces aquaticus*) (Mondo et al., 2017), XP_033546789 (*Lindgomyces ingoldianus*) (Haridas et al., 2020). Predicted signal peptides are underlined. Cysteine residues are in bold font and amino acid conservation is shown in blue, with dark blue representing strict conservation.

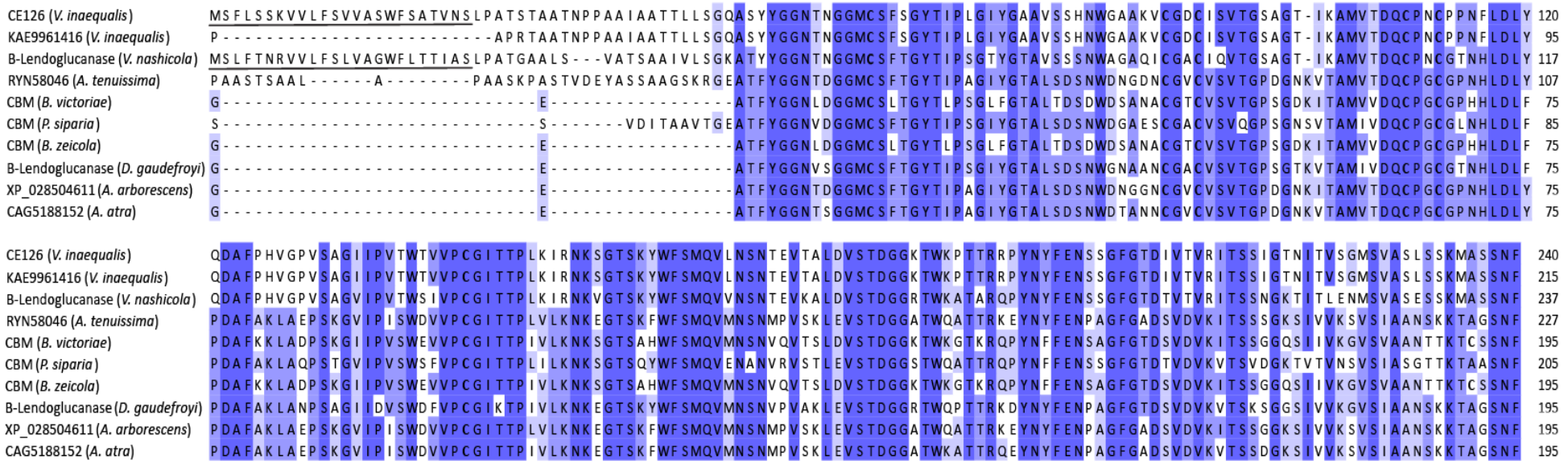

Figure 3.9. Candidate effector 126 (CE126) of *Venturia inaequalis* (MNH120) has sequence similarity to proteins from Dothideomycete fungi. CE126 was aligned with top nine similar proteins identified in the non-redundant (nr) protein database of NCBI using BLASTp. Protein IDs and species names are as follows: CE126 (*V. inaequalis*), hypothetical protein KAE9961416 (*V. inaequalis*) (Lichtner, 2018), barwin-like (B-L) endoglucanase TID19147 (*Venturia nashicola*) (Prokchorchik et al., 2019), hypothetical protein RYN58046 (*Alternaria tenuissima*) (Armitage et al., 2019), carbohydrate-binding module (CBM) family protein XP_014559948 (*Bipolaris victoriae*) (Condon et al., 2013), CBM family protein KAF2715297 (*Pleomassaria siparia*) (Haridas et al., 2020), CBM family protein XP_007707584 (*Bipolaris zeicola*) (Condon et al., 2013), barwin-like (B-L) endoglucanase KAF1838997 (*Decorospora gaudefroyi*) (Haridas et al., 2020), hypothetical protein XP_028504611 (*Alternaria arborescens*) (Armitage et al., 2019), unnamed protein CAG5188152 (*Alternaria atra*) (Stam, 2021). Predicted signal peptides are underlined. Cysteine residues are in bold font and amino acid conservation is shown in blue, with dark blue representing strict conservation. Signal peptides for larger proteins are not shown.

3.3.6 CE proteins of *V. inaequalis* that trigger cell death in *Nicotiana* species have structural similarity to proteins from plant-pathogenic fungi with characterized tertiary structures

To confirm that CE17 and CE126 have an Alt a 1- and expansin-type fold, respectively, and to gain further insights into the tertiary structure and thus virulence function of CE93, the tertiary structures of all three CEs were predicted using AlphaFold2 (Jumper et al., 2021). For CE17, AlphaFold2 predicted a tertiary structure with a pLDDT score of 86.02, and a predicted TM-score of 0.78 (Fig. 3.10). Consistent with the BLASTp similarity searches, comparison of the predicted CE17 tertiary structure with solved tertiary structures present in the RCSB Protein Data Bank using the Dali server (Holm, 2020) revealed that this protein has structural similarity to PevD1 (RCSB protein data bank (PDB) ID: 5XMZ) from *V. dahliae* (Zhou et al., 2017) and Alt a 1 (RSCB protein data bank (PDB) ID: 3V0R) from *A. alternata* (Chruszcz et al., 2012) (Fig. 3.10). The structure of these Alt a 1-like proteins has a unique β-barrel fold formed by 10 or 11 β-strands linked by two disulphide bonds (Fig. 3.10). As observed in Figure 3.7, all Alt a 1-like proteins possess 4 conserved cysteine residues to form intramolecular disulphide bonds (Chruszcz et al., 2012).

For CE93, AlphaFold2 predicted a tertiary structure with a pLDDT score of 87.54, and a predicted TM-score of 0.80 (Fig. 3.11). The comparison of the predicted structure of CE93 with previously solved structures present in the Protein Data Bank using the Dali server revealed structural similarity to lytic polysaccharide monooxygenases (LPMOs), specifically the LPMO AA15 from the insect *Thermobia domestica* (RSCB protein data bank (PDB) ID: 5MSZ) (Sabbadin et al., 2018), and the LPMO AA13 from *Aspergillus oryzae* (RSCB protein data bank (PDB) ID: 4OPB) (Hemsworth et al., 2014) (Fig. 3.11). These proteins are characterized by a central β-sandwich fold containing various loops and two or more disulfide bonds (Fig. 3.11).

For CE126, AlphaFold2 predicted tertiary structure with a pLDDT score of 93.12, and a predicted TM-score of 0.86 (Fig. 3.12). When comparing the predicted structure of CE126 with solved tertiary structures in structures present in the Protein Data Bank using the Dali server (Holm, 2020), structural similarity to bacterial and plant expansins

was shown, specifically to the expansin-like protein EXLX1 (RSCB PDB ID: 3D30) from the bacterium *Bacillus subtilis* (Kerff et al., 2008), and the beta-expansin EXPB1 from maize (RSCB PDB ID: 2HCZ) (Yennawar et al., 2006) (Fig. 3.12). Such proteins are characterized by a double psi-beta barrel fold (DPBB) (de Oliveira et al., 2011). However, similar to CE93, the predicted structure of CE126 appears to have a disordered region, but in this case at the N-terminus.

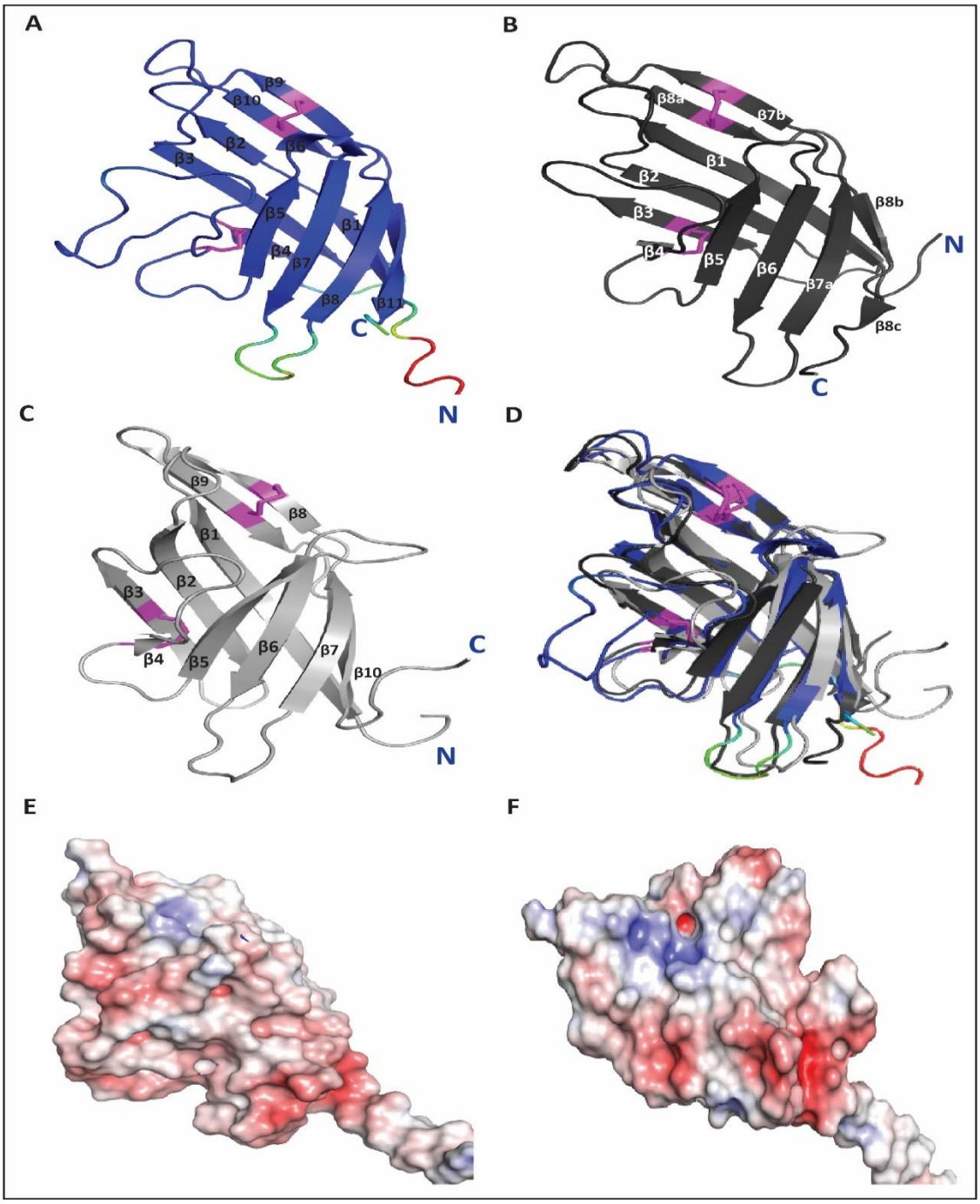

Figure 3.10. Predicted tertiary structure of Candidate Effector 17 (CE17) from *Venturia inaequalis.* (A) Tertiary structure of CE17 predicted by Alphafold2 (Jumper et al., 2021). Structure is coloured according to the pLDDT score: dark blue for highly confident predicted regions; light blue and green for regions of low confidence and red for disordered regions. Disulfide bonds are shown as purple sticks. **(B)** Solved crystal structure of Alt a 1 (RCSB protein data bank (PDB) ID: 3V0R) from *Alternaria alternata* (Chruszcz et al., 2012). **(C)** Solved crystal structure of PevD1 (RCSB protein data bank (PDB) ID: 5XMZ) from *Verticillium dahliae* (Zhou et al., 2017). The β strands and α helices are numbered sequentially. The N- and C-termini are labelled in each panel. **(D)** Structural superimposition of CE17, PevD1 and Alt a 1. **(E-F)** Surface charge potential of CE17 (rotated 180° around the y axis) Blue represents positive charge and red negative charge. Tertiary structures were superimposed, visualized and rendered using PyMol (https://pymol.org/2/) (The PyMOL Molecular Graphics System, 2015) (DeLano, 2002).

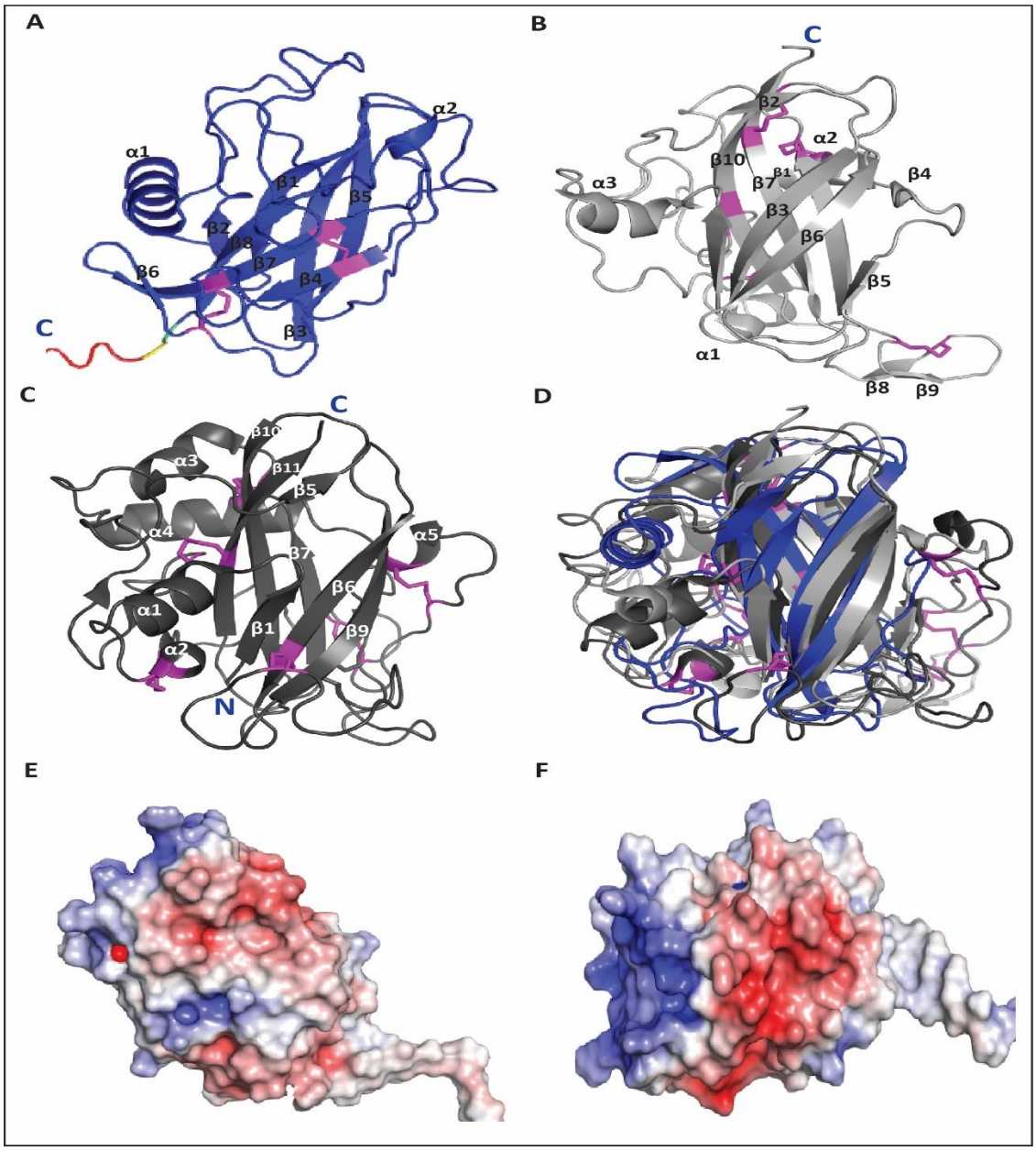

Figure 3.11. Predicted structure of candidate effector 93 (CE93) from *Venturia inaequalis.* (A) Tertiary structure of CE93 predicted by AlphaFold2 (Jumper et al., 2021). Structure is coloured according to the pLDDT score: dark blue for highly confident predicted regions; light blue and green for regions of low confidence and red for disordered regions. Disulfide bonds are shown as purple sticks. **(B)** Solved crystal structure of the lytic polysadccharide monooxygenase (LPMO) AA15 from the insect *Thermobia domestica* (RSCB protein data bank (PDB) ID: 5MSZ) (Sabbadin et al., 2018). **(C)** Solved crystal structure of LPMO AA13 from *Aspergillus oryzae* (RSCB protein data bank (PDB) ID: 4OPB) (Hemsworth et al., 2014). The β strands and α helices are numbered sequentially. The N- and/or C-termini are labelled in each panel. **(D)** Structural superimposition of CE93, LPMO AA15 and LPMO AA13. **(E-F)** Surface charge potential of CE93 (rotated 180° around the y axis). Blue represents positive charge and red negative charge. Tertiary structures were superimposed, visualized and rendered using PyMol (https://pymol.org/2/) (The PyMOL Molecular Graphics System, 2015) (DeLano, 2002).

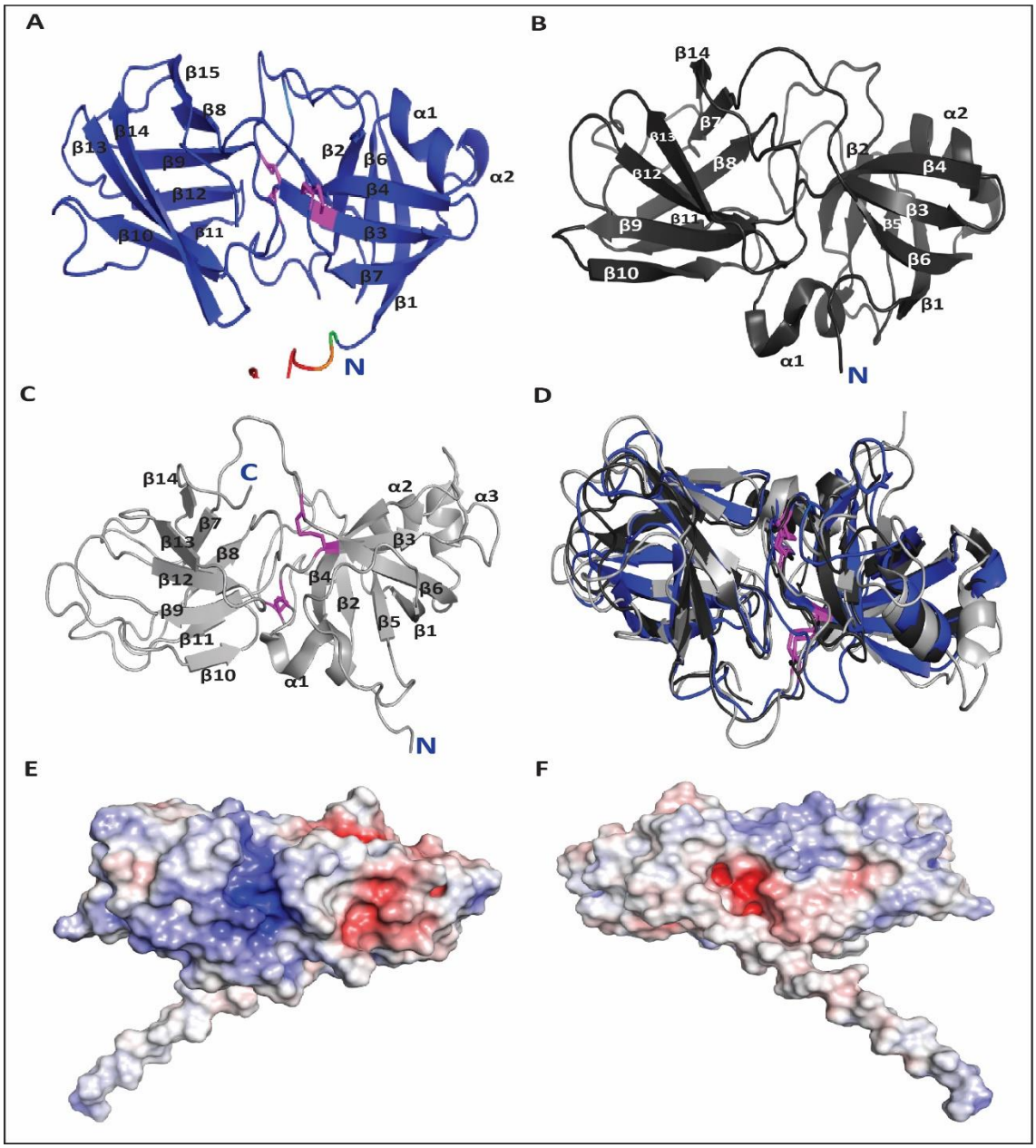

Figure 3.12. Predicted structure of candidate effector 126 (CE126) from *Venturia inaequalis.* **(A)** Tertiary structure of CE126 predicted by Alphafold (Jumper et al., 2021). Structure is coloured according to the pLDDT score: dark blue for highly confident predicted regions; light blue and green for regions of low confidence and red for disordered regions. Disulfide bonds are shown as purple sticks. **(B)** Solved crystal structure of EXLX1, an expansin-like protein from *Bacillus subtilis* (RSCB protein data bank (PDB) ID: 30D30) (Kerff et al., 2008). **(C)** Solved crystal structure of the beta-expansin EXPB1 from *Zea mays* (RSCB protein data bank (PDB) ID: 2HCZ) (Yennawar et al., 2006). The β strands and α helices are numbered sequentially. The N- and C-termini are labelled in each panel. **(D)** Structural superimposition of CE126, EXLX1 and EXPB1. **(E-F)** Surface charge potential of CE126 (rotated 180° around the y axis). Blue represents positive charge and red negative charge. Tertiary structures were superimposed, visualized and rendered using PyMol (https://pymol.org/2/) (The PyMOL Molecular Graphics System, 2015) (DeLano, 2002).

3.3.7 CEs that trigger cell death in *Nicotiana* species are variable in sequence between isolates of *V. inaequalis*

To analyze polymorphisms in the genes that encode the three cell death-eliciting CEs, 90 *V. inaequalis* isolates collected from around the world (Table A.4), were analyzed for allelic variation. Based on both nucleotide and protein sequence alignments, a total of 54 DNA modifications across the 90 strains were identified in the three *CE* genes (Fig. 3.13 and Table 3.2), the majority of which were single-nucleotide polymorphisms (SNPs), only one nucleotide insertion in *CE17* and no deletions. Twenty DNA polymorphisms were identified in *CE17*. Nine of them were nonsynonymous mutations altering the amino acid sequence of the protein, two in the signal peptide, and seven in the mature protein. Based on all DNA modifications, 14 alleles were identified for the *CE17* gene (Fig. 3.13 and Table 3.2). The gene with the least DNA modifications was *CE93*, with a total of 12 DNA polymorphisms and only four accounting for nonsynonymous mutations altering the amino acid sequence of the encoded protein (Fig. 3.13 and Table 3.2). For this *CE* gene, eight alleles were identified. In the *CE126* gene, 22 DNA modifications were observed; three of them altering amino acid residues in the signal peptide, and five of them altering the mature protein sequence (Fig. 3.13 and Table 3.2). For *CE126*, a total of 12 alleles were identified.

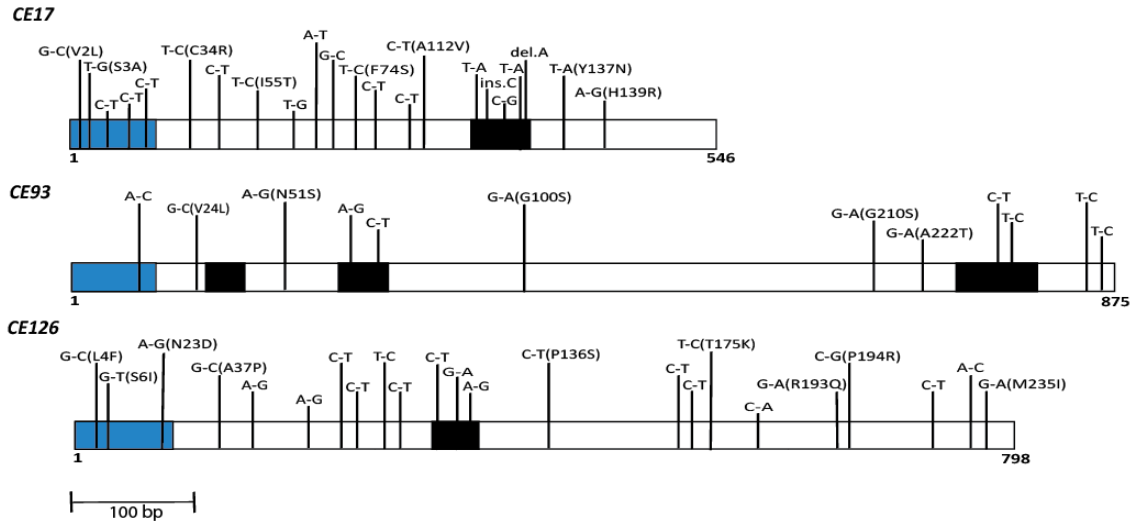

Figure 3.13. Sequence variation for three candidate effector (*CE*) genes across isolates of *Venturia inaequalis*. Blue boxes indicate parts of the genes encoding signal peptides. Predicted introns are shown as black boxes. DNA polymorphisms are shown for all genes; those resulting in an amino acid sequence alteration in the protein are indicated in brackets. Scale bar = 100 base pairs (bp).

Table 3.2. Allelic variation in three candidate effector (*CE*) genes of *Venturia inaequalis*

Candidate effector gene	Polymorphisms at DNA level	Mutations in protein	Candidate effector gene	Polymorphisms at DNA level	Mutations in protein	Candidate effector gene	Polymorphisms at DNA level	Mutations in protein
CE17	4G>C	Val2Leu	***CE93***	37A>C		***CE126***	12G>C	Leu4Phe
	7T>G	Ser3Ala		70G>C	Val24Leu		17G>T	Ser6Ile
	15C>T			201A>G	Asn51Ser		67A>G	Asn23Asp
	21C>T			280A>G			109G>C	Ala37Pro
	42C>T			320C>T			129A>G	
	100T>C	Cys34Arg		402G>A	Gly100Ser		162A>G	
	123C>T			732G>A	Gly210Ser		192C>T	
	164T>C	Ile55Thr		768G>A	Ala222Thr		198C>T	
	177T>G			801C>T			252T>C	
	183A>T			813T>C			264C>t	
	195G>C			866T>C			346C>T	
	221T>C	Phe74Ser		869T>C			349G>A	
	312C>T						353A>G	
	333C>T						447C>T	Pro136Ser
	335C>T	Ala112Val					481C>T	
	388T>A						483C>T	
	393ins.C						573T>C	Thr175Lys
	396T>A						599C>A	
	405del.A						653G>A	Arg193Gln
	406T>A	Tyr137Asn					656C>G	Pro194Arg
	467A>G	His139Arg					714C>T	
							729A>C	
							780G>A	Met235Ile

3.3.8 CE proteins of *V. inaequalis* do not trigger chlorosis and/or cell death in *Nicotiana* species when targeted to the plant cytoplasm

The Rvi15 resistance protein in apple that provides protection against *V. inaequalis* is a NBS-LRR, a class of R proteins known to localize to the plant cytoplasm (Schouten et al., 2013). Therefore, to determine whether CEs of *V. inaequalis* trigger chlorosis or cell death when expressed inside *N. benthamiana* and *N. tabacum* cells, and thus are potentially recognized by R proteins of these species, 56 *V. inaequalis* CEs were synthesized without a secretion signal (ΔSP) and produced in *N. benthamiana* and *N. tabacum* using ATTAs. The selected 56 CEs are the highest expressed genes derived from the *V. inaequalis* EU_B04–'Royal Gala' interaction. As expected, the INF1 positive control protein triggered a strong cell death in both *Nicotiana* species, and the negative control EV pICH86988 gave no response in both *Nicotiana* species (Fig. A.9). Like the negative control, none of the CEs without a signal peptide triggered chlorosis or cell death in either *Nicotiana* species (Fig. A.9). This suggests that none of the CE proteins were potentially recognized by intracellular IPRs.

3.4 Discussion

Effectors favour pathogen infection through avoidance and suppression of the plant defence responses. However, they can also be inadvertently perceived directly or indirectly by R proteins to activate a defence response. Current evidence in other Dothideomycetes suggests that *V. inaequalis* effectors could act and be perceived similarly. In this chapter, a total of 133 CEs identified in previous research were selected and analysed using web-based bioinformatic tools. Then, these CEs were expressed in the non-host plant species *N. benthamiana* and *N. tabacum* to determine whether they elicit a cell death or chlorotic response indicative of potential recognition by an R protein. In identifying these effectors, the corresponding R proteins in *N. benthamiana* and *N. tabacum* could be transferred to apple cultivars, or homologs could be identified in apple (i.e. by genome sequencing). Such homologs could be then screened to confirm the recognition of the same effector. In addition, this approach can lead to hints into effectors that target the plant immune system.

Consistent with other known effectors from fungal pathogens, most of the 133 CEs selected for analysis in this study were small secreted proteins that are highly expressed *in planta* and contain four or more cysteine residues (Bowen et al., 2009; Sperschneider et al., 2015; Thordal-Christensen et al., 2018). In total, 130 of these CEs were predicted by the ApoplastP server to be targeted to the plant apoplast, while only 100 were predicted to be effectors by the EffectorP 3.0 server. It should be mentioned, however, that these are mere predictions. As such, although 33 CEs were not predicted to be effectors by EffectorP 3.0, these proteins were not discarded for further analysis. In support of this decision, it has been shown that not all characterized effectors are correctly predicted using these servers (Sperschneider et al., 2018). For example, the effector Cmu1 from *Ustilago maydis* has been incorrectly predicted as non-effector (Sperschneider et al., 2016), while the cytoplasmic effector AvrPm2 from *Blumeria graminis* f. sp. *tritici* is incorrectly predicted as apoplastic effector (Sperschneider & Dodds, 2021). Likewise, it should be pointed out that the ApoplastP server did not predict the apoplastic effectors such as AvrLm1 from *L. maculans* and CfTom1 from *C. fulvum* as being apoplastic (Sperschneider et al., 2018).

In the early days of effector biology, it appeared that many fungal effector proteins were species-specific, lacking similar proteins in other fungi (De Wit, 1997). However, with larger numbers of fungal genomes being sequenced over the last two decades, it has become increasingly clear that many of these effector proteins do in fact have similar proteins in other fungal species (Stergiopoulos et al., 2010). In line with this, 126 CEs of *V. inaequalis* were found to have sequence similarity to uncharacterized proteins, while a further 7 have structural or amino acid sequence similarity to proteins with known function. These CEs represent conserved proteins that contribute to host adaptation in other plant-associated fungal species. CE10 (ViHyd1) shares similarity with the hydrophobin family of proteins that are only present in fungi. These proteins are known to mediate the attachment of hyphae to hydrophobic surfaces and have a role in appressorial development for efficient infection (Talbot et al., 1996; Wösten, 2001). One example of a hydrophobin is the *Magnaporthe oryzae* hydrophobin Mpg1, which has previously been shown to contribute to adhesion, germling differentiation and pathogenicity of this fungus in wheat (Inoue et al., 2016). Investigating structural similarity to other proteins also resulted in the identification of hydrophobins from Sordariomycete and Eurotiomycete fungal pathogens. ViHyd1, as in other filamentous pathogens, could potentially have a role in conidial attachment to the cuticle and appressorial formation to start the infection process. A potential role of this protein in infection can be investigated by deletion of the *ViHyd1* gene, to see if attachment and appressorial development are impaired.

CE11 (ViEcp6) shares similarity to lysin motif (LysM) domain-containing effectors previously described in other Dothideomycete pathogens. This protein is predicted to contain three LysM motifs as found in Ecp6 from *C. fulvum,* the most well-known and characterized example of a fungal LysM domain-containing effector protein (Bolton et al. 2008; de Jonge et al. 2010; Sanchez-Valet et al. 2013). Such LysM domains are known to be involved in binding peptidoglycan (Miya et al., 2007). Ecp6 sequesters chitin fragments released from the cell wall of the fungus to prevent chitin-triggered immunity (de Jonge et al., 2010). Other chitin-binding LysM proteins have been described in *Z. tritici* (Marshall et al., 2011). The predicted structure of ViEcp6 also displayed matches to chitin-binding proteins such as the LysM receptor-like protein (RLP) OsCEBiP from

Oryza sativa (rice) (Liu et al., 2016). The finding on a similar Ecp6 protein in *V. inaequalis* suggests that this fungus employs a similar strategy to *C. fulvum* and other fungal pathogens in that it secretes a protein with chitin-binding activity to outcompete apple chitin-binding receptors to prevent chitin-triggered immune responses.

CE12 (ViPNPL-5) and CE13 (ViPNPL-9) belong to the plant natriuretic peptide-like (PNPLs) family of proteins. Plant natriuretic peptides (PNPs) are molecules secreted into the apoplast under biotic and abiotic stress conditions to modulate salt and water homeostasis (Gehring & Irving, 2003; Turek et al., 2014). It has been reported that PNP homologs are produced by plant pathogens such as *V. dahliae* during infection to promote colonization. The effector VdAve1 from *V. dahliae* is a PNPL protein that triggers *Ve1*-mediated resistance in tomato and is required for full virulence (de Jonge et al., 2012). Recently, it has been demonstrated that VdAve1 manipulates the host microbiome composition by specifically suppressing antagonistic bacteria that affect *V. dahliae* growth (Snelders et al., 2020). Based on these examples in other pathogens, it is plausible that, to facilitate apple infection, *V. inaequalis* deploys PNPL effector proteins to modulate host cell physiology and the host microbiome.

As there is currently no high throughput method for CE expression in apple, the potential elicitor activity of 132 CEs was assessed using ATTAs in *Nicotiana* species with CEs targeted to the apoplast (using the tobacco signal peptide PR1α), or to the cytoplasm (without the tobacco signal peptide PR1α). Notably, as *V. inaequalis* growth is confined to the sub-cuticular space (Bowen et al., 2011), and because an extracellular PRR-type R protein, Rvi6, has been identified in *Malus* (Belfanti et al., 2004), screened CEs were initially fused to a plant signal peptide for extracellular targeting. However, as an intracellular NLR-type R protein, Rvi15, has also been described in apple that is active against *V. inaequalis* (Schouten et al., 2013), a second screen was carried out without signal peptides. The performed ATTAs resulted in the identification of two CEs that elicited a cell death response, and one CE that induced a chlorotic response. The differences in the observed responses triggered by each CE could reflect the divergence among R proteins in both *Nicotiana* species. However, these chlorotic/necrotic responses cannot be immediately assigned to an immunity response. Perhaps these CEs interact with different host targets to alter certain biological processes that can be

beneficial for the pathogen. For example, these responses may be interacting with a virulence target at the plant plasma membrane, which in *N. benthamiana* or *N. tabacum*, inadvertently leads to a necrotic or chlorotic response (i.e. through disruption or perturbation of the plant plasma membrane). To determine whether the necrotic cell death or chlorotic responses are based on the plant immune system, expression of *PR*-genes, accumulation of reactive oxygen species (ROS), or the production of ethylene in ATTA leaf samples could be assessed (Robert-Seilaniantz et al., 2007; Waszczak et al., 2018; Zhang et al., 2017). In addition, these CEs could be expressed in *BAK1/SOBIR1*-silenced plants. If a reduction in cell death/chlorosis induction is observed, this would indicate that the CEs are recognized in the apoplast by extracellular PRRs that require BAK1 and/or SOBIR1 to trigger signalling pathways that culminate in cell death or chlorosis (Kettles et al., 2017).

It was determined that the three CEs exclusively exert their elicitor activity in the apoplast (i.e. when targeted to the apoplast using a signal peptide), as their elicitor activity was lost using their respective versions without signal peptides. This outcome has been observed in related studies. For example, the cell death-inducing activity of eight CEs from the rice false smut fungus *Ustilaginoidea virens* depends on the presence of a secretion signal (Fang et al., 2016). It is important to mention, though, that signal peptides direct proteins through the Endoplasmic Reticulum (ER)-Golgi pathway (Alonso et al., 2020). Hence, non-secreted versions of CEs may lack post-translational processing occurring in the ER-Golgi secretory pathway that is required to be functional, correctly folded, and stable (Viotti, 2016). An inspection of the CE17 and CE93 sequences revealed they carry two and one ER-Golgi dependent N-glycosylation sites (NXS or NXT motifs), respectively. As such, it remains possible that CEs without a signal peptide lack post-translational modifications, such as glycosylation, required for the elicitation of cell death or chlorosis in *Nicotiana* species.

Despite the low amino acid sequence similarity to other Alt a 1-like proteins (AA1) unique to Dothideomycetes and Sordariomycetes classes of fungi (Chruszcz et al., 2012), CE17 was predicted to possess high structural similarity to the AA1 proteins Alt a 1 and PevD1. The AA1 family of proteins are characterized by a β-barrel fold containing 10 or 11 β-strands linked by two disulfide bonds that provide protein stability

(Chruszcz et al., 2012; Twaroch et al., 2012) (Fig. 3.10). The shared intramolecular pattern of the disulphide bonds among the Alt a 1 family can be observed from the conservation of their cysteine residues (Fig. 3.7). The role of AA1 proteins in plant-pathogen interactions has been pursued in the last years, revealing clues of their functionality. *A. alternata* can be generally found in vegetables, fruits, and cereals. Spores present in these foods produce components related to allergenicity, for example the major allergen Alt a 1 that elicits asthma responses in patients with *Alternaria* species allergy (Gómez-Casado et al., 2014). Alt a 1 is released from germinating spores as a tetramer, and then breaks down into a monomer in the acidic environment of the plant apoplast. These monomers function as enzymatic inhibitors of pathogenesis-related 5 (PR5) thaumatin-like proteins involved in plant defence responses such as ROS production (Garrido-Arandia et al., 2016; Gómez-Casado et al., 2014). PevD1 is one of the most abundant proteins secreted by the Sordariomycete *V. dahliae* and is highly expressed during infection, and also interacts with PR5-thaumatin-like proteins to inhibit their antifungal activity (Zhang et al., 2018). MoHrip1 from the Sordariomycete *M. oryzae* is another characterized member of the AA1 family, it is highly expressed during spore germination and infection of rice, it binds to the plasma membrane causing cell shrinkage and chloroplast disorganization (Zhang et al., 2017). The same study showed that MoHrip1 infiltration of tobacco leaves induced ROS accumulation, expression of defence-related genes and necrosis (Zhang et al., 2017).

Like CE17, the Alt a 1, PevD1 and MoHrip1 proteins are cell death elicitors in *Nicotiana* species (Garrido-Arandia et al., 2016; Zhang et al., 2018; Zhang et al., 2017). Furthermore, a recent study reported an Alt a 1-like protein from the pine pathogen *Dothistroma septosporum* that triggered cell death in the same model species (Hunziker et al., 2021). Remarkably, all of these AA1 family members share the same three-dimensional protein structure and induce the expression of defence-related genes, culminating in a cell death. Hence, it can be hypothesized that CE17 could potentially be perceived as an IP in *Nicotiana* species, inducing the expression of defence-related genes, ROS accumulation and necrosis. Moreover, the high expression of *CE17* during the first two days of infection by *V. inaequalis* on apple leaves suggest that this protein has a role in virulence at an early stage. The role of AA1-like proteins in virulence has

been demonstrated for example, by knocking out their encoding genes. Specifically, mutants of *V. dahliae* knocked out for the *PevD1* gene showed a significant decrease in virulence in cotton seedlings (Zhang et al., 2018). The same knockout approach has been pursued by successfully knocking out the gene encoding CE17 in *V. inaequalis* (Arshed et al., in progress). However, it remains to be determined whether CE17 has a role in promoting virulence or pathogenicity.

CE93 has sequence similarity to proteins across fungal species from different classes, hosts and lifestyles, including a human fungal pathogen (Fig. 3.8). However, these all are uncharacterized proteins. Using CE93 as a query in the InterProScan database revealed a potential clue regarding the function of this protein. CE93 was placed in the Egh16-like family of fungal proteins whose encoding genes are commonly highly expressed during early infection events, playing a role in conidial germination and appressorial formation (Xue et al., 2002). Examples include the Magas1 protein produced by the entomopathogenic fungus *Metarhizium acridum*, important for virulence and insect cuticle penetration (Cao et al., 2012), and Egh7 and Egh16 from the Leotiomycete *Blumeria graminis* (syn. *Erysiphe graminis* f. sp. *hordei*) involved in the maturation of conidia and hyphal growth, respectively (Justesen et al., 1996). Based on available information about Egh16-like family members and the high expression level of *CE93* at 24 hpi, 2 and 3 dpi (coinciding with *V. inaequalis* conidial germination, appressorial formation and cuticle penetration), it can be considered that CE93 has a potential role in the infection process. The role of Egh16-like proteins as virulence factors in phytopathogenic fungi has been studied in the rice blast fungus *M. oryzae*. The two highly expressed *Egh16*-like genes, *GAS1* and *GAS2* were identified during appressorial formation, and subsequently were deleted to observe any effects on infection structures or virulence (Xue et al., 2002). Conidiation and appressorial formation were not affected in deletion mutants, while appressorial penetration and lesion development were significantly reduced (Xue et al., 2002), demonstrating the role of GAS1 and GAS2 in *M. oryzae* virulence. The same approach could be pursued in *V. inaequalis* to determine the role of CE93 in virulence. Structural predictions of CE93 uncovered homology to lytic polysaccharide monooxygenases (LPMOs) which are ''auxiliary'' enzymes involved in cellulose digestion (Fig. 3.11). The term auxiliary is

adopted as these LPMOs facilitate the activity of other enzymes (e.g., endoglucanases) (Sabbadin et al., 2018). Such LPMOs are characterized by a central β-sandwich fold containing various loops and two or more disulfide bonds (Fig. 3.11) (Sabbadin et al., 2018). These clues perhaps reveal the role of CE93 in boosting the effect of other plant cell wall-degrading enzymes during infection. The possible enzymatic nature of this protein in combination with the potential substrates present in the plant apoplast, could explain the chlorotic response observed in *N. benthamiana*.

CE126 has sequence similarity to hypothetical proteins, barwin-like endoglucanases, and the carbohydrate-binding module (CBM) family of proteins across different classes of fungal pathogens (Fig. 3.9). Using CE126 as query in the InterProScan database placed this CE in the RlpA-like superfamily of proteins that contain the unique double psi-beta barrel DPPB domain (de Oliveira et al., 2011). This result coincides with the predicted structural similarity of CE126 to plant and bacterial expansins which are indeed characterized by a DBPP fold (Fig. 3.12). Plant expansins are non-enzymatic wall loosening proteins that regulate events (i.e. cell enlargement) involving cell wall modifications (Cosgrove, 2005). Aligned with the activity and tertiary structure of plant expansins, bacterial expansins can facilitate attachment and manipulation of plant cell walls by binding cellulose (Kerff et al., 2008). Expansin-like proteins are not only found in plants and bacteria, but also in filamentous fungi. For example, the EglD expansin-like protein from the Eurotiomycete *A. nidulans*, is a cell wall-localized protein presumably involved in cell wall remodelling during conidial germination (Bouzarelou et al., 2008). This theory was further supported by enzymatic treatment of conidiospore *EglD* deletion mutants, resulting in an altered cell wall structure compared to the wild type strain (Bouzarelou et al., 2008). The information on previously characterized expansin-like proteins, and the highest expression levels of *CE126* at 24 hpi could indicate a role of this protein in conidial attachment and cell wall remodelling to initiate germination. Localization and the role of CE126 could possibly be further studied using GFP-tagged versions of CE126 and *CE126* deletion mutants.

Another family of proteins containing a DBPP fold and a CBM domain are the cerato-platanins (CPPs), which are small secreted and cysteine-rich carbohydrate-binding proteins only found in filamentous fungi. However, contrary to expansins, these

cannot bind cellulose (Baccelli, 2015; Gaderer et al., 2014). CPPs are involved in conidial production, and also can act as virulence factors eliciting plant defence responses such as salicylic acid (SA) signalling, phytoalexin synthesis and cell death. One example of a CPP that is implicated in both conidial production and induction of plant defence responses is CgP1 from the rubber tree pathogen *Colletotrichum gloeosporioides* (Wang et al., 2018). A significant reduction of conidiation and a decrease in virulence were observed using *CgP1* knock-out mutants (Wang et al., 2018). In the same study, CgP1 was transiently expressed in tobacco leaves and rubber tree mesophyll protoplasts triggering a strong cell death and ROS accumulation, respectively. Several studies have shown that fungal CPPs act as IPs, triggering plant defence responses ending in a necrotic cell death in diverse plants (Frías et al., 2011; Li et al., 2019). For example the CPP BcSpl1 from *Botrytis cinerea* induces strong necrosis when infiltrated in tomato, tobacco and *Arabidopsis* leaves (Frías et al., 2011), and the CPP FocCP1 from *Fusarium oxysporum* triggers an HR in tobacco (Li et al., 2019). Based on studies of CPPs from other fungi, it can be inferred that CE126 is perceived as an IP by the host IPRs, activating plant defence responses that culminated in the observed necrosis in *N. tabacum* plants.

The allelic variation analysis of the three cell death or chlorosis elicitors across *V. inaequalis* isolates showed polymorphisms that altered the amino acid sequences in the three proteins. These changes could be derived from selection pressure mediated by yet-unknown R proteins in apple (i.e. to evade recognition), or could signify functional optimization, for example, to better interact with existing or new host virulence targets (Khajuria et al., 2018; Tanaka et al., 2014; Thierry & Balesdent, 2017). The sexual reproduction in *V. inaequalis,* which occurs once a year, combined with several cycles of asexual production per apple growing season, is expected to have resulted in this genetic variability amongst strains (Gladieux et al., 2008).

Notably, only three of the 132 screened CEs (2%) induced a cell death or chlorotic response in *Nicotiana* species. This rate was much lower compared to other studies using CEs from *Z. triciti* (22%) (Kettles et al., 2017) and *D. septosporum* (20%) (Hunziker et al., 2021). However, it is expected that rates of recognition will vary from species to species. It is of course possible that R proteins in *Nicotiana* species cannot recognize effectors directly as they have not co-evolved with *V. inaequalis* or that CEs do not

modulate the immune system in *N. benthamiana/N. tabacum,* or a component of the immune system that is guarded by R proteins is missing in such non-host plants. Hence, the majority of these CEs presumably only have activity in *Malus* species. The ideal scenario is to perform effectoromics using agroinfiltration in different apple accessions; however, this approach has been trialled in leaves without success. Transient expression assays have been developed only in apple fruits (Lv et al., 2019; Spolaore et al., 2001).

Identification (cloning) of genes encoding membrane-bound R proteins in *Nicotiana* species that respond to CEs and induce plant immune responses can be performed using virus-induced gene silencing (VIGS) (Wang et al., 2018). For example, identification of the IPR that recognizes XEG1 in *N. benthamiana* was achieved by silencing *IPR* genes that encode predicted RLPs and receptor-like kinases (RLKs) using tobacco rattle virus TRV-based constructs (Wang et al., 2018). By identifying R proteins that recognise a specific elicitor of *V. inaequalis* in non-host plants, genes encoding homologs of such R proteins could potentially be identified in *Malus* germplasm collections using genome sequencing, or these could be genetically engineered to be similar to non-host R proteins. Furthermore, R proteins from *Nicotiana* species could potentially be transferred by genetic modification into apple cultivars. Examples of R protein transfer across sexually incompatible plants have been reported. The gene encoding the immune receptor Ve1 from tomato was transferred to tobacco and cotton plants to confer Ave1-dependent resistance to *Verticillium* species (Song et al., 2018). Recently, the *Rvi6 R* gene from apple was transferred to pear clones, resulting in strong defence reactions and limited sporulation after inoculation with *V. pyrina,* showing the potential of intergenic *R* gene transfer among the *Rosaceae* family (Perchepied et al., 2021).

In conclusion, using ATTAs in *Nicotiana* species has facilitated the identification and characterization of virulence factors among diverse fungal pathogens. In this chapter, ATTAs uncovered three proteins that may play an important role in the *V. inaequalis*-apple pathosystem. Further characterization studies are needed to conclude a specific function for each CE protein, or whether these CEs are recognized by R proteins in apple.

Chapter 4: Identification of the Avr9B avirulence effector from *Cladosporium fulvum*

4.1 Introduction

Leaf mould, caused by *Cladosporium fulvum*, is one of the most important diseases of tomato (*Solanum lycopersicum*) worldwide, and is particularly prevalent in greenhouse and high tunnel environments, where it causes severe defoliation and yield losses (Thomma et al., 2005). During infection, *C. fulvum* primarily resides in the apoplastic space between mesophyll cells (Thomma et al., 2005), where it secretes an arsenal of effector proteins to promote host colonization (see Chapter 1 for more details) (Mesarich et al., 2018). Most of the *C. fulvum* effectors identified so far are small, secreted proteins (SSPs) of less than 300 amino acids in length with an even number of cysteine (Cys) residues (Mesarich et al., 2018; Stergiopoulos et al., 2007). In many cases, these Cys residues form disulphide bonds that function to promote stability of the effector proteins in the apoplastic environment, which is rich in plant proteases (Joosten et al., 1997; Luderer et al., 2002; van den Burg et al., 2003). Specific examples of *C. fulvum* effectors identified to date are detailed in Chapter 1.

The *C. fulvum*–tomato pathosystem has long been used as a model to understand the molecular basis of plant–pathogenic fungus interaction (Joosten & de Wit, 1999; Rivas & Thomas, 2005), with resistance and susceptibility known to be governed by a gene-for-gene relationship (Flor, 1971). Under this relationship, the product of an avirulence (*Avr*) effector gene from *C. fulvum* can be recognized by the product of a corresponding *Cf* resistance (*R*) gene from tomato to provide resistance (de Wit et al., 2009; Wulff et al., 2009). If either the *Avr* effector gene or the *Cf R* gene is missing from the pathogen or plant, respectively, then resistance does not occur (de Wit et al., 2009). Following this recognition event, an array of plant immune responses are activated, which can include a hypersensitive response (HR), which is a strong localized cell-death reaction that halts the growth of the pathogen (Heath, 2000). It is important to note, however, that the outcome of Cf-mediated resistance is not always accompanied by an HR. Indeed, it can also be characterized by a weaker response that cannot be observed as a HR, but can be determined by the accumulation of pathogenesis-related (PR)

proteins in the apoplast (e.g. cysteine proteases, β-1,3 glucanases and chitinases) (Kombrink et al., 1988; Laugé et al., 1998; Panter et al., 2002).

Cf-mediated immune responses can vary from weak to strong, depending on the Cf R protein involved. For example, differences in the necrotic patterns of Cf-9/Avr9- and Cf-4/Avr4-induced HR have been reported previously, with Cf-4 triggering a more severe necrotic response than the resistance mediated by Cf-9 (Cai et al., 2001). These differences may be the result of variation in the stability of the Avr effector in the apoplast that can determine the strength of perception by the cognate host virulence target Cf R protein. Alternatively, there can be differences in the length of the cytoplasmic tails of the Cf R proteins which impacts the subsequent immune signaling cascade which in turn affects the strength of the immune system output (van der Burgh & Joosten, 2019).

The *Cf R* genes of tomato encode membrane-anchored receptor-like proteins (RLPs) composed of extracellular amino (N)-terminal leucine-rich repeats (LRRs) and a short cytoplasmic carboxyl (C)-terminal domain (Kruijt et al., 2005; Thomas et al., 1998). Two well-characterized examples are Cf-4 and Cf-9, which activate plant immune responses, including an HR, upon recognition of the *C. fulvum* avirulence effector proteins Avr4 and Avr9, respectively (Jones et al., 1994; Thomas et al., 1997). These Cf R proteins share >91% amino acid identity, but differ in their number of LRRs, with Cf-4 containing 25 LRRs, and Cf-9 containing 27 LRRs. Despite their high amino acid identity, determinants that allow the specific recognition of the cognate Avr effector proteins have been identified. By performing domain swaps between the Cf-4 and Cf-9 R proteins, it was determined that Cf-mediated recognition specificity is governed by the LRR number and the sequence variation within the central LRRs (Thomas et al., 1997). Similar conclusions were also drawn after performing domain swaps between the Cf-5 and Cf-2 R proteins (Seear & Dixon, 2003).

Cf-9 and Cf-9B (R proteins responsible for recognizing the Avr9 and Avr9B Avr effectors, respectively) share 89% identity and 92% similarity to each other, and their differences are mainly located at the N-terminal regions of the protein. Despite their close similarity, there are specific determinants for each protein for recognition. By performing domain swaps between both R proteins, it was found that residues within

LRR 13 to 15 of Cf-9 confer recognitional specificity to Avr9, and residues in LRR 10 to 12 were required to elicit a strong HR. In contrast, it was determined that residues along the entire N-terminal half (up to LRR15) of Cf-9B were required for Cf-9B-mediated resistance, and residues in LRR 5 to 9 and 10 to 12 were required to induce a strong necrotic response in *N. benthamiana* (Chakrabarti et al., 2009). Crucially *C. fulvum* can overcome Cf-resistance by modifying its *Avr* effector genes through point mutations that lead to amino acid substitutions or frameshifts, or even through gene deletions (Stergiopoulos et al., 2007).

Many of the commercial tomato cultivars deployed worldwide carry the *Hcr9* (Homologues of *Cladosporium fulvum* resistance gene *Cf-9*) introgression segment from the wild tomato species *Solanum pimpinellifolium* (Jones et al., 1993). This segment, which spans 36.5 kb at the Milky Way locus on the short arm of tomato chromosome 1, is made up of five paralogous genes, namely *Hcr9-9A*, *Hcr9-9B* (*Cf-9B*), *Cf-9*, *Hcr9-9D* and *Hcr9-9E* (*Cf-9E*) (Fig. 4.1) (Jones et al., 1994; Parniske et al., 1999). Three of these genes provide protection against *C. fulvum*. More specifically, *Cf-9* provides resistance in both seedlings and mature plants, whereas *Cf-9B* and *Cf-9E* only provide resistance in mature plants (i.e., during flowering and fruiting) (Laugé et al., 1998; Panter et al., 2002). While *Cf-9*-mediated resistance involves an HR, *Cf-9B*-mediated resistance is only associated with reduced colonization of tomato leaves and a strong accumulation of PR proteins (Laugé et al., 1998; Panter et al., 2002). In the case of *Cf-9E*, the immune responses involved in the resistance response, which result in a delay of sporulation by one week, are currently unknown (Laugé et al., 1998). Furthermore, it has been previously shown that up-regulation of *Cf-9B* gene expression is not responsible for the mature onset of resistance (Panter et al., 2002).

Figure 4.1. The 36.5 kb *Hcr9* (Homologues of *Cladosporium fulvum* resistance gene *Cf-9*) introgression segment from wild tomato species *Solanum pimpinellifolium*. Black arrows and bars represent Lipoxygenase C exons, and the arrows indicate the polarity of transcription of the 3'-exon. Figure not to scale.

Resistance mediated by the *Hcr9* introgression segment has, for the most part, provided durable resistance against *C. fulvum*. This is despite the fact that *Cf-9*-mediated resistance has been overcome by *C. fulvum* through the deletion of the corresponding *Avr9* gene in many race 9 strains of the fungus worldwide (Bernal-Cabrera et al., 2021; Iida et al., 2010; Iida et al., 2015; Stergiopoulos et al., 2007; van Kan et al., 1991; Yoshida et al., 2021). A key component of this durability has been the *Cf-9B R* gene, which provides growers with protection against race 9 strains during flowering and fruiting. Notably, though, a New Zealand strain of *C. fulvum*, IPO 2679, was identified in 1998 that could overcome both *Cf-9* and *Cf-9B*-mediated resistance (Laugé et al., 1998). To understand the molecular mechanism involved in the circumvention of *Cf-9B*-mediated resistance, and to determine whether other strains collected from around the world have also overcome this resistance, the work described in this chapter set out to identify the corresponding *Avr* effector gene of *C. fulvum*, *Avr9B*. In identifying *Avr9B*, growers can identify *Cf-9B* resistance-breaking strains in the field (i.e. in commercial greenhouse and high tunnel settings), which will in turn direct tomato cultivar selection and deployment for protection against *C. fulvum*.

4.2 Materials and methods

4.2.1 Biological materials

Bacterial strains, fungal strains and plants used in this chapter are listed in Table 4.1. Plasmids and primers used in this chapter were designed using Geneious v. 9.1.8 software (www.geneious.com) (Kearse et al., 2012). All primers and generated plasmids are listed in Table A.1 and Table A.2, respectively.

Table 4.1. Bacterial and fungal strains, and plant material used in this chapter.

Organism/strain	Characteristics	References
Escherichia coli		
DH5α	*F⁻ endA1 glnV44 thi-1 recA1 relA1 gyrA96 deoR nupG* Φ80d*lacZ*ΔM15 Δ(*lacZYA-argF*)U169*, hsdR17*(r_K^- m_K^+), λ–.	Taylor et al. (1993); Invitrogen
Agrobacterium tumefaciens		
GV3101::pMP90	Disarmed strain carrying pMP90 (pTiC58) helper plasmid; C58C1; Rif^R ,$Gent^R$.	Koncz & Schell (1986); Hellens et al. (2000)
AGL1	pTiBo542ΔT-DNA; Rif^R.	Lazo et al. (1991)
1D1249	Wild armed strain. Kan^R.	C. Kado, UC Davis
Cladosporium fulvum		
0WU (CBS131901)	Wild type race 4E strain that overcomes resistance in tomato cultivars carrying the *Cf-4E* resistance gene (i.e. due to non-synonymous mutations in the *Avr4E* avirulence effector gene). Carries a functional copy of the *Avr2*, *Avr4*, *Avr5*, *Avr9* and *Avr9B* avirulence effector genes. Origin: The Netherlands (1997).	de Wit et al. (2012)
1	Wild type. Race 1 strain. Origin: The Netherlands	Lindhout et al. (1989)
2	Wild type race 2 strain that overcomes resistance in tomato cultivars carrying the *Cf-2* gene. Origin: The Netherlands (year unknown).	Lindhout et al. (1989)
4	Wild type race 4 strain that overcomes resistance in tomato cultivars carrying the *Cf-4* gene. Origin: The Netherlands (1971)	Lindhout et al. (1989)
5 (IPO 1979)	Wild type race 5 strain that overcomes resistance in tomato cultivars carrying the *Cf-5* gene. Origin: France (1979)	Lindhout et al. (1989)
2.4	Wild type race 2 and race 4 strain that overcomes resistance in tomato cultivars carrying the *Cf-2* and *Cf-4* genes. Origin: The Netherlands (1971)	Lindhout et al. (1989)
2.4.5	Wild type race 2, 4 and 5 strain that overcomes resistance in tomato cultivars carrying the *Cf-2, Cf-4* and *Cf-5* genes. Origin: The Netherlands (1977)	Lindhout et al. (1989)

Organism/strain	Characteristics	References
2.4.5.9	Wild type race 2, 4, 5 and strain that overcomes resistance in tomato cultivars carrying the *Cf-2*, *Cf-4*, *Cf-5* and *Cf-9* genes. Origin: The Netherlands (1980)	Lindhout et al. (1989)
2.4.9	Wild type race 2, 4 and 9 strain that overcomes resistance in tomato cultivars carrying the *Cf-2, Cf-4* and *Cf-9* genes. Origin: Japan (2018).	Yoshida et al. (2021)
2.4.9.11	Wild type race 2, 4, 9 and 11 strain that overcomes resistance in tomato cultivars carrying the *Cf-2, Cf-4* and *Cf-9* genes. Origin: Poland (year unknown).	Lindhout et al. (1989)
2.5	Wild type race 2 and race 5 strain that overcomes resistance in tomato cultivars carrying the *Cf-2* and *Cf-5* genes. Origin: Bulgaria	Laterrot et al., (1985)
2.5.9	Wild type race 2, 5 and 9 strain that overcomes resistance in tomato cultivars carrying the *Cf-2*, *Cf-5* and *Cf-9* genes. Origin: France (1987)	Lindhout et al. (1989)
2.9	Wild type race 2 and race 9 strain that overcomes resistance in tomato cultivars carrying the *Cf-2* and *Cf-9* genes. Origin: Japan (2008).	Iida et al. (2010)
IPO 2679	Wild type strain race 2, race 9 and race 9B strain that overcomes resistance in tomato cultivars carrying the *Cf-2*, *Cf-9* and *Cf-9B* genes. Carries a functional copy of the *Avr4*, *Avr4E* and *Avr5* avirulence effector genes. Origin: New Zealand (year unknown).	Laugé et al. (1998); Stergiopoulos et al. (2007)
ICMP 7320	Wild type race 2, race 4 and race 9 strain that overcomes resistance in tomato cultivars carrying the *Cf-2*, *Cf-4* and *Cf-9* genes. Carries a functional copy of the *Avr5* and *Avr9B* avirulence effector genes. It is not yet known whether this strain carries a functional copy of the *Avr4E* avirulence effector gene. Origin: New Zealand (1981).	Mesarich et al. (2018)
Nicotiana spp.		
Nicotiana benthamiana wild type	Solanaceous non-host of *C. fulvum*.	Dr. K. Sohn[a]
Nicotiana tabacum Wisconsin 38	Solanaceous non-host of *C. fulvum*.	Dr. K. Sohn[a]
Solanum lycopersicum		
Money Maker (MM)-Cf-0	Susceptible Money Maker cultivar of tomato that carries no Cf resistance proteins active against *C. fulvum*.	
MM-Cf-9	Money Maker cultivar of tomato that carries the *Hcr9* (Homologues of *Cladosporium fulvum* resistance gene *Cf-9*) introgression segment from *S. pimpinellifolium*, including the *Cf-9* and *Cf-9B* resistance genes, which provide resistance against *C. fulvum* strains carrying the *Avr9* and *Avr9B* avirulence effector genes, respectively.	

[a]Previously School of Agriculture and Environment (SAE), Massey University.

4.2.2 Growth conditions

4.2.2.1 Plant material

4.2.2.1.1 *Nicotiana* species

Seed of *Nicotiana* species were germinated, and the resulting plants grown, according to section 3.2.2.1.

4.2.2.1.2 *S. lycopersicum*

Seeds of *S. lycopersicum* cultivar Money Maker (Yates, Auckland, New Zealand) were germinated in 4 x 4 x 5 cm TEKU® pots (Pöppelmann, Lohne, Germany), containing Dalton's Premium Seed Mix (Fruitfed, New Zealand) for 10–12 days at 70% relative humidity at 23–25°C during the daytime, and 19–21°C at night with a 16 h light/8 h dark photoperiod. Following germination, seedlings were carefully transferred to 10 cm pots containing Dalton's Potting Mix and grown under the same conditions described above.

4.2.2.2 Fungal strains

4.2.2.2.1 PDA lawn cultures

Potato dextrose agar (PDA; Merck, Darmstadt, Germany) lawn cultures were initiated from preserved spore suspensions stored at -80˚C. Approximately 150 µl of spore suspension was spread onto PDA plates, which were then sealed with Parafilm® M (Pechiney Plastic Packaging; Chicago, IL, USA) and maintained under dark conditions at 22˚C.

4.2.2.2.2 PDB liquid cultures

Potato dextrose broth (PDB; Scharlab, Barcelona, Spain) liquid cultures were initiated from 2-week-old fungal cultures grown on PDA (section 4.2.2.2.1). Conidia were collected with sterile water, passed through a sterile layer of Miracloth (Merck) to remove fungal mycelia, followed by centrifugation at 4,000 *g* for 8 min. Conidia were washed with sterile water, collected again by centrifugation at the same speed, and diluted to a final concentration of 10^6 conidia ml^{-1}. Then, 1 ml of the conidial suspension was used to inoculate 50 ml of PDB and cultured at 22°C at 150 rpm (Bio-Line Incubator Shaker, Edwards Instrument Company, Wisconsin, USA) for 4 days.

4.2.2.3 Bacterial strains

4.2.2.3.1 *Escherichia coli*

E. coli was cultured according to section 3.2.2.2.1.

4.2.2.3.2 Preparation of chemically competent *E. coli* DH5α

E. coli DH5α from a glycerol stock was streaked onto LB agar and grown overnight at 37˚C. A single colony was then inoculated into 5 ml of LB medium and cultured overnight at 180 rpm at 37˚C. The next day, the overnight culture was inoculated into 500 ml of LB medium and incubated at 180 rpm at 30˚C until an OD_{600} of 0.4-0.6 was reached. Then, the culture was poured into pre-cooled sterile centrifuge tubes and chilled on ice for at least 10 min and spun down at 4,700 *g* (Heraeus Megafuge 16R, TX-400 rotor, Thermo Scientific) for 10 min at 4˚C. The supernatant was discarded and the pellet was gently resuspended in 100 ml of ice-cold CC buffer (10 mM Hepes, 15 mM $CaCl_2$, 55 mM $MnCl_24H_2O$, 250 mM KCl), and incubated on ice for 10 min. Then, the culture was spun down again at 4,700 *g* for 10 min at 4˚C and the obtained pellet was gently resuspended in 18.6 ml of ice-cold CC buffer and 1.4 ml DMSO. The cell suspension was incubated on ice for 10 min, then distributed in 200 µl aliquots to 1.5 microfuge tubes, and snap frozen in liquid nitrogen. Tubes were stored at -80˚C.

4.2.2.3.3 Transformation of chemically competent *E. coli* DH5α cells

Chemically competent cells were thawed on ice and mixed with 2-5 µl of ligation mixture (section 4.2.9.1) in a 1.5 ml microcentrifuge tube (Eppendorf, Hamburg, Germany). The mixture was placed on ice for 30 min, followed by a heat shock at 42˚C for 30 sec and then placed immediately back on ice for 2 min. Then, 950 µl of LB medium at room temperature (RT) was added to the tube and the cells incubated at 37˚C at 180 rpm (Bio-Line Incubator Shaker) for 1 h. Finally, 50-100 µl of cells were spread on selective LB agar plates as per section 3.2.2.2.1.

4.2.2.3.4 Cultivation of *A. tumefaciens*

A. tumefaciens strains were cultured according to section 3.2.2.2.2, with the following specifications. For the selection of *A. tumefaciens* AGL1 transformants, kanamycin (ACTGene) and rifampicin (ACTGene) were added to a final concentration of 50 µg/ml and 10 µg/ml, respectively. For selection of in *A. tumefaciens* 1D1249 transformants, kanamycin was added to a final concentration of 100 µg/ml.

4.2.3 Genomic DNA extraction

C. fulvum IPO 2679 was grown in PDB as per section 4.2.2.2.2 for two weeks in preparation for genomic DNA extraction, with fungal biomass subsequently harvested with sterile Miracloth (Merck, Darmstadt, Germany) and freeze-dried. Samples were then ground to a powder in liquid nitrogen, and genomic DNA was extracted as per section 2.2.5.1.

4.2.4 Genome sequencing

Genomic DNA from section 4.2.3 was supplied to the Massey Genome Service (MGS) facility (Palmerston North, New Zealand), with an A260/280 ratio of 1.65 and no obvious DNA degradation or RNA contamination (see section 2.2.5.2). The quality and quantity of the genomic DNA sample from section 4.2.3 was then validated by the MGS facility using a Qubit assay (Thermo Fisher Scientific), with the sample required to have a genomic DNA quality score (GQS) of at least 3.0 out of 5.0 (the GQS of the *C. fulvum* IPO 2679 genomic DNA was 4.0). Following these quality assurance steps, the genomic DNA sample was shipped to Novogene (Beijing, China), where Illumina TruSeq™ Nano library preparation and Illumina MiSeq™ paired-end 150 bp (PE150) sequencing on the Illumina MiSeq™ platform was carried out, with the aim of providing 100x coverage (8.7 Gb of raw data).

4.2.4.1 Genome assembly

Genome assemblies were performed by David Winter (Massey University, Palmerston North) as follows. As a starting point for genome assembly, fastp v.0.20.0 (Chen et al., 2018) was used to remove all low-quality bases from the sequencing reads of *C. fulvum* obtained in section 4.2.4. A *de novo* genome sequence was then assembled using SPAdes v3.11.1 (Bankevich et al., 2012), with the final assembly generated from a set of different kmers (21,33,55,77,99,127). Final genome assembly was assessed for quality using QUAST v5.0.2 (Gurevich et al., 2013) and searched for potential adapter (Illumina oligonucleotide sequence) contamination at the National Center for Biotechnology Information (NCBI) UniVec database using the Basic Local Alignment Search Tool (BLAST) (ftp://ftp.ncbi.nlm.nih.gov/pub/UniVec/). Genome sequences were visualized using Geneious v. 9.1.8 software (www.geneious.com) (Kearse et al., 2012).

4.2.5 Identification of candidate Avr9B avirulence effectors

To identify candidate Avr9B Avr effectors, alignments were performed between 119 candidate effector genes and their encoding protein sequences from the *C. fulvum* reference strain 0WU (which contains a functional copy of the *Avr9B Avr* effector gene) and *C. fulvum* strain IPO 2679 (which lacks a functional copy of the *Avr9B Avr* effector gene) using Geneious v. 9.1.8 software (Kearse et al., 2012). This set of 119 was made up of 75 apoplastic SSPs from Mesarich et al. (2018), 10 *C. fulvum* candidate effectors (CfCEs) from Mesarich et al. (2014), Ecp2-3 from Stergiopoulos et al. (2012), and a further 33 predicted SSPs that did not meet the criteria for inclusion in the Mesarich et al. (2014) study (i.e. they were not cysteine-rich and/or were encoded by genes that are highly expressed during growth of *C. fulvum* both *in planta* and in culture) (Mesarich et al. unpublished) present in the National Center for Biotechnology Information (NCBI) database or an in-house database.

4.2.5.1 Bioinformatic analysis of candidate Avr9B avirulence effectors

A series of bioinformatic tools were applied to candidate Avr9B Avr effectors from section 4.2.5 to confirm data obtained previously (Mesarich et al., 2014; Mesarich et al., 2018; Laugé et al., 2000). More specifically, ApoplastP was used to predict whether the proteins are targeted to the plant apoplast or cytoplasm (Sperschneider et al., 2018). EffectorP 3.0 was used to predict whether proteins are in fact effectors (Sperschneider & Dodds, 2021). SignalP 4.0 was used to predict whether the proteins possess a N-terminal signal peptide for secretion (Nielsen, 2017), and then TargetP to further validate these results by prediction of proteins that enter the secretory pathway (Emanuelsson et al., 2000). TMHMM 2.0 was used to predict whether proteins possessed transmembrane helices for integration into the fungal plasma membrane (Krogh et al., 2001), while Big-PI was used to predict whether proteins have a glycosylphosphatidylinositol (GPI)-anchor lipid modification site for fungal plasma membrane attachment (Eisenhaber et al., 1999). PONDR® VLXT was used to predict whether proteins possess disordered regions (IDRs) (Molecular Kinetics, Inc., Washington State University and the WSU Research Foundation). Sequence comparisons at the nucleotide and protein levels were performed using Geneious v. 9.1.8 software (Kearse et al., 2012), with DNA and protein sequence alignments carried out using Clustal Ω (Madeira et al., 2019). Sequence similarity searches using the

basic local alignment search tool (BLAST) server (Altschul et al., 1997) were carried out in publicly available databases (sequence read archive (SRA), as well as nucleotide, whole genome sequence and protein databases), at NCBI and the Joint Genome Institute (JGI), and were based on BLASTp, tBLASTn and BLASTn.

4.2.5.2 PCR amplification

Polymerase chain reactions (PCRs) were set up in a final volume of 25 µl containing 0.5 µl of each (10 mM) forward and reverse primer, 0.5 µl of (10 mM) dNTPs, 2.5 µl of 10X ThermoPol® Reaction Buffer, 0.125 µl Taq DNA polymerase (New England Biolabs) and 1 µl of DNA (100 ng/µl). The PCR cycling conditions were as follows: initial denaturation for 30 sec at 95°C, followed by 30 cycles of 30 sec at 95°C, 60 sec at 55°C, 60 sec at 68°C, and a final extension at 68°C for 5 min.

4.2.5.3 Agarose gel electrophoresis

DNA was mixed with 0.25 volumes of SDS loading dye (0.2% (w/v) Bromophenol Blue (Avantor Sciences Inc., Pennsylvania, USA), 20% (w/v) sucrose, 1% (w/v) SDS and 5 mM EDTA, pH 6.8) and resolved on a 0.8% (w/v) agarose (HyAgaroseTM, HydraGene) gel in 1x Tris/acetic acid/EDTA (TAE) buffer (190 mM Tris, 342 mM acetic acid (Emsure®, Merck, New Jersey, USA), 2.5 mM EDTA) at 80 V for 50 min. A 1 kb plus DNA ladder (Invitrogen, Massachusetts, USA) was used as a size marker. DNA was stained with ethidium bromide (1 µg/ml) for 15 min then visualized with the Molecular Imager® Gel Doc™ XR system and the Image LabTM Software (Bio-Rad, California, USA). PCR amplicons were purified using a gel purification kit (Omega Bio-tek, Georgia, USA) as per the manufacturer's instructions, and sequenced at the Massey Genome Service facility (Palmerston North, New Zealand).

4.2.6 Tomato infection assays

For relative expression experiments, *C. fulvum* strain 5 (IPO 1979) was cultured on PDA for 2 to 3 weeks as per section 4.2.2.2.1. Conidia from PDA cultures were gently scraped and collected using sterile water, passed through a layer of sterile Miracloth to remove fungal mycelia, and collected by centrifugation at 4,000 *g* for 8 min. Conidia were then washed with sterile water, collected again by centrifugation as above and diluted to a final concentration of 5 x 10^5 conidia ml^{-1}. To initiate infection, conidia were spray-inoculated with an atomizer onto the abaxial surface of four-week-old tomato

leaves. Plants were placed in plastic-covered cages for 48 h to ensure 100% relative humidity (RH), and maintained under a regime of 16/8 h light/dark photoperiod. Then, cages were opened to allow the disease development to progress with 70% RH, at 21°C under the same light/dark regime.

Tomato infections using complemented *C. fulvum* IPO 2679 strains were performed by Christiaan Schol (Wageningen University, The Netherlands) as follows: *C. fulvum* strains containing the empty vector pFBTS1, and the pFBTS1 vectors containing *Avr9B-C1* or *Avr9B-C2* were grown for 17 days as per section 4.2.2.2.1. Then, conidia were collected as mentioned above, diluted to a final concentration of 2 x 10^6 conidia ml^{-1}, and spray-inoculated with an atomizer onto the abaxial surface of whole eight-week-old tomato MM-Cf-0 and MM-Cf-9 plants. Finally, plants were placed at the same conditions as above.

4.2.7 RT-qPCR analysis of gene expression

Leaf samples from *C. fulvum* strain 5 (IPO 1979; carrying a functional copy of *Avr9B*)–*S. lycopersicum* MM-Cf-0 interactions at 2, 4, 8, 12 and 16 days post-inoculation (dpi), as well as fungal samples from 4-day-old *C.fulvum* IPO 1979 PDB liquid cultures, were collected as follows: The fourth composite leaf of infected tomato plants, or mycelia collected and blot-dried on filter paper, were harvested, placed in a Falcon™ tube and immediately flash frozen in liquid nitrogen. Total RNA was extracted from 100 mg of material ground in liquid nitrogen using 1 ml Trizol and purified with an RNeasy® Mini kit (Qiagen, Hilden, Germany). cDNA was synthesized from 5 µg of total RNA using the QuantiTect Reverse Transcription Kit (Qiagen). Genomic DNA was eliminated by the gDNA Wipeout Buffer contained in the same QuantiTect kit. Reverse transcriptase-quantitative PCR was performed in a LightCycler® 480 System (Roche). A 20 µl reaction containing 5 µl SensiFast SYBR mix (Meridian Bioscience, Ohio, USA), 0.4 µl of each forward and reverse primers (10 µM), 100 ng of template cDNA and 3.2 µl sterile MQ water. The cycling conditions were as follows: initial denaturation for 10 min at 95°C, followed by 40 cycles of 15 s at 95°C and annealing/extension for 45 s at 60°C. qCfActin-F/qCfActin-R, qAvr9BC1-F/qAvr9BC1-R and qAvr9BC2-F/qAvr9BC2-R oligonucleotide primer pairs were designed with PRIMER3. The efficiency and specificity of primers were determined with a dilution series of cDNA for *Avr9B* candidate genes, and genomic DNA for the *C. fulvum actin* before use. The *C. fulvum actin* gene was used as a reference for

normalization of gene expression as per Mesarich et al. (2014), and results were analyzed according to the $2^{-\Delta Ct}$ method described by Livak and Schmittgen (2001). The results were the average of three biological replicates.

4.2.8 *A. tumefaciens* infiltration of *Nicotiana* spp. and tomato

4.2.8.1 Vector construction

All binary vectors generated for use in *Agrobacterium tumefaciens*-mediated transient transformation assays (ATTAs) (see section 4.2.8.2) are listed in Table A.2. Candidate *Avr9B* effector genes *Avr9B-C1* and *Avr9B-C2*, as well as homologs of the *Avr9B-C2* gene from *Stemphylium lycopersici* strain CIDEFI-216 (protein ID: TW65_01570) (Franco et al., 2015) and *Pseudocercospora fuligena* strain CBS109729 (protein ID: HII31_03919) (Zaccaron, 2020), were synthesized directly into the expression vector pICH86988 (Addgene plasmid #48076; http://n2t.net/addgene:48076;RRID:Addgene_48076) (Weber et al., 2011) (Fig. A.2) by Twist Bioscience (San Francisco, California, USA) for use in ATTAs involving *Nicotiana* species and *S. lycopersicum* (see section 4.2.8.2). The nucleotide sequence encoding each mature candidate effector protein was fused to the nucleotide sequences encoding the *N. tabacum* PR protein 1α (PR1α) signal peptide sequence (for secretion into the plant apoplast) and a 3xFLAG tag (for detection by Western blotting) at its N-terminus.

To generate an Avr9B-C2 version without the PR1α signal peptide, fragments were amplified from the synthesized vector above using the PCR primer pair NSPCE2_BsaI-F/CE2_BsaI-R (442 bp), introducing *Bsa*I restriction sites, and assembled via the Golden Gate cloning system as per section 3.2.4.5. For Avr9B-C2 with Cys to Ser substitutions, a series of overlap PCRs were performed from the synthesized vector and assembled via Golden Gate as per section 3.2.4.5. Overlap PCR for the Cys77Ser mutation in Avr9B-C2 was performed with the primer pairs CE2_BsaI-F/CE2_Cys1-R (411 bp) and CE2_Cys1-F/CE2_BsaI-R (184 bp). Overlap PCR for the Cys80Ser mutation in Avr9B-C2 was performed using the primer pairs CE2_BsaI-F/CE2_Cys2-R (411 bp) and CE2_Cys2-F/CE2_BsaI-R (184 bp). All reactions were performed using a Phusion® High-Fidelity DNA Polymerase (New England Biolabs) (section 4.2.8.1.1). Amplicons were visualized and extracted as per section 4.2.5.3.

4.2.8.1.1 High-Fidelity PCR

PCRs were carried out in a total volume of 50 µl containing 10 µl of 5X Phusion HF Buffer, 1 µl dNTPs (10 mM), 2.5 µl Forward primer (10 µM), 2.5 µl Reverse primer (10 µM), 0.5 µl Phusion® High-Fidelity Polymerase and 1 µl of DNA (100 ng/µl). Cycling conditions were as follows: initial denaturation at 98˚C for 30 sec, followed by 30-35 cycles of 5-10 sec at 98°C, 10-30 sec at 55-62˚C and 30 sec per kb at 72 ˚C, and a final extension for 5-10 min at 72˚C.

4.2.8.2 *A.* transient transformation assays (ATTAs)

ATTAs in *Nicotiana* species were performed as described in section 3.2.5. For ATTAs involving tomato, *A. tumefaciens* 1D1249 cell suspensions were prepared as per section 3.2.5 and infiltrated into fully extended leaves of 4-to-5-week-old tomato plants.

4.2.8.3 Protein extraction and Western blotting

Protein extractions and detection via Western blot were carried out as per sections 3.2.6, 3.2.7 and 3.2.8.

4.2.9 Gene complementation

Genomic DNA from *C. fulvum* strain 0WU was extracted as per section 4.2.3. The genomic DNA fragments of *Avr9B-C1* and *Avr9B-C2*, containing the complete open reading frame, as well as their native promoter and terminator, were amplified by PCR using the primer pairs GibCE1-F/GibCE1-R (2,901 bp) and GibCE2-F/GibCE2-R (2,431 bp), which contained an additional 18-25 bp at the 5' end homologous to the pFBTS1 backbone. PCRs were performed as per section 4.2.8.1.1. Amplicons were resolved by agarose gel electrophoresis as per section 4.2.5.3, and extracted with the Wizard SV Gel and PCR clean-up kit (Promega) as per the manufacturer's instructions and ligated into pFBTS1 (Fig. A.4) (a modified version of pFBT004) (Bolton et al., 2008) using a Gibson Assembly approach (section 4.2.9.1) (Gibson et al., 2009). Amplification of the pFBTS1 backbone by PCR was performed with the primer pairs pFBTS1-F/CHM52-R (3,227 bp) and MR125-F/pFBTS1-R (2,791 bp). PCRs were carried out as per section 4.2.8.1.1, and amplicons were extracted as mentioned above. Ligations resulted in the constructs pFBTS1::Avr9B-C1 and pFBTS1::Avr9B-C2, which were transformed into chemically competent *E. coli* DH5α cells as per section 4.2.2.3.3. Transformed colonies were screened using the CloneChecker™ System (section 4.2.9.2). Confirmed constructs, and

the empty vector pFBTS1, were transformed into electrocompetent *A. tumefaciens* AGL1 cells by electroporation as per section 3.2.4.8. Then, constructs were introduced into *C. fulvum* IPO 2679 via *A. tumefaciens*-mediated transformation described by Ökmen et al. (2013) (section 4.2.9.3).

4.2.9.1 Gibson Assembly

Vector (50-100 ng) was mixed on ice with 5-fold excess of each insert to a total volume of 5 µl with water. The DNA solution was added to 5 µl of 2x Gibson Assembly master mix (5x isothermal buffer (25% v/v PEG-8000, 500 mM Tris-HCl pH 7.5, 50 mM $MgCl_2$, 50 mM DTT, 5 mM NAD, and 10 mM dNTPs), T5 exonuclease (10 U/ml) (New England Biolabs), Phusion polymerase (2 U/ml) (Thermo Fisher Scientific) and Taq ligase (40 U/ml) (New England Biolabs). The mix was placed in a thermocycler at 50°C for 1 h, and 2-5 µl of assembly reactions were used to transform chemically competent *E. coli* DH5α cells as per section 4.2.2.3.3. Transformed colonies were screened using the CloneChecker™ System (section 4.2.9.2).

4.2.9.2 CloneChecker™ System

A single transformed colony was selected and dipped in 8 µl of CloneChecker™ Green-Solution (0.1 M NaCl, 10 mM Tris-HCL, pH 8.0; 1 mM EDTA, pH 8.0; and 0.5% Triton X-100) in a PCR tube, followed by a 30 sec incubation at 100°C in a thermal cycler (Eppendorf). The sample was cooled down at RT and then 1.5 µl of digestion mix (1 µl of 10x reaction buffer and 0.5 µl of *Bam*HI-HF restriction enzyme (NEB)) was added following an incubation at 37 °C for 30 min. After incubation, 5 µl of SDS loading dye (0.2% (w/v) Bromophenol Blue (Avantor Sciences Inc), 20% (w/v) sucrose, 1% (w/v) SDS and 5 mM EDTA, pH 6.8) were added to the sample and resolved by electrophoresis on a 1% agarose gel (HyAgaroseTM, HydraGene) (section 4.2.5.3). DNA was visualized with the Molecular Imager® Gel Doc™ XR system and the Image LabTM Software (Bio-Rad). Positive colonies were confirmed by PCR using gene-specific primers and amplicon sequencing, and then transformed into *A. tumefaciens* AGL1 via electroporation (section 3.2.4.8).

4.2.9.3 *A. tumefaciens*-mediated transformation of *C. fulvum*

A. tumefaciens AGL1 cells carrying the pFBTS1, pFBTS1::Avr9B-C1 or pFBTS1::Avr9B-C2 plasmids were grown in minimal medium (MM; 10 mM K_2PO_4, 2.5

mM NaCl, 2 mM $MgSO_4$, 0.7 mM $CaCl_2$, 9 µM $FeSO_4$, 4 mM NH_4SO_4 and 10 mM glucose, adjusted to pH 5.5) supplemented with 10 µg/ml rifampicin and 50 µg/ml kanamycin for 2 days at 28°C. Cells were collected by centrifugation at 3,363 *g* for 8 min and resuspended in induction medium (IM; 40 mM 2-N-morpholino ethanesulfonic acid, pH 5.3; 0.5% glycerol (w/v); 200 µM acetosyringone) supplemented with 10 µg/ml rifampicin and 50 µg/ml kanamycin, to an optical density (OD_{600}) of 0.15. Prior to co-cultivation, *A. tumefaciens* AGL1 culture was incubated for 4-6 h at 28°C to an OD_{600} of 0.25. *C. fulvum* conidia were collected from PDA plates by rinsing with sterile water, and separated from other fungal debris using two layers of sterile Miracloth and adjusted to 1 x 10^6 conidia ml^{-1}. Then, 200 µl of *A. tumefaciens* AGL1 culture (OD_{600} of 0.25) was co-cultivated with 200 µl of conidial suspension, and plated on Hybond™-nitrocellulose membrane (Amersham Biosciences, Amersham, United Kingdom) overlaying IM plates, and incubated for 2 days at 20°C. After co-incubation, membranes were transferred to MM plates supplemented with 100 µg/ml hygromycin (Roche, Basel, Switzerland) and 200 µM cefotaxime, and incubated at 20°C for 2-3 weeks. *C. fulvum* transformants were single spored, sub-cultured two times on selective PDA plates and once on non-selective PDA plates. Subsequently, transformants were tested on PDA plates supplemented with 100 µg/ml hygromycin. In preparation for PCR screening, a rapid mini preparation of fungal DNA was performed (section 4.2.9.4).

4.2.9.4 Rapid mini preparation of fungal DNA for PCR

C. fulvum transformants were screened according to Liu et al. (2000) as follows. A small sample of mycelium was added to a 1.5 ml microcentrifuge tube containing 500 µl of lysis buffer (400 mM Tris-HCl [pH 8.0], 60 mM EDTA [pH 8.0], 150 mM NaCl, 1% (w/v) sodium dodecyl sulphate), and left at RT for 10 min. Then, 150 µl of potassium acetate (5 M, pH 4.8) was added and the tube was vortexed briefly and centrifuged at 13,000 *g* for 1 min. The supernatant was transferred to a new tube and an equal volume of isopropyl alcohol was added and mixed by inversion. The tube was centrifuged at 13,000 *g* for 2 min, and the resultant pellet was washed in 300 µl of 70% ethanol and centrifuged at 10,000 *g* for 1 min; the supernatant was discarded, and the pellet air-dried and dissolved in 20 µl of 10 mM Tris-HCl (pH 8.5). The purified DNA was used for PCR using the primer pairs Comp-F/CompCE1-R (2,431 bp) and Comp-F/GibCE2-R (2,970 bp).

4.2.10 Candidate Avr9B localization vector construction

4.2.10.1 Creation of GFP- and mCherry-tagged Avr9B-C2

For generation of an N-terminal GFP- and mCherry-tagged versions of Avr9B-C2, all fragments were amplified by PCR with primers containing *Bsa*I restriction sites to generate the final vector via Golden Gate as per section (section 3.2.4.5). The *PR1α* signal peptide (for secretion to the apoplast) fragment of 153 bp was amplified by PCR from the synthesized plasmid pICH86988::Avr9B-C2 using the primer pair PR1a_BsaI-F/PR1a_BsaI-R. The *GFP* and the linker coding sequence $(GGGS)_2$ were amplified from pBH83 (Hassing, 2019) with the primer combination N_GFP_mCherry-F/N_GFP-R (765 bp). The *mCherry* and the linker coding sequence $(GGGS)_2$ were amplified from pBH77 (Hassing, 2019) with the primer combination N_GFP_mCherry-F/N_mCherry-R (759 bp). The *Avr9B-C2* sequence was amplified from the synthesized plasmid pICH86988::Avr9B-C2 using the primer combination Ntag_Avr9B-F/Ntag_Avr9B-R (418 bp). Additionally, constructs without the PR1α signal peptide were created following the same protocol. The GFP and the linker sequence were amplified using the primer pair NSP_NmCherry-GFP-F/N_GFP-R (765 bp) and the *mCherry* and the linker sequence were amplified using the primer pair NSP_NmCherry-GFP-F/N_mCherry-R (759 bp). The Avr9B-C2 sequence was amplified using the primer combination Ntag_Avr9B-F/Ntag_Avr9B-R (418 bp). All PCRs were performed as per section 4.2.8.1.1, and assembly of the final construct was carried out using the Golden Gate protocol as per section 3.2.4.5. Constructs were sequenced and transformed into *A. tumefaciens* GV3101 electrocompetent cells for agroinfiltration as per section 3.2.4.8.

4.2.10.2 Fluorescent protein detection

Protein extractions, SDS-PAGE and Western blots were performed as per sections 3.2.6, 3.2.7 and 3.2.8 respectively, with the following modifications: for GFP detection, the membrane was incubated with 1:1,000-diluted anti-GFP antibody (Santa Cruz Biotechnology) produced in mouse and subsequently incubated with the secondary antibody (chicken anti-mouse; Santa Cruz Biotechnology), diluted 1:10,000. For mCherry detection, the membrane was incubated with 1:1,000-diluted anti-mCherry antibody (BioVision Inc, California, USA) produced in rabbit, and subsequently incubated with the secondary antibody (goat anti-rabbit; BioVision), diluted 1:10,000.

4.2.10.3 Microscopy

For analysis of Avr9B-C2-fluorophore fusion protein localization, *N. tabacum* leaves were infiltrated as per section 3.2.5, but cell suspensions were adjusted to an OD_{600} of 0.25 to avoid the chlorotic response induced by Avr9B-C2. Two days post-infiltration, *N. tabacum* leaves were collected, and cut into small squares surrounding the infiltration zone. For plasmolyzed samples, a 1 M sucrose solution was infiltrated into leaves immediately prior to dissection. Leaf samples were placed onto a microscopic slide, submerged with water and subsequently covered with a glass cover slip. Samples were analysed using a Zeiss LM 700 confocal laser-scanning microscope (Oberkochen, Germany). GFP and chlorophyll auto-fluorescence were viewed by exciting at 488 and 633 nm, and emission was recorded at 505-550 nm. Excitation of mCherry was carried out at 587 nm and emission was recorded at 565-610 nm.

4.2.11 Prediction of Avr9B-C2 tertiary structure

Prediction of the Avr9B-C2 tertiary structure was performed using AlphaFold2 (Jumper et al., 2021) and ColabFold (Mirdita et al., 2021) as per section 3.2.10.

4.3 Results

4.3.1 Genome sequencing of *C. fulvum* IPO 2679

As a starting point for the identification of Avr9B candidates, the genome of *C. fulvum* strain IPO 2679 was sequenced in order to make DNA and protein comparisons with the reference *C. fulvum* strain 0WU. The genome sequencing data, analyzed by David Winter (Massey University, Palmerston North), resulted in a N50 value of 36 kb and with ~97% of BUSCO genes represented as a single copy.

4.3.2 Nucleotide and protein sequence alignments reveal two Avr9B effector candidates

All 119 previously identified SSPs from *C. fulvum* strain 0WU (which contains a functional copy of the *Avr9B* effector gene), as well as the nucleotide sequences that encode them, were aligned with the SSP and gene sequences of IPO 2679 strain (which lacks a functional copy of the *Avr9B* avirulence effector gene) to identify any that have a mutation that may be correlated with a loss of recognition of Avr9B by Cf-9B.

Alignments uncovered synonymous mutations in only 4 of the 119 SSP-encoding genes (Table 4.2), whereas non-synonymous substitutions were observed in 10 of the 119 SSP-encoding genes (Table 4.2). Some of the differences in strain IPO 2679 were confirmed based on results previously determined by Stergiopoulos et al (2007), after PCR amplicon sequencing of selected *Avr* effector genes. More specifically, these was an R64I substitution in Ecp2-1 and both an L82F and T93M substitution in Avr4E (Table 4.2). Interestingly, though, two amino acid substitutions were identified that were not reported by Stergiopoulos et al. (2007). These were a V108G substitution in Ecp4, and a C30Y substitution in Ecp5 (Table 4.2), suggesting that these differences were missed by the previous study. The following substitutions were also identified in SSPs of strain IPO 2679: N342K in Ecp2-3, S65P in Ecp32-2, S58L in Ecp40, S54P in CFU_836861, T172I in CFU_840790, as well as D134Y, A166S, ins168G, G171D, M183I, T188K, E189S, M191T, L201M, L206W, Q211D, H213K, S224T, T243I, N246D, G247N, E248Q, E249P, Q251K, L266I, N271Q, M275K, S278E, K290S and N292P in CFU_830444 (Table 4.2). Although, CFU_830444 contained many amino acid substitutions, it was not selected as an Avr9B candidate as the expression the gene encoding this protein was found to be up-

regulated both in culture and *in planta* based on previous RNA-Seq data from Mesarich et al. (2014).

A further two of the SSP-encoding genes were found to be absent in strain IPO 2679, while another had a C-terminal deletion (Table 4.2) confirming again results from Stergiopolous et al. (2007). Specifically, *Avr2* had a C-terminal deletion that resulted in the loss of its last 25 amino acid residues (Table 4.2), and the *Avr9* gene had been deleted. The second deleted gene (not included in Stergiopolous et al. 2007) corresponds to *CfCE54* (Table 4.2). Collectively, based on these results, two Avr9B candidate effectors were selected for further analysis, Ecp5 and CfCE54, which from this point onwards will be named Avr9B Candidate 1 (Avr9B-C1) and Avr9B Candidate 2 (Avr9B-C2), respectively. These candidates were chosen because the differences between *C. fulvum* 0WU and *C. fulvum* IPO 2679, were consistent with mutations observed in *C. fulvum* strains known to break resistance mediated by other Cf R proteins, namely, the amino acid substitutions in Avr4 and the deletion of the *Avr9* coding gene, which enable the fungus to overcome Cf-4- and Cf-9-mediated resistance, respectively (Joosten et al., 1997; van Kan et al., 1991).

Table 4.2 DNA polymorphisms in the coding sequences of small secreted proteins (SSPs) from New Zealand *Cladosporium fulvum* strain IPO 2679 with respect to *C. fulvum* reference strain 0WU.

GenBank accession number	JGI protein number	SSP name	Polymorphism at DNA level	Predicted mutation in protein
CAA78401	197200	Ecp2-1	87 C>A	-
			191 G>T	R64I
CAC01609	186834	Ecp4	323 T>G	V108G
CAC01610*	-	**Ecp5***	86 G>A	C30Y
AQA29272	183790	Ecp32-2	93 G>A	-
			193 T>C	S65P
AQA29250	-	Ecp40	173 C>T	S58L
	-	CFU_836861	160 T>C	S54P
AQA29282		Ecp2-3	720 T>G	-
			1,026 T>A	N342K
			1,047 T>G	-
	-	CFU_840790	515 C>T	T172I
AAT28196	183814	Avr4E	244 C>T	L82F
			278 C>T	T93M
P22287	-	Avr9	deleted	no protein
AQA29257*	-	**CfCE54***	deleted	no protein
KAH3644934	188403	CFU_830444	400 G>T	D134Y
			465 T>C	-
			471 G>A	-
			483 C>T	-
			486 C>T	-
			496 G>T	-
			498 A>T	A166S
			501 ins. A	
			502 ins. G	ins168G
			503 ins. G	
			512 G>A	G171D
			525 G>C	
			534 C>T	
			537 C>T	
			546 C>T	
			549 G>C	M183I
			558 T>C	
			563 C>A	
			564 T>G	T188K
			565 G>T	E189S
			566 A>C	E189S
			567 G>A	E189S
			570 T>C	-
			572 T>C	M191T
			573 G>T	M191T

GenBank accession number	JGI protein number	SSP name	Polymorphism at DNA level	Predicted mutation in protein
KAH3644934	188403	CFU_830444	580 C>T	-
			585 C>A	-
			600 C>A	-
			601 C>A	L201M
			603 C>G	L201M
			606 C>T	-
			615 T>C	-
			616 C>T	L206W
			617 T>G	L206W
			618 C>G	L206W
			627 C>T	-
			630 G>A	-
			631 C>G	Q211D
			633 A>C	Q211D
			637 C>A	H213K
			639 C>G	H213K
			642 T>C	-
			645 T>C	-
			648 A>C	-
			651 T>C	-
			670 T>A	S224T
			671 T>C	S224T
			681 T>C	-
			705 C>T	-
			708 T>C	-
			728 C>T	T243I
			736 A>G	N246D
			739 G>A	G247N
			740 G>A	G247N
			742 G>C	E248Q
			745 G>C	E249P
			746 A>C	E249P
			747 G>A	E249P
			751 C>A	Q251K
			771 A>C	-
			786 T>C	-
			792 C>T	-
			796 C>A	L266I
			804 C>T	-
			807 G>A	-
			811 A>C	N271Q
			813 C>G	N271Q
			824 T>A	M275K
			832 A>G	S278E

GenBank accession number	JGI protein number	SSP name	Polymorphism at DNA level	Predicted mutation in protein
KAH3644934	188403	CFU_830444	833 G>A	S278E
			834 C>G	S278E
			840 T>C	-
			846 T>C	-
			868 A>T	K290S
			869 A>C	K290S
			870 G>T	K290S
			874 A>G	N292P
			876 C>T	N292P

***Avr9B effector candidates selected for follow-up experiments.

The first *Avr9B* candidate, *Avr9B-C1* (GenBank gene ID: CAC01610), is 796 nucleotides (nt) in length, and is made up of two introns (51 and 261 nt, respectively) and three exons (4, 86 and 261 nt, respectively). The *Avr9B-C1* gene is predicted to encode a protein of 115 amino acids in length, with five Cys residues and a predicted signal peptide of 17 amino acids in strain 0WU (Fig. 4.2A). PCR amplicon sequencing confirmed the non-synonymous mutation at position 89 of the coding sequence (TGC→TAC) in strain IPO 2679, which results in a Cys-to-Tyr substitution at position 30 of the protein sequence (Fig. 4.2A). This protein is not predicted to possess a transmembrane domain or GPI anchor modification site.

The second *Avr9B* candidate, *Avr9B-C2,* (GenBank gene ID: KX943086.1) is 566 nt in length and is made up of two introns (52 and 55 nt, respectively) and three exons (382, 57 and 20 nt, respectively). The *Avr9B-C2* gene is predicted to encode a protein of 152 amino acids with an N-terminal signal peptide of 21 amino acids, followed by a repeat-rich region made up of four direct 11-amino acid repeats, and a Cys-rich region with eight Cys residues (Fig. 4.2B). The repeat-rich region largely overlaps with an intrinsically disordered region (IDR) predicted by PONDR® (Fig. 4.2B). A PCR presence-or-absence screen, as well as PCR amplicon sequencing, were carried out on the *Avr9B-C2* gene across different *C. fulvum* strains collected from around the world (Table 4.1) to determine whether the gene is absent in any other strains and to assess the level of allelic variation for *Avr9B-C2*. The *Ecp11-1* effector gene (positive control; Mesarich et al., 2018) could be amplified from all strains tested, confirming that genomic DNA quality

was adequate for PCR (Fig. 4.3). PCR amplification confirmed that the *Avr9B-C2* gene is absent in strain IPO 2679 and showed that no other strains are missing the gene (Fig. 4.3). PCR amplicon sequencing revealed that the *Avr9B-C2* gene is pseudogenized in the Japanese strain, 2.9, with a premature stop codon identified at codon 2 (CGA→TGA; Arg-to-STOP) (Fig. 4.2B). A non-synonymous substitution was also observed at codon 97 (TGG→TGC) of the race 1 strain, resulting in a Trp-to-Cys substitution at position 97 of Avr9B-C2 (Fig. 4.2B). Synonymous substitutions were not observed in *Avr9B-C2*. Like Avr9B-C1, Avr9B-C2 was not predicted to possess a transmembrane domain or GPI anchor modification site. Please note that an allelic variation screen was not performed for the *Avr9B-C1* gene, as this had already been carried out by Stergiopoulos et al. (2007). In addition, ApoplastP predicted both proteins to localize to the apoplast (Avr9B-C1=0.88 and Avr9B-C2=0.6), and EffectorP 3.0 predicted Avr9B-C1 as an effector (0.969) and Avr9B-C2 as a non-effector (0.658).

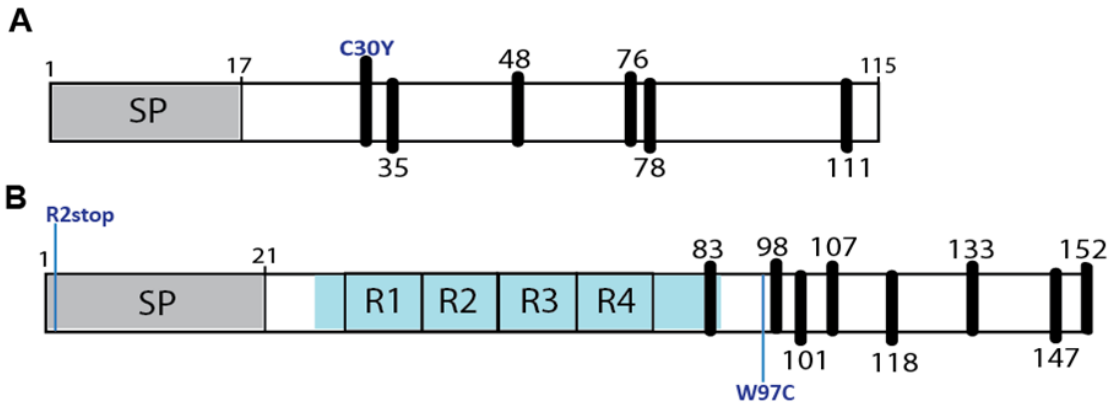

Figure 4.2. Schematic representation of the two candidate Avr9B avirulence effector proteins from strain 0WU of *Cladosporium fulvum*. Both proteins contain a putative signal peptide (SP) for secretion (highlighted in grey) and are cysteine-rich (shown by thick vertical bars). **(A)** Avr9B-C1 contains a Cys-to-Tyr substitution located at position 30 (in the allele from IPO 2679). **(B)** Avr9B-C2 contains four direct repeats (R1–R4) of 11 amino acids in length, which largely overlap with a predicted intrinsically disordered region (IDR; highlighted in blue). Allelic variation across 16 *C. fulvum* strains collected from around the world is shown in dark blue: a premature stop (Arg-to-Stop) at position 2 in the Japanese strain 2.9, and a Trp-to-Cys substitution at position 97 the race 1 strain.

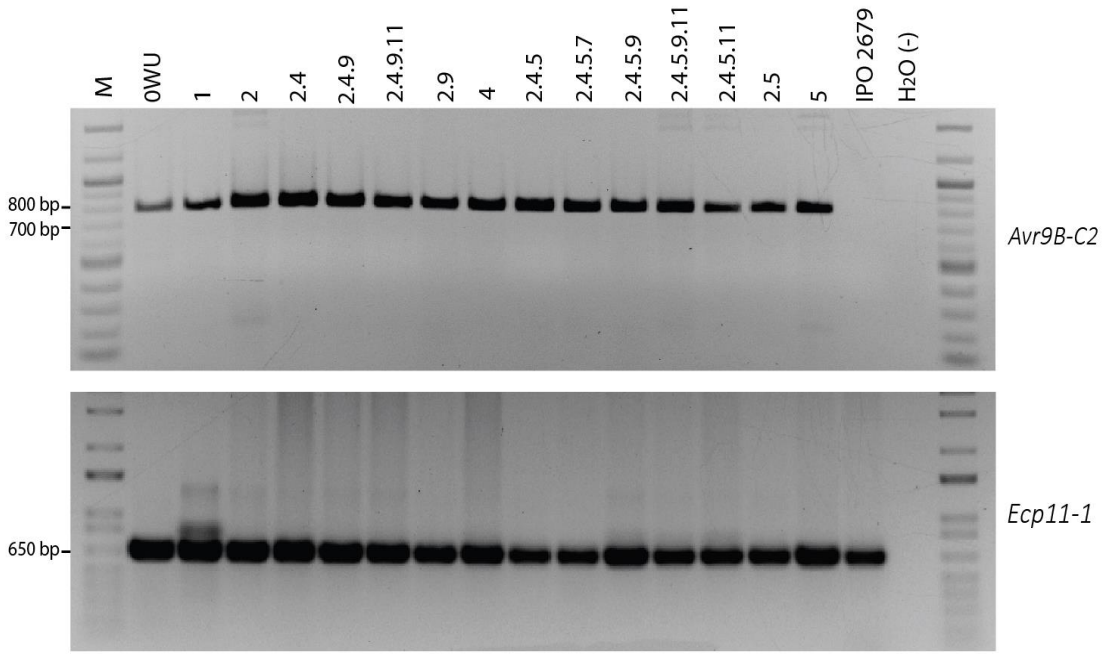

Figure 4.3. Presence-or-absence of *Avr9B-C2* across *Cladosporium fulvum* strains collected from around the world. The *Avr9B-C2* gene is only absent from strain IPO 2679. The *C. fulvum Ecp11-1* effector gene (positive control) is present across all strains investigated. Strain number, with the exception of IPO 2679 and 0WU, represents race status; M = 1 kb DNA ladder marker, H_2O (-) no template negative control. Expected PCR amplicon sizes: *Avr9B-C2* = 796 bp and *Ecp11-1* = 650 bp.

4.3.3 Candidate *Avr9B* avirulence effector genes are expressed during infection of tomato

All other *Avr* effector genes of *C. fulvum* are known to be upregulated during growth *in planta*, when compared to growth of the fungus in culture (Mesarich et al., 2014; Mesarich et al., 2018). Thus, to determine whether both candidate genes are expressed during infection, an RT-qPCR experiment was performed. Indeed, it was confirmed that both genes are strongly induced during infection, relative to expression in culture, reaching the highest expression at 8 dpi (Fig. 4.4). These expression profiles, specifically, reaching the highest expression at 8 dpi with a significant reduction at 12 dpi, are also reflected in previous RNA-Seq data obtained by Mesarich et al. (2014). However, in the mentioned study, expression of the *Avr9B-C2* gene was not detected at 4 dpi.

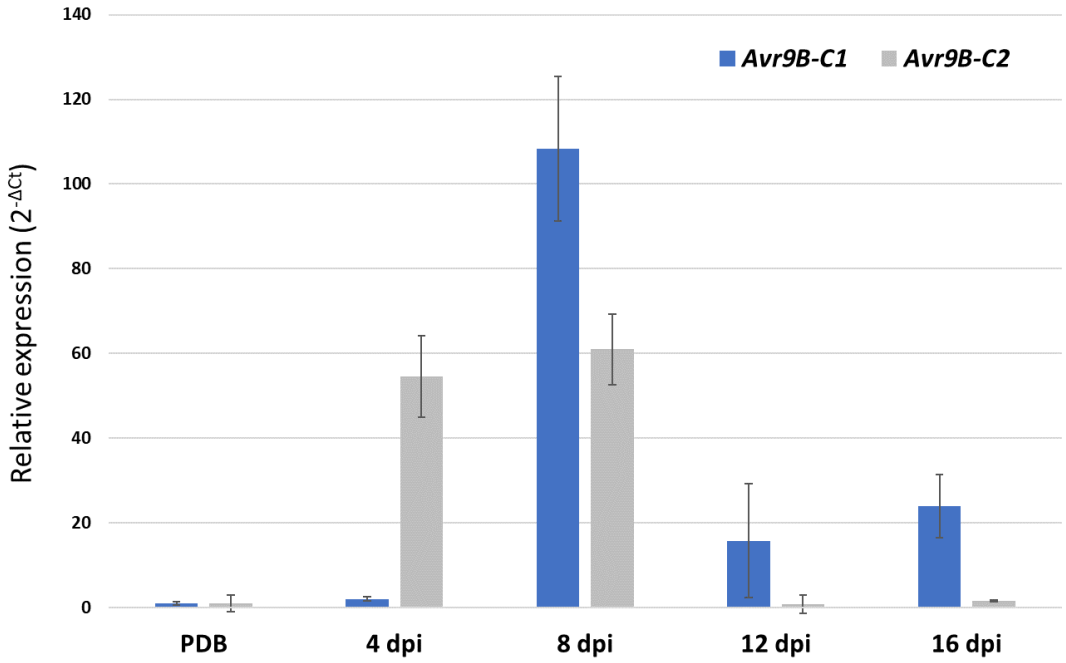

Figure 4.4. The *Avr9B* candidate genes are strongly induced *in planta*, relative to expression in culture. Expression was analyzed by a quantitative real-time polymerase chain reaction (RT-qPCR) experiment, from a compatible *Cladosporium fulvum* strain 5 (IPO 1979)–*Solanum lycopersicum* 'Money Maker' (Cf-0) interaction at 4, 8, 12 and 16 days post inoculation (dpi), as well as in culture in potato dextrose broth (PDB). Expression was normalized to the *actin* gene according to the $2^{-\Delta Ct}$ method. Error bars represent the standard deviation of three biological replicates.

4.3.4 Candidate Avr9 effectors have homologs in other fungal pathogens

To determine whether homologs of Avr9B-C1 and Avr9B-C2 are present in other fungi, each was screened against publicly available sequence databases in NCBI using BLASTp and tBLASTn. Using Avr9B-C1 as query resulted in a hit to a hypothetical protein in the Protea-associated Dothideomycete species, *Saccharata proteae* (GenBank ID KAF2088685; 61% amino acid identity) (Haridas et al., 2020), as well as hits to hypothetical proteins from Sordariomycete fungi, specifically the sweet potato pathogen *Fusarium denticulatum* (GenBank ID KAF5684395; 43% amino acid identity) (Kim et al., 2020) and the mango pathogen *F. mexicanum* (GenBank ID KAF5529800; 41% amino acid identity) (Kim et al., 2020) (Fig. 4.5).

Homology searches using Avr9B-C2 as a query uncovered similarity to hypothetical proteins present only in Dothideomycetes. These homologs could be

divided into two groups. The first group contained proteins with 8 conserved Cys residues and a predicted IDR (Fig. 4.6). Such IDRs varied in sequence, number of repeats, and others lacked any repeat units in their IDRs. Full-length homologs of this group were found in other fungal pathogens, for example, the maize and tomato pathogens *Curvularia geniculata* (NCBI genome ID: PQMW01000002, 27% amino acid identity) (de Siqueira et al., 2021; de Siqueira et al., 2018) and *Curvularia lunata* (NCBI genome ID: JFHG01001162, 27% amino acid identity) (Gao et al., 2014; Siqueira et al., 2017), the endophytic fungus *Curvularia papendorfii* (NCBI genome ID: JXCC01000110, 28% amino acid identity identity) (Kuan et al., 2015), the leaf grey spot pathogen of tomato *Stemphylium lycopersici* (GenBank ID TW65_01570, 33% amino acid identity) (Franco et al., 2015), and the causal agent of leaf blight in diverse plants (e.g., onion, garlic, asparagus, tomato), *Stemphylium vesicarium* (NCBI genome ID: VHPU01001430, VHPT01001605; 27% amino acid identity) (Gazzetti et al., 2019; Sharma et al., 2020) (Fig. 4.6). In addition, this group included two genes from *Alternaria gansuensis* and *C. geniculata* that are likely pseudogenized as they lack two Cys residues and contain a premature stop codon, respectively.

The second group contained a C-terminal extension with two extra Cys residues (10 in total), with only a few proteins in this group predicted to possess an IDR (Fig. 4.7). Full-length Avr9B-C2 homologs in this group appear among a wide diversity of pathogens affecting different crops, for example in the sorghum pathogen, *Bipolaris cookei* (23% amino acid identity) (Zaccaron & Bluhm, 2017). However, the gene in this pathogen appears to be a pseudogene; it is split across two scaffolds and is disrupted by other sequence. It could of course be, however, that the genome for this pathogen was not correctly assembled. Another Avr9B-C2 homolog is present in the Victoria blight pathogen of oats, *Bipolaris victoriae* (24% amino acid identity) (Condon et al., 2013). Nevertheless, the homolog in this species has non-canonical intron-exon splice sites, so may also be a pseudogene. Other homologs belong to *Curvularia* species (~20% amino acid identity) (de Siqueira et al., 2018; Gao et al., 2014), the leaf spot pathogen of cowpea, *Pseudocercospora cruenta* (22% amino acid identity) (Navathe et al., 2020), the corn leaf disease pathogen *Exserohilum rostratum* (22% amino acid identity) (Wang et al., 2021) the yellow Sigatoka pathogen *P. emusae* (15% amino acid identity) (Chang et al., 2016), the black leaf mould pathogen of tomato, *P. fuligena* (22% amino acid

identity) (Zaccaron, 2020), the husk spot pathogen of macadamia, *P. macadamiae* (19% amino acid identity) (Akinsanmi & Carvalhais, 2020), the pine pathogen *P. pini-densiflorae* (21% amino acid identity) (Sakalidis et al., 2017), the leaf blight pathogen of rubber, *P. ulei* (17% amino acid identity) (Guyot & Le Guen, 2018; Hora Júnior et al., 2014) and the yellow stunt and root rot of milk-vetch *Alternaria gansuensis* (13% amino acid identity) (Liu et al., 2016) (Fig. 4.7).

Figure 4.5. Avr9B-C1 from *Cladosporium fulvum* has similarity to uncharacterized proteins present in other fungal plant pathogens. Protein sequences were aligned using Clustal Ω. Protein IDs and species names are as follows: Avr9B-C1 (*Cladosporium fulvum* strain 0WU) (de Wit et al., 2012) , Ecp5 (*C. fulvum* strain IPO 2679), KAF2088685 (*Saccharata proteae*) (Haridas et al., 2020), KAF5684395 (*Fusarium denticulatum*) (Kim et al., 2020), KAF5529800 (*Fusarium mexicanum*) (Kim et al., 2020). Predicted signal peptides are underlined. Cysteine residues are shown in bold font. Amino acid conservation is shown in blue, with dark blue representing strict conservation.

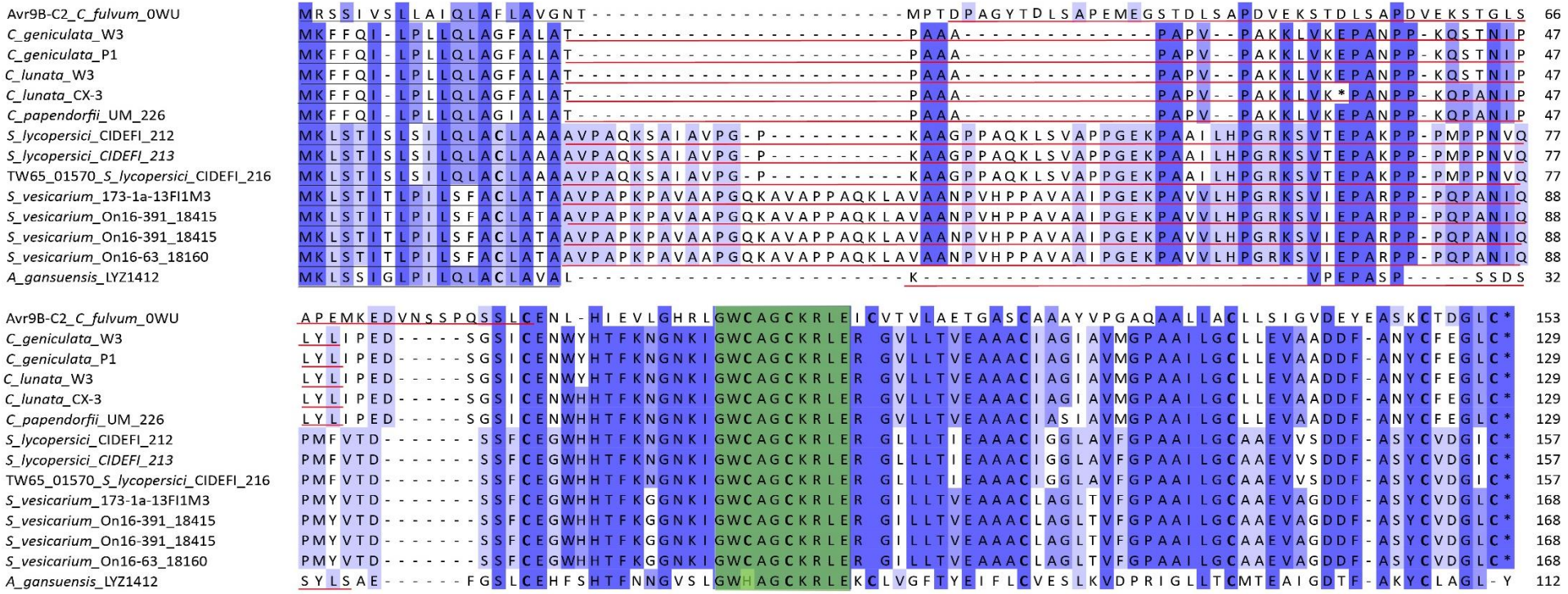

Figure 4.6. Avr9B-C2 from *Cladosporium fulvum* has similarity to uncharacterized proteins present in other fungal plant pathogens (Group 1). Protein sequences were aligned using Clustal Ω. Avr9B-C2 was aligned with similar proteins based on tBLASTn conducted in the NCBI server. Species names are as follows: *Curvularia geniculata* strain W3 and P1 (de Siqueira et al., 2021; de Siqueira et al., 2018) and *Curvularia lunata* strain W3 and CX-3 (Gao et al., 2014; Siqueira et al., 2017), *Curvularia papendorfii* (Kuan et al., 2015), *Stemphylium lycopersici* strains CIDEFI 212, CIDEFI 213 and CIDEFI 216 (Franco et al., 2015), *Stemphylium vesicarium* strains 173-1a-13FI1M3, On16-391 and On16-63 (Gazzetti et al., 2019; Sharma et al., 2020) and *Alternaria gansuensis* strain LYZ1412 (Liu et al., 2016). Predicted signal peptides are underlined in black. Cysteine residues are shown in bold font. Amino acid conservation is shown in blue, with dark blue representing strict conservation. Predicted intrinsically disordered regions are underlined in red. The most conserved region of the alignment is boxed in green.

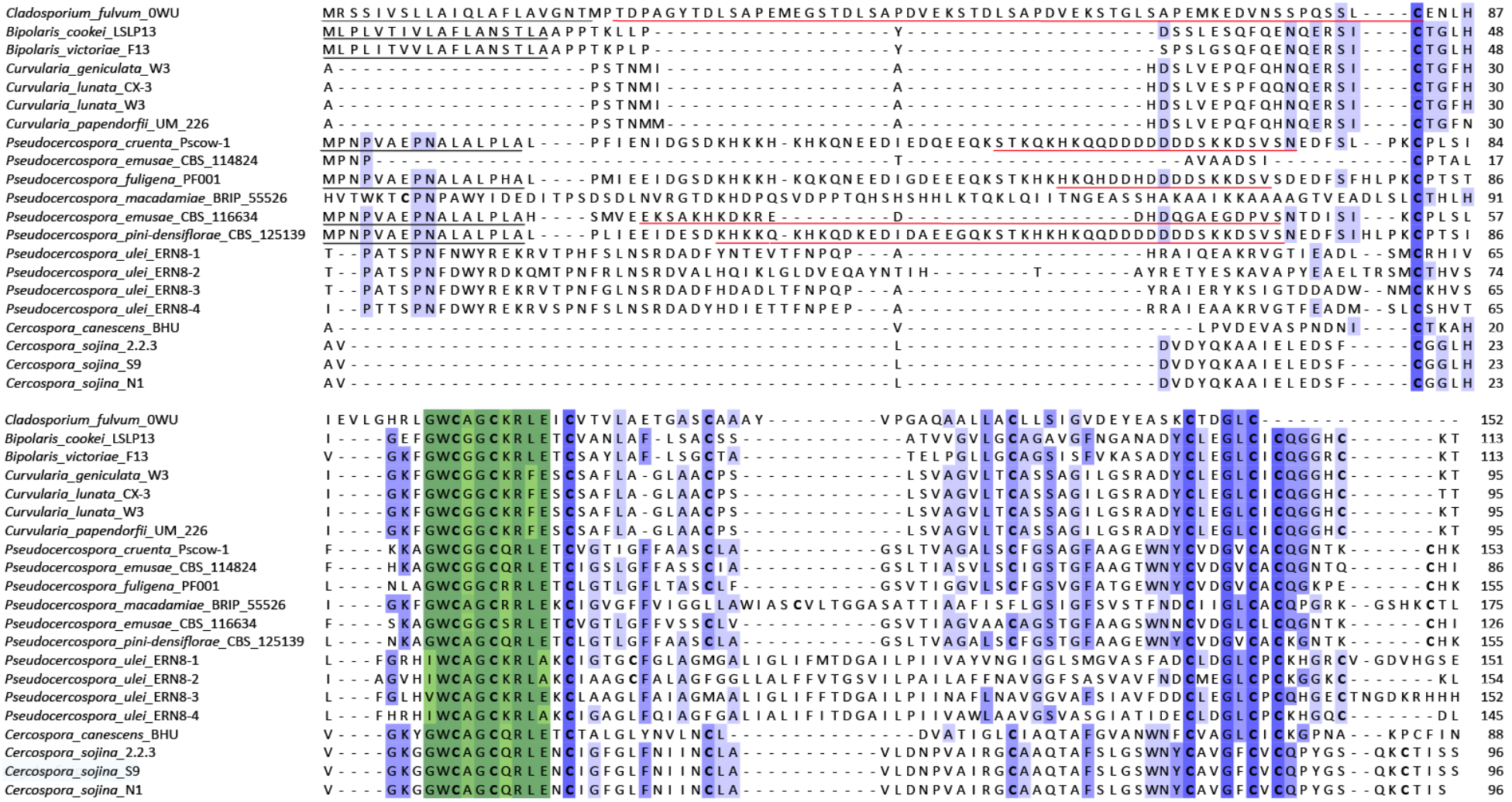

Figure 4.7. Legend on next page.

Figure 4.7. Avr9B-C2 from *Cladosporium fulvum* has similarity to uncharacterized proteins present in other fungal plant pathogens (Group 2). Protein sequences were aligned using Clustal Ω. Avr9B-C2 was aligned with similar proteins based on tBLASTn conducted in NCBI server. Species names are as follows: *Pseudocercospora ulei* strain ERN8 1-4 (Guyot & Le Guen, 2018; Hora Júnior et al., 2014), *Pseudocercospora macadamiae* strain RIP_55526 (Akinsanmi & Carvalhais, 2020), *Pseudocercospora pini-densiflorae* strain CBS 125139 (Sakalidis et al., 2017), *Pseudocercospora emusae* strains CBS_116634 and CBS_114824 (Chang et al., 2016), *Pseudocercospora fuligena* strain PF001 (Zaccaron, 2020), *Pseudocercospora cruenta* strain Pscow 1 (Navathe et al., 2020), *Exserohilum rostratum* strains B9826, B6284, B6272, B6207, B6177, B6171, B6096 and B6094 (Wang et al., 2021), *Bipolaris victoriae* strain F13 (Condon et al., 2013), *Bipolaris cookei* strain LSLP13 (Zaccaron & Bluhm, 2017), *Curvularia geniculata* strain P1 (de Siqueira et al., 2021), *Curvularia papendorfii* strain UM 226 (Kuan et al., 2015), *Curvularia lunata* strain W3 and CX-3 (Gao et al., 2014; Siqueira et al., 2017), *Curvularia geniculata* strain W3 (de Siqueira et al., 2018), *Cercospora sojina* strains S9, N1, 2.2.3, Race 15 (Fagundes et al., 2018; Luo et al., 2018; Xin, 2019; Zeng et al., 2017), *Cercospora canescens* strain BHU (Chand et al., 2014). Predicted signal peptides are underlined in black. Cysteine residues are shown in bold font. Amino acid conservation is shown in blue, with dark blue representing strict conservation. Predicted natural disordered regions are underlined in red. The most conserved region of the alignment is boxed in green.

4.3.5 *A. tumefaciens* transient expression transformation assays

4.3.5.1 Only one Avr9B effector candidate triggers a Cf-9B-dependent cell death response

As a starting point, it was first confirmed that Cf-9B triggers an HR when expressed alone in *N. benthamiana* (Fig. A.10). This is in line with the observation of a previous study (Chakrabarti et al., 2009), in which a component of the apoplastic wash fluid of *N. benthamiana* triggered a Cf-9B-dependent cell death response. Hence, *N. tabacum* was used for ATTAs. Each candidate Avr9B effector, fused to the PR1α *N. tabacum* secretion signal for delivery into the plant apoplast, and a 3xFLAG tag for detection via Western blot, was screened in *N. tabacum* separately and also in conjunction with Cf-9B to determine whether either candidate can trigger a Cf-9B-dependent HR. As anticipated, the positive control INF1, a elicitor protein from *Phytophtora infestans* (Kamoun et al., 1998), consistently triggered a strong cell death response upon recognition by a cell surface lectin-like receptor kinase pattern recognition receptor in *N. tabacum* (Kanzaki et al., 2008). Likewise, the negative control empty vector (EV; pICH86988) did not trigger a cell death or chlorotic response, but only a ring related to the mechanical damage from the needleless syringe (Fig. 4.8A-B). A chlorotic (or a very infrequently cell death) response was observed across the infiltration zone when expressing Avr9B-C2 by itself, whereas no response was observed for both versions of Avr9B-C1 (from *C. fulvum* strains 0WU and IPO 2679, respectively) (Fig. 4.8A). The inability of both Avr9B-C1 versions to trigger cell death with the R gene was not due to the lack of Avr9B-C1, as they could be detected via Western blotting (Fig 4.8C). The Cf-9 protein, which recognizes the Avr9 effector from *C. fulvum*, as expected, did not induce any response, whereas Cf-9B induced a negligible chlorotic-like response on its own (Fig. 4.8A). As predicted, co-expression of Cf-9 with Avr9B-C1 from 0WU, Avr9B-C1 from IPO 2679 or Avr9B-C2 did not induce any response (Fig. 4.8A). Similarly, no response was observed upon co-expression of Cf-9B with Avr9B-C1 from 0WU, or IPO 2679 (Fig. 4.8A). Interestingly, however, co-expression of Cf-9B with Avr9B-C2 induced a consistent strong cell death response covering the entire infiltration zone (Fig. 4.8A), suggesting that Avr9B-C2 is in fact Avr9B.

4.3.5.2 A signal peptide but not the repetitive region in Avr9B-C2 is required for a Cf-9B-dependent cell death response

ATTAs in the previous section were performed using Avr9B-C2 containing the PR1α signal peptide of *N. tabacum* for delivery into the apoplast, resulting in a chlorotic response alone or Cf-9B-dependent cell death. To determine if apoplastic localization is required to trigger such responses, Avr9B-C2 was expressed in *N. tabacum* using an ATTA, but without the PR1α signal peptide (ΔSP). In congruence with previous observations, the positive control INF1 triggered a consistent strong cell death response, whereas the negative control EV, triggered no response. In contrast to the observations in section 4.3.5.1, Avr9B-C2 without a signal peptide (ΔSP) failed to trigger a chlorotic response by itself or cell death when co-expressed with Cf-9B (Fig. 4.8B). To assess whether the repetitive IDR present in the Avr9B-C2 protein is required to trigger chlorosis alone or a Cf-9B-dependent cell death response in *N. tabacum*, a version of this protein was also expressed using an ATTA but without this IDR (containing repeats R1–R4) (Fig 4.8B). Unlike the observations of Avr9B-C2 (ΔSP) where chlorosis and Cf-9B-dependent cell death were abolished, IDR (R1–R4) in Avr9B-C2 was not required for these responses, as the responses were similar to those with the wild type version of Avr9B-C2 (Fig 4.8B). Taken together, these results suggest that apoplastic localization, but not the repetitive region, is required for the ability of the Avr9B-C2 protein to trigger a chlorotic response and Cf-9B-dependent cell death. It is important to mention that Avr9B-C2 could not be detected via Western blotting in any of the three tested versions (including the wild type allele) (Fig. 4.8C). Thus, it remains possible that the version of Avr9B-C2 without the PR1α signal peptide is not stable in the apoplast of *N. tabacum*.

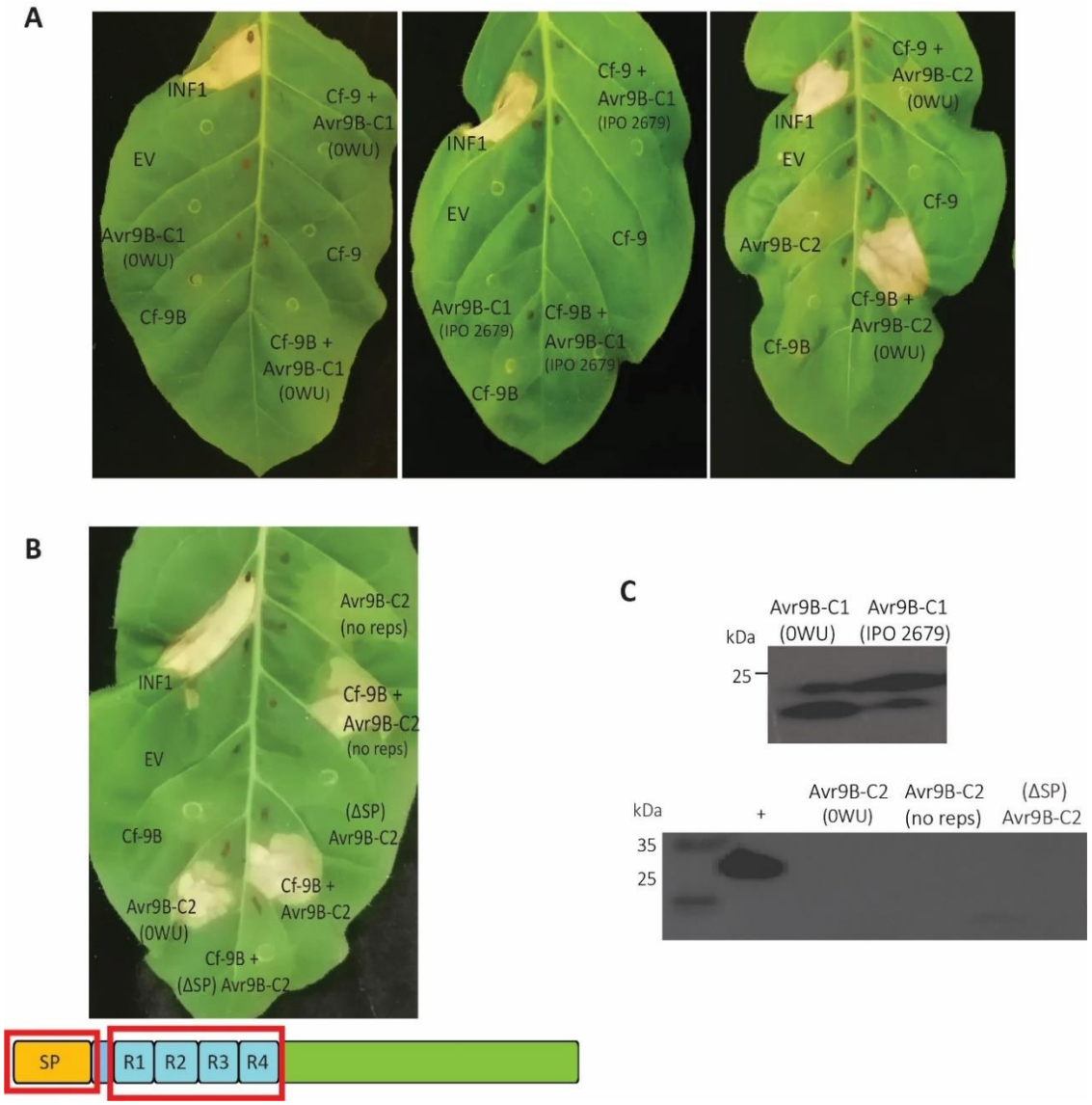

Figure 4.8. Co-expression of candidate Avr9B avirulence effectors Avr9B-C1 or Avr9B-C2 from *Cladosporium fulvum* with the Cf-9 or Cf-9B R proteins of tomato in the model non-host species *Nicotiana tabacum* using *Agrobacterium tumefaciens*-mediated transient transformation assays (ATTAs). The INF1 elicitin protein from *Phytophthora infestans* was used as a positive control and empty vector pICH86988 (EV) as a negative control. **(A)** Co-expression of Avr9B-C2 with Cf-9B, but not Avr9B-C1, triggered a strong cell death response. **(B)** Avr9B-C2 infrequently triggers a strong cell death response on its own. Co-expression of Avr9B-C2 without the Pathogenesis-Related protein 1α (PR1α) signal peptide (ΔSP) with Cf-9B did not trigger a cell death response. Co-expression of Avr9B-C2 without the repetitive region (no reps; R1–R4) with Cf-9B did not compromise the cell death response. The figure below the leaf indicates regions of the protein that were removed (red boxes). Photos were taken at 5 days post-infiltration and are representative of at least 3 independent ATTA experiments. **(C)** Protein detection by Western blotting (Avr9B-C2 could not be detected, likely due to inaccessibility to the FLAG tag). Protein samples were collected from leaf samples and the 3xFLAG tag was used for detection. Expected size for Avr9B-C1=17 kDa and the expected size for Avr9B-C2=20 kDa. Positive control (+) is a *Dothistroma septosporum* candidate effector (MW=25 kDa) (Tarallo, unpublished). Figures cropped for simplification, and original blots appear in Figure A.11.

4.3.5.3 Avr9B-C2 homologs from other fungal tomato pathogens trigger a chlorotic response or cell death responses when expressed alone in *Nicotiana* tabacum

To test whether Avr9B-C2 homologs from the tomato pathogens *S. lycopersici* (TW65_01570) and *P. fuligena* (HII31_03919) identified in section 4.3.4 could also trigger a Cf-9B-dependent HR, each protein, fused to the PR1α *N. tabacum* secretion signal for delivery into the plant apoplast and a 3xFLAG tag for detection via Western blot, was co-expressed with Cf-9B using ATTAs in *N. tabacum* and visualized at 5 days post-infiltration. As expected, the positive control INF1 triggered a strong cell death response, while the negative control EV triggered no response. TW65_01570 triggered a strong but 'patchy' cell death response in approximately 80% of the infiltration zone by itself (Fig. 4.9A). When co-expressing TW65_01570 with Cf-9 and Cf-9B, a similar cell death response was observed. Hence, it was not possible to determine whether TW65_01570 is recognized by Cf-9B (Fig. 4.9A). Similarly to Avr9B-C2, HII31_03919 triggered a chlorotic response by itself. However, in contrast to Avr9B-C2, no Cf-9B-dependent HR was observed (Fig. 4.9A), suggesting that this protein is not recognized by Cf-9B. Unlike Avr9B-C2, expression of the TW65_01570 and HII31_03919 proteins could be confirmed via Western blot (Fig. 4.9B).

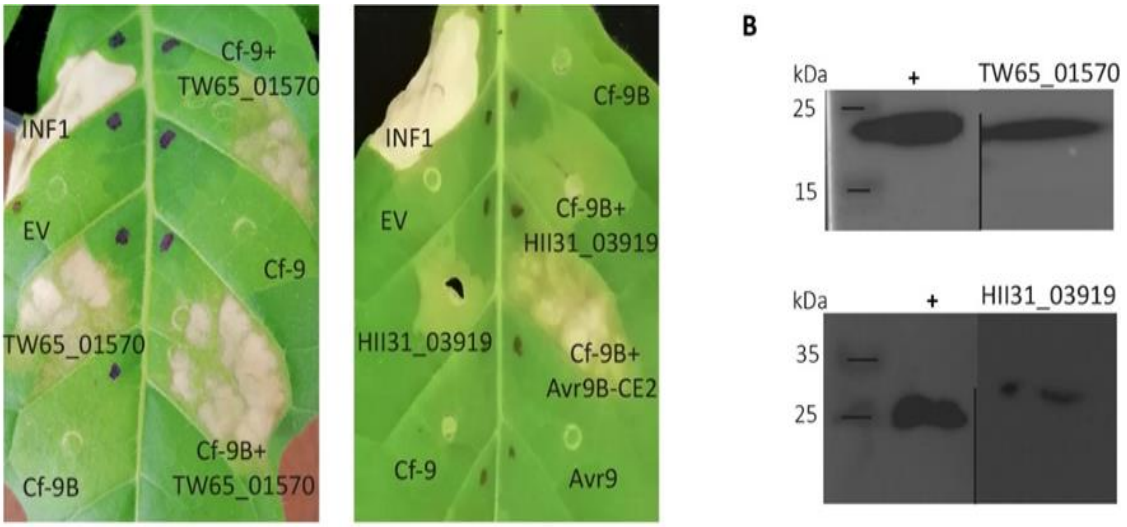

Figure 4.9. Co-expression of Avr9B-C2 homologs from the tomato pathogens *Stemphylium lycopersici* and *Pseudocercospora fuligena* with the Cf-9 or Cf-9B R proteins of tomato in the model non-host species *Nicotiana tabacum* using *Agrobacterium tumefaciens*-mediated transient transformation assays (ATTAs). The INF1 elicitin protein from *Phytophthora infestans* was used as a positive control and empty vector pICH86988 (EV) as a negative control. **(A)** The apoplastic localized TW65_01570 (*S. lycopersici*) and HII31_03919 (*P. fuligena*) triggered cell

death and chlorosis, independently of Cf-9B, respectively. Photos were taken at 5 days post-infiltration and are representative of at least 3 independent ATTA experiments. **(B)** Protein detection by Western blotting. Expected size for TW65_015E70=20 kDa, and the expected size for HII31_03919=24 kDa. Protein samples were collected from leaf samples and the 3xFLAG tag was used for detection. Positive control is a *Dothistroma septosporum* candidate effector (MW=25 kDa) (Tarallo, unpublished). Figures cropped for simplification; original blots appear in Figure A.11.

4.3.5.4 A cysteine-to-serine substitution at position 77 of Avr9B-C2 compromises recognition by Cf-9B

To investigate whether the cysteine residues in the 10 amino acid conserved sequence (GWCAGCKRLE) are determinants for Avr9B-C2 avirulence function (i.e. recognition), single Cys-to-Ser amino acid substitutions at positions 77 and 80 of the mature protein (following signal peptide cleavage) were performed (Fig. 4.10B). Both protein versions were assessed for recognition by Cf-9B using ATTAs. Similar to previous results, the negative control did not trigger a response, whereas the positive control INF1 elicited a strong cell death reaction (Fig. 4.10A). The wild type version of Avr9B-C2 triggered the characteristic chlorotic response and a Cf-9B-dependent cell death as observed in section 4.3.5.1 (Fig. 4.10A). The Cys-to-Ser substitution at position 77 in Avr9B-C2 (hereafter referred to as C77S), compromised the chlorotic response and the Cf-9B-dependent HR (Fig. 4.10A). The chlorotic response caused by the Cys-to-Ser substitution at position 80 (hereafter referred to as C80S) was almost indistinguishable compared to the wild type, whereas a Cf-9B-dependent cell death was not abolished (Fig. 4.10A). Notably, in contrast to the wild type version of the protein (Fig. 4.8) both mutated versions of Avr9B-C2 (containing the PR1α signal peptide) could be detected via Western blotting (Fig. 4.10C).

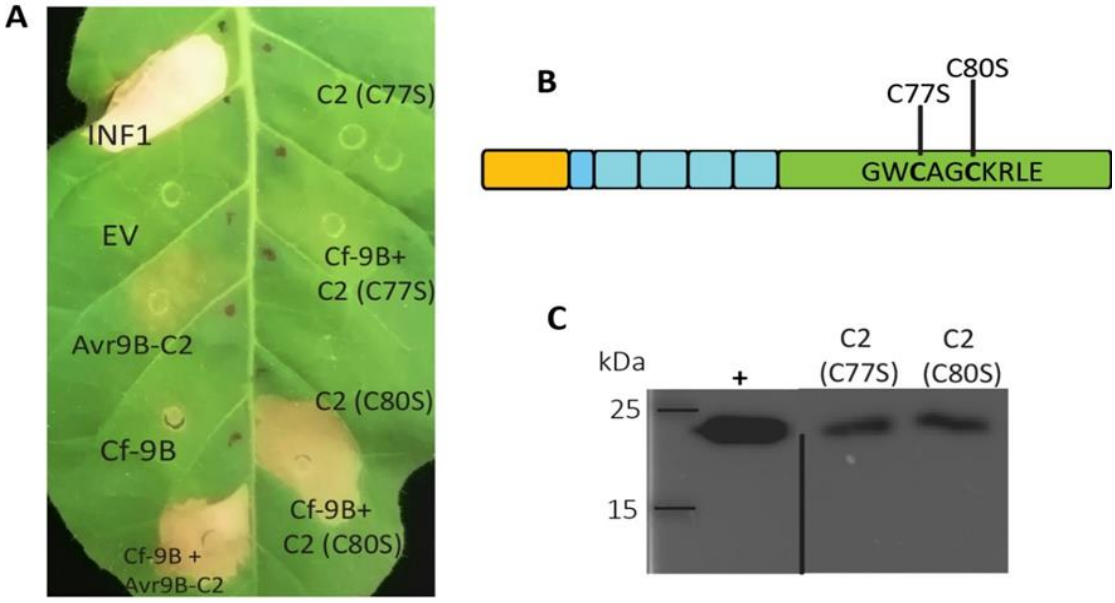

Figure 4.10. A cysteine to serine substitution at position 77 is indispensable for the Avr9B-C2 chlorotic response, as well as to trigger a Cf-9B-dependent hypersensitive response. (A) Cys-to-Ser substitutions in Avr9B-C2 protein were investigated using *Agrobacterium tumefaciens* transient transformation assays. The INF1 elicitin protein from *Phytophthora infestans* was used as a positive control and empty vector pICH86988 (EV) as a negative control. The wild type version of Avr9B-C2 was also used as positive control in conjunction with Cf-9B. The C77S substitution abolished chlorosis and the Cf-9B-dependent HR. The C80S substitution considerably reduced the chlorotic response, but not the Cf-9B-dependent HR. Photos were taken at 5 days post-infiltration and are representative of at least 3 independent ATTA experiments. **(B)** Figure representing the location of Cys-to-Ser substitutions in the conserved GWCAGCKRLE motif. **(C)** Protein detection by Western blotting. Protein samples were collected from leaf samples and the 3xFLAG tag was used for detection. Positive control is a *Dothistroma septosporum* candidate effector (MW=25 kDa) (Tarallo, unpublished). Figures cropped for simplification, original blots appear in Figure A.11.

4.3.5.5 ATTAs in tomato

To investigate whether the responses observed in *N. tabacum* could be reproduced in tomato MM-Cf-0, ATTAs were performed using the *A. tumefaciens* strain 1D1246 that was previously reported to induce high levels of transient expression in solanaceous plants without causing necrosis (Wroblewski et al., 2005). Unfortunately, however, necrotic responses were observed in the majority of the leaves infiltrated by the bacterium itself (Fig. A.12). As the Avr9B–Cf-9B interaction in tomato is characterized by accumulation of PR proteins (Laugé et al., 1998), apoplastic wash fluid was collected from infiltrated leaves at 2 days post-infiltration (before necrosis

occurred) and analyzed by SDS-PAGE to see whether PR proteins (e.g. P69, β-1,3-glucanases, chitinases, and P14) accumulate in the apoplast. Unfortunately, no differences were observed among samples (Fig. A.13), leading to inconclusive results.

4.3.6 Candidate Avr9B restores avirulence on MM-Cf-9 tomato plants

C. fulvum IPO 2679 circumvents *Cf-9* and *Cf-9B*-mediated resistance, and therefore is able to infect tomato lines carrying the *Hcr-9* introgression segment. Complementation experiments, in which a functional copy of the *Avr9B-C1* and *Avr9B-C2* genes from strain 0WU transformed into strain IPO 2679, were carried out to determine if avirulence on MM-Cf-9 could be restored. As expected, mock inoculation of plants displayed no disease symptoms, whereas all strains inoculated on MM-Cf-0 resulted in infection (no *Cf* genes; compatible interaction) that resulted in wilting of leaves (Fig. 4.11). As expected, the wild type strain, 7320 (carrying *Avr9B* but lacking *Avr9*) resulted in an incompatible interaction (no disease) on MM-Cf-9 plants (Figs. 4.11 and 4.12). Strains IPO 2619 containing the empty vector pFBTS1 or the *Avr9B-C1*, were virulent on MM-Cf-9 plants which can be observed as white patches or dark green sporulation spots (Figs. 4.11 and 4.12). However, avirulence was restored with transformants carrying the *Avr9B-C2* gene when inoculated of MM-Cf-9 plants, as disease symptoms were abolished on entire plants and leaves (Figs. 4.11 and 4.12). Therefore, it was confirmed that *Avr9B-C2* is indeed the *Avr9B* gene.

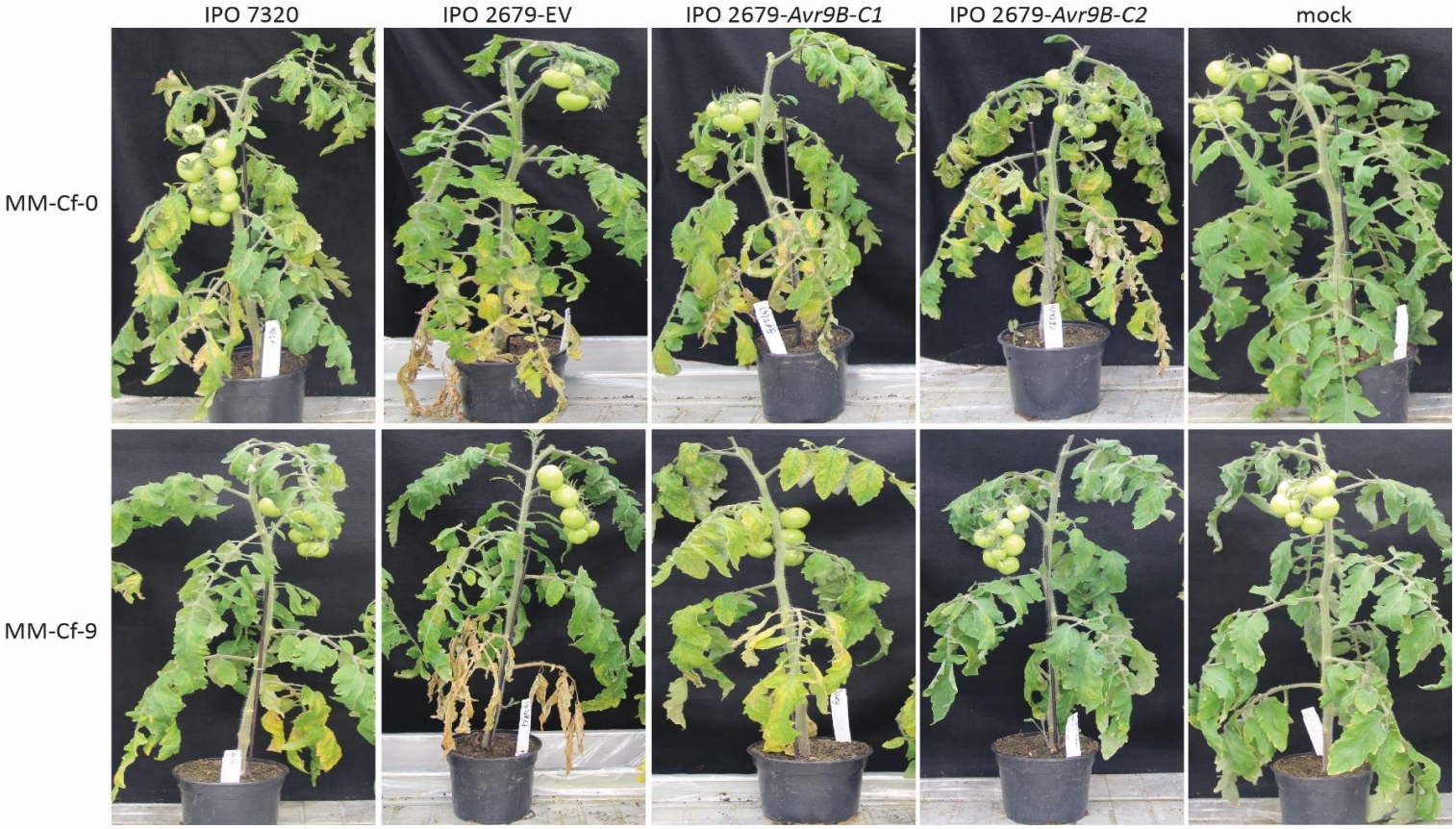

Figure 4.11. Strain IPO 2679 of *Cladosporium fulvum* complemented with *Avr9B-C1* or *Avr9B-C2*. Inoculation of MM-Cf-0 (carrying no *Cf* resistance genes) with all strains result in a compatible interaction (disease). Likewise, inoculation of MM-Cf-9 (carrying *Cf-9* and *Cf-9B*) with IPO2679 carrying the empty vector (EV) (pFBTS1; no insert) transformant or with IPO2679 transformant (4) carrying *Avr9B-C1,* results in a compatible interaction (disease). However, MM-Cf-9 plants inoculated with the wild type strain IPO 7320 (carrying *Avr9B* but lacking *Avr9*), or IPO 2679 transformant (4) carrying *Avr9B-C2*, results in an incompatible interaction (disease resistance). Results were representative of 5 transformants (except EV) assessed. Mock-inoculated plants show no disease. Photographs were taken 22 days post-inoculation.

Figure 4.12. *Avr9B-C2* of *Cladosporium fulvum* strain 0WU restores avirulence on MM-Cf-9. Inoculation of MM-Cf-0 (carrying no *Cf* resistance genes) with all strains result in a compatible interaction (disease). Likewise, inoculation of MM-Cf-9 (carrying *Cf-9* and *Cf-9B*) with IPO 2679 transformant carrying the empty vector (EV) (pFBTS1; no insert) or transformant (4) carrying *Avr9B-C1*, results in a compatible interaction (disease). MM-Cf-9 plants inoculated with the wild type IPO 7320 (carrying *Avr9B* but lacking *Avr9*), or IPO 2679 transformant (4) carrying *Avr9B-C2*, results in an incompatible interaction (disease resistance). Results are representative of 5 transformants (except EV) assessed. Photographs were taken 23 days post-inoculation.

4.3.7 Avr9B is likely localized to the plant plasma membrane

To investigate the localization of Avr9B *in planta*, Avr9B was fused to either mCherry or GFP at its N-terminus, after the PR1α signal peptide, and fluorescence visualized following ATTAs at 2 days post-infiltration in *N. tabacum* using confocal laser scanning microscopy. At the same time, the localization of versions without the PR1α signal peptide (ΔSP) were also investigated. As controls for secretion into the apoplast, mCherry and GFP were fused only to the PR1α signal peptide, which were localized in the cell periphery of plant cells (Figs. 4.13A and 4.14A). Likewise, Avr9B was observed to localize in the cell periphery of plant cells with both mCherry and GFP fusions (Figs. 4.13B and 4.14B). In contrast, the Avr9B versions without a PR1α signal peptide were found to localize at the cell periphery and the nucleus of plant cells (Figs. 4.13C and 4.14C). With the exception of the Avr9B-GFP tagged version, all proteins were detected via Western Blot (Figs. 4.13D and 4.14D). Nevertheless, free mCherry was observed in the blots, suggesting a small amount cleavage of the protein. To discern and distinguish with more detail the extracellular localization of Avr9B, plasmolysis was performed by infiltrating a sucrose solution into *N. tabacum* leaf samples expressing GFP-Avr9B immediately before microscope observations. Using this method, Avr9B appeared to localize to the plant plasma membrane (Fig. 4.15), however the signal using this method was weak.

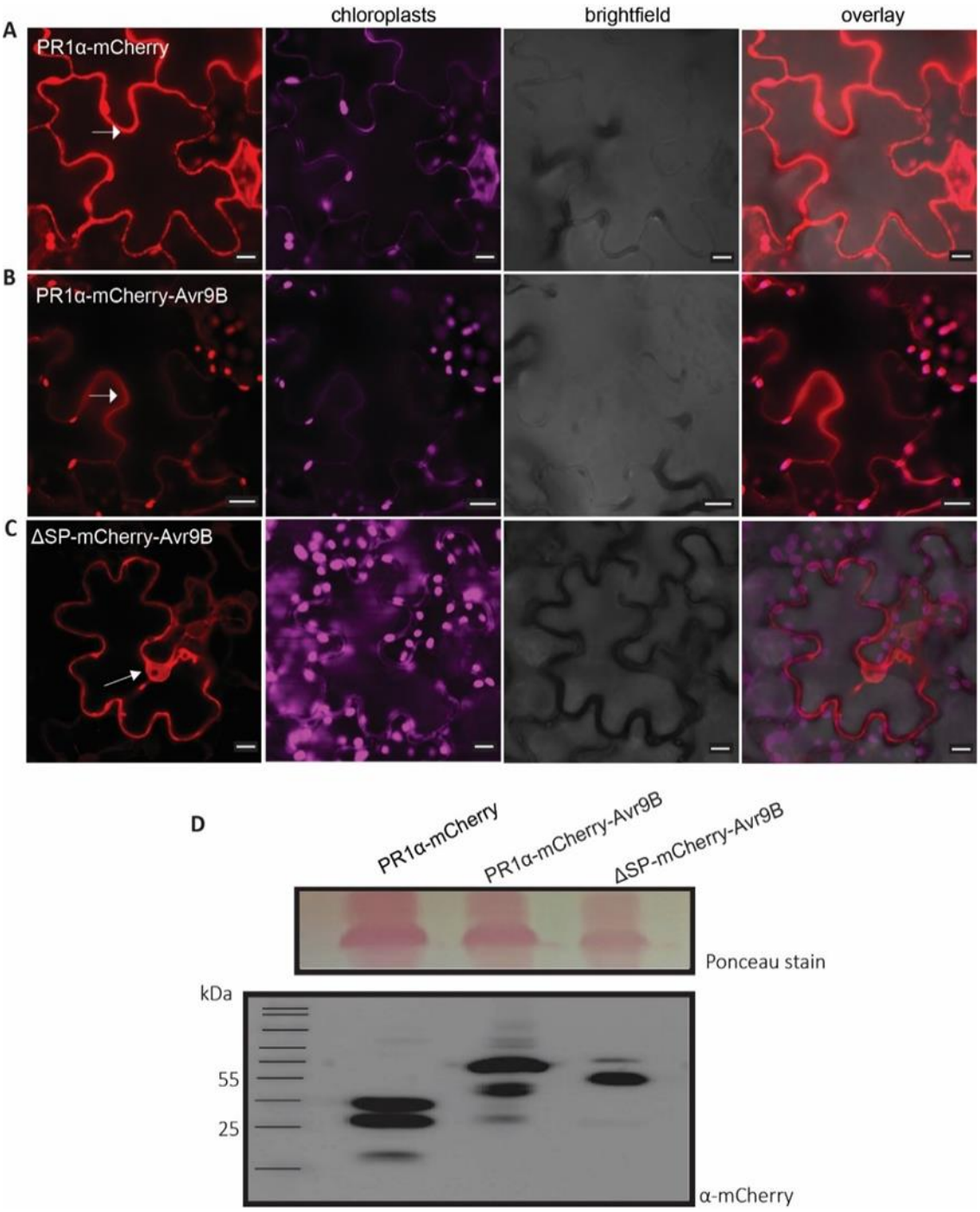

Figure 4.13. *In planta* localization of mCherry-Avr9B. *Agrobacterium tumefaciens* GV3101 carrying the expression vectors pICH86988::PRIα-mCherry, pICH86988::PRIα-mCherry-Avr9B and pICH86988::ΔSP-mCherry-Avr9B were infiltrated into *Nicotiana tabacum* leaves. Fusion proteins were visualized by confocal laser scanning microscopy at 2 days post-infiltration. **(A)** Apoplastic localisation of mCherry (white arrow); Bar= 10 µM. **(B)** mCherry-Avr9B appears to localise at the plant plasma membrane (white arrow); Bar= 20 µM. **(C)** No signal peptide (ΔSP) mCherry-Avr9B localises at cell periphery and the nucleus of plant cells (white arrow); Bar= 10 µM. Images shown are representative of at least 3 infiltrations. **(D)** Protein detection by Western blotting shows free mCherry. Total protein was collected from leaf samples and mCherry was used for detection with an anti-mCherry antibody. Expected sizes are: PR1α-mCherry=32 kDa, PRIα-mCherry-Avr9B=46 kDa, ΔSP-mCherry-Avr9B=41 kDa.

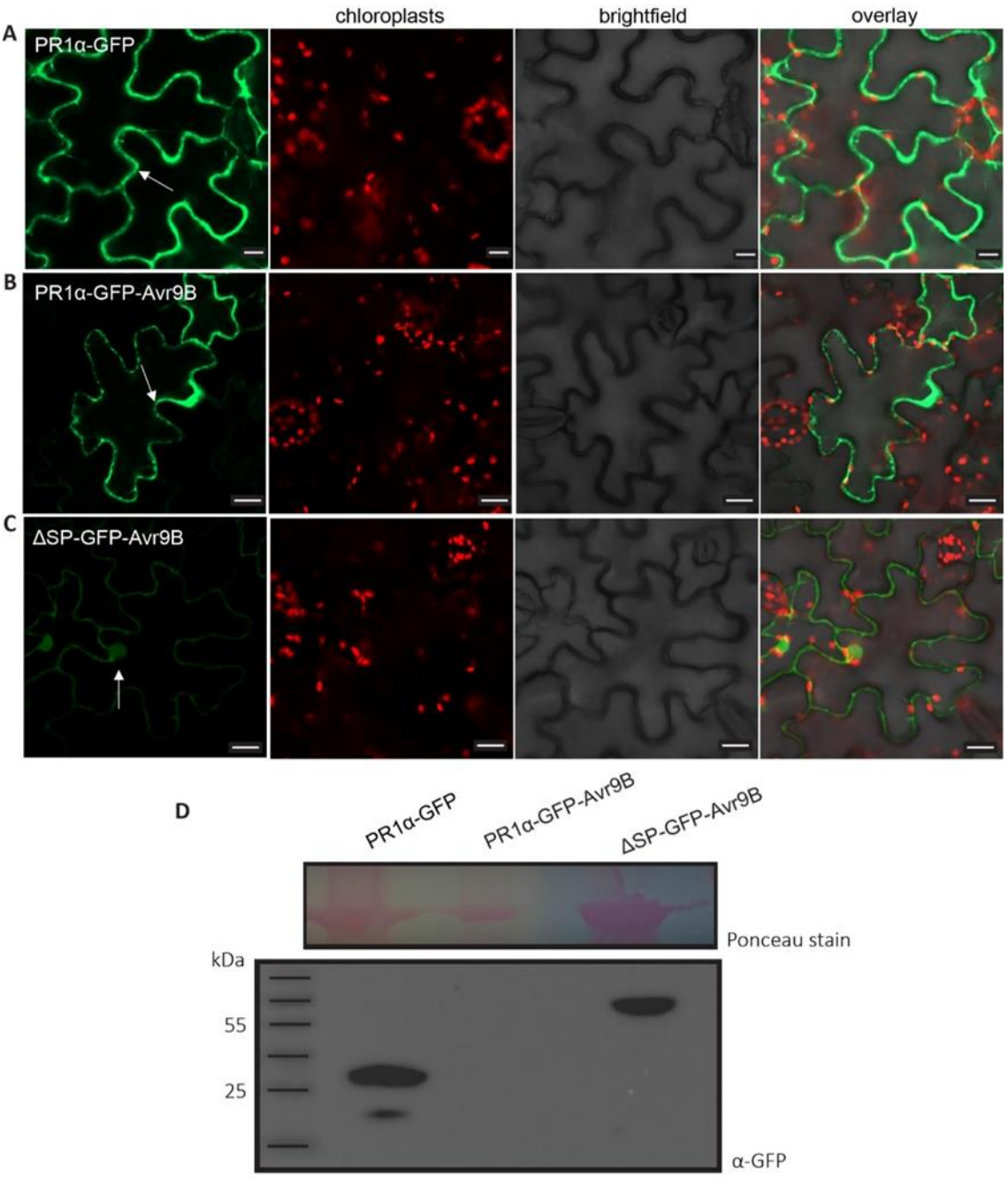

Figure 4.14. *In planta* localization of GFP-Avr9B. *Agrobacterium tumefaciens* GV3101 carrying the expression vectors pICH86988::PRIα-GFP, pICH86988::PRIα-GFP-Avr9B and pICH86988::ΔSP-GFP-Avr9B were infiltrated into *Nicotiana tabacum* leaves. Fusion proteins were analysed visualized by laser confocal laser scanning microscopy at 2 days post post-infiltration. **(A)** Apoplastic localization of GFP (white arrow); Bar= 10 µM. **(B)** GFP-Avr9B appears to localise at the plant plasma membrane (white arrow); Bar= 10 µM. **(C)** No signal peptide (ΔSP) GFP-Avr9B localises at the cell periphery and the nucleus of plant cells (white arrow); Bar= 20 µM. Images shown are representative at least 3 infiltrations. **(D)** Protein detection by Western blotting. Total protein samples were collected from leaf samples and the GFP was used for detection with an anti-GFP antibody. Expected sizes: PR1α-GFP=32 kDa, PR1α-GFP-Avr9B=46 kDa, ΔSP-GFP-Avr9B=41 kDa.

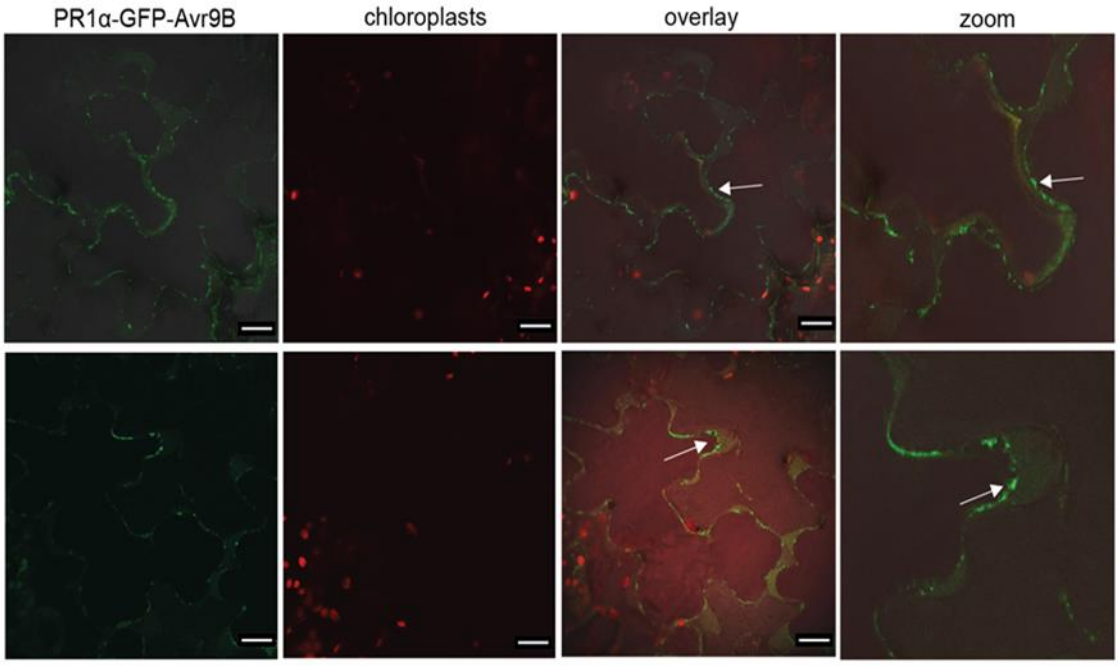

Figure 4.15. Plasmolysis of *Nicotiana tabacum* cells expressing GFP-Avr9B. *Agrobacterium tumefaciens* GV3101 carrying the expression vectors pICH86988::PRIα-GFP-Avr9B were infiltrated into *N. tabacum* leaves. White arrows indicate plant plasma membrane localization. GFP-Avr9B was visualized by confocal laser scanning microscopy at 2 days post-infiltration. To perform plasmolysis, a 1 M sucrose solution was infiltrated into leaf samples immediately prior to microscope observations. Bar= 20 µM.

4.3.8 Avr9B is predicted to adopt a novel tertiary fold

AlphaFold2, as part of the ColabFold server (Jumper et al., 2021; Mirdita et al., 2021) was used to predict the tertiary structure of Avr9B, based on a multiple sequence alignment of Avr9B and its homologs from other fungal species without their signal peptides or predicted IDRs. Predictions resulted in a tertiary structure with an pLDDT score of 90.81, and a predicted TM-score >0.75 (Fig. 4.16). The predicted structure is characterized by three alpha helices and two β-strands stabilized by four disulfide bonds (Fig. 4.16A). Comparison of the predicted Avr9B tertiary structure with solved tertiary structures present in the RCSB Protein Data Bank using the Dali server (Holm, 2020) revealed no significant structural similarity to any other protein (i.e. no hits with a Z score >2.0).

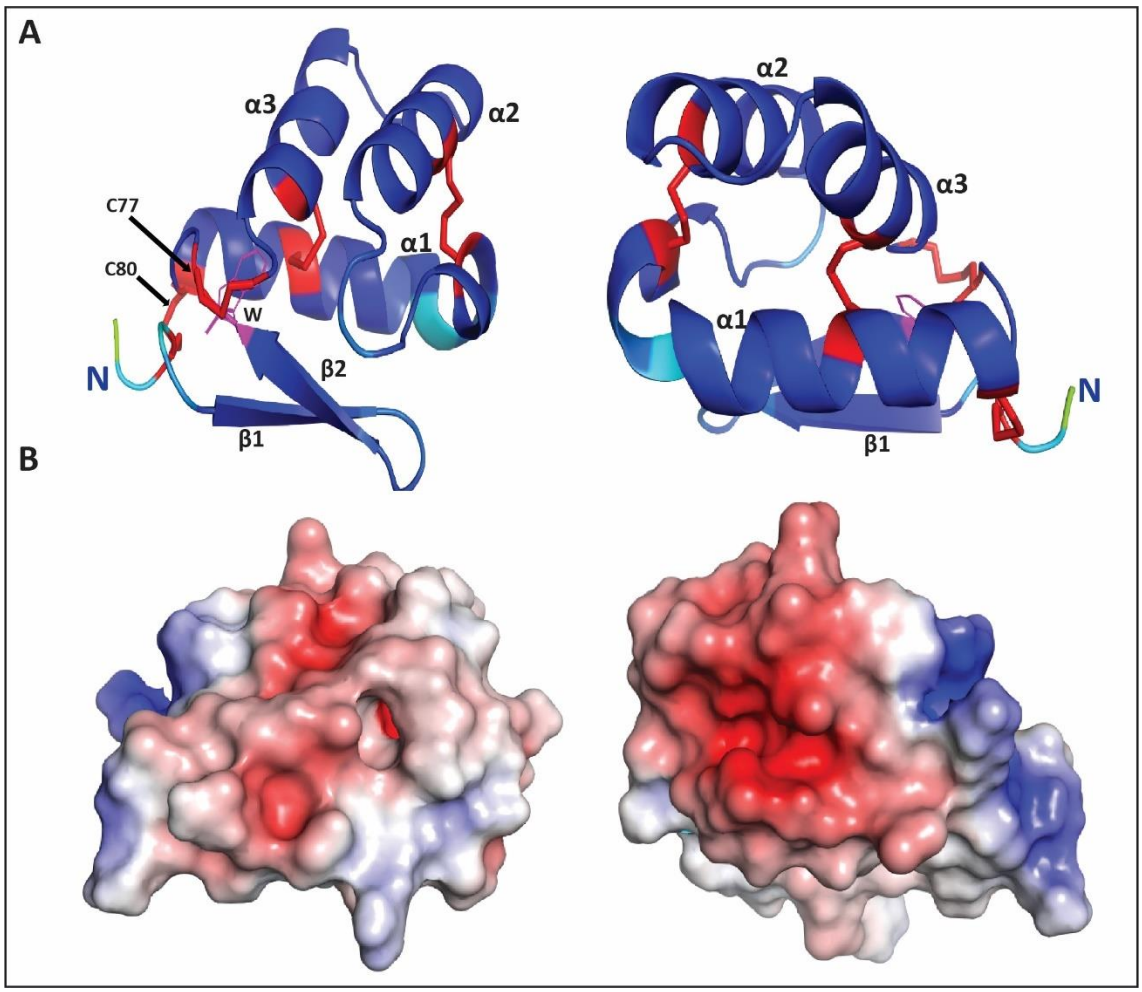

Figure 4.16. Predicted tertiary structure of Avr9B from *Cladosporium fulvum*. (A) Tertiary structure of Avr9B (frontal and back view without the putative N-terminal intrinsically disordered region) predicted by AlphaFold2 (Jumper et al., 2021). Structure is coloured according to the pLDDT score: dark blue for highly confident predicted regions while light blue and green for regions of low confidence. The β strands and α helices are numbered sequentially, and N-terminus is labeled. Disulfide bonds appear in red sticks. Cysteine residues substituted by a serine at positions 77 and 80, are indicated with black arrows. Tryptophan (W) substituted by cysteine in *C. fulvum* race 1 at position 97 appears in purple. **(B)** Surface charge potential of Avr9B (rotated 180° around the y axis). Blue represents positive charge and red negative charge. Tertiary structures were visualized and rendered using PyMol (https://pymol.org/2/) (The PyMOL Molecular Graphics System, 2015) (DeLano, 2002).

4.4 Discussion

Emerging strains overcoming Cf-9B resistance are a threat to commercial tomato production, hence Avr effector identification is crucial to understand the molecular mechanisms by which *C. fulvum* promotes colonization, as well activates and/or overcomes the plant immune system. Diverse studies have determined that such mechanisms are facilitated by selection pressure. As resistance is typically driven by single *R* genes in cultivated crops, this can lead to the rapid emergence of pathogen strains (races) that overcome resistance. Resistance can be overcome in a number of different ways, including deletion, disruption or mutation of the corresponding *Avr* effector gene (e.g., through non-synonymous and frame-shift mutations). These mechanisms can be influenced by the genomic location of effector genes and proximity of repetitive elements that can cause disruption by transposable elements (Gout et al., 2007) .

Various approaches have been deployed to identify *Avr* effector genes such as map-based cloning, reverse genetics, comparative genomics and transcriptomics. In many cases, these approaches rely on the identification of a deletion, disruption or mutation associated with circumvention of resistance (Kanja & Hammond-Kosack, 2020). In the case of *C. fulvum*, the majority of Avr effectors (i.e., Avr4, Avr4E and Avr9) have been identified using a reverse genetics approach that involves the presence of the protein in apoplastic wash fluid samples isolated from infected leaves, and infiltration into a plant host carrying a cognate R protein (Joosten et al., 1994; van Kan et al., 1991; Westerink et al., 2004). The latest Avr effector to be identified, Avr5, was found using a comparative transcriptomic approach (Mesarich et al., 2014). In the Avr5 study, 44 *C. fulvum* candidate effectors were identified and compared between strain 0WU (carries a functional copy of *Avr5*) and IPO 1979 (lacks a functional copy of *Avr5*), leading to the selection of two candidate Avr5 proteins with interesting mutations and one of these confirmed to be Avr5 through functional analyses (Mesarich et al., 2014). In this chapter, a combined whole genome sequencing and comparative SSP repertoire approach were used to identify the Avr9B effector from *C. fulvum.*

In this study, a total of 119 SSPs (<300aa, containing an N-terminal signal peptide and an even number of cysteines) expressed during infection from the reference strain of *C. fulvum* 0WU (carries a functional copy of *Avr9B*) (Mesarich et al., 2018; Mesarich

et al., 2014; Mesarich, unpublished), were compared with the sequenced New Zealand strain IPO 2679 (lacks a functional copy of *Avr9B*). Comparisons led to non-synonymous mutations in 10 of the SSP-encoding genes and two gene deletions. This low number of mutations is consistent with the Avr5 study, where very few SSPs with amino acid differences between strains were identified (Mesarich et al. 2014). From these differences, the mutations/amino acid differences in the known Avr effectors Avr2, Avr4E and Avr9 were previously identified in the allelic variation analysis performed by Stergiopolous et al. (2007) with the exception of a Cys-to-Tyr substitution at amino acid position 30 in Ecp5. From all the proteins differing between both strains, two were selected as the Avr9B effector candidates; Ecp5 (Avr9B-C1) that possesses a Cys-to-Tyr substitution, and CfCE54 (Avr9B-C2) which is encoded by a gene that is deleted in *C. fulvum* IPO 2679. Ecp5 (Avr9B-C1) was selected as the primary Avr9B candidate as it had already been reported as an Avr effector recognized by the tomato Cf-Ecp5 immune receptor. In addition, modifications in Ecp genes have been emerging recently, specifically a similar Cys-to-Tyr substitution in Ecp5 was found in four isolates (CIDEFI 318, 325, 330 and 332) of *C. fulvum* in Argentina, but at position 78 (Lucentini et al., 2021). Cys-to-Tyr substitutions identified in Avr4 were shown to not compromise the chitin-binding activity of the protein, but such substitutions altering disulfide bond pattern led to a less stable protein that is more sensitive to protease degradation in the apoplast, preventing a Cf-4 mediated response (van den Burg et al., 2003). It should be noted, however, that targeted mutation of Cys30 in Ecp5 did not lead to the circumvention of Cf-Ecp5-mediated resistance (Luderer et al., 2002).

Selection of the second Avr9B candidate protein was based on previous examples in which a gene is deleted in certain strains of *C. fulvum* to avoid recognition. Indeed, this mechanism of overcoming resistance has so far been observed for *Avr4E*, *Avr5* and *Avr9*, which are deleted in certain races of *C. fulvum* to circumvent *Cf-4E*-, *Cf-5*- and *Cf-9*-mediated resistance, respectively (Iida et al., 2015; Mesarich et al., 2014; Van den Ackerveken et al., 1992; van Kan et al., 1991; Yoshida et al., 2021). Hence, deletion of the *Avr9B-C2* gene in the strain IPO 2679 was of high interest. The *Avr9B-C1* gene is expressed in culture at a very low level and is highly expressed *in planta*, reaching the highest expression at 8 dpi. The *Avr9B-C2* gene is only expressed *in planta*, and also reaches its highest expression at 8 dpi. These expression profiles resemble other

C. fulvum Avr effector genes such as *Avr2*, *Avr5* and *Avr9*, whose peak expression is also at 8 dpi (Mesarich et al., 2014). Interestingly, homologs of both proteins are restricted to uncharacterized proteins in fungal pathogens. A third SSP gene (*CFU_830444*) with 20 non-synonymous substitutions between strain 0WU and IPO 2679 was not selected as a candidate for *Avr9B*, as the expression profile indicated that it is expressed not only *in planta* but also in culture.

Based on the consistent results from ATTA experiments using Avr9B-C2, further characterization experiments were performed on this protein. Avr9B-C2 has four repeats; a feature that is common in several other effector proteins from plant-associated organisms (Mesarich et al., 2015). The repeats of Avr9B-C2 are predicted to form the majority of an IDR; such regions do not possess a stable secondary and/or tertiary structure, but they can adapt and fold upon binding to their respective interactors to carry out their biological activities (Wright & Dyson, 1999). These proteins are characterized by their high content of charged residues and low proportion of hydrophobic residues, and are typically associated with recognition, signal transduction and transcriptional regulation (Uversky et al., 2005; Xue et al., 2014).

Disordered regions have also been predicted in effectors from bacteria (e.g. AvrPto from *Pseudomonas syringae*) whose structural flexibility has been assigned as an important feature for effector translocation, evasion of the plant immune system and host function mimicry (Marín et al., 2013). In addition, IDRs in oomycete effectors have been proposed to have a role in translocation or function. The cell death-inducing activity of the RxLR effectors PsAvh18 from *Phytophthora sojae* and PcAvh207 from *P. capsici* that contain IDRs of 37 and 18 amino acids, respectively, were tested by mutating disorder-promoting residues with the aim to convert the disordered structure into an ordered structure. Mutant versions of PsAvh18 and PcAvh207 tested via agroinfiltration in *N. benthamiana* abolished cell death-inducing activity, suggesting that IDRs might contribute to effector activity (Shen et al., 2017). To investigate if the predicted IDR in Avr9B compromised the function of the protein, an Avr9B version without the four repeats located within the predicted IDR was tested in ATTAs. Using Avr9B without the repeat region located at the N-terminus after signal peptide cleavage, surprisingly did not compromise Cf-9B-mediated cell death. This suggests that the C-terminus of Avr9B (i.e. the cysteine-rich region) is the relevant region of the protein for

recognition by Cf-9B; indeed this region contains all eight cysteine residues needed for proper protein folding, stability and recognition. The presence of predicted IDRs in all Avr9B homologs in group 1 (containing 8 cysteines) (Fig. 4.6), suggests positive evolutionary selection and relevance of such unorganized structures in virulence, as observed in effectors from bacterial and oomycete pathogens (Marín et al., 2013; Shen et al., 2017). Certainly, IDR prediction and functional characterization can enhance understanding of effector function as well as the prediction of new fungal effectors.

To determine the importance of secretion and apoplastic localization, an Avr9B version without the PR1α signal peptide for secretion to the apoplast was designed for ATTAs. Loss of the signal peptide abolished both the chlorotic activity of Avr9B and Cf-9B-mediated cell death. It should be noted, however, that the lack of a signal peptide can lead to a non-functional protein due to the absence of post-translational modifications that occur in the ER-Golgi pathway (Viotti, 2016).

As observed in Figures 4.6 and 4.7, Avr9B homologs appear only in fungal pathogens from the Dothideomycetes class, specifically the Pleosporales and Capnodiales orders, including several tomato pathogens. This suggests that these proteins may play an important role in tomato colonization. From all the homologs found, two proteins from tomato pathogens [one from group 1 (8 Cys) and one from group 2 (10 Cys)] were selected for ATTAs. TW65_01570 from the gray leaf mould necrotrophic pathogen *S. lycopersici,* and HII31_03919 from the black leaf mould pathogen *P. fuligena*. TW65_01570 consistently triggered a strong but 'patchy' cell death, therefore it was not possible to conclude a potential interaction with Cf-9B. Whereas, HII31_03919 by itself triggered a weak chlorotic response, with no cell death response when co-expressed with Cf-9B, suggesting that this protein likely does not interact with the Cf-9B R protein from tomato. Interestingly, TW65_01570, HII31_03919 and all Avr9B homologs in group 1 and 2 possess a 10 amino acid conserved GWCAGCKRLE sequence. To investigate whether the cysteine residues in this motif are crucial for Avr9B functionality, they were substituted with a serine. The difference between cysteine and serine is a single atom (sulfur versus oxygen). Substitution at position 77, resulted in a loss of chlorosis and Cf-9B-mediated cell death, whereas substitution at position 80 led to a partial reduction in chlorosis but did not compromise the Cf-9B-dependent cell death response. By analyzing the predicted structure of Avr9B,

it can be observed that cysteine to serine substitution at position 77 disrupts one of the disulfides bonds involving α-helices 1 and 3, and β-sheet 2. This disruption likely results in a highly unstable protein. The detection via Western blot of both versions of Avr9B with cys-to-ser substitutions, in contrast to the wild type protein could possibly be due to a change in the protein structure that can facilitate access of the FLAG antibody to the FLAG tag.

Previous effectoromics experiments using PVX in different tomato accessions, from which one of the expressed SSPs was Avr9B, revealed that this protein enhances the characteristic PVX symptoms in MM-Cf-0, and causes leaf curling, chlorosis and necrosis in the wild tomato species CGN14353 *Solanum pimpinellifolium* (Mesarich, unpublished). These strong responses contrast the weak resistance response observed in MM-Cf-9 plants, and may relate to previous observations in *Cf-Ecp5*- containing accessions (Iakovidis et al., 2020). Differences in the strength of defence responses were observed in multiple accessions carrying *Cf-Ecp5* when screened for Ecp5-induced HR (Iakovidis et al., 2020). Contrary to the previous concept of a single dominant *Cf-Ecp5* gene (Haanstra et al., 2000), four *Cf-Ecp5* loci were mapped on three different chromosomes (Iakovidis et al., 2020). Hence, these *Cf-Ecp5* genes evolved distinct Ecp5 recognition specificities and elements that regulate the strength of the HR (Iakovidis et al., 2020). In the same way, it could be that multiple *Cf-9* genes, with distinct Avr9B recognition specificities have evolved.

In order to determine subcellular localization of Avr9B, protein fusions using GFP and mCherry were developed for ATTAs using *N. tabacum* leaves and confocal laser scanning microscopy. Apart from Avr9B, integrity of GFP-tagged proteins were verified via Western blot, with no free GFP observed. All mCherry-tagged proteins were also verified via Western blot. However, free mCherry was observed, suggesting a cleavage of the fluorescent protein from the effector. Localization of PR1α-secreted mCherry and GFP was observed at the plant cell periphery. Green fluorescence derived from GFP-Avr9B was observed at the plant plasma membrane. Red fluorescence derived from mCherry-Avr9B was also observed at the plant plasma membrane, but at a lower intensity; such intensity variations are likely due to differences in gene expression among leaf samples, or the limited amount of expression, as the leaf samples were taken

before the onset of chlorosis, which is not ideal for reaching the highest levels of expression.

Plasma membrane localization has been reported for the SCRE2 effector from *Ustilaginoidea virens* (Fang et al., 2019). Avr9B-tagged versions without a signal peptide (ΔSP) were found to localize to the cell periphery and nucleus of plant cells. Such localization is similar to a previous report (Cao et al., 2018) in which *the Fusarium oxysporum* f. sp. *lycopercisi* effectors Avr2 and Six5 were expressed in *N. benthamiana* leaves without signal peptides. By performing cell plasmolysis to expand the apoplastic space, Avr9B appeared to localize to the plant plasma membrane. Interestingly, some of the Avr9B homologs from group 2 are predicted to possess a transmembrane domain (specifically homologs from *P. ulei* and *P. macadamiae*) which may indicate association with the plant plasma membrane. Moreover, of the *C. fulvum* effectors studied to date, only Avr9 is known to localize to high-affinity binding sites (HABS) in the plant plasma membrane (Kooman-Gersmann et al., 1996; Luderer et al., 2001). The chlorotic response of Avr9B of *N. tabacum* could be an indication of plasma membrane localization through membrane perturbation. For example, AvrB from the bacterium *P. syringae* pv. *glycinea,* is a plasma membrane-localized effector and induces cytotoxicity in *Arabidopsis* plants, indicating a possible virulence function (Nimchuk et al., 2000). Another possibility is that Avr9B could be interacting with an endogenous RLP of *N. tabacum*. To assess such outcome, SOBIR1-silenced plants could be used to determine if defence responses are impaired. In future experiments, plasma membrane localization can be further confirmed by using plasma membrane markers such as FM4-64 (Rigal et al., 2015), CD3-1007 (Nelson et al., 2007) or ACA8 (Bonza et al., 2000) to observe co-localization. The surface charge predicted for Avr9B (Fig. 4.16B) could be related to a membrane-localized protein as negative and positive charges are localized in opposite sides of the protein, the hydrophobic positively charged part of the protein interacting with membrane lipids and the hydrophilic negatively charged part of the protein facing into the cytoplasm. In addition, it could be also possible that the negatively charged site of the protein mediates interactions with positively charged ligands.

To conclude, genome comparisons between the *C. fulvum* reference strain 0WU and *C. fulvum* IPO 2679, in conjunction with a gene complementation experiment, have led to the identification of *Avr9B.* The *Avr9B* gene encodes an SSP with an intrinsically

disordered repeat-rich N-terminus, followed by a structured C-terminal cysteine-rich region. Structure prediction using AlphaFold2 revealed that Avr9B has novel fold consisting of three α-helices and two β-strands stabilized by four disulfide bonds. In identifying Avr9B, tomato growers can now identify Cf-9B resistance-breaking strains of *C. fulvum* in the field, which in turn will direct tomato cultivar selection for protection against *C. fulvum*. The research in this chapter suggests that other strains have evolved to overcome both Cf-9 and Cf-9B-mediated resistance, as indicated by sequencing of *Avr9B* gene in the race 9 strain from Japan (2.9). The loss of Cf-9 resistance exposed Cf-9B resistance through strong selection pressure to be overcome. It seems likely, given that a functional gene has only been lost from strains that have also lost the *Avr9* gene, that the loss of *Avr9B* may have occurred after *Avr9* was lost.

Chapter 5: Discussion and future directions

5.1 Introduction

There are a wide number of publications regarding the discovery and characterization of proteinaceous Avr effectors from *C. fulvum*, as well as the Cf R proteins that recognize them (reviewed in Wulff et al., 2009; de Wit, 2016; Mesarich et al., 2018). This large volume of research is, in part, a result of the ease with which the *C. fulvum*–tomato pathosystem can be studied. Indeed, *C. fulvum* can be easily cultured and transformed, tomato infection and effectoromics-based assays are both feasible and effective, apoplastic wash fluid containing Avr effector proteins from compatible *C. fulvum*–tomato interactions can be readily isolated and analyzed, and both near-isogenic and more diverse lines of tomato carrying one or more specific *Cf R* genes are available. These features, together with the fact that tomato is a fast growing, readily fruiting annual plant, have helped to rapidly expand our knowledge on the *C. fulvum*–tomato pathosystem. Despite this, many observations remained insufficiently explained prior to this thesis. Among them is the peculiar late resistance mechanism provided by the Cf-9B R protein of tomato, its interaction with the corresponding Avr9B Avr effector, and the strategies *C. fulvum* deploys to overcome Cf-9B-mediated resistance, a resistance central to fruit production in many commercial tomato cultivars.

In contrast to the *C. fulvum*–tomato pathosystem, molecular research on the *V. inaequalis*–apple pathosystem is still in its infancy, with only two *Rvi R* genes and one *Avr* effector gene cloned prior to the start of this thesis (Schouten et al., 2013; Collemare et al., 2018), despite the gene-for-gene nature of this interaction having been recognised genetically in the 1950s (Boone & Keitt, 1957; Williams & Shay, 1957). Unlike tomato, apple is a perennial tree crop that can take several years to fruit. Furthermore, while *V. inaequalis* can be easily cultured and transformed (Fitzgerald et al., 2003), and infection assays are relatively straight forward, apoplastic wash fluid cannot be isolated as leaves are difficult to infiltrate with water or buffer, and no effectoromics assay involving *Agrobacterium tumefaciens* has been established. One advantage over *C. fulvum*, however, is the ability to sexually cross isolates of *V. inaequalis* in culture,

which provides the opportunity to identify fungal genes of interest using, for example, map-based cloning and genotype–phenotype association experiments.

To better understand how *V. inaequalis* and *C. fulvum* cause disease or overcome resistance, and to monitor the occurrence of resistance-breaking isolates or strains in the field, Avr effectors from these pathogens must be identified and functionally characterized. With this in mind, the focus of this thesis was to identify and characterize proteinaceous Avr effectors from *V. inaequalis* and *C. fulvum*. This chapter summarizes the findings of this thesis and emphasizes future experiments that are required to extend knowledge on this research.

5.2 Chapter 2: Progress towards the identification of a candidate AvrRvi4 effector from *V. inaequalis*

In Chapter 2, a combined comparative genomics and phenotyping approach based on progeny from a sexual cross between *V. inaequalis* isolates that differ in their ability to overcome the *Rvi4 R* gene in apple was used to identify what is presumed to be the corresponding *Avr* effector gene, *AvrRvi4*, from *V. inaequalis*. This putative *Avr* gene encodes a cysteine-rich SSP that forms part of an expanded family consisting of six members in *V. inaequalis* reference isolate MNH120. If the candidate is subsequently confirmed to be AvrRvi4, it would be one of the only three Avr effectors/candidate Avr effectors identified from fungal tree pathogens, after AvrRvi6 from *V. inaequalis* and the candidate AvrMlp7 effector from the poplar rust fungus, *Melampsora larici-populina* (Collemare et al., 2018; Louet et al., 2021). Features and characterization of the AvrRvi6 Avr effector, as well as the molecular mechanism involved in the Rvi6-mediated resistance breakdown are still yet to be published. The candidate *AvrMlp7* effector from *M. larici-populina*, however, was recently shown to encode a 219-amino acid protein with no canonical signal peptide, and to have putatively broken *RMlp7*-mediated resistance in poplar through a nonsynonymous mutation and gene deletion of the corresponding candidate *AvrMlp7* gene (Louet et al., 2021). For the *AvrRvi4* candidate, multiple types of mutation were identified that could be responsible for the circumvention of *Rvi4*-mediated resistance in apple, including disruption by transposon insertion, deletions and point mutations, as commonly reported for other fungal

pathogens (Louet et al., 2021; Luderer et al., 2002; Wu et a., 2015; Zhou et al., 2007). Thus, provided that the candidate can subsequently be confirmed as AvrRvi4, this thesis, will have for the first time uncovered the molecular mechanisms leading to the emergence of *Rvi4* resistance-breaking strains of *V. inaequalis*.

Notably, genes encoding homologs of the AvrRvi4 protein were found to be restricted to the *Venturia* genus, with no homologs identified in other Dothideomycetes or other fungal genera. Indeed, *V. asperata*, *V. orbiculata*, *V. pyrina* and *V. nashicola*, which are scab pathogens of apple, rowan, European pear and Asian pear, respectively, were all found to possess at least one gene encoding a protein with homology to AvrRvi4. Interestingly, though, no homologs were identified in *V. effusa*, *V. carpophila* and *V. oleaginea*, which cause scab diseases of pecan, peach and olive, respectively, suggesting that members of the *AvrRvi4* family are restricted to *Venturia* pathogens infecting plants of the Malinae subtribe. Contrary to highly conserved effectors in plant-pathogenic fungi, taxon-specific effectors, such as the candidate *AvrRvi4*-type effectors found in this thesis, are known to determine host specificity in other plant–fungus pathosystems (Schulze-Lefert & Panstruga, 2011). Examples include the *PWL*, *AvrPi-ta*, *Avr-Pia*, *AVR-Pik/km/kp* and *Avr-Pii Avr* effectors from *M*. *oryzae* (Orbach et al., 2000; Yoshida et al., 2009). As such, the *AvrRvi4* candidate, if confirmed, would follow this pattern of determining host specificity.

All members of the candidate AvrRvi4 effector family are characterized by an identical cysteine pattern, a conserved N-terminal pro-domain ending in a putative Kex2 protease cleavage site, a predicted β-sandwich fold structure with a long intrinsically disordered region (IDR). Structural predictions using AlphaFold2 and CollabFold (Jumper et al., 2021; Mirdita et al., 2021), and comparisons to other proteins present in the Protein Data Bank using the Dali server (Berman et al., 2000; Holm, 2020), revealed that all AvrRvi4 members from *V. inaequalis* share a similar β-sandwich fold to the ToxA effector from *Pyrenophora tritici* f. sp. *repentis* and Avr2 effector from *Fusarium oxysporum* f. sp. *lycopersici.* However, given that the candidate AvrRvi4 effector possesses a different β-sheet topology to ToxA and Avr2, and because the ToxA and Avr2 lack both a long IDR and have a different disulfide bond configuration, it seems unlikely that the candidate AvrRvi4 effector shares a similar virulence function to ToxA and Avr2. Interestingly, the AvrLm567 Avr family from the flax rust fungus *Melampsora lini* (Wang

et al., 2007), the MAX effectors from *Pyrenophora tritici-repentis* and *M. oryzae* (de Guillen et al., 2015; Seong & Krasileva, 2021), as well as several other effector protein families from *V. inaequalis* (Rocafort et al. in preparation), also possess or are predicted to adopt a β-sandwich fold, albeit with different β-sheet topologies. This thesis therefore expands the repertoire of known β-sandwich-type effectors deployed by fungal pathogens, and adds to growing evidence that observed fungal effector proteins adopt a limited array of structural folds (Daniel et al., 2021; de Guillen et al., 2015; Lazar et al., 2021; Rocafort et al. in preparation; Seong & Krasileva, 2021). One reason why the β-sandwich is emerging as an important fold in effector biology could be that it may aid with the protein stability necessary to cope with the conditions in the apoplast or plant cells. Another reason could be that such a fold facilitates binding to multiple or specific host targets (Seong & Krasileva, 2021). With the advent of accurate protein structure prediction in the form of AlphaFold2, it will be interesting to determine whether the effector repertoires of other fungal pathogens are indeed enriched for proteins with β-sandwich folds.

5.2.1 Future research concerning the candidate AvrRvi4 effector from *V. inaequalis*

5.2.1.1 Gene complementation of NZ203.1 race (1,4)

To confirm the discovery of the *AvrRvi4* effector, a gene complementation experiment should be performed in *V. inaequalis* NZ203.1 race (1,4) to determine if avirulence on apple plants can be restored. This experiment requires *Agrobacterium tumefaciens*-mediated transformation (ATMT) or protoplast-mediated transformation of strain NZ203.1 (Fitzgerald et al., 2003; Rocafort et al., 2021) with a vector containing a wild-type copy of *AvrRvi4*, together with its native promoter and terminator regions, from isolate J222 race (1) or MNH120 race (1). After screening and single sporing transformants to ensure that they carry the wild-type *AvrRvi4* gene, these should then be inoculated onto apple leaves carrying the *Rvi4 R* gene as in Chapter 2, to see if a pin-point pit hypersensitive response (HR) is triggered (i.e. as a result of recognition of AvrRvi4 by Rvi4).

5.2.1.2 Assessment of the role that the candidate AvrRvi4 effector family members play in virulence or pathogenicity

The role in virulence and pathogenicity of many effectors from plant-pathogenic fungi has been determined by silencing or knocking out the genes that encode them (Fang et al., 2019; Zhang et al., 2019). However, while this approach is often sufficient for single-copy genes, functional redundancy can make this more difficult for genes that belong to families. Thus, the role of the candidate *AvrRvi4* effector family in virulence and pathogenicity should be assessed using CRISPR-Cas9 technology to disrupt all family members, followed by the reintroduction of single or different gene combinations using conventional complementation transformation. Importantly, this gene editing technology has already been successfully applied to *V. inaequalis* by inactivating the *trihydroxynaphthalene reductase* (*THN*) gene, to impair melanin biosynthesis (Rocafort et al., 2021). Mutant strains should then be inoculated onto susceptible apple cultivar 'Royal Gala' to determine the severity of the disease. The latter could be determined by observing and measuring symptoms by confocal microscopy, in conjunction with biomass quantification (Gusberti et al., 2012). It should be noted, however, that biomass quantification in *V. inaequalis* does not distinguish between aerial (leaf surface) and sub-cuticular growth. Hence, a stromata (sub-cuticular infection structure)-specific gene could be used for quantification (Prencipe et al., 2020).

5.2.1.3 Assessment of the role that the IDR of the candidate AvrRvi4 protein plays in triggering Rvi4-mediated resistance

To explore the role of the IDR of the candidate AvrRvi4, complementation of the isolate NZ203.1 with a mutated version of *AvrRvi4* gene (without the nucleotide sequence encoding the IDR) should be performed. Then, *V. inaequalis* transformants carrying the mutated version could be inoculated on *Rvi4* apple leaves, to determine if the IDR is necessary for a Rvi4-mediated HR. Additionally, IDR swaps between the AvrRvi4 family and homologs found in other *Venturia* species could be carried out, to determine specificities amongst these IDRs.

5.2.1.4 *In planta* and in culture localization of the AvrRvi4 effector family

To gain a better understanding of the virulence or pathogenicity function of AvrRvi4 family members, the localization of each protein during the infection process *in*

planta and in culture within cellophane membranes should be investigated. Here, each member could be fused to enhanced yellow fluorescent protein (eYFP) (Mesarich, 2011), and transformed into *V. inaequalis* isolate MNH120 or J222 via ATMT or protoplast-mediated transformation (Fitzgerald et al., 2003; Rocafort et al., 2021). Then, transformants could be inoculated onto 'Royal Gala' leaves or cellophane membranes to observe eYFP fluorescence using confocal microscopy.

5.2.1.5 Protein interaction experiments

To identify potential virulence targets, protein pull-downs and yeast two hybrid assays could be performed using AvrRvi4 with an affinity ligand to determine interacting proteins (He et al., 2018).

5.2.1.6 Assessment of the repetitive element in the *AvrRvi4* gene

Interestingly, two long repetitive regions containing three tandem repeats of 12 bp, and one extra 12-bp repeat outside the long repetitive region, were also located in the promoter region of the candidate *AvrRvi4* gene, suggesting a significant role for these repetitive elements in regulating the expression level of this gene during infection. Notably, it has been recently found that SSP-encoding genes of *V. inaequalis* are expressed in waves during infection of apple leaves (Rocafort et al., in preparation). With this in mind, a future experiment could investigate whether the promoter region of *AvrRvi4*, together with the promoter regions of other SSP-encoding genes that are in the same wave as the *AvrRvi4* family, contain shared motifs responsible for regulating their expression *in planta*.

Tandem repeats in promoter regions have been previously found, and their relevance has been studied, in other fungal effector genes (Sweigard et al., 1995; Zhu et al., 2021). To determine the role of the repetitive promoter element in the expression pattern of the candidate *AvrRvi4* gene, fluorophore-promoter fusions could be generated. For example, constructs containing the original promoter fragment of the candidate *AvrRvi4* gene, a promoter deleted for one or more of the repeats, or a promoter with additional repeats could be fused to GFP and transformed into *V. inaequalis* MNH120 or J222 using ATMT (Fitzgerald et al., 2004). Selected transformants could then be inoculated onto leaves of apple cultivar 'Royal Gala' and confocal microscopy used to examine, quantify and compare fluorescence intensity for

each construct. To measure gene expression, RT-qPCR could be performed (as specified in Section 5.2.2) from leaf samples collected at 12 and 24 hpi, as well as 3, 5 and 7 dpi.

5.2.1.7 Identification of the *Rvi4* gene

As a first step to identify the Rvi4 gene, it could be possible to sequence the apple accession TSR33T239 which carries *Rvi4*. Then, by using the available molecular markers associated with *Rvi4* (Baldi et al., 2004; Jänsch et al., 2015), it could be possible to identify *RLP* or *NLR* genes within the genome regions flanked by those markers. Then two approaches could be followed; the first one would involve cloning and co-expressing each gene with the candidate *AvrRvi4* gene in *Nicotiana* species to look for an HR. The second approach consists in the introduction of each gene into the susceptible cultivar 'Royal Gala' to see if an HR is triggered when inoculating with *AvrRvi4* carrying isolates MNH120 or J222. This approach has already been conducted with success using *Rvi15* (Schouten et al., 2013). Upon identifying Rvi4, it will be possible to determine if there is direct interaction with AvrRvi4.

Complementation of the NZ203.1 race (1,4) isolate with a functional copy of each one of the homologs found in other *Venturia* species could be performed in order to see if one of these proteins is recognized by the Rvi4 R protein in apple (i.e. triggering a pinpoint pit HR). If recognition occurs, then it may be feasible to transfer the *Rvi4* gene to European pear, for example, to provide protection against *V. pyrina*. Notably, this approach has recently been successfully applied to European pear. In this example, the *Rvi6 R* gene, which corresponds to the *AvrRvi6 Avr* effector of *V. inaequalis*, was introduced into European pear to confer resistance to *V. pyrina* (Perchepied et al., 2021). It is anticipated, although not yet confirmed, that Rvi6 is recognizing one of the AvrRvi6 homologs in *V. pyrina* to provide resistance.

5.3 Chapter 3: Identification of candidate effectors from *V. inaequalis* that trigger defence responses in non-host plants

In Chapter 3, 132 candidate effectors (CEs) from *V. inaequalis* were screened for their ability to trigger defence responses (i.e. cell death or chlorosis) in the non-host model plants *Nicotiana benthamiana* and *N. tabacum*, signifying potential recognition by an R protein in these species using *Agrobacterium tumefaciens* transient expression assays (ATTAs or agroinfiltrations). Based on this approach, three CEs were found to trigger cell death or chlorosis in one or both *Nicotiana* species. Moreover, by using versions without the tobacco signal peptide PR1α, it was concluded that the three CEs needed to be secreted to the apoplast via the Endoplasmic Reticulum (ER)-Golgi pathway to trigger these defence responses. Despite the low amino acid sequence similarity to other proteins, the three proteins that triggered a response shared structural similarity to previously characterized proteins, providing clues on their possible functions.

CE17 (Alt a 1-like) triggered a weak and strong cell death in *N. benthamiana* and *N. tabacum,* respectively. This protein shares a predicted β-barrel fold with Alt a 1 from *Alternaria alternata* and PevD1 from *Verticillium dahliae* (Chruszcz et al., 2012; Zhou et al., 2017). These proteins contain four conserved cysteine residues, forming two disulfide bonds, that link the β-strands of the protein. Due to the structural similarity, it is possible that CE17, like Alt a 1, interacts with host pathogenesis-related (PR) proteins to suppress their action. CE93 triggered a chlorotic response only in *N. benthamiana*. CE93 structural prediction revealed a β-sandwich fold containing various loops, as observed in lytic polysaccharide monooxygenases (LPMOs), specifically the LPMO AA15 from the insect *Thermobia domestica* (Sabbadin et al., 2018) and the LPMO AA13 from *Aspergillus oryzae* (Hemsworth et al., 2014). Based on the structural prediction of CE93 and its similarity to LPMOs, it is possible that this protein acts as an auxiliary enzyme to facilitate cellulose digestion. Interestingly, based on its amino acid sequence, CE93 was found to be similar to Egh16-like proteins which have been recently found to be effectors with chitinase activity (EWCA) (Martínez-Cruz et al., 2021). These effectors which seem to be widely distributed among fungal pathogens, are secreted to break

down chitin oligomers into smaller molecules, to avoid the oligomerization of the plant chitin elicitor receptor kinase (CERK1), and in this way, suppress the activation of plant defence responses (Hammoudi, 2021). With this in mind, it could be that *V. inaequalis* also uses EWCAs to avoid chitin-triggered immunity. CE126 triggered a strong cell death only in *N. tabacum*. This protein shares structural similarity with the expansin-like protein EXLX1 from *Bacillus subtilis* and the beta-expansin EXPB1 from maize (Kerff et al., 2008; Yennawar et al., 2006). These proteins are characterised by a double psi-β barrel fold (DPBB) (de Oliveira et al., 2011). The potential function of this protein corresponding with the structural similarity to expansins, is presumably cell wall remodelling during conidial attachment and germination.

In contrast to other studies where the percentage of CE proteins eliciting a defence response in *Nicotiana* species was higher (e.g. Hunziker et al., 2021; Kettles et al., 2017), in this study only 2% of CEs induced a chlorotic or cell death response. However, there are other reports where no elicitor activity was observed when screening CE proteins. For instance, from 70 selected CEs from the apple-pathogenic fungus *Valsa mali*, none could induce cell death when expressed in *N. benthamiana,* but seven of them could suppress the pro-apoptotic activity of the mouse protein BAX (BAX-induced cell death), suggesting that these CEs supress host defence responses rather than elicit them (Li et al., 2015). Considering that *V. mali* is a necrotroph, it is often thought that effectors from this type of pathogen must promote cell death. Intriguingly, suppressing host cell death could be a function of effectors at a very early stage of the infection by necrotrophic fungi in order to facilitate disease progress (i.e. as part of a very short biotrophic phase) (Li et al., 2015). As cell death suppression activity from CEs is more likely related with biotrophy, this may provide an explanation as to why so few CEs of *V. inaequalis* triggered defence responses in the two *Nicotiana* species tested. In the studies carried out by Hunziker et al. (2021) and Kettles et al. (2017), the pathogens studied were hemibiotrophs that therefore have a necrotrophic growth phase. It could therefore be that in these two studies, a higher proportion of CEs from these pathogens were inadvertently selected that triggered defence responses as part of their necrotrophic growth phase.

A common theme among CEs that trigger cell death in *Nicotiana* species is however emerging. For example, Alt a 1-like CEs from several plant-pathogenic fungi

have been shown to trigger cell death (Wang et al., 2012; Zhang et al., 2017). One possible explanation for this is that these CEs have a conserved virulence target across host and non-host species, or that the virulence target of these CEs is commonly guarded by R proteins to provide protection against a wide range of pathogens. In contrast, as highlighted above, most CEs tested do not appear to trigger defence responses in *Nicotiana* species. This may reflect the fact that these plant species have evolved separately (i.e. in absence of the plant pathogens from which the effectors were derived).

5.3.1 Future research concerning CEs of *V. inaequalis* that trigger defence responses in non-host plants

5.3.1.1 Infiltration of apple hypocotyls with apoplastic wash fluid containing CEs

Infiltrations in apple leaves from cultivar 'Royal Gala' and other cultivars carrying different *Rvi R* genes were planned using apoplastic wash fluid collected from *N. benthamiana* leaves expressing CEs (i.e. to determine whether the CEs could trigger visible defence responses in these apple cultivars). However due to the hardness of the apple leaf cuticle, it proved impossible to infiltrate apoplastic wash fluid using a needleless syringe, which also caused considerable mechanical damage leading to necrosis in all the infiltration zones. Application of vacuum did not improve infiltration. In addition, the low volumes of apoplastic wash fluid obtained from *N. benthamiana* leaves meant that a high number of plants and a more extensive growth room facility space would have been required to carry out robust experiments. Due to the unsuccessful infiltrations of apple leaves, syringe or vacuum infiltration of apple hypocotyls from different apple cultivars with the apoplastic wash fluid samples could be trialled to observe a potential response. However, as mentioned above, the volumes of apoplastic wash fluid obtained from *N. benthamiana* leaves may not be sufficient for such experiments. Instead, *Pichia pastoris* could be used (Kombrink, 2012) for the heterologous production of CEs to obtain larger volumes of protein.

5.3.1.2 Deletion of *CE* genes

CE proteins from Chapter 3 with amino acid sequence or structural similarity to previously characterized proteins, could be studied individually to elucidate their role in

virulence or pathogenicity. Using the aforementioned CRISPR-Cas9 approach (Rocafort et al., 2021), it would be possible to knock-out the genes encoding the hydrophobin CE10 (ViHyd1), the LysM domain-containing protein CE11 (ViEcp6), the plant natriuretic peptide-likes CE12 (ViPNPL-5) and CE13 (ViPNPL-9), and the elicitors CE93 and CE126. Regarding the *CE27* (*Alt a 1-like*) gene, it has already been knocked out (Arshed et al., unpublished results), it would be worth to follow up the corresponding infection experiments using the modified strain.

5.3.1.3 Assess that the chlorotic and necrotic responses observed in *Nicotiana* species are immune responses

To determine if the chlorotic or necrotic response triggered by the three CEs of *V. inaequalis* in *Nicotiana* species are due to an immune response and not to a toxic effect on plant cells (e.g. through membrane perturbation), different approaches could be pursued. One of the strategies widely used is to measure reactive oxygen species (ROS) accumulation in leaves following ATTAs involving CEs (Apel & Hirt, 2004; Fang et al., 2019; Shetty et al., 2007). Here, ROS generation is visualized by bright field microscopy following the staining of ROS in *Nicotiana* leaves by 3,3'-diaminobenzidine (DAB). PR proteins are induced either locally or systemically when plants are threatened by pathogens (Liu et al., 2019). Expression of genes encoding PR proteins (e.g. PR1, PR2 and PR3 family) could also be analysed in *Nicotiana* spp. by RT-qPCR (Cutt et al., 1988; Dubin et al., 2021).

5.3.1.4 Cell death suppression assays

CE proteins of *V. inaequalis* could be screened for their ability to suppress plant immune system activation (cell death) by a known effector and R–Avr protein pairs in *N. benthamiana* using ATTAs (i.e. to gain insights into their possible virulence function). Cell death activators to be used could be INF1 from *P. infestans* (Kamoun et al., 1998), the extracellular R–Avr protein pair Cf-4–Avr4 from tomato and *C. fulvum*, respectively (Van der Hoorn et al., 2000), and the intracellular R–Avr protein pair R3a–Avr3a from potato and *P. infestans*, respectively (Bos et al., 2006).

5.3.1.5 Identification of R protein homologs or genetic modification of apple

Identification of potential R proteins in *N. benthamiana* that recognize specific pathogen effectors has been achieved through silencing candidate *R* genes (Brendolise

et al., 2017). If an R protein from *N. benthamiana* that is able to recognize a specific *V. inaequalis* CE was found, a gene encoding a potential homolog of this R protein could be identified in *Malus* germplasm collections by genome sequencing and potentially transferred to apple cultivars to engineer scab resistance (Song et al., 2018). The latter, provided that the virulence target (if the CE is not recognized directly) is also present in apple. Remarkably, it is now possible to engineer R proteins to recognize distinct effectors (Zhang & Coaker, 2017). With this in mind, it could be feasible to engineer an existing R protein to recognize or to enhance the recognition (in case there is an R protein with a weak response) of AvrRi4.

5.4 Chapter 4: Identification of the Avr9B effector from *C. fulvum*

In Chapter 4, a comparative genomics approach based on *in planta*-expressed CEs from *C. fulvum*, as well as functional assays, were used to identify the *Avr9B* effector gene from *C. fulvum*, which corresponds to the *Cf-9B R* gene of tomato. Unlike many other Dothideomycete fungi, *C. fulvum* has a well-characterized inventory of CEs, with many now confirmed to be secreted into the apoplastic environment of tomato during host colonization (Mesarich et al., 2018). Comparing this protein inventory between *C. fulvum* strain 0WU (containing a functional copy of *Avr9B*) and the New Zealand strain IPO 2679 (lacking a functional copy of *Avr9B*), it was possible to show that *Avr9B* had been deleted in IPO 2679. The presence of this gene was assessed among other *C. fulvum* races, and it was further determined that indeed, the gene was deleted only in the New Zealand strain. The *Avr9B* gene encodes a protein of 152 amino acids, with four repeats that overlap with a large predicted N-terminal IDR. The finding that, like the candidate AvrRvi4 protein, Avr9B has a large predicted IDR is interesting, and suggests that IDRs are likely a common feature of many fungal effector proteins. This is certainly the case for other effectors from bacteria and oomycetes, where IDRs have been shown to play a role in virulence or evasion of recognition by the host immune system (Marín et al., 2013; Shen et al., 2017; Yang et al., 2020).

Using ATTAs, Avr9B was co-expressed with the corresponding tomato Cf-9B immune receptor in *N. tabacum*. Surprisingly, this co-expression resulted in a strong cell death response, which is different to what is known about Cf-9B-mediated resistance in

tomato, where no HR is observed (Laugé et al., 1998). Such different resistance outcomes have been observed previously. For example, the *V. dahliae* Avr effector Ave1, when co-expressed with its corresponding R protein Ve1 in *N. tabacum*, led to a strong cell death or HR, whereas no HR was observed when co-expressed in *N. benthamiana* (Zhang, van Esse, et al., 2013). Another example illustrating the absence of an HR in a resistance response, occurred using *Ve1*-expressing *Arabidopsis* plants challenged with *V. dahliae* (carrying *Ave1*), supporting the premise that disease resistance and HR do not always happen simultaneously (Zhang et al., 2013). These discrepancies in resistance responses, may be due to a missing component involved in signal transduction in a certain host (Zhang et al., 2013). In any case, this thesis has provided an Avr effector that can be further used to dissect resistance mechanisms that do not involve an HR, for which we know relatively little about. Curiously, the cell death response observed in *N. tabacum* was not dependent on the presence of the repetitive region within the IDR. Whether this IDR is required for its virulence function (i.e. outside of recognition) remains to be determined.

BLASTp and tBLASTn searches led to the identification of diverse Avr9B-like proteins restricted to other plant pathogens of the Dothideomycete class. These proteins can be divided into two groups; the first group consists of proteins containing eight cysteine residues and N-terminal IDRs, whereas the second group consists of proteins containing 10 cysteine residues with only three of them predicted to contain an IDR. One protein from each group belonging to other tomato pathogens, were selected for ATTAs; TW64_01570 from *Stemphylium lycopersici* and HII31_03919 from *Pseudocercospora fuligena*, the causal agents of gray and black leaf mould of tomato, respectively. TW64_01570 caused strong cell death in *N. tabacum* by itself, therefore it was not possible to determine an interaction when co-expressed with Cf-9B. HII31_03919 caused chlorosis when expressed by itself and when co-expressed with Cf-9B, hence no interaction was likely to occur. Amino acid sequence alignments in both groups, revealed a 10-amino acid conserved region encompassing two cysteine residues. Both cysteine residues within the 10 amino acid region were independently substituted by a serine in Avr9B, and surprisingly, the Cf-9B-mediated cell death response was abolished only by the substitution of the first cysteine (position 77). This is possibly caused by a disulfide bond disruption leading to an unstable protein that is

easier to degrade in the apoplast and is no longer recognized by Cf-9B. Importantly, complementation of the New Zealand strain IPO 2679 with a functional copy of the *Avr9B* gene restored avirulence in tomato plants carrying the *Cf-9B* gene, validating the discovery of the *Avr9B* effector.

To investigate the localization of Avr9B, N-terminal protein fusions with both green fluorescent protein (GFP) and mCherry were performed. Confocal microscope observations led to preliminary localization of Avr9B to the plasma membrane.

Finally, structural prediction of Avr9B revealed a novel fold consisting of three alpha helices and two β-strands stabilized by four disulfide bonds, and no structural similarity to other proteins available at the Protein Data Bank. While no structural similarity was identified to this protein in this thesis, it will be interesting to see whether other plant-pathogenic fungi possess effectors with a similar fold to Avr9B that cannot be identified through sequence similarity alone (i.e. through the use of AlphaFold2). Indeed, so far, effector catalogues of only three fungal species have been studied in detail using AlphaFold2; i.e. from *Magnaporthe oryzae* (Seong & Krasileva, 2021), *Fusarium oxysporum* f. sp. *lycopersici* (Yu et al., 2021) and *V. inaequalis* (Rocafort et al. in preparation). No homologs of Avr9B have been identified in these pathogens, but other pathogens more closely related to *C. fulvum* have not yet been assessed.

5.4.1 Future research concerning the Avr9B effector from *C. fulvum*

5.4.1.1 Assessment of Avr9B-like proteins for recognition by Cf-9B

More of the identified Avr9B-like proteins could be co-expressed with Cf-9B using ATTAs in *N. tabacum* to determine if one of them also triggers a *Cf-9B*-mediated cell death, as has been performed for homologs of *C. fulvum* Avr4 by tomato Cf-4 (de Wit et al., 2012; Mesarich et al., 2016; Stergiopoulos et al., 2010). Based on this information, region swaps and targeted amino acid substitutions could be performed between Avr9B-like proteins that do and do not trigger Cf-9B-mediated resistance using the same ATTAs to identify key regions or amino acid residues required for HR induction.

5.4.1.2 Assessment of the chlorotic response triggered by Avr9B in *SOBIR1*-silenced plants of *N. benthamiana*

Diverse membrane-anchored RLPs lacking a kinase domain are coupled with SOBIR1 for intracellular signal transduction (Liebrand et al., 2013). This includes the Cf R proteins of tomato (Liebrand et al., 2013; Postma et al., 2016). To determine if the chlorotic response triggered by Avr9B in *N. benthamiana* in the absence of Cf-9B results from an interaction with an endogenous RLP, or whether the chlorotic response is instead due to some other phenomenon (e.g. perturbation of the plant plasma membrane), ATTAs involving *Avr9B* should be carried out in *SOBIR1*-silenced plants to determine if the chlorotic response is compromised. If the chlorotic response is not compromised, it is likely that this response is not RLP-dependent.

5.4.1.3 Confirmation that Avr9B is targeted to the plasma membrane

Membrane localization has been confirmed for other fungal effectors using membrane-specific fluorophores (Fang et al., 2019). To confirm the preliminary observations in this thesis regarding Avr9B localization, membrane-specific markers such as ACA8 and FM4-64 could be used in order to observe co-localization with the existing GFP- and mCherry- tagged Avr9B proteins from this thesis (Bonza et al., 2000; Rigal et al., 2015).

5.4.1.4 Protein interaction experiments

To identify potential virulence targets, protein pull-downs and yeast-two-hybrid (Y2H) assays involving Avr9B could be performed to identify virulence targets in tomato and *N. tabacum*, and to determine the regions of the Avr9B Avr protein determining interaction (Zhang et al., 2018). Furthermore, co-immunoprecipitations and confocal microscopy co-localization experiments could be pursued to determine if Avr9B and Cf-9B interact directly (Dagvadorj et al., 2021). Additionally, co-localization with the identified virulence target would help to reveal if this target is also localized to the plant plasma membrane.

5.5 Conclusion

With an increasing population expected to reach by 9.6 billion in 2050 (Gerland et al., 2014), challenges to meet future food demand are imminent. One of these challenges is the prevention of fungal diseases that not only affect yields, quality and availability of food expected to meet the consumers demand, but also have a high impact on the livelihood of numerous people whose income depend on crop production (Fones et al., 2020; Godfray et al., 2016). Current agricultural practices mainly rely on fungicide applications and the deployment of single *R* genes as a source of resistance (Fisher et al., 2012; Fones et al., 2020). As we have learned from history, practices relying on a single source of resistance can have serious consequences, when resistance-breaking isolates or strains appear in the field.

In terms of apple and tomato, cultivars deployed around the world also often make use of single *R* genes, and in several cases, these have been rapidly overcome by isolates or strains of *V. inaequalis* and *C. fulvum*, respectively. Indeed, for *C. fulvum*, strains have emerged that can overcome one or more of all cloned *R* genes used in resistant cultivars (i.e. *Cf-2.1/Cf2.2*, *Cf-4*, *Cf-4E*, *Cf-5*, *Cf-9* and *Cf-9B*) (Dixon et al., 1996; Jones et al., 1994; Parniske et al., 1999; Takken et al., 1999; Thomas et al., 1998; Thomas et al., 1997). Of these, *Cf-9B* is of particular importance to growers, as it provides protection against leaf mould disease during fruit production. For *V. inaequalis*, isolates have been identified that overcome one or more *R* genes in apple, including *Rvi6*, which is present in many commercial scab-resistant cultivars, as well as *Rvi4* and *Rvi5*, which are not as widely deployed (Patocchi et al., 2020).

In this thesis, a strong candidate for the *AvrRvi4* gene from *V. inaequalis* (corresponding to *Rvi4*) was identified. Likewise, the *Avr9B* gene (corresponding to *Cf-9B*) was also discovered. These genes encode proteins with features typical of most other fungal Avr effectors identified to date, further reinforcing the finding that Avrs from fungi are predominantly cysteine-rich SSPs. Importantly, in identifying the *AvrRvi4* candidate and *Avr9B*, this thesis has contributed to our understanding of how *V. inaequalis* and *C. fulvum* overcome *Rvi4*- and *Cf-9B*-mediated resistance, respectively. It has also shown that the mechanisms deployed by these fungi to overcome *Rvi4*- and *Cf-9B*-mediated resistance are similar to those reported for other fungal species known

to circumvent resistance mediated by single *R* genes. The identification of *AvrRvi4* and *Avr9B* will also enable the rapid identification of *Rvi4* and *Cf-9B* resistance-breaking isolates or strains of *V. inaequalis* and *C. fulvum* in the field (e.g. through PCR diagnostics). This is crucial, as it has the potential to direct the deployment of tomato cultivars resistant against *Cf-9B*-breaking strains of *C. fulvum* in commercial settings. In the case of apple, which is a woody perennial plant, *AvrRvi4* could be monitored across diverse populations of *V. inaequalis* to assess the frequency of *Rvi4* resistance breakdown and their geographical distribution. This monitoring could then be used to decide whether the *Rvi4* gene should be pyramided into apple cultivars to provide durable resistance against scab disease. Finally, the identification of AvrRvi4 and Avr9B will enable future experiments to be carried out to determine their roles in promoting host colonization (i.e. in the absence of Rvi4 and Cf-9B respectively). This will in turn provide valuable information on how *V. inaequalis* and *C. fulvum* cause disease, which could be used to inform novel disease control strategies.

In addition to the candidate AvrRvi4 protein and Avr9B, three CEs of *V. inaequalis* were identified that triggered defense in the non-host plants *N. benthamiana* and/or *N. tabacum*. These CEs may represent novel Avrs of *V. inaequalis*, and as such, could be used to identify new sources of resistance in apple germplasm collections. In addition, these CEs could be used to better understand how *V. inaequalis* activates the plant immune system (i.e. by identifying their plant virulence targets), which like that described above, could be used to inform novel disease control strategies.

Appendix

Table A.1. List of primers used in this thesis. All sequences are ordered (5' -3').

Chapter 2	
Amplification of candidate *AvrRvi4*	
atg6122-F	CGACGGTAAGAGTACTATATTACGAC
atg6122-R	AAAGTTTTCCCTGTCCCAAGATT
Ins-F	ATCTCATAAATCAGACCCTTCC
Ins-R	ACCCTTCCTCTATGTGTTTTTGG
Chapter 3	
Amplification of synthesized candidate effectors in pTWIST plasmid	
M13-F	GCCAGGGTTTTCCCAGTCACGA
M13-R	GCGGATAACAATTTCACACAGG
pICH86988-F	AGGACACGCTCGAGTATAAG
pICH86988-R	CTCTTCGGATACTAGCGTAC
Cin1-F	GGTCTCGCAAGTTGCCAGCTG
Cin1-R	GGTCTCAAAGCCTAGTATCCTCCTGGAC
Cin3-F	GGTCTCGCAAGTTCACTGTTCCGTC
Cin3-R	GGTCTCAAAGCCTAGGCCTTTTG
Cin1L1-F	GGTCTCGCAAGATGCCAACAGCCATC
Cin1L1-R	GGTCTCAAAGCTCAATAGCCGCG
Cin1L2-F	GGTCTCGCAAGCTTCCAAACGAAGCAAC
Cin1L2-R	GGTCTCAAAGCCTAGTTGTGGTAGTTC
16969-F	GGTCTCGCAAGATGCCAGCAGCTCAATG
16969-R	GGTCTCAAAGCCTAGCACGGCTTCTC
15505-F	GGTCTCGCAAGACTCCGATTGATAGC
15505-R	GGTCTCAAAGCTCAATGCTTCCAGGGAC
18699-F	GGTCTCGCAAGATCAAATACCCTCCAC
18699-R	GGTCTCAAAGCCTAACAAAGGACGTCGC
24527-F	GGTCTCGCAAGTATGAGTGCCCTATAAAAC
24527-R	GGTCTCAAAGCTTAATACCCTGTTG
13533-F	GGTCTCGCAAGGTACCAAACACAAACG
13533-R	GGTCTCAAAGCTCATTTGTTCCCCGAG
13636-F	GGTCTCGCAAGGACTGGCACATCATCAAC
13636-R	GGTCTCAAAGCCTAGTTCTCTTTGATG
14801-F	GGTCTCGCAAGGCCGACTCATTAACCTAC
14801-R	GGTCTCAAAGCTCAGGAGGTGTACGTTG
15961-F	GGTCTCGCAAGAGCCCATTCAC
15961-R	GGTCTCAAAGCCTAGGCGCTCTGGACCAT
16394-F	GGTCTCGCAAGGGCGTCATAGACCACAG
16394-R	GGTCTCAAAGCCTAGAGCTCAAAG
682.7-F	GGTCTCGCAAGGACTGGGAAATCTACAC
682.7-R	GGTCTCAAAGCCTAATTACAATAATCAC
21582-F	GGTCTCGCAAGCAAGGTCTAAATGTCAC
21582-R	GGTCTCAAAGCTCATGGAGGTGAGAC
25058-F	GGTCTCGCAAGAACCCTGTTCCTCAGTC

Table A.1. Continued.

Chapter 3	
Amplification of synthesized candidate effectors in pTWIST plasmid	
25058-R	GGTCTCAAAGCCTACTGGACCAAG
17864-F	GGTCTCGCAAGTTGCCTCAGCCGGATG
17864-R	GGTCTCAAAGCTCACTGGTTTCTATCGAC
Candidate effectors without signal peptide	
NSP_BsaI-F	GGTCTCGAATGGACTACAAGG
15961-R	GGTCTCAAAGCCTAGGCGCTCTGGACCAT
NSP_CE93-R	GGTCTCAAAGCTTACTCATCATC
NSP_CE126-R	GGTCTCAAAGCTCAAAAGTTACTAC
Chapter 4	
Gene presence/absence screen and allelic variation	
Avr9B_C1-F	CTACTCCTGGCCACACTCCCACTG
Avr9B_C2-R	CATCAAACGTCAAATGCGCAACCCCTG
Avr9B_C2-F	CATATATAAACTCCTCGCTCGCCCTC
Avr9B_C2-R	CACCGAGCACTATCATTTCACATGC
***Avr9B*-C2 variations for ATTAs**	
pICH86988-F	AGGACACGCTCGAGTATAAG
pICH86988-R	CTCTTCGGATACTAGCGTAC
CE2_BsaI-F	GGTCTCGAATGATGGGATTTG
CE2_BsaI-R	GGTCTCAAAGCCTAACACAAC
CE2_Cys1-F	GTTGGAGTGCGGGTTGTAAAC
CE2_Cys1-R	AACCCGCACTCCAACCGAG
CE2_Cys2-F	GCGGGTAGTAAACGACTTG
CE2_Cys2-R	AGTCGTTTACTACCCGCAC
NSPCE2_BsaI-F	GGTCTCGAATGGACTACAAGG
Gene complementation	
pFBTS1-F	GCACGTGAGAACGCTAATAGCCCTTTCAGATCAACAGCTT
pFBTS1-R	CTATTAGCGTTCTCACGTGC
MR125-F	TTGATATCGAATTCCTGCAGC
CHM52-R	AGCTTGATATCTGTTAGTAATC
GibCE1-F	GATTACTAACAGATATCAAGCTGATTCAGCTTCTCGCTATAG
GibCE1-R	GCTGCAGGAATTCGATATCAACTCTACACGGGCGCGACTGC
GibCE2-F	GATTACTAACAGATATCAAGCTCCTATCGTAAAGCGCCTGAG
GibCE2-R	GCTGCAGGAATTCGATATCAAGATGGATCCCTACTTCGCCTTC
Transformant screening	
Comp-F	TGTTATTGCCAGTGCCGCTTCAATTCATGATG
CompCE1-R	CGCCACTAGTCTCGAGTTAATTAACCG
GibCE2-R	GCTGCAGGAATTCGATATCAAGATGGATCCCTACTTCGCCTTC
Reverse transcription–quantitative real-time PCR (RT-qPCR)	
qCfActin-F	GGCACCAATCAACCCAAAG
qCfActin-R	TACGACCAGAAGCGTACAG
qAvr9BC1-F	TACGACACGACTGGAGAAC
qAvr9BC1-R	CGAACATCAAACGTCAAATGC
qAvr9BC2-F	GATTTGCGTCACCGTTCTCG
qAvr9BC2-R	CCGATTGAGAGCAAACAGGC

Table A.1. Continued.

Chapter 3	
Localization	
PR1a_BsaI-F	GGTCTCAAATGGGATTTGTTCTCTTTTCAC
PR1a_BsaI-R	GGTCTCTGATGTCGTGGTCCTTGTAG
Ntag_CfCE54-F	GGTCTCAATCTATGCCGACCGACCCTG
Ntag_CfCE54-R	GGTCTCTAAGCCTAACACAACCCATCGGTAC
N_GFP_mCherry-F	GGTCTCACATCATGGTGAGCAAGGGC
N_mCherry-R	GGTCTCTAGATCCACCTCCACCAGAACCTCCACCTCCAGATCTGTACAGCT CG
N_GFP-R	GGTCTCTAGATCCACCTCCACCAGAACC
ControlGFP_mCherry-F	GGTCTCACATCGGAGGTGGAGGTTCT
NSP_NmCherry-GFP-F	GGTCTCAAATGGTGAGCAAGGGCGA

Table A.2. List of plasmids used in this thesis.

Chapter 3			
Plasmid	Characteristics	Antibiotic^R	Reference
pTWIST	Shuttle vector with *Bsa*I sites, PR1a secretion signal from *N. tabacum*, 3XFLAG Tag, and candidate effector (synthesized), Amp^R	Amp	This study
pICH86988	Binary vector, 35S CaMV promoter and NosT terminator, LacZ	Kan	Webber et al. 2011
pINF1	pBC302-3 containing INF1	Kan	Bos et al. 2006
pCE1	pICH86988 containing 5'PRIα-3xFLAG-CE1	Kan	This study
pCE2	pICH86988 containing 5'PRIα-3xFLAG-CE2	Kan	This study
pCE3	pICH86988 containing 5'PRIα-3xFLAG-CE3	Kan	This study
pCE4	pICH86988 containing 5'PRIα-3xFLAG-CE4	Kan	This study
pCE5	pICH86988 containing 5'PRIα-3xFLAG-CE5	Kan	This study
pCE6	pICH86988 containing 5'PRIα-3xFLAG-CE6	Kan	This study
pCE7	pICH86988 containing 5'PRIα-3xFLAG-CE7	Kan	This study
pCE8	pICH86988 containing 5'PRIα-3xFLAG-CE8	Kan	This study
pCE9	pICH86988 containing 5'PRIα-3xFLAG-CE9	Kan	This study
pCE10	pICH86988 containing 5'PRIα-3xFLAG-CE10	Kan	This study
pCE11	pICH86988 containing 5'PRIα-3xFLAG-CE11	Kan	This study
pCE12	pICH86988 containing 5'PRIα-3xFLAG-CE12	Kan	This study
pCE13	pICH86988 containing 5'PRIα-3xFLAG-CE13	Kan	This study
pCE14	pICH86988 containing 5'PRIα-3xFLAG-CE14	Kan	This study
pCE15	pICH86988 containing 5'PRIα-3xFLAG-CE15	Kan	This study
pCE16	pICH86988 containing 5'PRIα-3xFLAG-CE16	Kan	This study
pCE17	pICH86988 containing 5'PRIα-3xFLAG-CE17	Kan	This study
pCE18	pICH86988 containing 5'PRIα-3xFLAG-CE18	Kan	This study
pCE19	pICH86988 containing 5'PRIα-3xFLAG-CE19	Kan	This study
pCE20	pICH86988 containing 5'PRIα-3xFLAG-CE20	Kan	This study
pCE21	pICH86988 containing 5'PRIα-3xFLAG-CE21	Kan	This study
pCE22	pICH86988 containing 5'PRIα-3xFLAG-CE22	Kan	This study
pCE23	pICH86988 containing 5'PRIα-3xFLAG-CE23	Kan	This study
pCE24	pICH86988 containing 5'PRIα-3xFLAG-CE24	Kan	This study
pCE25	pICH86988 containing 5'PRIα-3xFLAG-CE25	Kan	This study
pCE26	pICH86988 containing 5'PRIα-3xFLAG-CE26	Kan	This study
pCE27	pICH86988 containing 5'PRIα-3xFLAG-CE27	Kan	This study
pCE28	pICH86988 containing 5'PRIα-3xFLAG-CE28	Kan	This study
pCE29	pICH86988 containing 5'PRIα-3xFLAG-CE29	Kan	This study
pCE30	pICH86988 containing 5'PRIα-3xFLAG-CE30	Kan	This study
pCE31	pICH86988 containing 5'PRIα-3xFLAG-CE31	Kan	This study
pCE32	pICH86988 containing 5'PRIα-3xFLAG-CE32	Kan	This study
pCE33	pICH86988 containing 5'PRIα-3xFLAG-CE33	Kan	This study
pCE34	pICH86988 containing 5'PRIα-3xFLAG-CE34	Kan	This study
pCE35	pICH86988 containing 5'PRIα-3xFLAG-CE35	Kan	This study
pCE36	pICH86988 containing 5'PRIα-3xFLAG-CE36	Kan	This study
pCE37	pICH86988 containing 5'PRIα-3xFLAG-CE37	Kan	This study
pCE38	pICH86988 containing 5'PRIα-3xFLAG-CE38	Kan	This study
pCE39	pICH86988 containing 5'PRIα-3xFLAG-CE39	Kan	This study

Table A.2. Continued.

Plasmid	Characteristics	Antibiotic^R	Reference
pCE40	pICH86988 containing 5'PRIα-3xFLAG-CE40	Kan	This study
pCE41	pICH86988 containing 5'PRIα-3xFLAG-CE41	Kan	This study
pCE42	pICH86988 containing 5'PRIα-3xFLAG-CE42	Kan	This study
pCE43	pICH86988 containing 5'PRIα-3xFLAG-CE43	Kan	This study
pCE44	pICH86988 containing 5'PRIα-3xFLAG-CE44	Kan	This study
pCE45	pICH86988 containing 5'PRIα-3xFLAG-CE45	Kan	This study
pCE46	pICH86988 containing 5'PRIα-3xFLAG-CE46	Kan	This study
pCE47	pICH86988 containing 5'PRIα-3xFLAG-CE47	Kan	This study
pCE48	pICH86988 containing 5'PRIα-3xFLAG-CE48	Kan	This study
pCE49	pICH86988 containing 5'PRIα-3xFLAG-CE49	Kan	This study
pCE50	pICH86988 containing 5'PRIα-3xFLAG-CE50	Kan	This study
pCE51	pICH86988 containing 5'PRIα-3xFLAG-CE51	Kan	This study
pCE52	pICH86988 containing 5'PRIα-3xFLAG-CE52	Kan	This study
pCE53	pICH86988 containing 5'PRIα-3xFLAG-CE53	Kan	This study
pCE54	pICH86988 containing 5'PRIα-3xFLAG-CE54	Kan	This study
pCE55	pICH86988 containing 5'PRIα-3xFLAG-CE55	Kan	This study
pCE56	pICH86988 containing 5'PRIα-3xFLAG-CE56	Kan	This study
pCE57	pICH86988 containing 5'PRIα-3xFLAG-CE57	Kan	This study
pCE58	pICH86988 containing 5'PRIα-3xFLAG-CE58	Kan	This study
pCE59	pICH86988 containing 5'PRIα-3xFLAG-CE59	Kan	This study
pCE60	pICH86988 containing 5'PRIα-3xFLAG-CE60	Kan	This study
pCE61	pICH86988 containing 5'PRIα-3xFLAG-CE61	Kan	This study
pCE62	pICH86988 containing 5'PRIα-3xFLAG-CE62	Kan	This study
pCE63	pICH86988 containing 5'PRIα-3xFLAG-CE63	Kan	This study
pCE64	pICH86988 containing 5'PRIα-3xFLAG-CE64	Kan	This study
pCE65	pICH86988 containing 5'PRIα-3xFLAG-CE65	Kan	This study
pCE66	pICH86988 containing 5'PRIα-3xFLAG-CE66	Kan	This study
pCE67	pICH86988 containing 5'PRIα-3xFLAG-CE67	Kan	This study
pCE68	pICH86988 containing 5'PRIα-3xFLAG-CE68	Kan	This study
pCE69	pICH86988 containing 5'PRIα-3xFLAG-CE69	Kan	This study
pCE70	pICH86988 containing 5'PRIα-3xFLAG-CE70	Kan	This study
pCE71	pICH86988 containing 5'PRIα-3xFLAG-CE71	Kan	This study
pCE72	pICH86988 containing 5'PRIα-3xFLAG-CE72	Kan	This study
pCE73	pICH86988 containing 5'PRIα-3xFLAG-CE73	Kan	This study
pCE74	pICH86988 containing 5'PRIα-3xFLAG-CE74	Kan	This study
pCE75	pICH86988 containing 5'PRIα-3xFLAG-CE75	Kan	This study
pCE76	pICH86988 containing 5'PRIα-3xFLAG-CE76	Kan	This study
pCE77	pICH86988 containing 5'PRIα-3xFLAG-CE77	Kan	This study
pCE78	pICH86988 containing 5'PRIα-3xFLAG-CE78	Kan	This study
pCE79	pICH86988 containing 5'PRIα-3xFLAG-CE79	Kan	This study
pCE80	pICH86988 containing 5'PRIα-3xFLAG-CE80	Kan	This study
pCE81	pICH86988 containing 5'PRIα-3xFLAG-CE81	Kan	This study
pCE82	pICH86988 containing 5'PRIα-3xFLAG-CE82	Kan	This study
pCE83	pICH86988 containing 5'PRIα-3xFLAG-CE83	Kan	This study
pCE84	pICH86988 containing 5'PRIα-3xFLAG-CE84	Kan	This study

Table A.2. Continued.

Plasmid	Characteristics	Antibiotic^{R}	Reference
pCE85	pICH86988 containing 5'PRIα-3xFLAG-CE85	Kan	This study
pCE86	pICH86988 containing 5'PRIα-3xFLAG-CE86	Kan	This study
pCE87	pICH86988 containing 5'PRIα-3xFLAG-CE87	Kan	This study
pCE88	pICH86988 containing 5'PRIα-3xFLAG-CE88	Kan	This study
pCE89	pICH86988 containing 5'PRIα-3xFLAG-CE89	Kan	This study
pCE90	pICH86988 containing 5'PRIα-3xFLAG-CE90	Kan	This study
pCE91	pICH86988 containing 5'PRIα-3xFLAG-CE91	Kan	This study
pCE92	pICH86988 containing 5'PRIα-3xFLAG-CE92	Kan	This study
pCE93	pICH86988 containing 5'PRIα-3xFLAG-CE93	Kan	This study
pCE94	pICH86988 containing 5'PRIα-3xFLAG-CE94	Kan	This study
pCE95	pICH86988 containing 5'PRIα-3xFLAG-CE95	Kan	This study
pCE96	pICH86988 containing 5'PRIα-3xFLAG-CE96	Kan	This study
pCE97	pICH86988 containing 5'PRIα-3xFLAG-CE97	Kan	This study
pCE98	pICH86988 containing 5'PRIα-3xFLAG-CE98	Kan	This study
pCE99	pICH86988 containing 5'PRIα-3xFLAG-CE99	Kan	This study
pCE100	pICH86988 containing 5'PRIα-3xFLAG-CE100	Kan	This study
pCE101	pICH86988 containing 5'PRIα-3xFLAG-CE101	Kan	This study
pCE102	pICH86988 containing 5'PRIα-3xFLAG-CE102	Kan	This study
pCE103	pICH86988 containing 5'PRIα-3xFLAG-CE103	Kan	This study
pCE104	pICH86988 containing 5'PRIα-3xFLAG-CE104	Kan	This study
pCE105	pICH86988 containing 5'PRIα-3xFLAG-CE105	Kan	This study
pCE106	pICH86988 containing 5'PRIα-3xFLAG-CE106	Kan	This study
pCE107	pICH86988 containing 5'PRIα-3xFLAG-CE107	Kan	This study
pCE108	pICH86988 containing 5'PRIα-3xFLAG-CE108	Kan	This study
pCE109	pICH86988 containing 5'PRIα-3xFLAG-CE109	Kan	This study
pCE110	pICH86988 containing 5'PRIα-3xFLAG-CE110	Kan	This study
pCE111	pICH86988 containing 5'PRIα-3xFLAG-CE111	Kan	This study
pCE112	pICH86988 containing 5'PRIα-3xFLAG-CE112	Kan	This study
pCE113	pICH86988 containing 5'PRIα-3xFLAG-CE113	Kan	This study
pCE114	pICH86988 containing 5'PRIα-3xFLAG-CE114	Kan	This study
pCE115	pICH86988 containing 5'PRIα-3xFLAG-CE115	Kan	This study
pCE116	pICH86988 containing 5'PRIα-3xFLAG-CE116	Kan	This study
pCE117	pICH86988 containing 5'PRIα-3xFLAG-CE117	Kan	This study
pCE118	pICH86988 containing 5'PRIα-3xFLAG-CE118	Kan	This study
pCE119	pICH86988 containing 5'PRIα-3xFLAG-CE119	Kan	This study
pCE120	pICH86988 containing 5'PRIα-3xFLAG-CE120	Kan	This study
pCE121	pICH86988 containing 5'PRIα-3xFLAG-CE121	Kan	This study
pCE122	pICH86988 containing 5'PRIα-3xFLAG-CE122	Kan	This study
pCE123	pICH86988 containing 5'PRIα-3xFLAG-CE123	Kan	This study
pCE124	pICH86988 containing 5'PRIα-3xFLAG-CE124	Kan	This study
pCE125	pICH86988 containing 5'PRIα-3xFLAG-CE125	Kan	This study
pCE126	pICH86988 containing 5'PRIα-3xFLAG-CE126	Kan	This study
pCE127	pICH86988 containing 5'PRIα-3xFLAG-CE127	Kan	This study
pCE128	pICH86988 containing 5'PRIα-3xFLAG-CE128	Kan	This study
pCE129	pICH86988 containing 5'PRIα-3xFLAG-CE129	Kan	This study

Table A.2. Continued.

Plasmid	Characteristics	Antibiotic^R	Reference
pCE130	pICH86988 containing 5'PRIα-3xFLAG-CE130	Kan	This study
pCE131	pICH86988 containing 5'PRIα-3xFLAG-CE131	Kan	This study
pCE132	pICH86988 containing 5'PRIα-3xFLAG-CE132	Kan	This study
pCE133	pICH86988 containing 5'PRIα-3xFLAG-CE133	Kan	This study
PCE27_NSP	pICH86988 containing 5'-3xFLAG-CE27	Kan	This study
pCE93_NSP	pICH86988 containing 5'-3xFLAG-CE93	Kan	This study
pCE126_NSP	pICH86988 containing 5'-3xFLAG-CE126	Kan	This study
Chapter 4			
Plasmid	**Characteristics**	**Antibiotic^R**	**Reference**
pICH86988	Binary vector, 35S CaMV promoter and NosT terminator, LacZ	Kan	Webber et al. (2011)
pINF1	pBC302-3 containing INF1	Kan	Joe Win
pSLJ9601	pSLJ9601 containing Cf-9	Kan	Chakrabarti et al. (2009)
pCBJ200	pCBJ200 containing Cf-9B	Kan	Chakrabarti et al. (2009)
pAvr9	pICH86988 containing 5'PRIα-3xFLAG-Avr9	Kan	This study
pAvr9B-C1_0WU	pICH86988 containing 5'PRIα-3xFLAG-Avr9B-C1_OWU	Kan	This study
PAvr9B-C1_IPO2679	pICH86988 containing 5'PRIα-3xFLAG-Avr9B-C1_IPO2679	Kan	This study
PAvr9B-C2	pICH86988 containing 5'PRIα-3xFLAG-Avr9B-C2	Kan	This study
pNSPAvr9B-C2	pICH86988 containing 5'3xFLAG-Avr9B-C2	Kan	This study
pNDRAvr9B-C2	pICH86988 containing 5'PRIα-3xFLAG-CE1NDR	Kan	This study
pAvr9B-C2Cys1	pICH86988 containing 5'PRIα-3xFLAG-CE1Cys77Ser	Kan	This study
pAvr9B-C2Cys2	pICH86988 containing 5'PRIα-3xFLAG-CE1Cys80Ser	Kan	This study
pTW65_01570	pICH86988 containing 5'PRIα-3xFLAG-TW65_01570	Kan	This study
pHII31_03919	pICH86988 containing 5'PRIα-3xFLAG-HII31_03919	Kan	This study
pFBTS1	Used for complementation experiments	Kan, Hyg	Bolton et al. (2008)
pFBTS1-CfCE54	pFBTS1 containing *Avr9B-C1* with native promoter and terminator	Kan, Hyg	This study
pFBTS1-Ecp5	pFBTS1 containing *Avr9B-C2* with native promoter and terminator	Kan, Hyg	This study
p_mCherry	pICH86988 containing 5'PRIα-mCherry	Kan	This study
p_GFP	pICH86988 containing 5'PRIα-GFP	Kan	This study
p_mCherry-Avr9B	pICH86988 containing 5'PRIα-mCherry-Avr9B	Kan	This study
p_GFP-Avr9B	pICH86988 containing 5'PRIα-GFP-Avr9B	Kan	This study
p_NSP-mCherry-Avr9B	pICH86988 containing 5'-mCherry-Avr9B	Kan	This study
p_NSP-GFP-Avr9B	pICH86988 containing 5'-GFP-Avr9B	Kan	This study

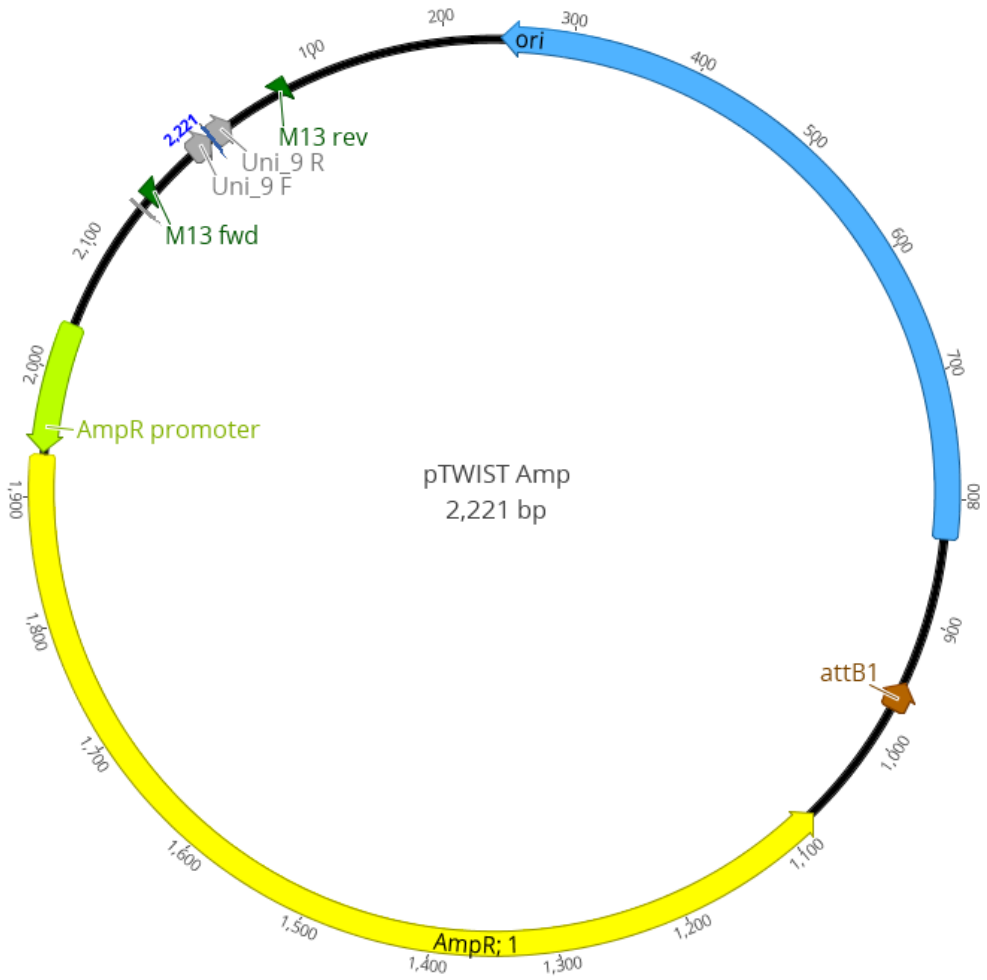

Figure A.1. pTWIST Amp high copy number vector map. Figure from the TWIST Bioscience website (https://www.twistbioscience.com/). Key features of interest: AmpR; ampicillin resistance gene. Standard M13 fwd and rev primers; bp = base pairs.

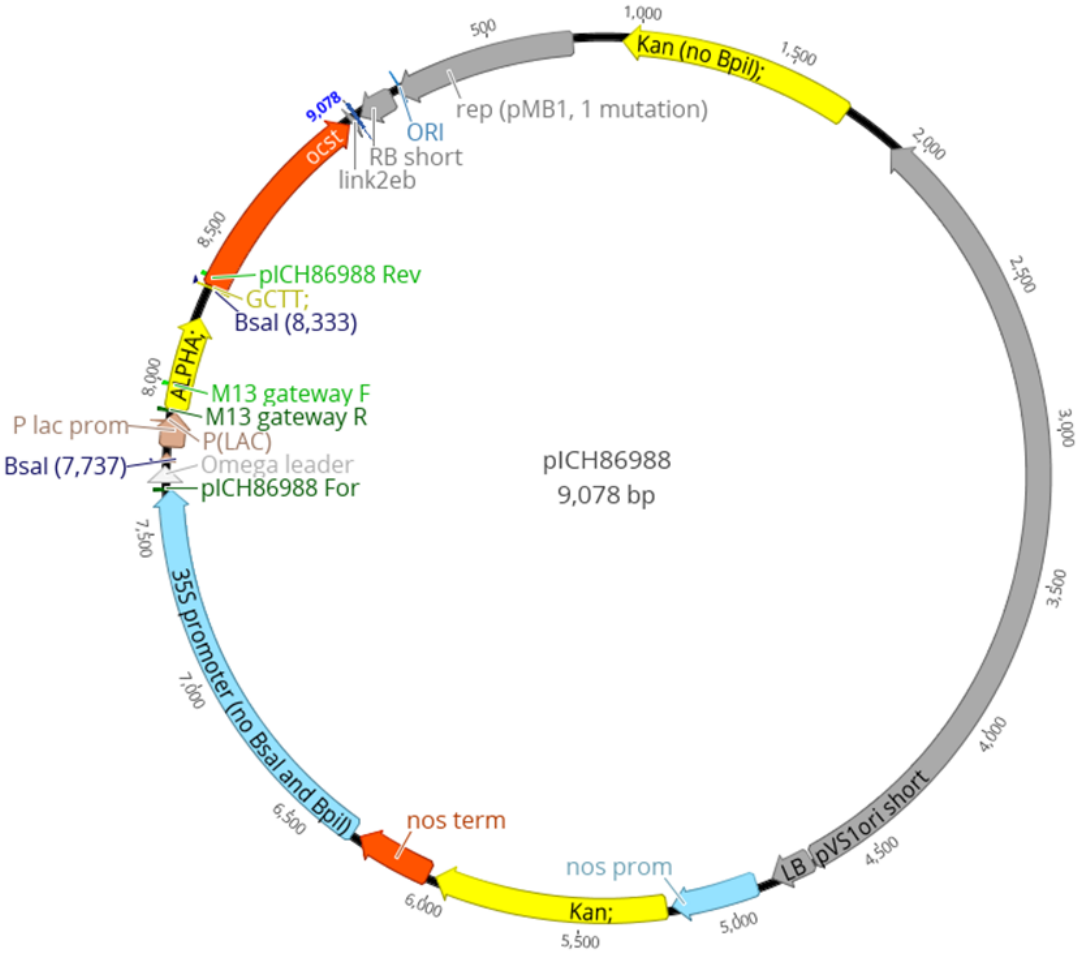

Figure A.2. Map of pICH86988. (Weber et al., 2011). Key features of interest: 35S caulifower mosaic virus (CaMV) 35S promoter region, *ocst*, *octopine synthase* gene (enhancer of transcription in plant cells). NosT terminator, LacZ, Kan, kanamycin resistance cassete; pICH86988 For and Rev primers for to sequence inserts; *Bsa*I restriction sites for Golden Gate Assembly; bp = base pairs.

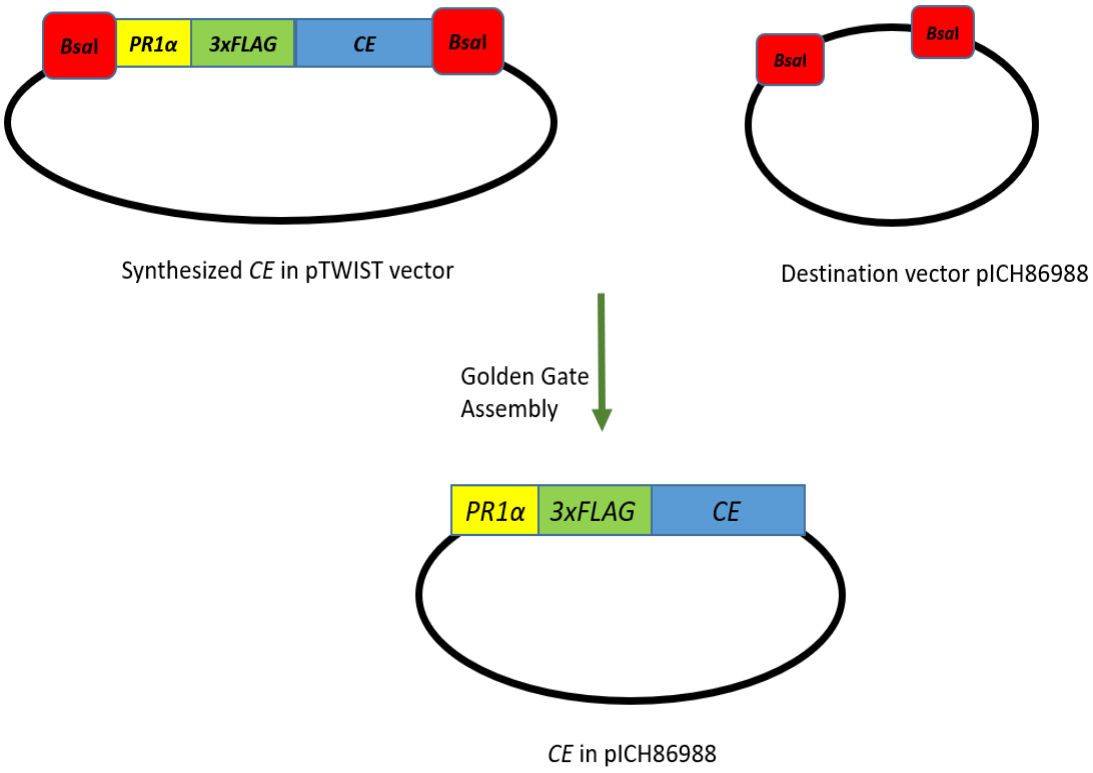

Figure A.3. Example of a Golden Gate Assembly reaction. Synthesized pTWIST plasmid containing the candidate effector (*CE*) gene of interest, a PR1α signal peptide and a 3xFLAG tag for detection (with flanking *Bsa*I restriction sites), is mixed with the destination vector pICH86988 (containing *Bsa*I restriction sites), in a one step Golden Gate reaction to generate the final expression vector. In some cases, the genes were directly synthesized in the destination vector.

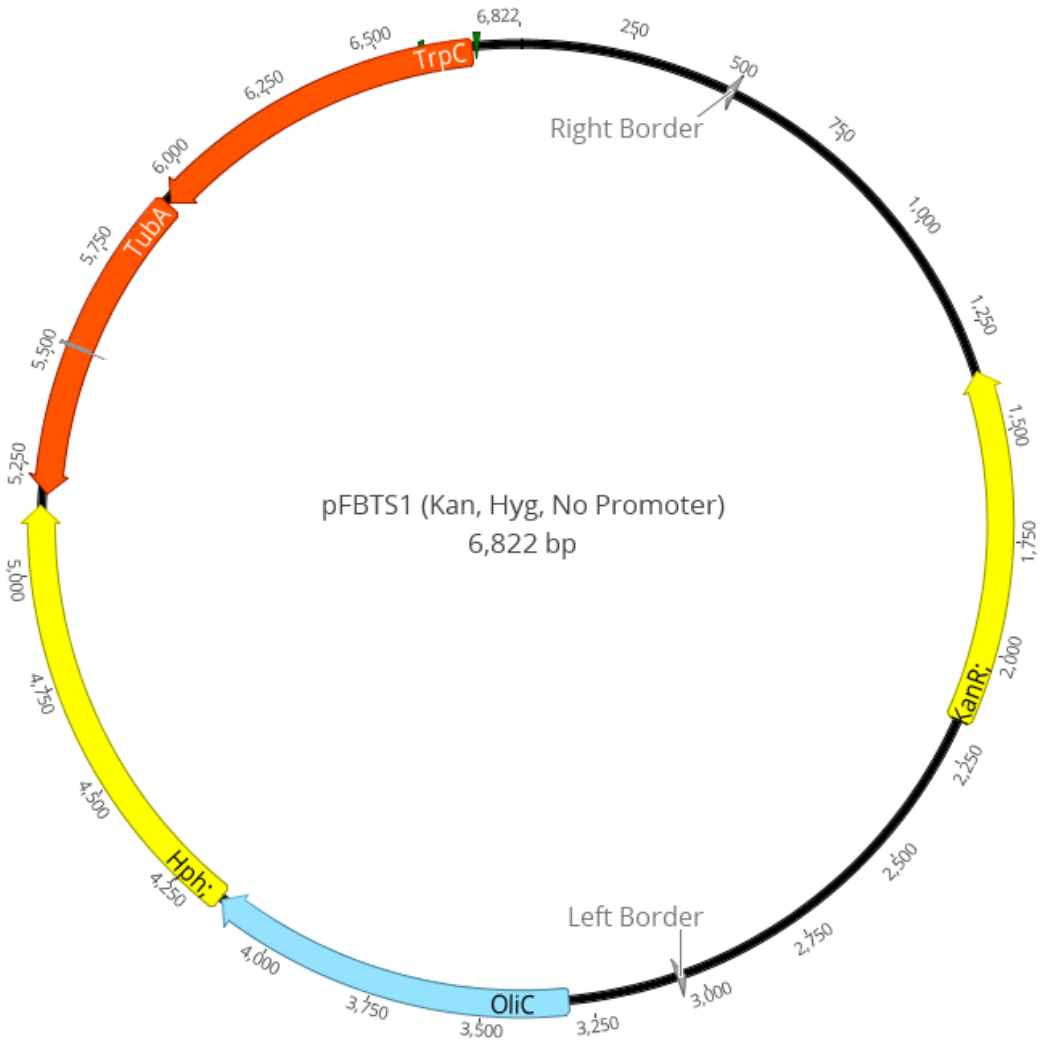

Figure A.4. Map of pFBTS1. A modified version of pFBT004 (Bolton et al., 2008), used for complementation experiments. Key features of interest: KanR; kanamycin resistance cassete, Hph; *hygromycin B phosphotransferase* gene.

>Candidate 1_ KAE9977539
MKATLISAILLTLSAVDAKKHRLCCCYGIDEDAPGKWSDKSAVCVQKPNEQIVASSKGYFIMSNQLWN
YNKDKRYPLEVESKNWFYAADIDFGNDNWVGGNEASDLCNAKGYNSKCFSPGSNDYRNPGTYQKRSQN
VDQDGKFVDVKGDSPILERDLVERKANGTKSTHKKGKTSSHKHSSHKNSTSHSSSHKKNSTSHSSTHK
KNSTSTKHHPKPSTTAVADFIERDLMERDLMERKANGTKSTHKKGKSSSHKNSTSHSSSHKKNSTSHS
STHKKNSTSTKHHSKPATTAVADFIERDLMERDLVERKANGTKSTKNHGTGHGKNTTSTHGKNTTSTH
AKNTTSTKHHYTPSTTPIAHLKHVDKQTNGTHVNATKPHHASGKPWTTFSQVTKSHHHYGNGTNAALG
HANATGGYAKPTGTATPSSGIVYCNQYWKAPGCVDKPDPAATPVVCGQYWKAKGCVPAKTGSS*
>Candidate 2_ atg11569
MKLTSTLLVAATTLLAPPVSANSYTLCCCTKLTYPQDSMDFRIFYDPRSRDLNIPSKQCDRAATKTIV
DIMHGHFAFTTHFWYAQKNVPRYRGDSYIYATAIDGDDNLIGQKEMEGWCAKQKAQRYCWSPGPEDLY
DYKGVKLKGTP*
>Candidate3_ atg10296
MHFQTPLLSILFAHPTSAYSCCFEIVGATYYKNFRTVMQSGALQVWRPTGGADDCMIVVDRDGANCKQ
WKYKIPESACIAYRPYKHVGVTGAATCY*
>Candidate4
MYAQTLLLPAILLVQPSFAAPYYCCFEIIKGATNGQPATIYSTMLLSGGTEIWSPLSDCKIRVVKTGT
GCGSWTGSIYSSSFDCRSMYPVGHMGVAEAWHCPNGGSGRI*
>Candidate 5_ KAE9973409
MQFQTLLPAILFAQSSFAYTCCFEYVGKGDFAYAEYLGSGGLQVWRPTGSPTCEIMINKSGKSCADWK
HSIAQNSCASSRPYRHIGVTEAGMCSSTYGA*
>Candidate 6_ atg12048
MRLQNLLLPAILFTQSSVALYACCYQVVGKGSVSKTFTSGGTETWVIDPDCQAFITKTGENCSQWTSE
VTGTCSRLAPVTHYGVAPASRCPPE*
>Candidate 7_ atg7739
MKFAIFSALFLAAGIANAQTGPGTVTCVKAFDTGRCFKWNSQNRGELYAECLARSPCQKDGDQCVLKS
EVHNGNYFSTCSGVKKGHV*
>Candidate 8_ atg3658
MKFTLALALAFLSATVSAISSVHPRMACLPVLWENGYCRVYLTNNPKQVTAQQYLCLKSSPCTTNENG
CTLEVAADGVLYGRCSG*
>Candidate 9_ atg12027
MKLLLISAVLALSSQVALGCQCKTSVSQRGKVPLYTRTACFDCSGRIDPNTSECGGSQHACFNRKCRE
LGGIEYGPPSTCYP*
>Candidate 10_ atg8503
MKLLLVSAFLGLFSQIASACQCKAPNGSVYWKRTQDSCGLCNGSWDTPAKGECSHVGHECFLAACKQL
TKNDGKVGTVSSCY*
>Candidate 11_
MKFQTTLLLLIGTTTALLPRNKETSEAGTTLFDLEHCSEWGQCCFPSCGSDCCDGLRCKGERLPGREN
KWRNVCRIHLH*
>Candidate 12_ KAE9966577
MPFSTILALPFFFISALAAPPFTNAIFPRGLSSVGQTGATQAAEQICFLGHCLDLGKDLGNHGPKGVM
AHSHCNLMQCVTAPGSTFATCASHQLNPTATAWTTAYCATGILKLGGDMPLPCKDCIGKLKLFSGGR*
>Candidate 13_ atg6122
MKFTQTLLLPFVLLAGSIEAVTQQKSVMVIFPKGTPDNIVTQARDAVIAAGGVITHDYENLLQGFAAT
ASAKAFDTVHELTSAYNPSIEEDQIISVAHDS*
>Candidate 14_ KAE9981873
MRPSTILLCSYTLLAPSPTTAVTNITFSNIKIHPTSTPTSTIFSTSTSSTTSTSTSTAITSTTIATNP
QIFDNQKFFEQAQEIADEETKTSDEDKAARLFLSGVPELRDWIRGLIW*
>Candidate 15_ atg6605
MYITHLLLFLSLFVLLFPCSRFCEALSVDRELSKAETPLNGGDIKRPDREIPSEEVGYGSTVSVAMVG
YCTERHVECASCELEVRRAIIAAKSSFVRPSTLVRLFSGGRNGQWR*
>Candidate 16
MYITHLLLFLSLFVLLFPCSRFCEALSVDRELSKAETPLNGGDIKRPDREIPSEEVGYGSTVSVAMVG
YCTERHVECASCELEVRRAIIAAKSSFVRPSTLVRLFSGGRNGQWR*

Figure A.5. Amino acid sequence of 16 SSP AvrRvi4 candidates from *Venturia inaequalis.* Cysteine residues appear in bold font. Signal peptides are underlined.

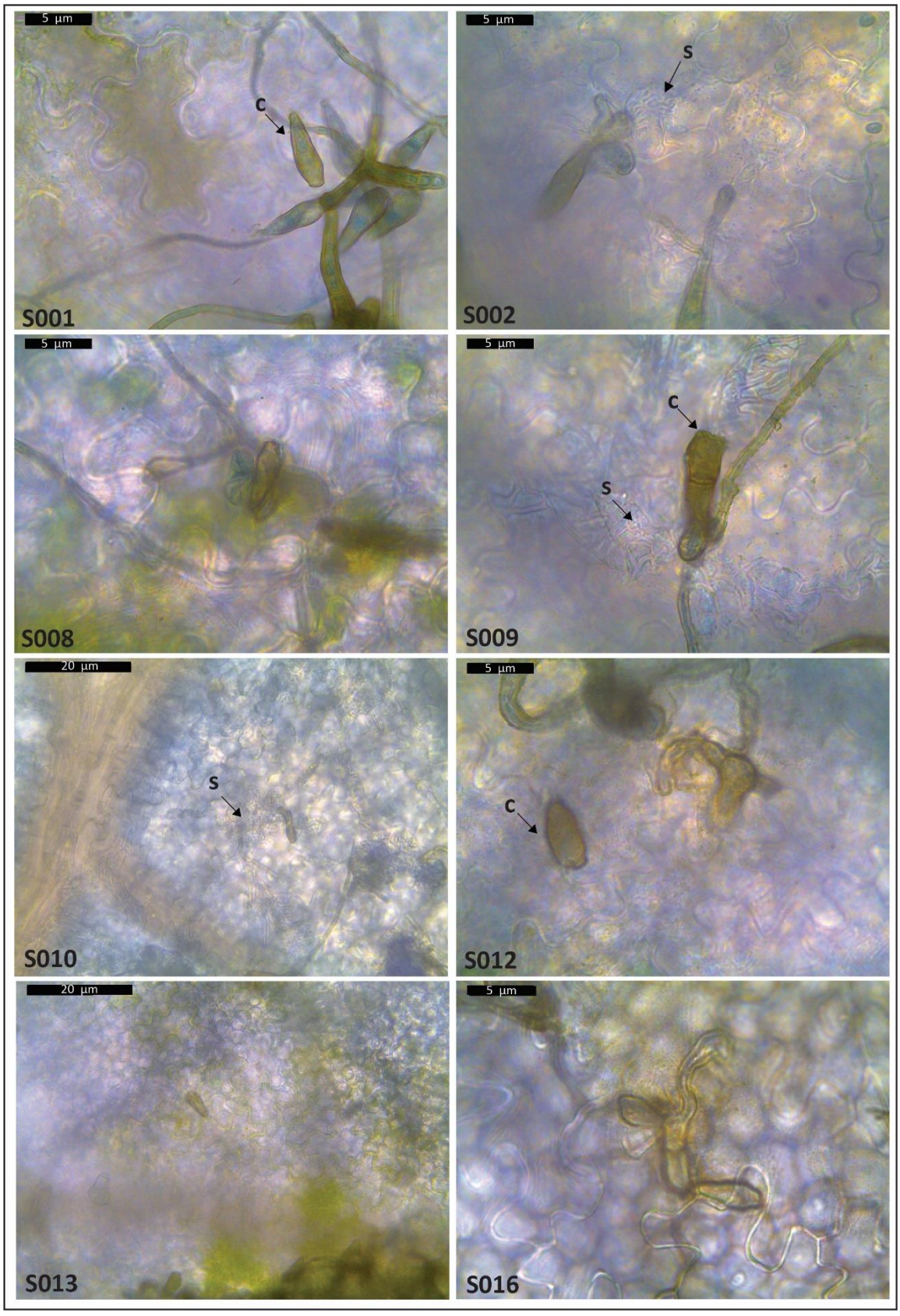

Figure A.6. Legend in page 245.

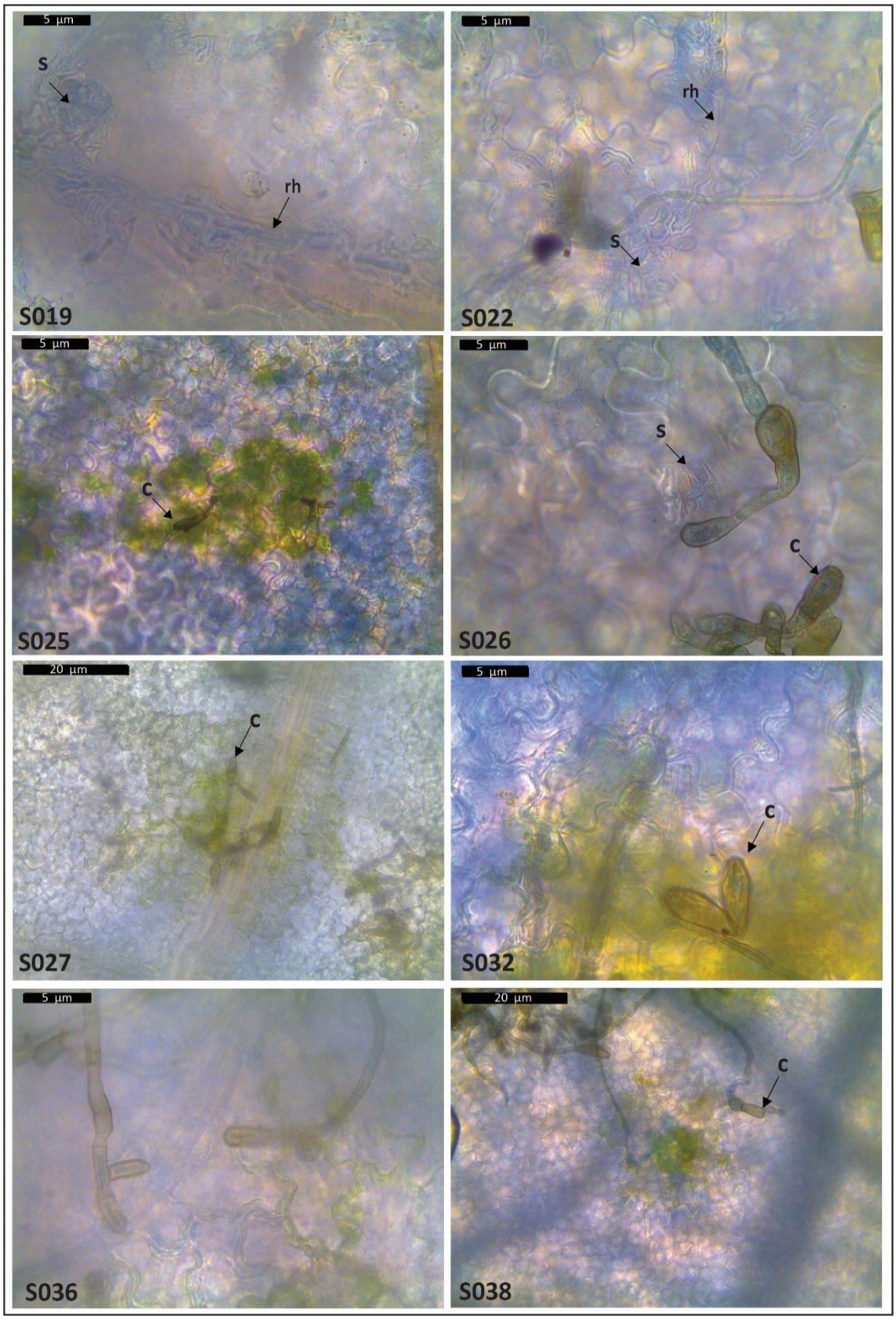

Figure A.6. Legend in page 245.

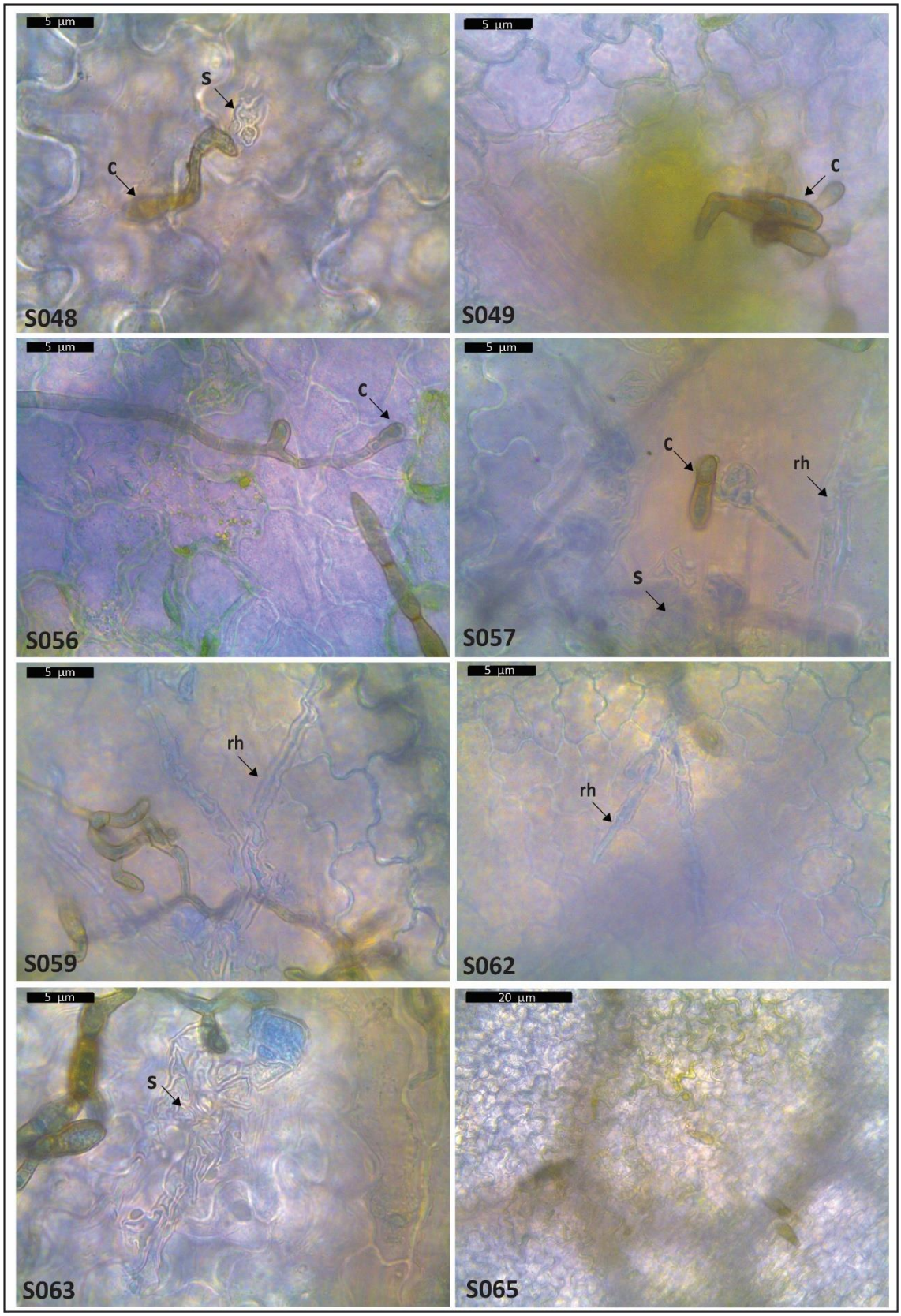

Figure A.6. Legend in page 245.

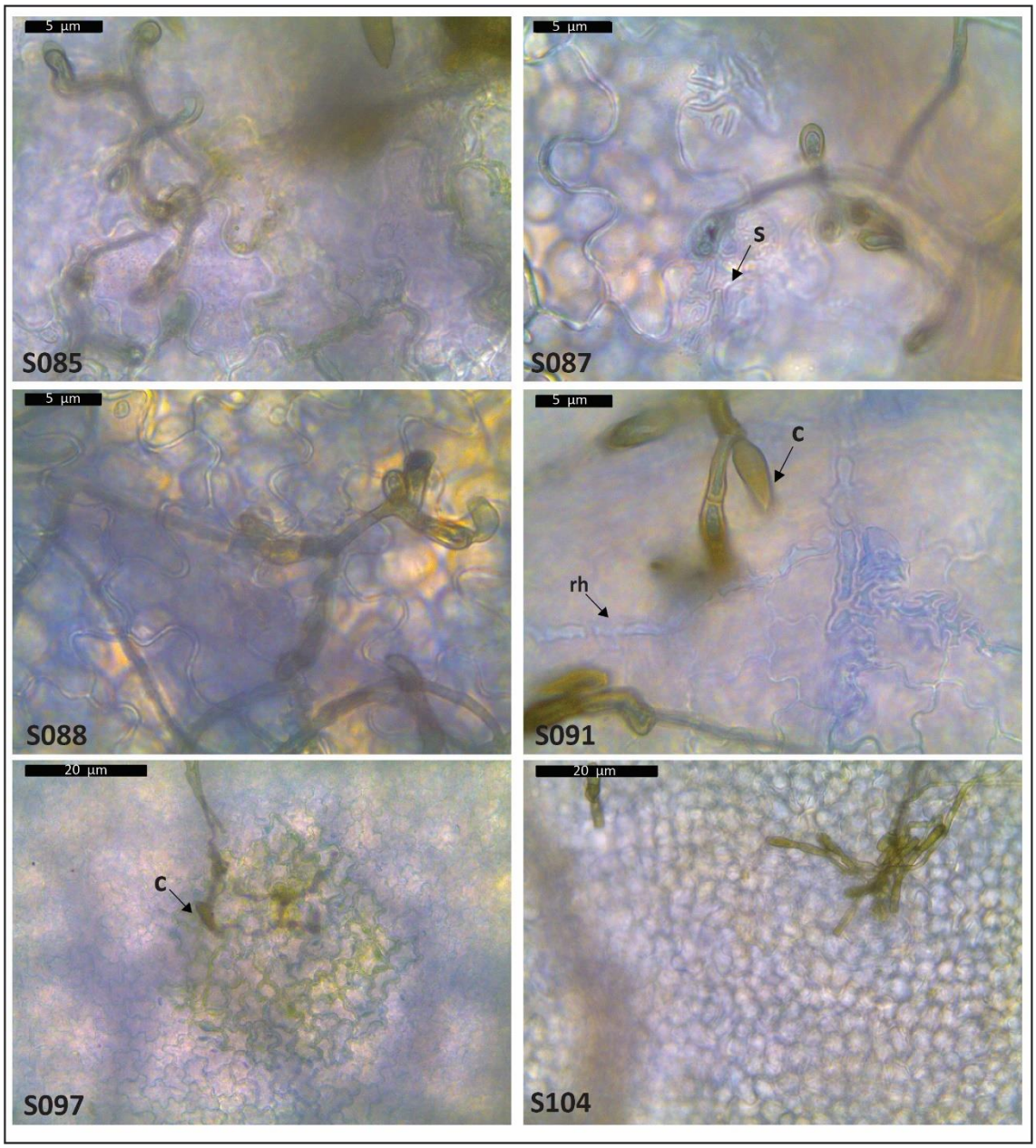

Figure A.6. Microscopic observations of *Venturia inaequalis* isolates inoculated on *Rvi4* apple leaves. Hypersensitive response (HR) triggered by isolates S001, S008, S012, S013, S016, S025, S027, S032, S036, S038, S049, S056, S065, S085, S097, S104. Subcuticular stromata (s) and runner hyphae (rh) formed by progeny isolates S002, S009, S019, S022, S026, S048, S057, S059, S062, S063, S087 and S091. Arrows indicate infection structures. (c)= conidium. All progeny isolates are derived from a cross between parental isolates J222 and NZ203.1. Samples observed correspond to leaves at 4 days post-inoculation.

Table A.3. Regions in the *Venturia inaequalis* NZ203.1 race (1,4) genome that have the best correlation between single nucleotide variants (SNVs) and an inability of progeny from a cross between isolates J222 and NZ203.1 to trigger a hypersensitive response (HR) on *Rvi4* apple.

minus	plus	ambif	p_minus	p_plus	chrom	pos	pval	padj
0	19	8	1	0	NODE_510_length_33946_cov_13.0851	2263	5.39E-10	0.000401
0	19	10	1	0	NODE_84_length_156639_cov_13.546	10849	5.39E-10	0.000401
0	18	9	1	0	NODE_31_length_236765_cov_12.7941	231638	8.62E-09	0.006416
0	18	9	1	0	NODE_31_length_236765_cov_12.7941	231745	8.62E-09	0.006416
0	18	10	1	0	NODE_84_length_156639_cov_13.546	17021	8.62E-09	0.006416
0	18	10	1	0	NODE_84_length_156639_cov_13.546	25992	8.62E-09	0.006416
1	19	10	1	0	NODE_175_length_104725_cov_13.1158	92705	1.08E-08	0.00802
1	19	10	1	0	NODE_175_length_104725_cov_13.1158	92789	1.08E-08	0.00802
1	19	10	1	0	NODE_175_length_104725_cov_13.1158	94332	1.08E-08	0.00802
1	19	10	1	0	NODE_175_length_104725_cov_13.1158	94374	1.08E-08	0.00802
1	19	10	1	0	NODE_175_length_104725_cov_13.1158	94398	1.08E-08	0.00802
1	19	10	1	0	NODE_175_length_104725_cov_13.1158	94544	1.08E-08	0.00802
1	19	10	1	0	NODE_175_length_104725_cov_13.1158	97607	1.08E-08	0.00802
1	19	10	1	0	NODE_175_length_104725_cov_13.1158	97612	1.08E-08	0.00802
1	19	10	1	0	NODE_175_length_104725_cov_13.1158	98352	1.08E-08	0.00802
1	19	10	1	0	NODE_175_length_104725_cov_13.1158	99197	1.08E-08	0.00802
1	19	10	1	0	NODE_175_length_104725_cov_13.1158	99277	1.08E-08	0.00802
1	19	9	1	0	NODE_175_length_104725_cov_13.1158	99369	1.08E-08	0.00802
1	19	10	1	0	NODE_175_length_104725_cov_13.1158	103286	1.08E-08	0.00802

Table A.3. Continued

minus	plus	ambif	p_minus	p_plus	chrom	pos	pval	padj
1	19	10	1	0	NODE_31_length_236765_cov_12.7941	214554	1.08E-08	0.00802
1	19	10	1	0	NODE_31_length_236765_cov_12.7941	214555	1.08E-08	0.00802
1	19	10	1	0	NODE_31_length_236765_cov_12.7941	214556	1.08E-08	0.00802
1	19	10	1	0	NODE_31_length_236765_cov_12.7941	214557	1.08E-08	0.00802
1	19	10	1	0	NODE_31_length_236765_cov_12.7941	214952	1.08E-08	0.00802
1	19	10	1	0	NODE_31_length_236765_cov_12.7941	215018	1.08E-08	0.00802
1	19	10	1	0	NODE_31_length_236765_cov_12.7941	217540	1.08E-08	0.00802
1	19	10	1	0	NODE_31_length_236765_cov_12.7941	217590	1.08E-08	0.00802
1	19	10	1	0	NODE_31_length_236765_cov_12.7941	218683	1.08E-08	0.00802
1	19	10	1	0	NODE_31_length_236765_cov_12.7941	219030	1.08E-08	0.00802
1	19	10	1	0	NODE_31_length_236765_cov_12.7941	220523	1.08E-08	0.00802
1	19	10	1	0	NODE_31_length_236765_cov_12.7941	220547	1.08E-08	0.00802
1	19	10	1	0	NODE_31_length_236765_cov_12.7941	220571	1.08E-08	0.00802
1	19	10	1	0	NODE_31_length_236765_cov_12.7941	220629	1.08E-08	0.00802
1	19	10	1	0	NODE_31_length_236765_cov_12.7941	220699	1.08E-08	0.00802
1	19	10	1	0	NODE_31_length_236765_cov_12.7941	220708	1.08E-08	0.00802
1	19	10	1	0	NODE_31_length_236765_cov_12.7941	220709	1.08E-08	0.00802
1	19	10	1	0	NODE_31_length_236765_cov_12.7941	220715	1.08E-08	0.00802
1	19	10	1	0	NODE_31_length_236765_cov_12.7941	220717	1.08E-08	0.00802
1	19	10	1	0	NODE_31_length_236765_cov_12.7941	220757	1.08E-08	0.00802

Table A.4. *Venturia inaequalis* isolates assessed for allelic variation analyses. Source: Le Cam et al., 2019.

ID	Isolate	Country of origin	Year of isolation	Host	Reference
2222	Vina_2222_CAM	Kazakhstan	2006	*Malus sieversii*	De Gracia et al. 2015
2223	Vina_2223_CAM	Kazakhstan	2006	*Malus sieversii*	De Gracia et al. 2015
2225	Vina_2225_CAM	Kazakhstan	2006	*Malus sieversii*	De Gracia et al. 2015
2226	Vina_2226_CAM	Kazakhstan	2006	*Malus sieversii*	De Gracia et al. 2015
2446	Vina_2446_CAM	Kazakhstan	2006	*Malus sieversii*	De Gracia et al. 2015
2447	Vina_2447_CAM	Kazakhstan	2006	*Malus sieversii*	De Gracia et al. 2015
2448	Vina_2448_CAM	Kazakhstan	2006	*Malus sieversii*	De Gracia et al. 2015
2449	Vina_2449_CAM	Kazakhstan	2006	*Malus sieversii*	De Gracia et al. 2015
2450	Vina_2450_CAM	Kazakhstan	2006	*Malus sieversii*	De Gracia et al. 2015
2451	Vina_2451_CAM	Kazakhstan	2006	*Malus sieversii*	De Gracia et al. 2015
2452	Vina_2452_CAM	Kazakhstan	2006	*Malus sieversii*	De Gracia et al. 2015
2453	Vina_2453_CAM	Kazakhstan	2006	*Malus sieversii*	De Gracia et al. 2015
2454	Vina_2454_CAM	Kazakhstan	2006	*Malus sieversii*	De Gracia et al. 2015
2455	Vina_2455_CAM	Kazakhstan	2006	*Malus sieversii*	De Gracia et al. 2015
2456	Vina_2456_CAM	Kazakhstan	2006	*Malus sieversii*	De Gracia et al. 2015
2457	Vina_2457_CAM	Kazakhstan	2006	*Malus sieversii*	De Gracia et al. 2015
2458	Vina_2458_CAM	Kazakhstan	2006	*Malus sieversii*	De Gracia et al. 2015
2459	Vina_2459_CAM	Kazakhstan	2006	*Malus sieversii*	De Gracia et al. 2015
2460	Vina_2460_CAM	Kazakhstan	2006	*Malus sieversii*	De Gracia et al. 2015
2461	Vina_2461_CAM	Kazakhstan	2006	*Malus sieversii*	De Gracia et al. 2015
2227	Vina_2227_CAP	Kazakhstan	2006	*Malus sieversii*	De Gracia et al. 2015
2228	Vina_2228_CAP	Kazakhstan	2006	*Malus sieversii*	De Gracia et al. 2015
2229	Vina_2229_CAP	Kazakhstan	2006	*Malus sieversii*	De Gracia et al. 2015

Table A.4. Continued.

ID	Isolate	Country of origin	Year of isolation	Host	Reference
2230	Vina_2230_CAP	Kazakhstan	2006	*Malus sieversii*	De Gracia et al. 2015
2232	Vina_2232_CAP	Kazakhstan	2006	*Malus sieversii*	De Gracia et al. 2015
2462	Vina_2462_CAP	Kazakhstan	2006	*Malus sieversii*	De Gracia et al. 2015
2463	Vina_2463_CAP	Kazakhstan	2006	*Malus sieversii*	De Gracia et al. 2015
2464	Vina_2464_CAP	Kazakhstan	2006	*Malus sieversii*	De Gracia et al. 2015
2465	Vina_2465_CAP	Kazakhstan	2006	*Malus sieversii*	De Gracia et al. 2015
2466	Vina_2466_CAP	Kazakhstan	2006	*Malus sieversii*	De Gracia et al. 2015
2467	Vina_2467_CAP	Kazakhstan	2006	*Malus sieversii*	De Gracia et al. 2015
2468	Vina_2468_CAP	Kazakhstan	2006	*Malus sieversii*	De Gracia et al. 2015
2469	Vina_2469_CAP	Kazakhstan	2006	*Malus sieversii*	De Gracia et al. 2015
2470	Vina_2470_CAP	Kazakhstan	2006	*Malus sieversii*	De Gracia et al. 2015
2471	Vina_2471_CAP	Kazakhstan	2006	*Malus sieversii*	De Gracia et al. 2015
2472	Vina_2472_CAP	Kazakhstan	2006	*Malus sieversii*	De Gracia et al. 2015
2473	Vina_2473_CAP	Kazakhstan	2006	*Malus sieversii*	De Gracia et al. 2015
2474	Vina_2474_CAP	Kazakhstan	2006	*Malus sieversii*	De Gracia et al. 2015
2475	Vina_2475_CAP	Kazakhstan	2006	*Malus sieversii*	De Gracia et al. 2015
2476	Vina_2476_CAP	Kazakhstan	2006	*Malus sieversii*	De Gracia et al. 2015
2493	Vina_2493_domASIA	China, Jiling	2008	*Malus* x *domestica* 'Haitang'	scabbed leaf provided by Zhang XG, Shandong University, Taian, China

Table A.4. Continued.

ID	Isolate	Country of origin	Year of isolation	Host	Reference
2508	Vina_2508_domASIA	Japan	2008	*Malus* x *domestica* 'Fuji'	scabbed leaf provided by Ishii H, Kobe University, Kobe, Japan
104	Vina_104_domEU	France	1978	*Malus* x *domestica* 'Golden'	Bénaouf and Parisi 2000
301	Vina_301_domEU	Germany	1988	*Malus* x *domestica* '81/19-53'	Bénaouf and Parisi 2000
2492	Vina_2492_domEU	France	2003	*Malus* x *domestica* 'Judor'	Lemaire et al., 2016
2498	Vina_2498_domEU	Sweden	2005	*Malus* x *domestica* 'Gala'	Gladieux et al. 2008
2499	Vina_2499_domEU	Spain	2005	*Malus* x *domestica* 'Golden'	Gladieux et al. 2008
EU-B04	Vina_EUB04_domEU	Belgium	1998	*Malus* x *domestica* 'Golden'	Parisi et al., 2004
1286	Vina_1286_RVI6	France	1996	*Malus* x *domestica* 'Judeline'	Guérin et al. 2007
1680	Vina_1680_RVI6	France	2001	*Malus* x *domestica* 'Judeline'	Caffier et al., 2015
2199	Vina_2199_RVI6	Denmark	2003	*Malus* x *domestica* 'Florina'	Caffier et al., 2015
2491	Vina_2491_RVI6	United Kingdom	2000	*Malus* x *domestica* 'Florina'	collected by Roberts T, East Malling Research, East Malling, England
EU-NL24	Vina_EUNL24_RVI6	The Netherlands	1998	*Malus* x *domestica* 'Prima'	Parisi et al., 2004
1066e	Vina_1066e_flo	United Kingdom	1993	*Malus floribunda* '821'	Roberts and Crute, 1994
1180	Vina_1180_flo	Germany	1995	*Malus floribunda* '54-1'	na
1393	Vina_1393_flo	Germany	1999	*Malus floribunda*	collected by Kollar A, JKI, Dossenheim, Germany

Table A.4. Continued.

ID	Isolate	Country of origin	Year of isolation	Host	Reference
2490	Vina_2490_flo	Spain	2003	*Malus floribunda*	collected by Dapena E, SERIDA, Villaviciosa, Spain
2263	Vina_2263_loq	Spain	2006	*Eriobotrya japonica* 'Algerie'	Gladieux et al. 2010a
2503	Vina_2503_loq	Spain	2006	*Eriobotrya japonica*	Gladieux et al. 2010a
2504	Vina_2504_loq	Spain	2006	*Eriobotrya japonica* 'Algerie'	Gladieux et al. 2010a
2505	Vina_2505_loq	Iran	2006	*Eriobotrya japonica*	Gladieux et al. 2010a
2506	Vina_2506_loq	France	2004	*Eriobotrya japonica*	Gladieux et al. 2010a
2389	Vina_2389_sor	France	2005	*Sorbus aucuparia*	collected by Le Cam B and Gladieux P, INRA, Angers, France
2484	Vina_2484_ori	Armenia	2009	*Malus orientalis*	scabbed leaf provided by Gladieux P, INRA, Montpellier, France
2485	Vina_2485_ori	Armenia	2009	*Malus orientalis*	scabbed leaf provided by Gladieux P, INRA, Montpellier, France
2486	Vina_2486_ori	Armenia	2009	*Malus orientalis*	scabbed leaf provided by Gladieux P, INRA, Montpellier, France
2487	Vina_2487_ori	Armenia	2009	*Malus orientalis*	scabbed leaf provided by Gladieux P, INRA, Montpellier, France
2488	Vina_2488_ori	Armenia	2009	*Malus orientalis*	scabbed leaf provided by Gladieux P, INRA, Montpellier, France
2489	Vina_2489_ori	Armenia	2009	*Malus orientalis*	scabbed leaf provided by Gladieux P, INRA, Montpellier, France

Table A.4. Continued

ID	Isolate	Country of origin	Year of isolation	Host	Reference
1669	Vina_1669_pyr	USA, KY	2001	*Pyracantha*	Gladieux et al. 2010a
2266	Vina_2266_pyr	France	1993	*Pyracantha 'Mohave'*	Gladieux et al. 2010a
2269	Vina_2269_pyr	Sweden	2003	*Pyracantha*	Gladieux et al. 2010a
2507	Vina_2507_pyr	Chili	2004	*Pyracantha coccinea*	Gladieux et al. 2010a
2478	Vina_2478_syl	France	2005	*Malus sylvestris*	Gladieux et al., 2010b
2479	Vina_2479_syl	France	2005	*Malus sylvestris*	Gladieux et al., 2010b
2480	Vina_2480_syl	France	2005	*Malus sylvestris*	Gladieux et al., 2010b
2481	Vina_2481_syl	France	2005	*Malus sylvestris*	Gladieux et al., 2010b
2482	Vina_2482_syl	France	2005	*Malus sylvestris*	Gladieux et al., 2010b
2483	Vina_2483_syl	France	2005	*Malus sylvestris*	Gladieux et al., 2010b

CE1
>Cin1_atg5511
MQYSSLLATIVALSATTTSALPAAAADVFDPPTQYGYDGKPLDASFCRTAGSREKDCRKDVQACDKKY
DDQGRETACAKGIREKYKPAVVYGYDGKPLDLGFCTLAGIREVDCRKDAQTCDKKYESDKCLNAIKEK
YKPVVDPNPPAYGYDGKPLDASFCRSFGAKENECRKDVLACDKKFDNEGRESACSKAIREKYKPFYVA
PPPVYGYDGKPLDASFCRSFGAKENECRKDILACDKKFDNEGRESACSKAIREKYKPFYVAPPVYGYD
GKPLDASFCKGAGSKENECKKDILACDKKYDNEGRETACAKAIREKYKTSTTTPVNYGYDGKPLDASF
CKKFPSREAECRKDVENCDRKFDDQGRETKCSKDIKEKYKEEKKADEKKEKDGKRQPTNADFCKRAGT
SVLEAECRKAVKECDKKYQNIGHEKECSRDLEDKYTKGSSSYGSGSGSYGPGGY*
CE2
>Cin3_atg4061
MHFSQVAPFLFGISLAFTVPSNDKQEGSDAVNTRYLAKRQSDIPTYHKLWDEEKESGVKAAYKVVDGQ
EVKGQVEKRQSDIPTYHKLWDEEKESGVKAAYKVVDGQEVKGQVEKRQSDAPYYHKLWDEENGAVAKA
AYRAVDGQEVKGQVEKRQSDAPYYHKLWDEENGATTKSAYKVVDGQEVKGQVEKRQSDAPYYHKLWDE
ENGATVKAAYQADEAGAQADAQKA*
CE3
>Cin1L1_atg5172
MQFINSLTAALVAFNGVVSAMPTAIADGAEVAEVAKVAEVAEVATNANVADPPRNYGGSGYGSSGYGI
SSYGTSSYGTASYGSDYNGGSDYGDRFDPSRGDRDYGSERRGKKLDDSFCKKYGSEKDECKERVKKCD
KKTADFSEDERKCREKVERHFEDEKRKGNNRGY*
CE4
>Cin1L2_atg6798
MRFAAIISMAFATFSMTSAMALPNEATFEVSKDDPKKTDKLPVGTGAQGVGAVNGDLHHVKTSYCKAL
TDAKKRSPCLKALEACEKERTENKEEACQNKVKKNYHN*
CE5
>16969_atg3864
MRILFTLSATAALLGSCLAMPAAQCSPDTSVAPVVTPSTDGLEVQDQANACPSGAVERYACRLITTGF
CPRTELSGYTKSCCGASPYCADGGCYVIGDYKNFDNCITDGGRRKDIIPSEKPC*
CE6
>15505_atg1429
MKPTAFLASLLTFAVMAAATPIDSIGRAASIQAAIEMNNALDVYNRMQTDESAMIGHTLCACQFDKHA
NLYLDATISACADLGGEMDIRDRKAGLGGIDFFGKYCRPHDSVKLDGKGFNIACRNHYAIASSCPWKH
*
CE7
>18699_atg4475
MRFQLLSMAFLAAVQVASAIKYPPLGHVAGGYQGKKTPVYGYCYAVGKKTIIYTCPNFEDTSCDTSCN
QAQAKAGSRVQCDVLC*
CE8
>24527_atg9241
MLYSTLIISTLLATLTAGYECPIKHKLITTGGCVYRHRCVRDKQEDADAFCNQQGSKRSTGQHIANVV
GPSGHLNGDRITYICCAPIPNWDGNVYPYDPSTGY*
CE9
>13533_atg11760
MLFRSLLLFAFTSLSIAVAVPNTNDDALRRAAAAACDNLCNRSDQNRSSCVQCVMNKITSSAAPCPAF
DNRRQGQRGCGHVEQSSRGGLSGTPDPYSGNK*
CE10
>ViHyd1_atg24541
MFSKAILFFSVLSIAMAAPGSKTTAPGTFSVEDQSCGDGQQVSCCDSDTAGSLLGLTCVVPILNACAQ
GNSAACCKTEQTGLINVGLDCIPIAL*
CE11
>ViEcp6_atg11994
MVSLFTLLVAAAPAPELLSARELCNGTITLDERVQKYTIASGDSLGAIATKFNRGICDIATANKITNI
NFVTAGQVLTIPAQVCIPDNASCQPKTPEATATSILGGPGFYIVVSGDTLTAIAKNFQITLQSLIAAN
PAITNPDLILVGQVIIIPVLPGSSCTISPYVIKSGDIFFDLAAKFGTTAGQLLSLNTGTDPTKLAIGQ
TVTIASGCKSA*

Figure A.7. Legend in page 263.

CE12
>ViPNPL-5_QDH43451
MKFTTALLALSSFAHLGLCIVGVVTTYRPPYLPTKCYGSNQGQFPAGNLFGAVGPGLWDNGAACGRYY
AIRCINPIYGSGHCVPGARITVKIVEGRLGSRAPLISLSMQAAQMLYTGSGSFKAEFGEVPG*
CE13
>ViPNPL-9_QDH43453
MKVITTLIALSSLAYLGLCDAGVATTYKSPYLPTRCHGNDQGQFPPEYLFAAIGPGQWNNGAACDRHY
IIRCTSPIGGIGQCKPGYITVKIVEGRLGNRAPDFSIPPQAVEKIYTGAGRFKIEFGEA*
CE14
>atg11273
MQYSTLLLAFVSVAQANIVCQPVPTSFTKYPCTALSDKSYCLNACDSHCPGKQNIWCILSGNPKVKFD
CWCG*
CE15
>13636_atg12276
MVKLSSAAAFLAAASSVAVADWHIINWEAGCARSGCFYIFNVTGPASEDGKIPSFGASCNAYEYRKPQ
AFTPCGINDSGAGNRGVSAKFVPRVEPNGILEKVAVSFAFTDLKTGAVRNFTGTTNIQINQFVAPRQN
YTISDIKENIKEN*
CE16
>14801_atg3212
MVATTPSLLSSVLFALLATAAPLLPRDASAADSLTYCAAISDTICSSTSDLASTAVVTLPAGWYGHFE
CYATVDGIDRYFAGHPPIAPGSGQSQVCWATASALGPAQGGTGRQACLKSQLANCCEMTHLSIQGLQC
PAPTNKVAGLAADTTYTS*
CE17
>15961(Alta1-like)_atg2494
MVSFTTLFATVAATASIVAASPFTRPDPPTTSACGGSNDEVLKITDFFSRKYDGINIATLGFNISATN
GGELNFRCAPYDPAIDATAAQFEDKRVYFCAKDSSFSFSFENAANQLYLWQTIVTDTNILVGNGTIPN
YCHAGGSSQTDMVCQQVADVNITMVQSA*
CE18
>16394_atg2434
MKFTIVLPLLIAIAYAGVIDIHIDTTGDVIQADCYWDGTAPFCAGACGPGYQECGRSASGGGQPCVTG
TKAMCCSQSCPAMQFTEPARVQPPKEEVVEALGSCYWEGTAPFCGGSCSKGYNECARSDTGDGESCVT
GSKALCCTKECPNNVADQKPLFALGSVARGSALCANGEKLWCAPGATSNEECRCAPQNFEL*
CE19
>682.7_atg4496
MRFTTITLAALAALFTTPILADWEIYTGTCSNFGETGYPYPNTLEPVTCDQCGECGRSGNYDGDPENG
EPFTSTNPCCADEDCRGDYSLTYIPNNQYHNIYLNDEQIGYCEPQGYHAGECNPNGVYSCTIGSVRIC
HSDYCN*
CE20
>21582_atg6993
MNFSISLLQLLGLSIAPTFVTPQGLNVTAISATNGVSVLECWSLASPPQNARGAANYDIGNFEDAFIG
VIAPRTRIGYAHAPSIQFVSPP*
CE21
>25058_atg13108
MQFSTALLSLAALATFSSANPVPQSGFTGTSKWWYWTVTDLTLTSTPLVPKYQYKFNIQHYSQTLKAN
CSGPAEKIVCSDQSYTISVQEGRESTTFKITQKLYQSSGLATLTGETKLNVSCLASDGVSPEFTKTVC
TDPAFKVDSNLVQ*
CE22
>17864_atg5488
MNLTTIIAASLALLRSTIMALPQPDDHVAPAEGIIVPINQGPNCQGNSGLNLFNGIKGTGKCDEYSIS
NDGTCMRFNPFFNIRSVHLADGAQCILYSSKTCKIESKDDHKAPLLHSVDDLFADQAGSPALTFYPRG
WKCYYWPPKAASVPVARSLDTTADAHELAPGTLMLCNKAKGLGNCGIWSFKNNNCVSIADDFTIVSIY
IDDKTQCWIYNNRVCNTDLSLNDKWAPLLKSTDDVIADGLGYNPHSWKCVDRNQ*

Figure A.7. Legend in page 263.

CE23
>g9438_atg1395
MLFSQAFVTFLLSATALAMPGDWQKDHEYEKSVCKTKTKYDYETYTDKIYKTVTNYKTDVETKFKTDV
ETKYKTDVETKYKTEVKTVLETKTVPYEEKKTVAFYETKTVPWPSTITGFTPVVKTGEVFETVCKTEL
VGDHYDYDDGNKGWKKV*
CE24
>g4401_atg5327
MYGLNQFLVLALATSALACKCTENGLKNGPSDNQATVGACQFATGHMVGDDCQKACHVSFDRWCGDLT
GYYTKLKNLRSSCGADRAFC*
CE25
>g9336_atg5420
MRFTAALAIAALSSSALAYPAQASVDTTLSANHDEPPVKPGTDPKLDPKTAKPKTKLKIYEFPEKCKV
DDDWDWTKPVLLPHACKLPKGFHFPAFDAEKQKLEKTIKNEKGEKEKKKFTFEWPKECELPKEADWKK
GVAIPHECELPKGFLIPKALVPVVPGVKQEKPKEEKPKTEKPKEEKPKETKPKEEKPKTEKPKEEKPK
ETKPKTEKPKGEKPNGEPPKGTDADPNDK*
CE26
>g3042_KAE9992730
MLFAKSSVAMVSLFTLLVAAAPAPELLSARELCNGTITLDERVQSYTIASGDSLGAIATKFNRGICNI
ATANKITNINFITAGQVLTIPAQVCIPDNTSCQPKTPEATATSILGGPGFYIVVSGDTLTAIAKNFQI
TLQSLIAANPAITNPDLILVGQVIIIPVLPGSSCTISPYVIKSGDIFFDLAAKFGTTAGQLLSLNTGT
DPTKLAIGQTVTIASGCKNATATTGENKYWKGQWGGPGGKWEGKWGN*
CE27
>g13163_atg5361
MKASIIGSVLFAVSALASPFAHGPDDDDHTPPAKTPELKSASETATAAGLTALVAALTKSGLAATVDG
LKDVTIFAPTNEAFAKVASTTSGLGKEALGDILKYHIVKKVIKSTDLKTGDKVPTLYGPIITVTLAEK
KVLINKATVVKADVPFKGGIVHVIDAVLTPPPKN*
CE28
>g1277_atg5929
MQFQALLLPAILFAQSSVAYNCCFQVGVKGARGGYHKIFGSGPTENWVLASDCTVAVFKPGNDCSRWY
ARATAGTSCSGLGNWEGKSVPGNSCT*
CE29
>g12222_atg12663
MLKSLWLIFVFFSITLACDPVYHNCCWNNRCVDNSGCETYLNTYCGICVKRHDGCRNQRRRGKDDCNK
GTLNAQKCSDDLSNKCGNADCCDSKTGAPIGCPGKNGKRLVDSV*
CE30
>g14234_atg6441_RDI86726
MKFSAILLLAASALATPIVDPNAPPAEEVTITSAVTSGNGCPSGTVQTTFSPDKTVATFGFDAFQTYI
GPKTKPQDHSKNCQIHLSLKYPGGFQFSLFEATYHGYARLDAGVTGSFTSSYYFSQAATKTSISKATI
SGPDYLNGLIYTKADVIENASLIWSPCGANGILNINNRITLTAPSEGKAAGELANDDATVKFTQLLAF
KWRKCTN*
CE31
>g9700_atg2705_RDI83167
MKFISAAILFAVAVVAQSGEMEVRNELDFYKHMTKRSPNENPLQKRYFCGDGWPTFDACQKAGCVFSP
CIQKNNRKGQSTWQCCTYVNRDDCC*
CE32
>g8959
MKFAIFSVLFLAFGISNADFPTGTCVLAFDYGRCVIYNAQGRPAKYAQCRSSNPCTKKGNNCSFNGVC
T*
CE33
>g9061_atg4321
MKLLLIPAVLGLFAQLASGCQCVDPNGIFLLTITKQACGRCGGSYDIPVQNHCFRPVHRCFDIYCKSL
SGRSYIKSSCA*
CE34
>g7375_atg10823
MHFSIILTLLLPALTLAHSCGGGKLLIKLGTCNPSACWDLSQDDVNRQCGKPGGKYFTARSQYPGEKV
MYICC*

Figure A.7. Legend in page 263.

CE35
>g11637_atg644_RDI85799
MKSTSFLLIVAAALGLPELSWACSDVFPLQEARCECNYGDTTRCAIPGVRHGAGWACKCSDCPRSYQG
HFLGDVSAISKSAYSYRRKCRDN*
CE36
>g14256_atg8668_KAE9970676
MRFVMPILALLAVQLQALPSPANEISRTSVNEALTLPILSKRLDPEPAPANDLFLGSPGNEAATDPKP
LGSESAPANEVPGTSPNEAFSVAKRPIFAGFGQCGGQLALWPRVQYLFFPPRPQRITVDMRMARHSWR
GFIHVFDDDTRVETVTVVPLWNDVTGAFGTTVEAWNRTEWPMRLVIIVEVSGVNGLGRYEEHRMNLDL
PGGLHYAKTKCMISTFGKDKRVNMYLWIEKLKVSPP*
CE37
>g3687_atg11932
MKFTLALAIAFLSATTSANRTACRITTGPYGDGHCVVYDKVHWDQPTKEEYDCITASPCTVAQNGCTI
FKQDGVKKARCSG*
CE38
>g10504_atg4427_ RDI87518
MKIQTILLLIGTATALVPRNKETSEVGSNIFASEVRKCSKWGECCPPTCSDKCCDQLKCHNREIPTDP
GVWEATCKIN*
CE39
>g13513
MKSVQTFVAFLLATTVSAEYYKCKTGHTTGTKSGKCFAYQDGTNNIIPYRTERLCRDLAPCRADGTKC
TYHGEQVQGTWYSNC*
CE40
>g13878_atg2807_KAE9974018
MLSPLTVLALSSAVSAHFHLTVPYWRGDSFAANRSQWTYPCANVDQSNSSTNRTAWPLDGGSLLASFS
HPWAYTYVNLGLGNAVTGFNISLVEGFNQTGNGTFCLGKTGRRVLEGLNLAEGQNGSVQVIQISHSGA
ALYNCADITFSSKATLLDEGVCRNGTGVGGVALQNAGTVMAAAGNGTAAASKSSGAVGGVRVKGCVVF
GALMVGVWALIM*
CE41
>g1250_atg8558?_RDI80995
MQFLSITAVLLNLVLIQDVAAVNAVKAAIPNPMCQYRPDNCVANDCSTIYQNAHSTCKSRCNGAGTAI
CCGTQLYCWGGSTFVTRLV*
CE42
>g12572
MKLLLITAVLGLFSQLASGCQCKAMTPSAVRVYTQRACTRCRGNFDAEPYECGGSNHACFNSACTAST
GITVKPSTCP*
CE43
>g13647_atg11273
MQYSTLLLAFVSVAQANIICQPVPTSFTKYPCTALSDKSYCLNACDKNCPGKQDIWCVISGNPKVKFD
CWCG*
CE44
>g3498_atg7515
MKLTSTLLLCLAVNSLAADAVDWPWTCYQRKGTTGVCRQAKANIPGAGDLPQACLQGSQCEKPEHACT
PNQFIDPGTGYKYATCGE*
CE45
>g4360_atg1069
MKFISAAILFSIAVAQSVEDKDVNKYYESMSNKDVNKYYKSMPKRSPNENQSPNDKHVFTKRYMCGDG
KNTFQECQNNGCVYSPCVQKQGKWGMTWMCCKPPGINDCC*
CE46
>g11778_atg6591
MLLQTLLPAILFAQSTLAYACCYQIRAQYGGRKASSILFSGNNEVWHPDPNSECEIAVYKNGKSSCAG
WTYSIVLGCNVFQPTSAYVGPVAAKECGY*

Figure A.7. Legend in page 263.

CE47
>g2403_atg829
MQFTTAFALAALSIGQAAAGTLNHRHFHMRSAAHAPIAEVEERDILSTLASSLISTLGIQAGTNAAAN
NGGVWLGKDGDYTNDFINNSTEDIVVAVWGPAGSWVNAIKPLITVAVPSKSTKTVSFANGASGAWAAI
YPDTKLTQYGQIGQTWGEFTFAGQWSTVDVSREVLMTGRGMRIETPKCVSDMETCVFVCDSGSTCLTG
YTLKNCAAGSQPGAQIGTYAGAASGGCSGMGDKAALKTYFY*
CE48
>g10970_atg6878_KAE9970717
MYFSFILPLALLAAFLPDVLACTARKQNCCWGGTDNGFVGCYNQHNFSDNLCRDKKYTADYCSRHKIS
AKDCSSDCCDIKTKKGIKCPGAKHGIQLPSFLNGLGSLTPQDLGAPKGGGSGGDPSGGLIPGLGSIFG
GGSAGAQPSKPTGKRMVRRFMS*
CE49
>g3143
MKFTSALAIASLSISVSAIGTPRMACRLPPSGKKADVYGYCVVYDAHDWTKATREEYQCLSESPCKKD
QNGCTLTKYGTLAGQCSGLVPGRN*
CE50
>g14092
MKFAIITALFLAAGASAAYVPKDDGTYTVCTPNDKAGICKKYDRNNKPTGLQEDCRWVKPCNHNGNGC
IMDFAGTGRANCSG*
CE51
>g9851_atg6627
MKLLLIPAILGLFSQLASGCQCIDAIGNVLPTSSKSACGPCGGSWDAPVAGQCSHPNHICFKAWCKDV
THKGSTRSTCN*
CE52
>g1678_RDI86109
MKLATLIPTVILALFTTTTIGCATYKVCWCELLNITYKGKPNQNVPWDDMTQAACREPGQIQYRNMYN
HKVCWRFNERIFITAQGIDNCSWKNQCEDEYEKKLKEKYKKGMITGHCAERAN*
CE53
>g3841
MKFPSALAIAFLSITVSAVPNRTACRLPAVPADIKDQFGYCIVYSIIDPFRPLQPEKKYQCVPTSPCR
VDQNGCMKIVSFTGKEYANCSG*
CE54
>g3533_atg8817
MKFTSALAIAFLSITVSAVRTACRLPDSSNKRDTGHCVVYDAKKWWKPTKEEYPCYMDWPCKEAQNGC
TLDEYSWGKVGKCSGGG*
CE55
>g912_atg4567_KAE9973739.1
MHYSSALFLVVGAGKVLAQAGGCSPLHFIYARAPTEQGYGAVGASIFSNVAKLIPGITGYPVSYPASS
GGNQCASEDTGVSDMLKQIANKAIECPRQKFVLGGYSQGGIIAVRTINKMPVDLLPKIIAVTLVGSPE
CPASVKGRCKSFCNAGDAICSTGRAYTSACDGSRGAAKGFPRTSSPAKTEHKPTRREMAGMDTRSVEV
GGNAEVAGFDLKSICDGPEPAEKGHKVLKDPHTAYSEDGYYVYAAACYIQKMFSGRR*
CE56
>g12877
MYTYTLKQLLVLALAGSGLACKCTRNGYKGAPVDTKATEVNCPLSGGRVVNPGTPNVDCLGACHLNFG
QLCARSTGQYSSIPYLGNDCGTDTAYCHNGK*
CE57
>g9007_RDI77214.1
MKATFFALLLSTFAYAAPILEERQSTGTTANEYTRSGCKDIIFFFARGSTEVGNMGSSVGPPTADGIK
SAFGSSRVAVEGVDYGALLSTNFNPGGADYAGISEMKSLFQDAASKCPNSAIVAGGYSQGAALVHRAI
ENLSSSVKDKIVGVVTYGDTQNLQDGGQIPNFPRAKVLVICNTGDAVCAGTLTILAPHLDYVRRVPEA
VSFLNGKLTAAGK*
CE58
>g9793_atg1373
MKLLLIPVVVGLFSQLASGCRCIPKPSEISMTNTYTHVACDVCHGQYDPNTHECGGVGHTCFQLRCQK
QTGLYTVSPSCQP*

Figure A.7. Legend in page 263.

CE59
>g7408
MKFTTSLLLCLAVNSVAARHWECVPRQGYQGFCRLLDDSNQVVLGSSQECRQASPCLTNHHACQPNKF
QDAGGSYANCNEAHSTS*
CE60
>g12428_atg12924_KAE9986115
MKFLSLVVLATAASANYLDAVNARRSPNAVEARQPHGPEKSNVPLAARHGPGDYDTPKMVGRSAHGPG
DYDTPKATRVVARKPHGPDGDDDHTIPKSTRVVARKPHGPDGDDDHTGGKKGGGYRRRQVPQPKASAP
TMPEMPGMAGMGHS*
CE61
>g8715_KAE9963057.1
MKLTTILLPALYCNIAASRATSSWFSANDDSQLRLQNDDPLSVPGENPLLFCADPKDNILAITKADLN
PNPPKAGTTLSISAEGYLNEDIEDGAKVHITVKYGVITLINQETDLCEQTHNVDLECPLEKGELQLTK
DVDLPKEIPPGNYHVLADVYTKDGKKITCLTAAVSFRRG*
CE62
>g4805_KAE9981396
MKFSATIPLFLAAFSSAAPIEDSSNVDPEPSGIFVKDIKYNGSGCPAGSVSSQFSDDRKIFTVTFNKY
EANIGPKVQLRSDARKNCQLNLKLNYPSGFQYSVVGFITRGYADIDADVTAEIGSIYYFSGQSQQTTS
RNTIKGPFHASYTKEDNINVATAVWSPCDAQGLANINTDIRLTAPPNSPAAGSLTVDSIDGKFGTKFE
YRLQWRSAQCGTKRRAVDDAPVLNEMNMEANSFVVDN*
CE63
>g12872
MKLLLLPVIMGLCSQFASACQCKSLDGYTSPTKTSEECHPCGGHYNYGSKECNEANHRCFNEACNRRF
GQPLDTVASTCGRGY*
CE64
>g9279 _ACM90099.1
MKYSLAASFALAALVGAAPLNNKRDTVYSTATVEEWVTEWLTTTVWEDEAPYAAATSTPAGGFYEVAH
SASASSTKTRAAARPSNIVNSASSSYSTPAAPVVVSSTSSSSSTSTSIAAPTTPTTPAYVAPTTPSST
YVAPTSTSTYVAPVVVTPTTTAVPVVPTSTAPAYVAPAATTSKVAAVYASTSSGGSGTSTGDMTYYDV
SVGLTSCGLTGSNSDFLVAMNKPDMANGVNPNNNPNCNKFINIYYNGAGPFLGKVVDTCPECVSGAID
VTDSLFKAVAPSGDGRVHGVSWSWA*
CE65
>g10511
MKFLYPLLVSLLTASVSASKWRLCCCAGWNDCNQFVCDSDSAQNIVDLLSGTYVRSKKLWDRYTGSPI
GGLDGWIYAKDDGFIGGNEMSDKCSRDYGLSSRCFDPKLKTGEYSDYSNDGKKIGSRQTLDGGLGGVG
AQLKPKKPKSKGGGGGDDPPRQELMERSGRKERSQRREKKRTRTRIIGQFASDVQSHTLAKDL*
CE66
>g1500_atg2922
MKLLLIPIALGYFSRLALGCQCIPPGGETSVIGTLRACSPCNGNYDGVTHECGGANHGCFIDRCAKLT
GVKGKSSTCQ*
CE67
>g121
MYGLKQLLVLALAGTALACQCRTDGLTTGTLDIPATDAACRSTGGTVHNAQTENIECADACHYNFEQK
CRQLSRIYTDVPRLRSTCGGNKYGCK*
CE68
>g11287
MRPQTLLPAILFAQSSFAYSCCFEVLGQRDVATGVFANGGVFTWAPRTDCIIEINTNAESCSGWRWRY
LSGTSCKSLGLPLAYLGTAPRSQCN*
CE69
>g10061_atg11917
MRFLPFLPAAFLAAVQPVSGLALPEVGVVARSAASYITLSGFCPGPGYTSLMYTCPGGIPTRCEAPCA
GKGVETHCYASCG*
CE70
>g13842_atg2850
MKFTSALAIAFLSITASAARTACRLPKSKQESGRCVVYDEKDWRKPTDQTYSCFTDSPCKTAQNGCTL
IKWGDTYYAECSG*

Figure A.7. Legend in page 263.

CE71
>g13809_atg10584
MHFQTILLPAVLFAQSSVAYWCCYEIYTAGHFDKRVARYFWSGGYEDWTPAAGCTIRIHKDGKSCANW
TDQLVGGLCSAFRPIGYYGPAPATDCPPPGT*
CE72
>g12228_atg12491
MQFLSVTAVLLNLVLIHEVAAVEAVEATIAMCQQVPKYCPKQNDCGYFFSDRHASCRAKCGVGANAAI
CCDQQLYCWSAGGGIGT*
CE73
>g3582_atg5886
MKSFVSITFAALFASVTLAAPQAGGTFMGFSMPPACATGCITPEVQGAGCGTIPNIACVCKAEKVVNA
LKTCVPTKCNAEEIAKFEPTINSACKGNPGYPMKLGKGAK*
CE74
>g865_atg12640
MKFTLALVIAFLSATVSAGPRTACLALPGKDQWGYCVVYMANNWQQATAEQYPCLPESPCNVNEHGCI
LVKRNGKVVGKCNG*
CE75
>g10970_atg3532
MRFLVSLAAAVVSLPTALAAAGCPPLELIYARATTEPKGLGAAGGLLAKDLAKDLPAATVYPVNYPAS
MGSLNTCEGPMDLIKQVKTRVDSCPGIKLALGGHSQGGAVVTATISKIPAKYLKSIVAVTLFGAPPCS
DLTKSTVPGVAEVGARCKSFCNYKDQICDSTGAMGNGGPRASCTLPKSFVPRRRDVEVKDFGLGYPAY
VEPRPLSEQESLRVNRFNKQAAATCGEDERGHKAGSMTGLAAHMAYKSDGYYVAAASCYIAKMFKAAG
GSGPPAAEAAQ*
CE76
>g8761_atg1995
MYGLKQLLVLALAPSALACQCRVDGLPDGLLDIQATQTACDWTDGGIKNPGTPIIQCERACHSSFMVK
CMRLTGLYTQFPRLKSNCKPDNKWC*
CE77
>g8276_atg437_RDI88990
MKLIVILLSCTAAVLAFPIANPIANPVANPNPMAKPAPAPIPQSRYGPGRGEPDRPVGDRPKPQPAKP
NPAYPKPDPNIGG*
CE78
>g3875_ KAE9980336
MRVSSIVFGLFTSFAMAAPLASYNGGSDTTGTLAPVVGSNLGSVVGTGSGNKASADGNSATGNGNGNG
DGNAAGNGNSVGNGSGSGNAVGTGSGNGNEASANGNTIGNDIGNVNVGLPSTITINPNIDAPITL*
CE79
>g13066_atg2104
MSYTRYLSLALAASFAHAYPQAPAAGAPPAAGAPSAAGAPSAAGSPSAWRAPADLPASTSQECKAILQ
DAGVRAADGEIIPNKYMVELKPFATEATVKEIAAALKVKPTLTYKKKAQPGFAAELTYDQVCSVYKNA
AVDHVEADIKPANAQKPASQLVSDHDSDAYGNWPVGQANFTGTPDITGLDADCAKIVWYTVLSVDPAK
AVKGVFQATFKTFAKQADVEKMLQNAELKDLKLKASDSDSGGKKDWDDSFEIKFLVASMTPKAVCFLT
HHELVSFIAPSTHEEKPPTV*
CE80
>g4565_atg9444.t1
MKSSSFLLIVATALGLPELSWACDDAYAPREGRCQCNYYGLNENGDTIRCVFHGVSHGNRWLCACASC
PPGYRGYSLRDVDAISQPKYNGRHKCRDNENDQP*
CE81
>g4116_atg9255
MGIQPRCRSERKTRCIPVVYRPHRGFLDYCETQISKLNALSKSLTDTKGAFEREERKVYIRPISLHQF
QNHQQQQLQSTIIITIFHSTTPPTKTPPKNPKSINMFSKAILFFSVLSIAMAAPGSKTTAPGTFSVED
QSCGDGQQVSCCDSDTAGSLLGLTCVVPILNACAQGNSAACCKTEQTGLINVGLDCIPIAL*
CE82
>g4568_atg2596
MYFPTFVAALSSLLVLTSAQFPKVQIPPGHDMERGCCNPDNGGAWKNKATTDCCNSGPIAGFPWHWDR
PNGGRIACRFDKDQKEDFMQCCIKAGQVLHTEDWRACRLI*

Figure A.7. Legend in page 263.

CE83
>g11651_atg4507
MKFTLAIASILAAVSAQSIPGLPTCGVSCMITAATGAKGCGFTDSKCFCGLPAITEALKTCVPQNCSA
TPADIKATYELANKSCAGAKGFTPLTPPA*
CE84
>g13068_atg2102
MKASVILSILLTVVSAAPPSNKAKREELNWYQIATKGKVGTPNFLSQKGGKIGGFNGTRESAANAGKF
FTAVGAGGTLQLLAGNWDHQVGLKASNSSKGVMELVDLGSGPTAAIIPADAPGSVEWGVFAVSEAGEI
TVKDGADVPTRQWISYLDTDGAYYVALWDGVTKQPRSFANVSLIATKTEGLWT*
CE85
>g10873_atg6534
MILLILTIASFALTGTANPTLRARAVTAVYCQFQCFTNEVYEVSRLQESGELIDYIAGCQISNQYCQI
RCADEQEPSCRALGTGNGKVDWRFECVKTAPTQPIVPPAAEPIVPPATQPIVPPASQPIVPPATQPIL
PPATQPEPKPKTKPPTKGCATCTGAPIIKPGNPLCLKNKSKCDPLRAPGCCSGWCSEGKCLPRT*
CE86
>g2970_atg3579
MVLLRTISNMHFLPAILALSLYASEAAAQDQRSTKCYLDRTNGGKTWFPTANCDLLPHNLYLCAHGTT
IVHKETLIEIHSGSAAGTWLVGCNNKPYFLHCPAHEYGAFRILDCKDTVESVDNLQA*
CE87
>g866_atg12630
MKFTLALAIAFFSTVSAGARKACLKPSGPGQAGWCRVYMESIWQQVTAEQYPCLPESPCNVNENGCIL
VKRNGVTYGKCSG*
CE88
>g1114_atg2985
MLGLAFISSLALATVSAQTVSTSYALNISTTPSLWDGQCTYPVADRSFNLTSYLGRWYQVAGTRASFT
SSCSCVYAQYTANANGTVNVFNGCQVGNSSINIEGTATPADPIYGDAGVLRVQFPVSGAPACPGPNYI
VQQATSEWAIVQASNFSTLFLLSRVQTPARADIDFWLNRAGALGSNLANVISTNQTGCLFT*
CE89
>g8315_atg4299
MQFATLLSFSLAAFFFAPTILACYWNSDPSKSQDCCWGGKTARGRPYGYAGCYMQHATTNPCSDPSYQ
DDYCLNHGVHESDCDGDCCQVSTKKKMKCPS*
CE90
>g512_atg2126
MKFTSALAIALLSITTSASFPKAGISLPNPRTACETKKGPNHAGVCKVYEVLDATKETGEQVNCMKEH
PCMVNQNGCVIWVKNGKKVAKCTG*
CE91
>g7268_atg4154
MLKVRWIVSSEIVQSLPSIIRSTTYSTIYLSIPTTMKFIVITALYLASGAASRPGTDPNQDPAYVPAA
GDGSYTVCTPYDMPGICKRYKKDGTATKEVAKCRSARQCWVNGNGCTMVGNGFANCSG*
CE92
>g7836_atg5204
MQLITPILALLVVQIQALPSPATNVPEISGNEALTLPTVSKQLDFESPPANEVPGTSPNEALTLATST
KRLDRRVFGFGGCGSTSAWPTVQAVFFPPRPRRIDINMQQAQHNVEGFRHNWETVTFPIESEVTVPLW
NPATGSFGTIVSVWNRTEQSRRVVVIVEVAPNRGTRGRIVEHRINIEVPGGLSHSIQSCMIKYFGANK
NVKMYMWIEGPGS*
CE93
>g8349_atg1169
MLFQSSMVALFAASTLVAGHGAIVKAVGDQGGVGAAIGVDPDTPRDGTRRNPFQQDSTRFKGDNADTC
GQTLGGGENDIIAGTKAVMAMMGGTLPQISAGGEISMTLHQVNGDGGGPYTCQIDPAGDGSAFVDMKV
TTQVAGTNSRSNAKAVDLPLKAAIPAGQTCSGNVAGMNNICMVRCMNAARAGPFGGCVPVQMANAAVS
NSAAVGNSTAAGNSTAPAKRFAQAVETTEDEEDDE*
CE94
>g4289_atg7104
MKLPTLLILLFPLANHVSASGYYSTSCRKSVPYGNCELWLHNGEGTQELIDSQPCVKKHPCIKESTSQ
CTIRGNGQKAADCQ*

Figure A.7. Legend in page 263.

CE95
>g1587_atg3066
MKLSTTLLLCLTVNSVAAGGTYWQCYKFKGTQGYCRQYEDNHIPVPGSKQECRQASPCTQDNHKCTPN
KFQKAGVGSYANCNDPDP*
CE96
>g7240_atg3209
MNRTTALSSSPLNLKSSISKMQFLSITAVLLNLVLIQDVSAAICTTGRPAQCQEVPCKTLTNEPGFVC
SNECNGANSIVCCSGKIYCWHGHQGFTTRLV*
CE97
>g253_atg8470
MFGFKQLLVLALAGSALACQCRQDGVRAANKRVDVSATEEACTNAHGTLYNAGTVNVECAAVCNRNFF
DECLKLQGQNSDIPDIRSTCRRDNIGCR*
CE98
>g14452_atg5693
MRFQLVLSTLLTTTLATNKCFWDVYGTTQTIEAGDSIKINGVGIACGTTSSPTFGVFAKCKVAYDQKV
GTCDTYAFGKSTDTIKCVYKKSGTPNYGTCKEVST*
CE99
>g9009_atg10983
MVQLLSILSMGLISSATAIALPSAAGDLSACGNTNIIFTGLPPYHPLVISQGFDPKMVDQNLKADAKA
IVAAGYNLKTVFMGPDQDISVFSKFLDGTQWQGAGVGFGIRGSRVPELTVRLEDILKVYKEKAEKAEV
VFNYSPNSTLWALQRRLPLPKECGPGKELGYTEVCTICKQ*
CE100
>g2966_atg4199
MQFSAKAVMLCIAMASQLTSAQFCGTSVGTPVEQGCNHEDCNQTYKDCWKICRQQCSKTYNQQTGYKG
SITCCSGRLYCP*
CE101
>g987_atg221
MYLQTLLPAILFAQSTLAYACCFQIKGTRNGAKKASSILFSGPTESWHPTSNLDCAVYVYKDGTSCGT
WAGRINTGCDVFTPLAYAKSVPASECGY*
CE102
>g11652_atg4506
MKFFIAISAVIAAVSAQGLPPGVAACSLPCWASAAGIKDCAQGGDPKCFCGKPAVQEALKTCVPQKCT
DKADVKGVYDMANKMCAGATGFTPLTPPA*
CE103
>g1325_atg3320
MLFTSALAIALLSITASASPQPQIVGTYNSPPRTACETRMGIDKAGICKIYDANNWTKATREHVNCLV
TSPCMVGENGCRIFINKAGQRVAKCSG*
CE104
>g13264_atg12023
MMWPFIRAFEVWAVARLLSSPTFHRGVGKVAKTVHRIQHGTPMEELGGTKLERKGPSLFQHFKDEIKQ
QLNIKDHNNNKRL*
CE105
>g4795_atg956
MKFSIFAVGASIASLVSAQAGAAEPPKCGTTIMIAAISSSGCGITEVQCMCKNNNLIKTVQAKIPKAC
LLEADRAVFAMFFNSQCIGQAGFPITIGEGEKSASTTGGGNKQSASGKSDARTTRVSVGVLAIAGVIA
VALT*
CE106
>g13458_atg2861
MKLLLIPAFLALFSQLASGCACSGNSEQSRLRTKQACDRCGGHVVQERRQCDRPIHACFNTKCKELGS
QPNYPSSCPS*
CE107
>g9048_KAE9963288_atg12172
MATKFCYAVLLMTAIVSASPVHVIRGVEDVSAGPHGKPSPKEKPASGLFSSLSSLTSGFGAGSAGSAA
DGAVDLTAGMKSGKNTAAPKSTMETKAAGMLEQSITTAGTNIGEALGKSVGISIGRSIGTSIGGTLGT
KLSSMLSGNTKFVLVDGEPMEVERQAGEEESRQSLVYDDHLATSVQDESEASVGYAHRMARSAENEPT
KKDAGY*

Figure A.7. Legend in page 263.

CE108
>g7965_atg7917_RDI89068.1
MKVQTILLFVGTAMAVGPPGFALSHPGFDEKYGSRFGSGSGSQPYCYPYGSPCGAGTSSCCQPYQCRP
FAGRGVSVYRCH*
CE109
>g477_RDI89936.1
MKIQTIFLLIGTAAALVPRMEQSSAVGNAFDIAACSGAGGCCGVTCNRSCCSPYKCKRRLEPGTSNSY
EDACL*
CE110
>g12950_atg3546
MKLLLIPAFLGLFPQLALGCLCINIMGDREYGISSNGCSKCGGSWDTPTKGTCNHPDHECFGKVCREY
GSRPTCK*
CE111
>g1193_atg11536
MKLLSLSVVLFMAATHVVADYSTCIHGPATEGTSGFCVTYNDNGGQKNQQSCRGAKPCNVKGNGCIRD
REFWQGGWYANCS*
CE112
>g2802_ KAE9981362
MKFFALVASTLIAQAIATADPDFAEVQVGGIVKRDSGPSPGGGNLKDSGGSVEFGEVEVGGVVRRDSG
PSPGGGNHHSRSGSRKRRDSGPSPGTPHISNGGDGVDFEEVEVGGVVKRESGPSPGVGNHPYPSYPGG
PKRRDSGPSPGTPHISNGGDSVGFEEVEVGGVVRRASGPSPGGGNRL*
CE113
>g4453_atg6711
MYEFKQLLVLALASTALACQCKKDGATDGILDVQATQFACTRAGGQIRNKGTKSVFCEKGCHDDFYTY
CHHYGGYEWGFPKSGSTCPKDYAWCKTP*
CE114
>g3896_atg3658
MKFTLALALAFLSATVSAISSVHPRMACLPVLWENGYCRVYLTNNPKQVTAQQYLCLKSSPCTTNENG
CTLEVAADGVLYGRCSG*
CE115
>g3666_atg3999
MKFVSALAIALLSVTASAAPQGLPAPPAKGGPKPRTACETYSGPFHAGVCKVYDRTDYTKPTGDQVNC
LITSPCGVNQNGCVIYYKDGKRVAKCTG*
CE116
>g10668_atg4017
MAPSISLFSINAILILSADDGSRLYSKYYQSPHPPLGTPAGSTNYAGASAYPTLSSQKAFETGLREKT
VKTNADVILYDNRVVTFKTEGDVILYVVGSADENEILLFNAILALRDSLTILLKSSVDKRTILENYDL
VTLAIDELCDDGVLLETDPVTVSMRVSRAPAQDMAGAKGIDLSEQGLLNAWEFAKMKGLERLRQGL*
CE117
>g1969_atg10454
MKSSSFLLVVAALVLPELSWGCKDAVGPPLGRCECNYDGQDDKGNTIRCAFHGVTYGKRWLCRCSDCP
LTYGGKGLRDVDTISQPKYNVRHKCRDN*
CE118
>g287_atg4048
MLLQTLLPAILFAQSTLAYSCCFQIRSKVGKKASSILFSEGTNPLWYPDPNIDCAVAVYKDGTSCGTW
KAKVVVGCGVFQPIGFLGSVAASECGY*
CE119
>g3879_ atg3764
MKLLLLPTILALSSQLQSVSACQCQDPTGYIYKDYTRNACGPCGGTYNTPTAEQCNGSRHICFDDTCQ
KVSGSKYIKSSCGRL*
CE120
>g7152_atg4893
MKIQTILLLVGTAIAMAPPYSEAELKAGKFLHKRCQAKGESCGAASTGKSCCAPNTCGLVKAYGMKAE
AYYKCK*

Figure A.7. Legend in page 263.

CE121
>g3941_ RDI79975.1_atg8806
MQFLSITAVVLNLVLLQNVAAQKCNGIFEPSPCQTIPCNTLFNKPLDVCARGCPGTNRATCCSGNIFC
WTQPGVMTRLV*
CE122
>g3837_atg5113
MRLQTLVPAILFAQSTLAIYYCCMQIQAQPPKQWNIASIILASGQPEIWWPRGTIEKCAVAVYKKGNS
CASWESNIFWGCENFLPLSHLKPVVGTECARSSSS*
CE123
>g486_atg12115
MKIPTILLFIGTATALVPRQPETSEVGNNVFAKRACAKWGKTCPPTGLDDCCPDLKCKDELIPGLART
YQSICRIN*
CE124
>g14218_atg9439
MYGLKQLLFLALAGSALACQCTVGGLRSGTLDISATDTACRFSQIGIIQNPGTSNIECKGACHKTFDD
GCVSYSKRDYAVKGLRSTCGTYGGPC*
CE125
>g1770_atg9819
MQFQTLLPAILFAQSTFAYTCCFEIRGTGNYALFHSNMPNGGIQVWRPWGSNECEMMVNKSGATCKDW
KYSIAQNSCNHLKPFKHIGTTGEATCRYTGGGN*
CE126
>g14206_atg9666
MKSTPALAIALLSMTVSASRKACTLPTGSGDSGYCVVYEEKNWWKPTKERYACLEHSPCLVDQNGCFP
VQRSVYTLAKCSG*
CE127
>g10123_RDI80873
MKSTPALAIALLSMTVSASRKACTLPTGSGDSGYCVVYEEKNWWKPTKERYACLEHSPCLVDQNGCFP
VQRSVYTLAKCSG*
CE128
>g13369_atg12287
MKFTTTLTLTLLSLTVSADRTACELPTHPDALGYCILYSESEPNNRKYKYQCLPTSPCLVDQNGCIIV
RRDMKLRANCSG*
CE129
>g14258_atg1497
MKFSAVIALSIAALASAQVPKGSGADAPKIPAGIKCALTCLAPLKESGCKIDGIFPKGAGTGATRIAG
RPPGDLAKPAGQVVDTPQMRKVRRQGDSPAKAPPKISPETIAAAKTARDCFCAAPAMKTVQPCITSGC
ASAPDGGAAAVKGINAACKAVTSFTPLTPAPAAAGGAAPPA*
CE130
>g234_atg5397
MGKPLLCPLLAVILFGQLINASTSDQVVFKGDSTNHMKIRQELLDAEIIPTVIDDFIPAFTLTVSWPN
KTAKLGNTIDPDELQDAPIIKLHGSHHKGLSGLQYTIALTDPDAPSRDNPEWSEMCHWIATNIPVTSS
SFVEGSKSKKLKEIMPYKPPGPPPNTGKHRYVFLAFAPANQTTKKLRLSKPSDRQHWGTGKKRHGVRD
WAAQNGLAPVAANFIYSQNEKQ*
CE131
>g10046_atg6166
MKFTVIAALFLAAGAAGAPPKHKPSPLDGSYTVCTPDDAGGMCQRFFKNGNPTNSFQDCDGPKPCLTI
GNGCTMNYINRGKAACSA*
CE132
>g917_ KAE9967354
MRLQTFLPAIIFAQSSNAVYWCCYKFQATVTFTQYVSSGGVGRWTIGSGCLIRIDKTGPNCGSWKSEL
VGKTCDGLGEVKSYGVVAAGECK*
CE133
>g9080
MRFQLLSMAFLAAVQVASAIKYPPLGHVAGGYQGKKTPVYGYCYAVGKKTIIYTCPNFEDTSCDTSCN
QAQVKAGSRVQCDVLC*

Figure A.7. Amino acid sequence of 133 candidates effectors from *Venturia inaequalis.* All proteins (with exception of the first CE; Cin1) were screened in *Nicotiana* species. Candidates starting with the letter 'g' correspond to *V. inaequalis* isolate EU_B04 (Le Cam et al., 2019). The Joint Genome Institute (JGI) gene atg number and/or the National Center for Biotechnology Information (NCBI) gene ID, appear beside the candidate name. Cysteine residues appear in bold font. Signal peptides are underlined.

Table A.5. Bioinformatic analysis of 133 candidate effectors (CEs) from *Venturia inaequalis*.

CE number	CE name[a]	atg/GenBank no.[b]	Protein length (aa)	No. cysteine residues[c]	SignalP[d]	EffectorP[e]	ApoplastP[f]	TMHMM[g]	TargetP[h]	Big-Pi[i]	NCBI BlastP (e^{-5})[j]
CE1	Cin1	atg5511	463	28	20	Non-effector p=0.5	Non-apoplastic p=0.81	No	S	No	Similar to hypothetical proteins
CE2	Cin3	atg4061	229	0	16	Non-effector p=0.649	Non-apoplastic p=0.96	No	S	No	Similar to hypothetical proteins
CE3	Cin1L1	atg5172	170	4	20	Unlikely effector p=0.527	Non-apoplastic p=0.7	No	S	No	Similar to hypothetical proteins
CE4	Cin1L2	atg6798	107	4	21	Effector p=0.751	Non-apoplastic p=0.78	No	S	No	Cellophane-induced protein 1-like 2 (*Venturia pyrina*)
CE5	16969	atg3864	123	10	19	Effector p=0.897	Apoplastic p=0.76	No	S	No	Similar to hypothetical proteins
CE6	15505	atg1429	137	6	19	Effector p=0.887	Non-apoplastic p=0.53	No	S	No	Similar to hypothetical proteins
CE7	18699	atg4475	85	6	19	Effector p=0.927	Apoplastic p=0.75	No	S	No	Similar to hypothetical proteins
CE8	24527	atg9241	104	6	18	Effector p=0.965	Apoplastic p=0.93	No	S	No	Similar to hypothetical proteins
CE9	13533	atg11760	101	6	17	Effector p=0.894	Apoplastic p=0.68	No	S	No	Similar to hypothetical proteins
CE10	ViHyd1	atg24541	95	8	17	Effector p=0.691	Apoplastic p=0.82	No	S	No	Similar to hydrophobin-like proteins

Table A.5. Continued.

CE number	CE name[a]	atg/GenBank no.[b]	Protein length (aa)	No. cysteine residues[c]	SignalP[d]	EffectorP[e]	ApoplastP[f]	TMHMM[g]	TargetP[h]	Big-Pi[i]	NCBI BlastP (e^{-5})[j]
CE11	ViEcp6	atg11994	216	6	20	Non-Effector p=0.684	Apoplastic p=0.83	No	S	No	Similar to putative peptidoglycan-binding lysin proteins
CE12	ViPNPL5	QDH43451	131	4	19	Unlikely effector p=0.504	Apoplastic p=0.61	No	S	No	Similar to hypothetiA1:L13cal proteins. Similar to plant natriuretic peptide like proteins
CE13	ViPNPL9	QDH43453	128	4	21	Effector p=0.863	Apoplastic p=0.75	No	S	No	Similar to hypothetical proteins. Similar to plant natriuretic peptide like proteins
CE14	11273	atg11273	73	8	16	Effector p=0.87	Apoplastic p=0.82	No	S	No	Similar to hypothetical proteins
CE15	13636	atg12276	150	4	20	Effector p=0.952	Apoplastic p=0.77	No	S	No	Similar to hypothetical proteins
CE16	14801	atg3212	155	8	30	Non-effector 0.806	Apoplastic p=0.88	No	S	No	Similar to hypothetical proteins
CE17	15961	atg2494	165	5	20	Non-effector p=0.5	Apoplastic p=0.73	No	S	No	Allergen Ste b 1 (Cercospora beticola). Alt a 1 (Alternaria alternata)
CE18	16394	atg2434	198	20	16	Effector p=0.836	Apoplastic p=0.69	No	S	No	Similar to hypothetical proteins
CE19	682.7	atg4496	143	12	21	Effector p=0.815	Apoplastic p=0.78	No	S	No	Similar to hypothetical proteins

Table A.5. Continued.

CE number	CE name[a]	atg/GenBank no.[b]	Protein length (aa)	No. cysteine residues[c]	SignalP[d]	EffectorP[e]	ApoplastP[f]	TMHMM[g]	TargetP[h]	Big-Pi[i]	NCBI BlastP (e^{-5})[j]
CE20	21582	atg6993	91	1	22	Non-effector p=0.525	Non-apoplastic p=0.51	No	S	No	Enolase (*V. inaequalis*)
CE21	25058	atg13108	150	4	19	Non-effector p=0.826	Apoplastic p=0.66	No	S	No	Similar to hypothetical proteins
CE22	17864	atg5488	259	12	20	Effector p=0.668	Apoplastic p=0.85	No	S	No	Similar to hypothetical proteins
CE23	g9438	atg1395	153	2	18	Non-effector p=0601	Non-apoplastic p=0.64	No	S	No	Similar to hypothetical proteins
CE24	g4401	atg5327	88	8	18	Effector p=1	Apoplastic p=0.83	No	S	No	Similar to hypothetical proteins
CE25	g9336	atg5420	233	4	18	Non-effector p=0.805	Non-apoplastic p=0.73	No	S	No	Similar to hypothetical proteins
CE26	g3042	KAE9962589.1	251	6	20	Non-effector p=0.954	Apoplastic p=0.78	No	S	No	LysM domain/ putative peptidoglycan-binding lysin subgroup protein
CE27	g13163	atg5361	170	0	17	Effector p=0.994	Apoplastic p=0.69	No	S	No	Fasciclin domain (4 repeated domains)
CE28	g1277	atg5929	94	6	19	Effector p=0.79	Apoplastic p=0.87	No	S	No	Similar to hypothetical proteins
CE29	g12222	atg12663	112	14	17	Effector p=0.952	Apoplastic p=0.61	No	S	No	Similar to hypothetical proteins

Table A.5. Continued.

CE number	CE name[a]	atg/GenBank no.[b]	Protein length (aa)	No. cysteine residues[c]	SignalP[d]	EffectorP[e]	ApoplastP[f]	TMHMM[g]	TargetP[h]	Big-Pi[i]	NCBI BlastP (e^{-5})[j]
CE30	g14234	atg6441/RDI86726.1	211	4	15	Effector p=0.653	Apoplastic p=0.89	No	S	No	Candidate effector 16 [*Venturia inaequalis*]
CE31	g9700	atg2705	93	8	18	Effector p=0.992	Apoplastic p=0.53	No	S	No	Similar to hypothetical proteins
CE32	g8959	N/A	69	6	18	Effector p=0.889	Apoplastic p=0.89	No	S	No	Leucine carboxyl methyltransferase 1 [*Venturia inaequalis*]
CE33	g9061	atg4321	79	8	19	Effector p=0.938	Apoplastic p=0.66	No	S	No	Similar to hypothetical proteins
CE34	g7375	atg10823	73	6	17	Effector p=875	Non-apoplastic p=0.63	No	S	No	Similar to hypothetical proteins
CE35	g11637	atg644	91	8	22	Effector p=0.951	Apoplastic p=0.61	No	S	No	Similar to hypothetical proteins
CE36	g14256	atg8668	240	2	17	Unlikely effector p=0.525	Non-poplastic p=0.93	No	S	No	Similar to hypothetical proteins
CE37	g3687	atg11932	81	6	18	Effector p=0.978	Apoplastic p=0.86	No	S	No	Similar to hypothetical proteins
CE38	g10504	atg4427	78	8	15	Effector p=0.969	Non-poplastic p=0.57	No	S	No	Similar to hypothetical proteins
CE39	g13513	N/A	83	6	18	Effector p=0.985	Apoplastic p=0.76	No	S	No	Similar to hypothetical proteins

Table A.5. Continued.

CE number	CE name[a]	atg/GenBank no.[b]	Protein length (aa)	No. cysteine residues[c]	SignalP[d]	EffectorP[e]	ApoplastP[f]	TMHMM[g]	TargetP[h]	Big-Pi[i]	NCBI BlastP (e^{-5})[j]
CE40	g13878	atg2807	216	5	16	Non-effector p=0.666	Apoplastic p=0.72	No	S	No	Lysophospholipase 1 [*Venturia inaequalis*]
CE41	g1250	atg8558	87	8	21	Effector p=0.768	Apoplastic p=0.87	No	S	No	Similar to hypothetical proteins
CE42	g12572	N/A	75	8	19	Effector p=0.897	Apoplastic p=0.77	No	S	No	Similar to hypothetical proteins
CE43	g13647	atg11273	72	8	16	Effector p=0.947	Apoplastic p=0.83	No	S	No	Similar to hypothetical proteins
CE44	g3498	atg7515	86	6	20	Effector p=0.96	Apoplastic p=0.9	No	S	No	Similar to hypothetical proteins
CE45	g4360	atg1069	108	8	17	Effector p=0.914	Apoplastic p=0.63	No	S	No	Similar to hypothetical proteins
CE46	g11778	atg6591	97	6	20	Effector p=0.828	Non-apoplastic p=0.7	No	S	No	Similar to hypothetical proteins
CE47	g2403	atg829	245	6	19	Non-effector p=0.655	Apoplastic p=0.83	No	S	No	Similar to hypothetical proteins
CE48	g10970	atg6878	158	10	21	Effector p=0.901	Apoplastic p=0.7	No	S	No	Similar to hypothetical proteins
CE49	g3143	atg11319	92	6	18	Effector p=0.926	Apoplastic p=0.76	No	S	No	Similar to hypothetical proteins
CE50	g14092	N/A	82	6	17	Effector p=0.951	Apoplastic p=0.88	No	S	No	Similar to hypothetical proteins

Table A.5. Continued.

CE number	CE name[a]	atg/GenBank no.[b]	Protein length (aa)	No. cysteine residues[c]	SignalP[d]	EffectorP[e]	ApoplastP[f]	TMHMM[g]	TargetP[h]	Big-Pi[i]	NCBI BlastP (e^{-5})[j]
CE51	g9851	atg6627	79	8	19	Effector p=902	Apoplastic p=0.89	No	S	No	Similar to hypothetical proteins
CE52	g1678	RDI86109	121	8	23	Effector p=0.949	Non-apoplastic p=0.5	No	S	No	Similar to hypothetical proteins
CE53	g3841	N/A	90	6	18	Effector p=0.957	Apoplastic p=0.66	No	S	No	Similar to hypothetical proteins
CE54	g3533	atg8817	85	6	18	Effector p=0.902	Apoplastic p=0.57	No	S	No	Similar to hypothetical proteins
CE55	g912	atg4567	261	10	18	Effector p=0.703	Apoplastic p=0.6	No	S	No	Cutinase (uperfamily containing proteases, lipases, peroxidases, esterases, epoxide hydrolases and dehalogenases) / alpha-beta hydrolase family
CE56	g12877	N/A	99	8	20	Effector p=0.926	Apoplastic p=0.95	No	S	No	Similar to hypothetical proteins
CE57	g9007	RDI77214.1	217	4	16	Effector p=0.707	Apoplastic p=0.69	No	S	No	cutinase
CE58	g9793	atg1373	81	8	19	Effector p=0.919	Apoplastic p=0.75	No	S	No	Similar to hypothetical proteins
CE59	g7408	N/A	85	6	18	Effector p=0.937	Apoplastic p=0.59	No	S	No	Similar to hypothetical proteins

Table A.5. Continued.

CE number	CE name[a]	atg/GenBank no.[b]	Protein length (aa)	No. cysteine residues[c]	SignalP[d]	EffectorP[e]	ApoplastP[f]	TMHMM[g]	TargetP[h]	Big-Pi[i]	NCBI BlastP (e^{-5})[j]
CE60	g12428	atg12924	150	0	15	Non-effector p=0.691	Non-apoplastic p=0.53	No	S	No	Similar to hypothetical proteins
CE61	g8715	KAE9963057.1	175	4	20	Non-effector p=0.525	Non-apoplastic p=0.73	No	S	No	Similar to hypothetical proteins
CE62	g4805	KAE9981396.1	241	4	17	Effector p=0.768	Non-apoplastic p=0.55	No	S	No	Similar to hypothetical proteins
CE63	g12872	N/A	83	8	19	Effector p=0.965	Non-apoplastic p=0.53	No	S	No	Similar to hypothetical proteins
CE64	g9279	ACM90099.1	297	4	17	Non-effector p=0.988	Non-apoplastic p=0.82	No	S	No	Candidate effector 10 [*Venturia inaequalis*]
CE65	g10511	N/A	199	7	18	Effector p=0.555	Non-poplastic p=0.77	No	S	No	Similar to hypothetical proteins
CE66	g1500	atg2922	78	8	19	Effector p=0.959	Apoplastic p=0.81	No	S	No	Similar to hypothetical proteins
CE67	g121	N/A	94	8	18	Effector p=0.905	Apoplastic p=0.76	No	S	No	Similar to hypothetical proteins
CE68	g11287	N/A	93	6	20	Effector p=0.737	Apoplastic p=0.57	No	S	No	Similar to hypothetical proteins
CE69	g10061	atg11917	81	6	20	Unlikely effector p=0.507	Apoplastic p=0.69	No	S	No	Similar to hypothetical proteins

Table A.5. Continued.

CE number	CE name[a]	atg/GenBank no.[b]	Protein length (aa)	No. cysteine residues[c]	SignalP[d]	EffectorP[e]	ApoplastP[f]	TMHMM[g]	TargetP[h]	Big-Pi[i]	NCBI BlastP (e^{-5})[j]
CE70	g13842	atg2850	81	6	18	Effector p=0.98	Apoplastic p=0.59	No	S	No	Similar to hypothetical proteins
CE71	g13809	atg10584	99	6	19	Effector p=0.861	Apoplastic p=0.8	No	S	No	Similar to hypothetical proteins
CE72	g12228	atg12941	85	8	21	Effector p=0.958	Apoplastic p=0.64	No	S	No	Similar to hypothetical proteins
CE73	g3582	atg5886	108	8	19	Effector p=0.855	Apoplastic p=0.79	No	S	No	8-cysteine region, CFEM domain
CE74	g865	atg12640	82	6	18	Effector p=0.917	Apoplastic p=0.77	No	S	No	Similar to hypothetical proteins
CE75	g10970	atg3532	283	10	19	Non-effector p=0.591	Apoplastic p=0.61	No	S	No	alpha/beta hydrolase family
CE76	g8761	atg1995	93	8	18	Effector p=0.914	Apoplastic p=0.61	No	S	No	Similar to hypothetical proteins
CE77	g8276	atg437	81	0	16	Non-effector p=0.668	Apoplastic p=0.7	No	S	No	Similar to hypothetical proteins
CE78	g3875	KAE9980336.1	133	0	17	Non-effector p=0.83	Apoplastic p=0.85	No	S	No	Similar to hypothetical proteins
CE79	g13066	atg2104	292	4	18	Non-effector p=0.809	Apoplastic p=0.61	No	S	No	Similar to hypothetical proteins
CE80	g4565	atg9444	103	8	22	Effector p=0.983	Apoplastic p=0.67	No	S	No	Similar to hypothetical proteins

Table A.5. Continued.

CE number	CE name[a]	atg/GenBank no.[b]	Protein length (aa)	No. cysteine residues[c]	SignalP[d]	EffectorP[e]	ApoplastP[f]	TMHMM[g]	TargetP[h]	Big-Pi[i]	NCBI BlastP (e^{-5})[j]
CE81	g4116	atg9255	198	10	19	Effector p=0.898	Apoplastic p=0.7	No	Other	No	Similar to hypothetical proteins
CE82	g4568	atg2596	109	8	19	Effector p=0.909	Apoplastic p=0.64	No	S	No	Similar to hypothetical proteins
CE83	g11651	atg4507	98	8	16	Non-Effector p=0.507	Apoplastic p=0.83	No	S	No	Similar to hypothetical proteins
CE84	g13068	atg2102	190	0	16	Effector p=0.606	Apoplastic p=0.71	No	S	No	Similar to hypothetical proteins
CE85	g10873	atg6534	201	15	17	Effector p=0.773	Apoplastic p=0.72	No	S	No	Similar to hypothetical proteins
CE86	g2970	atg3579	126	6	28	Effector p=0.825	Apoplastic p=0.65	No	S	No	Similar to hypothetical proteins
CE87	g866	atg12630	82	6	19	Effector p=0.899	Apoplastic p=0.63	No	S	No	Similar to hypothetical proteins
CE88	g1114	atg2985	198	5	17	Non-Effector p=0.688	Apoplastic p=0.83	No	S	No	Similar to hypothetical proteins
CE89	g8315	atg4299	100	10	22	Effector p=0.945	Apoplastic p=0.81	Yes	S	No	Similar to hypothetical proteins
CE90	g512	atg2126	93	6	18	Effector p=0.948	Apoplastic p=0.79	No	S	No	Similar to hypothetical proteins
CE91	g7268	atg4154	127	6	15	Effector p=0.878	Apoplastic p=0.75	No	S	No	Similar to hypothetical proteins

Table A.5. Continued.

CE number	CE name[a]	atg/GenBank no.[b]	Protein length (aa)	No. cysteine residues[c]	SignalP[d]	EffectorP[e]	ApoplastP[f]	TMHMM[g]	TargetP[h]	Big-Pi[i]	NCBI BlastP (e^{-5})[j]
CE92	g7836	atg5204	218	2	17	Effector p=0.581	Non-apoplastic p=0.68	No	S	No	Similar to hypothetical proteins
CE93	g8349	atg1169	240	6	19	Non-Effector p=0.775	Apoplastic p=0.81	No	S	No	Similar to hypothetical proteins
CE94	g4289	atg7104	83	6	19	Effector p=0.978	Apoplastic p=0.67	No	S	No	Similar to hypothetical proteins
CE95	g1587	atg3066	87	6	18	Effector p=0.946	Apoplastic p=0.79	No	S	No	Similar to hypothetical proteins
CE96	g7240	atg3209	100	8	41	Effector p=0.781	Apoplastic p=0.8	No	S	No	Similar to hypothetical proteins
CE97	g253	atg8470	97	8	18	Effector p=0.959	Apoplastic p=0.56	No	S	No	Similar to hypothetical proteins
CE98	g14452	atg5693	104	6	16	Effector p=0.785	Apoplastic p=0.96	No	S	No	Similar to hypothetical proteins
CE99	g9009	atg10983	177	4	18	Effector p=0.766	Non-apoplastic p=0.7	No	S	No	Similar to hypothetical proteins
CE100	g2966	atg4199	81	9	21	Effector p=0.929	Apoplastic p=0.76	No	S	No	Similar to hypothetical proteins
CE101	g987	atg221	97	6	20	Effector p=0.869	Apoplastic p=0.8	No	S	No	Similar to hypothetical proteins
CE102	g11652	atg4506	98	8	16	Effector p=0.82	Apoplastic p=0.84	No	S	No	Similar to hypothetical proteins

Table A.5. Continued.

CE number	CE name[a]	atg/GenBank no.[b]	Protein length (aa)	No. cysteine residues[c]	SignalP[d]	EffectorP[e]	ApoplastP[f]	TMHMM[g]	TargetP[h]	Big-Pi[i]	NCBI BlastP (e^{-5})[j]
CE103	**g1325**	atg3320	96	6	18	Effector p=0.947	Apoplastic p=0.82	No	S	No	Similar to hypothetical proteins
CE104	**g13264**	atg12023	82	0	19	Non-Effector p=0.602	Non-apoplastic p=0.74	No	M	No	Similar to hypothetical proteins
CE105	**g4795**	atg956	141	6	18	Non-Effector p=0.555	Apoplastic p=0.8	No	S	Yes	Similar to hypothetical proteins
CE106	**g13458**	atg2861	79	8	19	Effector p=0.964	Non-apoplastic p=0.54	No	S	No	Similar to hypothetical proteins
CE107	**g9048**	KAE9963288.1	211	0	18	Non-Effector p=0.861	Non-apoplastic p=0.51	No	S	No	Similar to hypothetical proteins
CE108	**g7965**	atg7917	81	8	15	Effector p=0.731	Apoplastic p=0.75	No	S	No	Similar to hypothetical proteins
CE109	**g477**	RDI89936.1	74	8	15	Effector p=0.95	Apoplastic p=0.75	No	S	No	Guanine nucleotide-binding protein subunit beta-like protein
CE110	**g12950**	atg3546	76	8	19	Effector p=0.965	Apoplastic p=0.72	Yes	S	No	Similar to hypothetical proteins
CE111	**g1193**	atg11536	82	6	19	Effector p=0.959	Apoplastic p=0.85	No	S	No	D-lactate dehydrogenase [cytochrome] [*Venturia inaequalis*]
CE112	**g2802**	KAE9981362.1	184	0	19	Non-Effector p=0.667	Non-apoplastic p=0.69	No	S	No	Similar to hypothetical proteins

Table A.5. Continued.

CE number	CE name[a]	atg/GenBank no.[b]	Protein length (aa)	No. cysteine residues[c]	SignalP[d]	EffectorP[e]	ApoplastP[f]	TMHMM[g]	TargetP[h]	Big-Pi[i]	NCBI BlastP (e^{-5})[j]
CE113	g4453	atg6711	97	8	18	Effector p=0.972	Apoplastic p=0.81	No	S	No	Similar to hypothetical proteins
CE114	g3896	atg3658	86	6	18	Effector p=0.77	Apoplastic p=0.76	No	S	No	Similar to hypothetical proteins
CE115	g3666	atg3999	97	6	18	Effector p=0.898	Apoplastic p=0.92	No	S	No	Similar to hypothetical proteins
CE116	g10668	atg4017	207	1	18	Non-Effector p=0.519	Non-apoplastic p=0.92	No	Other	No	Similar to hypothetical proteins
CE117	g1969	atg10454	97	8	21	Effector p=0.908	Apoplastic p=0.56	No	S	No	Similar to hypothetical proteins
CE118	g287	atg4048	96	6	18	Effector p=0.759	Apoplastic p=0.67	No	S	No	Similar to hypothetical proteins
CE119	g3879	atg3764	84	8	21	Effector p=0.951	Apoplastic p=0.79	No	S	No	Similar to hypothetical proteins
CE120	g7152	atg4893	75	6	23	Effector p=0.888	Apoplastic p=0.56	No	S	No	Similar to hypothetical proteins
CE121	g3941	RDI79975.1	80	8	21	Effector p=0.733	Apoplastic p=0.78	No	S	No	Similar to hypothetical proteins
CE122	g3837	atg5113	104	6	18	Unlikely Effector p=0.507	Non-apoplastic p=0.62	No	S	No	Similar to hypothetical proteins
CE123	g486	atg12115	77	6	15	Effector p=0.96	Apoplastic p=0.68	No	S	No	Similar to hypothetical proteins

Table A.5. Continued.

CE number	CE name[a]	atg/GenBank no.[b]	Protein length (aa)	No. cysteine residues[c]	SignalP[d]	EffectorP[e]	ApoplastP[f]	TMHMM[g]	TargetP[h]	Big-Pi[i]	NCBI BlastP (e^{-5})[j]
CE124	g14218	atg9439	95	8	18	Effector p=0.931	Apoplastic p=0.88	No	S	No	Similar to hypothetical proteins
CE125	g1770	atg9819	102	6	18	Effector p=0.962	Apoplastic p=0.76	No	S	No	Similar to hypothetical proteins
CE126	g14206	atg9666	241	6	24	Non-Effector p=0.936	Apoplastic p=0.82	No	S	No	Similar to hypothetical proteins
CE127	g10123	RDI80873.1	82	6	18	Effector p=0.88	Apoplastic p=0.65	No	S	No	Similar to hypothetical proteins
CE128	g13369	atg12287	81	6	18	Effector p=0.842	Apoplastic p=0.67	No	S	No	Similar to hypothetical proteins
CE129	g14258	atg1497	178	8	17	Non-Effector p=0.841	Apoplastic p=0.77	No	S	No	Similar to hypothetical proteins
CE130	g234	atg5397	227	1	21	Effector p=0.739	Apoplastic p=0.56	No	S	No	Similar to hypothetical proteins
CE131	g10046	atg6166	87	6	17	Effector p=0.914	Apoplastic p=0.81	No	S	No	Similar to hypothetical proteins
CE132	g917	KAE9967354.1	91	6	18	Effector p=0.922	Apoplastic p=0.83	No	S	No	Similar to hypothetical proteins
CE133	g9080	N/A	85	6	19	Effector p=0.927	Apoplastic p=0.76	No	S	No	Similar to hypothetical proteins.

Details of superscript letters from Table A.5.

[a]Candidate effector names starting with 'g' correspond to *V. inaequalis* isolate EU-B04.

[b]The Joint Genome Institute (JGI) gene atg number or the National Center for Biotechnology Information (NCBI) gene ID numbers appear in the column after the CE name. N/A = not available.

[c]Number of cysteine residues in the mature protein (i.e. after signal peptide cleavage)

[d]The length of the signal peptide using the SignalP server

[e]Prediction of effector proteins was performed with EffectorP server

[f]Localization to the plant apoplast was predicted with ApoplastP server

[g]Presence of transmembrane helices were predicted with the TMHMM server

[h]The TargetP server predicted the localization of all CEs in the secretory pathway (S)

[i]The presence of a putative C-terminal GPI (glycosylphosphatidylinositol) lipid modification (anchor) sites was analysed using the Big-Pi server

[j]BlastP analysis at cut off E-value of $1e^{-5}$

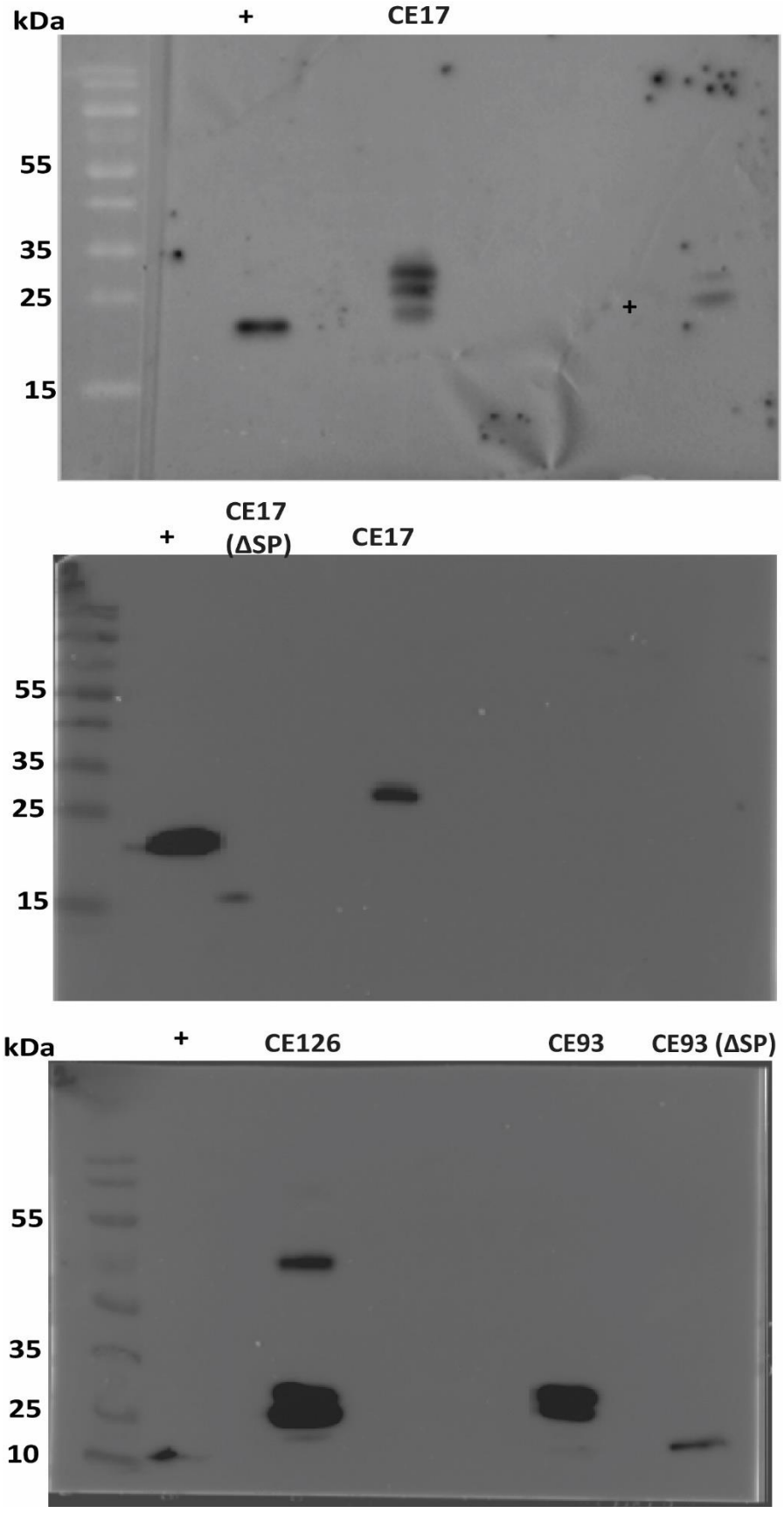

Figure A.8. Legend in the next page.

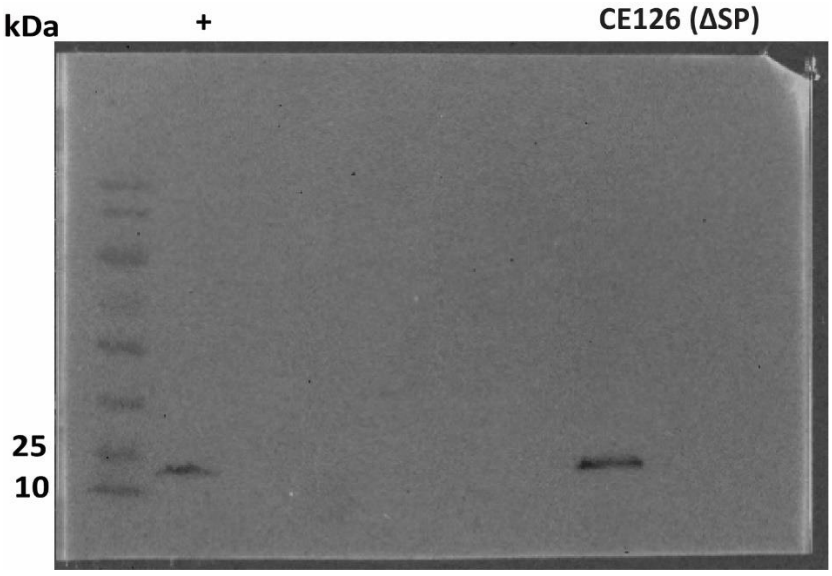

Figure A.8. Full pictures of Western blots in chapter 3. Protein detection of candidate effectors (CEs) triggering a response in *Nicotiana benthamiana* and/or *Nicotiana tabacum* by Western blotting. Protein samples were collected from leaf samples and the 3xFLAG tag was used for detection. Positive controls are a *Dothistroma septosporum* CE MW=10 kDa (Tarallo, unpublished), and a *Phytophthora agathidicida* RxLR effector MW=24 kDa (Guo et al., 2020).

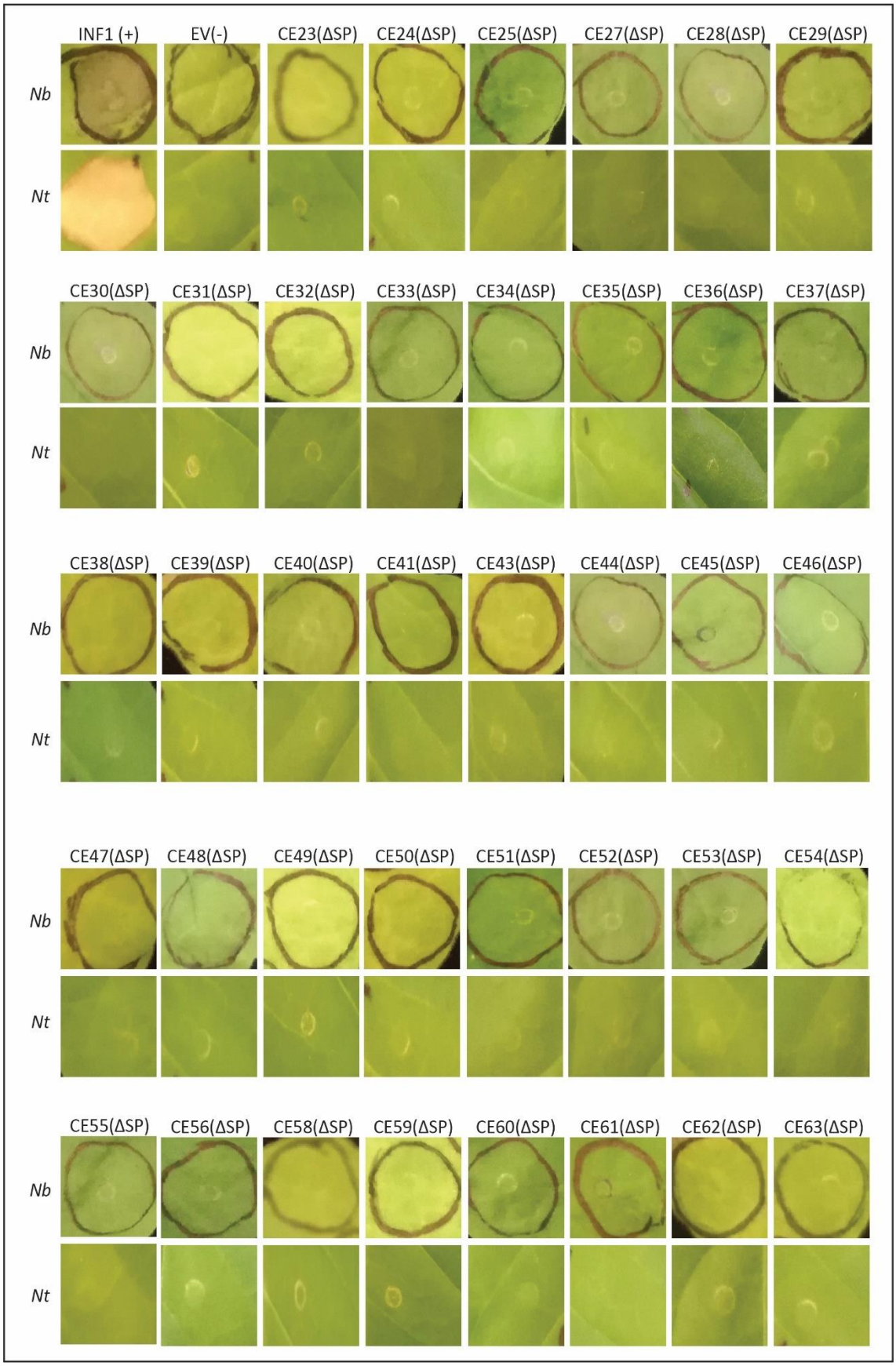

Figure A.9. Legend in the next page.

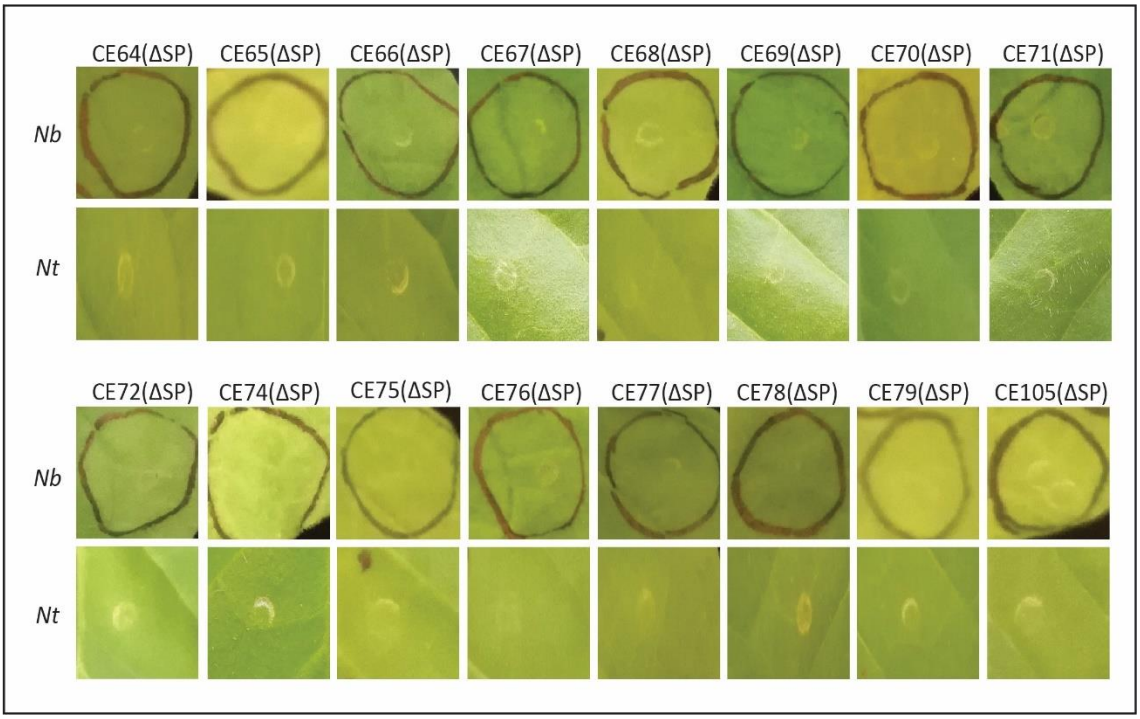

Figure A.9. Candidate effectors (CEs) of *Venturia inaequalis* do not trigger chlorosis and/or cell death when expressed in the cytoplasm of model non-host species *Nicotiana benthamiana* (*Nb*) and *Nicotiana tabacum* (*Nt*) using an *Agrobacterium tumefaciens*-mediated transient expression assay (ATTA). The INF1 elicitin protein from *Phytophthora infestans* was used as positive control and empty vector pICH86988 (EV) as negative control. CEs were expressed without a PR1α signal peptide (ΔSP) to ensure targeting to the plant cytoplasm. Photos were taken at 7 days post-inoculation (dpi). Photos are representative of at least three independent ATTA experiments.

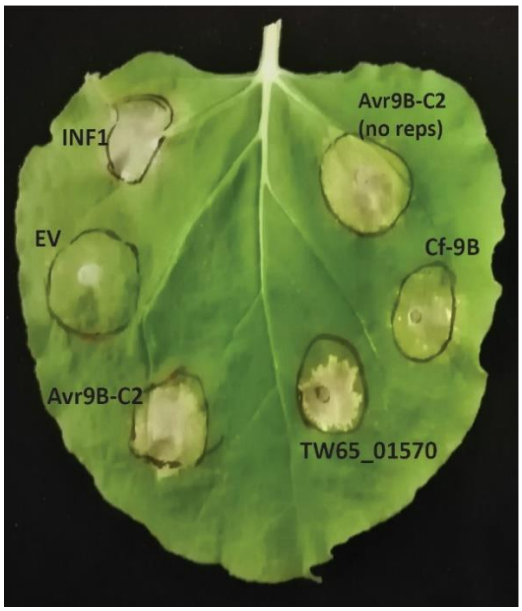

Figure A.10. Expression of Cf-9B triggers cell death and/or chlorosis in *Nicotiana benthamiana.* *Agrobacterium tumefaciens* transient transformation assays (ATTAs) were performed to express different proteins. The INF1 elicitin protein from *Phytophthora infestans* was used as a positive control and empty vector pICH86988 (EV) as a negative control. Full length and version without the repetitive region of Avr9B-C2 from *Cladosporium fulvum* caused cell death, as well as TW65_01570 from *Stemphilium lycopersici*. Photo taken 5 days post infiltration.

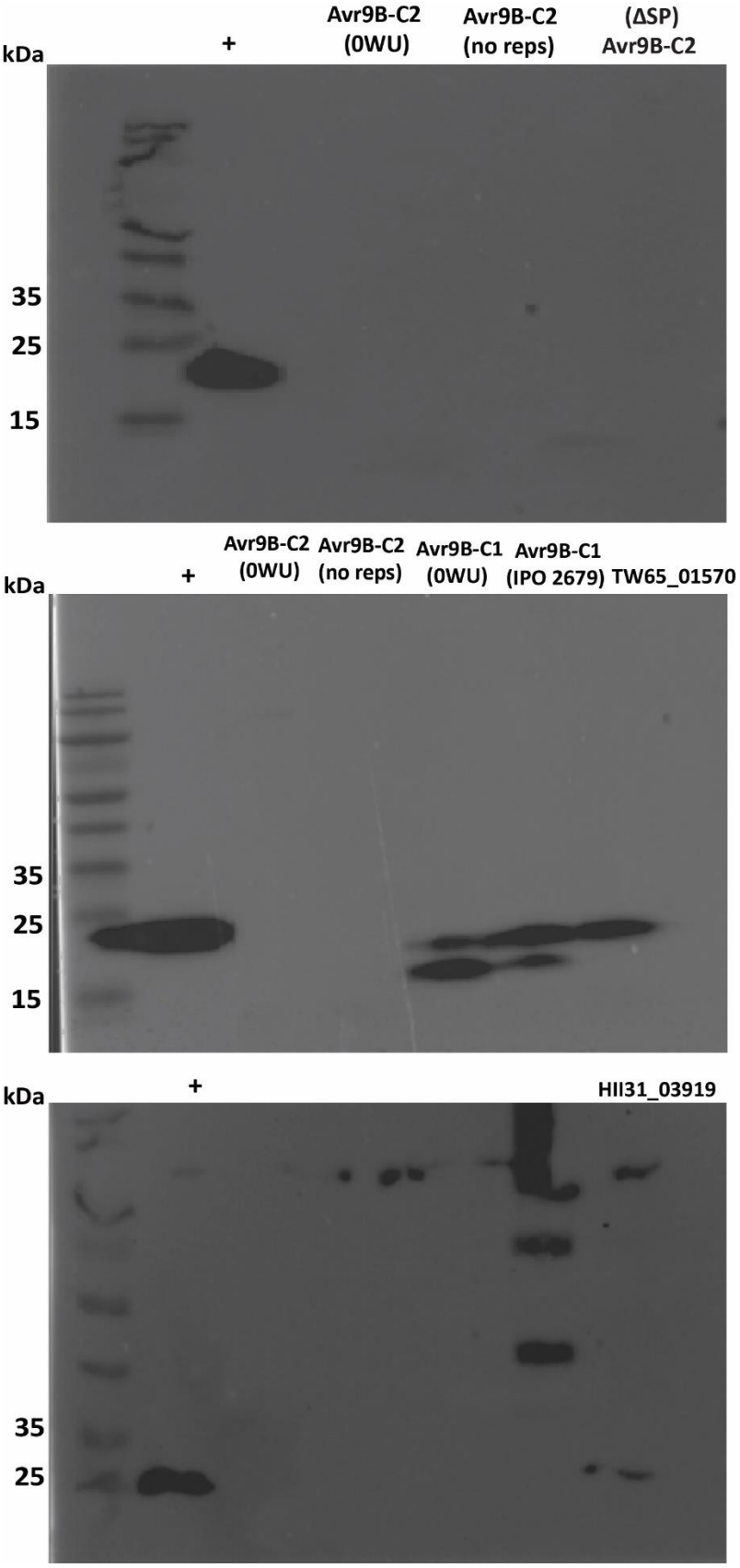

Figure A.11. Legend in the next page.

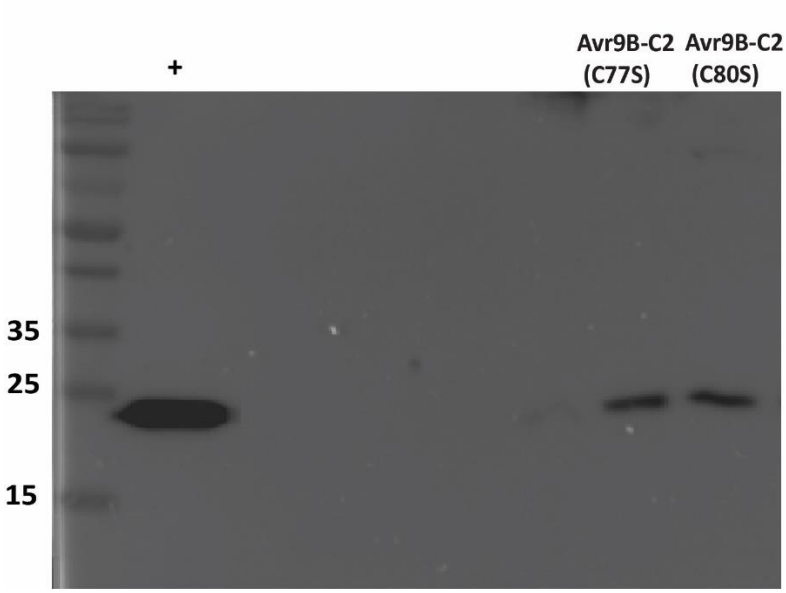

Figure A.11. Full pictures of Western blots in chapter 4. Protein detection by Western blotting. Protein samples were collected from leaf samples and the 3xFLAG tag was used for detection. Positive control is a Dothistroma septosporum candidate effector (MW=25 kDa) (Tarallo, unpublished).

Figure A.12. Example of *Agrobacterium tumefaciens*-mediated transient expression assays (ATTAs) in tomato. ATTAs performed in tomato using the wild *A. tumefaciens* 1D1249 strain, triggered necrosis in the majority of leaf samples regardless the construct carried by each strain.

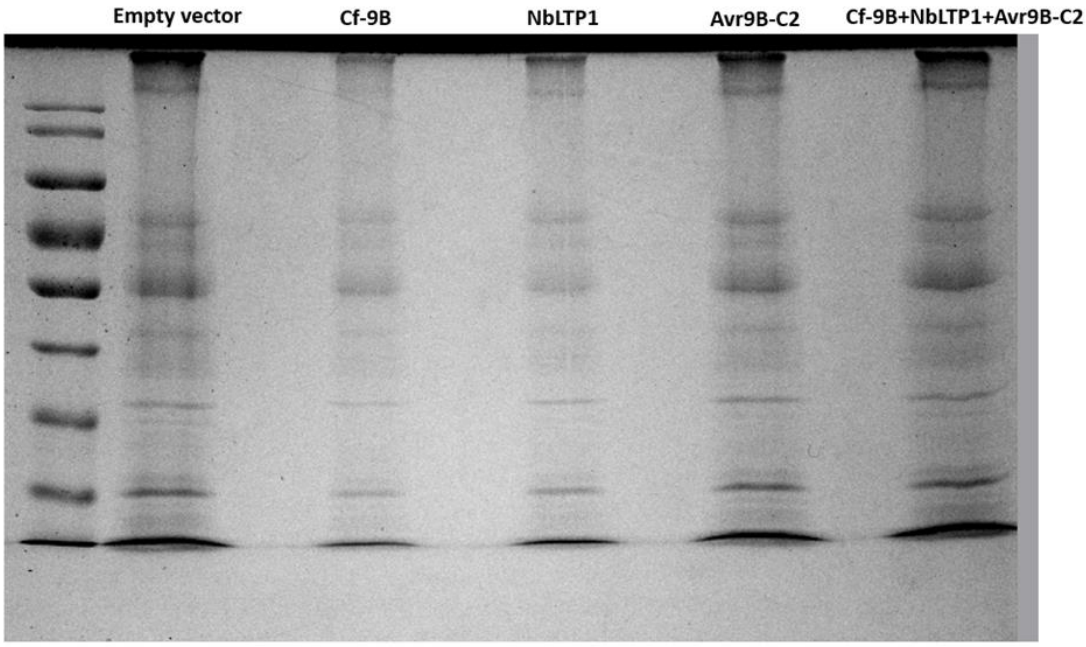

Figure A.13. Analysis of apoplastic fluid isolated by sodium dodecyl sulfate-polyacrylamide gel electrophoresis (SDS-PAGE). Apoplastic fluid was isolated from tomato 'Money Maker' leaflets 2 days post infiltration with *Agrobacterium tumefaciens* 1D1249 strains carrying the empty vector (pICH86988), *Cf-9B*, a *Nicotiana benthamiana* lipid transfer protein (*NbLTP1*) (Chakrabarti et al., unpublished) and *Avr9B-C2*. Accumulation of pathogenesis-related proteins (e.g. P69, chitinases and β-1,3-glucanases), or significant differences among samples were not observed.

MASSEY UNIVERSITY
TE KUNENGA KI PŪREHUROA
UNIVERSITY OF NEW ZEALAND

GRADUATE RESEARCH SCHOOL

Note for Examiners
Explanation of COVID-19 Impacts

Thank you for taking the time to examine this thesis, which has been undertaken during the Covid-19 pandemic. The New Zealand Government's response to Covid-19 includes a system of Alert Levels which have impacted upon researchers. Our University's pandemic plan applied the Government's expectations to our research environment to ensure the health and safety of our researchers, however, research was impacted by restrictions and disruptions, as outlined below.

For a six-week period from March 26 to April 27 2020, New Zealand was placed under very strict lockdown conditions (Level 4 – Lockdown), with students and staff unable to physically access University facilities, unless they were involved in essential research related to Covid-19. All field work ceased and data collection with humans was restricted to online methods, if appropriate. The restrictions were partially lifted on April 27, but students and staff were not generally allowed back into University facilities until May 13.

Ongoing disruptions have also been encountered for some students due to uncertainties over the potential for future Covid-19-related restrictions on activities, and a Covid-19 cluster outbreak based in Auckland in New Zealand on 12 August 2020 led to the imposition of rolling Level 2 (Reduce) and Level 3 (Restrict) conditions until 23 September 2020. Auckland campus based students remained on Level 2 until 7 October 2020.

This Alert Level system continues to be utilised throughout 2021, and in particular from 17 August 2021 when the whole of New Zealand again moved to Level 4 lockdown for an extended period. The Auckland region remained in alert level 3 or 4 for a number of months. Please see the NZ Government website for more information on lockdown dates.

These changing Alert Levels have meant that some research students had experimental, clinical, laboratory, field work, and/or data collection or analysis interrupted, and consequently may have had to adjust their research plans. For some students, the impacts of Covid-19 have been substantial as they may have had to significantly revise their research plans.

Overseas travel is not permitted by the University and restrictions have been placed on the New Zealand borders which are closed to non-New Zealand citizens and permanent residents. This meant that international students who were based offshore at the time of lockdown, were unable to return to New Zealand. A small number of offshore students were provided permission to return to New Zealand in early 2021. Many students have also suffered from anxiety and stress-related issues, and have had financial impacts, meaning their research progress has been significantly delayed.

This form, as completed by the supervisor and student, outlines the extent that the research has been affected by Covid-19 conditions.

Approved by DRC 10/Feb/2021
DRC 21/02/03
Updated September 2021

Please consider the factors listed below in your assessment of the work.

This statement has been prepared by the candidate's supervisor in consultation with the student and has been endorsed by the relevant Head of Academic Unit.

Student Name:	Silvia de la Rosa	ID Number:	[redacted]
Supervisor Name:	Carl H. Mesarich	Date:	31-Jan-22
Thesis title:	Identification of novel avirulence effectors in the Dothideomycete plant pathogens, Venturia inaequalis and Cladosporium fulvum		

Considerations to be taken into account. Note: This statement will remain in the final copy of the thesis which will be available from the Massey University Library following the examination process.
[*Enter key considerations here for the examiners. This can include but is not limited to change of scope, scale, topic, focus; limitations in relation to data collection, access to necessary literature or archival materials, laboratories, field sites; disruptions as a result of lockdown and various alert levels, medical or health considerations etc*]

Chapter 2: A bioinformatics collaborator on the project from Massey University was assigned the task of assembling the Venturia inaequalis genomes and identifying single nucleotide variants (SNVs) that co-segregated with an inability of this fungus to trigger disease resistance in apple plants carrying the Rvi4 resistance gene. Around mid-2021, the bioinformatician took up a position at the Institute of Environmental Science and Research (ESR), where they were responsible for the sequencing and analysis of Covid-19 genomes from people infected with the virus. As the number of infected people increased, coincident with the arrival of delta and omicron variants at the border and in the community, the bioinformatician struggled to get the V. inaequalis data to the student quickly, and thus the student was unable to identify the corresponding AvrRvi4 candidate in a timely manner. This meant that the student was unable to perform the genetic complementation experiment involving the candidate AvrRvi4 gene of V. inaequalis. This experiment will instead be carried out by collaborators at the New Zealand Institute for Plant and Food Research. With regards to the first nation-wide Covid-19 lockdown, all grafted Rvi4 apple plants for use in Chapter 2 could not be watered, and therefore died. These grafted plants were already over one year old when they were lost. As a consequence of this setback, apple seeds had to be sought and seedlings carrying the Rvi4 gene identified. This process took up to two months to complete.

Chapter 3: As a consequence of the first and second nation-wide Covid-19 lockdowns, all Nicotiana benthamiana and Nicotiana tabacum used by the student in Agrobacterium tumefaciens-mediated transient expression assays involving candidate effectors of V. inaequalis could not be watered, and therefore died. The plants that were lost were ready for experimental work, and it took at least six weeks for new Nicotiana plants to be ready for research (i.e. from seed germination).

Chapter 4: The only physical containment level 2 (PC2) glasshouse available for growing larger plants like tomato at Massey University in Palmerston North (Science Tower D glasshouse) lost all heating and climate control during the student's research project. Due to financial restrains imposed on the university by the Covid-19 pandemic, this glasshouse could not be repaired (and is still yet to be repaired). As a consequence of this, all pilot experiments involving Potato virus X (PVX) infection of tomato plants, which could only be performed in the Science Tower D glasshouse according to a Massey University safe operating procedure (SOP), failed, resulting in a significant loss of time (it takes at least four weeks to complete this experiment). These experiments will now have to be carried out by collaborators abroad. The failure of the heating and climate control in the Science Tower D glasshouse also meant that the student was unable to perform the genetic complementation experiment involving the candidate Avr9B genes of Cladosporium fulvum. This experiment instead had to carried out by collaborators abroad.

To partially compensate for the lost time described above, the student was awarded a three-month extension (retrospective three-month suspension of study). This time extension covered her fees for this period, but not her stipend, meaning that she had to take on a paid position outside of her PhD research (part-time employment).

Approved by DRC 10/Feb/2021
DRC 21/02/03
Updated September 2021

Confidential for Examiners Only: [*Please enter any other considerations which are confidential for examiners only and should not be placed in the final thesis version submitted to Library following the examination process]*

Signed, confirming this is a fair reflection of the impact of Covid-19 on this research.

Student	Silvia de la Rosa	Digitally signed by Silvia de la Rosa DN: cn=Silvia de la Rosa, c=NZ, o=Massey University, email=s.delarosa@massey.ac.nz Reason: I agree to the specified portions of this document Location: Massey University, Palmerston North Date: 2022.01.26 17:23:20 +13'00'
Supervisor	Carl Mesarich	Digitally signed by Carl Mesarich Date: 2022.01.25 19:58:46 +13'00'
Head of Academic Unit (or nominee)	Peter Tozer	Digitally signed by Peter Tozer Date: 2022.01.26 12:21:22 +13'00'

Approved by DRC 10/Feb/2021
DRC 21/02/03
Updated September 2021

References

Acosta Morel, W., Anta Fernández, F., Baroncelli, R., Becerra, S., Thon, M. R., van Kan, J. A. L., Díaz-Mínguez, J. M., & Benito, E. P. (2021). A major effect gene controlling development and pathogenicity in *Botrytis cinerea* identified through genetic analysis of natural mycelial non-pathogenic isolates [Original Research]. *Frontiers in Plant Science*, *12*. https://doi.org/10.3389/fpls.2021.663870

Agrios, G. N. (1988). *Plant pathology*. <Go to ISI>://CABI:19932329351

Akinsanmi, O. A., & Carvalhais, L. C. (2020). Draft genome of the macadamia husk spot pathogen, *Pseudocercospora macadamiae*. *Phytopathology*, *110*(9), 1503-1506. https://doi.org/10.1094/phyto-12-19-0460-a

Alonso, A. P. M., Ali, S., Song, X., Linning, R., & Bakkeren, G. (2020). UhAVR1, an HR-triggering avirulence effector of *Ustilago hordei* is secreted via the ER-Golgi pathway to the cytosol of barley coleoptile cells and contributes to virulence early in infection. *bioRxiv*, 2020.2008.2017.254789. https://doi.org/10.1101/2020.08.17.254789

Altschul, S. F., Madden, T. L., Schäffer, A. A., Zhang, J., Zhang, Z., Miller, W., & Lipman, D. J. (1997). Gapped BLAST and PSI-BLAST: a new generation of protein database search programs. *Nucleic Acids Res*, *25*(17), 3389-3402. https://doi.org/10.1093/nar/25.17.3389

Andersen, M. R., Salazar, M. P., Schaap, P. J., van de Vondervoort, P. J., Culley, D., Thykaer, J., Frisvad, J. C., Nielsen, K. F., Albang, R., Albermann, K., Berka, R. M., Braus, G. H., Braus-Stromeyer, S. A., Corrochano, L. M., Dai, Z., van Dijck, P. W., Hofmann, G., Lasure, L. L., Magnuson, J. K., Menke, H., Meijer, M., Meijer, S. L., Nielsen, J. B., Nielsen, M. L., van Ooyen, A. J., Pel, H. J., Poulsen, L., Samson, R. A., Stam, H., Tsang, A., van den Brink, J. M., Atkins, A., Aerts, A., Shapiro, H., Pangilinan, J., Salamov, A., Lou, Y., Lindquist, E., Lucas, S., Grimwood, J., Grigoriev, I. V., Kubicek, C. P., Martinez, D., van Peij, N. N., Roubos, J. A., Nielsen, J., & Baker, S. E. (2011). Comparative genomics of citric-acid-producing *Aspergillus niger* ATCC 1015 versus enzyme-producing CBS 513.88. *Genome Research*, *21*(6), 885-897. https://doi.org/10.1101/gr.112169.110

Anderson, C., Khan, M. A., Catanzariti, A.-M., Jack, C. A., Nemri, A., Lawrence, G. J., Upadhyaya, N. M., Hardham, A. R., Ellis, J. G., Dodds, P. N., & Jones, D. A. (2016). Genome analysis and avirulence gene cloning using a high-density RADseq linkage map of the flax rust fungus, *Melampsora lini*. *BMC Genomics*, *17*(1), 667. https://doi.org/10.1186/s12864-016-3011-9

Anh, V. L., Inoue, Y., Asuke, S., Vy, T. T. P., Anh, N. T., Wang, S., Chuma, I., & Tosa, Y. (2018). *Rmg8* and *Rmg7*, wheat genes for resistance to the wheat blast fungus, recognize the same avirulence gene *AVR-Rmg8*. *Molecular Plant Pathology*, *19*(5), 1252-1256. https://doi.org/https://doi.org/10.1111/mpp.12609

Apel, K., & Hirt, H. (2004). Reactive oxygen species: metabolism, oxidative stress, and signal transduction. *Annual Review of Plant Biology*, *55*, 373-399.

Arango, R., Diaz-Trujillo, C., Dhillon, B., Aerts, A., Carlier, J., Crane, C. F., V. de Jong, T., de Vries, I., Dietrich, R., Farmer, A. D., Fortes Fereira, C., Garcia, S., Guzman, M., Hamelin, R. C., Lindquist, E. A., Mehrabi, R., Quiros, O., Schmutz, J., Shapiro, H., Reynolds, E., Scalliet, G., Souza, M., Jr., Stergiopoulos, I., Van der Lee, T. A. J., De Wit, P. J. G. M., Zapater, M.-F., Zwiers, L.-H., Grigoriev, I. V., Goodwin, S. B., & Kema, G. H. J. (2016). Combating a global threat to a clonal crop: banana black

sigatoka pathogen *Pseudocercospora fijiensis (*Synonym *Mycosphaerella fijiensis*) genomes reveal clues for disease control. *PLoS genetics*, *12*(8), e1005876. https://doi.org/10.1371/journal.pgen.1005876

Armitage, A. D., Cockerton, H. M., Sreenivasaprasad, S., Woodhall, J., Lane, C., Harrison, R. J., & Clarkson, J. P. (2019). Genomics, evolutionary history and diagnostics of the *Alternaria alternata* species group including apple and Asian pear pathotypes. *Frontiers in Microbiology*. https://doi.org/https://doi.org/10.3389/fmicb.2019.03124

Asai, S., & Shirasu, K. (2015). Plant cells under siege: plant immune system versus pathogen effectors. *Current Opinion in Plant Biology*, *28*, 1-8. https://doi.org/10.1016/j.pbi.2015.08.008

Avenot, H. F., & Michailides, T. J. (2010). Progress in understanding molecular mechanisms and evolution of resistance to succinate dehydrogenase inhibiting (SDHI) fungicides in phytopathogenic fungi. *Crop Protection*, *29*(7), 643-651. https://doi.org/https://doi.org/10.1016/j.cropro.2010.02.019

Ayer, K. M., Choi, M.-W., Smart, S. T., Moffett, A. E., Cox, K. D., & Cann, I. (2020). The effects of succinate dehydrogenase inhibitor fungicide dose and mixture on development of resistance in *Venturia inaequalis*. *Applied and Environmental Microbiology*, *86*(17), e01196-01120. https://doi.org/doi:10.1128/AEM.01196-20

Ayer, K. M., Villani, S. M., Choi, M.-W., & Cox, K. D. (2019). Characterization of the *VisdhC* and *VisdhD* genes in *Venturia inaequalis*, and sensitivity to fluxapyroxad, pydiflumetofen, inpyrfluxam, and benzovindiflupyr. *Plant Disease*, *103*(6), 1092-1100. https://doi.org/10.1094/pdis-07-18-1225-re

Babu, M. M., Kriwacki, R. W., & Pappu, R. V. (2012). Versatility from Protein Disorder. *Science*, *337*(6101), 1460-1461. https://doi.org/doi:10.1126/science.1228775

Baccelli, I. (2015). Cerato-platanin family proteins: one function for multiple biological roles? *Frontiers in Plant Science*, *5*, 769-769. https://doi.org/10.3389/fpls.2014.00769

Backes, A., Guerriero, G., Ait Barka, E., & Jacquard, C. (2021). *Pyrenophora teres*: taxonomy, morphology, interaction with barley, and mode of control [Review]. *Frontiers in Plant Science*, *12*(509). https://doi.org/10.3389/fpls.2021.614951

Baggs, E., Dagdas, G., & Krasileva, K. V. (2017). NLR diversity, helpers and integrated domains: making sense of the NLR IDentity. *Current Opinion in Plant Biology*, *38*, 59-67. https://doi.org/https://doi.org/10.1016/j.pbi.2017.04.012

Bailey, T. L., Johnson, J., Grant, C. E., & Noble, W. S. (2015). The MEME Suite. *Nucleic Acids Res*, *43*(W1), W39-49. https://doi.org/10.1093/nar/gkv416

Baker, D., Shiau, A. K., & Agard, D. A. (1993). The role of pro regions in protein folding. *Current opinion in cell biology*, *5*(6), 966-970.

Baldi, P., Patocchi, A., Zini, E., Toller, C., Velasco, R., & Komjanc, M. (2004). Cloning and linkage mapping of resistance gene homologues in apple. *Theoretical and Applied Genetics*, *109*(1), 231-239.

Balesdent, M.-H., Fudal, I., Ollivier, B., Bally, P., Grandaubert, J., Eber, F., Chèvre, A.-M., Leflon, M., & Rouxel, T. (2013). The dispensable chromosome of *Leptosphaeria maculans* shelters an effector gene conferring avirulence towards *Brassica rapa*.

New Phytologist, *198*(3), 887-898. https://doi.org/https://doi.org/10.1111/nph.12178

Bankevich, A., Nurk, S., Antipov, D., Gurevich, A. A., Dvorkin, M., Kulikov, A. S., Lesin, V. M., Nikolenko, S. I., Pham, S., Prjibelski, A. D., Pyshkin, A. V., Sirotkin, A. V., Vyahhi, N., Tesler, G., Alekseyev, M. A., & Pevzner, P. A. (2012). SPAdes: a new genome assembly algorithm and its applications to single-cell sequencing. *Journal of computational biology : a journal of computational molecular cell biology*, *19*(5), 455-477. https://doi.org/10.1089/cmb.2012.0021

Bashi, Z. D., Hegedus, D. D., Buchwaldt, L., Rimmer, S. R., & Borhan, M. H. (2010). Expression and regulation of *Sclerotinia sclerotiorum* necrosis and ethylene-inducing peptides (NEPs) [Article]. *Molecular Plant Pathology*, *11*(1), 43-53. https://doi.org/10.1111/j.1364-3703.2009.00571.X

Bebber, D. P., Ramotowski, M. A. T., & Gurr, S. J. (2013). Crop pests and pathogens move polewards in a warming world. *Nature Climate Change*, *3*(11), 985-988. https://doi.org/10.1038/nclimate1990

Becker, M. G., Zhang, X., Walker, P. L., Wan, J. C., Millar, J. L., Khan, D., Granger, M. J., Cavers, J. D., Chan, A. C., Fernando, D. W. G., & Belmonte, M. F. (2017). Transcriptome analysis of the *Brassica napus–Leptosphaeria maculans* pathosystem identifies receptor, signaling and structural genes underlying plant resistance. *The Plant Journal*, *90*(3), 573-586. https://doi.org/https://doi.org/10.1111/tpj.13514

Belfanti, E., Silfverberg-Dilworth, E., Tartarini, S., Patocchi, A., Barbieri, M., Zhu, J., Vinatzer, B. A., Gianfranceschi, L., Gessler, C., & Sansavini, S. (2004). The *HcrVf2* gene from a wild apple confers scab resistance to a transgenic cultivated variety. *Proceedings of the National Academy of Sciences of the United States of America*, *101*(3), 886-890. https://doi.org/10.1073/pnas.0304808101

Bénaouf, G., & Parisi, L. (2000). Genetics of host-pathogen relationships between *Venturia inaequalis* races 6 and 7 and *Malus* species. *Phytopathology*, *90*(3), 236-242. https://doi.org/10.1094/phyto.2000.90.3.236

Beresford, R. M., Wright, P. J., Wood, P. N., & Park, N. M. (2012). Sensitivity of *Venturia inaequalis* to myclobutanil penconazole and dodine in relation to fungicide use in Hawkes Bay apple orchards. *New Zealand Plant Protection*, *65*(0), 106-113. https://doi.org/10.30843/nzpp.2012.65.5396

Berman, H. M., Westbrook, J., Feng, Z., Gilliland, G., Bhat, T. N., Weissig, H., Shindyalov, I. N., & Bourne, P. E. (2000). The Protein Data Bank. *Nucleic Acids Res*, *28*(1), 235-242. https://doi.org/10.1093/nar/28.1.235

Bernal-Cabrera, A., Martínez-Coca, B., Herrera-Isla, L., Ynfante-Martínez, D., Peteira-Delgado, B., Portal, O., Leiva-Mora, M., & de Wit, P. J. G. M. (2021). The first report on the occurrence race 9 of the tomato leaf mold pathogen *Cladosporium fulvum* (syn. *Passalora fulva*) in Cuba. *European Journal of Plant Pathology*, *160*(3), 731-736. https://doi.org/10.1007/s10658-021-02261-4

Birren, B., Lander, E., Galagan, J., Nusbaum, C., Devon, K., Ma, L.-J., Jaffe, D., Butler, J., Alvarez, P., Gnerre, S., Grabherr, M., Kleber, M., Mauceli, E., Brockman, W., MacCallum, I. A., Young, S., LaButti, K., DeCaprio, D., Crawford, M., Koehrsen, M., Engels, R., Montgomery , P., Pearson, M., Howarth , C., Larson, L., White, J., Yandava , C., Kodira, C., Guigo, R., Borodovsky, M., Zeng , Q., O'Leary, S., Alvarado, L., Pandelova, I., & Ciuffetti, L. (2008). Genome Sequence of *Pyrenophora tritici-repentis*. *Unpublished*.

Blanco-Ulate, B., Rolshausen, P. E., & Cantu, D. (2013). *Genome sequence of Neofusicoccum parvum isolate UCR-NP2*

Blum, M., Chang, H.-Y., Chuguransky, S., Grego, T., Kandasaamy, S., Mitchell, A., Nuka, G., Paysan-Lafosse, T., Qureshi, M., Raj, S., Richardson, L., Salazar, G. A., Williams, L., Bork, P., Bridge, A., Gough, J., Haft, D. H., Letunic, I., Marchler-Bauer, A., Mi, H., Natale, D. A., Necci, M., Orengo, C. A., Pandurangan, A. P., Rivoire, C., Sigrist, C. J. A., Sillitoe, I., Thanki, N., Thomas, P. D., Tosatto, S. C. E., Wu, C. H., Bateman, A., & Finn, R. D. (2020). The InterPro protein families and domains database: 20 years on. *Nucleic Acids Res*, *49*(D1), D344-D354. https://doi.org/10.1093/nar/gkaa977

Bohm, H., Albert, I., Oome, S., Raaymakers, T. M., Van den Ackerveken, G., & Nurnberger, T. (2014). A conserved peptide pattern from a widespread microbial virulence factor triggers pattern-Iinduced immunity in *Arabidopsis* [Article]. *PLOS Pathogens*, *10*(11), 11, Article e1004491. https://doi.org/10.1371/journal.ppat.1004491

Boller, T., & Felix, G. (2009). A renaissance of elicitors: perception of microbe-associated molecular patterns and danger signals by pattern-recognition receptors. *Annual Review of Plant Biology*, *60*(1), 379-406. https://doi.org/10.1146/annurev.arplant.57.032905.105346

Bolton, M. D., Van Esse, H. P., Vossen, J. H., De Jonge, R., Stergiopoulos, I., Stulemeijer, I. J. E., Van Den Berg, G. C. M., Borrás-Hidalgo, O., Dekker, H. L., De Koster, C. G., De Wit, P. J. G. M., Joosten, M. H. A. J., & Thomma, B. P. H. J. (2008). The novel *Cladosporium fulvum* lysin motif effector Ecp6 is a virulence factor with orthologues in other fungal species. *Molecular Microbiology*, *69*(1), 119-136. https://doi.org/10.1111/j.1365-2958.2008.06270.x

Bond, T. E. T. (1938). Infection experiments with *Cladosporium fulvum* Cooke and related species *Annals of Applied Biology*, *25*(2), 277-307. https://doi.org/10.1111/j.1744-7348.1938.tb02335.x

Bonza, M. C., Morandini, P., Luoni, L., Geisler, M., Palmgren, M. G., & De Michelis, M. I. (2000). At-ACA8 encodes a plasma membrane-localized calcium-ATPase of *Arabidopsis* with a calmodulin-binding domain at the N terminus. *Plant Physiology*, *123*(4), 1495-1506. https://doi.org/10.1104/pp.123.4.1495

Boone, D. M., & Keitt, G. W. (1957). *Venturia inaequalis* (Cke.) Wint. XII. Genes controlling pathogenicity of wild-type lines. . *Phytopathology*(47).

Bos, J. I. B., Kanneganti, T. D., Young, C., Cakir, C., Huitema, E., Win, J., Armstrong, M. R., Birch, P. R. J., & Kamoun, S. (2006). The C-terminal half of *Phytophthora infestans* RXLR effector AVR3a is sufficient to trigger R3a-mediated hypersensitivity and suppress INF1-induced cell death in *Nicotiana benthamiana* [Article]. *The Plant Journal*, *48*(2), 165-176. https://doi.org/10.1111/j.1365-313X.2006.02866.x

Boudichevskaia, A., Flachowsky, H., Fischer, C., Hanke, V., & Dunemann, F. (2004). Development of molecular markers for *Vr1*, a scab resistance factor from R12740-7A apple.

Boudichevskaia, A., Flachowsky, H., Peil, A., Fischer, C., & Dunemann, F. (2006). Development of a multiallelic SCAR marker for the scab resistance gene *Vr1*/*Vh4*/*Vx* from R12740-7A apple and its utility for molecular breeding. *Tree Genetics & Genomes*, *2*, 186-195. https://doi.org/10.1007/s11295-006-0043-3

Bouzarelou, D., Billini, M., Roumelioti, K., & Sophianopoulou, V. (2008). EglD, a putative endoglucanase, with an expansin like domain is localized in the conidial cell wall of *Aspergillus nidulans*. *Fungal Genetics and Biology*, *45*(6), 839-850. https://doi.org/https://doi.org/10.1016/j.fgb.2008.03.001

Bowen, J. K., Mesarich, C. H., Bus, V. G., Beresford, R. M., Plummer, K. M., & Templeton, M. D. (2011). *Venturia inaequalis*: the causal agent of apple scab. *Molecular Plant Pathology*, *12*(2), 105-122. https://doi.org/10.1111/j.1364-3703.2010.00656.x

Bowen, J. K., Mesarich, C. H., Rees-George, J., Cui, W., Fitzgerald, A., Win, J., Plummer, K. M., & Templeton, M. D. (2009). Candidate effector gene identification in the ascomycete fungal phytopathogen *Venturia inaequalis* by expressed sequence tag analysis. *Molecular Plant Pathology*, *10*(3), 431-448. https://doi.org/10.1111/j.1364-3703.2009.00543.x

Braun, U., Crous, P. W., Dugan, F., Groenewald, J. Z., & Sybren De Hoog, G. (2003). Phylogeny and taxonomy of *Cladosporium*-like hyphomycetes, including *Davidiella* gen. nov., the teleomorph of *Cladosporium* s. str. *Mycological Progress*, *2*(1), 3-18. https://doi.org/10.1007/s11557-006-0039-2

Brendolise, C., Montefiori, M., Dinis, R., Peeters, N., Storey, R. D., & Rikkerink, E. H. (2017). A novel hairpin library-based approach to identify NBS-LRR genes required for effector-triggered hypersensitive response in *Nicotiana benthamiana*. *Plant Methods*, *13*, 32. https://doi.org/10.1186/s13007-017-0181-7

Broggini, G. A., Le Cam, B., Parisi, L., Wu, C., Zhang, H. B., Gessler, C., & Patocchi, A. (2007). Construction of a contig of BAC clones spanning the region of the apple scab avirulence gene *AvrVg*. *Fungal Genetics and Biology*, *44*(1), 44-51. https://doi.org/10.1016/j.fgb.2006.07.001

Bruzzese, E., & Hasan, S. (1983). A whole leaf clearing and staining technique for host specificity studies of rust fungi. *Plant Pathology*, *32*(3), 335-338. https://doi.org/10.1111/j.1365-3059.1983.tb02841.x

Bus, V., Rikkerink, E., Aldwinckle, H. S., Caffier, V., Durel, C. E., Gardiner, S., Gessler, C., Groenwold, R., Laurens, F., Le Cam, B., Luby, J., Meulenbroek, B., Kellerhals, M., Parisi, L., Patocchi, A., Plummer, K., Schouten, H. J., Tartarini, S., & van de Weg, W. E. (2009). A proposal for the nomenclature of *Venturia inaequalis* races

Bus, V. G. (2006). *Differential host-pathogen interactions of Venturia inaequalis and Malus* ResearchSpace@ Auckland].

Bus, V. G., Rikkerink, E. H., Caffier, V., Durel, C. E., & Plummer, K. M. (2011). Revision of the nomenclature of the differential host-pathogen interactions of *Venturia inaequalis* and *Malus*. *Annual Review of Phytopathology*, *49*, 391-413. https://doi.org/10.1146/annurev-phyto-072910-095339

Bus, V. G. M., Laurens, F. N. D., van de Weg, W. E., Rusholme, R. L., Rikkerink, E. H. A., Gardiner, S. E., Bassett, H. C. M., Kodde, L. P., & Plummer, K. M. (2005a). The *Vh8* locus of a new gene-for-gene interaction between *Venturia inaequalis* and the wild apple *Malus sieversii* is closely linked to the *Vh2* locus in *Malus pumila* R12740-7A. *New Phytologist*, *166*(3), 1035-1049. https://doi.org/10.1111/j.1469-8137.2005.01395.x

Bus, V. G. M., Rikkerink, E. H. A., van de Weg, W. E., Rusholme, R. L., Gardiner, S. E., Bassett, H. C. M., Kodde, L. P., Parisi, L., Laurens, F. N. D., Meulenbroek, E. J., &

Plummer, K. M. (2005b). The *Vh2* and *Vh4* scab resistance genes in two differential hosts derived from Russian apple R12740-7A map to the same linkage group of apple. *Molecular Breeding*, *15*(1), 103-116. https://doi.org/10.1007/s11032-004-3609-5

Butler, E., & Jones, S. (1949). Tomato leaf mould, *Cladosporium fulvum* Cooke. *Plant Pathology*, 672-678.

Caffier, V., Le Cam, B., Expert, P., Tellier, M., Devaux, M., Giraud, M., & Chevalier, M. (2012). A new scab-like disease on apple caused by the formerly saprotrophic fungus *Venturia asperata*. *Plant Pathology*, *61*(5), 915-924. https://doi.org/https://doi.org/10.1111/j.1365-3059.2011.02583.x

Caffier, V., Patocchi, A., Expert, P., Bellanger, M. N., Durel, C. E., Hilber-Bodmer, M., Broggini, G. A. L., Groenwold, R., & Bus, V. G. M. (2015). Virulence characterization of *Venturia inaequalis* reference isolates on the differential set of *Malus* hosts [Article]. *Plant Disease*, *99*(3), 370-375. https://doi.org/10.1094/pdis-07-14-0708-re

Cai, X., Takken, F. L. W., Joosten, M. H. A. J., & De Wit, P. J. G. M. (2001). Specific recognition of Avr4 and Avr9 results in distinct patterns of hypersensitive cell death in tomato, but similar patterns of defence-related gene expression. *Molecular Plant Pathology*, *2*(2), 77-86. https://doi.org/10.1046/j.1364-3703.2001.00053.x

Cao, L. X., Blekemolen, M. C., Tintor, N., Cornelissen, B. J. C., & Takken, F. L. W. (2018). The *Fusarium oxysporum* Avr2-Six5 effector pair alters plasmodesmatal exclusion selectivity to facilitate cell-to-cell movement of Avr2 [Article]. *Molecular Plant*, *11*(5), 691-705. https://doi.org/10.1016/j.molp.2018.02.011

Cao, Y., Zhu, X., Jiao, R., & Xia, Y. (2012). The *Magas1* gene is involved in pathogenesis by affecting penetration in *Metarhizium acridum*. *Journal of Microbiology and Biotechnology*, *22*(7), 889-893. https://doi.org/10.4014/jmb.1111.11055

Carbone, M. J., Alaniz, S., Bentancur, O., & Mondino, P. (2021). Sensitivity of *Venturia inaequalis* to dodine in Uruguay. *Tropical Plant Pathology*, *46*(6), 643-650. https://doi.org/10.1007/s40858-021-00467-9

Catanzariti, A.-M., Dodds, P. N., Lawrence, G. J., Ayliffe, M. A., & Ellis, J. G. (2005). Haustorially expressed secreted proteins from flax rust are highly enriched for avirulence elicitors. *The Plant Cell*, *18*(1), 243-256. https://doi.org/10.1105/tpc.105.035980

Chakrabarti, A., Panter, S. N., Harrison, K., Jones, J. D. G., & Jones, D. A. (2009). Regions of the Cf-9B disease resistance protein able to cause spontaneous necrosis in *Nicotiana benthamiana* lie within the region controlling pathogen recognition in tomato. *Molecular Plant-Microbe Interactions*, *22*(10), 1214-1226. https://doi.org/10.1094/mpmi-22-10-1214

Chaloner, T. M., Gurr, S. J., & Bebber, D. P. (2021). Plant pathogen infection risk tracks global crop yields under climate change. *Nature Climate Change*, *11*(8), 710-715. https://doi.org/10.1038/s41558-021-01104-8

Chand, R., Singh, V., Singh, V. K., Kumar, M., Pal, C., Kumar, P., & Chowdappa, P. (2014). *De novo* whole genome sequencing of *Cercospora canescens*. *Unpublished*.

Chang, T. C., Salvucci, A., Crous, P. W., & Stergiopoulos, I. (2016). Comparative genomics of the Sigatoka disease complex on banana suggests a link between parallel

evolutionary changes in *Pseudocercospora fijiensis* and *Pseudocercospora eumusae* and increased virulence on the banana host. *PLoS genetics*, *12*(8), e1005904. https://doi.org/10.1371/journal.pgen.1005904

Chen, C., Bock, C. H., & Wood, B. W. (2017). Draft genome sequence of *Venturia carpophila*, the causal agent of peach scab. *Standards in genomic sciences*, *12*(1), 1-8.

Chen, L.-H., Kracun, S. K., Nissen, K. S., Mravec, J., Jorgensen, B., Labavitch, J., & Stergiopoulos, I. (2021). A diverse member of the fungal Avr4 effector family interacts with de-esterified pectin in plant cell walls to disrupt their integrity. *Science Advances*, *7*(19), Article eabe0809. https://doi.org/10.1126/sciadv.abe0809

Chen, S., Huang, T., Zhou, Y., Han, Y., Xu, M., & Gu, J. (2017). AfterQC: automatic filtering, trimming, error removing and quality control for fastq data. *BMC Bioinformatics*, *18*(Suppl 3), 80-80. https://doi.org/10.1186/s12859-017-1469-3

Chevalier, M., Lespinasse, Y., & Renaudin, S. (1991). A microscopic study of the different classes of symptoms coded by the *Vf* gene in apple for resistance to scab *(Venturia inaequalis)*. *Plant Pathology*, *40*(2), 249-256. https://doi.org/doi:10.1111/j.1365-3059.1991.tb02374.x

Chruszcz, M., Chapman, M. D., Osinski, T., Solberg, R., Demas, M., Porebski, P. J., Majorek, K. A., Pomés, A., & Minor, W. (2012). *Alternaria alternata* allergen Alt a 1: A unique β-barrel protein dimer found exclusively in fungi. *Journal of Allergy and Clinical Immunology*, *130*(1), 241-247.e249. https://doi.org/doi:10.1016/j.jaci.2012.03.047

Ciuffetti, L. M., Manning, V. A., Pandelova, I., Betts, M. F., & Martinez, J. P. (2010). Host-selective toxins, Ptr ToxA and Ptr ToxB, as necrotrophic effectors in the *Pyrenophora tritici-repentis*-wheat interaction. *New Phytologist*, *187*(4), 911-919. https://doi.org/10.1111/j.1469-8137.2010.03362.x

Ciuffetti, L. M., Tuori, R. P., & Gaventa, J. M. (1997). A single gene encodes a selective toxin causal to the development of tan spot of wheat. *The Plant Cell*

9(2), 135-144. https://doi.org/10.1105/tpc.9.2.135

Coleine, C., Masonjones, S., & Stajich, J. E. (2019). Genomes of endolithic fungi from Antarctica. *Unpublished*.

Collemare, J., Lemaire, C., Sannier, M., Bellanger, M., Expert, P., & Schouten, H. (2018, 15-19/01/2018). Evolutionary history of *AvrRvi6*, the first avirulence gene identified in the apple scab fungus *Venturia inaequalis* Journées Jean Chevaugeon, Aussois, France.

Condon, B. J., Leng, Y., Wu, D., Bushley, K. E., Ohm, R. A., Otillar, R., Martin, J., Schackwitz, W., Grimwood, J., MohdZainudin, N., Xue, C., Wang, R., Manning, V. A., Dhillon, B., Tu, Z. J., Steffenson, B. J., Salamov, A., Sun, H., Lowry, S., LaButti, K., Han, J., Copeland, A., Lindquist, E., Barry, K., Schmutz, J., Baker, S. E., Ciuffetti, L. M., Grigoriev, I. V., Zhong, S., & Turgeon, B. G. (2013). Comparative genome structure, secondary metabolite, and effector coding capacity across *Cochliobolus* pathogens. *PLoS genetics*, *9*(1), e1003233. https://doi.org/10.1371/journal.pgen.1003233

Cook, D. E., Mesarich, C. H., & Thomma, B. P. (2015). Understanding plant immunity as a surveillance system to detect invasion. *Annual Review of Phytopathology*, *53*, 541-563. https://doi.org/10.1146/annurev-phyto-080614-120114

Cooke, M. C. (1883). New American fungi. *Grevillea*, *12*, 22-33. https://ci.nii.ac.jp/naid/10021182468/en/

Cordero-Limon, L., Shaw, M. W., Passey, T. A., Robinson, J. D., & Xu, X. (2021). Cross-resistance between myclobutanil and tebuconazole and the genetic basis of tebuconazole resistance in *Venturia inaequalis*. *Pest Management Science*, *77*(2), 844-850. https://doi.org/https://doi.org/10.1002/ps.6088

Cornille, A., Gladieux, P., Smulders, M. J. M., Roldán-Ruiz, I., Laurens, F., Le Cam, B., Nersesyan, A., Clavel, J., Olonova, M., Feugey, L., Gabrielyan, I., Zhang, X.-G., Tenaillon, M. I., & Giraud, T. (2012). New insight into the history of domesticated apple: secondary contribution of the European wild apple to the genome of cultivated varieties. *PLoS genetics*, *8*(5), e1002703-e1002703. https://doi.org/10.1371/journal.pgen.1002703

Cosgrove, D. J. (2005). Growth of the plant cell wall. *Nature Reviews Molecular Cell Biology*, *6*(11), 850-861. https://doi.org/10.1038/nrm1746

Couto, D., & Zipfel, C. (2016). Regulation of pattern recognition receptor signalling in plants [Review Article]. *Nature Reviews Immunology*, *16*, 537. https://doi.org/10.1038/nri.2016.77

Cramer, R. A., & Lawrence, C. B. (2003). Cloning of a gene encoding an Alt a 1 isoallergen differentially expressed by the necrotrophic fungus *Alternaria brassicicola* during *Arabidopsis* infection [Article]. *Applied and Environmental Microbiology*, *69*(4), 2361-2364. https://doi.org/10.1128/aem.69.4.2361-2364.2003

Cuomo, C., de Hoog, S., Gorbushina, A., Stielow, B., Teixiera, M., Abouelleil, A., Chapman, S. B., Priest, M., Young, S. K., Wortman, J., Nusbaum, C., & Birren, B. (2016). *The genome sequence of Ochroconis gallopava CBS43764*

Cutt, J. R., Dixon, D. C., Carr, J. P., & Klessig, D. F. (1988). Isolation and nucleotide sequence of cDNA clones for the pathogenesis-related proteins PR1a, PR1b and PR1c of *Nicotiana tabacum* cv. Xanthi nc induced by TMV infection. *Nucleic Acids Res*, *16*(20), 9861-9861. https://doi.org/10.1093/nar/16.20.9861

Dagvadorj, B., Outram, M. A., Williams, S. J., & Solomon, P. S. (2021). The necrotrophic effector ToxA from *Parastagonospora nodorum* interacts with wheat NHL proteins to facilitate *Tsn1*-mediated necrosis. *bioRxiv*, 2021.2009.2022.461440. https://doi.org/10.1101/2021.09.22.461440

Dalio, R. J. D., Herlihy, J., Oliveira, T. S., McDowell, J. M., & Machado, M. (2018). Effector biology in focus: a primer for computational prediction and functional characterization. *Molecular Plant-Microbe Interactions*, *31*(1), 22-33. https://doi.org/10.1094/MPMI-07-17-0174-FI

Danecek, P., Bonfield, J. K., Liddle, J., Marshall, J., Ohan, V., Pollard, M. O., Whitwham, A., Keane, T., McCarthy, S. A., Davies, R. M., & Li, H. (2021). Twelve years of SAMtools and BCFtools. *GigaScience*, *10*(2). https://doi.org/10.1093/gigascience/giab008

Dangl, J. L., & Jones, J. D. G. (2001). Plant pathogens and integrated defence responses to infection. *Nature*, *411*(6839), 826-833. https://doi.org/10.1038/35081161

de Guillen, K., Ortiz-Vallejo, D., Gracy, J., Fournier, E., Kroj, T., & Padilla, A. (2015). Structure analysis uncovers a highly diverse but structurally conserved effector

family in phytopathogenic fungi. *PLOS Pathogens*, *11*(10), e1005228. https://doi.org/10.1371/journal.ppat.1005228

De Jonge, R., Ebert, M. K., Suttle, J. C., Jurick Ii, W. M., Secor, G. A., Thomma, B. P., Van De Peer, Y., & Bolton, M. D. (2018). The cercosporin biosynthetic gene cluster was horizontally transferred to several fungal lineages and shown to be expanded in *Cercospora beticola* based on microsynteny with recipient genomes. *Unpublished*.

de Jonge, R., Peter van Esse, H., Kombrink, A., Shinya, T., Desaki, Y., Bours, R., van der Krol, S., Shibuya, N., Joosten, M. H. A. J., & Thomma, B. P. H. J. (2010). Conserved fungal LysM effector Ecp6 prevents chitin-triggered immunity in plants. *Science*, *329*(5994), 953-955. https://doi.org/10.1126/science.1190859

de Jonge, R., & Thomma, B. P. H. J. (2009). Fungal LysM effectors: extinguishers of host immunity? *Trends in Microbiology*, *17*(4), 151-157. https://doi.org/https://doi.org/10.1016/j.tim.2009.01.002

de Jonge, R., van Esse, H. P., Maruthachalam, K., Bolton, M. D., Santhanam, P., Saber, M. K., Zhang, Z., Usami, T., Lievens, B., Subbarao, K. V., & Thomma, B. P. (2012). Tomato immune receptor Ve1 recognizes effector of multiple fungal pathogens uncovered by genome and RNA sequencing. *Proceedings of the National Academy of Sciences*, *109*(13), 5110-5115. https://doi.org/10.1073/pnas.1119623109

de Oliveira, A. L., Gallo, M., Pazzagli, L., Benedetti, C. E., Cappugi, G., Scala, A., Pantera, B., Spisni, A., Pertinhez, T. A., & Cicero, D. O. (2011). The structure of the elicitor Cerato-platanin (CP), the first member of the CP fungal protein family, reveals a double ψβ-barrel fold and carbohydrate binding. *Journal of Biochemical Chemistry*, *286*(20), 17560-17568. https://doi.org/10.1074/jbc.M111.223644

de Siqueira, K. A., Senabio, J. A., Pietro-Souza, W., de Oliveira Mendes, T. A., & Soares, M. A. (2021). *Aspergillus* sp. A31 and *Curvularia geniculata* P1 mitigate mercury toxicity to *Oryza sativa* L. *Archives of Microbiology*, *203*(9), 5345-5361. https://doi.org/10.1007/s00203-021-02481-6

de Siqueira, K. A., Souza, W. P., Mendes, T. A. O., & Soares, M. A. (2018). Genomes of the mercury-resistant fungi *Curvularia geniculata*-W3 and *Aspergillus terreus*-W25. *Unpublished*.

de Wit, P. D., Joosten, M., Thomma, B., & Stergiopoulos, I. (2009). Gene for gene models and beyond: the *Cladosporium fulvum*-tomato pathosystem.

de Wit, P. J. (2016). *Cladosporium fulvum* effectors: weapons in the arms race with tomato. *Annual Review of Phytopathology*, *54*, 1-23. https://doi.org/10.1146/annurev-phyto-011516-040249

de Wit, P. J., Laugé, R., Honée, G., Joosten, M. H., Vossen, P., Kooman-Gersmann, M., Vogelsang, R., & Vervoort, J. J. (1997). Molecular and biochemical basis of the interaction between tomato and its fungal pathogen *Cladosporium fulvum*. *Antonie Van Leeuwenhoek International Journal of General and Molecular Microbiology*, *71*(1-2), 137-141. https://doi.org/10.1023/a:1000102509556

De Wit, P. J. G. M. (1977). A light and scanning-electron microscopic study of infection of tomato plants by virulent and avirulent races of *Cladosporium fulvum*. *Netherlands Journal of Plant Pathology*, *83*(3), 109-122. https://doi.org/10.1007/BF01981556

de Wit, P. J. G. M., van der Burgt, A., Ökmen, B., Stergiopoulos, I., Abd-Elsalam, K. A., Aerts, A. L., Bahkali, A. H., Beenen, H. G., Chettri, P., Cox, M. P., Datema, E., de Vries, R. P., Dhillon, B., Ganley, A. R., Griffiths, S. A., Guo, Y., Hamelin, R. C., Henrissat, B., Kabir, M. S., Jashni, M. K., Kema, G., Klaubauf, S., Lapidus, A., Levasseur, A., Lindquist, E., Mehrabi, R., Ohm, R. A., Owen, T. J., Salamov, A., Schwelm, A., Schijlen, E., Sun, H., van den Burg, H. A., van Ham, R. C. H. J., Zhang, S., Goodwin, S. B., Grigoriev, I. V., Collemare, J., & Bradshaw, R. E. (2012). The genomes of the fungal plant pathogens *Cladosporium fulvum* and *Dothistroma septosporum* reveal adaptation to different hosts and lifestyles but also signatures of common ancestry. *PLoS genetics*, *8*(11), e1003088. https://doi.org/10.1371/journal.pgen.1003088

Debler, J. W., Henares, B. M., & Lee, R. C. (2021). Agroinfiltration for transient gene expression and characterisation of fungal pathogen effectors in cool-season grain legume hosts. *Plant Cell Reports*, *40*(5), 805-818. https://doi.org/10.1007/s00299-021-02671-y

Degrave, A., Wagner, M., George, P., Coudard, L., Pinochet, X., Ermel, M., Gay, E. J., Fudal, I., Moreno-Rico, O., Rouxel, T., & Balesdent, M.-H. (2021). A new avirulence gene of *Leptosphaeria maculans*, *AvrLm14*, identifies a resistance source in American broccoli (*Brassica oleracea*) genotypes. *Molecular Plant Pathology*, *22*(12), 1599-1612. https://doi.org/https://doi.org/10.1111/mpp.13131

DeLano, W. (2002). Pymol: An open-source molecular graphics tool. *CCP4 Newsletter on protein crystallography*, *40*(1), 82-92.

Deng, C. H., Plummer, K. M., Jones, D. A. B., Mesarich, C. H., Shiller, J., Taranto, A. P., Robinson, A. J., Kastner, P., Hall, N. E., Templeton, M. D., & Bowen, J. K. (2017). Comparative analysis of the predicted secretomes of *Rosaceae* scab pathogens *Venturia inaequalis* and *V. pirina* reveals expanded effector families and putative determinants of host range. *BMC Genomics*, *18*(1), 339. https://doi.org/10.1186/s12864-017-3699-1

Di, X., Cao, L., Hughes, R. K., Tintor, N., Banfield, M. J., & Takken, F. L. W. (2017). Structure-function analysis of the *Fusarium oxysporum* Avr2 effector allows uncoupling of its immune-suppressing activity from recognition. *New Phytologist*, *216*(3), 897-914. https://doi.org/10.1111/nph.14733

Dixon, M. S., Golstein, C., Thomas, C. M., Van der Biezen, E. A., & Jonathan, D. G. J. (2000). Genetic complexity of pathogen perception by plants: the example of *Rcr3*, a tomato gene required specifically by *Cf-2*. *Proceedings of the National Academy of Sciences of the United States of America*, *97*(16), 8807-8814. http://www.jstor.org/stable/123086

Dixon, M. S., Jones, D. A., Keddie, J. S., Thomas, C. M., Harrison, K., & Jones, J. D. G. (1996). The tomato *Cf-2* disease resistance locus comprises two functional genes encoding leucine-rich repeat proteins. *Cell*, *84*(3), 451-459. https://doi.org/10.1016/S0092-8674(00)81290-8

Djamei, A., Schipper, K., Rabe, F., Ghosh, A., Vincon, V., Kahnt, J., Osorio, S., Tohge, T., Fernie, A. R., Feussner, I., Feussner, K., Meinicke, P., Stierhof, Y.-D., Schwarz, H., Macek, B., Mann, M., & Kahmann, R. (2011). Metabolic priming by a secreted fungal effector [Article]. *Nature*, *478*(7369), 395-398. https://doi.org/10.1038/nature10454

Dodds, P. N., Lawrence, G. J., Catanzariti, A. M., Teh, T., Wang, C. I. A., Ayliffe, M. A., Kobe, B., & Ellis, J. G. (2006). Direct protein interaction underlies gene-for-gene specificity and coevolution of the flax resistance genes and flax rust avirulence genes [Article]. *Proceedings of the National Academy of Sciences of the United States of America*, *103*(23), 8888-8893. https://doi.org/10.1073/pnas.0602577103

Dubin, A., Likhanov, A., Klyachenko, O., Subin, A., & Kluvadenko, A. (2021). Effect of chitosan formulations on different biological origin on tobacco (*Nicotiana tabacum* L.) PR-genes expression *Journal of microbiology, biotechnology and food sciences*, *9*(6), 1141-1144. https://office2.jmbfs.org/index.php/JMBFS/article/view/4488

Eisenhaber, B., Bork, P., & Eisenhaber, F. (1999). Prediction of potential GPI-modification sites in proprotein sequences. *Journal of Molecular Biology*, *292*(3), 741-758. https://doi.org/10.1006/jmbi.1999.3069

Emanuelsson, O., Nielsen, H., Brunak, S., & von Heijne, G. (2000). Predicting subcellular localization of proteins based on their N-terminal amino acid sequence. *Journal of Molecular Biology*, *300*(4), 1005-1016. https://doi.org/doi:10.1006/jmbi.2000.3903

Fagundes, W. C., Zaccaron, A. Z., & Bluhm, B. H. (2018). Molecular basis of pathogenesis in *Cercospora sojina* revealed through pool sequencing. *Unpublished*.

Fang, A., Gao, H., Zhang, N., Zheng, X., Qiu, S., Li, Y., Zhou, S., Cui, F., & Sun, W. (2019). A novel effector gene *SCRE2* contributes to full virulence of *Ustilaginoidea virens* to rice. *Frontiers in Microbiology*, *10*, 845. https://doi.org/10.3389/fmicb.2019.00845

Fang, A., Han, Y., Zhang, N., Zhang, M., Liu, L., Li, S., Lu, F., & Sun, W. (2016). Identification and characterization of plant cell death–inducing secreted proteins from *Ustilaginoidea virens*. *Molecular Plant-Microbe Interactions*, *29*(5), 405-416. https://doi.org/10.1094/mpmi-09-15-0200-r

Faris, J. D., Zhang, Z., Lu, H., Lu, S., Reddy, L., Cloutier, S., Fellers, J. P., Meinhardt, S. W., Rasmussen, J. B., Xu, S. S., Oliver, R. P., Simons, K. J., & Friesen, T. L. (2010). A unique wheat disease resistance-like gene governs effector-triggered susceptibility to necrotrophic pathogens. *Proceedings of the National Academy of Sciences*, *107*(30), 13544-13549. https://doi.org/10.1073/pnas.1004090107

Félix, C., Meneses, R., Gonçalves, M. F. M., Tilleman, L., Duarte, A. S., Jorrín-Novo, J. V., Van de Peer, Y., Deforce, D., Van Nieuwerburgh, F., Esteves, A. C., & Alves, A. (2019). A multi-omics analysis of the grapevine pathogen *Lasiodiplodia theobromae* reveals that temperature affects the expression of virulence- and pathogenicity-related genes. *Scientific Reports*, *9*(1), 13144. https://doi.org/10.1038/s41598-019-49551-w

Fernandes, I., De Jonge, R., Van De Peer, Y., Devreese, B., Alves, A., & Esteves, A. C. (2016). *Proteomics and genomics reveal pathogen-plant mechanisms compatible with a hemibiotrophic lifestyle of Diplodia corticola*

Fiaccadori, R., Cicognani, E., Alberoni, G., Collina, M., & Brunelli, A. (2011). Sensitivity to strobilurin fungicides of Italian *Venturia inaequalis* populations with different origin and scab control. *Pest Management Science*, *67*(5), 535-540. https://doi.org/10.1002/ps.2090

Fisher, M. C., Henk, D. A., Briggs, C. J., Brownstein, J. S., Madoff, L. C., McCraw, S. L., & Gurr, S. J. (2012). Emerging fungal threats to animal, plant and ecosystem health [Review]. *Nature*, *484*(7393), 186-194. https://doi.org/10.1038/nature10947

Fitzgerald, A. M., Mudge, A. M., Gleave, A. P., & Plummer, K. M. (2003). *Agrobacterium* and PEG-mediated transformation of the phytopathogen *Venturia inaequalis.* . *Mycological Research*, *107*(7), 803-810. https://doi.org/10.1017/S0953756203008086

Flor, H. H. (1971). Current status of the Gene-For-Gene concept. *Annual Review of Phytopathology*, *9*(1), 275-296. https://doi.org/10.1146/annurev.py.09.090171.001423

Fones, H. N., Bebber, D. P., Chaloner, T. M., Kay, W. T., Steinberg, G., & Gurr, S. J. (2020). Threats to global food security from emerging fungal and oomycete crop pathogens. *Nature Food*, *1*(6), 332-342. https://doi.org/10.1038/s43016-020-0075-0

Fradin, E. F., Abd-El-Haliem, A., Masini, L., van den Berg, G. C. M., Joosten, M. H. A. J., & Thomma, B. P. H. J. (2011). Interfamily transfer of tomato Ve1 mediates *Verticillium* resistance in *Arabidopsis* *Plant Physiology*, *156*(4), 2255-2265. https://doi.org/10.1104/pp.111.180067

Fradin, E. F., Zhang, Z., Juarez Ayala, J. C., Castroverde, C. D. M., Nazar, R. N., Robb, J., Liu, C.-M., & Thomma, B. P. H. J. (2009). Genetic dissection of *Verticillium* wilt resistance mediated by tomato *Ve1* *Plant Physiology*, *150*(1), 320-332. https://doi.org/10.1104/pp.109.136762

Franceschetti, M., Maqbool, A., Jiménez-Dalmaroni, M. J., Pennington, H. G., Kamoun, S., & Banfield, M. J. (2017). Effectors of filamentous plant pathogens: commonalities amid diversity. *Microbiology and Molecular Biology Reviews*, *81*(2), e00066-00016. https://doi.org/doi:10.1128/MMBR.00066-16

Franco, M. E., López, S., Medina, R., Saparrat, M. C., & Balatti, P. (2015). Draft genome sequence and gene annotation of *Stemphylium lycopersici* strain CIDEFI-216. *Genome Announcements*, *3*(5). https://doi.org/10.1128/genomeA.01069-15

Frías, M., González, C., & Brito, N. (2011). BcSpl1, a cerato-platanin family protein, contributes to Botrytis cinerea virulence and elicits the hypersensitive response in the host. *New Phytologist*, *192*(2), 483-495. https://doi.org/10.1111/j.1469-8137.2011.03802.x

Friesen, T. L., Meinhardt, S. W., & Faris, J. D. (2007). The *Stagonospora nodorum*-wheat pathosystem involves multiple proteinaceous host-selective toxins and corresponding host sensitivity genes that interact in an inverse gene-for-gene manner. *The Plant Journal*, *51*(4), 681-692. https://doi.org/10.1111/j.1365-313X.2007.03166.x

Fudal, I., Ross, S., Brun, H., Besnard, A.-L., Ermel, M., Kuhn, M.-L., Balesdent, M.-H., & Rouxel, T. (2009). Repeat-induced point mutation (RIP) as an alternative mechanism of evolution toward virulence in *Leptosphaeria maculans*. *Molecular Plant-Microbe Interactions*, *22*(8), 932-941. https://doi.org/10.1094/mpmi-22-8-0932

Fudal, I., Ross, S., Gout, L., Blaise, F., Kuhn, M. L., Eckert, M. R., Cattolico, L., Bernard-Samain, S., Balesdent, M. H., & Rouxel, T. (2007). Heterochromatin-like regions as ecological niches for avirulence genes in the *Leptosphaeria maculans* genome:

map-based cloning of *AvrLm6*. *Molecular Plant-Microbe Interactions*, *20*(4), 459-470. https://doi.org/10.1094/mpmi-20-4-0459

Gaderer, R., Bonazza, K., & Seidl-Seiboth, V. (2014). Cerato-platanins: a fungal protein family with intriguing properties and application potential. *Applied Microbiology and Biotechnology*, *98*(11), 4795-4803. https://doi.org/10.1007/s00253-014-5690-y

Gao, S., Li, Y., Gao, J., Suo, Y., Fu, K., Li, Y., & Chen, J. (2014). Genome sequence and virulence variation-related transcriptome profiles of *Curvularia lunata*, an important maize pathogenic fungus. *BMC Genomics*, *15*(1), 627. https://doi.org/10.1186/1471-2164-15-627

Garcia, O., Macedo, J. A. N., Tiburcio, R., Zaparoli, G., Rincones, J., Bittencourt, L. M. C., Ceita, G. O., Micheli, F., Gesteira, A., Mariano, A. C., Schiavinato, M. A., Medrano, F. J., Meinhardt, L. W., Pereira, G. A. G., & Cascardo, J. C. M. (2007). Characterization of necrosis and ethylene-inducing proteins (NEP) in the basidiomycete *Moniliophthora perniciosa*, the causal agent of witches' broom in *Theobroma cacao* [Article]. *Mycological Research*, *111*, 443-455. https://doi.org/10.1016/j.mycres.2007.01.017

Garrido-Arandia, M., Silva-Navas, J., Ramirez-Castillejo, C., Cubells-Baeza, N., Gomez-Casado, C., Barber, D., Pozo, J. C., Melendi, P. G., Pacios, L. F., & Diaz-Perales, A. (2016). Characterisation of a flavonoid ligand of the fungal protein Alt a 1 [Article]. *Scientific Reports*, *6*, 9, Article 33468. https://doi.org/10.1038/srep33468

Gauthier, N. (2018). *Apple Scab* https://doi.org/10.1094/PHI-I-2000-1005-01

Gazzetti, K., Diaconu, E. L., Nanni, I. M., Ciriani, A., & Collina, M. (2019). Genome sequence resource for *Stemphylium vesicarium*, causing brown spot disease of pear. *Molecular Plant-Microbe Interactions*, *32*(8), 935-938. https://doi.org/10.1094/mpmi-11-18-0299-a

Gehring, C. A., & Irving, H. R. (2003). Natriuretic peptides - a class of heterologous molecules in plants [Article]. *International Journal of Biochemistry & Cell Biology*, *35*(9), 1318-1322. https://doi.org/10.1016/s1357-2725(03)00032-3

Gerland, P., Raftery, A. E., Sevčíková, H., Li, N., Gu, D., Spoorenberg, T., Alkema, L., Fosdick, B. K., Chunn, J., Lalic, N., Bay, G., Buettner, T., Heilig, G. K., & Wilmoth, J. (2014). World population stabilization unlikely this century. *Science*, *346*(6206), 234-237. https://doi.org/10.1126/science.1257469

Gessler, C., Patocchi, A., Sansavini, S., Tartarini, S., & Gianfranceschi, L. (2006). *Venturia inaequalis* resistance in apple. *Critical Reviews in Plant Sciences*, *25*(6), 473-503. https://doi.org/10.1080/07352680601015975

Ghanbarnia, K., Fudal, I., Larkan, N. J., Links, M. G., Balesdent, M.-H., Profotova, B., Fernando, W. G. D., Rouxel, T., & Borhan, M. H. (2015). Rapid identification of the *Leptosphaeria maculans* avirulence gene *AvrLm2* using an intraspecific comparative genomics approach. *Molecular Plant Pathology*, *16*(7), 699-709. https://doi.org/https://doi.org/10.1111/mpp.12228

Ghanbarnia, K., Ma, L., Larkan, N. J., Haddadi, P., Fernando, W. G. D., & Borhan, M. H. (2018). *Leptosphaeria maculans* AvrLm9: a new player in the game of hide and seek with AvrLm4-7. *Molecular Plant Pathology*, *19*(7), 1754-1764. https://doi.org/https://doi.org/10.1111/mpp.12658

Gibson, D. G., Young, L., Chuang, R. Y., Venter, J. C., Hutchison, C. A., 3rd, & Smith, H. O. (2009). Enzymatic assembly of DNA molecules up to several hundred kilobases. *Nature Methods*, *6*(5), 343-345. https://doi.org/10.1038/nmeth.1318

Giraldo, M. C., & Valent, B. (2013). Filamentous plant pathogen effectors in action [Article]. *Nature Reviews Microbiology*, *11*(11), 800-814. https://doi.org/10.1038/nrmicro3119

Gisi, U., Sierotzki, H., Cook, A., & McCaffery, A. (2002). Mechanisms influencing the evolution of resistance to Qo inhibitor fungicides. *Pest Management Science*, *58*(9), 859-867. https://doi.org/10.1002/ps.565

Gladieux, P., Caffier, V., Devaux, M., & Le Cam, B. (2010a). Host-specific differentiation among populations of *Venturia inaequalis* causing scab on apple, pyracantha and loquat. *Fungal Genetics and Biology*, *47*(6), 511-521. https://doi.org/https://doi.org/10.1016/j.fgb.2009.12.007

Gladieux, P., Zhang, X. G., Afoufa-Bastien, D., Valdebenito Sanhueza, R. M., Sbaghi, M., & Le Cam, B. (2008). On the origin and spread of the scab disease of apple: out of central Asia. *PLoS One*, *3*(1), e1455. https://doi.org/10.1371/journal.pone.0001455

Gladieux, P., Zhang, X. G., Roldan-Ruiz, I., Caffier, V., Leroy, T., Devaux, M., Van Glabeke, S., Coart, E., & Le Cam, B. (2010b). Evolution of the population structure of *Venturia inaequalis*, the apple scab fungus, associated with the domestication of its host [Article]. *Molecular Ecology*, *19*(4), 658-674. https://doi.org/10.1111/j.1365-294X.2009.04498.x

Godfray, H. C., Mason-D'Croz, D., & Robinson, S. (2016). Food system consequences of a fungal disease epidemic in a major crop. *Philosopical Transactions 371*(1709). https://doi.org/10.1098/rstb.2015.0467

Gómez-Casado, C., Murua-García, A., Garrido-Arandia, M., González-Melendi, P., Sánchez-Monge, R., Barber, D., Pacios, L. F., & Díaz-Perales, A. (2014). Alt a 1 from *Alternaria* interacts with PR5 thaumatin-like proteins. *FEBS Letters*, *588*(9), 1501-1508. https://doi.org/doi:10.1016/j.febslet.2014.02.044

Gómez-Gómez, L., & Boller, T. (2000). FLS2: An LRR Receptor–like kinase involved in the perception of the bacterial elicitor flagellin in *Arabidopsis*. *Molecular Cell*, *5*(6), 1003-1011. https://doi.org/https://doi.org/10.1016/S1097-2765(00)80265-8

Gonzalez-Dominguez, E., Armengol, J., & Rossi, V. (2017). Biology and epidemiology of *Venturia* species affecting fruit crops: a review. *Frontiers in Plant Science*, *8*, 1496. https://doi.org/10.3389/fpls.2017.01496

Gout, L., Fudal, I., Kuhn, M. L., Blaise, F., Eckert, M., Cattolico, L., Balesdent, M. H., & Rouxel, T. (2006). Lost in the middle of nowhere: the *AvrLm1* avirulence gene of the Dothideomycete *Leptosphaeria maculans*. *Molecular Microbiology*, *60*(1), 67-80. https://doi.org/doi:10.1111/j.1365-2958.2006.05076.x

Gout, L., Kuhn, M. L., Vincenot, L., Bernard-Samain, S., Cattolico, L., Barbetti, M., Moreno-Rico, O., Balesdent, M.-H., & Rouxel, T. (2007). Genome structure impacts molecular evolution at the *AvrLm1* avirulence locus of the plant pathogen *Leptosphaeria maculans*. *Environmental Microbiology*, *9*(12), 2978-2992. https://doi.org/https://doi.org/10.1111/j.1462-2920.2007.01408.x

Grabherr, M. G., Haas, B. J., Yassour, M., Levin, J. Z., Thompson, D. A., Amit, I., Adiconis, X., Fan, L., Raychowdhury, R., Zeng, Q., Chen, Z., Mauceli, E., Hacohen, N., Gnirke, A., Rhind, N., di Palma, F., Birren, B. W., Nusbaum, C., Lindblad-Toh, K., Friedman,

N., & Regev, A. (2011). Full-length transcriptome assembly from RNA-Seq data without a reference genome. *Nature biotechnology*, *29*(7), 644-652. https://doi.org/10.1038/nbt.1883

Guldener, U. (2018). *Direct submission*

Guo, Y., Dupont, P.-Y., Mesarich, C. H., Yang, B., McDougal, R. L., Panda, P., Dijkwel, P., Studholme, D. J., Sambles, C., Win, J., Wang, Y., Williams, N. M., & Bradshaw, R. E. (2020). Functional analysis of RXLR effectors from the New Zealand kauri dieback pathogen *Phytophthora agathidicida*. *Molecular Plant Pathology*, *21*(9), 1131-1148. https://doi.org/https://doi.org/10.1111/mpp.12967

Gurevich, A., Saveliev, V., Vyahhi, N., & Tesler, G. (2013). QUAST: quality assessment tool for genome assemblies. *Bioinformatics*, *29*(8), 1072-1075. https://doi.org/10.1093/bioinformatics/btt086

Gusberti, M., Patocchi, A., Gessler, C., & Broggini, G. A. L. (2012). Quantification of *Venturia inaequalis* growth in *Malus* × *domestica* with quantitative real-time polymerase chain reaction. *Plant Disease*, *96*(12), 1791-1797. https://doi.org/10.1094/pdis-12-11-1058-re

Gust, A. A., & Felix, G. (2014). Receptor like proteins associate with SOBIR1-type of adaptors to form bimolecular receptor kinases [Review]. *Current Opinion in Plant Biology*, *21*, 104-111. https://doi.org/10.1016/j.pbi.2014.07.007

Guyot, J., & Le Guen, V. (2018). A review of a century of studies on South American leaf blight of the rubber tree. *Plant Disease*, *102*(6), 1052-1065. https://doi.org/10.1094/pdis-04-17-0592-fe

Haanstra, J. P. W., Laugé, R., Meijer-Dekens, F., Bonnema, G., de Wit, P. J. G. M., & Lindhout, P. (1999). The *Cf-Ecp2* gene is linked to, but not part of, the *Cf-4/Cf-9* cluster on the short arm of chromosome 1 in tomato. *Molecular and General Genetics*, *262*(4), 839-845. https://doi.org/10.1007/s004380051148

Haanstra, J. P. W., Meijer-Dekens, F., Laugé, R., Seetanah, D., Joosten, M. H. A. J., de Wit, P. J. G. M., & Lindhout, P. (2000). Mapping strategy for resistance genes against *Cladosporium fulvum* on the short arm of Chromosome 1 of tomato: *Cf-ECP5* near the *Hcr9* Milky Way cluster. *Theoretical and Applied Genetics*, *101*, 661-668.

Haddadi, P., Larkan, N. J., Van de Wouw, A., Zhang, Y., Neik, T. X., Beynon, E., Bayer, P., Edwards, D., Batley, J., & Borhan, H. (2021). *Brassica napus* genes *Rlm4* and *Rlm7*, conferring resistance to *Leptosphaeria maculans*, are alleles of the *Rlm9* wall-associated kinase-like resistance locus. *bioRxiv*.

Hammoudi, V. (2021). The art of passing unnoticed: pathogenic fungi remain incognito thanks to EWCA effectors. *The Plant Cell*, *33*(4), 1097-1098. https://doi.org/10.1093/plcell/koab017

Haridas, S., Albert, R., Binder, M., Bloem, J., LaButti, K., Salamov, A., Andreopoulos, B., Baker, S. E., Barry, K., Bills, G., Bluhm, B. H., Cannon, C., Castanera, R., Culley, D. E., Daum, C., Ezra, D., González, J. B., Henrissat, B., Kuo, A., Liang, C., Lipzen, A., Lutzoni, F., Magnuson, J., Mondo, S. J., Nolan, M., Ohm, R. A., Pangilinan, J., Park, H. J., Ramírez, L., Alfaro, M., Sun, H., Tritt, A., Yoshinaga, Y., Zwiers, L. H., Turgeon, B. G., Goodwin, S. B., Spatafora, J. W., Crous, P. W., & Grigoriev, I. V. (2020). 101 Dothideomycetes genomes: A test case for predicting lifestyles and emergence of pathogens. *Studies in Mycology*, *96*, 141-153. https://doi.org/https://doi.org/10.1016/j.simyco.2020.01.003

Hassing, B. (2019). *Genetic analysis of candidate genes that regulate the Epichloë festucae-Lolium perenne mutualistic symbiotic interaction* [Doctoral, Massey University]. Palmerston North, NZ. http://hdl.handle.net/10179/15395

He, Q., Naqvi, S., McLellan, H., Boevink, P. C., Champouret, N., Hein, I., & Birch, P. R. (2018). Plant pathogen effector utilizes host susceptibility factor NRL1 to degrade the immune regulator SWAP70. *Proceedings of the National Academy of Sciences*, *115*(33), E7834-E7843.

He, Y., Zhou, J., Shan, L., & Meng, X. (2018). Plant cell surface receptor-mediated signaling – a common theme amid diversity. *Journal of Cell Science*, *131*(2). https://doi.org/10.1242/jcs.209353

Heath, M. C. (2000). Hypersensitive response-related death. *Plant Molecular Biology Reporter*, *44*(3), 321-334. https://doi.org/10.1023/a:1026592509060

Heidrich, K., Blanvillain-Baufumé, S., & Parker, J. E. (2012). Molecular and spatial constraints on NB-LRR receptor signaling. *Current Opinion in Plant Biology*, *15*(4), 385-391. https://doi.org/https://doi.org/10.1016/j.pbi.2012.03.015

Hemetsberger, C., Herrberger, C., Zechmann, B., Hillmer, M., & Doehlemann, G. (2012). The *Ustilago maydis* effector Pep1 suppresses plant immunity by inhibition of host peroxidase activity. *PLOS Pathogens*, *8*(5), e1002684. https://doi.org/10.1371/journal.ppat.1002684

Hemmat, M., Brown, S. K., & Weeden, N. F. (2002). Tagging and mapping scab resistance genes from R12740-7A apple. *Journal of the American Society for Horticultural Science jashs*, *127*(3), 365-370. https://doi.org/10.21273/jashs.127.3.365

Hemsworth, G. R., Henrissat, B., Davies, G. J., & Walton, P. H. (2014). Discovery and characterization of a new family of lytic polysaccharide monooxygenases. *Nat Chem Biol*, *10*(2), 122-126. https://doi.org/10.1038/nchembio.1417

Holm, L. (2020). Using Dali for protein structure comparison. In Z. Gáspári (Ed.), *Structural Bioinformatics: Methods and Protocols* (pp. 29-42). Springer US. https://doi.org/10.1007/978-1-0716-0270-6_3

Hopp, T. P., Prickett, K. S., Price, V. L., Libby, R. T., March, C. J., Pat Cerretti, D., Urdal, D. L., & Conlon, P. J. (1988). A short polypeptide marker sequence useful for recombinant protein identification and purification. *Nature biotechnology*, *6*(10), 1204-1210. https://doi.org/10.1038/nbt1088-1204

Hora Júnior, B. T. d., de Macedo, D. M., Barreto, R. W., Evans, H. C., Mattos, C. R. R., Maffia, L. A., & Mizubuti, E. S. G. (2014). Erasing the past: a new identity for the damoclean pathogen causing South American leaf blight of rubber. *PLoS One*, *9*(8), e104750. https://doi.org/10.1371/journal.pone.0104750

Houterman, P. M., Ma, L., van Ooijen, G., de Vroomen, M. J., Cornelissen, B. J., Takken, F. L., & Rep, M. (2009). The effector protein Avr2 of the xylem-colonizing fungus *Fusarium oxysporum* activates the tomato resistance protein I-2 intracellularly. *The Plant Journal*, *58*(6), 970-978. https://doi.org/10.1111/j.1365-313X.2009.03838.x

Hu, M., Gu, L., Li, M., Jeffrey, P. D., Gu, W., & Shi, Y. (2006). Structural basis of competitive recognition of p53 and MDM2 by HAUSP/USP7: implications for the regulation of the p53-MDM2 pathway. *Plos Biology*, *4*(2), e27. https://doi.org/10.1371/journal.pbio.0040027

Huang, J.-S. (2001). Penetration of cuticles by plant pathogens. In *Plant pathogenesis and resistance: biochemistry and physiology of plant-microbe interactions* (pp. 3-

48). Springer Netherlands. https://doi.org/10.1007/978-94-017-2687-0_1

Hunziker, L., Tarallo, M., Gough, K., Guo, M., Hargreaves, C., Loo, T. S., McDougal, R. L., Mesarich, C. H., & Bradshaw, R. E. (2021). Apoplastic effector candidates of a foliar forest pathogen trigger cell death in host and non-host plants. *bioRxiv*, 2021.2008.2006.455341. https://doi.org/10.1101/2021.08.06.455341

Hurlburt, N. K., Chen, L.-H., Stergiopoulos, I., & Fisher, A. J. (2018). Structure of the *Cladosporium fulvum* Avr4 effector in complex with (GlcNAc)6 reveals the ligand-binding mechanism and uncouples its intrinsic function from recognition by the Cf-4 resistance protein. *PLOS Pathogens*, *14*(8), e1007263. https://doi.org/10.1371/journal.ppat.1007263

Hyde, K. (1993). Tropical Australian freshwater fungi. VI. *Tiarosporella paludosa* and *Clohesyomyces aquaticus* gen. et sp. nov. (Coelomycetes). *Australian Systematic Botany*, *6*(2), 169-173. https://doi.org/https://doi.org/10.1071/SB9930169

Iakovidis, M., Soumpourou, E., Anderson, E., Etherington, G., Yourstone, S., & Thomas, C. (2020). Genes encoding recognition of the *Cladosporium fulvum* effector protein Ecp5 are encoded at several loci in the tomato genome. *G3 Genes|Genomes|Genetics*. https://doi.org/10.1534/g3.120.401119

Iida, Y., Iwadate, Y., Kubota, M., & Terami, F. (2010). Occurrence of a new race 2.9 of leaf mold of tomato in Japan. *Journal of General Plant Pathology*, *76*(1), 84-86. https://doi.org/10.1007/s10327-009-0207-8

Iida, Y., van 't Hof, P., Beenen, H., Mesarich, C., Kubota, M., Stergiopoulos, I., Mehrabi, R., Notsu, A., Fujiwara, K., Bahkali, A., Abd-Elsalam, K., Collemare, J., & de Wit, P. J. (2015). Novel mutations detected in avirulence genes overcoming tomato *Cf* resistance genes in isolates of a Japanese population of *Cladosporium fulvum*. *PLoS One*, *10*(4), e0123271. https://doi.org/10.1371/journal.pone.0123271

Inoue, K., Kitaoka, H., Park, P., & Ikeda, K. (2016). Novel aspects of hydrophobins in wheat isolate of *Magnaporthe oryzae*: Mpg1, but not Mhp1, is essential for adhesion and pathogenicity [Article]. *Journal of General Plant Pathology*, *82*(1), 18-28. https://doi.org/10.1007/s10327-015-0632-9

Ishii, H., & Yanase, H. (2000). *Venturia nashicola*, the scab fungus of Japanese and Chinese pears: a species distinct from *V. pirina*. *Mycological Research*, *104*(6), 755-759. https://doi.org/https://doi.org/10.1017/S0953756299001720

Islam, M. S., Haque, M. S., Islam, M. M., Emdad, E. M., Halim, A., Hossen, Q. M., Hossain, M. Z., Ahmed, B., Rahim, S., Rahman, M. S., Alam, M. M., Hou, S., Wan, X., Saito, J. A., & Alam, M. (2012). Tools to kill: genome of one of the most destructive plant pathogenic fungi *Macrophomina phaseolina*. *BMC Genomics*, *13*, 493. https://doi.org/10.1186/1471-2164-13-493

Jaber, M. Y., Bao, J., Gao, X., Zhang, L., He, D., Wang, X., Wang, A., Wang, Z., & Wang, B. (2020). Genome sequence of *Venturia oleaginea*, the causal agent of olive leaf scab. *Molecular Plant-Microbe Interactions*, *33*(9), 1095-1097. https://doi.org/10.1094/mpmi-03-20-0070-a

Jänsch, M., Broggini, G. A., Weger, J., Bus, V. G., Gardiner, S. E., Bassett, H., & Patocchi, A. (2015). Identification of SNPs linked to eight apple disease resistance loci. *Molecular Breeding*, *35*(1), 1-21.

Jänsch, M., Paris, R., Amoako-Andoh, F., Keulemans, W., Davey, M. W., Pagliarani, G., Tartarini, S., & Patocchi, A. (2013). A Phenotypic, molecular and biochemical characterization of the first cisgenic scab-resistant apple variety 'Gala'. *Plant Molecular Biology Reporter*, *32*(3), 679-690. https://doi.org/10.1007/s11105-013-0682-0

Jeffress, S., Ash, G., Arun Chinnappa, K., & Stodart, B. (2020). Genome mining of the citrus pathogen *Elsinoe fawcettii*; prediction and prioritisation of candidate effectors, cell wall degrading enzymes and secondary metabolite gene clusters.

Jenkins, J. A. (1948). The origin of the cultivated tomato. *Economic Botany*, *2*(4), 379-392. https://doi.org/10.1007/BF02859492

Jennings, Z., Kable, K., Halliday, C. L., Nankivell, B. J., Kok, J., Wong, G., & Chen, S. C. A. (2016). *Verruconis gallopava* cardiac and endovascular infection with dissemination after renal transplantation: Case report and lessons learned. *Medical mycology case reports*, *15*, 5-8. https://doi.org/10.1016/j.mmcr.2016.12.006

Jha, G., Thakur, K., & Thakur, P. (2009). The *Venturia*-Apple pathosystem: pathogenicity mechanisms and plant defense responses. *Journal of Biomedicine and Biotechnology*, *2009*, 680160. https://doi.org/10.1155/2009/680160

Johnson, S., Jones, D., Thrimawithana, A. H., Deng, C. H., Bowen, J. K., Mesarich, C. H., Ishii, H., Won, K., Bus, V. G. M., & Plummer, K. M. (2019). Whole genome sequence resource of the Asian pear scab pathogen *Venturia nashicola*. *Molecular Plant-Microbe Interactions*, *32*(11), 1463-1467. https://doi.org/10.1094/mpmi-03-19-0067-a

Jombart, T., & Ahmed, I. (2011). adegenet 1.3-1: new tools for the analysis of genome-wide SNP data. *Bioinformatics*, *27*(21), 3070-3071.

Jones, D. A., Dickinson MJ, Balint-Kurti PJ, Dixon MS, & JDG, J. (1993). Two complex resistance loci revealed in tomato by classical and RFLP mapping of the *Cf-2*, *Cf-4*, *Cf-5*, and *Cf-9* gene for resitance to *Cladosporium fulvum*. *Molecular Plant-Microbe Interactions*, *6*, 348–357.

Jones, D. A., Thomas, C. M., Hammond-Kosack, K. E., Balint-Kurti, P. J., & Jones, J. D. (1994). Isolation of the tomato *Cf-9* gene for resistance to *Cladosporium fulvum* by transposon tagging. *Science*, *266*(5186), 789-793. https://doi.org/10.1126/science.7973631

Jones, J. D., & Dangl, J. L. (2006). The plant immune system. *Nature*, *444*(7117), 323-329. https://doi.org/10.1038/nature05286

Jones, J. D. G., Vance, R. E., & Dangl, J. L. (2016). Intracellular innate immune surveillance devices in plants and animals. *Science*, *354*(6316), aaf6395. https://doi.org/doi:10.1126/science.aaf6395

Joosten, M., Cozijnsen, T. J., & Dewit, P. (1994). Host-resistance to a fungal tomato pathogen lost by a single base-pair change in an avirulence gene [Article]. *Nature*, *367*(6461), 384-386. https://doi.org/10.1038/367384a0

Joosten, M., & de Wit, P. (1999). The tomato–*Cladosporium fulvum* interaction: a versatile experimental system to study plant-pathogen interactions. *Annual Review of Phytopathology*, *37*(1), 335-367. https://doi.org/10.1146/annurev.phyto.37.1.335

Joosten, M. H., Vogelsang, R., Cozijnsen, T. J., Verberne, M. C., & De Wit, P. J. (1997). The biotrophic fungus *Cladosporium fulvum* circumvents Cf-4-mediated resistance by

producing unstable Avr4 elicitors. *Plant Cell*, *9*(3), 367-379. https://doi.org/10.1105/tpc.9.3.367

Joosten, M. H. A. J., & de Wit, P. J. G. M. (1988). Isolation, purification and preliminary characterization of a protein specific for compatible *Cladosporium fulvum* (syn. *Fulvia fulva*)-tomato interactions. *Physiological and Molecular Plant Pathology*, *33*(2), 241-253. https://doi.org/https://doi.org/10.1016/0885-5765(88)90024-0

Joosten, M. H. A. J., Hendrickx, L. J. M., & De Wit, P. J. G. M. (1990). Carbohydrate composition of apoplastic fluids isolated from tomato leaves inoculated with virulent or avirulent races of *Cladosporium fulvum* (syn. *Fulvia fulva*). *Netherlands Journal of Plant Pathology*, *96*(2), 103-112. https://doi.org/10.1007/BF02005134

Jumper, J., Evans, R., Pritzel, A., Green, T., Figurnov, M., Ronneberger, O., Tunyasuvunakool, K., Bates, R., Žídek, A., Potapenko, A., Bridgland, A., Meyer, C., Kohl, S. A. A., Ballard, A. J., Cowie, A., Romera-Paredes, B., Nikolov, S., Jain, R., Adler, J., Back, T., Petersen, S., Reiman, D., Clancy, E., Zielinski, M., Steinegger, M., Pacholska, M., Berghammer, T., Bodenstein, S., Silver, D., Vinyals, O., Senior, A. W., Kavukcuoglu, K., Kohli, P., & Hassabis, D. (2021). Highly accurate protein structure prediction with AlphaFold. *Nature*. https://doi.org/10.1038/s41586-021-03819-2

Justesen, A., Somerville, S., Christiansen, S., & Giese, H. (1996). Isolation and characterization of two novel genes expressed in germinating conidia of the obligate biotroph *Erysiphe graminis* f.sp. *hordei*. *Gene*, *170*(1), 131-135. https://doi.org/https://doi.org/10.1016/0378-1119(95)00875-6

Kamoun, S., van West, P., Vleeshouwers, V. G. A. A., de Groot, K. E., & Govers, F. (1998). Resistance of *Nicotiana benthamiana* to *Phytophthora infestans* Is Mediated by the Recognition of the Elicitor Protein INF1. *The Plant Cell*, *10*(9), 1413-1425. https://doi.org/10.1105/tpc.10.9.1413

Kang, S., Sweigard, J. A., & Valent, B. (1995). The PWL host specificity gene family in the blast fungus *Magnaporthe grisea*. *Molecular Plant Microbe Interactions*, *8*(6), 939-948.

Kanja, C., & Hammond-Kosack, K. E. (2020). Proteinaceous effector discovery and characterization in filamentous plant pathogens [Review]. *Molecular Plant Pathology*, *21*(10), 1353-1376. https://doi.org/10.1111/mpp.12980

Kanzaki, H., Saitoh, H., Takahashi, Y., Berberich, T., Ito, A., Kamoun, S., & Terauchi, R. (2008). NbLRK1, a lectin-like receptor kinase protein of *Nicotiana benthamiana*, interacts with *Phytophthora infestans* INF1 elicitin and mediates INF1-induced cell death. *Planta*, *228*(6), 977-987. https://doi.org/10.1007/s00425-008-0797-y

Kapos, P., Devendrakumar, K. T., & Li, X. (2019). Plant NLRs: From discovery to application. *Plant Science*, *279*, 3-18. https://doi.org/https://doi.org/10.1016/j.plantsci.2018.03.010

Kearse, M., Moir, R., Wilson, A., Stones-Havas, S., Cheung, M., Sturrock, S., Buxton, S., Cooper, A., Markowitz, S., Duran, C., Thierer, T., Ashton, B., Meintjes, P., & Drummond, A. (2012). Geneious Basic: An integrated and extendable desktop software platform for the organization and analysis of sequence data. *Bioinformatics*, *28*(12), 1647-1649. https://doi.org/10.1093/bioinformatics/bts199

Kerff, F., Amoroso, A., Herman, R., Sauvage, E., Petrella, S., Filée, P., Charlier, P., Joris, B., Tabuchi, A., Nikolaidis, N., & Cosgrove, D. J. (2008). Crystal structure and activity of *Bacillus subtilis* YoaJ (EXLX1), a bacterial expansin that promotes root colonization. *Proceedings of the National Academy of Sciences of the United States of America*, *105*(44), 16876-16881. https://doi.org/10.1073/pnas.0809382105

Kettles, G. J., Bayon, C., Canning, G., Rudd, J. J., & Kanyuka, K. (2017). Apoplastic recognition of multiple candidate effectors from the wheat pathogen *Zymoseptoria tritici* in the nonhost plant *Nicotiana benthamiana*. *New Phytologist*, *213*(1), 338-350. https://doi.org/https://doi.org/10.1111/nph.14215

Khajuria, Y. P., Kaul, S., Wani, A. A., & Dhar, M. K. (2018). Genetics of resistance in apple against *Venturia inaequalis* (Wint.) Cke. *Tree Genetics & Genomes*, *14*(2). https://doi.org/10.1007/s11295-018-1226-4

Kildea, S., Sheppard, L., Cucak, M., & Hutton, F. (2021). Detection of virulence to septoria tritici blotch (STB) resistance conferred by the winter wheat cultivar Cougar in the Irish *Zymoseptoria tritici* population and potential implications for STB control. *Plant Pathology*, *n/a*(n/a). https://doi.org/https://doi.org/10.1111/ppa.13432

Kim, H.-S., Lohmar, J. M., Busman, M., Brown, D. W., Naumann, T. A., Divon, H. H., Lysøe, E., Uhlig, S., & Proctor, R. H. (2020). Identification and distribution of gene clusters required for synthesis of sphingolipid metabolism inhibitors in diverse species of the filamentous fungus *Fusarium*. *BMC Genomics*, *21*(1), 510. https://doi.org/10.1186/s12864-020-06896-1

Kim, Y.-K., Li, D., & Kolattukudy, P. E. (1998). Induction of Ca2+-calmodulin signaling by hard-curface contact primes *Colletotrichum gloeosporioides* conidia to germinate and form appressoria. *Journal of Bacteriology*, *180*(19), 5144-5150. http://jb.asm.org/content/180/19/5144.abstract

Kirk, P., Cannon, P., Minter, D., & Stalpers, J. (2008). *Ainsworth and Bisby's dictionary of the fungi*. Cabi. https://doi.org/10.1079/9780851998268.0000

Knaus, B. J., & Grünwald, N. J. (2017). vcfr: a package to manipulate and visualize variant call format data in R. *Molecular ecology resources*, *17*(1), 44-53.

Köller, W. (1992). Antifungal agents with target sites in sterol functions and biosynthesis. *Target sites of fungicide action*, *7*, 119e206.

Koller, W., Parker, D. M., & Becker, C. M. (1991). Role of cutinase in the penetration of apple leaves by *Venturia inaequalis* [Article]. *Phytopathology*, *81*(11), 1375-1379. https://doi.org/10.1094/Phyto-81-1375

Köller, W., Wilcox, W. F., & Jones, A. L. (1999). Quantification, persistence, and status of dodine resistance in New York and Michigan orchard populations of *Venturia inaequalis*. *Plant Disease*, *83*(1), 66-70. https://doi.org/10.1094/pdis.1999.83.1.66

Kombrink, A. (2012). Heterologous production of fungal effectors in *Pichia pastoris*. *Methods in molecular biology*, *835*, 209-217. https://doi.org/10.1007/978-1-61779-501-5_13

Kombrink, A., Sánchez-Vallet, A., & Thomma, B. P. H. J. (2011). The role of chitin detection in plant–pathogen interactions. *Microbes and Infection*, *13*(14), 1168-1176. https://doi.org/https://doi.org/10.1016/j.micinf.2011.07.010

Kombrink, E., Schröder, M., & Hahlbrock, K. (1988). Several pathogenesis-related proteins in potato are 1,3-β-glucanases and chitinases. *Proceedings of the National Academy of Sciences*, *85*(3), 782-786. https://doi.org/10.1073/pnas.85.3.782

Kooman-Gersmann, M., Honee, G., Bonnema, G., & DeWit, P. (1996). A high-affinity binding site for the AVR9 peptide elicitor of *Cladosporium fulvum* is present on plasma membranes of tomato and other *Solanaceous* plants [Article]. *Plant Cell*, *8*(5), 929-938. <Go to ISI>://WOS:A1996UP10900016

Kourelis, J., Malik, S., Mattinson, O., Krauter, S., Kahlon, P. S., Paulus, J. K., & van der Hoorn, R. A. L. (2020). Evolution of a guarded decoy protease and its receptor in solanaceous plants. *Nature Communications*, *11*(1), 4393. https://doi.org/10.1038/s41467-020-18069-5

Krenek, P., Samajova, O., Luptovciak, I., Doskocilova, A., Komis, G., & Samaj, J. (2015). Transient plant transformation mediated by *Agrobacterium tumefaciens*: principles, methods and applications. *Biotechnology Advances*

33(6 Pt 2), 1024-1042. https://doi.org/10.1016/j.biotechadv.2015.03.012

Krogh, A., Larsson, B., von Heijne, G., & Sonnhammer, E. L. (2001). Predicting transmembrane protein topology with a hidden Markov model: application to complete genomes. *Journal of Molecular Biology*, *305*(3), 567-580. https://doi.org/10.1006/jmbi.2000.4315

Kruger, J., Thomas, C. M., Golstein, C., Dixon, M. S., Smoker, M., Tang, S. K., Mulder, L., & Jones, J. D. G. (2002). A tomato cysteine protease required for Cf-2-dependent disease resistance and suppression of autonecrosis [Article]. *Science*, *296*(5568), 744-747. https://doi.org/10.1126/science.1069288

Kruijt, M., Brandwagt, B. F., & de Wit, P. J. G. M. (2004). Rearrangements in the *Cf-9* disease resistance gene cluster of wild tomato have resulted in three genes that mediate Avr9 responsiveness. *Genetics*, *168*(3), 1655-1663. https://doi.org/10.1534/genetics.104.028985

Kruijt, M., MJ, D. E. K., & de Wit, P. J. (2005). Receptor-like proteins involved in plant disease resistance. *Molecular Plant Pathology*, *6*(1), 85-97. https://doi.org/10.1111/j.1364-3703.2004.00264.x

Kuan, C. S., Yew, S. M., Toh, Y. F., Chan, C. L., Ngeow, Y. F., Lee, K. W., Na, S. L., Yee, W. Y., Hoh, C. C., & Ng, K. P. (2015). Dissecting the fungal biology of *Bipolaris papendorfii*: from phylogenetic to comparative genomic analysis. *DNA Research*, *22*(3), 219-232. https://doi.org/10.1093/dnares/dsv007

Kucheryava, N., Bowen, J. K., Sutherland, P. W., Conolly, J. J., Mesarich, C. H., Rikkerink, E. H., Kemen, E., Plummer, K. M., Hahn, M., & Templeton, M. D. (2008). Two novel *Venturia inaequalis* genes induced upon morphogenetic differentiation during infection and in vitro growth on cellophane. *Fungal Genetics and Biology*, *45*(10), 1329-1339. https://doi.org/10.1016/j.fgb.2008.07.010

Larkan, N. J., Ma, L., & Borhan, M. H. (2015). The *Brassica napus* receptor-like protein RLM2 is encoded by a second allele of the *LepR3/Rlm2* blackleg resistance locus. *Plant Biotechnology Journal*, *13*(7), 983-992. https://doi.org/https://doi.org/10.1111/pbi.12341

Larkan, N. J., Ma, L., Haddadi, P., Buchwaldt, M., Parkin, I. A., Djavaheri, M., & Borhan, M. H. (2020). The *Brassica napus* wall-associated kinase-like (WAKL) gene *Rlm9* provides race-specific blackleg resistance. *The Plant Journal*, *104*(4), 892-900.

Laugé, R., Dmitriev, A. P., Joosten, M. H. A. J., & De Wit, P. J. G. M. (1998). Additional resistance gene(s) against *Cladosporium fulvum* present on the *Cf-9* introgression segment are associated with strong PR protein accumulation. *Molecular Plant-Microbe Interactions*, *11*(4), 301-308. https://doi.org/10.1094/mpmi.1998.11.4.301

Laugé, R., Joosten, M. H. A. J., Van den Ackerveken, G. F. J. M., Van den Broek, H. W. J., & De Wit, P. J. G. M. (1997). The *in planta*-produced extracellular proteins ECP1 and ECP2 of *Cladosporium fulvum* are virulence factors. *Molecular Plant-Microbe Interactions*, *10*(6), 725-734. https://doi.org/10.1094/mpmi.1997.10.6.725

Laugé., Goodwin, P. H., de Wit, P. J., & Joosten, M. H. (2000). Specific HR-associated recognition of secreted proteins from *Cladosporium fulvum* occurs in both host and non-host plants. *The Plant Journal*, *23*(6).

Lazar, N., Mesarich, C. H., Petit-Houdenot, Y., Talbi, N., de la Sierra-Gallay, I. L., Zélie, E., Blondeau, K., Gracy, J., Ollivier, B., Blaise, F., Rouxel, T., Balesdent, M.-H., Idnurm, A., van Tilbeurgh, H., & Fudal, I. (2021). A new family of structurally conserved fungal effectors displays epistatic interactions with plant resistance proteins. *bioRxiv*, 2020.2012.2017.423041. https://doi.org/10.1101/2020.12.17.423041

Lazarovits, G., & Higgins, V. J. (1976). Histological comparison of *Cladosporium fulvum* race 1 on immune, resistant, and susceptible tomato varieties. *Canadian Journal of Botany*, *54*(3-4), 224-234. https://doi.org/10.1139/b76-022

Le Cam, B., Parisi, L., & Arene, L. (2002). Evidence of two formae speciales in *Venturia inaequalis*, responsible for apple and pyracantha scab. *Phytopathology*, *92*(3), 314-320. https://doi.org/10.1094/phyto.2002.92.3.314

Le Cam, B., Sargent, D., Gouzy, J., Amselem, J., Bellanger, M.-N., Bouchez, O., Brown, S., Caffier, V., De Gracia, M., Debuchy, R., Duvaux, L., Payen, T., Sannier, M., Shiller, J., Collemare, J., & Lemaire, C. (2019). Population genome sequencing of the scab fungal species *Venturia inaequalis*, *Venturia pirina*, *Venturia aucupariae* and *Venturia asperata*. *G3 Genes|Genomes|Genetics*, *9*(8), 2405-2414. https://doi.org/10.1534/g3.119.400047

Leushkin, E. V., Logacheva, M. D., Penin, A. A., Sutormin, R. A., Gerasimov, E. S., Kochkina, G. A., Ivanushkina, N. E., Vasilenko, O. V., Kondrashov, A. S., & Ozerskaya, S. M. (2015). Comparative genome analysis of *Pseudogymnoascus* spp. reveals primarily clonal evolution with small genome fragments exchanged between lineages. *BMC Genomics*, *16*(1), 400. https://doi.org/10.1186/s12864-015-1570-9

Li, H. (2013). Aligning sequence reads, clone sequences and assembly contigs with BWA-MEM. *arXiv preprint arXiv:1303.3997*.

Li, H., & Durbin, R. (2010). Fast and accurate long-read alignment with Burrows-Wheeler transform. *Bioinformatics*, *26*(5), 589-595. https://doi.org/10.1093/bioinformatics/btp698

Li, H., Handsaker, B., Wysoker, A., Fennell, T., Ruan, J., Homer, N., Marth, G., Abecasis, G., & Durbin, R. (2009). The sequence alignment/map format and SAMtools. *Bioinformatics*, *25*(16), 2078-2079.

Li, S., Dong, Y., Li, L., Zhang, Y., Yang, X., Zeng, H., Shi, M., Pei, X., Qiu, D., & Yuan, Q. (2019). The novel cerato-platanin-like protein FocCP1 from *Fusarium oxysporum*

triggers an immune response in plants. *International Journal of Molecular Sciences*, *20*(11), 2849. https://www.mdpi.com/1422-0067/20/11/2849

Li, Z., Yin, Z., Fan, Y., Xu, M., Kang, Z., & Huang, L. (2015). Candidate effector proteins of the necrotrophic apple canker pathogen *Valsa mali* can suppress BAX-induced PCD [Original Research]. *Frontiers in Plant Science*, *6*. https://doi.org/10.3389/fpls.2015.00579

Lichtner, F. J. (2018). *Venturia inaequalis genome resource*

Lichtner, F. J., Jurick, W. M., Ayer, K. M., Gaskins, V. L., Villani, S. M., & Cox, K. D. (2020). A genome resource for several North American *Venturia inaequalis* isolates with multiple fungicide resistance phenotypes. *Phytopathology*, *110*(3), 544-546. https://doi.org/10.1094/phyto-06-19-0222-a

Liebrand, T. W. H., van den Berg, G. C. M., Zhang, Z., Smit, P., Cordewener, J. H. G., America, A. H. P., Sklenar, J., Jones, A. M. E., Tameling, W. I. L., Robatzek, S., Thomma, B. P. H. J., & Joosten, M. H. A. J. (2013). Receptor-like kinase SOBIR1/EVR interacts with receptor-like proteins in plant immunity against fungal infection. *Proceedings of the National Academy of Sciences*, *110*(24), 10010-10015. https://doi.org/10.1073/pnas.1220015110

Liu, Song, T. Q., Zhang, X., Yuan, H. B., Su, L. M., Li, W. L., Xu, J., Liu, S. H., Chen, L. L., Chen, T. Z., Zhang, M. X., Gu, L. C., Zhang, B. L., & Dou, D. L. (2014). Unconventionally secreted effectors of two filamentous pathogens target plant salicylate biosynthesis [Article]. *Nature Communications*, *5*, 10, Article 4686. https://doi.org/10.1038/ncomms5686

Liu, D., Coloe, S., Baird, R., & Pedersen, J. (2000). Rapid Mini-Preparation of Fungal DNA for PCR. *Journal of Clinical Microbiology*, *38*(1), 471-471. https://doi.org/10.1128/jcm.38.1.471-471.2000

Liu, J., Li, Y., & Creamer, R. (2016). A re-examination of the taxonomic status of *Embellisia astragali*. *Current Microbiology*, *72*(4), 404-409. https://doi.org/10.1007/s00284-015-0962-z

Liu, S., Wang, J., Han, Z., Gong, X., Zhang, H., & Chai, J. (2016). Molecular mechanism for fungal cell wall recognition by rice chitin receptor OsCEBiP. *Structure*, *24*(7), 1192-1200.

Liu, Y., Liu, Q., Tang, Y., & Ding, W. (2019). NtPR1a regulates resistance to *Ralstonia solanacearum* in *Nicotiana tabacum* via activating the defense-related genes. *Biochemical and Biophysical Research Communications*, *508*(3), 940-945. https://doi.org/https://doi.org/10.1016/j.bbrc.2018.12.017

Livak, K. J., & Schmittgen, T. D. (2001). Analysis of relative gene expression data using real-time quantitative PCR and the 2(-Delta Delta C(T)) Method. *Methods*, *25*(4), 402-408. https://doi.org/10.1006/meth.2001.1262

Lo Presti, L., Lanver, D., Schweizer, G., Tanaka, S., Liang, L., Tollot, M., Zuccaro, A., Reissmann, S., & Kahmann, R. (2015). Fungal effectors and plant susceptibility. *Annual Review of Plant Biology*, *66*, 513-545. https://doi.org/10.1146/annurev-arplant-043014-114623

Louet, C., Saubin, M., Andrieux, A., Persoons, A., Gorse, M., Pétrowski, J., Fabre, B., De Mita, S., Duplessis, S., Frey, P., & Halkett, F. (2021). A point mutation and large deletion at the candidate avirulence locus *AvrMlp7* in the poplar rust fungus correlate with poplar *RMlp7* resistance breakdown. *Molecular Ecology*, *n/a*(n/a). https://doi.org/https://doi.org/10.1111/mec.16294

Lu, S., Faris, J. D., Sherwood, R., Friesen, T. L., & Edwards, M. C. (2014). A dimeric PR-1-type pathogenesis-related protein interacts with ToxA and potentially mediates ToxA-induced necrosis in sensitive wheat. *Molecular Plant Pathology*, *15*(7), 650-663. https://doi.org/https://doi.org/10.1111/mpp.12122

Lucentini, C. G., Medina, R., Franco, M. E. E., Saparrat, M. C. N., & Balatti, P. A. (2021). *Fulvia fulva* [syn. *Cladosporium fulvum*, Passalora fulva] races in Argentina are evolving through genetic changes and carry polymorphic avr and ecp gene sequences. *European Journal of Plant Pathology*, *159*(3), 525-542. https://doi.org/10.1007/s10658-020-02181-9

Luderer, De Kock, M. J. D., Dees, R., H. L., De Wit, P., J. G. M., & Joosten, H. A. J. (2002). Functional analysis of cysteine residues of ECP elicitor proteins of the fungal tomato pathogen *Cladosporium fulvum*. *Molecular Plant Pathology*, *3*(2), 91-95. https://doi.org/https://doi.org/10.1046/j.1464-6722.2001.00095.x

Luderer, R., Rivas, S., Nürnberger, T., Mattei, B., Van den Hooven, H. W., Van der Hoorn, R. A. L., Romeis, T., Wehrfritz, J.-M., Blume, B., Nennstiel, D., Zuidema, D., Vervoort, J., De Lorenzo, G., Jones, J. D. G., De Wit, P. J. G. M., & Joosten, M. H. A. J. (2001). No evidence for binding between resistance gene product Cf-9 of tomato and avirulence gene product AVR9 of *Cladosporium fulvum*. *Molecular Plant-Microbe Interactions*, *14*(7), 867-876. https://doi.org/10.1094/mpmi.2001.14.7.867

Luderer, R., Takken, F. L. W., de Wit, P. J. G. M., & Joosten, M. H. A. J. (2002). *Cladosporium fulvum* overcomes Cf-2-mediated resistance by producing truncated Avr2 elicitor proteins. *Molecular Microbiology*, *45*(3), 875-884. https://doi.org/10.1046/j.1365-2958.2002.03060.x

Luo, X., Cao, J., Huang, J., Wang, Z., Guo, Z., Chen, Y., Ma, S., & Liu, J. (2018). Genome sequencing and comparative genomics reveal the potential pathogenic mechanism of *Cercospora sojina* Hara on soybean. *DNA Research*, *25*(1), 25-37. https://doi.org/10.1093/dnares/dsx035

Lv, Y., Zhang, M., Wu, T., Wu, T., & Zhong, Y. (2019). The infiltration efficiency of *Agrobacterium*-mediated transient transformation in four apple cultivars. *Scientia Horticulturae*, *256*, 108597. https://doi.org/https://doi.org/10.1016/j.scienta.2019.108597

Ma, L., & Borhan, M. H. (2015). The receptor-like kinase SOBIR1 interacts with *Brassica napus* LepR3 and is required for *Leptosphaeria maculans* AvrLm1-triggered immunity [Original Research]. *Frontiers in Plant Science*, *6*. https://doi.org/10.3389/fpls.2015.00933

Ma, L., Houterman, P. M., Gawehns, F., Cao, L., Sillo, F., Richter, H., Clavijo-Ortiz, M. J., Schmidt, S. M., Boeren, S., Vervoort, J., Cornelissen, B. J. C., Rep, M., & Takken, F. L. W. (2015). The AVR2–SIX5 gene pair is required to activate I-2-mediated immunity in tomato. *New Phytologist*, *208*(2), 507-518. https://doi.org/https://doi.org/10.1111/nph.13455

Ma, L., Lukasik, E., Gawehns, F., & Takken, F. L. (2012). The use of agroinfiltration for transient expression of plant resistance and fungal effector proteins in *Nicotiana benthamiana* leaves. *Methods in molecular biology*, *835*, 61-74. https://doi.org/10.1007/978-1-61779-501-5_4

Ma, S., Lapin, D., Liu, L., Sun, Y., Song, W., Zhang, X., Logemann, E., Yu, D., Wang, J., Jirschitzka, J., Han, Z., Schulze-Lefert, P., Parker, J. E., & Chai, J. (2020). Direct pathogen-induced assembly of an NLR immune receptor complex to form a

holoenzyme. *Science*, *370*(6521), eabe3069. https://doi.org/doi:10.1126/science.abe3069

Ma, Z., & Michailides, T. J. (2005). Advances in understanding molecular mechanisms of fungicide resistance and molecular detection of resistant genotypes in phytopathogenic fungi. *Crop Protection*, *24*(10), 853-863. https://doi.org/https://doi.org/10.1016/j.cropro.2005.01.011

Ma, Z., Proffer, T. J., Jacobs, J. L., & Sundin, G. W. (2006). Overexpression of the 14α-demethylase target gene (*CYP51*) mediates fungicide resistance in *Blumeriella jaapii*. *Applied and Environmental Microbiology*, *72*(4), 2581-2585.

MacHardy, W. E. (1996). *Apple scab: biology, epidemiology, and management*. American Phytopathological Society (APS Press).

Madeira, F., Park, Y. M., Lee, J., Buso, N., Gur, T., Madhusoodanan, N., Basutkar, P., Tivey, A. R. N., Potter, S. C., Finn, R. D., & Lopez, R. (2019). The EMBL-EBI search and sequence analysis tools APIs in 2019. *Nucleic Acids Res*, *47*(W1), W636-W641. https://doi.org/10.1093/nar/gkz268

Manning, V. A., Hamilton, S. M., Karplus, P. A., & Ciuffetti, L. M. (2008). The Arg-Gly-Asp-containing, solvent-exposed loop of Ptr ToxA is required for internalization [Article]. *Molecular Plant-Microbe Interactions*, *21*(3), 315-325. https://doi.org/10.1094/mpmi-21-3-0315

Manning, V. A., Hardison, L. K., & Ciuffetti, L. M. (2007). Ptr ToxA interacts with a chloroplast-localized protein. *Molecular Plant-Microbe Interactions*, *20*(2), 168-177. https://doi.org/10.1094/mpmi-20-2-0168

Marín, M., Uversky, V. N., & Ott, T. (2013). Intrinsic disorder in pathogen effectors: protein flexibility as an evolutionary hallmark in a molecular arms race. *The Plant Cell*, *25*(9), 3153-3157. https://doi.org/10.1105/tpc.113.116319

Marshall, R., Kombrink, A., Motteram, J., Loza-Reyes, E., Lucas, J., Hammond-Kosack, K. E., Thomma, B. P. H. J., & Rudd, J. J. (2011). Analysis of two in planta expressed LysM effector homologs from the fungus *Mycosphaerella graminicola* reveals novel functional properties and varying contributions to virulence on wheat. *Plant Physiology*, *156*(2), 756-769. https://doi.org/10.1104/pp.111.176347

Martin, R., Qi, T., Zhang, H., Liu, F., King, M., Toth, C., Nogales, E., & Staskawicz, B. J. (2020). Structure of the activated ROQ1 resistosome directly recognizing the pathogen effector XopQ. *Science*, *370*(6521), eabd9993. https://doi.org/doi:10.1126/science.abd9993

Martínez-Cruz, J., Romero, D., Hierrezuelo, J., Thon, M., de Vicente, A., & Pérez-García, A. (2021). Effectors with chitinase activity (EWCAs), a family of conserved, secreted fungal chitinases that suppress chitin-triggered immunity. *The Plant Cell*, *33*(4), 1319-1340. https://doi.org/10.1093/plcell/koab011

Masny, S. (2017). Occurrence of *Venturia inaequalis* races in Poland able to overcome specific apple scab resistance genes. *European Journal of Plant Pathology*, *147*(2), 313-323. https://doi.org/10.1007/s10658-016-1003-x

McKirdy, S., Mackie, A., & Kumar, S. (2011). Apple scab successfully eradicated in Western Australia. *Australasian Plant Pathology*, *30*, 371.

Medina, R., López, S. M. Y., Franco, M. E. E., Rollan, C., Ronco, B. L., Saparrat, M. C. N., De Wit, P. J. G. M., & Balatti, P. A. (2015). A Survey on occurrence of *Cladosporium fulvum* identifies race 0 and race 2 in tomato-growing areas of

Argentina. *Plant Disease*, *99*(12), 1732-1737. https://doi.org/10.1094/pdis-12-14-1270-re

Meinhardt, S. W., Cheng, W., Kwon, C. Y., Donohue, C. M., & Rasmussen, J. B. (2002). Role of the arginyl-glycyl-aspartic motif in the action of Ptr ToxA produced by *Pyrenophora tritici-repentis*. *Plant Physiology*, *130*(3), 1545-1551.

Mentlak, T. A., Kombrink, A., Shinya, T., Ryder, L. S., Otomo, I., Saitoh, H., Terauchi, R., Nishizawa, Y., Shibuya, N., Thomma, B. P. H. J., & Talbot, N. J. (2012). Effector-mediated suppression of chitin-triggered immunity by *Magnaporthe oryzae* is necessary for rice blast disease. *The Plant Cell*, *24*(1), 322-335. https://doi.org/10.1105/tpc.111.092957

Mesarich. (2011). *Investigating the structure and function of ViCin1, a novel repeat protein from the apple scab fungus Venturia inaequalis* University of Auckand]. Auckland, New Zealand.

Mesarich, Bowen, J. K., Hamiaux, C., & Templeton, M. D. (2015). Repeat-containing protein effectors of plant-associated organisms. *Frontiers in Plant Science*, *6*, 872. https://doi.org/10.3389/fpls.2015.00872

Mesarich, Griffiths, S. A., van der Burgt, A., Okmen, B., Beenen, H. G., Etalo, D. W., Joosten, M. H., & de Wit, P. J. (2014). Transcriptome sequencing uncovers the *Avr5* avirulence gene of the tomato leaf mold pathogen *Cladosporium fulvum*. *Molecular Plant-Microbe Interactions*, *27*(8), 846-857. https://doi.org/10.1094/MPMI-02-14-0050-R

Mesarich, Okmen, B., Rovenich, H., Griffiths, S. A., Wang, C., Karimi Jashni, M., Mihajlovski, A., Collemare, J., Hunziker, L., Deng, C. H., van der Burgt, A., Beenen, H. G., Templeton, M. D., Bradshaw, R. E., & de Wit, P. (2018). Specific hypersensitive response-associated recognition of new apoplastic effectors from *Cladosporium fulvum* in wild tomato. *Molecular Plant-Microbe Interactions*, *31*(1), 145-162. https://doi.org/10.1094/MPMI-05-17-0114-FI

Mesarich, Schmitz, M., Tremouilhac, P., McGillivray, D. J., Templeton, M. D., & Dingley, A. J. (2012). Structure, dynamics and domain organization of the repeat protein Cin1 from the apple scab fungus. *Biochimica et Biophysica Acta*, *1824*(10), 1118-1128. https://doi.org/10.1016/j.bbapap.2012.06.015

Mesarich, C. H., Stergiopoulos, I., Beenen, H. G., Cordovez, V., Guo, Y., Karimi Jashni, M., Bradshaw, R. E., & de Wit, P. J. (2016). A conserved proline residue in Dothideomycete Avr4 effector proteins is required to trigger a Cf-4-dependent hypersensitive response. *Molecular Plant Pathology*, *17*(1), 84-95. https://doi.org/10.1111/mpp.12265

Michelmore, R. W., Paran, I., & Kesseli, R. V. (1991). Identification of markers linked to disease-resistance genes by bulked segregant analysis: a rapid method to detect markers in specific genomic regions by using segregating populations. *Proceedings of the National Academy of Sciences*, *88*(21), 9828-9832. https://doi.org/10.1073/pnas.88.21.9828

Mirdita, M., Ovchinnikov, S., & Steinegger, M. (2021). ColabFold - Making protein folding accessible to all. *bioRxiv*, 2021.2008.2015.456425. https://doi.org/10.1101/2021.08.15.456425

Miya, A., Albert, P., Shinya, T., Desaki, Y., Ichimura, K., Shirasu, K., Narusaka, Y., Kawakami, N., Kaku, H., & Shibuya, N. (2007). CERK1, a LysM receptor kinase, is essential for chitin elicitor signaling in *Arabidopsis*. *Proceedings of the National*

Academy of Sciences, *104*(49), 19613-19618. https://doi.org/10.1073/pnas.0705147104

Möller, M., & Stukenbrock, E. H. (2017). Evolution and genome architecture in fungal plant pathogens. *Nature Reviews Microbiology*, *15*(12), 756-771. https://doi.org/10.1038/nrmicro.2017.76

Mondo, S. J., Dannebaum, R. O., Kuo, R. C., Labutti, K., Haridas, S., Kuo, A., Salamov, A., Ahrendt, S. R., Lipzen, A., Sullivan, W., Andreopoulos, W. B., Clum, A., Lindquist, E., Daum, C., Ramamoorthy, G. K., Gryganskyi, A., Culley, D., Magnuson, J. K., James, T. Y., O'Malley, M. A., Stajich, J. E., Spatafora, J. W., Visel, A., & Grigoriev, I. V. (2017). Widespread adenine N6-methylation of active genes in fungi. *Nature genetics*. https://doi.org/10.1038/ng.3859

Morales-Cruz, A., Amrine, K. C., Blanco-Ulate, B., Lawrence, D. P., Travadon, R., Rolshausen, P. E., Baumgartner, K., & Cantu, D. (2015). Distinctive expansion of gene families associated with plant cell wall degradation, secondary metabolism, and nutrient uptake in the genomes of grapevine trunk pathogens. *BMC Genomics*, *16*(1), 469. https://doi.org/10.1186/s12864-015-1624-z

Mueller, A. N., Ziemann, S., Treitschke, S., Aßmann, D., & Doehlemann, G. (2013). Compatibility in the *Ustilago maydis*–maize interaction requires inhibition of host cysteine proteases by the fungal effector Pit2. *PLOS Pathogens*, *9*(2), e1003177. https://doi.org/10.1371/journal.ppat.1003177

Narasimhan, V., Danecek, P., Scally, A., Xue, Y., Tyler-Smith, C., & Durbin, R. (2016). BCFtools/RoH: a hidden Markov model approach for detecting autozygosity from next-generation sequencing data. *Bioinformatics*, *32*(11), 1749-1751.

Navathe, S., Sinha, S., Chand, R., & Kharwar, R. (2020). Draft genome sequence of *Pseudocercospora cruenta* (Sacc.) Deighton, causing leaf spot of cowpea. *Mendeley Data*. https://doi.org/10.17632/g39mv8yp87.1

Nei, M., & Rooney, A. P. (2005). Concerted and birth-and-death evolution of multigene families. *Annual review of genetics*, *39*, 121-152. https://doi.org/10.1146/annurev.genet.39.073003.112240

Nelson, B. K., Cai, X., & Nebenführ, A. (2007). A multicolored set of *in vivo* organelle markers for co-localization studies in *Arabidopsis* and other plants. *The Plant Journal*, *51*(6), 1126-1136. https://doi.org/https://doi.org/10.1111/j.1365-313X.2007.03212.x

Nielsen, H. (2017). Predicting secretory proteins with SignalP. *Methods in molecular biology 1611*, 59-73. https://doi.org/10.1007/978-1-4939-7015-5_6

Nierman, W. C., Pain, A., Anderson, M. J., Wortman, J. R., Kim, H. S., Arroyo, J., Berriman, M., Abe, K., Archer, D. B., Bermejo, C., Bennett, J., Bowyer, P., Chen, D., Collins, M., Coulsen, R., Davies, R., Dyer, P. S., Farman, M., Fedorova, N., Fedorova, N., Feldblyum, T. V., Fischer, R., Fosker, N., Fraser, A., García, J. L., García, M. J., Goble, A., Goldman, G. H., Gomi, K., Griffith-Jones, S., Gwilliam, R., Haas, B., Haas, H., Harris, D., Horiuchi, H., Huang, J., Humphray, S., Jiménez, J., Keller, N., Khouri, H., Kitamoto, K., Kobayashi, T., Konzack, S., Kulkarni, R., Kumagai, T., Lafon, A., Latgé, J. P., Li, W., Lord, A., Lu, C., Majoros, W. H., May, G. S., Miller, B. L., Mohamoud, Y., Molina, M., Monod, M., Mouyna, I., Mulligan, S., Murphy, L., O'Neil, S., Paulsen, I., Peñalva, M. A., Pertea, M., Price, C., Pritchard, B. L., Quail, M. A., Rabbinowitsch, E., Rawlins, N., Rajandream, M. A., Reichard, U., Renauld, H., Robson, G. D., Rodriguez de Córdoba, S., Rodríguez-Peña, J. M., Ronning, C. M., Rutter, S., Salzberg, S. L., Sanchez, M., Sánchez-Ferrero, J. C., Saunders, D.,

Seeger, K., Squares, R., Squares, S., Takeuchi, M., Tekaia, F., Turner, G., Vazquez de Aldana, C. R., Weidman, J., White, O., Woodward, J., Yu, J. H., Fraser, C., Galagan, J. E., Asai, K., Machida, M., Hall, N., Barrell, B., & Denning, D. W. (2005). Genomic sequence of the pathogenic and allergenic filamentous fungus *Aspergillus fumigatus*. *Nature*, *438*(7071), 1151-1156. https://doi.org/10.1038/nature04332

Nilsson, J., Grahn, M., & Wright, A. P. (2011). Proteome-wide evidence for enhanced positive Darwinian selection within intrinsically disordered regions in proteins. *Genome biology*, *12*(7), 1-17.

Nimchuk, Z., Marois, E., Kjemtrup, S., Leister, R. T., Katagiri, F., & Dangl, J. L. (2000). Eukaryotic fatty acylation drives plasma membrane targeting and enhances function of several type III effector proteins from *Pseudomonas syringae*. *Cell*, *101*(4), 353-363. https://doi.org/10.1016/S0092-8674(00)80846-6

Nirmala, J., Drader, T., Lawrence, P. K., Yin, C. T., Hulbert, S., Steber, C. M., Steffenson, B. J., Szabo, L. J., von Wettstein, D., & Kleinhofs, A. (2011). Concerted action of two avirulent spore effectors activates reaction to *Puccinia graminis 1* (*Rpg1*)-mediated cereal stem rust resistance [Article]. *Proceedings of the National Academy of Sciences of the United States of America*, *108*(35), 14676-14681. https://doi.org/10.1073/pnas.1111771108

Niu, J., Ram, A. F. J., & Punt, P. J. (2020). Meeting a challenge: a view on studying transcriptional control of genes involved in plant biomass degradation in *Aspergillus niger*. In H. Nevalainen (Ed.), *Grand Challenges in Fungal Biotechnology* (pp. 211-235). Springer International Publishing. https://doi.org/10.1007/978-3-030-29541-7_8

Novak, A., Ćosić, J., Vrandečić, K., Jurković, D., Plavec, J., Križanac, I., & Ivić, D. (2021). Characterization of tomato leaf mould pathogen, *Passalora fulva*, in Croatia. *Journal of Plant Diseases and Protection*, *128*(4), 1041-1049. https://doi.org/10.1007/s41348-020-00419-6

Nováková, M., Šašek, V., Trdá, L., Krutinová, H., Mongin, T., Valentová, O., Balesdent, M.-H., Rouxel, T., & Burketová, L. (2016). *Leptosphaeria maculans* effector AvrLm4-7 affects salicylic acid (SA) and ethylene (ET) signalling and hydrogen peroxide (H2O2) accumulation in *Brassica napus*. *Molecular Plant Pathology*, *17*(6), 818-831. https://doi.org/https://doi.org/10.1111/mpp.12332

Ohm, R. A., Feau, N., Henrissat, B., Schoch, C. L., Horwitz, B. A., Barry, K. W., Condon, B. J., Copeland, A. C., Dhillon, B., Glaser, F., Hesse, C. N., Kosti, I., LaButti, K., Lindquist, E. A., Lucas, S., Salamov, A. A., Bradshaw, R. E., Ciuffetti, L., Hamelin, R. C., Kema, G. H. J., Lawrence, C., Scott, J. A., Spatafora, J. W., Turgeon, B. G., de Wit, P. J. G. M., Zhong, S., Goodwin, S. B., & Grigoriev, I. V. (2012). Diverse lifestyles and strategies of plant pathogenesis encoded in the genomes of eighteen *Dothideomycetes* fungi. *PLOS Pathogens*, *8*(12), e1003037. https://doi.org/10.1371/journal.ppat.1003037

Ökmen, B. (2013). *Identification and characterization of novel effectors of Cladosporium fulvum* (Publication Number Proefschrift Wageningen) s.n.]]. [S.l. https://edepot.wur.nl/266200

Ökmen, B., Etalo, D. W., Joosten, M., Bouwmeester, H. J., de Vos, R. C. H., Collemare, J., & de Wit, P. (2013). Detoxification of α-tomatine by *Cladosporium fulvum* is

required for full virulence on tomato [Article]. *New Phytologist*, *198*(4), 1203-1214. https://doi.org/10.1111/nph.12208

Olukayode, T., Quime, B., Shen, Y.-C., Yanoria, M. J., Zhang, S., Yang, J., Zhu, X., Shen, W.-C., von Tiedemann, A., & Zhou, B. (2019). Dynamic insertion of Pot3 in *AvrPib* prevailing in a field rice blast population in the Philippines led to the high virulence frequency against the resistance gene *Pib* in rice. *Phytopathology*, *109*(5), 870-877. https://doi.org/10.1094/phyto-06-18-0198-r

Orbach, M. J., Farrall, L., Sweigard, J. A., Chumley, F. G., & Valent, B. (2000). A telomeric avirulence gene determines efficacy for the rice blast resistance gene *Pi-ta*. *The Plant Cell*, *12*(11), 2019-2032.

Ori, N., Eshed, Y., Paran, I., Presting, G., Aviv, D., Tanksley, S., Zamir, D., & Fluhr, R. (1997). The I2C family from the wilt disease resistance locus I2 belongs to the nucleotide binding, leucine-rich repeat superfamily of plant resistance genes. *The Plant Cell*, *9*(4), 521-532. https://doi.org/10.2307/3870504

Outram, M. A., Solomon, P. S., & Williams, S. J. (2021). Pro-domain processing of fungal effector proteins from plant pathogens. *PLOS Pathogens*, *17*(10), e1010000. https://doi.org/10.1371/journal.ppat.1010000

Padder, B. A., Sofi, T. A., Ahmad, M., Shah, M.-U.-D., Hamid, A., Saleem, S., & Ahanger, F. A. (2013). Virulence and molecular diversity of *Venturia inaequalis* in commercial apple growing regions in Kashmir. *Journal of Phytopathology*, *161*(4), 271-279. https://doi.org/https://doi.org/10.1111/jph.12061

Panter, S. N., Hammond-Kosack, K. E., Harrison, K., Jones, J. D. G., & Jones, D. A. (2002). Developmental control of promoter activity is not responsible for mature onset of Cf-9B mediated resistance to leaf mold in tomato. *Molecular Plant-Microbe Interactions*, *15*(11), 1099-1107. https://doi.org/10.1094/mpmi.2002.15.11.1099

Papp, D., Singh, J., Gadoury, D., & Khan, A. (2020). New North American isolates of *Venturia inaequalis* can overcome apple scab resistance of *Malus floribunda* 821. *Plant Disease*, *104*(3), 649-655. https://doi.org/10.1094/pdis-10-19-2082-re

Parisi, L., Lespinasse, Y., Guillaumes, J., & Krueger, J. (1993). A new race of *Venturia inaequalis* virulent to apples with resistance due to the *Vf* gene. *Phytopathology*, *83*, 533-537.

Parisi, L., Fouillet, V., Schouten, H., Groenwold, R., Laurens, F., Didelot, F., Evans, K., Fischer, C., Gennari, F., & Kemp, H. (2004). Variability of the pathogenicity of *Venturia inaequalis* in Europe. *Acta Hortic*, *663*(1), 107-113.

Parisi, L., Lespinasse, Y., Guillaumes, J., & Kruger, J. (1994). *A new race of Venturia inaequalis virulent to apples with resistance due to the Vf gene*. Kluwer Academic Publishers. <Go to ISI>://CABI:19961600025

Parlange, F., Daverdin, G., Fudal, I., Kuhn, M.-L., Balesdent, M.-H., Blaise, F., Grezes-Besset, B., & Rouxel, T. (2009). *Leptosphaeria maculans* avirulence gene *AvrLm4-7* confers a dual recognition specificity by the *Rlm4* and *Rlm7* resistance genes of oilseed rape, and circumvents Rlm4-mediated recognition through a single amino acid change. *Molecular Microbiology*, *71*(4), 851-863. https://doi.org/https://doi.org/10.1111/j.1365-2958.2008.06547.x

Parniske, M., Wulff, B. B. H., Bonnema, G., Thomas, C. M., Jones, D. A., & Jones, J. D. G. (1999). Homologues of the *Cf-9* disease resistance gene (*Hcr9s*) are present at multiple loci on the short arm of tomato chromosome 1. *Molecular Plant-*

Microbe Interactions, *12*(2), 93-102. https://doi.org/10.1094/mpmi.1999.12.2.93

Passey, T. A., & Armitage, A. D. (2018). *Venturia inaequalis* strain 05/172. *Unpublished*.

Passey, T. A. J., Armitage, A. D., Sobczyk, M. K., Shaw, M. W., & Xu, X. (2020). Genomic sequencing indicates non-random mating of *Venturia inaequalis* in a mixed cultivar orchard. *Plant Pathology*, *69*(4), 669-676. https://doi.org/https://doi.org/10.1111/ppa.13150

Passey, T. A. J., Armitage, A. D., Xu, X., & Rokas, A. (2018). Annotated draft genome sequence of the apple scab pathogen *Venturia inaequalis*. *Microbiology Resource Announcements*, *7*(12), e01062-01018. https://doi.org/doi:10.1128/MRA.01062-18

Patocchi, A., Bigler, B., Koller, B., Kellerhals, M., & Gessler, C. (2004). *Vr2:* a new apple scab resistance gene. *Theoretical and Applied Genetics*, *109*(5), 1087-1092. https://doi.org/10.1007/s00122-004-1723-8

Patocchi, A., Bigler, B., Liebhard, R., Koller, B., & Gessler, C. (2003). *Mapping of Vr2, a third apple scab resistance gene of Russian seedling (R127407A)* Plant & Animal Genomes XI Conference,

Patocchi, A., Wehrli, A., Dubuis, P.-H., Auwerkerken, A., Leida, C., Cipriani, G., Passey, T., Staples, M., Didelot, F., Philion, V., Peil, A., Laszakovits, H., Rühmer, T., Boeck, K., Baniulis, D., Strasser, K., Vávra, R., Guerra, W., Masny, S., Ruess, F., Le Berre, F., Nybom, H., Tartarini, S., Spornberger, A., Pikunova, A., & Bus, V. G. M. (2020). Ten Years of VINQUEST: first insight for breeding new apple cultivars with durable apple scab resistance. *Plant Disease*, *104*(8), 2074-2081. https://doi.org/10.1094/pdis-11-19-2473-sr

Pedersen, B. S., & Quinlan, A. R. (2018). Mosdepth: quick coverage calculation for genomes and exomes. *Bioinformatics*, *34*(5), 867-868.

Pennington, H. G., Jones, R., Kwon, S., Bonciani, G., Thieron, H., Chandler, T., Luong, P., Morgan, S. N., Przydacz, M., & Bozkurt, T. (2019). The fungal ribonuclease-like effector protein CSEP0064/BEC1054 represses plant immunity and interferes with degradation of host ribosomal RNA. *PLOS Pathogens*, *15*(3), e1007620.

Perchepied, L., Chevreau, E., Ravon, E., Gaillard, S., Pelletier, S., Bahut, M., Berthelot, P., Cournol, R., Schouten, H. J., & Vergne, E. (2021). Successful intergeneric transfer of a major apple scab resistance gene (*Rvi6*) from apple to pear and precise comparison of the downstream molecular mechanisms of this resistance in both species. *BMC Genomics*, *22*(1), 843. https://doi.org/10.1186/s12864-021-08157-1

Petit-Houdenot, Y., Degrave, A., Meyer, M., Blaise, F., Ollivier, B., Marais, C.-L., Jauneau, A., Audran, C., Rivas, S., Veneault-Fourrey, C., Brun, H., Rouxel, T., Fudal, I., & Balesdent, M.-H. (2019). A two genes –for– one gene interaction between *Leptosphaeria maculans* and *Brassica napus*. *New Phytologist*, *223*(1), 397-411. https://doi.org/https://doi.org/10.1111/nph.15762

Petit-Houdenot, Y., & Fudal, I. (2017). Complex interactions between fungal avirulence genes and their corresponding plant resistance genes and consequences for disease resistance management. *Frontiers in Plant Science*, *8*, 1072. https://doi.org/10.3389/fpls.2017.01072

Pieczul, K. (2021). First report of *Alternaria alternata* on *Echinacea purpurea* flowers in Poland. *Unpublished*.

Plissonneau, C., Daverdin, G., Ollivier, B., Blaise, F., Degrave, A., Fudal, I., Rouxel, T., & Balesdent, M.-H. (2016). A game of hide and seek between avirulence genes *AvrLm4-7* and *AvrLm3* in *Leptosphaeria maculans*. *New Phytologist*, *209*(4), 1613-1624. https://doi.org/https://doi.org/10.1111/nph.13736

Plissonneau, C., Rouxel, T., Chèvre, A.-M., Van De Wouw, A. P., & Balesdent, M.-H. (2018). One gene-one name: the *AvrLmJ1* avirulence gene of *Leptosphaeria maculans* is *AvrLm5*. *Molecular Plant Pathology*, *19*(4), 1012-1016. https://doi.org/https://doi.org/10.1111/mpp.12574

Polat, Z., & Bayraktar, H. (2021). Resistance of *Venturia inaequalis* to multiple fungicides in Turkish apple orchards. *Journal of Phytopathology*, *169*(6), 360-368. https://doi.org/https://doi.org/10.1111/jph.12990

Postma, J., Liebrand, T. W. H., Bi, G. Z., Evrard, A., Bye, R. R., Mbengue, M., Kuhn, H., Joosten, M., & Robatzek, S. (2016). Avr4 promotes Cf-4 receptor-like protein association with the BAK1/SERK3 receptor-like kinase to initiate receptor endocytosis and plant immunity [Article]. *New Phytologist*, *210*(2), 627-642. https://doi.org/10.1111/nph.13802

Pradhan, A., Ghosh, S., Sahoo, D., & Jha, G. (2021). Fungal effectors, the double edge sword of phytopathogens. *Current Genetics*, *67*(1), 27-40. https://doi.org/10.1007/s00294-020-01118-3

Prencipe, S., Sillo, F., Garibaldi, A., Gullino, M. L., & Spadaro, D. (2020). Development of a sensitive TaqMan qPCR assay for detection and quantification of *Venturia inaequalis* in apple leaves and fruit and in air samples. *Plant Disease*, *104*(11), 2851-2859. https://doi.org/10.1094/pdis-10-19-2160-re

Prokchorchik, M., Won, K., Lee, Y., Choi, E. D., Segonzac, C., & Sohn, K. H. (2019). *High contiguity whole genome sequence and gene annotation resource for two Venturia nashicola isolates*

The PyMOL Molecular Graphics System. In. (2015). (Version 2.0) Schrödinger, LLC.

Quaedvlieg, W., Verkley, G. J. M., Shin, H. D., Barreto, R. W., Alfenas, A. C., Swart, W. J., Groenewald, J. Z., & Crous, P. W. (2013). Sizing up Septoria. *Studies in Mycology*, *75*, 307-390. https://doi.org/https://doi.org/10.3114/sim0017

Ranatunga, C., Gardiner, S., Bssett, H., Rikkerink, E., & Bus, V. (1999). Marker assisted selection for pest and disease resistance in the New Zealand apple breeding programme. Eucarpia symposium on Fruit Breeding and Genetics 538,

Ranf, S., Gisch, N., Schäffer, M., Illig, T., Westphal, L., Knirel, Y. A., Sánchez-Carballo, P. M., Zähringer, U., Hückelhoven, R., Lee, J., & Scheel, D. (2015). A lectin S-domain receptor kinase mediates lipopolysaccharide sensing in *Arabidopsis thaliana*. *Nature Immunology*, *16*(4), 426-433. https://doi.org/10.1038/ni.3124

Rigal, A., Doyle, S. M., & Robert, S. (2015). Live cell imaging of FM4-64, a tool for tracing the endocytic pathways in *Arabidopsis* root cells. *Methods in molecular biology*, *1242*, 93-103. https://doi.org/10.1007/978-1-4939-1902-4_9

Rivas, S., & Thomas, C. M. (2005). Molecular interactions between tomato and the leaf mold pathogen *Cladosporium fulvum*. *Annual Review of Phytopathology*, *43*(1), 395-436. https://doi.org/10.1146/annurev.phyto.43.040204.140224

Robert-Seilaniantz, A., Navarro, L., Bari, R., & Jones, J. D. (2007). Pathological hormone imbalances. *Current Opinion in Plant Biology*, *10*(4), 372-379. https://doi.org/10.1016/j.pbi.2007.06.003

Robert-Siegwald, G., Vallet, J., Abou-Mansour, E., Xu, J., Rey, P., Bertsch, C., Rego, C., Larignon, P., Fontaine, F., & Lebrun, M.-H. (2017). *Draft genome sequence of Diplodia seriata F98.1, a fungal species involved in grapevine trunk diseases*

Roberts, A., & Crute, I. (1994). Apple scab resistance from *Malus floribunda* 821 (*Vf*) is rendered ineffective by isolates of *Venturia inaequalis* from *Malus floribunda*. *Norwegian Journal of Agricultural Sciences*

Robinson, J. T., Thorvaldsdóttir, H., Winckler, W., Guttman, M., Lander, E. S., Getz, G., & Mesirov, J. P. (2011). Integrative genomics viewer. *Nature biotechnology*, *29*(1), 24-26.

Rocafort, M., Arshed, S., Hudson, D., Singh, J., Bowen, J. K., Plummer, K. M., Bradshaw, R. E., Johnson, R. D., Johnson, L. J., & Mesarich, C. H. (2021). CRISPR-Cas9 gene editing and rapid detection of gene-edited mutants using high-resolution melting in the apple scab fungus, *Venturia inaequalis*. *bioRxiv*, 2021.2002.2004.428760. https://doi.org/10.1101/2021.02.04.428760

Rocafort, M., Fudal, I., & Mesarich, C. H. (2020). Apoplastic effector proteins of plant-associated fungi and oomycetes. *Current Opinion in Plant Biology*, *56*, 9-19. https://doi.org/https://doi.org/10.1016/j.pbi.2020.02.004

Rodriguez-Moreno, L., Ebert, M. K., Bolton, M. D., & Thomma, B. (2018). Tools of the crook- infection strategies of fungal plant pathogens. *The Plant Journal*, *93*(4), 664-674. https://doi.org/10.1111/tpj.13810

Rooney, H. C. E. (2005). *Cladosporium* Avr2 inhibits tomato Rcr3 protease required for Cf-2-dependent disease resistance [Correction]. *Science*, *310*(5745), 54-54. <Go to ISI>://WOS:000232477000024

Rouxel, T., Grandaubert, J., Hane, J. K., Hoede, C., van de Wouw, A. P., Couloux, A., Dominguez, V., Anthouard, V., Bally, P., Bourras, S., Cozijnsen, A. J., Ciuffetti, L. M., Degrave, A., Dilmaghani, A., Duret, L., Fudal, I., Goodwin, S. B., Gout, L., Glaser, N., Linglin, J., Kema, G. H., Lapalu, N., Lawrence, C. B., May, K., Meyer, M., Ollivier, B., Poulain, J., Schoch, C. L., Simon, A., Spatafora, J. W., Stachowiak, A., Turgeon, B. G., Tyler, B. M., Vincent, D., Weissenbach, J., Amselem, J., Quesneville, H., Oliver, R. P., Wincker, P., Balesdent, M. H., & Howlett, B. J. (2011). Effector diversification within compartments of the *Leptosphaeria maculans* genome affected by Repeat-Induced Point mutations. *Nature Communications*, *2*, 202. https://doi.org/10.1038/ncomms1189

Ryder, L. S., & Talbot, N. J. (2015). Regulation of appressorium development in pathogenic fungi [Review]. *Current Opinion in Plant Biology*, *26*, 8-13. https://doi.org/10.1016/j.pbi.2015.05.013

Sabbadin, F., Hemsworth, G. R., Ciano, L., Henrissat, B., Dupree, P., Tryfona, T., Marques, R. D. S., Sweeney, S. T., Besser, K., Elias, L., Pesante, G., Li, Y., Dowle, A. A., Bates, R., Gomez, L. D., Simister, R., Davies, G. J., Walton, P. H., Bruce, N. C., & McQueen-Mason, S. J. (2018). An ancient family of lytic polysaccharide monooxygenases with roles in arthropod development and biomass digestion. *Nature Communications*, *9*(1), 756. https://doi.org/10.1038/s41467-018-03142-x

Saintenac, C., Lee, W.-S., Cambon, F., Rudd, J. J., King, R. C., Marande, W., Powers, S. J., Bergès, H., Phillips, A. L., & Uauy, C. (2018). Wheat receptor-kinase-like protein Stb6 controls gene-for-gene resistance to fungal pathogen *Zymoseptoria tritici*. *Nature genetics*, *50*(3), 368-374.

Sakalidis, M., Feau, N., Dhillon, B., Taylor, G. A., Birol, I., Jones, S. J., & Hamelin, R. C. (2017). *Mycosphaerella gibsonii* genome sequencing. *Unpublished*.

Sallato, B. V., Latorre, B. A., & Aylwin, G. (2006). First report of practical resistance to QoI fungicides in *Venturia inaequalis* (apple scab) in Chile. *Plant Disease*, *90*(3), 375. https://doi.org/10.1094/pd-90-0375a

Sanchez-Vallet, A., Saleem-Batcha, R., Kombrink, A., Hansen, G., Valkenburg, D. J., Thomma, B., & Mesters, J. R. (2013). Fungal effector Ecp6 outcompetes host immune receptor for chitin binding through intrachain LysM dimerization [Article]. *Elife*, *2*, 16, Article e00790. https://doi.org/10.7554/eLife.00790

Sandskär, B., & Liljeroth, E. (2005). Incidence of races of the apple scab pathogen (*Venturia inaequalis*) in apple growing districts in Sweden. *Acta Agriculturae Scandinavica, Section B — Soil & Plant Science*, *55*(2), 143-150. https://doi.org/10.1080/09064710510029042

Sarma, G. N., Manning, V. A., Ciuffetti, L. M., & Karplus, P. A. (2005). Structure of Ptr ToxA: an RGD-containing host-selective toxin from *Pyrenophora tritici-repentis*. *The Plant Cell*, *17*(11), 3190-3202. https://doi.org/10.1105/tpc.105.034918

Saunders, D. G. O., Breen, S., Win, J., Schornack, S., Hein, I., Bozkurt, T. O., Champouret, N., Vleeshouwers, V., Birch, P. R. J., Gilroy, E. M., & Kamoun, S. (2012). Host protein BSL1 associates with *Phytophthora infestans* RxLR effector AVR2 and the *Solanum demissum* immune receptor R2 to mediate disease resistance [Article]. *Plant Cell*, *24*(8), 3420-3434. https://doi.org/10.1105/tpc.112.099861

Savary, S., Willocquet, L., Pethybridge, S. J., Esker, P., McRoberts, N., & Nelson, A. (2019). The global burden of pathogens and pests on major food crops. *Nature Ecology & Evolution*, *3*(3), 430-439. https://doi.org/10.1038/s41559-018-0793-y

Scherrer, S., & Honegger, R. (2003). Inter- and intraspecific variation of homologous hydrophobin (H1) gene sequences among *Xanthoria* spp. (lichen-forming ascomycetes). *New Phytologist*, *158*(2), 375-389. https://doi.org/https://doi.org/10.1046/j.1469-8137.2003.00740.x

Schnabel, G., & Jones, A. L. (2001). The 14α-Demethylasse (*CYP51A1*) gene is overexpressed in *Venturia inaequalis* strains resistant to Myclobutanil. *Phytopathology*, *91*(1), 102-110. https://doi.org/10.1094/phyto.2001.91.1.102

Schneider, D., Saraiva, A., Azzoni, A., Miranda, H., de Toledo, M., Pelloso, A., & Souza, A. (2010). Overexpression and purification of PWL2D, a mutant of the effector protein PWL2 from *Magnaporthe grisea*. *Protein expression and purification*, *74*(1), 24-31.

Schottens-Toma, I. M. J., & de Wit, P. J. G. M. (1988). Purification and primary structure of a necrosis-inducing peptide from the apoplastic fluids of tomato infected with *Cladosporium fulvum* (syn. Fulvia fulva). *Physiological and Molecular Plant Pathology*, *33*(1), 59-67. https://doi.org/https://doi.org/10.1016/0885-5765(88)90043-4

Schouten, H. J., Brinkhuis, J., van der Burgh, A., Schaart, J. G., Groenwold, R., Broggini, G. A. L., & Gessler, C. (2013). Cloning and functional characterization of the *Rvi15*

(*Vr2*) gene for apple scab resistance. *Tree Genetics & Genomes*, *10*(2), 251-260. https://doi.org/10.1007/s11295-013-0678-9

Schulze-Lefert, P., & Panstruga, R. (2011). A molecular evolutionary concept connecting nonhost resistance, pathogen host range, and pathogen speciation. *Trends in Plant Science*, *16*(3), 117-125.

Schuster, M., & Steinberg, G. (2020). The fungicide dodine primarily inhibits mitochondrial respiration in *Ustilago maydis*, but also affects plasma membrane integrity and endocytosis, which is not found in *Zymoseptoria tritici*. *Fungal Genetics and Biology*, *142*, 103414. https://doi.org/https://doi.org/10.1016/j.fgb.2020.103414

Schwessinger, B., & McDonald, M. (2017). High quality DNA from fungi for long read sequencing e.g. PacBio, Nanopore MinION. *protocols.io dx.doi.org/10.17504/protocols.io.k6qczdw*. https://doi.org/dx.doi.org/10.17504/protocols.io.k6qczdw

Seear, P. J., & Dixon, M. S. (2003). Variable leucine-rich repeats of tomato disease resistance genes *Cf-2* and *Cf-5* determine specificity [Article]. *Molecular Plant Pathology*, *4*(3), 199-202. https://doi.org/10.1046/j.1364-3703.2003.00162.x

Seong, K., & Krasileva, K. V. (2021). Computational structural genomics unravels common folds and novel families in the secretome of fungal phytopathogen *Magnaporthe oryzae*. *Molecular Plant-Microbe Interactions*, *34*(11), 1267-1280. https://doi.org/10.1094/mpmi-03-21-0071-r

Sharma, S., Hay, F. S., & Pethybridge, S. J. (2020). Genome resource for two *Stemphylium vesicarium* isolates causing Stemphylium leaf blight of onion in New York. *Molecular Plant-Microbe Interactions*.

Shay, J.R., & Williams, E.B. (1956). Identification of three physiological races of *Venturia inaequalis*. *Phytopathology*, *46*, 190-193.

Shen, D., Li, Q., Sun, P., Zhang, M., & Dou, D. (2017). Intrinsic disorder is a common structural characteristic of RxLR effectors in oomycete pathogens. *Fungal Biology*, *121*(11), 911-919. https://doi.org/https://doi.org/10.1016/j.funbio.2017.07.005

Shetty, N. P., Mehrabi, R., Lütken, H., Haldrup, A., Kema, G. H. J., Collinge, D. B., & Jørgensen, H. J. L. (2007). Role of hydrogen peroxide during the interaction between the hemibiotrophic fungal pathogen *Septoria tritici* and wheat. *New Phytologist*, *174*(3), 637-647. https://doi.org/https://doi.org/10.1111/j.1469-8137.2007.02026.x

Shiller, J., Van de Wouw, A. P., Taranto, A. P., Bowen, J. K., Dubois, D., Robinson, A., Deng, C. H., & Plummer, K. M. (2015). A large family of *AvrLm6*-like genes in the apple and pear scab pathogens, *Venturia inaequalis* and *Venturia pirina*. *Frontiers in Plant Science*, *6*, 980. https://doi.org/10.3389/fpls.2015.00980

Sierotzki, H., & Scalliet, G. (2013). A review of current knowledge of resistance aspects for the next-generation succinate dehydrogenase inhibitor fungicides. *Phytopathology*, *103*(9), 880-887. https://doi.org/10.1094/phyto-01-13-0009-rvw

Silva, R. S., Kumar, L., Shabani, F., & PicanÇO, M. C. (2017). Assessing the impact of global warming on worldwide open field tomato cultivation through CSIRO-Mk3·0

global climate model. *The Journal of Agricultural Science*, *155*(3), 407-420. https://doi.org/10.1017/S0021859616000654

Simons, G., Groenendijk, J., Wijbrandi, J., Reijans, M., Groenen, J., Diergaarde, P., Van der Lee, T., Bleeker, M., Onstenk, J., de Both, M., Haring, M., Mes, J., Cornelissen, B., Zabeau, M., & Vos, P. (1998). Dissection of the *Fusarium I2* gene cluster in tomato reveals six homologs and one active gene copy. *Plant Cell*, *10*(6), 1055-1068. https://doi.org/10.1105/tpc.10.6.1055

Siqueira, K. A., Souza W.P., Mendes T.A.O., & M.A., S. (2017). Genomes of the *Curvularia lunata* and *Aspergillus terreus*, mercury-resistant fungi. *Unpublished*.

Sivanesan, A. (1977). *The taxonomy and pathology of Venturia species* (Vol. 59).

Smereka, K. J., Machardy, W. E., & Kausch, A. P. (1987). Cellular differentiation in *Venturia inaequalis* ascospores during germination and penetration of apple leaves. *Canadian Journal of Botany*, *65*(12), 2549-2561. https://doi.org/10.1139/b87-346

Snelders, N. C., Rovenich, H., Petti, G. C., Rocafort, M., van den Berg, G. C. M., Vorholt, J. A., Mesters, J. R., Seidl, M. F., Nijland, R., & Thomma, B. P. H. J. (2020). Microbiome manipulation by a soil-borne fungal plant pathogen using effector proteins. *Nature Plants*, *6*(11), 1365-1374. https://doi.org/10.1038/s41477-020-00799-5

Sonah, H., Deshmukh, R. K., & Belanger, R. R. (2016). Computational prediction of effector proteins in fungi: opportunities and challenges. *Frontiers in Plant Science*, *7*, 126. https://doi.org/10.3389/fpls.2016.00126

Song, R., Li, J., Xie, C., Jian, W., & Yang, X. (2020). An overview of the molecular genetics of plant resistance to the Verticillium wilt pathogen *Verticillium dahliae*. *International Journal of Molecular Sciences*, *21*(3), 1120. https://www.mdpi.com/1422-0067/21/3/1120

Song, Y., Liu, L. L., Wang, Y. D., Valkenburg, D. J., Zhang, X. L., Zhu, L. F., & Thomma, B. (2018). Transfer of tomato immune receptor Ve1 confers Ave1-dependent *Verticillium* resistance in tobacco and cotton [Article]. *Plant Biotechnology Journal*, *16*(2), 638-648. https://doi.org/10.1111/pbi.12804

Soumpourou, E., Iakovidis, M., Chartrain, L., Lyall, V., & Thomas, C. M. (2007). The *Solanum pimpinellifolium Cf-Ecp1* and *Cf-Ecp4* genes for resistance to *Cladosporium fulvum* are located at the Milky Way locus on the short arm of chromosome 1. *Theoretical and Applied Genetics*, *115*(8), 1127-1136. https://doi.org/10.1007/s00122-007-0638-6

Spanu, P. D. (2017). Cereal immunity against powdery mildews targets RNase-Like Proteins associated with Haustoria (RALPH) effectors evolved from a common ancestral gene. *New Phytologist*, *213*(3). https://doi.org/ https://doi.org/10.1111/nph.14386

Sperschneider, J., & Dodds, P. N. (2021). EffectorP 3.0: prediction of apoplastic and cytoplasmic effectors in fungi and oomycetes. *bioRxiv*, 2021.2007.2028.454080. https://doi.org/10.1101/2021.07.28.454080

Sperschneider, J., Dodds, P. N., Gardiner, D. M., Manners, J. M., Singh, K. B., & Taylor, J. M. (2015). Advances and challenges in computational prediction of effectors from plant pathogenic fungi. *PLOS Pathogens*, *11*(5), e1004806. https://doi.org/10.1371/journal.ppat.1004806

Sperschneider, J., Dodds, P. N., Singh, K. B., & Taylor, J. M. (2018). ApoplastP: prediction of effectors and plant proteins in the apoplast using machine learning. *New Phytologist*, *217*(4), 1764-1778. https://doi.org/10.1111/nph.14946

Sperschneider, J., Gardiner, D. M., Dodds, P. N., Tini, F., Covarelli, L., Singh, K. B., Manners, J. M., & Taylor, J. M. (2016). EffectorP: predicting fungal effector proteins from secretomes using machine learning. *New Phytologist*, *210*(2), 743-761. https://doi.org/10.1111/nph.13794

Spolaore, S., Trainotti, L., & Casadoro, G. (2001). A simple protocol for transient gene expression in ripe fleshy fruit mediated by *Agrobacterium*. *Journal of experimental botany*, *52*(357), 845-850. http://www.jstor.org/stable/23696706

Stam, R. (2021). *Direct submission*

Stanke, M., & Morgenstern, B. (2005). AUGUSTUS: a web server for gene prediction in eukaryotes that allows user-defined constraints. *Nucleic Acids Res*, *33*(Web Server issue), W465-W467. https://doi.org/10.1093/nar/gki458

Steinberg, G., & Gurr, S. J. (2020). Fungi, fungicide discovery and global food security. *Fungal Genetics and Biology*, *144*, 103476. https://doi.org/https://doi.org/10.1016/j.fgb.2020.103476

Stergiopoulos, I., De Kock, M. J. D., Lindhout, P., & De Wit, P. J. G. M. (2007). Allelic variation in the effector genes of the tomato pathogen *Cladosporium fulvum* reveals different modes of adaptive evolution. *Molecular Plant-Microbe Interactions*, *20*(10), 1271-1283. https://doi.org/10.1094/MPMI-20-10-1271

Stergiopoulos, I., van den Burg, H. A., Okmen, B., Beenen, H. G., van Liere, S., Kema, G. H. J., & de Wit, P. (2010). Tomato Cf resistance proteins mediate recognition of cognate homologous effectors from fungi pathogenic on dicots and monocots [Article]. *Proceedings of the National Academy of Sciences of the United States of America*, *107*(16), 7610-7615. https://doi.org/10.1073/pnas.1002910107

Stotz, H. U., Mitrousia, G. K., de Wit, P. J., & Fitt, B. D. (2014). Effector-triggered defence against apoplastic fungal pathogens. *Trends in Plant Science*, *19*(8), 491-500. https://doi.org/10.1016/j.tplants.2014.04.009

Strelkov, S. E., & Lamari, L. (2003). Host–parasite interactions in tan spot *Pyrenophora tritici-repentis* of wheat. *Canadian Journal of Plant Pathology*, *25*(4), 339-349. https://doi.org/10.1080/07060660309507089

Sutton, T. B., Walgenbach, J. F., Aldwinckle, H. S., Agnello, A., & Society, A. P. (2014). *Compendium of apple and pear diseases and pests*. APS Press/The American Phytopathological Society. https://books.google.co.nz/books?id=OAHpvgEACAAJ

Sweigard, J. A., Carroll, A. M., Kang, S., Farrall, L., Chumley, F. G., & Valent, B. (1995). Identification, cloning, and characterization of PWL2, a gene for host species specificity in the rice blast fungus. *The Plant Cell*, *7*(8), 1221-1233.

Tai, Y. S., Bragg, J., Lu, H., Edwards, M., Faris, J., Friesen, T., & Meinhardt, S. (2007). Functional characterization of Ptr ToxA and molecular identification of its intracellular targeting protein in wheat. Plant and Animal Genome VX Conference Abstracts2007,

Takken, F. L., & Goverse, A. (2012). How to build a pathogen detector: structural basis of NB-LRR function. *Current Opinion in Plant Biology*, *15*(4), 375-384. https://doi.org/10.1016/j.pbi.2012.05.001

Takken, F. L. W., Thomas, C. M., Joosten, M. H. A. J., Golstein, C., Westerink, N., Hille, J., Nijkamp, H. J. J., De Wit, P. J. G. M., & Jones, J. D. G. (1999). A second gene at the tomato *Cf-4* locus confers resistance to *Cladosporium fulvum* through recognition of a novel avirulence determinant. *The Plant Journal*, *20*(3), 279-288. https://doi.org/https://doi.org/10.1046/j.1365-313X.1999.00601.x

Talbot, N. J., Kershaw, M. J., Wakley, G. E., De Vries, O., Wessels, J., & Hamer, J. E. (1996). *MPG1* encodes a fungal hydrophobin involved in surface interactions during infection-related development of *Magnaporthe grisea*. *The Plant Cell*, *8*(6), 985-999. https://doi.org/10.1105/tpc.8.6.985

Tanaka, S., Brefort, T., Neidig, N., Djamei, A., Kahnt, J., Vermerris, W., Koenig, S., Feussner, K., Feussner, I., & Kahmann, R. (2014). A secreted *Ustilago maydis* effector promotes virulence by targeting anthocyanin biosynthesis in maize. *Elife*, *3*, e01355. https://doi.org/10.7554/eLife.01355

Tanaka, T., Nakayama, M., Takahashi, T., Nanatani, K., Yamagata, Y., & Abe, K. (2017). Analysis of the ionic interaction between the hydrophobin RodA and two cutinases of *Aspergillus nidulans* obtained via an *Aspergillus oryzae* expression system [Article]. *Applied Microbiology and Biotechnology*, *101*(6), 2343-2356. https://doi.org/10.1007/s00253-016-7979-5

Taylor, P. (2020). *Bipolaris victoriae (Victoria blight of oats)* https://doi.org/10.1079/ISC.14698.20210200787

Team, R. C. (2013). R: A language and environment for statistical computing.

Thakur, K., Chawla, V., Bhatti, S., Swarnkar, M. K., Kaur, J., Shankar, R., & Jha, G. (2013). *De novo* transcriptome sequencing and analysis for *Venturia inaequalis*, the devastating apple scab pathogen. *PLoS One*, *8*(1), e53937. https://doi.org/10.1371/journal.pone.0053937

Thierry, R., & Balesdent, M. H. (2017). Life, death and rebirth of avirulence effectors in a fungal pathogen of Brassica crops, *Leptosphaeria maculans*. *New Phytologist*, *214*(2), 526-532. https://doi.org/doi:10.1111/nph.14411

Thomas, C. M., Dixon, M. S., Parniske, M., Golstein, C., & Jones, J. D. (1998). Genetic and molecular analysis of tomato *Cf* genes for resistance to *Cladosporium fulvum*. *Philosophical transactions of the Royal Society of London. , 353*(1374), 1413-1424. https://doi.org/10.1098/rstb.1998.0296

Thomas, C. M., Jones, D. A., Parniske, M., Harrison, K., Balint-Kurti, P. J., Hatzixanthis, K., & Jones, J. D. (1997). Characterization of the tomato *Cf-4* gene for resistance to *Cladosporium fulvum* identifies sequences that determine recognitional specificity in Cf-4 and Cf-9. *The Plant Cell*, *9*(12), 2209-2224. https://doi.org/10.1105/tpc.9.12.2209

Thomma, B. P. H. J., Nürnberger, T., & Joosten, M. H. A. J. (2011). Of PAMPs and effectors: the blurred PTI-ETI dichotomy. *The Plant Cell*, *23*(1), 4-15. https://doi.org/10.1105/tpc.110.082602

Thomma, B. P. H. J., VAN ESSE, H. P., CROUS, P. W., & DE WIT, P. J. G. M. (2005). *Cladosporium fulvum* (syn. *Passalora fulva*), a highly specialized plant pathogen as a model for functional studies on plant pathogenic Mycosphaerellaceae.

Molecular Plant Pathology, *6*(4), 379-393. https://doi.org/10.1111/j.1364-3703.2005.00292.x

Thordal-Christensen, H., Birch, P. R. J., Spanu, P. D., & Panstruga, R. (2018). Why did filamentous plant pathogens evolve the potential to secrete hundreds of effectors to enable disease? *Molecular Plant Pathology*, *19*(4), 781-785. https://doi.org/10.1111/mpp.12649

Tomas, A., Feng, G. H., Reeck, G. R., Bockus, W. W., & Leach, J. E. (1990). Purification of a cultivar-specific toxin from *Pyrenophora-tritici-repentis*, causal agent of tan spot of wheat *Molecular Plant-Microbe Interactions*, *3*(4), 221-224. https://doi.org/10.1094/mpmi-3-221

Toruno, T. Y., Stergiopoulos, I., & Coaker, G. (2016). Plant-pathogen effectors: cellular probes interfering with plant defenses in spatial and temporal manners. *Annual Review of Phytopathology*, *54*, 419-441. https://doi.org/10.1146/annurev-phyto-080615-100204

Troncoso-Rojas, R., & Tiznado-Hernández, M. E. (2014). *Alternaria alternata* (Black Rot, Black Spot). In S. Bautista-Baños (Ed.), *Postharvest Decay* (pp. 147-187). Academic Press. https://doi.org/https://doi.org/10.1016/B978-0-12-411552-1.00005-3

Tuori, R. P., Wolpert, T. J., & Ciuffetti, L. M. (2000). Heterologous expression of functional Ptr ToxA. *Molecular Plant Microbe Interactions*, *13*(4), 456-464. https://doi.org/10.1094/mpmi.2000.13.4.456

Turek, I., Marondedze, C., Wheeler, J. I., Gehring, C., & Irving, H. R. (2014). Plant natriuretic peptides induce proteins diagnostic for an adaptive response to stress [Original Research]. *Frontiers in Plant Science*, *5*(661). https://doi.org/10.3389/fpls.2014.00661

Turgeon, B. G., & Yoder, O. C. (2000). Proposed nomenclature for mating type genes of filamentous ascomycetes. *Fungal Genetics and Biology*, *31*(1), 1-5. https://doi.org/10.1006/fgbi.2000.1227

Twaroch, T. E., Arcalís, E., Sterflinger, K., Stöger, E., Swoboda, I., & Valenta, R. (2012). Predominant localization of the major *Alternaria allergen* Alt a 1 in the cell wall of airborne spores. *Journal of Allergy and Clinical Immunology*, *129*(4), 1148-1149. https://doi.org/10.1016/j.jaci.2011.10.008

Uversky, V. N., Oldfield, C. J., & Dunker, A. K. (2005). Showing your ID: intrinsic disorder as an ID for recognition, regulation and cell signaling. *Journal of Molecular Recognition*, *18*(5), 343-384. https://doi.org/https://doi.org/10.1002/jmr.747

Van de Wouw, A. P., Lowe, R. G. T., Elliott, C. E., Dubois, D. J., & Howlett, B. J. (2014). An avirulence gene, *AvrLmJ1*, from the blackleg fungus, *Leptosphaeria maculans*, confers avirulence to *Brassica juncea* cultivars. *Molecular Plant Pathology*, *15*(5), 523-530. https://doi.org/https://doi.org/10.1111/mpp.12105

Van den Ackerveken, G. F., Van Kan, J. A., & De Wit, P. J. (1992). Molecular analysis of the avirulence gene avr9 of the fungal tomato pathogen *Cladosporium fulvum* fully supports the gene-for-gene hypothesis. *Plant Journal*, *2*(3), 359-366. https://doi.org/10.1111/j.1365-313x.1992.00359.x

Van den Ackerveken, G. F., Van Kan, J. A., Joosten, M. H., Muisers, J. M., Verbakel, H. M., & De Wit, P. J. (1993). Characterization of two putative pathogenicity genes of the fungal tomato pathogen *Cladosporium fulvum*. *Molecular Plant-Microbe Interactions*, *6*(2), 210-215. https://doi.org/10.1094/mpmi-6-210

Van den Ackerveken, G. F., Vossen, P., & De Wit, P. J. (1993). The Avr9 race-specific elicitor of *Cladosporium fulvum* is processed by endogenous and plant proteases. *Plant Physiology*, *103*(1), 91-96. https://doi.org/10.1104/pp.103.1.91

van den Burg, H. A., Harrison, S. J., Joosten, M., Vervoort, J., & de Wit, P. (2006). *Cladosporium fulvum* Avr4 protects fungal cell walls against hydrolysis by plant chitinases accumulating during infection [Article]. *Molecular Plant-Microbe Interactions*, *19*(12), 1420-1430. https://doi.org/10.1094/mpmi-19-1420

van den Burg, H. A., Westerink, N., Francoijs, K. J., Roth, R., Woestenenk, E., Boeren, S., de Wit, P. J., Joosten, M. H., & Vervoort, J. (2003). Natural disulfide bond-disrupted mutants of Avr4 of the tomato pathogen *Cladosporium fulvum* are sensitive to proteolysis, circumvent Cf-4-mediated resistance, but retain their chitin binding ability. *Journal of Biochemical Chemistry*, *278*(30), 27340-27346. https://doi.org/10.1074/jbc.M212196200

van der Burgh, A. M., & Joosten, M. (2019). Plant immunity: thinking outside and inside the box. *Trends in Plant Science*, *24*(7), 587-601. https://doi.org/10.1016/j.tplants.2019.04.009

Van der Hoorn, R. A. L., Laurent, F., Roth, R., & De Wit, P. (2000). Agroinfiltration is a versatile tool that facilitates comparative analyses of Avr9/Cf-9-induced and Avr4/Cf-4-induced necrosis [Article]. *Molecular Plant-Microbe Interactions*, *13*(4), 439-446. https://doi.org/10.1094/mpmi.2000.13.4.439

van Esse, H. P., Bolton, M. D., Stergiopoulos, I., de Wit, P., & Thomma, B. (2007). The chitin-binding *Cladosporium fulvum* effector protein Avr4 is a virulence factor [Article]. *Molecular Plant-Microbe Interactions*, *20*(9), 1092-1101. https://doi.org/10.1094/mpmi-20-9-1092

van Esse, H. P., van't Klooster, J. W., Bolton, M. D., Yadeta, K. A., van Baarlen, P., Boeren, S., Vervoort, J., de Wit, P., & Thomma, B. (2008). The *Cladosporium fulvum* virulence protein Avr2 inhibits host proteases required for basal defense [Article]. *Plant Cell*, *20*(7), 1948-1963. https://doi.org/10.1105/tpc.108.059394

van Kan, J. A., van den Ackerveken, G. F., & de Wit, P. J. (1991). Cloning and characterization of cDNA of avirulence gene *Avr9* of the fungal pathogen *Cladosporium fulvum*, causal agent of tomato leaf mold. *Molecular Plant-Microbe Interactions*, *4*(1), 52-59. https://doi.org/10.1094/mpmi-4-052

Varet, A., Hause, B., Hause, G., Scheel, D., & Lee, J. (2003). The *Arabidopsis NHL3* gene encodes a plasma membrane protein and its overexpression correlates with increased resistance to *Pseudomonas syringae* pv. tomato DC3000. *Plant Physiology*, *132*(4), 2023-2033. https://doi.org/10.1104/pp.103.020438

Veloukas, T., Bardas, G. A., Karaoglanidis, G. S., & Tzavella-Klonari, K. (2007). Management of tomato leaf mould caused by *Cladosporium fulvum* with trifloxystrobin. *Crop Protection*, *26*(6), 845-851. https://doi.org/https://doi.org/10.1016/j.cropro.2006.08.005

Villani, S. M., Hulvey, J., Hily, J.-M., & Cox, K. D. (2016). Overexpression of the *CYP51A1* gene and repeated elements are associated with differential sensitivity to DMI fungicides in *Venturia inaequalis*. *Phytopathology*, *106*(6), 562-571. https://doi.org/10.1094/phyto-10-15-0254-r

Vinatzer, B. A., Patocchi, A., Gianfranceschi, L., Tartarini, S., Zhang, H.-B., Gessler, C., & Sansavini, S. (2001). Apple contains receptor-like genes homologous to the *Cladosporium fulvum* resistance gene family of tomato with a cluster of genes

cosegregating with *Vf* apple scab resistance. *Molecular Plant-Microbe Interactions*, *14*(4), 508-515. https://doi.org/10.1094/MPMI.2001.14.4.508

Viotti, C. (2016). ER to Golgi-dependent protein secretion: the conventional pathway. In A. Pompa & F. De Marchis (Eds.), *Unconventional Protein Secretion: Methods and Protocols* (pp. 3-29). Springer New York. https://doi.org/10.1007/978-1-4939-3804-9_1

Vleeshouwers, V. G., & Oliver, R. P. (2014). Effectors as tools in disease resistance breeding against biotrophic, hemibiotrophic, and necrotrophic plant pathogens. *Molecular Plant-Microbe Interactions*, *27*(3), 196-206. https://doi.org/10.1094/MPMI-10-13-0313-IA

Vleeshouwers, V. G., Rietman, H., Krenek, P., Champouret, N., Young, C., Oh, S. K., Wang, M., Bouwmeester, K., Vosman, B., Visser, R. G., Jacobsen, E., Govers, F., Kamoun, S., & Van der Vossen, E. A. (2008). Effector genomics accelerates discovery and functional profiling of potato disease resistance and *Phytophthora infestans* avirulence genes. *PLoS One*, *3*(8), e2875. https://doi.org/10.1371/journal.pone.0002875

Wan, J., Tanaka, K., Zhang, X.-C., Son, G. H., Brechenmacher, L., Nguyen, T. H. N., & Stacey, G. (2012). LYK4, a lysin motif receptor-like kinase, is important for chitin signaling and plant innate immunity in *Arabidopsis* *Plant Physiology*, *160*(1), 396-406. https://doi.org/10.1104/pp.112.201699

Wang, Xu, Y., Sun, Y., Wang, H., Qi, J., Wan, B., Ye, W., Lin, Y., Shao, Y., Dong, S., Tyler, B. M., & Wang, Y. (2018). Leucine-rich repeat receptor-like gene screen reveals that *Nicotiana* RXEG1 regulates glycoside hydrolase 12 MAMP detection. *Nature Communications*, *9*(1), 594. https://doi.org/10.1038/s41467-018-03010-8

Wang, B. N., Yang, X. F., Zeng, H. M., Liu, H., Zhou, T. T., Tan, B. B., Yuan, J. J., Guo, L. H., & Qiu, D. W. (2012). The purification and characterization of a novel hypersensitive-like response-inducing elicitor from *Verticillium dahliae* that induces resistance responses in tobacco [Article]. *Applied Microbiology and Biotechnology*, *93*(1), 191-201. https://doi.org/10.1007/s00253-011-3405-1

Wang, F., Lin, Y., Yin, W.-X., Peng, Y.-L., Schnabel, G., Huang, J.-B., & Luo, C.-X. (2015). The Y137H mutation of *VvCYP51* gene confers the reduced sensitivity to tebuconazole in *Villosiclava virens*. *Scientific Reports*, *5*(1), 17575. https://doi.org/10.1038/srep17575

Wang, J., Hu, M., Wang, J., Qi, J., Han, Z., Wang, G., Qi, Y., Wang, H.-W., Zhou, J.-M., & Chai, J. (2019). Reconstitution and structure of a plant NLR resistosome conferring immunity. *Science*, *364*(6435), eaav5870. https://doi.org/doi:10.1126/science.aav5870

Wang, W., An, B., Feng, L., He, C., & Luo, H. (2018). A *Colletotrichum gloeosporioides* cerato-platanin protein, CgCP1, contributes to conidiation and plays roles in the interaction with rubber tree. *Canadian Journal of Microbiology*, *64*(11), 826-834. https://doi.org/10.1139/cjm-2018-0087

Wang, X., Guo, B., Gao, Y., Mu, W., & Liu, F. (2017). The toxicity of six triazole fungicides to *Cladosporium fulvum* and their safety and field efficacy in the control of tomato leaf mold. *Journal of Plant Protection*, *44*(4), 671-678. <Go to ISI>://CABI:20173350867

Wang, Y., Liu, W., & Wu, H. (2021). Genomic sequence resource of *Exserohilum rostratum*, an important pathogen causing corn leaf disease. *Unpublished*.

Wang, Y., & Wang, Y. (2018). Trick or treat: microbial pathogens evolved apoplastic effectors modulating plant susceptibility to infection. *Molecular Plant-Microbe Interactions*, *31*(1), 6-12. https://doi.org/10.1094/mpmi-07-17-0177-fi

Wang, Y., Wang, Y. C., & Wang, Y. M. (2020). Apoplastic proteases: powerful weapons against pathogen infection in plants [Review]. *Plant Communications*, *1*(4), 10, Article 100085. https://doi.org/10.1016/j.xplc.2020.100085

Waszczak, C., Carmody, M., & Kangasjärvi, J. (2018). Reactive oxygen species in plant signaling. *Annual Review of Plant Biology*, *69*(1), 209-236. https://doi.org/10.1146/annurev-arplant-042817-040322

Watanabe, H., Horinouchi, H., Muramoto, Y., & Ishii, H. (2017). Occurrence of azoxystrobin-resistant isolates in *Passalora fulva*, the pathogen of tomato leaf mould disease. *Plant Pathology*, *66*(9), 1472-1479. https://doi.org/https://doi.org/10.1111/ppa.12701

Weber, E., Engler, C., Gruetzner, R., Werner, S., & Marillonnet, S. (2011). A modular cloning system for standardized assembly of multigene constructs. *PLoS One*, *6*(2), e16765. https://doi.org/10.1371/journal.pone.0016765

Weiland, J., & Koch, G. (2004). Sugarbeet leaf spot disease (*Cercospora beticola* Sacc.)dagger. *Molecular Plant Pathology*, *5*(3), 157-166. https://doi.org/10.1111/j.1364-3703.2004.00218.x

Westerink, N., Brandwagt, B. F., De Wit, P. J. G. M., & Joosten, M. H. A. J. (2004). *Cladosporium fulvum* circumvents the second functional resistance gene homologue at the *Cf-4* locus (*Hcr9-4E*) by secretion of a stable avr4E isoform. *Molecular Microbiology*, *54*(2), 533-545. https://doi.org/10.1111/j.1365-2958.2004.04288.x

Wheeler, J., Jones, D. A., Kastner, P., Taranto, A. P., Cooke, I. R., Boshoven, J. C., Shiller, J. B., Mesarich, C. H., Thomma, B. P. H. J., Deng, C. H., Bowen, J. K., & Plummer, K. M. (2019). Characterisation of an expanded family of plant natriuretic peptide-like proteins in the apple and pear scab pathogens. *Unpublished*.

Wijayawardene, N. N., Hyde, K. D., Rajeshkumar, K. C., Hawksworth, D. L., Madrid, H., Kirk, P. M., Braun, U., Singh, R. V., Crous, P. W., Kukwa, M., Lücking, R., Kurtzman, C. P., Yurkov, A., Haelewaters, D., Aptroot, A., Lumbsch, H. T., Timdal, E., Ertz, D., Etayo, J., Phillips, A. J. L., Groenewald, J. Z., Papizadeh, M., Selbmann, L., Dayarathne, M. C., Weerakoon, G., Jones, E. B. G., Suetrong, S., Tian, Q., Castañeda-Ruiz, R. F., Bahkali, A. H., Pang, K.-L., Tanaka, K., Dai, D. Q., Sakayaroj, J., Hujslová, M., Lombard, L., Shenoy, B. D., Suija, A., Maharachchikumbura, S. S. N., Thambugala, K. M., Wanasinghe, D. N., Sharma, B. O., Gaikwad, S., Pandit, G., Zucconi, L., Onofri, S., Egidi, E., Raja, H. A., Kodsueb, R., Cáceres, M. E. S., Pérez-Ortega, S., Fiuza, P. O., Monteiro, J. S., Vasilyeva, L. N., Shivas, R. G., Prieto, M., Wedin, M., Olariaga, I., Lateef, A. A., Agrawal, Y., Fazeli, S. A. S., Amoozegar, M. A., Zhao, G. Z., Pfliegler, W. P., Sharma, G., Oset, M., Abdel-Wahab, M. A., Takamatsu, S., Bensch, K., de Silva, N. I., De Kesel, A., Karunarathna, A., Boonmee, S., Pfister, D. H., Lu, Y.-Z., Luo, Z.-L., Boonyuen, N., Daranagama, D. A., Senanayake, I. C., Jayasiri, S. C., Samarakoon, M. C., Zeng, X.-Y., Doilom, M., Quijada, L., Rampadarath, S., Heredia, G., Dissanayake, A. J., Jayawardana, R. S., Perera, R. H., Tang, L. Z., Phukhamsakda, C., Hernández-Restrepo, M., Ma, X.,

Tibpromma, S., Gusmao, L. F. P., Weerahewa, D., & Karunarathna, S. C. (2017). Notes for genera: *Ascomycota*. *Fungal Diversity*, *86*(1), 1-594. https://doi.org/10.1007/s13225-017-0386-0

Williams, E., & Shay, J. (1957). The relationship of genes for pathogenicity and certain other characters in *Venturia inaequalis* (Cke.) Wint. *Genetics*, *42*(6), 704.

Wösten, H. A. B. (2001). Hydrophobins: multipurpose proteins. *Annual Review of Microbiology*, *55*(1), 625-646. https://doi.org/10.1146/annurev.micro.55.1.625

Wright, P. E., & Dyson, H. J. (1999). Intrinsically unstructured proteins: re-assessing the protein structure-function paradigm. *Journal of Molecular Biology*, *293*(2), 321-331. https://doi.org/https://doi.org/10.1006/jmbi.1999.3110

Wu, H., Schoch, C., Boonmee, S., Bahkali, A., Chomnunti, P., & Hyde, K. (2011). A reappraisal of *Microthyriaceae*. *Fungal Diversity*, *51*, 189-248. https://doi.org/10.1007/s13225-011-0143-8

Wu, J., Kou, Y., Bao, J., Li, Y., Tang, M., Zhu, X., Ponaya, A., Xiao, G., Li, J., Li, C., Song, M.-Y., Cumagun, C. J. R., Deng, Q., Lu, G., Jeon, J.-S., Naqvi, N. I., & Zhou, B. (2015). Comparative genomics identifies the *Magnaporthe oryzae* avirulence effector *AvrPi9* that triggers *Pi9*-mediated blast resistance in rice. *New Phytologist*, *206*(4), 1463-1475. https://doi.org/https://doi.org/10.1111/nph.13310

Wubben, J. P., Eijkelboom, C. A., & De Wit, P. J. G. M. (1993). Accumulation of pathogenesis-related proteins in the epidermis of tomato leaves infected by *Cladosporium fulvum*. *Netherlands Journal of Plant Pathology*, *99*(3), 231-239. https://doi.org/10.1007/BF03041412

Wubben, J. P., Joosten, M. H., & De Wit, P. J. (1994). Expression and localization of two in planta induced extracellular proteins of the fungal tomato pathogen *Cladosporium fulvum*. *Molecular plant-microbe interactions 7*(4), 516-524. https://doi.org/10.1094/mpmi-7-0516

Wulff, B. B., Thomas, C. M., Smoker, M., Grant, M., & Jones, J. D. (2001). Domain swapping and gene shuffling identify sequences required for induction of an Avr-dependent hypersensitive response by the tomato Cf-4 and Cf-9 proteins. *Plant Cell*, *13*(2), 255-272. https://doi.org/10.1105/tpc.13.2.255

Wulff, B. B. H., Chakrabarti, A., & Jones, D. A. (2009). Recognitional specificity and evolution in the tomato–*Cladosporium fulvum* pathosystem. *Molecular Plant-Microbe Interactions*, *22*(10), 1191-1202. https://doi.org/10.1094/mpmi-22-10-1191

Xin, G. (2019). Comparative genomics and association analysis identifies virulence genes of *Cercospora sojin*a on soybean. *Unpublished*.

Xu, J., & Zhang, S. (2015). Mitogen-activated protein kinase cascades in signaling plant growth and development. *Trends in Plant Science*, *20*(1), 56-64. https://doi.org/10.1016/j.tplants.2014.10.001

Xu, X. M., & Robinson, J. (2005). Modelling the effects of wetness duration and fruit maturity on infection of apple fruits of Cox's Orange Pippin and two clones of Gala by *Venturia inaequalis*. *Plant Pathology*, *54*(3), 347-356. https://doi.org/doi:10.1111/j.1365-3059.2005.01177.x

Xue, B., Blocquel, D., Habchi, J., Uversky, A. V., Kurgan, L., Uversky, V. N., & Longhi, S. (2014). Structural disorder in viral proteins. *Chemical Reviews*, *114*(13), 6880-6911. https://doi.org/10.1021/cr4005692

Xue, C., Park, G., Choi, W., Zheng, L., Dean, R. A., & Xu, J.-R. (2002). Two novel fungal virulence genes specifically expressed in appressoria of the rice blast fungus. *The Plant Cell*, *14*(9), 2107-2119. https://doi.org/10.1105/tpc.003426

Yan, L., Chen, J., Zhang, C., & Ma, Z. (2008). Molecular characterization of benzimidazole-resistant isolates of *Cladosporium fulvum*. *FEMS Microbiology Letters*, *278*(2), 242-248. https://doi.org/10.1111/j.1574-6968.2007.00999.x

Yang, L.-N., Liu, H., Duan, G.-H., Huang, Y.-M., Liu, S., Fang, Z.-G., Wu, E.-J., Shang, L., & Zhan, J. (2020). The *Phytophthora infestans* AVR2 effector escapes R2 recognition through effector disordering. *Molecular Plant-Microbe Interactions*, *33*(7), 921-931. https://doi.org/10.1094/mpmi-07-19-0179-r

Yennawar, N. H., Li, L. C., Dudzinski, D. M., Tabuchi, A., & Cosgrove, D. J. (2006). Crystal structure and activities of EXPB1 (*Zea m* 1), a beta-expansin and group-1 pollen allergen from maize. *Proceedings of the National Academy of Sciences*, *103*(40), 14664-14671. https://doi.org/10.1073/pnas.0605979103

Yoshida, K., Asano, S., Sushida, H., & Iida, Y. (2021). Occurrence of tomato leaf mold caused by novel race 2.4.9 of *Cladosporium fulvum* in Japan. *Journal of General Plant Pathology*, *87*(1), 35-38. https://doi.org/10.1007/s10327-020-00963-x

Yoshida, K., Saitoh, H., Fujisawa, S., Kanzaki, H., Matsumura, H., Yoshida, K., Tosa, Y., Chuma, I., Takano, Y., & Win, J. (2009). Association genetics reveals three novel avirulence genes from the rice blast fungal pathogen *Magnaporthe oryzae*. *The Plant Cell*, *21*(5), 1573-1591.

Young, C. A., Cox, M. P., Ganley, A. R. D., & David, W. J. (2019). *Finished genome of Venturia effusa*

Yu, C., Diao, Y., Lu, Q., Zhao, J., Cui, S., Peng, C., He, B., & Liu, H. (2020). *Genome assembly and annotation of Botryosphaeria dothidea sdau 11-99, a latent pathogen of apple fruit ring rot in China*

Yu, D. S., Outram, M. A., Smith, A., McCombe, C. L., Khambalkar, P. B., Rima, S. A., Sun, X., Ma, L., Ericsson, D. J., Jones, D. A., & Williams, S. J. (2021). The structural repertoire of *Fusarium oxysporum* f. sp. *lycopersici* effectors revealed by experimental and computational studies. *bioRxiv*, 2021.2012.2014.472499. https://doi.org/10.1101/2021.12.14.472499

Yuzo, Y., & Yuri, A. (1987). Interaction of azole antifungal agents with cytochrome P-45014DM purified from *Saccharomyces cerevisiae* microsomes. *Biochemical pharmacology*, *36*(2), 229-235.

Zaccaron, A. (2020). *Draft genome resource of the tomato pathogen Pseudocercospora fuligena*. University of California.

Zaccaron, A., & Stergiopoulos, I. (2021). A chromosome-scale genome assembly of the tomato pathogen *Cladosporium fulvum* reveals a compartmentalized genome architecture and the presence of a dispensable chromosome. *Unpublished*.

Zaccaron , A. Z., & Bluhm, B. H. (2017). The genome sequence of *Bipolaris cookei* reveals mechanisms of pathogenesis underlying target leaf spot of sorghum. *Scientific Reports*. https://doi.org/https://doi.org/10.1038/s41598-017-17476-x

Zaynab, M., Fatima, M., Abbas, S., Sharif, Y., Umair, M., Zafar, M. H., & Bahadar, K. (2018). Role of secondary metabolites in plant defense against pathogens. *Microbial Pathogenesis*, *124*, 198-202. https://doi.org/https://doi.org/10.1016/j.micpath.2018.08.034

Zeng, F., Wang, C., Zhang, G., Wei, J., Bradley, C. A., & Ming, R. (2017). Draft genome sequence of *Cercospora sojina* isolate S9, a fungus causing frogeye leaf spot (FLS) disease of soybean. *Genomics Data*, *12*, 79-80. https://doi.org/10.1016/j.gdata.2017.02.014

Zhan, J., Pettway, R. E., & McDonald, B. A. (2003). The global genetic structure of the wheat pathogen *Mycosphaerella graminicola* is characterized by high nuclear diversity, low mitochondrial diversity, regular recombination, and gene flow. *Fungal Genetics and Biology*, *38*(3), 286-297. https://doi.org/10.1016/s1087-1845(02)00538-8

Zhang, Gao, Y., Liang, Y., Dong, Y., Yang, X., & Qiu, D. (2018). *Verticillium dahliae* Alt a 1-like protein PevD1 targets cotton PR5-like protein and contributes to fungal infection. *Journal of experimental botany*. https://doi.org/10.1093/jxb/ery351

Zhang, Liang, Y., Dong, Y., Gao, Y., Yang, X., Yuan, J., & Qiu, D. (2017). The *Magnaporthe oryzae* Alt A 1-like protein MoHrip1 binds to the plant plasma membrane. *Biochemical and Biophysical Research Communications*, *492*(1), 55-60. https://doi.org/doi:10.1016/j.bbrc.2017.08.039

Zhang, M., & Coaker, G. (2017). Harnessing effector-triggered immunity for durable disease resistance. *Phytopathology*, *107*(8), 912-919. https://doi.org/10.1094/phyto-03-17-0086-rvw

Zhang, M., Xie, S., Zhao, Y., Meng, X., Song, L., Feng, H., & Huang, L. (2019). Hce2 domain-containing effectors contribute to the full virulence of *Valsa mali* in a redundant manner. *Molecular Plant Pathology*, *20*(6), 843-856. https://doi.org/10.1111/mpp.12796

Zhang, Z., Fradin, E., de Jonge, R., van Esse, H. P., Smit, P., Liu, C.-M., & Thomma, B. P. H. J. (2013). Optimized agroinfiltration and virus-induced gene silencing to study Ve1-mediated *Verticillium* resistance in tobacco. *Molecular Plant-Microbe Interactions*, *26*(2), 182-190. https://doi.org/10.1094/mpmi-06-12-0161-r

Zhang, Z., van Esse, H. P., van Damme, M., Fradin, E. F., Liu, C.-M., & Thomma, B. P. H. J. (2013). Ve1-mediated resistance against *Verticillium* does not involve a hypersensitive response in Arabidopsis. *Molecular Plant Pathology*, *14*(7), 719-727. https://doi.org/https://doi.org/10.1111/mpp.12042

Zhong, Z., Marcel, T. C., Hartmann, F. E., Ma, X., Plissonneau, C., Zala, M., Ducasse, A., Confais, J., Compain, J., Lapalu, N., Amselem, J., McDonald, B. A., Croll, D., & Palma-Guerrero, J. (2017). A small secreted protein in *Zymoseptoria tritici* is responsible for avirulence on wheat cultivars carrying the *Stb6* resistance gene. *New Phytologist*, *214*(2), 619-631. https://doi.org/10.1111/nph.14434

Zhou, E., Jia, Y., Singh, P., Correll, J. C., & Lee, F. N. (2007). Instability of the *Magnaporthe oryzae* avirulence gene AVR-Pita alters virulence. *Fungal Genetics and Biology*, *44*(10), 1024-1034. https://doi.org/https://doi.org/10.1016/j.fgb.2007.02.003

Zhou, R., Zhu, T., Han, L., Liu, M., Xu, M., Liu, Y., Han, D., Qiu, D., Gong, Q., & Liu, X. (2017). The asparagine-rich protein NRP interacts with the *Verticillium* effector PevD1 and regulates the subcellular localization of cryptochrome 2. *Journal of experimental botany*, *68*(13), 3427-3440. https://doi.org/10.1093/jxb/erx192

Zhou, Y., Zhang, L., Fan, F., Wang, Z.-Q., Huang, Y., Yin, L.-F., Yin, W.-X., & Luo, C.-X. (2021). Genome sequence of *Venturia carpophila*, the causal agent of peach scab. *Molecular Plant-Microbe Interactions*, *34*(7), 852-856. https://doi.org/10.1094/mpmi-11-20-0321-a

Zhu, J., Jeong, J. S., & Khang, C. H. (2021). Tandem DNA repeats contain cis-regulatory sequences that activate biotrophy-specific expression of *Magnaporthe* effector gene *PWL2*. *Molecular Plant Pathology*, *22*(5), 508-521. https://doi.org/10.1111/mpp.13038

Zhuang, M., Calabrese, M. F., Liu, J., Waddell, M. B., Nourse, A., Hammel, M., Miller, D. J., Walden, H., Duda, D. M., Seyedin, S. N., Hoggard, T., Harper, J. W., White, K. P., & Schulman, B. A. (2009). Structures of SPOP-substrate complexes: insights into molecular architectures of BTB-Cul3 ubiquitin ligases. *Molecular Cell*, *36*(1), 39-50. https://doi.org/10.1016/j.molcel.2009.09.022

Zipfel, C. (2014). Plant pattern-recognition receptors [Review]. *Trends in Immunology*, *35*(7), 345-351. https://doi.org/10.1016/j.it.2014.05.004